THE PHYSICAL REVIEW

A journal of experimental and theoretical physics established by E. L. Nichols in 1893

Published by the American Institute of Physics for the

AMERICAN PHYSICAL SOCIETY

Officers

President

F. W. LOOMIS
University of Illinois
Urbana, Illinois

Vice-President

I. I. RABI
Columbia University
New York, New York

Secretary

K. K. DARROW
Bell Telephone Laboratories
Office:
Columbia University
New York 27, New York

Treasurer

G. B. PEGRAM
Columbia University
New York 27, New York

Local Secretary for the Pacific Coast

J. KAPLAN
University of California at Los Angeles
Los Angeles, California

Managing Editor

JOHN T. TATE
University of Minnesota
Minneapolis, Minnesota

BOARD OF EDITORS

Editor

JOHN T. TATE

Assistant Editor

J. W. BUCHTA

Associate Editors

H. A. BETHE	S. A. GOUDSMIT	W. E. LAMB, JR.
L. A. RINGHOUR	E. M. PURCELL	R. G. HERB
W. G. ZACHARIASEN	V. F. WEISSKOPF	J. BARDEEN

Manuscripts for publication should be submitted to John T. Tate, University of Minnesota, Minneapolis, Minnesota. The authors' institutions are requested to pay a publication charge of $4 per page which, if honored, entitles them to 100 free reprints. Instructions will be sent with galley proofs.

Proof and all correspondence concerning papers in the process of publication should be addressed to the Publication Manager, American Institute of Physics, 57 East 55 Street, New York 22, New York.

Subscription Price

United States and Canada.....$15.00
Elsewhere.....$16.50

Back Numbers[1]

Ready back number rate when complete year is available: $20.00.
Single copies: $2.00 each, prior to July, 1929;
$1.00 each, July, 1929–December, 1941;
$2.00 each, January, 1942–December, 1946.
Current issues: $1.00 each.
General index, 1893–1920: $4.00.

Subscriptions and orders for back numbers should be addressed to Prince and Lemon Streets, Lancaster, Pennsylvania, or to the American Institute of Physics, 57 East 55 Street, New York 22, New York.

Changes of address in the case of members of the American Physical Society should be addressed to the Treasurer; in the case of other subscribers to the Physical Review, to the Business Manager, American Institute of Physics.

[1] See Series I Register of Physics Department, Cornell University, Ithaca, New York.

The Physical Review is published bimonthly at Prince and Lemon Streets, Lancaster, Pennsylvania.

Entered as second-class matter March 6, 1918, at the Post Office at Lancaster, Pennsylvania, under the Act of March 3, 1879.

Acceptance for mailing at special rate of postage provided for in paragraph 4, section 538, P. L. & R., authorized January 27, 1925.

THE
PHYSICAL REVIEW

A journal of experimental and theoretical physics established by E. L. Nichols in 1893

SECOND SERIES, VOL. 75, NO. 12 JUNE 15, 1949

Capture Cross Sections for Fast Neutrons

D. J. HUGHES, W. D. B. SPATZ, AND N. GOLDSTEIN
Argonne National Laboratory, Chicago, Illinois
(Received January 27, 1949)

The neutron capture cross sections at an effective energy of one Mev have been measured for 32 isotopes, including 4 isomeric pairs. Unmoderated fission neutrons were used as the source, and the high intensities available by this method have made it possible to measure fast cross sections as low as 10^{-4} barn. The cross sections (except those for a few "magic number" nuclei) show a smooth variation with atomic weight, ranging from 10^{-1} b at $A=100$ to 10^{-4} b at $A=20$. The rapid change in cross section is a measure of the change in level spacing of the compound nucleus formed after neutron capture. A survey is made of all the existing data on absorption cross sections as functions of A and neutron energy.

I. INTRODUCTION

CROSS-SECTION measurements made with neutrons from chain-reacting piles have been mainly those at or near thermal energy. Although piles have a high flux of neutrons extending all the way from fission energies to thermal the great spread in energy has made cross-section measurements at specific energies exceedingly difficult. It was the purpose of the present measurements to isolate a particular group of fast neutrons, the nascent fission neutrons of energy about one Mev, and use them for measurement of absorption cross sections. Although the fission neutrons themselves show a large spread in energy, the measured cross sections can be correctly interpreted because of the smooth variation of cross section with energy in the one-Mev region. The absorption cross section for thermal neutrons varies irregularly from isotope to isotope depending on the proximity of the closest resonance level. As the neutron energy is raised, however, the width and density of the levels increase until even with a monoenergetic neutron source the observed cross section becomes an average over several levels. The absorption cross section at such high energies thus depends on the average behavior of the resonances, and is expected to be a slowly varying function of neutron energy and atomic weight. The disadvantage of the energy spread is further compensated by the large available flux, absolute calibration, and steadiness of the pile as a neutron source.

The theory of resonance absorption of neutrons in terms of the "Breit-Wigner" formula has been treated by many authors. The discussion of Feshbach, Peaslee, and Weisskopf[1] is quite convenient for the present measurements. FPW show that the average absorption cross section for fast neutrons in a small energy band ΔE at E is given by

$$\sigma_a{}^l=\frac{\pi}{k^2}(2l+1)\frac{2\pi(\Gamma_{nl}\Gamma_{al})_{\rm av}}{D_l[(\Gamma_{nl})_{\rm av}+(\Gamma_{al})_{\rm av}]} \qquad (1)$$

where $\sigma_a{}^l$ is the contribution to the cross section of neutrons with angular momentum $l\hbar$ and wave number k. Γ_{nl} and Γ_{al} are the neutron and absorption widths for the many levels involved ("av" signifies average value) and D_l is the level spacing. Considering only $l=0$, it is seen that where $\Gamma_n>\Gamma_a$ (neutron energy >10 kev) the variation of cross section with energy will be as $1/E$. As the neutron energy is raised, the capture cross section falls off less rapidly as higher l scattering becomes important. The onset of inelastic scattering, however, decreases the capture cross section and the energy dependence at one Mev will be the resultant of the higher l and the inelastic scattering effects. Any variation of cross section from isotope to isotope in

[1] H. Feshbach, D. C. Peaslee, and V. F. Weisskopf, Phys. Rev. 71, 145 (1947).

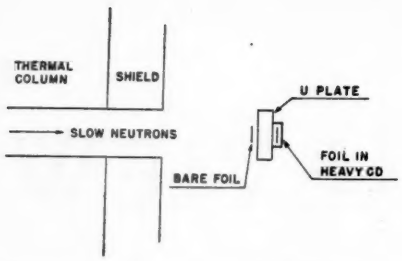

FIG. 1. Apparatus for measurement of activation cross sections for fission neutrons.

this energy region would reflect the variation mainly in level spacing, D. Thus it would be expected that the cross section at one Mev would increase with atomic weight rapidly at first (as D decreases with increasing complexity of the nucleus) then would change only slowly for heavy nuclei (as D changes slowly—see FPW, p. 155). Of course any unusual values of the neutron binding energy might be expected to give unusual values of D and hence of cross section. Measurements of absorption cross sections thus give information on the average level behavior, particularly the level spacing, D. It is because of this dependence of the cross section on the average level behavior that the spread in energy of the fission neutron distribution does not prove to be a serious complicating factor in the present measurements.

At the time the present experiments were begun, some experimental results were available on absorption cross sections for neutrons in the region of one Mev, based on work with cyclotrons, Van de Graaffs, Ra-α-Be, and photo-neutron sources. The reported cross sections were mainly for heavy nuclei (large cross sections) and in general were quite uncertain in regard to absolute calibration because of the difficulty of measuring fast neutron flux, although some of the Los Alamos results were based on careful flux calibration. The present method was devised to improve the absolute cross-section values and to extend them to the light elements for which no values existed.

TABLE I. Neutron cross sections at 1 Mev effective energy.

Isotope	Activity	Isotopic Activation Cross-Sections Thermal*	Fast	Remarks
Na^{23}	14.8 hr.	0.55 barns	0.29 mb	
Mg^{28}	10.2 min.	0.049	0.60	
Al^{27}	2.4 min.	0.23	0.40	
Cl^{37}	37 min.	0.61	0.80	
K^{41}	12.4 hr.	1.0	2.9	
V^{51}	3.9 min.	5.5	2.2	
Co^{59}	10.7 min.	0.72	0.23 } 9.2	The total σ_a is based on the assumption that the isomeric ratio of 30/0.72 holds for fast neutrons.
	5 yr.	30	— }	
Mn^{55}	2.6 hr.	11.5	3.5	
Ni^{64}	2.6 hr.	3.4	6.7	See text
Cu^{63}	12.8 hr.	3.1	8.9	
Cu^{65}	5 min.	2.0	6.0	
Zn^{68}	57 min.	0.89	7.1 } 20.1	Isomeric ratio: Thermal 10.5; fast 0.55
	13.8 hr.	0.085	13.0 }	
Ga^{69}	20 min.	1.52	22.7	
As^{75}	26.8 hr.	4.2	23	
Br^{79}	18 min.	8.9	30 } 44	Isomeric ratio: Thermal 3.0; fast 2.1
	4.4 hr.	3.0	14 }	
Br^{81}	34 hr.	2.3	17	
Cb^{93}	6.6 min.	1.4	52	See text
Mo^{98}	67 hr.	0.39	32	
Mo^{100}	14.6 min.	0.22	15	
Rh^{103}	44 sec.	150	103 } 119.5	Isomeric ratio: Thermal 11.7; fast 6.3
	4.2 min.	12.8	16.5 }	
Ag^{107}	2.3 min.	48	127	
Ag^{109}	22 sec.	108	225	
In^{115}	13 sec.	57	63 } 243	Isomeric ratio: Thermal 0.36; fast 0.35
	54 min.	157	180 }	
Sb^{121}	2.8 day	6.8	90	
I^{127}	25 min.	6.8	107	
Ba^{138}	86 min.	0.56	2.6	
W^{186}	23 hr.	37	66	
Pt^{198}	31 min.	3.6	59	
Au^{197}	2.7 day	96	121	
Hg^{204}	5.5 min.	0.37	88	
Pb^{208}	3 hr.	0.00046	1.8	
Bi^{209}	5 day	0.015	3.0	

* Values taken from Seren's survey (see reference 4), or from unreported work at Argonne Laboratory.

II. EXPERIMENTAL METHOD

Unmoderated fission neutrons were obtained (Fig. 1) by irradiating a plate of uranium metal in a beam of slow neutrons from the thermal column of the Argonne heavy water pile. A foil placed inside heavy Cd near such a plate receives only unmoderated fission neutrons if all slowing down materials are carefully excluded. As the capture cross section varies as $1/E$, the presence of only a small number of moderated neutrons can vitiate the results. The flux of fast neutrons at the foil can be determined as accurately as the thermal flux can be measured, for the ratio of the fast fission flux to the thermal flux can be calculated from the geometry of the plate and the nuclear constants of uranium.

The procedure, in brief, is to activate a cadmium covered foil of the material of interest with fission neutrons while an identical bare foil is simultaneously activated with thermal (plus fission) neutrons. The two foils are then counted on a G-M counter.

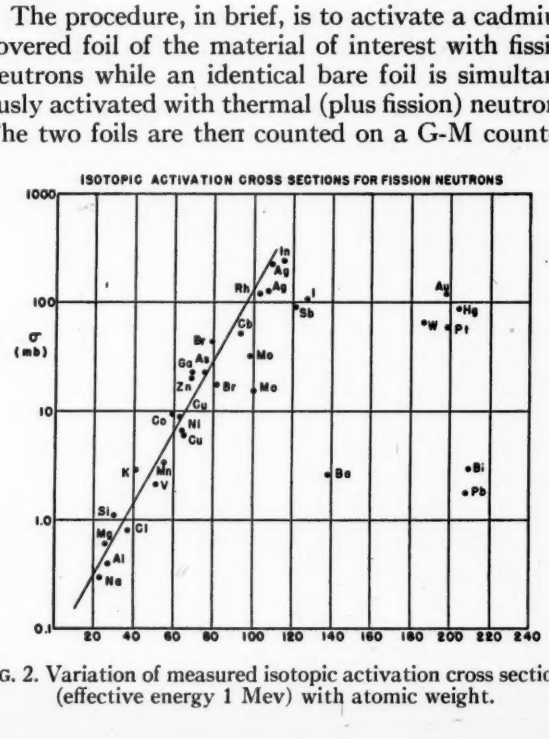

FIG. 2. Variation of measured isotopic activation cross sections (effective energy 1 Mev) with atomic weight.

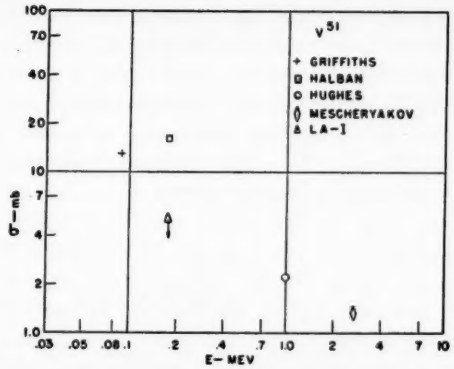

FIG. 3. Figures 3–17 are activation cross sections as a function of neutron energy for various isotopes. All available data are included, those of some observers being adjusted to obtain agreement for Au^{197}. See text for identification and description of the sources of data.

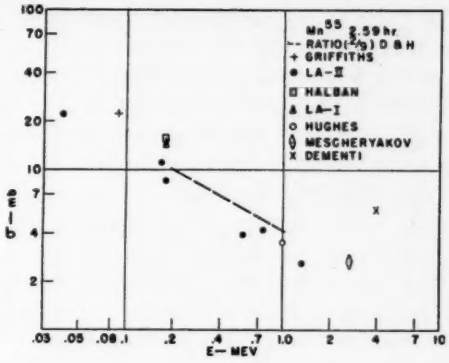

FIG. 4.

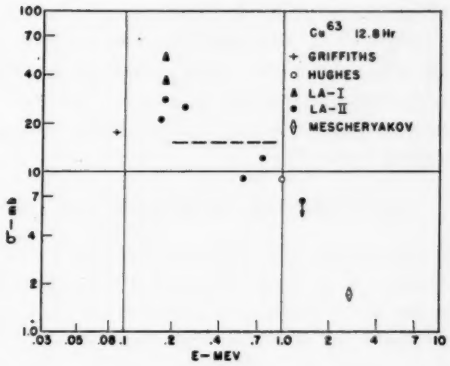

FIG. 5.

The fast activation cross section is obtained directly from the counting rate ratio, the known thermal cross section for the particular activity detected and the calculated ratio of fast to slow flux at the plate (which is approximately unity). In this way no corrections are necessary for self absorption in the foil, complicated decay schemes, or efficiency of the counter. In some cases where the thermal cross section was doubtful, it was determined from the bare foil activation, taking into consideration the thermal flux and the counter efficiency. Because the fast cross section is often only one-thousandth of the thermal it was found extremely important to use a thick, tight Cd cover for the fast irradiation to prevent significant leakage of thermal neutrons. A slight activation sometimes resulted from the small number of resonance neutrons present in the thermal column if the substance had a high resonance cross section. The resonance activation could be estimated easily, however, by running a Cd-covered foil with the uranium plates removed. The cross section obtained by this method is an average over the fission spectrum but, because the variation of $\sigma(n,\gamma)$ with energy is about the same for different elements near 1 Mev (approximately $1/E$), the measured cross section can be correctly considered as the capture cross section at 1 Mev neutron energy (as calculated from the known fission spectrum and a $1/E$ energy dependence).

The technique was first checked by measuring Au^{197}, I^{127} and In^{115} which have large activation cross sections which had already been measured as a function of energy. The results for these isotopes plotted at 1 Mev agreed well with the previous activation cross section values as is shown in Figs. 17, 15, and 14. From these first results it was concluded that the method gave the correct absolute capture cross sections at the calculated effective energy of 1 Mev. As the first elements had been done quite easily the measurements were then extended to elements of lower atomic weight for which no cross sections were available. The method proved quite powerful in measuring the light elements because the high flux made activations possible for extremely low cross sections. A rough survey soon showed: (1) a rapid decrease of the activation cross section, σ_{act} (isotopic), with decreasing atomic weight, A, for $A<100$; in this region σ varied nearly as A^4; (2) a rather smooth dependence of σ on A; the deviations from a smooth curve were not greater than the large experimental uncertainties associated with activation cross-section measurements.

It was seen that if the smooth dependence of σ_{act} (isotopic) on A for $A<100$ were true, then the total radiative capture cross section of an element for fast neutrons could be determined even if only one isotope of small abundance could be activated. This would be so because σ_a, total absorption, would be equal to σ_{act} (isotopic) for any isotope. The smooth dependence on A would also mean that the total absorption cross section of an element with no measurable activation could be predicted; thus it would be expected that iron would have a cross section of 6.5 millibarns (mb $=10^{-3}$ barn) at 1 Mev and would increase about as $1/E$ (see Section IV) for lower energies for at least several hundred kilovolts. The effect of structural materials and fission products in a "fast" pile could then be

predicted which is, of course, impossible for a thermal pile. Although the first measurements included only a few cross sections for heavy elements, it was obvious that the situation for $A>100$ was not simple, as Bi and Pb showed much lower cross sections than the other heavy elements, all of which were in the 100–200 mb range.

After the early measurements, which were undertaken mainly to aid in fast pile design, a great many more cross sections were determined because the method proved to be useful from the standpoint of basic nuclear theory. Recently, Alpher, Bethe, and Gamow[2] have shown an interesting relationship between the fast cross sections and the abundance of the elements and have interpreted the relationship in terms of a neutron-capture theory of the origin of the elements. The work was done at irregular intervals during the past several years but only the final results brought up to date will be presented here.

III. DISCUSSION OF RESULTS

Table I contains the final cross-section values for 32 isotopes, for 4 of which, both activities of isomeric pairs were measured. For each isotope the activity studied, its thermal isotopic activation cross section, and the fast activation cross section (which, barring unknown isomers, and to the extent that the isotopic cross sections follow a smooth curve will be equal to the atomic absorption cross section of the normal element, σ_a) are given. Figure 2 shows the cross sections plotted as a function of atomic weight where it is seen how the values for $A<100$ follow a rapidly rising smooth curve within a factor of about two. Thermal cross sections of course do not behave in such a regular manner and the curve of Fig. 2 can actually be used to infer peculiarities in the thermal cross section if the fast cross section (based on the thermal) does not fall on the curve. Examples of this behavior will be given among the following discussions of individual isotopes.

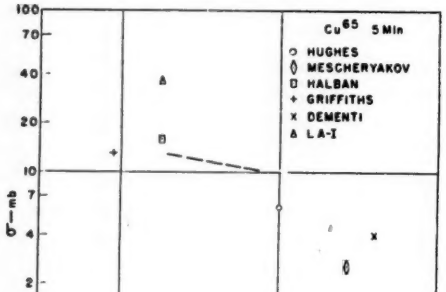

FIG. 6.

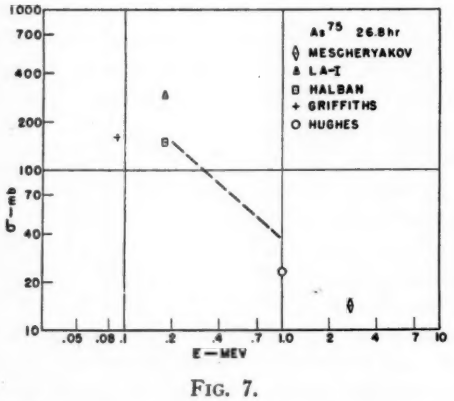

FIG. 7.

Cb93

At the time the present work was begun it was thought that the thermal activation cross section for 6.6 m Cb^{94} was only 0.01 b while the total thermal absorption (as measured by the effect on the pile) was known to be 1.4 b. The fast cross section measured in the present experiments, if based on a thermal value of 1.4 b, turned out to be 52 mb, which is "on" the smooth curve. This result implied that the total thermal activation cross section should be 1.4 b and not 0.01 b (i.e. that the difference was not caused by impurities as had been expected). The correctness of this procedure was shown when it was found by Goldhaber and Sturm[3] that Cb^{94} decayed by isomeric transition and the 0.01 b value was low by just the efficiency factor for γ-detection of a G-M counter, the correct activation cross section being about 1.4 barns.

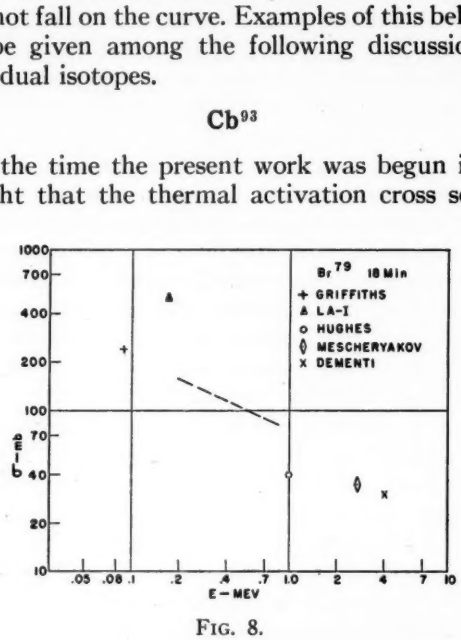

FIG. 8.

Co59

With thermal neutrons, a strong 5 year and a 10.7 minute isomer are produced, with cross section in the ratio 41 (this ratio may actually be lower

[2] R. A. Alpher, H. A. Bethe, and G. Gamow, Phys. Rev. **73**, 1803 (1948); R. A. Alpher, Phys. Rev. **74**, 1577 (1948).

[3] M. Goldhaber and W. Sturm, Phys. Rev. **70**, 111 (1946).

because of uncertainty in the fraction of the 10.7 minute activity which grows into the 5 yr.). In the present experiments only the 10.7 minute activity was measured and the total fast activation cross section was obtained by multiplying the 10.7 minute isomeric cross section by 41. The agreement of the result, 9.2 mb, with the curve indicates that there is no large shift in isomeric ratio with neutron energy in this case.

Ni^{64}

The early results of the present method, based on the extant thermal cross sections, gave a fast cross section far off the curve. It was then decided to remeasure the thermal cross section. The resulting *atomic* activation cross section for the 2.6 hour activity was 0.030 b as compared to the old 0.017 b (Seren's[4] value). In the meantime it was shown by Swartout *et al.*,[5] that the 2.6 hour activity was Ni^{64} (0.88 percent) and not Ni^{62} (3.88 percent). The combined effect of these two corrections was to

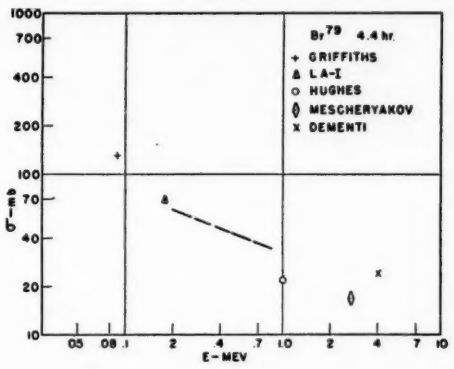

FIG. 9.

raise the fast isotopic cross section by a factor of about 7 and to bring it into agreement with the smooth curve.

Zn^{68}

Measurements of the isomeric activities (57 m and 13.8 h) again gave values off the curve when the listed values[4] of the thermal cross section were used. The thermal measurements were then repeated with the result that the reported 1.09 b isotopic value for the 57 m activity was lowered to 0.89 b and the 13.8 h lowered from 0.31 to 0.085 b. The new thermal cross sections led to a fast total activation of 20.1 mb again in agreement with the curve.

For the four isotopes for which both members of isomeric pairs were measured, the isomeric ratios

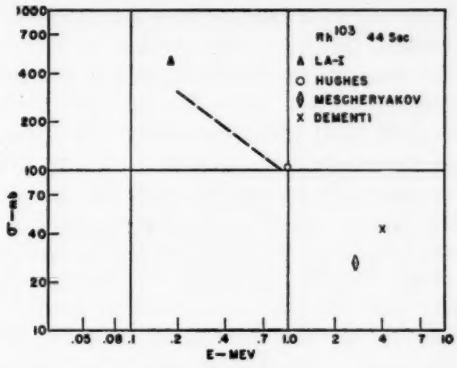

FIG. 10.

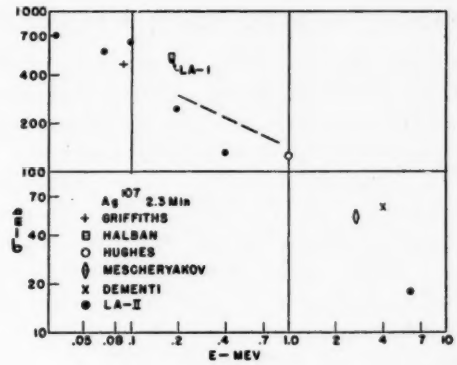

FIG. 11.

(ratios of activation cross sections for the isomers) for thermal and fast neutrons are also given in Table I. In the cases of In^{115}, Rh^{103} and Br^{79} the ratio is the same within experimental error for fast and for slow activation. For Zn^{68}, however, the ratio changes from a thermal value of 10.5 to 0.55 for fast neutrons. The fast isomeric ratio is of course the average of the ratio over many resonance levels of the compound nucleus and might be expected to be different (and closer to unity) than the thermal ratio which usually refers to a single level. The results, for the four isomeric pairs discussed although rough, are not inconsistent with this view as the changes which do show are in the correct direction. The behavior of Co^{59}, however, seems to indicate a large isomeric ratio which does not change greatly with neutron energy.

Among the heavy isotopes, there are several marked exceptions to the general rule that the cross sections are roughly constant, namely Ba^{138}, Pb^{208}, and Bi^{209}. Feshbach, Peaslee, and Weisskopf[1] had already pointed out that lead and bismuth, because of their low absorption, must have an unusually large level spacing D which would mean an unusually low neutron binding energy. However, as the same behavior in Ba^{138} was unexpected, attempts were made to find something wrong in the measurement or interpretation. Weisskopf sug-

[4] L. Seren, H. Friedlander, and S. Turkel, Phys. Rev. **72**, 888 (1947).
[5] J. A. Swartout, G. E. Boyd, A. E. Cameron, C. P. Keim, and C. E. Larson, Phys. Rev. **70**, 232 (1946).

gested that perhaps competition by inelastic scattering caused the low cross section in Ba^{138}. This possibility was checked by measuring the neutron capture cross section with Na-Be (900 kev) and Na-D_2O (230 kev) photo-neutrons. The cross section was unusually low, however, even at 230 kev where no inelastic scattering would be present. In the meantime Mayer[6] had shown that certain numbers of neutrons in nuclei formed stable "shells" and that the binding energy for the next neutron is extremely low. The low cross section for Ba^{138} was then easily explained because it contains 82 neutrons, forming a closed shell (Pb^{208} and Bi^{209} each contain 126 neutrons, also a closed shell).

IV. COMPARISON WITH OTHER MEASUREMENTS

As already discussed, the results for Au, I, and In were compared with the existing data on cross sections *vs.* energy as a check on the general method before proceeding with the light elements. After the other measurements had been made, an exhaustive survey by Way and the isotope information group at Clinton showed that there were quite a number of old results on capture cross section for neutrons of various energies with which the present results could be compared. In many cases the energies were not well defined and the absolute cross-section values were not good. However, if the cross sections of a given experimenter are multiplied by a constant to bring his value for a standard substance, say Au^{197}, into agreement with Fig. 17, then a comparison of the different values is possible. It is assumed in this procedure that the relative values of a given observer are correct even when his reported absolute values are definitely wrong.

Curves based on all the available data for a number of isotopes are given in Figs. 3–17. All those isotopes are shown for which more than 3 points were available above 0.1 Mev. The sources of data, as marked on the figures, are as follows:

"DEMENTI": V. S. Dementi and D. V. Timoshuk, Comptes Rendus de l'Acadamie des Sciences de l'URSS **27**, 929 (1940). Activation measurements using a Rn-Be neutron source, with a reported predominant energy of 200 kev. The reported cross sections are much too low if plotted at 200 kev and it seems more reasonable to assume an energy of about 4 Mev (as K. Way has done in her compilation) for which value the results are in line with the other measurements.

"D & H" (dashed line): P. Demers, H. H. Halban, R. Allen and G. R. Bishop. Nature **161**, 727 (1948). Measurements of the ratio of the cross sections at 220 kev (ThC"-D_2O photo-neutrons) to those at 950 kev (ThC"-Be). Only the ratio was measured, which is shown by the slope of the dotted line, the ordinate being arbitrary.

"WATTENBERG": R. Fields, B. Russell and A. Wattenberg: Unpublished activation measurements using Na-D_2O (230 kev) and Na-Be (900 kev) photo-neutron sources.

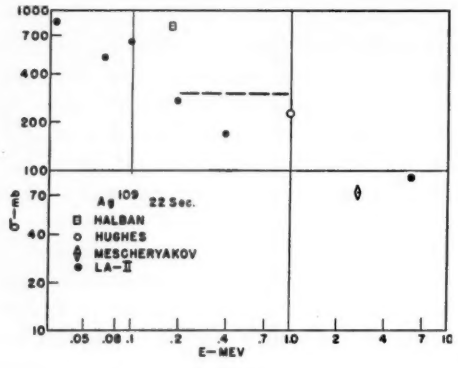

FIG. 12.

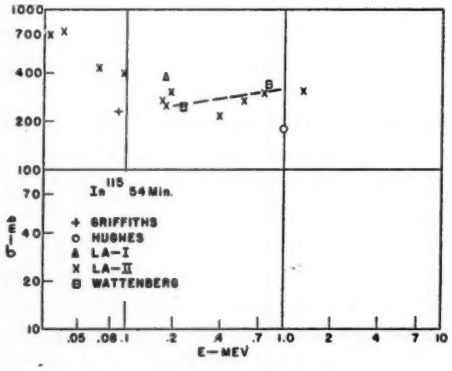

FIG. 13.

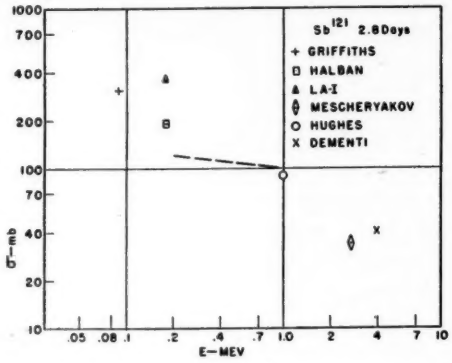

FIG. 14.

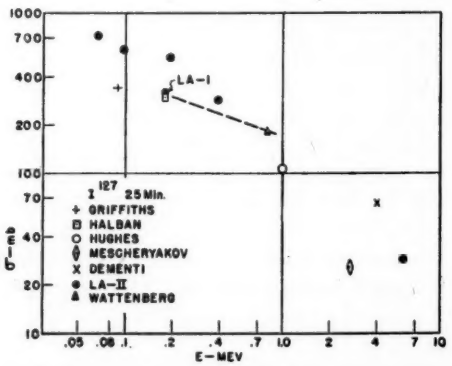

FIG. 15.

[6] M. G. Mayer, Phys. Rev. **74**, 235 (1948).

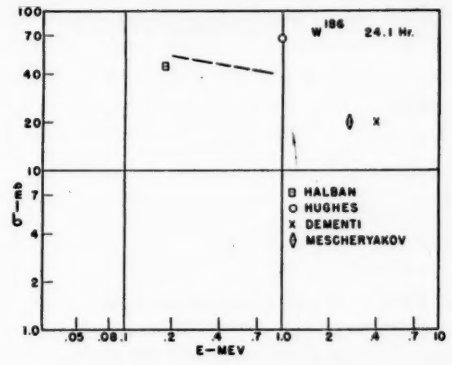

FIG. 16.

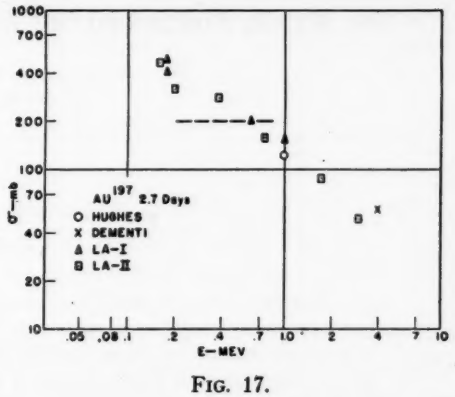

FIG. 17.

The cross sections were measured relative to gold, taking the value for gold from the data of Fig. 17.

"GRIFFITHS": J. H. E. Griffiths. Proc. Roy. Soc. **A170**, 513 (1939). Cross sections measured with a Ra-γ-Be source, using a calculated neutron flux from the source for obtaining absolute cross-section values. In plotting Griffiths points, we have followed K. Way in selecting 90 kev as the effective neutron energy which means that the cross section must be multiplied by 4.9 to fit the Au curve.

"HALBAN": H. H. Halban and L. Kowarski: Nature **142**, 392 (1938). Used ThC″-D_2O photo-neutron source of energy 220 kev. It was necessary to multiply the cross sections by the surprisingly large factor of 17 to secure agreement with the curve for gold given in Fig. 17.

"HUGHES": Present results.

"MESCHERYAKOV": M. G. Mescheryakov. Comptes Rendus URSS **48**, 555 (1945). Activations measured using $D(d,n)$ cyclotron neutrons of energy 2.7 Mev. Reported cross sections have been multiplied by 0.13 to agree with Fig. 17.

"LA–I": Photo-neutron measurements made at Los Alamos by:

M. Deutsch, M. B. Fischer, S. L. Friedman, A. O. Hanson, C. D. Klema, G. A. Linenberger, M. L. Perlman, E. Segrè, J. H. Williams

"LA–II": Van de Graaff measurements made at Los Alamos by:

J. M. Blair, M. Deutsch, K. I. Greisen, A. O. Hanson, G. A. Linenberger, J. A. Miskel, R. F. Taschek, C. M. Turner, J. H. Williams

The curves of Figs. 3–17 show that once the absolute cross-section values are adjusted for a given isotope there is quite good agreement for the others. The variation of cross section with energy is quite similar for most of the isotopes, that is, approximately a $1/v$ dependence at low energies which changes over to $1/E$ in the region of several hundred kilovolts. This change in slope would be expected to take place where the neutron width becomes greater than the gamma-width and its location in the experimental curves is quite reasonable. The continuation of the $1/E$ slope to energies well above one Mev indicates that the increase in capture (relative to $1/E$) caused by high l values must be approximately compensated by the decrease caused by inelastic scattering. The only definite exception to the general behavior seems to be In^{115} (and to a smaller extent, Ag^{109} and Sb^{121}) which changes much more slowly with energy than the other isotopes.

The measurements are being continued at the present time with special reference to the "magic number" nuclei containing 50, 82 and 126 neutrons. The unusually low binding energy for the next neutron of these nuclei should be shown quite well in their fast neutron capture cross section because of the rapid variation of level spacing with excitation energy.

PHYSICAL REVIEW VOLUME 75, NUMBER 12 JUNE 15, 1949

The Meson Fields and the Equation of Motion of a Spinning Particle

R. C. MAJUMDAR
University of Delhi, Delhi, India

AND

S. GUPTA
Tata Institute of Fundamental Research, Bombay, India

(Received April 20, 1948)

Following Riesz, the meson fields generated by a point dipole at a point outside the world line have been defined in terms of the derivatives of an integral which is an analytical function of a parameter, α, and converges for α lying between $2<\alpha<3$. It is then shown that by the process of analytical continuation of the parameter to the value $\alpha=2$ for which the Riesz fields satisfy the fundamental meson field equations, we not only obtain the classical Liénard-Wiechert-Bhabha fields at a point outside the world line but also a field at a point on the world line itself which is finite and represents the reaction of the field correctly. The equations for rotational and translational motions follow immediately from the usual electrodynamical equations of a dipole given by Frenkel. The equations thus obtained are free from singularities and do not contain any arbitrary constant except the mass and spin angular momentum of the dipole.

INTRODUCTION

IT is now well known that the meson field differs fundamentally from the electromagnetic field in its interaction with the nuclear particles, neutron and proton. Whereas the interaction of the electron of charge e with the electromagnetic field is completely described in classical electrodynamics by the four potentials of the field, the interaction of the nucleon with the meson field requires for its description not only a charge g_1 but also a dipole moment g_2 which has an explicit spin interaction with the meson field. It is this dipole type interaction which is absent in the electron case although it could always be introduced mathematically[1] and it leads to a scattering of mesons which increases as the square of their energy. Following Lorentz, Heisenberg[2] first derived an equation of motion for an extended dipole in a meson field and showed that the effect of the reaction of the proper field of the nucleon gives rise to an inertia of the motion of its spin which considerably reduces the scattering at high energies. Heisenberg's theory was, however, not relativistically invariant in that he assumed a dipole having finite extension. A relativistically invariant theory of the motion of a point dipole in a meson-field was first developed by Bhabha and Corben[3] and by Bhabha[4] following a method first initiated by Dirac.[5] The method of Lorentz had to be abandoned as the equations of motion of a particle involve the field at its world line which is infinite for a point particle in the usual classical theory. It is therefore necessary to calculate first the flow of energy, momentum and the angular momentum out of a portion of a thin tube surrounding the world line of the point particle, the radius of which is ultimately made to tend to zero. The equations of motion are then obtained from the principle of conservation of energy and momentum according to which this inflow must depend only on the conditions at the two ends of the tube. The infinities which appear in the expressions for the flow of energy, momentum and angular momentum when the tube shrinks to the world line are perfect differentials and are therefore subtracted away. The field which finally contributes fundamentally to the equations of motion is found to be the *so-called* radiation field which is defined as half the retarded minus the advanced field, and is finite on the world line. It has already been shown by Wentzel[6] that by introducing a time like four vector λ it is possible to form the limiting values of the field at the world point of the particle by finally putting $\lambda=0$ (λ-limiting process), this limiting value representing the radiation field. Harish-Chandra[7]

[1] W. Pauli, *Handbuch der Physik* (Springer, Verlag-Berlin, 1933), Quantentheorie Band 24/1.
[2] W. Heisenberg, Zeits. f. physik. **113**, 61 (1939).
[3] H. J. Bhabha and H. C. Corben, Proc. Roy. Soc. **A178**, 273 (1941).
[4] H. J. Bhabha, Proc. Roy. Soc. **A178**, 314 (1941).
[5] P. A. M. Dirac, Proc. Roy. Soc. **A167**, 148 (1938).
[6] G. Wentzel, Zeits. f. physik **86**, 479 (1933).
[7] Harish-Chandra, Proc. Nat. Acad. of Sci. (India) **14**, 195 (1945). (Just published.)

has also been able to construct an effective field expressed as an integral of the actual field at a world point, the integral being taken over a small closed three dimensional surface. The effective field reduces to the radiation field on the world line of the particle. The final equations obtained by Bhabha and Corben and by Bhabha can, therefore, be taken to represent the fundamental equations of motion of a point particle. However, there is an element of arbitrariness in the subtraction of the singular terms and the introduction of radiation field. Further, the equations are extremely complicated and involve a number of arbitrary constants which are not determined uniquely.

Recently Riesz[8] has developed an elegant method for solving the differential equations of the hyperbolic type, in which the well known divergent difficulties, first studied by Hadamard, are eliminated by a process of analytical continuation of an integral which is an analytical function of a parameter α. The method admits of a calculation of the meson fields generated by the point nucleon not only at a point outside the world line but also at a point on the world line occupied by the nucleon itself. The field quantities are first defined for values of α large enough for the integrals to be convergent. Then by analytical continuation with regard to the parameter α the potentials and the fields are determined. Riesz's method has been recently applied by Gustafson[9] to the problem of the self-energy of a point particle and by Fremberg[10] in obtaining the classical equation of a charged particle in a meson field. In the present paper we shall show that by defining a Riesz potential for the dipole which is convergent for a parameter α lying between $2<\alpha<5$ and by analytical continuation to $\alpha=2$ for which the field quantities are found to satisfy the fundamental meson equations, we can obtain not only the field quantities generated by a point dipole at a point outside the world line, but also finite values on the world line itself. The latter fields describe the reaction of the field correctly. The equations of motion of a point dipole then follow immediately from the usual equation for the dipole given by Frenkel.[11] The equations are free from singularities and do not contain any arbitrary constant except those which appear as mass and spin angular momentum of the dipole.

[8] M. Riesz, Conférence de la Réunion internat. des. math., tenue à Paris en Juillet 1937 (Paris) 1939.
[9] T. Gustafson, Nature **157**, 734 (1946); Nature, **158**, 273 (1946).
[10] N. E. Fremberg, Medd. Fran. Lunds. Uni. Mat. Sem. Band 7 (1946); Proc. Roy. Soc. **A188**, 18 (1946).
[11] J. Frenkel Zeits. f. physik. **37**, 243 (1926).

1. THE MESON FIELD OF A DIPOLE

We shall use the ordinary tensor notation throughout and take the fundamental metric tensor $g_{\mu\nu}$ in the form $g_{00}=1$, $g_{11}=g_{22}=g_{33}=-1$ with all other components vanishing. We shall put the velocity of light c equal to unity for convenience. The particle shall be treated as a point, its co-ordinates being z_μ which are functions of the proper time, τ, measured from an arbitrary point on the world line of the particle. The spin of the particle will be described by an antisymmetrical tensor, $S_{\mu\nu}$, which will also be considered as a function of τ and which together with its derivatives up to a certain order is continuous and bounded for $\tau\to-\infty$. The meson field generated by the spinning particle is described by potentials, φ_μ, and by field strengths, $G_{\mu\nu}$, which satisfy the following fundamental equations

$$\frac{\partial G_{\mu\nu}}{\partial x_\mu}+\chi^2\varphi_\nu=4\pi g_2\frac{\partial S_{\mu\nu}}{\partial x_\mu} \tag{1}$$

where

$$G_{\mu\nu}=\frac{\partial\varphi_\nu}{\partial x^\mu}-\frac{\partial\varphi_\mu}{\partial x^\nu}. \tag{2}$$

Now assuming

$$\partial\varphi_\nu/\partial x_\nu=0, \tag{3}$$

we obtain

$$\frac{\partial^2\varphi_\nu}{\partial x_\rho\partial x^\rho}+\chi^2\varphi_\nu=4\pi g_2\frac{\partial S_{\mu\nu}}{\partial x_\mu} \tag{4}$$

and

$$\frac{\partial G_{\mu\nu}}{\partial x^\lambda}+\frac{\partial G_{\nu\lambda}}{\partial x^\mu}+\frac{\partial G_{\lambda\mu}}{\partial x^\nu}=0. \tag{5}$$

We define the Riesz potential for the dipole at a point $P(x^\mu)$ outside the world line in the form

$$\varphi_\nu{}^\alpha(P)=\frac{g_2\chi^{4-\alpha}}{2^{(\alpha-2)/2}\Gamma(\alpha/2)}\frac{\partial}{\partial x_\mu}\int_{-\infty}^{\tau_0}S_{\mu\nu}(\tau)\times(\chi s)^{(\alpha-4)/2}J_{(\alpha-4)/2}(\chi s)d\tau \tag{6}$$

where $J_n(x)$ is the Bessel function of order n and s the four dimensional distance given by

$$s^2=s_\mu s^\mu,\quad s_\mu=x_\mu-z_\mu. \tag{7}$$

τ_0 is the retarded proper time determined by $s^2=0$. The integral in (6) is convergent for $2<\alpha<3$.

We assume that the world line has a time-like asymptote for $\tau\to-\infty$ and that for a large value of τ,

$$z^\mu(\tau)=v_{-\infty}{}^\mu\tau+\sum_{\kappa=0}^{\infty}C_\kappa{}^\mu\tau^{-\kappa}\quad(v_{-\infty}{}^\mu=\lim_{\tau\to-\infty}v^\mu). \tag{8}$$

As the integrand in (6) is singular at $\tau=\tau_0$ care should be taken to carry out differentiation under the integration sign. We introduce s as an integration variable and consider s and x_μ as independent variables. z_μ and consequently τ then become functions of s and x_μ. We thus obtain on differentiation and changing the variable again to τ

$$\varphi_\nu{}^\alpha(P)=\frac{g_2\chi^{4-\alpha}}{2^{(\alpha-2)/2}\Gamma(\alpha/2)}\int_{-\infty}^{\tau_0}\frac{\partial}{\partial\tau}\left(\frac{s^\mu S_{\mu\nu}}{\kappa}\right)\times(\chi s)^{(\alpha-4)/2}J_{(\alpha-4)/2}(\chi s)d\tau \tag{9}$$

where we have used

$$\frac{ds}{d\tau}=-\frac{\kappa}{s},\quad\frac{\partial\tau}{\partial x^\mu}=\frac{s_\mu}{\kappa};\quad\kappa=s_\mu v^\mu. \tag{10}$$

The integral (9) converges for $2<\alpha<5$.

Correspondingly, we define the Riesz field of the dipole by the equation

$$G_{\mu\nu}{}^\alpha=(\partial\varphi_\nu{}^\alpha/\partial x^\mu)-(\partial\varphi_\mu{}^\alpha/\partial x^\nu). \tag{11}$$

Differentiation of the potentials (9) in the manner described above, taking s and x_μ as independent variables, gives

$$G_{\mu\nu}{}^\alpha=\frac{g_2\chi^{4-\alpha}}{2^{(\alpha-2)/2}\Gamma(\alpha/2)}\int_{-\infty}^{\tau_0}\left[2\frac{\partial}{\partial\tau}\left(\frac{S_{\mu\nu}}{\kappa}\right)+\frac{\partial}{\partial\tau}\left\{\frac{1}{\kappa}\frac{\partial}{\partial\tau}\left(\frac{s_\mu s^\rho S_{\rho\nu}-s_\nu s^\rho S_{\rho\mu}}{\kappa}\right)\right\}\right]\times(\chi s)^{(\alpha-4)/2}J_{(\alpha-4)/2}(\chi s)d\tau \tag{12}$$

which converges for $2<\alpha<7$. It is to be observed that formulae (9) and (12) are exactly what we would have obtained by carrying out directly formal differentiation in (6) and (9) under the sign of integration.

Now it follows from (9) that outside the world line

$$\operatorname{div}\varphi^\alpha=g^{\mu\nu}(\partial\varphi_\nu{}^\alpha/\partial x^\mu)=0, \tag{13}$$

and

$$\Box\varphi_\mu{}^\alpha+\chi^2\varphi_\mu{}^\alpha=\varphi_\mu{}^{\alpha-2}. \tag{14}$$

Further, defining Riesz current density by

$$(\partial S_{\mu\nu}{}^\alpha/\partial x_\mu)=(1/4\pi)\varphi_\nu{}^{\alpha-2}(P), \tag{15}$$

it can be proved that the introduced field quantities satisfy the fundamental meson equations (3) to (5). In particular, by analytical continuation to $\alpha=2$, we have $\varphi_\mu{}^{(0)}=0$ outside the world line and consequently

$$\Box\varphi_\mu{}^{(2)}+\chi^2\varphi_\mu{}^{(2)}=0. \tag{16}$$

We shall frequently use the following formulae

$$J_{n-1}(x)=(2n/x)J_n(x)-J_{n+1}(x), \tag{17}$$

$$(d/dx)(x^{-n}J_n(x))=-x^{-n}J_{n+1}(x), \tag{18}$$

$$(d/dx)(x^nJ_n(x))=x^nJ_{n-1}(x), \tag{19}$$

$$\lim_{x\to0}(J_n(x)/x^n)=1/(2^n\cdot n!). \tag{20}$$

Using formula (17), the potentials (9) may be expressed as

$$\varphi_\nu{}^\alpha(P)=\frac{g_2\chi^{4-\alpha}(\alpha-2)}{2^{(\alpha-2)/2}\Gamma(\alpha/2)}\int_{-\infty}^{\tau_0}\frac{\partial}{\partial\tau}\left(\frac{s^\mu S_{\mu\nu}}{\kappa}\right)\times(\chi s)^{(\alpha-6)/2}J_{(\alpha-2)/2}(\chi s)d\tau-\frac{g_2\chi^{4-\alpha}}{2^{(\alpha-2)/2}\Gamma(\alpha/2)}\int_{-\infty}^{\tau_0}\frac{\partial}{\partial\tau}\left(\frac{s^\mu S_{\mu\nu}}{\kappa}\right)\times(\chi s)^{(\alpha-4)/2}J_{\alpha/2}(\chi s)d\tau \tag{21}$$

where the first integral converges for $2<\alpha<7$ and the second for $0<\alpha<5$. We introduce s as the integration variable and perform analytical continuation to $\alpha=2$ with the help of the lemma

$$\lim_{\beta\to+0}\beta\int_0^\infty f(t,\beta)t^{\beta-1}dt=f(0,0), \tag{22}$$

which is valid if the integral converges for $\beta>0$ and $f(t,\beta)$ is continuous in $t=\beta=0$. The potential at a point $P(x^\mu)$ lying outside the world line is thus given by

$$\varphi_\nu{}^{\alpha=2}(P)=\varphi_\nu{}^{\mathrm{ret}}(P)=g_2\left[\frac{1}{\kappa}\frac{\partial}{\partial\tau}\left(\frac{s^\rho S_{\rho\nu}}{\kappa}\right)\right]_0-g_2\chi\int_{-\infty}^{\tau_0}\frac{\partial}{\partial\tau}\left(\frac{s^\rho S_{\rho\nu}}{\kappa}\right)\frac{J_1(\chi s)}{s}d\tau$$
$$=g_2\left[\frac{1}{\kappa}\frac{\partial}{\partial\tau}\left(\frac{s^\rho S_{\rho\nu}}{\kappa}\right)\right]_0-\tfrac{1}{2}g_2\chi^2\left[\frac{s^\rho S_{\rho\nu}}{\kappa}\right]_0+g_2\chi^2\int_{-\infty}^{\tau_0}s^\rho S_{\rho\nu}\frac{J_2(\chi s)}{s^2}d\tau, \tag{23}$$

where the index 0 implies that the value of the

function is to be taken at the point retarded with respect to P.

Similarly, expressing the field (12) in the form

$$G_{\mu\nu}{}^{\alpha}=\frac{g_2\chi^{4-\alpha}}{2^{(\alpha-2)/2}\Gamma(\alpha/2)}(\alpha-2)\int_{-\infty}^{\tau_0}\left[2\frac{\partial}{\partial\tau}\left(\frac{S_{\mu\nu}}{\kappa}\right)+\frac{\partial}{\partial\tau}\left\{\frac{1}{\kappa}\frac{\partial}{\partial\tau}\left(\frac{s_\mu s^\rho S_{\rho\nu}-s_\nu s^\rho S_{\rho\mu}}{\kappa}\right)\right\}\right]\times(\chi s)^{(\alpha-6)/2}J_{(\alpha-2)/2}(\chi s)d\tau$$
$$-\frac{g_2\chi^{4-\alpha}}{2^{(\alpha-2)/2}\Gamma(\alpha/2)}\int_{-\infty}^{\tau_0}\left[2\frac{\partial}{\partial\tau}\left(\frac{S_{\mu\nu}}{\kappa}\right)+\frac{\partial}{\partial\tau}\left\{\frac{1}{\kappa}\frac{\partial}{\partial\tau}\left(\frac{s_\mu s^\rho S_{\rho\nu}-s_\nu s^\rho S_{\rho\mu}}{\kappa}\right)\right\}\right]\times(\chi s)^{(\alpha-4)/2}J_{\alpha/2}(\chi s)d\tau, \quad (24)$$

analytical continuation to $\alpha=2$ and repeated partial integrations give the field at a point $P(x^\mu)$ outside the world line:

$$G_{\mu\nu}{}^{\alpha=2}(P)=G_{\mu\nu}{}^{\mathrm{ret}}(P)=g_2\left\{2\left[\frac{1}{\kappa}\frac{\partial}{\partial\tau}\left(\frac{S_{\mu\nu}}{\kappa}\right)\right]_0+\left[\frac{1}{\kappa}\frac{\partial}{\partial\tau}\left(\frac{1}{\kappa}\frac{\partial}{\partial\tau}\left(\frac{\mathrm{K}_{\mu\nu}}{\kappa}\right)\right)\right]_0\right\}-g_2\chi^2\left[\frac{S_{\mu\nu}}{\kappa}\right]_0$$
$$-\frac{g_2\chi^2}{2}\left[\frac{1}{\kappa}\frac{\partial}{\partial\tau}\left(\frac{\mathrm{K}_{\mu\nu}}{\kappa}\right)\right]_0+2g_2\chi^2\int_{-\infty}^{\tau_0}S_{\mu\nu}\frac{J_2(\chi s)}{s^2}d\tau$$
$$+\frac{g_2\chi^4}{8}\left[\frac{\mathrm{K}_{\mu\nu}}{\kappa}\right]_0-g_2\chi^3\int_{-\infty}^{\tau_0}\mathrm{K}_{\mu\nu}\frac{J_3(\chi s)}{s^3}d\tau, \quad (25)$$

where

$$\mathrm{K}_{\mu\nu}=(s_\mu s^\rho S_{\rho\nu}-s_\nu s^\rho S_{\rho\mu}). \quad (26)$$

Expressions (23) and (25) were first obtained by Bhabha, and by Bhabha and Corben.

2. REACTIONS OF THE FIELD

We now proceed to calculate the fields at a point P on the world line. They will obviously represent the reaction of the field on the motion of the particle itself. We consider $\varphi_\nu{}^{\alpha}(P)$ as given by the expression (21) of which the first integral converges for $2<\alpha<7$ and the second for $0<\alpha<5$ even when P is on the world line. We divide the first integral into two parts, one in the interval $-\infty$ to $\tau_0-\epsilon$ and the other from $\tau_0-\epsilon$ to τ_0. The first part converges for $\alpha<7$ and therefore vanishes, especially for $\alpha=2$ on account of the factor $(\alpha-2)$. For the second part we expand the integrands in power series of $(\tau-\tau_0)$. We take $\tau_0=0$ for simplicity and have

$$s_\mu=-\tau[v_\mu+(1/2)\dot{v}_\mu\tau+(1/6)v_\mu{}^{\mathrm{ii}}\tau^2+(1/24)v_\mu{}^{\mathrm{iii}}\tau^3+(1/120)v_\mu{}^{\mathrm{iv}}\tau^4+O(\tau^5)],$$
$$s^2=\tau^2[1-(1/12)\dot{v}^2\tau^2-(1/12)(\dot{v}v^{\mathrm{ii}})\tau^3-\{(1/40)(\dot{v}v^{\mathrm{iii}})+(1/45)v^{\mathrm{ii}2}\}\tau^4+O(\tau^5)], \quad (27)$$
$$\kappa=-\tau[1-(1/6)\dot{v}^2\tau^2-(5/24)(\dot{v}v^{\mathrm{ii}})\tau^3-\{(3/40)(\dot{v}v^{\mathrm{iii}})+(1/15)v^{\mathrm{ii}2}\}\tau^4+O(\tau^5)].$$

In order to perform the analytical continuation of the potential $\varphi_\nu{}^{\alpha}$ to $\alpha=2$ we expand the quantities in the first of the integrals of (21) with the help of the expansions (27) and directly put $\alpha=2$ in the second integral. We thus obtain for the potentials on the world line:

$$\varphi_\nu{}^{\alpha=2}=\varphi_\nu{}^{\mathrm{ret}}=-g_2\{\tfrac{1}{3}\dot{v}^2v^\rho S_{\rho\nu}+\tfrac{1}{3}v^{\mathrm{ii}\rho}S_{\rho\nu}+\dot{v}^\rho\dot{S}_{\rho\nu}+v^\rho S_{\rho\nu}{}^{\mathrm{ii}}\}-(g_2\chi^2/2)v^\rho S_{\rho\nu}+g_2\chi^2\int_{-\infty}^{\tau_0}s^\rho S_{\rho\nu}\frac{J_2(\chi s)}{s^2}d\tau. \quad (28)$$

For the calculation of the field, $F_{\mu\nu}{}^{\alpha}(P)$, we consider (24) of which the first integral converges for $4<\alpha<9$ and the second for $2<\alpha<7$ when P is on the world line. By partial integration and using (18) we can express the second integral in the form

$$-\frac{g_2\chi^{6-\alpha}(\alpha-2)}{2^{(\alpha-2)/2}\Gamma(\alpha/2)}\int_{-\infty}^{\tau_0}\left\{2S_{\mu\nu}+\frac{\partial}{\partial\tau}\left(\frac{\mathrm{K}_{\mu\nu}}{\kappa}\right)\right\}\times(\chi s)^{(\alpha-8)/2}J_{\alpha/2}(\chi s)d\tau$$
$$+\frac{g_2\chi^{6-\alpha}}{2^{(\alpha-2)/2}\Gamma(\alpha/2)}\int_{-\infty}^{\tau_0}\left\{2S_{\mu\nu}+\frac{\partial}{\partial\tau}\left(\frac{\mathrm{K}_{\mu\nu}}{\kappa}\right)\right\}\times(\chi s)^{(\alpha-6)/2}J_{(\alpha+2)/2}(\chi s)d\tau, \quad (29)$$

where the first integral converges for $2<\alpha<7$ and the second for $0<\alpha<5$. Analytical continuation to $\alpha=2$, carried out as before, gives

for the fields on the world line

$$
\begin{aligned}
G_{\mu\nu}{}^{\alpha=2} = G_{\mu\nu}{}^{\mathrm{ret}} = g_2\{&\tfrac{2}{3}S_{\mu\nu}(\dot{v}v^{\mathrm{ii}}) \\
&+\tfrac{2}{3}\dot{S}_{\mu\nu}\dot{v}^2+\tfrac{2}{3}S_{\mu\nu}{}^{\mathrm{iii}}+[(4/3)v_\mu S_\nu{}''' \\
&+2v_\mu S_\nu{}'\dot{v}^2+\tfrac{1}{3}v_\mu{}^{\mathrm{iii}}\$_\nu-\tfrac{2}{3}v_\mu{}^{\mathrm{ii}}\dot{v}^\rho S_{\rho\nu} \\
&+(4/3)v_\mu{}^{\mathrm{ii}}S_\nu{}'-(4/3)v_\mu v^{\mathrm{ii}\rho}\dot{S}_{\rho\nu} \\
&-\tfrac{2}{3}\dot{v}_\mu v^{\mathrm{ii}\rho}S_{\rho\nu}-\tfrac{1}{3}v_\mu v^{\mathrm{iii}\rho}S_{\rho\nu} \\
&-2v_\mu\dot{v}^\rho S_{\rho\nu}{}^{\mathrm{ii}}+2\dot{v}_\mu S_\nu{}''-2\dot{v}_\mu\dot{v}^\rho\dot{S}_{\rho\nu} \\
&+2v_\mu\$_\nu(\dot{v}v^{\mathrm{ii}})-v_\mu\dot{v}^\rho S_{\rho\nu}\dot{v}^2+\dot{v}_\mu\$_\nu\dot{v}^2]_- \\
&+\chi^2[\tfrac{1}{2}\dot{S}_{\mu\nu}+v_\mu S_\nu{}'-\tfrac{1}{2}v_\mu\dot{v}^\rho S_{\rho\nu}+\tfrac{1}{2}\dot{v}_\mu\$_\nu]_-\} \\
&+2g_2\chi^2\int_{-\infty}^{\tau_0}S_{\mu\nu}\frac{J_2(\chi s)}{s^2}d\tau \\
&-g_2\chi^3\int_{-\infty}^{\tau_0}[s_\mu s^\rho S_{\rho\nu}]_-\frac{J_3(\chi s)}{s^3}d\tau, \qquad (30)
\end{aligned}
$$

where

$$
\$_\nu = S_{\nu\rho}v^\rho, \quad S_\nu{}' = \dot{S}_{\nu\rho}v^\rho, \quad S_\nu{}'' = S_{\nu\rho}{}^{\mathrm{ii}}v^\rho,
$$

$$
S_\nu{}''' = S_{\nu\rho}{}^{\mathrm{iii}}v^\rho, \qquad (31)
$$

and the minus sign as subscript denotes that the terms inside the brackets are to be subtracted with interchanges of μ and ν.

It is to be noted that the field given by (30) is the retarded field at the point τ_0 on the world line. This field agrees with the *so-called* radiation field, i.e. $\frac{1}{2}$ (retarded$-$advanced) field, as calculated by Bhabha and Corben, and by Bhabha provided we take $k_1=\frac{1}{3}$, $k_2=-(7/15)$, $k_3=\frac{1}{3}$; $k_4=(4/3)$, $k_6=0$ in expression (140) of B&C and $k=2$ in expression (10) of Bhabha. There is, however, disagreement in regard to terms with constant k_5 as has also been noticed by Harish Chandra[12] whose calculation of the radiation field by retaining only the finite and unambiguous terms of the field given by Bhabha agrees with our result (30).

3. THE EQUATION OF MOTION

A. The equation of rotational motion is now obtained directly from the equation of a dipole given by Frenkel

$$
I\dot{S}_{\lambda\mu} = g_2[S\cdot G^{\mathrm{ext}}]_{\lambda\mu}+g_2[S\cdot G^{\mathrm{react}}]_{\lambda\mu}, \qquad (32)
$$

where I is the spin angular momentum. The field $G_{\mu\nu}{}^{\mathrm{react}}$ is given by (30) and it represents the reaction of the field.

We now derive the equations of motion of the spinning particle in which the dipole always remains a pure magnetic dipole in the system in which the particle is at rest. This is expressed as

$$
S_{\mu\nu}v^\nu = 0 \qquad (33)
$$

and is one which is of physical interest. The rotational equation (32) is now to be modified to

$$
\begin{aligned}
I\{&\dot{S}_{\lambda\mu}+v_\lambda S_\mu{}'-v_\mu S_\lambda{}'\} \\
&=g_2[S_\lambda{}^\sigma\{G_{\sigma\mu}{}^{\mathrm{ext}}-(G_{\sigma\nu}{}^{\mathrm{ext}}v^\nu v_\mu \\
&\qquad -G_{\mu\rho}{}^{\mathrm{ext}}v^\rho v_\sigma)\}]_-+g_2[S_\lambda{}^\sigma D_{\sigma\mu}{}^{\mathrm{react}}]_- \qquad (34)
\end{aligned}
$$

with

$$
D_{\sigma\mu}{}^{\mathrm{react}} = G_{\sigma\mu}{}^{\mathrm{react}}-(G_{\sigma\nu}{}^{\mathrm{react}}v^\nu v_\mu - G_{\mu\nu}{}^{\mathrm{react}}v^\nu v_\sigma)
$$

where $G_{\sigma\mu}{}^{\mathrm{react}}$ is given by (30). Thus

$$
\begin{aligned}
D_{\sigma\mu}{}^{\mathrm{react}} = g_2\{&\tfrac{2}{3}S_{\sigma\mu}(\dot{v}v^{\mathrm{ii}})+\tfrac{2}{3}S_{\sigma\mu}{}^{\mathrm{iii}} \\
&+\tfrac{2}{3}\dot{S}_{\sigma\mu}\dot{v}^2-[\tfrac{2}{3}S_\sigma{}'''v_\mu+(4/3)S_\sigma{}'v_\mu\dot{v}^2 \\
&+\tfrac{2}{3}S_\sigma{}'v_\mu{}^{\mathrm{ii}}+(4/3)S_\sigma{}''\dot{v}_\mu \\
&+\tfrac{2}{3}\dot{S}_{\sigma\rho}\dot{v}^\rho\dot{v}_\mu]_-+\chi^2[\tfrac{1}{2}\dot{S}_{\sigma\mu}-S_\sigma{}'v_\mu]_-\} \\
&+\tilde{G}_{\sigma\mu}-(\tilde{G}_{\sigma\rho}v^\rho v_\mu-\tilde{G}_{\mu\rho}v^\rho v_\sigma), \qquad (35)
\end{aligned}
$$

$$
\begin{aligned}
\tilde{G}_{\sigma\mu} = &2g_2\chi^2\int_{-\infty}^{\tau_0}\frac{S_{\sigma\mu}J_2(\chi s)}{s^2}d\tau \\
&+g_2\chi^3\int_{-\infty}^{\tau_0}[s_\sigma S_{\mu\rho}s^\rho]_-\frac{J_3(\chi s)}{s^3}d\tau. \qquad (36)
\end{aligned}
$$

Equation (34) agrees with the corresponding equation given by Bhabha and Corben provided we take $d=-\frac{2}{3}$.

It must be noticed that the equation (34) ensures the condition

$$
S_{\mu\nu}S^{\mu\nu} = \text{constant}. \qquad (37)
$$

B. The equation for the translational motion of the dipole can also be taken over directly from the corresponding equation given by Frenkel

$$
\begin{aligned}
m\dot{v}_\mu+\frac{d}{d\tau}\{&IS_\mu{}'-\tfrac{1}{2}g_2v_\mu S^{\lambda\sigma}G_{\lambda\sigma}{}^{\mathrm{ext}}-g_2S_\mu{}^\lambda G_{\lambda\rho}{}^{\mathrm{ext}}v^\rho\} \\
&=T_\mu{}^{\mathrm{self}}-\tfrac{1}{2}g_2S^{\lambda\sigma}\frac{\partial G_{\lambda\sigma}{}^{\mathrm{ext}}}{\partial x^\mu}, \qquad (38)
\end{aligned}
$$

[12] Harish-Chandra, Proc. Roy. Soc. **A185**, 269 (1946).

where

$$T_\mu^{\text{self}} = -\frac{1}{2}g_2 S^{\lambda\sigma}\frac{\partial G_{\lambda\sigma}^{\text{react}}}{\partial x^\mu} + \frac{1}{2}\frac{d}{d\tau}(g_2 v_\mu S^{\lambda\sigma} G_{\lambda\sigma}^{\text{react}}) + \frac{d}{d\tau}(g_2 S_\mu^{\lambda} G_{\lambda\rho}^{\text{react}} v^\rho). \quad (39)$$

It is to be noted that $\partial G_{\lambda\sigma}^{\text{react}}/\partial x^\mu$ cannot be obtained from (30) by direct differentiation. It is to be found out by evaluating the value of $\partial G_{\lambda\sigma}{}^{\alpha}/\partial x^\mu$ for $\alpha=2$ on the world line. For this we first differentiate $G_{\lambda\sigma}{}^{\alpha}$ as given by (24) and get

$$\frac{\partial G_{\lambda\sigma}{}^{\alpha}}{\partial x^\mu} = \frac{g_2\chi^{4-\alpha}}{2^{(\alpha-2)/2}\Gamma(\alpha/2)}\int_{-\infty}^{\tau_0}\left[2\frac{\partial}{\partial\tau}\left\{\frac{1}{\kappa}\frac{\partial}{\partial\tau}\left(\frac{s_\mu S_{\lambda\sigma}}{\kappa}\right)\right\} + \frac{\partial}{\partial\tau}\left\{\frac{1}{\kappa}\frac{\partial}{\partial\tau}\left(\frac{s_\lambda S_{\mu\sigma} - s_\sigma S_{\mu\lambda}}{\kappa}\right)\right\} + \frac{\partial}{\partial\tau}\left\{\frac{1}{\kappa}\frac{\partial}{\partial\tau}(g_{\lambda\mu}S^\rho S_{\rho\sigma} - g_{\sigma\mu}S^\rho S_{\rho\lambda})\right\} + \frac{\partial}{\partial\tau}\left\{\frac{1}{\kappa}\frac{\partial}{\partial\tau}\left(\frac{1}{\kappa}\frac{\partial}{\partial\tau}\left(\frac{s_\lambda s_\mu S^\rho S_{\rho\sigma} - s_\sigma s_\mu S^\rho S_{\rho\lambda}}{\kappa}\right)\right)\right\}\right] \times (\chi s)^{(\alpha-4)/2} J_{(\alpha-4)/2}(\chi s)\, d\tau. \quad (40)$$

Then by analytical continuation to $\alpha=2$ we evaluate $\partial G_{\lambda\sigma}{}^{\alpha=2}/\partial x^\mu$ on the world line. The calculations are cumbersome and lengthy and we simply give the final result

$$T_\mu^{\text{self}} = T_\mu^{\text{self},0} + T_\mu^{\text{self},\chi}, \quad (41)$$

where

$$\begin{aligned} T_\mu^{\text{self},0} = g_2^2\big[& v_\mu\{(1/3)(\dot{S}S^{\text{iii}}) \\ & -(2/3)S'^2 - (8/3)(S'\dot{S}\dot{v}) - 2(S'S''') \\ & -2(S'S^{\text{ii}}\dot{v}) + (2/3)(\dot{v}\dot{S}\dot{S}\dot{v}) \\ & -2(S'\dot{S}v^{\text{ii}}) - (1/5)S^2 v^{\text{ii}2} \\ & -(4/15)S^2(\dot{v}v^{\text{iii}}) + \dot{S}^2\dot{v}^2 - 4S'^2\dot{v}^2 \\ & -(1/3)S^2\dot{v}^4\} + \dot{v}_\mu\{(\dot{S}S^{\text{ii}}) - 4(S'S'') \\ & -4(S'\dot{S}\dot{v}) - (2/3)S^2(\dot{v}v^{\text{ii}})\} \\ & +v_\mu{}^{\text{ii}}\{(2/3)\dot{S}^2 - 2S'^2 - \tfrac{1}{3}S^2\dot{v}^2\} \\ & -(1/15)v_\mu{}^{\text{iv}}S^2 - (2/3)S_{\mu\sigma}{}^{\text{iii}}S'^\sigma \\ & -(4/3)S_{\mu\sigma}{}^{\text{ii}}\dot{S}^{\sigma\rho}\dot{v}_\rho - (2/3)S_{\mu\sigma}{}^{\text{ii}}S''^\sigma \\ & -(2/3)\dot{S}_{\mu\sigma}S'''^\sigma - 2\dot{S}_{\mu\sigma}S^{\text{ii}\sigma\rho}\dot{v}_\rho \\ & -(8/15)S_{\mu\sigma}\dot{S}^{\sigma\rho}v_\rho{}^{\text{iii}} - (2/3)\dot{S}_{\mu\sigma}S'^\sigma\dot{v}^2 \\ & -(4/3)\dot{S}_{\mu\sigma}\dot{S}^{\sigma\rho}v_\rho{}^{\text{ii}} - (2/15)S_{\mu\sigma}S''''^\sigma \\ & -(6/5)S_{\mu\sigma}S^{\text{iii}\sigma\rho}\dot{v}_\rho - (22/15)S_{\mu\sigma}S^{\text{ii}\sigma\rho}v_\rho{}^{\text{ii}} \\ & +\tfrac{2}{3}S_{\mu\sigma}S''^\sigma\dot{v}^2 + (\tfrac{1}{3}-\tfrac{1}{3})S_{\mu\sigma}\dot{S}^{\sigma\rho}\dot{v}_\rho\dot{v}^2 \\ & +\tfrac{2}{3}S_{\mu\sigma}S'^\sigma(\dot{v}v^{\text{ii}})\big], \end{aligned} \quad (42)$$

the invariants formed by any combination of tensors and vectors having been written in the usual matrix notations; as for example

$$(\dot{v}S^{\text{ii}}\dot{S}v) = \dot{v}^\mu S_{\mu\rho}{}^{\text{ii}}\dot{S}^{\rho\nu}v_\nu,$$

and

$$\begin{aligned} T_\mu^{\text{self},\chi} = g_2^2\chi^2\big[& v_\mu(\tfrac{1}{2}\dot{S}^2 - S'^2 - \tfrac{1}{6}\dot{v}^2S^2) \\ & -\tfrac{1}{6}v_\mu{}^{\text{ii}}S^2 + \tfrac{2}{3}S_{\mu\sigma}S''^\sigma + \tfrac{1}{3}S_{\mu\sigma}\dot{S}^{\sigma\rho}\dot{v}^\rho\} \\ & -\tfrac{1}{8}g_2^2\chi^4 v_\mu S^2 - \tfrac{1}{2}g_2 S^{\lambda\sigma}\tilde{G}_{\lambda\sigma,\mu} \\ & +\frac{1}{2}\frac{d}{d\tau}(g_2 v_\mu S^{\lambda\sigma}\tilde{G}_{\lambda\sigma}) + \frac{d}{d\tau}(g_2 S_\mu{}^{\lambda}\tilde{G}_{\lambda\rho}v^\rho), \end{aligned} \quad (43)$$

where

$$\begin{aligned} \tilde{G}_{\lambda\sigma,\mu} = & -g_2\chi^3\int_{-\infty}^{\tau_0}\{2S_{\lambda\sigma}s_\mu + (g_{\mu\lambda}S^\rho S_{\rho\sigma} - g_{\mu\sigma}S^\rho S_{\rho\lambda}) \\ & +(s_\lambda S_{\mu\sigma} - s_\sigma S_{\mu\lambda})\}\frac{J_3(\chi s)}{s^3}d\tau \\ & +g_2\chi^4\int_{-\infty}^{\tau_0} s_\mu(s_\lambda S^\rho S_{\rho\sigma} - s_\sigma S^\rho S_{\rho\lambda})\frac{J_4(\chi s)}{s^4}d\tau, \end{aligned} \quad (44)$$

and $\tilde{G}_{\lambda\sigma}$ is given by (36). The results agree with those of Bhabha[13] if we put his constant $d=-\frac{2}{3}$. The disagreement in the coefficients of $\dot{v}_\mu(S'\dot{S}\dot{v})$ may, however, be noted.

Part of the present work was done during one of the author's (R.C.M.) visits at the Tata Institute of Fundamental Research in Bombay as visiting Professor of Theoretical Physics. The authors are thankful to Professor H. J. Bhabha, the director of the Institute, for having afforded them every facility during the progress of the work.

[13] H. J. Bhabha, Proc. India. Acad. Sci. **A11**, 247 (1940).

Energies of Neutrons from MsTh-D, La-D, Y-Be, and Sb-Be Photo-Neutron Sources*

A. O. HANSON**
Los Alamos Scientific Laboratory, Los Alamos, New Mexico
(Received February 28, 1949)

The energies of neutrons from several neutron sources have been compared with those of neutrons of calculable energies from the Li(p,n) reaction by observing the maximum pulse heights of proton recoils in a hydrogen filled proportional counter. The values found for the average neutron energy from the various sources are: MsTh-D, 197±10 kev; MsTh-Be, 827±30 kev; Y-Be, 158±5 kev; La-D, 151±8 kev; and Sb-Be, 24±3 kev.

These values are consistently lower than those expected from the measured gamma-ray energies and the usually accepted photo-neutron thresholds. Better agreement could be obtained if the photo-neutron thresholds of deuterium and beryllium were taken as 2.23 and 1.68 Mev.

The energies of the effective gamma-rays from Y^{88} and La^{140} are obtained from the neutron energies and are found to be 1.86 Mev and 2.53 Mev, respectively.

INTRODUCTION

ALTHOUGH a considerable amount of work has been reported on the measurement of neutron energies from photo-neutron sources, certain discrepancies have appeared and it was considered worth while to determine these energies with a somewhat different technique.[1,2] The present method consists of measuring the maximum pulse heights of neutron-produced proton recoils in a hydrogen-filled proportional counter which was calibrated by using neutrons of accurately known energies from the Li(p,n) reaction. Since the energies of the neutrons from the various photo-neutron sources lie within the range of energies obtained from the Li(p,n) reaction, the problem is simply that of matching the photo-neutron energies with known neutron energies.

SOURCES AND INSTRUMENTS

The gamma-ray sources used were: (1) A 500-mc MsTh source which was prepared commercially. (2) A radiolanthanum source made of barium fission products which is the parent of the 40-hour La^{140}. Its half-life is essentially that of the 12.2-day barium. (3) A 200-mc yttrium source (Y^{88}) prepared from strontium bombarded by deuterons in the Berkeley cyclotron.[3] Its half-life is approximately 105 days. (4) A 300-mc antimony source (Sb^{124}) which was prepared by exposing antimony to neutrons in the Argonne pile. It has a half-life of about 60 days.

The photo-neutrons were produced by placing the gamma-ray sources at the center of a deuterium sphere 2.5 inches in diameter and of a beryllium sphere 1.5 inches in diameter. In most of the runs these sources were placed inside a lead shield about 1.25 inches thick in order to reduce the number of low energy gamma-rays incident on the counter.

The proportional counter used was a rather large one. It was three inches in diameter and had a 0.010-inch central wire which had an active length of 3 inches. A guard ring which defined the active length of the 10-mil wire was made of $\frac{1}{16}$th-inch O.D. boron-free glass which was coated with Aquadag. This exterior conducting coating was connected to ground. The general construction of the counter is shown in Fig. 1. For most of the work the counter was filled with hydrogen or deuterium through a palladium leak to a pressure of about 50 cm. It was operated with about −3000 volts on the outer electrode. This voltage gave a gas multiplication of about a factor of five or more.

The counter was connected to a model 100 amplifier which had a rise time of about 1 microsecond and a minimum RC coupling which had a decay time of 5 microseconds. The counter and analyzing system were tested by filling the counter with nitrogen and observing the pulse height distribution due to the protons released by the capture of slow neutrons in N^{14} as described by Koontz and Hall.[4] In all cases the output of the amplifier was connected to a 10-channel pulse height analyzer so that all pulses in a small pulse height range were recorded in a single channel.[5] The relative magnitudes of the pulses recorded in the different channels, as well as the channel widths, were determined by using small pulses of known magnitudes fed into the first stage of the amplifier.

The neutrons of known energies which were used for calibrating the counter were obtained from the

* This article is based on work which was described in a declassified document LADC 63 and MDDC 149 December 10, 1945. The document has been revised and is presented for wider publication at this time because of its bearing on the values of the deuterium and beryllium neutron binding energies.

** Present address: Department of Physics, University of Illinois, Urbana, Illinois.

[1] Albert Wattenberg, Phys. Rev. **71**, 497 (1947).

[2] William E. Stephens, Rev. Mod. Phys. **19**, 19 (1947).

[3] M. Kahn, La225.

[4] P. G. Koontz and T. A. Hall, Rev. Sci. Inst. **18**, 643 (1947).

[5] The ten-channel pulse height analyzer was one designed at Los Alamos by Dr. K. I. Greisen.

Li(p,n) reaction.[6] The protons were furnished by the Wisconsin electrostatic generators then at Los Alamos. The energies of the protons are given in terms of the Li(p,n) threshold which is taken as 1.88 Mev.[7] The automatic regulators kept the voltages constant to about 2 kilovolts so that the error in the neutron energies is of the order of a few kev.

The neutrons from the various photo-neutron sources are fairly monoergic but there is a small distribution in energies due to the momentum carried into the system by the incident gamma-ray.

In general the energy of the emitted neutron depends on the angle (θ) between the direction of the emitted neutron and the direction of the incident gamma-ray. This energy is given approximately by the following relation:

$$E_n=\frac{A-1}{A}(E-Q)+\frac{E}{A}\left[2\left(\frac{A-1}{A}\right)\frac{(E-Q)}{931}\right]^{\frac{1}{2}}\cos\theta,$$

where E is the energy of the gamma-ray in Mev, Q is the neutron binding energy in Mev, and A is the mass number of the initial nucleus. The first term in the equation represents the average energy of the emitted neutrons (and protons in the case of deuterium). The second term gives the variation in the neutron energy as a function of the angle. The neutrons from the MsTh-D source are found to have energies distributed between 170 kev and 224 kev. In this case the maximum energies measured in this work must be reduced by 27 kev in order to obtain the average energy of the emitted neutrons or protons. The number of neutrons per unit energy interval within the above range can be represented approximately by a parabola with its vertex at the average energy.[8]

RESULTS

The relative pulse height distributions in the proportional counter when exposed to the neutrons from the Y-Be source and to neutrons of various energies from the Li(p,n) reaction are shown in Figs. 2 and 3. The abscissa on all graphs is the relative pulse height as determined by pulses of known magnitudes fed into the amplifier and the ordinate is the number of pulses in each given pulse height interval. The points are plotted to correspond to the average value of the pulse height range accepted by each channel. The data in Fig. 2 were obtained with the counter in front of the Li target while those in Fig. 3 were obtained with the counter at an angle of 120° from the forward direction. In the latter run the tail of large pulses is due to higher energy neutrons which were emitted in the forward direction but which have been scattered back by material around the target. Both runs indicate a value of 160 kev for the energy of the Y-Be neutrons. Since the protons from the generator are not strictly monoergic and since the counter subtends a finite angle, one would estimate that the maximum energies of the neutrons incident upon the counter from the Li(p,n) source would be about 2 kev greater than the energy indicated. The maximum energy of the Y-Be neutrons may, therefore, be specified as 162 kev with an error which may be estimated as about 5 kev.

The pulse height distributions with the same counter exposed to the neutrons from the MsTh-D, La-D, and Y-Be sources are shown in Fig. 4. If one assumes that the maximum neutron energies are proportional to the maximum pulse heights, the maximum energy of the neutrons from the MsTh-D and La-D sources are found to be 220 kev and 171 kev, respectively. A direct check on the proportionality between the pulse height and the neutron energy can be obtained from the data shown in Fig. 2. These data indicate that the proportionality is satisfactory within the accuracy of the measurements. They also indicate that the spread in the pulse height distribution introduced by the proportional counter is essentially a certain fraction of the pulse height. The preliminary experiments with nitrogen as well as the data shown in Fig. 5 indicate that this spread in pulse height is about ±5 percent.

Other comparisons of the MsTh-D and La-D neutron energies with that from Y-Be were obtained by observing the protons from the disintegration of deuterium in the proportional counter. The data shown in Fig. 5 were taken with the counter filled with 30 cm of deuterium and 25 cm of hydrogen and those in Fig. 6 with 55 cm of deuterium in the counter. If we again use the maximum pulse heights as a measure of the maximum energies these data indicate that the maximum energies of the neutrons from MsTh-D and La-D are 226 and 174 kev. If it is assumed that the maximum pulse heights are

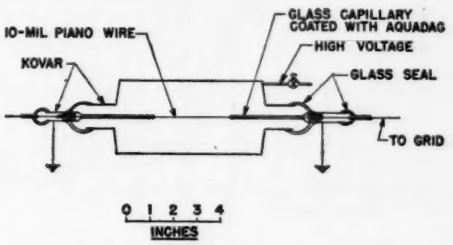

FIG. 1. Proportional counter.

[6] R. F. Taschek and A. Hemmendinger, Phys. Rev. **73**, 373 (1948).

[7] A. O. Hanson and D. L. Benedict, Phys. Rev. **65**, 33 (1944); Shoupp, Jennings, Jones, and Garbuny, Phys. Rev. **75**, 336 (1949); Herb, Snowden, and Sala, Phys. Rev. **75**, 246 (1949).

[8] J. R. Richardson and L. Emo, Phys. Rev. **53**, 234 (1938).

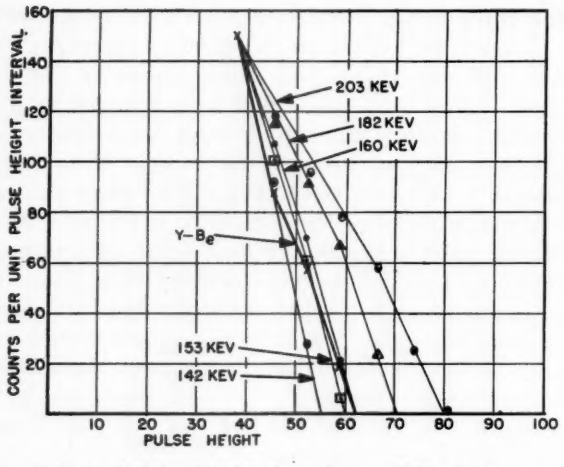

FIG. 2. Pulse height distributions due to Y-Be neutrons and Li(p,n) neutrons at 0°.

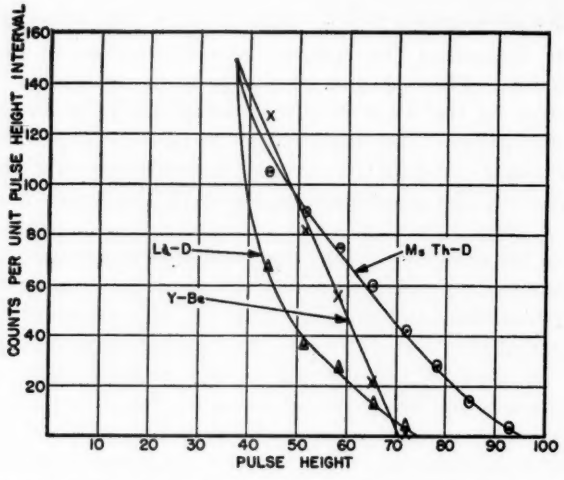

FIG. 4. Pulse height distributions due to neutrons from Y-Be, MsTh-D and La-D sources.

increased by the spread of 5 percent but that this pulse spread does not affect the position of the maximum in the observed pulse height distribution curve, the position of the maximum can be used to estimate the average neutron energies from MsTh-D and La-D sources. The average energies estimated in this way are found to be 195 kev and 151 kev. If one uses the values of 224 and 173 for the observed maximum energies reduced by the calculated energy spreads the corresponding average energies are 197 kev and 151 kev. These values are thought to be the most reliable but the uncertainty is difficult to estimate. The measurements seem to be consistent to within about 5 kev but the error could be as large as 10 kev.

A comparison of the pulse height distribution due to 890-kev Li(p,n) neutrons with that due to MsTh-Be neutrons is shown in Fig. 7. The data were taken with the counter filled with 20 cm of hydrogen and 50 cm of argon. The maximum energy of MsTh-Be neutrons can be estimated to be about 840 kev which gives an average energy of 827 kev.

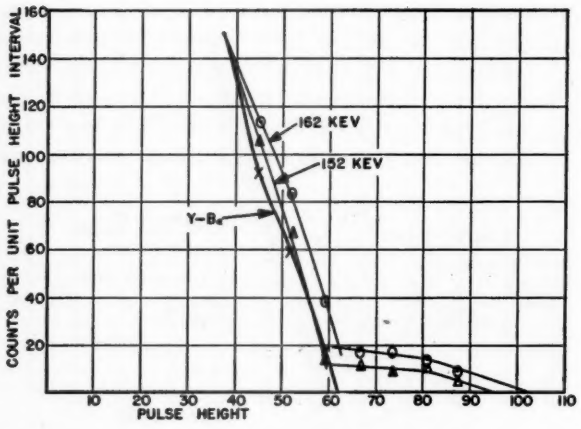

FIG. 3. Pulse height distributions due to Y-Be neutrons and Li(p,n) neutrons at 120°.

The data on the Sb-Be source were obtained with the same counter filled with 3 cm of hydrogen and ½ cm of methane. With only pure hydrogen in the counter at this pressure, the gas multiplication in the counter was very unstable. The addition of a small amount of methane greatly increased the stability.

A comparison of the pulse heights due to Sb-Be neutrons and those from the Li(p,n) reaction just at threshold is shown in Fig. 8A. The energy of the neutrons from this reaction at the threshold is 29.6 kev. For protons just 1 kev above the threshold, however, the energy turns out to be 40 kev. It is therefore difficult to estimate the effective energy with any accuracy. We have used a value of 35±5 kev, which would give a value of 25 kev for those from Sb-Be. The minimum value for these threshold neutrons would give an energy of 22 kev.

The dependence of the energy of the neutrons on that of the incident protons is much less critical at 120°. At this angle (for 30-kev neutrons) the neutron energy will change by only 1 kev for a 2-kev change in the proton energy. The spread in the neutron energy due to the finite solid angle subtended by the counter (3°) is about 3 kev. The results of the comparison at 120° is shown in Fig. 8B. It appears that the maximum energy of the Sb-Be neutrons is slightly lower than that of the 23 kev neutrons from Li. If one tries to take into account the spread in the energies from the Li(p,n) source one should increase these energies by about 3 kev. The maximum energy of the Sb-Be neutrons can therefore be specified as 25±3 kev and the average energy as 24±3 kev.

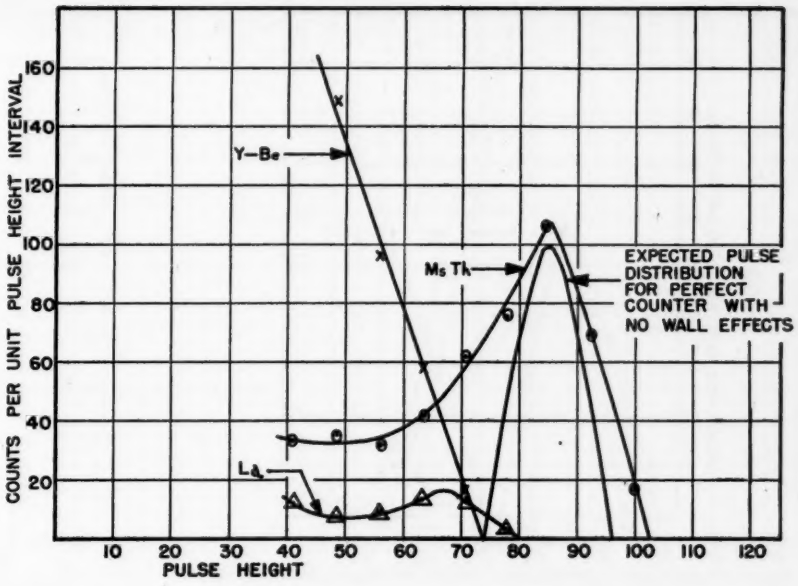

FIG. 5. Pulse height distributions due to Y-Be neutrons and the photo-protons from MsTh and La gamma-rays. The proportional counter was filled with 25 cm of hydrogen and 30 cm of deuterium.

DISCUSSION

Since the neutron energies depend on the difference between the gamma-ray energies and the binding energies of deuterium and beryllium, the present results can be used to obtain additional information about one or the other. The energy of the gamma-ray from MsTh is 2.623 ± 0.005 Mev[9] and has long been considered one of the most accurately known gamma-ray energies. The energy of the strong gamma-ray from the 60-day antimony has recently been measured and found to be 1.708 ± 0.010 Mev.[10] These two sources can be used with the present data on neutron energies to obtain values for the deuterium and beryllium binding energies. The average neutron energies from the Y-Be and the La-D sources can be used to obtain more accurate values for the energies of the effective gamma-rays from these sources. The data on the neutron energies and these simple correlations are summarized in Table I.

The value obtained for the deuterium binding energy (2.229 Mev) is much higher than the usually accepted value of 2.187 Mev and agrees reasonably well with the value (of 2.237 Mev) reported by Bell and Elliott for the energy of the gamma-rays due to the capture of slow neutrons by hydrogen.[11]

The value of 1.681 Mev for the binding energy of beryllium, obtained from the data on the anti-

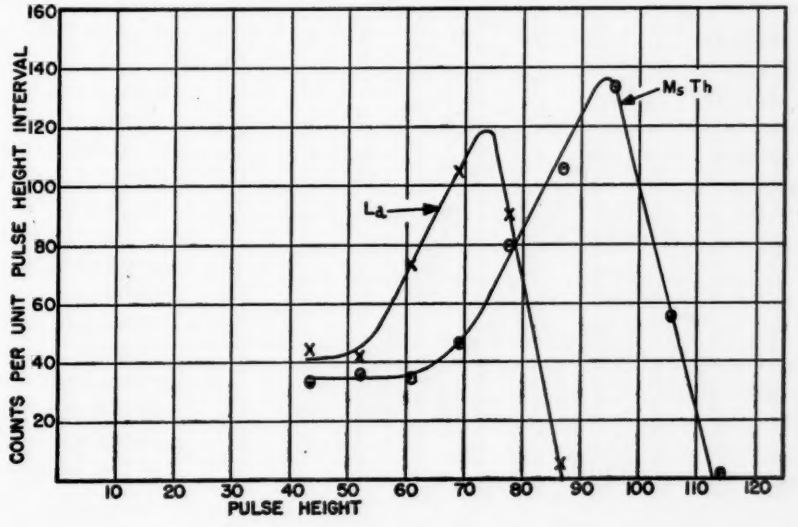

FIG. 6. Pulse height distributions due to photo-protons from MsTh and La gamma-rays with 55 cm of deuterium in the counter.

[9] C. D. Ellis, Proc. Roy. Soc. **138**, 318 (1932).
[10] C. S. Cook and L. M. Langer, Phys. Rev. **73**, 1149 (1948).
[11] R. E. Bell and L. G. Elliott, Phys. Rev. **74**, 1553L (1948).

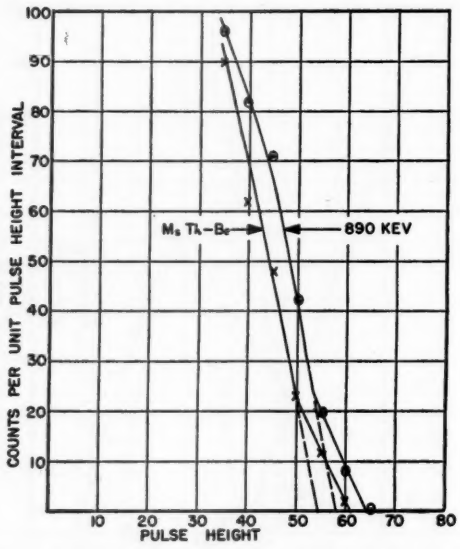

FIG. 7. Pulse height distributions due to MsTh-Be and 890-kev Li(p,n) neutrons.

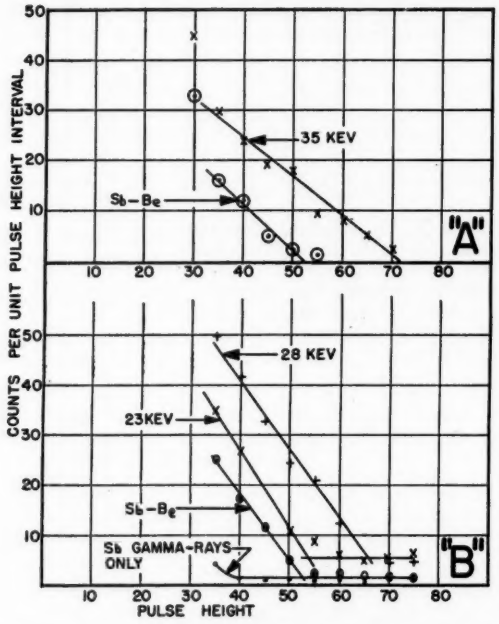

FIG. 8. Data on the comparison of the energy of Sb-Be neutrons with Li(p,n) neutrons at threshold (A), and with Li(p,n) neutrons at 120° (B).

mony source, is at first rather startling since it represents a difference of about 3 percent from the usually accepted value of 1.63 Mev.[2] It should, however, be more precise than the value obtained for the deuterium threshold.

There are two other measurements which can be used to correlate these two binding energies. One is the difference between the binding energies as obtained from the reaction energy for the $Be^9(p,d)Be^8$ reaction. The most recent value reported for this energy is 0.555 ± 0.003 Mev.[12] The present value of 1.681 ± 0.013 for the beryllium binding energy would, therefore, lead to a value of 2.236 ± 0.014 for the binding energy of deuterium which is essentially the same as that obtained by Bell and Elliott. The other measurement which seems to be well established is the ratio of the two thresholds. The value of this ratio is 1.338 ± 0.004.[13] This ratio and the present value for the beryllium binding energy would give a value of 2.249 Mev for deuterium. Although this value seems somewhat high, it is in agreement with the preceding value within the probable experimental errors. It seems likely that the energy assigned to the antimony gamma-ray may be slightly high. Further measurements on this gamma-ray, as well as that from the yttrium, would be desirable in order to use the present neutron energies to establish the binding energy of beryllium with greater precision.

The difference in energy between the Y and Sb gamma-rays can be determined in terms of the difference between the energies of the neutrons from the Y-Be and the Sb-Be sources. The present neutron measurements indicate that the energy of the gamma-ray from Y is 0.151 Mev greater than that from Sb. The energy obtained in this way is, therefore, 1.859 ± 0.015 Mev. Similarly the energy of the La gamma-ray is found to be 0.092 Mev less

TABLE I. Neutron energies.

Neutron source	Gamma-ray energy (Mev)	Average neutron energies (kev) Ref	This work	Other work	Ref	Thresholds
MsTh-D	2.623 ±0.005	9	197 ±10	218	2	2.229 ±0.020
MsTh-Be	2.623		827 ±30			1.693 ±0.030
Sb-Be	1.708 ±0.010	10	24 ±3	29 ±15	1	1.681 ±0.013
Y-Be	1.92 ±0.03	a	158 ±5	220	c	1.74
	1.89 ±0.05	b				1.71
	1.859 ±0.015	†				
La-D	2.3	d	151 ±8	160 ±20	1	
	2.531 ±0.010	†				

† These gamma-ray energies are based on the present neutron measurements.

[a] J. Reginald Richardson, Phys. Rev. **60**, 188 (1941).
[b] Downing, Deutsch, and Roberts, Phys. Rev. **60**, 471L (1941).
[c] G. Scharff-Goldhaber, Phys. Rev. **59**, 937A (1941).
[d] W. Rall and R. G. Wilkinson, Phys. Rev. **71**, 321L (1947).

[12] Tollestrup, Lauritsen, and Fowler, Phys. Rev. **75**, 1463 (1949); Allison, Skaggs, and Smith, Phys. Rev. **57**, 550L (1940).

[13] B. Waldman and W. M. Miller, Phys. Rev. **74**, 122A (1948).

than that from MsTh and can be specified as 2.531 ± 0.010 Mev.

ACKNOWLEDGMENTS

The author is indebted to Dr. E. Segrè and his group for making these sources available for this work, to Dr. A. Hemmindinger for his collaboration in the work with the Sb-Be source, and to Dr. J. H. Williams for his support and interest in this work.

Note added in Proof.—Peacock and Jones have reported a value of 1.853 ± 0.03 for the energy of the yttrium gamma-ray which is in agreement with the value deduced from the present work (W. C. Peacock and J. W. Jones, Plutonium Project Record CNL14 (February, 1948).

PHYSICAL REVIEW VOLUME 75, NUMBER 12 JUNE 15, 1949

Neutrinos from P 32

CHALMERS W. SHERWIN
Department of Physics, University of Illinois, Urbana, Illinois
(Received February 21, 1949)

Sources of P 32 which come close to being true monolayers are prepared by evaporation in a vacuum. The characteristics of these sources are maintained for 5 to 10 days with the aid of radiant heating. Surface charges are neutralized by periodic "baths" of thermal electrons. The momentum of the electrons is measured with a magnetic spectrometer and the momentum of the recoil ions is measured by observing their time of flight in a field free space.

The momentum measurements show that the missing momentum disappears in one package. Separate energy measurements determine the amount of energy which disappears. The observed ratio of the missing energy to the missing momentum is equal to the velocity of light (±20 percent), as required by the hypotheses that one neutrino is emitted in beta-decay.

After experimentally determined corrections are made for the effects of surface scattering of the recoil ions, it is concluded that the missing momentum vector (i.e., the neutrino) most probably enters the same hemisphere as the electron. The experimental points fit best on a curve of the form, $(1+v/c\cos\theta)$. This is in disagreement with previous tentative conclusions by the author which are now shown to be in error due to surface losses and scattering of the recoil ions.

I. INTRODUCTION

IN a recent review article, H. R. Crane[1] has described the search for the neutrino through its effect on the parent nucleus during the process of beta-decay. Experiments, performed over the past decade, have conclusively shown that momentum is not conserved in beta-decay, and there is some more or less tentative evidence[2,3] that the neutrino direction is either approximately random, or favors the opposite hemisphere with respect to the electron.

Both Crane[1] and Allen[2] point out that no recoil experiments have yet demonstrated that a single neutrino is emitted in beta-decay. However, in the Fermi theory[4] the bell shaped momentum distribution of the electrons is a consequence of the emission of two fast particles. The main factor which controls the shape of the electron momentum spectrum at high momenta is the number of cells in momentum space that are available to the electron and the neutrino.[5] If there were two neutrinos the electron spectrum would be quite different than observed.[6] Recoil experiments are also capable of giving information on this point, either by observing monoenergetic recoils from K capture as Crane[1] has suggested, or as in the present experiments, observing monoenergetic recoils associated with monoenergetic electrons.

An important objective of these experiments is to determine as much as possible about the angular correlation between the electron and the neutrino. Different forms of the neutrino-electron interaction predict different angular correlations.[7] Also the angular momentum change which determines the "forbiddeness" of the transition should affect the neutrino-electron angular correlation. Hamilton[7] shows that as the forbiddeness increases, the neutrino tends to go more and more in the same direction the electron, this correlation being greatest when the electron and neutrino momenta are equal. This effect can be visualized by the following simple classical picture. There is only a definite amount of energy available for the electron and the neutrino. Consequently, a limited amount of linear momentum can be carried by the two particles. If this linear momentum leaves the

[1] H. R. Crane, Rev. Mod. Phys. **20**, 278 (1948).
[2] James S. Allen, Am. J. Phys. **16**, 451 (1948); Allen, Paneth, and Morrish, Phys. Rev. **75**, 570 (1949).
[3] Chalmers W. Sherwin, Phys. Rev. **73**, 216 (1948); **73**, 1173 (1948).
[4] Enrico Fermi, Zeits. Physik **88**, 161 (1934).
[5] Emil J. Konopinski, Rev. Mod. Phys. **15**, 209 (1943).
[6] J. Blatt, private communication.
[7] Donald R. Hamilton, Phys. Rev. **71**, 456 (1947).

nucleus at some distance from the center it can produce the required change in angular momentum. When the electron and neutrino have about the same momentum, they must go in the same general direction in order that their total momentum can cause an angular momentum change in the nucleus. Near either end of the electron momentum spectrum, one particle has almost all the momentum, the direction of the other particle no longer appreciably affects their total momentum, and the angular momentum change no longer tends to correlate the direction of the neutrino and the electron.

II. THE PRINCIPLES OF THE EXPERIMENTAL METHOD

Some of the beta-decay recoil experiments performed to date have measured the recoil ion momentum distribution associated with the electrons traveling in a selected direction, but with no selection of the magnitude of the electron momentum.[2,3] The addition of a magnetic deflection beta-spectrometer makes possible the selection of the magnitude as well as the direction of the electron momentum. The direction of the recoil ion can be selected by means of slits, and its velocity determined by measuring its time of flight in a field free space. Thus, the beta-spectrometer and the recoil time of flight spectrometer permit direct measurements of the electron and recoil momentum vectors. If one assumes the conservation of momentum, the neutrino momentum can be immediately inferred by vector subtraction.

The same apparatus permits an independent measurement of the neutrino energy. The beta-spectrograph also specifies the electron energy, so the balance of the available energy can be assigned, assuming the conservation of energy, to the neutrino.

The ratio of the neutrino energy of the neutrino momentum must be equal to the velocity of light

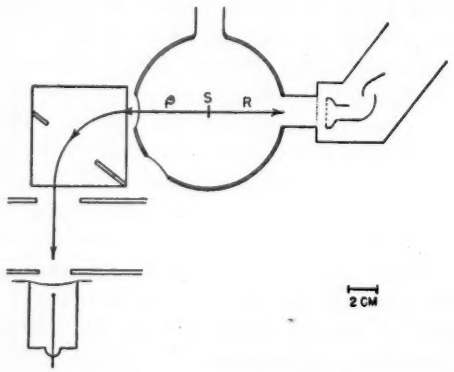

FIG. 1. Apparatus for neutrino recoil measurements. The P 32 source faces the electron multiplier. The velocity of the recoil ions is determined by measuring their time of flight. The momentum of the electrons is measured by the 90° deflection spectrometer.

for all cases where the energy is large compared to the rest mass. Since it requires a neutrino of several hundred thousand electron volts to impart a few electron volts energy to even a light nucleus, and since the rest mass of the neutrino is known to be less than 5 kev,[8,9] recoil experiments are very insensitive to the neutrino rest mass.

A convenient expression for the magnitude of the neutrino momentum, p_ν, is

$$p_\nu/m_e c=(E_0/m_e c^2+1)-((p_e/m_e c)^2+1)^{\frac{1}{2}}, \quad (1)$$

where p_e is the electron momentum in oersted-cm, $m_e c$ is 1700 oersted-cm, $m_e c^2$ is 0.51 Mev, and E_0 is the upper end point of the electron kinetic energy spectrum in Mev. This expression is obtained using only the conservation of energy and the assumption that the neutrino rest mass is negligible ($p_\nu=E_\nu/c$).

III. A BRIEF DESCRIPTION OF THE APPARATUS

A simplified sketch of the apparatus is shown in Fig. 1. A source of P 32 (~50 microcuries) on an area of about $\frac{1}{4}$ square centimeter is mounted on the blown glass film, S (0.4 mg/cm²). The active deposit faces the electron multiplier. The beta-particles are deflected by the 90° spectrometer and are detected in the Geiger counter which starts a 17-microsecond sweep on a cathode-ray tube. The electron multiplier pulse is clipped by a pulse or line, and is applied as intensity modulation on the cathode-ray tube, making a dot about $\frac{1}{5}$ microsecond in duration. A continuously moving film records the position of the electron multiplier pulses. Every six minutes a row of one microsecond calibration dots automatically appears on the sweep. The recoil ion time of flight distribution is plotted directly from the film record.

An important part of the equipment, not shown in Fig. 1, is a heater (two 0.075-cm diameter tungsten wires each one cm long) located 2 or 3 mm to the left of the source film. This heater serves two important functions. One is to keep the surface continuously warm by radiation from the dull red heater wires. This continuous heating permits the P 32 surface to maintain its original characteristics for 5 to 10 days. The second purpose of the heater is to give the radioactive surface a thermal electron "bath" for a few seconds every twelve hours. These electrons, emitted from the heater while it is run for short times at a high temperature, drift around to the front of the surface and neutralize the positive surface charge built up by the departing beta-particles.

The surface S is a blown Pyrex film freshly coated in the same vacuum system with a just visible gold film. On top of the gold is evaporated a LiF or

[8] J. L. Berggren and R. K. Osborne, Phys. Rev. **74**, 1240 (A) (1948).
[9] Cook, Langer, and Price, Phys. Rev. **74**, 548 (1948).

MgF_2 film. These insulating films have a "work function" which is high enough, at least in spots, to let some of the recoil ions (sulfur, 10.3-ev ionization potential) escape charged. Potentials of 10 to 15 volts still can build up in a period of 3 or 4 days, so that regular "baths" of electrons are necessary to keep surface charges from influencing the recoil ions. The heater cannot be continuously hot enough to emit appreciable numbers of electrons because this causes the electron multiplier to have a very high background. Even before this limit is reached there is some evidence that operating above a dull red temperature causes a deterioration of the surface (possibly diffusion of the P 32 atoms into the substrate) and slow evaporation of the P 32 atoms. The effects of too high heater temperatures are to noticeably increase, in 5 to 10 hours, the relative numbers of low momentum recoil ions, and to cause the electron multiplier background to increase steadily.

With the aid of the heater and a good vacuum (10^{-7} mm of Hg) surfaces show no noticeable changes for 4 to 6 days, but between 10 to 16 days there is some evidence that surface losses on the part of the recoil ions is on the increase. Without a heater, the surfaces badly deteriorate in a few hours. This remarkable and unexpectedly long life of the P 32 surfaces makes possible measurements that would otherwise be very difficult, if not impossible, to perform. When working with coincidence type experiments in which the effects are the order of the background, only efficient geometry and long observation time are of any avail in obtaining precision results.

It is interesting to consider the purity requirements on the radioactive material. To form a 50-microcurie monolayer source of P 32 on a 0.25 cm^2 surface requires that $\sim 1/500$ of the available surface area be occupied by P 32 atoms. This in turn requires that the maximum amount of inert atoms accompanying the P 32 as it is evaporated onto the final surface is about one microgram per millicurie. All of the significant data reported here was obtained from two shipments specially purified carrier free P 32 in weak acid solution obtained from Oak Ridge. One shipment had less than 40 micrograms and the other about 80 micrograms of non-volitile matter per millicurie. This material is twice evaporated in forming the final surface. After the first evaporation the active deposit becomes invisible, giving a separation factor of at least 20:1. After the second evaporation, the performance of the recoil ions is the only test of source thinness.

It should be noted that initially the P 32 atoms are on the average widely separated. They do not evaporate easily except at temperatures above 600°C, but their migration on the surface may still occur. Migration of barium on a tungsten surface

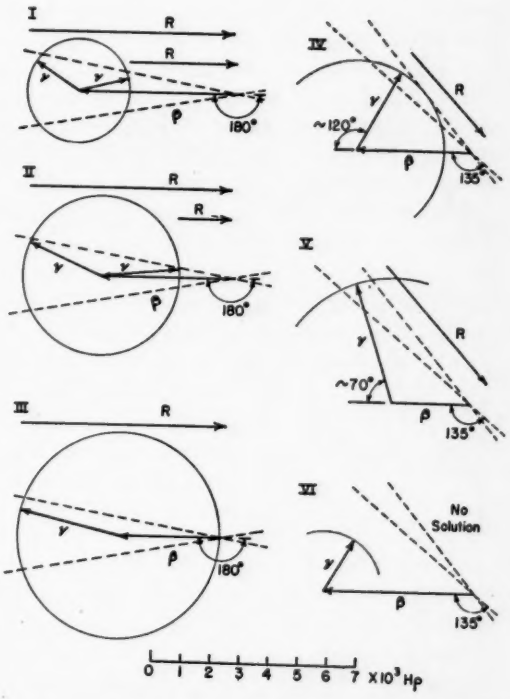

FIG. 2. Some vector diagrams of momenta in the beta-decay of P 32. The diagrams show six different geometrical arrangements of the electron (β), recoil ion (R), and neutrino (ν) momentum vectors that were tested experimentally. The dotted lines show the "cone of sensitivity" set by the slit widths of the detection system, into which the recoil ion must go in order to be detected. The magnitude of the neutrino momentum vector is calculated from the conservation of energy.

is known to occur 250 degrees below the evaporation temperature,[10, 11] and it occurs in mercury at liquid air temperature.[12]

The beta-spectrometer in Fig. 1 can be used at the 180° (electron-recoil angle) position as shown, or it can be moved to the 135° window. In the latter position, the spectrometer is rotated through 90° so the electrons are deflected perpendicular to the plane of the paper. Because of the shape of the slits, this reduces by a factor of two, the possible variation in angle between the electron and the recoil ions being detected. There is some scattering of the beta-particles in the exit window (8 mg/cm^2) of the vacuum system and in the air of the spectrograph chamber. The wide exit slit of the spectrometer (2.2 cm) and the width of the source (0.5 cm) already make the resolution of the instrument broad. The scattering has been generously allowed for using the observations of Slawsky and Crane[13] on 0.9-Mev electrons. The measurements reported

[10] J. H. de Boer, *Electron Emission and Absorption Phenomena* (Cambridge University Press, London, 1935), p. 112.
[11] J. A. Becker, Trans. Faraday Soc. **28**, 155 (1932).
[12] I. Estermann, Zeits. Physik. Chemie **106**, 403 (1923).
[13] M. M. Slawsky and H. R. Crane, Phys. Rev. **56**, 1203 (1939).

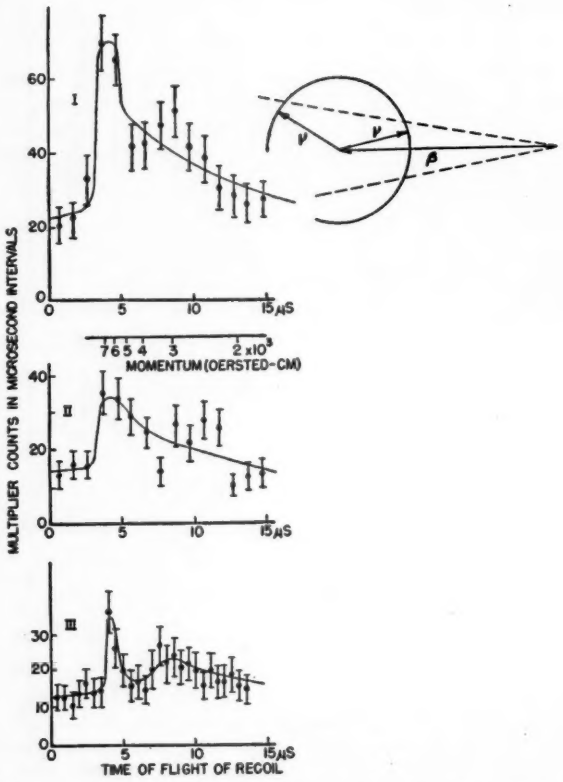

FIG. 3. Time of flight of recoil ions from three "poor" surfaces. There are far too many low momentum recoil ions for the geometry shown. These surfaces are thought to be over-laid with varying amounts of inert material.

here were made with electrons between 0.5 and 1.2 Mev.

The spectrometer is calibrated by measuring the complete beta-spectrum of the actual P 32 sources used in the recoil experiments. The beta-spectrum does not deviate from a straight line on a Fermi plot down to 3600 $H\rho$, and at 2600 $H\rho$ the points fall 10 percent below the line as the effects of scattering and absorption become noticeable.

The electron multiplier aperture subtends a solid angle of 38 square degrees, as viewed from S.

Improved equipment should have a vacuum spectrometer located at 180°, 135°, and 90° each recording data simultaneously from the same electron multiplier.

IV. SOME PREDICTIONS WITH MOMENTUM VECTORS

An hypothesis is tested by making predictions and then testing these predictions experimentally. The hypothesis that the neutrino acts like an ordinary particle or photon and carries away momentum whose magnitude is determined by the missing energy can be tested using the apparatus in Fig. 1. Some predictions, made easily by graphical methods, are shown in Fig. 2. The length of the neutrino momentum vector is fixed by the conservation of energy and is calculated from Eq. (1). Its direction is indeterminate although it may be influenced by some unknown angular correlation with respect to the electron. Dotted lines show the "cone of sensitivity" into which the recoil vector must fall for the recoil ion to be detected. Thus, the slits of the experimental apparatus permit only those neutrinos which have certain specified directions to produce detectable recoil ions. From the intensity of these groups of recoil ions, one can calculate the intensities of the neutrino groups that cause them, thus, measuring the neutrino-electron angular correlation.

For electron energies in excess of 0.5 Mev, the sum of the magnitudes of the neutrino and electron momenta is nearly constant (7000 to 7200 oersted-cm).

In interpreting the vector diagrams of Fig. 2 one must remember that the electron momentum vectors are only the center values of a group whose spread is ± 15 to ± 20 percent in length, and whose spread in direction is ± 5 to ± 10 degrees. An averaging of the effects of these variations must be made, and the time resolution (0.5 microsecond) of the time of flight measurements be taken into account, before exact predictions are possible regarding experimental results.

Consider first the geometry of case I. Here the electron momentum is $\frac{3}{4}$ of the maximum value of 7200 oersted-cm. The neutrino momentum, from Eq. (1), is very nearly $\frac{1}{4}$ of 7200 oersted-cm (or $H\rho$). For "forward" neutrinos, a high momentum (7200 $H\rho$) recoil is formed. For "backward" neutrinos a low momentum ($\frac{1}{2}\times 7200\ H\rho$) recoil is formed. For neutrinos having an angle of about 90° with respect to the electrons, the recoil should be outside the cone of sensitivity, and not be detected. Thus, for case I of Fig. 2, one should observe two distinct groups of recoil ions. As will be shown later, the high momentum recoils are clearly visible experimentally. A careful search for the lower momentum group of recoils has thus far been unsuccessful. These low momentum recoils are hard to observe for three reasons: (1) the solid angle available to the backward neutrino is only $\frac{1}{4}$ that available to the forward neutrino; (2) the spread (about $\pm 800\ H\rho$) in electron momentum causes the low momentum recoils to be spread over $\pm 1600\ H\rho$ around an average value of 3600 $H\rho$. This same uncertainty in the electron momentum causes, however, a negligible spread in the recoils due to the forward neutrinos since, to a good approximation, the electron's loss is the neutrino's gain and the two vectors add up to the same value of nearly 7200 $H\rho$; (3) the low momentum peak is hard to observe against the random background since, on a time of flight scale, a given momentum interval centered at 3600 $H\rho$ is spread over about

four times as many microseconds as is the same momentum interval centered at 7200 $H\rho$. These three effects attentuate and smear out the low momentum peak, making it hard to distinguish above the random background.

Case II is similar to I except that the low momentum peak due to the backward neutrino is even weaker and more diffuse than before. The high momentum peak should still have a value of 7200 $H\rho$, but its intensity per beta-particle should be lower since the solid angle available to the neutrino is less.

Case III has only one possible solution, namely recoils of about 7000 $H\rho$. These recoils should be only $\frac{1}{4}$ as intense per beta-particle as in case I since the solid angle available to the neutrino is only $\frac{1}{4}$ as large. This prediction assumes that the angular correlation function of the electron and neutrino does not change rapidly over the angles involved (0 to 60°). This case is particularly important since it is here possible to detect the presence of low momentum recoils which are spurious, due most probably to scattering and surface losses of the recoils. Since there is only one possible solution of the momentum triangle for a single neutrino, the presence of recoils at low energies can be explained by multiple neutrinos or by a poor surface, the latter explanation being far more likely. A sharp high momentum peak of recoils followed by no low energy recoils is thus considered to be the best test of a true monolayer surface. If there were multiple neutrinos with any randomness in their relative directions, one would not obtain the sharp high momentum peak predicted by cases I, II, and III since, on the average, their momenta would partially cancel each other. This would cause a diffuse group of recoil ions.

Cases I, II, and III of Fig. 2 form a sort of null method of detect for the neutrino. The mere presence of a sharp high momentum group of recoils coincident with lower momentum groups of electrons shows that there is a unique amount of momentum missing in each of the three cases and that the missing momentum increases in direct proportion to the missing energy. A further important prediction is that there should be a progressive change in the intensity per beta particle of the high momentum recoil peak due to the change of the solid angle available to the neutrino.

Case IV has nearly the same electron momentum as case III. One is looking for recoils in a different direction, 135° with respect to the electron instead of 180°. The neutrino, though backward, now has an appreciable available solid angle, and can form low momentum recoil ions in the region of 3000 to 5000 $H\rho$.

Case V differs from the previous one only by having a lower electron momentum. This predicts a higher average recoil momentum because of the new shape of the triangle. Thus, comparing the cases IV and V, the lower momentum electrons are associated with the higher momentum recoils—an effect that is most unlikely except on the neutrino hypothesis. This effect also gives more information about the surface, for if the average recoil groups observed in IV and V actually shift momentum as predicted it is unlikely that they are all due to some spurious effect such as scattering.

Case VI is a triangle that is insoluable by the efforts of the neutrino alone. At best the neutrino can make a group of medium momentum recoils which fail to enter the cone of sensitivity by 20 or 30 degrees. If there is no scattering of the recoils at the surface, one should obtain no recoil ions above the chance background. This test therefore makes possible an estimate of the effects of surface scattering which is potentially the most important sources of error in this type of experiment.

In addition, to the six cases shown in Fig. 2, some measurements were also taken, intermediate to cases IV and V, where the electron-neutrino angle is about 90°.

The rest of the paper consists of a description of

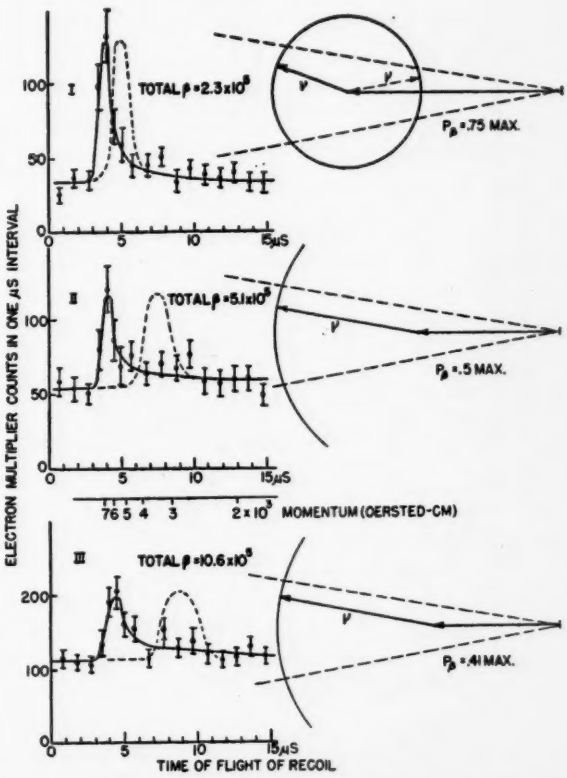

FIG. 4. Time of flight of recoil ions from surface A. The dotted curves (arbitrary amplitude) show what the recoil ion spectra would look like if there were no neutrino. The continued presence of the high momentum peak of recoils as the electron momentum is progressively reduced is evidence for a single neutrino. "Total β" means the total number of electrons detected during the observation of the complete curve.

the experimental observations made under the various conditions shown in Fig. 2. It can be stated, in anticipation, that for some sources the predictions of Fig. 2 are indeed fulfilled, and that scattering effects, though noticeable, are not so large as to obscure the essential agreement between theory and experiment.

V. EXPERIMENTAL RESULTS

Most of the sources have recoil spectra similar to the three shown in Fig. 3. There is evidence of a peak at about 7000 $H\rho$ as predicted by case I of Fig. 2, but there is a strong low momentum (long time of flight) "tail." This tail varies in intensity through a wide range for different sources. It might be explained by multiple neutrinos, but surface scattering due to the thickness of the source is far more likely. As will shortly be described, other surfaces for which the 7000 $H\rho$ peak stands out much better compared to the background show practically no evidence of a low momentum tail. The assumption is made that it is a spurious effect caused by the surface.

The tendency to form a second peak in the neighborhood of 8 or 10 microseconds also appears to be a spurious effect and not due, as was first supposed, to a strongly backward neutrino. When carefully studied, this second peak proves to be erratic and never to be really distinct above the background. When the highest purity radioactive material is used, this second peak simply vanishes.

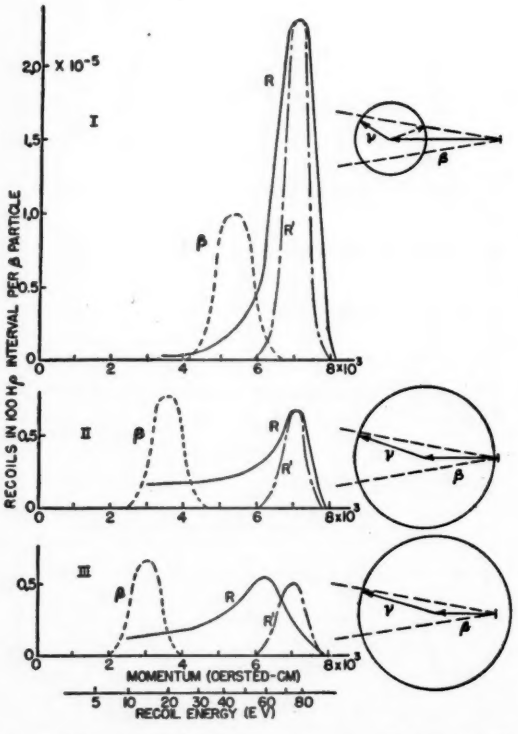

FIG. 5. Momentum spectra of the recoil ions in Fig. 4. β = the electron spectrum (arbitrary amplitude), R = the observed recoil momentum spectra (less background), R' = the calculated recoil momentum spectrum, normalized in amplitude to the observed spectrum, assuming a single neutrino, and taking into account the finite resolving power of the apparatus. The observed decrease in intensity of the high momentum recoil peak is predicted by the decrease in the solid angle available to the neutrino inside the cone of sensitivity.

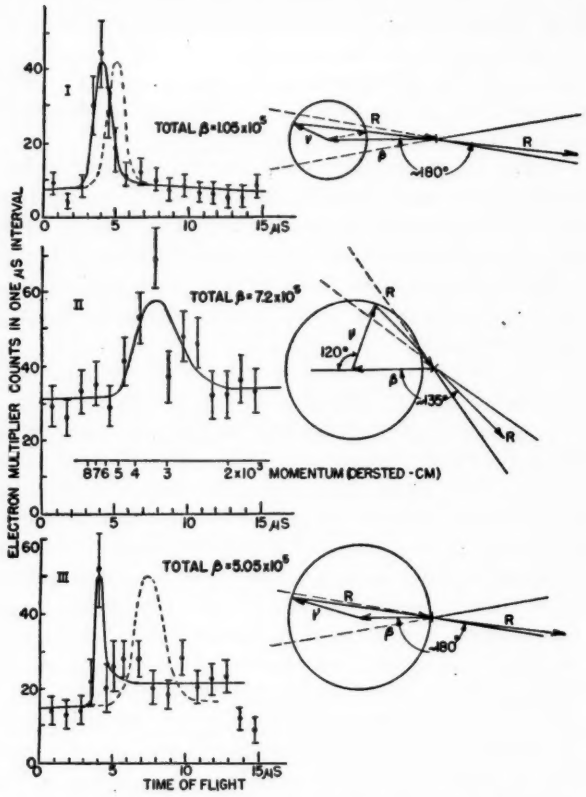

FIG. 6. Time of flight of recoil ions from surface B. An interesting point about these data is the difference between curves II and III. The only difference in the apparatus for these two cases is that the beta-spectrometer is moved from the 180° window to the 135° window (see Fig. 1). The dotted curves show what the recoil spectra would look like if the recoils received momentum only from the electrons.

Figure 4 shows recoil ion time of flight spectra for a typical "good" surface. Figure 5 shows the momentum spectra for the same data, background subtracted, along with the recoil spectra predicted by the neutrino. Several conclusions can be drawn from these data.

(a) The clear cut distinction between the observed recoil momentum and the electron momentum argues for a single neutrino for which the energy momentum is c (± 20 percent, estimated error). The fairly sharp recoil group shows that the recoil ions escape without too much interference from the source, in any case, the improvement over the data in Fig. 3 is very marked.

(b) The progressive decrease in the absolute intensity, Fig. 5, of the 7000 $H\rho$ peak as the solid angle available to the neutrino decreases, is pre-

dicted by a neutrino whose angular correlation with respect to the electron does not change rapidly between 0° and 60°. For example, in curves I and II of Fig. 5, the neutrino vector changes length by a factor of two making the available solid angle change by a factor of four, and the observed intensity of the peaks changes by 4.

(c) There is no evidence above background of a second low momentum (4500 to 2500 $H\rho$) peak due to the backward neutrinos. This peak would be about twice background if there were a backward $(1-v/c\cos\theta)$ neutrino-electron angular correlation. On some surfaces a small low momentum "tail" appears, following the 7000 $H\rho$ peak, for the geometry of curve I, Fig. 4. One might think this to be due to backward neutrinos, but an examination of the data obtained with the geometry of curve II, Fig. 4 also shows a similar low momentum tail. For this second case, the neutrino cannot possibly produce a low momentum peak. One concludes that the tail is due to scattering of that fraction of the recoil ions that are overlaid or otherwise obstructed by inert atoms.

A second "good" surface of P 32 on a LiF substrate is shown in Figs. 6 and 7. The top and bottom graphs support the same conclusions as just discussed above. In addition, the distinctly different recoil spectrum for the center case (electron-recoil angle 135°, electron momentum slightly over $\frac{1}{2}$ maximum) gives some additional information.

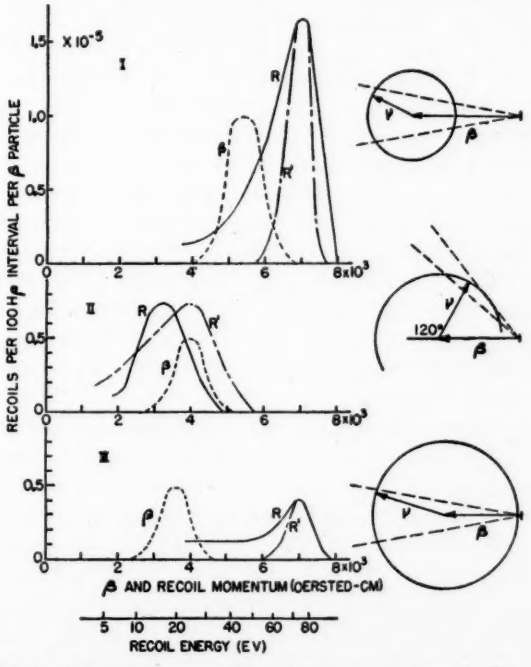

FIG. 7. Momentum spectra of the recoil ions in Fig. 6. β=electron spectrum (arbitrary amplitude). R=observed recoil momentum spectrum, less background. R'=calculated recoil momentum spectrum, normalized in amplitude to the observed spectrum, and taking into account the finite resolving power of the apparatus.

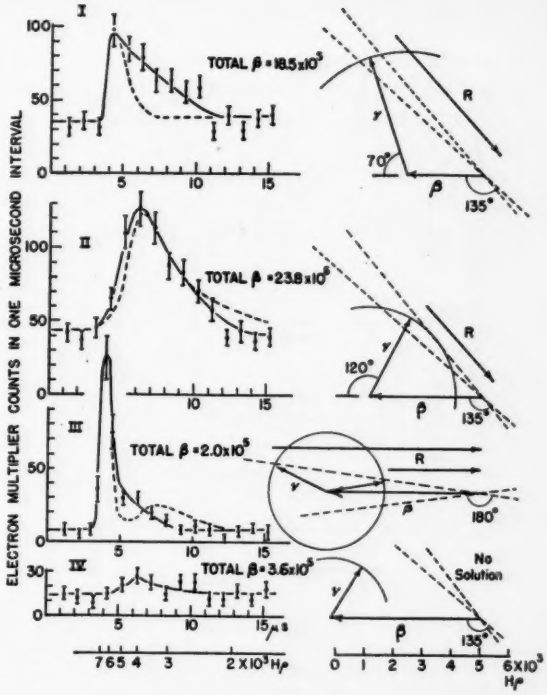

FIG. 8. Time of flight of recoil ions from surface C. The dotted lines show the calculated shape (arbitrary amplitude) of the recoil time of flight spectra taking into account the resolving power of the apparatus. The small low momentum peak in curve III was calculated assuming a random neutrino. This peak would be about 7 times larger for a backward $(1-v/c\cos\theta)$ neutrino, and about five times smaller for a forward $(1+v/c\cos\theta)$ neutrino. Curve IV shows that there are some spurious low momentum recoils that are not caused by neutrinos alone.

(a) Note that the essential difference between the geometry of curves II and III of Fig. 6 is the direction of the recoils with respect to the electrons. Since the recoils are always examined approximately perpendicular to the surface, the two figures differ only in the location of the beta spectrometer (see Fig. 1). We conclude that the high momentum recoil groups are not noticeably scattered through 45°. Otherwise, the spectra would not be so distinctly different. There is a low momentum "tail" on curve III which must be spurious, and whose total intensity is about 7×10^{-5} recoils per beta-particle. On the other hand, the recoil group in curve II has a total intensity of 16×10^{-5} recoils per beta-particle. If the spurious low momentum recoils present in III are also scattered through angles up to 45 degrees with any appreciable intensity, we estimate that up to $\frac{7}{16}$ of the recoils in curve II may be spurious. This method of making a correction for scattering is not very precise. It does, however, give the approximate magnitude of the correction, and more important, the direction of the correction. Furthermore, as will be pointed out when discussing observations with the insolu-

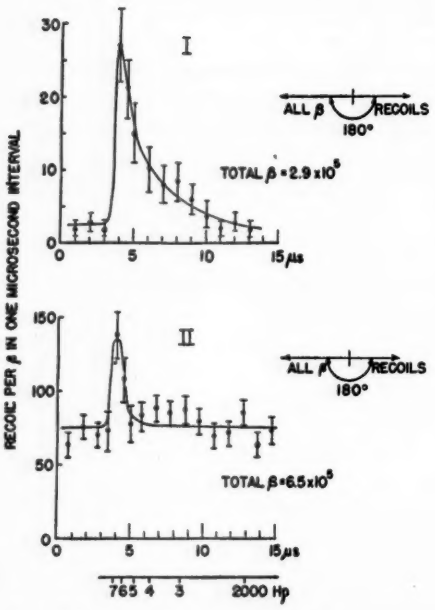

FIG. 9. Recoil ions from the complete electron momentum spectrum. The upper curve is from earlier published data by the author and its shape agrees rather well with that predicted by backward $(1-v/c\cos\theta)$ neutrino-electron angular correlation function. The lower curve is taken from the same surface as Fig. 4, and agrees only with a forward, or at most a random neutrino. The difference in the relative magnitude of the backgrounds is due to the much higher intensity of the source for II. The low momentum "tail" on curve I is apparently due to surface losses and scattering of the recoil ions which, without a beta-spectrometer, is hard to distinguish from a backward neutrino.

able triangle of case VI, Fig. 2, a different geometry suggests approximately the same correction.

(b) The presence of what appear to be genuine recoils at 3 to 4 thousand $H\rho$ on curve II suggests that recoils of this low energy really escape from the surface and can be detected. This removes one possible explanation of why the second low momentum peak in curve I is not observed, namely that some unknown surface effect prevents the recoil ions of initially low energy from escaping at all, or if they do escape, makes them neutral and thus undetectable.

(c) The predictions of the neutrino hypothesis agree rather well with all three observed recoil spectra as can be seen from Fig. 7.

Further information can be obtained by studying the observations on a third "good" surface. These data are plotted in Fig. 8. This source was several times weaker than the two others already discussed, and required longer observation time, the curves I through IV requiring 40, 47, 8½, and 21 hours, respectively. These observations were not made in the simple sequence suggested by the drawing, but are compiled from 16 different films with each successive film having a different geometry. This same procedure was also followed on the other surfaces described here.

We shall now discuss the significance of the data in Fig. 8, starting with curve III since it tests the monolayer character of the source.

(a) At first sight, curve III shows more of a low momentum tail than the same geometry in the earlier surfaces, and one might suspect it of being inferior. However, the random background is considerably lower, and it may be that the imperfection is no worse than for the earlier surfaces, but merely more easily noticed. Furthermore, this tail is not due to a backward neutrino since it also appears for the geometry of case III, Fig. 2 where the neutrino can not be the cause. The dotted curve in III, Fig. 8, shows the low intensity low momentum peak which would be caused by a random neutrino. A more forward neutrino, which is implied by the other observations, would make this peak still smaller and more obscure. Failure to observe it is not surprising. In any case, a strongly backward neutrino is rejected.

(b) A comparison of curves I and II of Fig. 8 shows that there is a distinct difference in the average momentum of the observed recoil groups. One group has a maximum at about 5 to 6 thousand $H\rho$, and the other at 3 to 4 thousand $H\rho$. This effect is predicted by the neutrino hypothesis as can be seen from the vector drawings and the dotted curves. Here is direct experimental evidence that the higher momentum recoils are associated with the lower energy electrons, as the neutrino hypothesis requires. The presence of a low momentum "tail" on curve I in contrast to the predictions indicates that there are some surface losses. How many of the recoils in the tail are initially due to the 70-degree neutrino group under study, and how many are due to entirely irrelevant neutrinos followed by surface scattering, is not certain. The dotted curves are arbitrarily normalized to the peak values of the solid experimental curves merely to show relative shapes. It is probable that over half the recoils in I are really due to the 70° neutrino group. The same characteristic shift in the neutrino momentum, visible in curves I and II of Fig. 8, is also observed on other surfaces, but with poorer statistical accuracy.

(c) We now consider the implications of the data of curve IV where there are supposed to be no recoils which can enter the cone of sensitivity. Actually, there is evidence of a peak of recoils in the 3 to 4 thousand $H\rho$ region. This peak must be due to scattering through 20 or more degrees of those recoils which are formed by the electron and neutrino vectors selected by the particular geometry. The total intensity of this spurious peak is $\sim 6\times 10^{-5}$ recoils per beta-particle. One can obtain an independent estimate of the intensity of the spurious low momentum recoil ions from a different geometry, the data for which is not shown in Fig. 8.

This geometry is the same as that of case III, Fig. 2, which, for the surface of Fig. 8, shows low momentum spurious recoils of intensity 5×10^{-5} recoils per beta-particle. Thus, the spurious recoil intensity is about the same at both 180° and 135° with respect to the beta-particles. This suggests that there is a diffuse group of low energy recoils of approximately constant intensity spread over a wide angle with respect to the electrons. One infers that these recoils are so badly scattered that they have lost most of their original correlation with the electron and neutrino, and form a sort of background against which the true events must be distinguished. For the surfaces in Figs. 6 and 8 this background, presumably due to scattering, has about the same intensity, and makes necessary a minus 45 percent correction to the observed intensity of the recoil groups in case II of each figure.

One of the big advantages of using a beta-spectrometer for neutrino recoil studies is now apparent. It is possible to make quantitative estimates of the effects of scattering of the recoils by the surface. Scattering is probably the most serious source of error in this type of measurement, and is very difficult if not impossible to detect if the whole beta-spectrum is used. In fact, the previous results of the author[3] using the entire electron spectrum, in which the data favored a backward neutrino, were obtained from what is now recognized as a "thick" or at least partially overlaid source. This is demonstrated graphically in Fig. 9 where the recoil spectrum at ~180° with respect to the whole electron spectrum is plotted. Curve I is from Fig. 3 of the earlier paper on P 32, and curve II is for the same surface as shown in Fig. 4 of this paper. The difference in the intensity of the random background is due to the fact that the source used in II is much more intense than that used in I. For the more recent source, II, the smaller number of low momentum recoils is apparent. Whereas the earlier curve, I, agrees rather well with the $(1-v/c\cos\theta)$ neutrino, curve II agrees well with any angular correlation that is random or more forward than random. Thus, the unexplained abundance of low momentum recoils in this early data, which made the conclusions about the neutrino-electron angular correlation tentative, is now definitely assignable to surface scattering and losses.

We now consider the question about the recoil ions of different velocities escaping in the charged state. Since, as will shortly be shown, only about 3 to 6 percent of the recoil ions from a LiF substrate, and $1\frac{1}{2}$ to 3 percent from a MgF_2 substrate, escape charged, the problem naturally arises whether the fraction that escapes charged depends on the recoil velocity. The angular correlation between electron and neutrino is determined from the measured intensity of recoil ion groups whose average velocity ranges from 4×10^6 cm/sec. for 7000 $H\rho$ to 2×10^6 cm/sec. for 3500 $H\rho$. If the chance of escaping charged is appreciably velocity dependent, then the observed recoil intensities, even after scattering corrections are made, are still in error.

Unlike the scattering corrections described above, there seems to be no presently feasible way to make an experimental correction for the effect of the ion velocity upon its chance of escaping charged. Fortunately, a simple theoretical argument gives a definite answer to the neutralization problem, whereas theoretical analysis of surface scattering is hopelessly complicated.

The theoretical argument hinges on the fact that the departure of the recoil atom from the surface is, from the viewpoint of the electronic states, an adiabatic process. If the separation of the atom from the surface were infinitely slow, the electron density near the substrate and near the recoil atom depends only on the form of the Hamiltonian, and not on its rate of change. The electronic state existing during this adiabatic process will be called the initial state, m. If, however, the recoil atom moves with appreciable speed, the changing Hamiltonian can excite an electronic state, k, in which the relative electron density near the substrate and near the recoil atom may be different than for state m. The criterion for the validity of the adiabatic approximation is that the change in H during the Bohr period for the transition $m\rightarrow k$ is small in comparison with the energy difference between these two states. The magnitude $|a_k|$ of the probability amplitude for state k is given by,[14]

$$|a_k| \sim \left|\frac{(1/\omega_{km})(\partial H/\partial t)}{E_k-E_m}\right|, \qquad (2)$$

where $\omega_{km}=(E_k-E_m)/\hbar$. We now assume that H changes most rapidly during the time Δt that the atom, of velocity v, moves the first angstrom unit of its path as it departs from the substrate. We also assume that the change ΔH is the order of 5 ev, and that $E_k-E_m\simeq5$ ev. These energy values cannot be too far off since the first ionization potential of the sulfur recoil atom is 10.3 ev, and the upper limit of the recoil spectrum shows that the loss in energy of the recoil ion is less than 8 ev. For a recoil atom moving with a velocity of 4×10^6 cm/sec., $|a_k|\sim1/20$, and a_k^2, the probability of the system being in the excited state k, is 1/400. For the slower recoil atoms moving at 2×10^6 cm/sec., a_k^2 is 1/1600. Therefore, the chance that the motion of the recoil ion will excite a state different than the ground state is seen to be small, and the adiabatic approximation is justified. Only at considerably higher velocities would the value of

[14] L. I. Schiff, *Quantum Mechanics* (McGraw Hill Book Company, Inc., New York, 1949), p. 210.

$\partial H/\partial t$ be large enough to excite higher electronic states and thus affect the relative density of electrons at the substrate and at the recoil atom.

The recoil ions are all singly charged. This is known by measuring their velocity after being artificially accelerated with energies large compared to their initial energy. A sharp row of dots appears on the film at an e/m value of singly charged, mass 32.

Although all of the data discussed thus far are from P 32 surfaces on a LiF substrate, one good surface was formed on a MgF_2 substrate. The shapes of the recoil spectra from this source are in excellent agreement with the corresponding spectra from sources on a LiF substrate. Only in one respect is there any significant difference, and that is in the intensity of the recoil groups per beta-particle. The recoil groups from MgF_2 are only about $\frac{1}{2}$ as intense as are the corresponding groups from a LiF substrate.

According to L. G. Shultz,[15] in a layer which averages about 20 angstroms in thickness, MgF_2 shows by x-ray analysis, no structure, while the LiF of the same average thickness shows structure

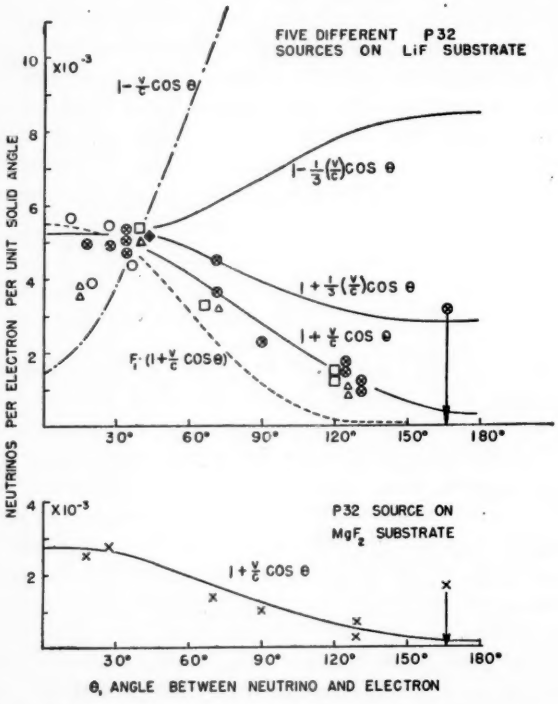
FIVE DIFFERENT P32 SOURCES ON LiF SUBSTRATE
NEUTRINOS PER ELECTRON PER UNIT SOLID ANGLE
X10⁻³
1−(v/c) cos θ
1−(1/3)(v/c) cos θ
1+(1/3)(v/c) cos θ
1+(v/c) cos θ
F₁(1+(v/c) cos θ)
30° 60° 90° 120° 150° 180°
X10⁻³
P32 SOURCE ON MgF₂ SUBSTRATE
1+(v/c) cos θ
30° 60° 90° 120° 150° 180°
θ, ANGLE BETWEEN NEUTRINO AND ELECTRON

FIG. 10. Experimental neutrino-electron angular correlation. The point at 165° with the downward pointing arrow means that the correlation function cannot lie above the value indicated, although it can lie anywhere below. Each point is the average probability over an interval in neutrino-electron angle ranging from ±15° to ±35°. $F_1(1+v/c\cos\theta)$ is the theoretical correlation for a first forbidden transition if the neutrino-electron interaction by itself would predict a correlation of $(1+v/c\cos\theta)$. Surface A (Fig. 4) = ○, Surface B (Fig. 6) = △, Surface C (Fig. 8) = ⊗.

[15] L. G. Shultz, private communication.

of the order of 50 angstroms. Blown glass films like those used as the foundation surfaces of these experiments have remarkably small vertical irregularities, of the order of 5 angstrom units in height, according to R. C. Williams.[16] Thus, it is probable that the MgF_2 substrate is smoother than the LiF on a 5 to 50 angstrom scale. That there is any improvement on the atomic (1–2 angstroms) scale is not likely.

The effects of scattering on the MgF_2 substrate can be described by the following numbers. The total intensity of the recoil group for the geometry of case IV, Fig. 2 is 7.2×10^{-5} recoils/beta-particle, or about half as intense as for the LiF case. The total intensity of spurious low momentum recoils measured with geometry III of Fig. 2 is 3.6×10^{-5}, again about half as intense as for LiF. No recoils are visible above the random background for geometry VI of Fig. 2, but if there were as many as $\sim3\times10^{-5}$ spurious recoils per beta-particle, a peak would have been visible. Thus, this second case sets an upper limit on the intensity of the spurious low momentum recoil ions which are scattered through $\sim30°$ at $\sim3\times10^{-5}$. The conclusion is that the scattering for a MgF_2 substrate is no worse, and possibly better than for LiF substrate.

The intensity of these low momentum, spurious recoils makes possible an estimate of the fraction of the P 32 atoms that are scattered. To make this estimate, we must make an assumption about the violence of the scattering. A fairly pessimistic estimate is that the scattering, when it occurs at all, removes practically all of the original angular correlation that the recoil had with the electron and the neutrino. For example, suppose that these recoils are scattered uniformily through 2π steradians. We further assume that the neutrino-electron angular correlation is $(1+v/c\cos\theta)$ which, as will shortly be demonstrated, agrees best with the observations. Now, to account for the observed intensities of (a) the unscattered recoils (i.e., the sharp high momentum recoil groups at electron-recoil angles of 180°), and (b) the diffuse, scattered recoils ($\sim6\times10^{-5}$ recoils in 38 square degrees/beta-particle, LiF substrate), a simple calculation shows that it is necessary that two things be simultaneously true: (1) 6 percent of all the recoils escape charged, and (2) 50 percent of the recoils are scattered and 50 percent are unscattered.

If, alternatively, we assume that the scattered recoils are spread over only one steradian, which is the region over which they have been observed, we then must conclude: (1) $3\frac{1}{2}$ percent escape charged, and (2) 15 percent are scattered and 85 percent are not scattered. Since one actually observes scattering through a solid angle of one

[16] Robley C. Williams, J. App. Phys. 20, 98 (1949).

TABLE I. Inferences about the form of the neutrino-electron interaction, based on the data of Fig. 10.

Type of transition	Form of neutrino-electron interaction		
	Most probable	Possible	Rejected
allowed	polar vector $(1+v/c\cos\theta)$	tensor $(1+\frac{1}{3}v/c\cos\theta)$	scalar and pseudo scalar $(1-v/c\cos\theta)$ axial vector $(1-\frac{1}{3}v/c\cos\theta)$
first forbidden	tensor $(1+\frac{1}{3}v/c\cos\theta)$ axial vector $(1-\frac{1}{3}v/c\cos\theta)$	polar vector $(1+v/c\cos\theta)$	scalar and pseudo scalar $(1-v/c\cos\theta)$

steradian, the figure of 15 percent scattered recoils is a minimum.

Similarly, for the MgF_2 substrate, $1\frac{3}{4}$ to 3 percent of the recoils escape charged, and 15 to 50 percent are scattered.

Presumably the P 32 atoms from which these scattered recoils come are hidden in cracks or behind surface obstructions so they have no direct path of escape toward the electron multiplier. If they were completely overlaid by inert material they probably would not escape at all. Since surfaces will usually be "rough" on an atomic scale there may be little hope of ever making a surface that is completely free from scattering, and therefore even "good" surfaces will have 15 to 50 percent of the escaping recoil ions badly scattered.

One might suppose that this amount of scattering would completely obscure the influence of the neutrino. Actually it is not as bad as it seems, since the extra randomness, in direction and time of flight, caused by the scattering makes these recoils to appear very much like the ordinary random background, making it higher than usual in the region of 5 to 15 microseconds. This extra background is identified, and corrected for, by studying recoil spectra for those cases where the neutrino by itself cannot cause true coincidences.

VI. THE EXPERIMENTAL DETERMINATION OF THE NEUTRINO-ELECTRON ANGULAR CORRELATION FUNCTION

The data from six different P 32 sources, all qualifying as "good" and corrected for scattering by the experimental method described in the previous section, are used to calculate the neutrino density per unit solid angle at various directions with respect to the electron. Figure 10 shows the experiment's points and also various angular correlation functions predicted by the different formulations of the Fermi theory.[7] v is the velocity of the electron. The function $F_1\cdot(1+v/c\cos\theta)$ is for a first forbidden transition when $(1+v/c\cos\theta)$ is the angular correlation for an allowed transition. Hamilton[7] shows that F_1 has the form, $(p/2q+q/2p+\cos\theta)$ where p is the electron momentum and q is the neutrino momentum. In the center region of the electron spectrum where $p\approx q$, F_1 has the approximate form $(1+\cos\theta)$. For the accuracy of observations made here, this approximation is good enough. For the most extreme case, $p=3q$ for the points at $\theta=35°$. Thus, $F_1(1+v/c\cos\theta)$ is very nearly $(1+\cos\theta)^2$.

The points at 165° with the vertical arrow beneath them are merely upper limits to the angular correlation function set by the failure to observe recoils from the backward neutrinos for the geometry of I, Fig. 2. If the angular correlation function is really as small near 180° as the other points imply, it is clear that recoils from the backward neutrinos are hopelessly obscured by the background.

The points in Fig. 10 represent an average over an appreciable neutrino electron angle. Those points at values of θ less than 50° are averages for all neutrinos from 0 to 2θ. These points are all taken with the beta-spectrometer at the 180° window (geometry of I–III, Fig. 2). The points at 70°, 90° and 120° are averages of neutrinos with angular spreads of ±15, ±20, and ±35 degrees, respectively.

An encouraging feature about the data in Fig. 10 is the smooth joining of the points with $\theta<50°$ to those with $\theta>50°$. This is significant since the first group of points is taken with an electron-recoil angle of ~180°, and the second group with an electron-recoil angle of ~135°. This involves a physical shift of the beta-spectrometer from the 180° window to the 135° window (Fig. 1), and also its rotation through 90°, making the electron deflection perpendicular to the plane of the figure.

The experimental points at 70°, 90°, and 120° in Fig. 10 have been reduced, before plotting, by empirically determined scattering corrections of 20 percent, 35 percent, and 45 percent.

Even after the above corrections are made, one is not quite sure that the ordinates of the points in Fig. 10 due to high momentum recoils ($\theta<50°$), and those due to the low momentum recoils ($\theta>90°$) have the correct relative values. The reason for this uncertainty lies in the fact that the lower energy recoils (15 to 25 ev) are more easily deflected by surface binding forces than are the high energy recoils (~75 ev). However, the LiF and MgF_2 substrates, which have rather different surface condition as shown by the different fractions of recoils escaping charged, both give the same relative intensities of high and low momentum recoils. This suggests, but does not conclusively prove, that the deflections due to surface binding forces are unimportant.

The result of these considerations is that the only estimate of error of the points in Fig. 10 is the fallible one given by the self-consistency of the different surfaces.

VII. CONCLUSIONS

The observation of distinct groups of recoil ions coincident with electron groups of much lower momentum seems explainable only on the hypothesis that a neutrino takes away the missing momentum in one package. Separate measurement of the missing energy shows it to have the correct magnitude required by the neutrino momentum. One cannot prove, without actually detecting the neutrino later, that it actually carries off the missing energy in the same direction as the missing momentum, but one is hard put to imagine a more likely place for the energy to be located.

Even without applying corrections for surface scattering of the recoils, a backward neutrino is convincingly rejected.

A summary of inferences about the form of the neutrino-electron interaction, based on the data of Fig. 10, is shown in Table I.

If the P 32 transition is second forbidden, the extreme forwardness of the neutrino with respect to the electron required by the angular momentum change, makes it unlikely that observations of the accuracy reported here could distinguish the original correlation due to the basic neutrino-electron interaction.

VIII. ACKNOWLEDGMENTS

Appreciation is extended to Mr. J. A. Cox and his staff at the Oak Ridge National Laboratory for their considerable effort in preparing the samples of highly purified P 32 without which these experiments would be impossible.

Mr. E. McNeil assisted in the operation of the equipment and in the plotting of the data from the film records. Helpful discussions with Professors A. Nordsieck and S. M. Dancoff are also appreciated.

This work was supported by the ONR and the United States AEC.

PHYSICAL REVIEW VOLUME 75, NUMBER 12 JUNE 15, 1949

Polarization Effects of Vector-Mesons

GREGOR WENTZEL
Institute for Nuclear Studies, University of Chicago, Chicago, Illinois
(Received February 24, 1949)

Adopting a vector-meson model for the π-meson we study (I) the polarization of π-mesons produced in nucleon-nucleon-collisions; (II) the angular distribution of μ-mesons resulting from π-μ-disintegrations, as depending on the polarization of the π-mesons; (III) the effect of electromagnetic fields on this polarization, in particular; (IV) the depolarization caused by the electric fields in matter. The theoretical results are encouraging for an experimental investigation.

INTRODUCTION

IN a previous paper[1] it was pointed out that if π-mesons have spin 1 it is very likely that polarized π-meson beams can be produced, and that various observable effects might result from this polarization. In order to substantiate these expectations, we want to present some theoretical estimates of certain polarization effects for vector-mesons. The choice of the vector-meson model may be justified by recalling that the π-mesons show a strong resemblance to the Yukawa mesons of the field theory of nuclear forces, indicating integer spin. In particular the fact that negative π-mesons captured by nuclei frequently produce large stars favors the assumption that the interaction of these mesons with nucleons is of the Yukawa type.[2] On the other hand, there is hardly any evidence so far to distinguish between spin 0 and spin 1. To decide this question, the most direct approach would be to prove or to disprove experimentally the existence of polarization effects.

I. MESON PRODUCTION

First we want to study the polarization of vector-mesons produced by nucleon-nucleon-collisions. Let nucleons of momentum $\mathbf{p}_0$ impinge on a target; the nucleons embedded in the target shall be described in terms of a given (nuclear) potential field, which seems a reasonable approximation. The initial state of the system is represented by a superposition of plane waves (Dirac eigenfunctions of free spin $\frac{1}{2}$ particles, normalized):

$$\phi_{p_0\lambda_0}(\mathbf{r},\sigma)=u_{p_0\lambda_0}(\mathbf{r},\sigma)+\sum_{p'\lambda'}u_{p'\lambda'}(\mathbf{r},\sigma)(p'\lambda'|R|p_0\lambda_0).$$

R, or rather $S=1+R$, is the scattering matrix corresponding to the target potential assumed. The suffix λ may be used to distinguish the charge states (proton, neutron) as well as the spin states of the nucleon. The transition to be studied, involving

[1] G. Wentzel, Helv. Phys. Acta 22 (1949), in press.
[2] J. A. Wheeler and J. Tiomno, Phys. Rev. 75, 1306 (1949).

meson emission, is characterized by the matrix element

$$\phi_{p\lambda}{}^{*}H\phi_{p_0\lambda_0}, \quad H=g_lH_l+g_tH_t,$$

where H_l and H_t stand for the well-known interaction operators of the conventional vector-meson theories. The suffixes l and t refer to the fact that for nucleons at rest, i.e., in the "static" approximation, H_l and H_t describe the nuclear coupling of longitudinal and transverse mesons, respectively.[3]

We use the following notations: $\hbar=c=1$; M=nucleon mass; $\boldsymbol{\alpha}$ and β=Dirac matrices of the nucleon, $\boldsymbol{\sigma}$ is its spin matrix ($\sigma_x=i\alpha_y\alpha_z$); τ=isotopic spin operator, describing transitions from the proton to the neutron state, or *vice versa*; m=meson mass, $\mathbf{k}$ and $\omega_k=(m^2+k^2)^{\frac{1}{2}}$ its momentum and energy; $\mathbf{a}_k{}^{*}$=meson creation operator (the x, y, z-components of this vector are the creation operators for mesons polarized parallel to the x, y, z axis, respectively). Then

$$H_l=\exp(-i\mathbf{k}\cdot\mathbf{r})\mathbf{a}_k{}^{*}\cdot\{\boldsymbol{\alpha}-\mathbf{k}/m+(\omega_k/m-1)((\boldsymbol{\alpha}\cdot\mathbf{k})\mathbf{k}/k^2)\}(m/\omega_k)^{\frac{1}{2}}\tau, \quad (1)$$

$$H_t=\exp(-i\mathbf{k}\cdot\mathbf{r})\mathbf{a}_k{}^{*}\cdot\{\boldsymbol{\alpha}+i[\mathbf{k}/\omega_k\times\boldsymbol{\sigma}]+(m/\omega_k-1)((\boldsymbol{\alpha}\cdot\mathbf{k})\mathbf{k}/k^2)\}\beta i(\omega_k/m)^{\frac{1}{2}}\tau. \quad (2)$$

These expressions are to be inserted in

$$\phi_{p\lambda}{}^{*}H\phi_{p_0\lambda_0}=\sum_{p'\lambda'}(p\lambda|R^{*}|p'\lambda')(p'\lambda'|H|p_0\lambda_0)+\sum_{p''\lambda''}(p\lambda|H|p''\lambda'')(p''\lambda''|R|p_0\lambda_0)+\sum_{p'\lambda'p''\lambda''}(p\lambda|R^{*}|p'\lambda')(p'\lambda'|H|p''\lambda'')\times(p''\lambda''|R|p_0\lambda_0). \quad (3)$$

Here, the term $(p\lambda|H|p_0\lambda_0)$ has been omitted because the simple meson emission without scattering is forbidden by energy-momentum conservation. In the Born approximation, where the last term in (3) (as being quadratic in R) is neglected, the unitarity of the S-matrix requires $R^{*}=-R$.[4]

We want to show that in the particular case that the energy of the impinging nucleon, $E_0=(M^2+p_0^2)^{\frac{1}{2}}$, is just slightly above the threshold energy $M+m$, the polarization of the emitted mesons can be large, even almost complete, according to the Born approximation. Indeed, if E_0 approaches $M+m$, the velocities of the meson and of the outgoing nucleon (k/ω_k and p/E) become very small compared with $v_0=p_0/E_0$. Therefore, in $(p'\lambda'|H|p_0\lambda_0)$, where $\mathbf{p}'=\mathbf{p}_0-\mathbf{k}$, $\mathbf{k}/m$ can be neglected against $\boldsymbol{\alpha}$, so that the curly brackets in (1) and (2) reduce to $\boldsymbol{\alpha}$. Indeed, as is easily derived by a Lorentz-transformation:

$$(p'\lambda'|\exp(-i\mathbf{k}\cdot\mathbf{r})\boldsymbol{\alpha}\tau|p_0\lambda_0)\approx(p_0\lambda'|\boldsymbol{\alpha}\tau|p_0\lambda_0)=\mathbf{v}_0(\lambda'|\tau|\lambda_0),$$

$$(p'\lambda'|\exp(-i\mathbf{k}\cdot\mathbf{r})\boldsymbol{\alpha}\beta i\tau|p_0\lambda_0)\approx(p_0\lambda'|\boldsymbol{\alpha}\beta i\tau|p_0\lambda_0)=\mathbf{v}_0\times(\lambda'|\boldsymbol{\sigma}\tau|\lambda_0),$$

where the matrices $(\lambda'|\cdots|\lambda_0)$ refer to a nucleon at rest. Hence, neglecting the other small terms:

$$(p'\lambda'|H_l|p_0\lambda_0)\approx(\mathbf{a}_k{}^{*}\cdot\mathbf{v}_0)(\lambda'|\tau|\lambda_0),$$

$$(p'\lambda'|H_t|p_0\lambda_0)\approx[\mathbf{a}_k{}^{*}\times\mathbf{v}_0]\cdot(\lambda'|\boldsymbol{\sigma}\tau|\lambda_0).$$

On the other hand, in the second term in (3), because $\mathbf{p}$ and $\mathbf{p}''=\mathbf{p}+\mathbf{k}$ are small momenta,

$$|(p\lambda|H|p''\lambda'')|\ll|(p'\lambda'|H|p_0\lambda_0)|$$

while

$$|(p''\lambda''|R|p_0\lambda_0)|\approx|(p\lambda|R^{*}|p'\lambda')|$$

since $\mathbf{p}_0$ and $\mathbf{p}''$ are almost the same momenta as $\mathbf{p}'$ and $\mathbf{p}$; moreover, $\mathbf{p}''-\mathbf{p}_0=\mathbf{p}-\mathbf{p}'=\mathbf{p}+\mathbf{k}-\mathbf{p}_0$. Therefore, in the Born approximation, the first term in (3) is by far the largest, and the matrix element reduces to

$$g_l(\mathbf{a}_k{}^{*}\cdot\mathbf{v}_0)\textstyle\sum_{\lambda'}(p\lambda|R^{*}|p'\lambda')(\lambda'|\tau|\lambda_0)+g_t[\mathbf{a}_k{}^{*}\times\mathbf{v}_0]\cdot\sum_{\lambda'}(p\lambda|R^{*}|p'\lambda')(\lambda'|\boldsymbol{\sigma}\tau|\lambda_0). \quad (4)$$

Now, consider the two simple cases of "pure" coupling:

(a) $g_l\neq0$ and $g_t=0$. The matrix element is proportional to $(\mathbf{a}_k{}^{*}\cdot\mathbf{v}_0)$, indicating that mesons with polarization perpendicular to $\mathbf{v}_0$ are not emitted.

(b) $g_l=0$, $g_t\neq0$. In this case the component of $\mathbf{a}_k{}^{*}$ parallel to $\mathbf{v}_0$ gives no contribution, i.e., polarization in this direction will not occur.

In these two cases we therefore expect complete polarization, parallel or perpendicular to the direction of the producing nucleon beam, respectively. In the case of a mixed interaction (both g_l and $g_t\neq0$) the degree of polarization will of course depend on the coupling ratio $|g_l/g_t|$. The polarization will also be somewhat lessened if the last term in (3) (quadratic in R) is appreciable. Finally it should be noted that we have disregarded intermediate states involving nucleon pair creation, but their contribution will be small since $Mv_0^2/2\approx m\ll M$.

Although the assumption of a fixed nuclear potential in the target certainly is an oversimplification, one may nevertheless conclude that mesons of spin 1, produced in nucleon-nucleon-collisions, can be expected to be polarized to a considerable extent, as long as the velocities of the meson and

[3] See G. Wentzel, *Quantentheorie der Wellenfelder* (Vienna 1943); English translation (New York 1949), §14.

[4] Generally: $S^{*}S=(1+R^{*})(1+R)=1$; $R^{*}+R+R^{*}R=0$.

the nucleon in the final state remain small as compared with the initial nucleon velocity v_0.

II. π-μ-DISINTEGRATION

Turning to the π-μ-decay, we consider the disintegration of a vector-meson into two particles of spin $\frac{1}{2}$, with rest-masses μ and ν, where ν may be zero. The theory of this process is well known from older β-theories since the μ-meson, except for its larger mass, behaves like an electron. The matrix element of the transition may be written

$$u_{\mu p\lambda}{}^{*}Ku_{\nu p_0\lambda_0}, \tag{5}$$

where u_ν refers to a negative energy anti-neutrino wave function. The operator K may again be a linear combination of two terms similar to $H_l(1)$ and $H_t(2)$. In the rest system of the π-meson ($\mathbf{k}=0$) they reduce to

$$K_l=(\mathbf{a}\cdot\boldsymbol{\alpha}), \tag{6}$$

$$K_t=(\mathbf{a}\cdot\boldsymbol{\alpha})\beta i. \tag{7}$$

If the polarization of the initial π-meson is linear, $\mathbf{a}$ may be replaced by the unit vector in the direction of polarization; otherwise appropriate averages of the squared matrix elements must be taken.

Assuming a pure coupling of the type (6) or (7), one finds by standard methods for the probability that a μ-meson is emitted into the solid angle $d\Omega$, in the rest system of the π-meson:

$$\text{const.}d\Omega\{1+(1-v_\mu{}^2)^{\frac{1}{2}}(1-v_\nu{}^2)^{\frac{1}{2}}\mp v_\mu v_\nu\cos 2\theta\}, \tag{8}$$

where the upper and lower signs refer to the coupling types (6) and (7), respectively; v_μ and v_ν are the velocities (magnitudes, in units c) of the μ-meson and the "neutrino," as determined by energy and momentum conservation; θ denotes the angle which the direction of emission ($\mathbf{v}_\mu$ or $\mathbf{v}_\nu$) forms with the polarization vector $\mathbf{a}$. If the rest mass of the neutrino vanishes ($v_\nu=1$), (8) becomes

$$\text{const.}d\Omega\{1\mp v_\mu\cos 2\theta\},\quad v_\mu=(m^2-\mu^2)/(m^2+\mu^2). \tag{9}$$

Adopting the experimental value $m/\mu=1.32$, we have $v_\mu=0.27$, and the anisotropy ratio would be $(1+v_\mu)/(1-v_\mu)=1.74$. Although this optimum ratio can only be reached in the case of a pure coupling (K_l or K_t) and linear polarization, the effect seems large enough to be detectable even under less favorable conditions.

III. EFFECTS OF ELECTROMAGNETIC FIELDS

In order to judge the observational possibilities, it is necessary to investigate how the polarization of the π-meson may be altered during its lifetime. Here, nuclear effects can be disregarded as unlikely, but electromagnetic forces, caused by external fields and by the matter traversed, may be important.

In this problem, since creation and annihilation processes are of no concern, it is convenient to describe the π-mesons by a non-quantitized wave field ψ_ν, of four-vector character. In a given electromagnetic field

$$F_{\nu\mu}=\partial A_\mu/\partial x_\nu-\partial A_\nu/\partial x_\mu$$

($x_4=it$) the ψ-wave propagates according to the field equations[5]

$$\partial_\mu(\partial_\mu\psi_\nu-\partial_\nu\psi_\mu)-i\gamma eF_{\nu\mu}\psi_\mu=m^2\psi_\nu \qquad [\partial_\mu=\partial/\partial x_\mu-ieA_\mu], \tag{10}$$

where γ is an arbitrary numerical factor accounting for an anomalous magnetic moment of the π-meson. The four components ψ_ν are not independent, for it follows from (10) that

$$m^2\partial_\nu\psi_\nu=i(1-\gamma)eF_{\nu\mu}\partial_\nu\psi_\mu-i\gamma e(\partial F_{\nu\mu}/\partial x_\nu)\psi_\mu. \tag{11}$$

Here, the identity

$$\partial_\nu\partial_\mu-\partial_\mu\partial_\nu=-ieF_{\nu\mu}$$

has been used which may also serve to rewrite (10) in the form

$$\partial_\mu{}^2\psi_\nu-\partial_\nu(\partial_\mu\psi_\mu)-i(1+\gamma)eF_{\nu\mu}\psi_\mu=m^2\psi_\nu, \tag{12}$$

where $(\partial_\mu\psi_\mu)$ can now be eliminated by inserting (11).

In order to study the change of polarization caused by the field F, let us express ψ_ν, according to

$$\psi_\nu=\varphi a_\nu,$$

by a scalar field φ obeying the field equation

$$\partial_\mu{}^2\varphi=m^2\varphi.$$

φ describes the motion of a spinless particle of mass m under the same electromagnetic forces. Assuming that a_ν is a slowly varying field (i.e., neglecting second derivatives) we obtain from (12)

$$2(\partial_\mu\varphi)\partial a_\nu/\partial x_\mu=i(1+\gamma)eF_{\nu\mu}\psi_\mu+\partial_\nu(\partial_\mu\psi_\mu).$$

In the last term we want to neglect the derivatives of the a_μ and of the $F_{\nu\mu}$, supposing that both fields vary slowly in regions with dimensions m^{-1}; then

$$2(\partial_\mu\varphi)\partial a_\nu/\partial x_\mu =ie\{(1+\gamma)\varphi F_{\nu\mu}+(1-\gamma)m^{-2}(\partial_\nu\partial_\lambda\varphi)F_{\lambda\mu}\}a_\mu. \tag{13}$$

For the discussion of a small space region, we can choose a frame of reference in which the particle is almost at rest and, gauging away the potentials A_μ in this region, we will have

$$\varphi\approx e^{-imt},\quad \partial_\mu\dot{\varphi}\approx-m\varphi\delta_{4\mu}. \tag{14}$$

[5] See H. C. Corben and J. Schwinger, Phys. Rev. **58**, 953 (1940); G. Wentzel, reference 3, §13.

Then from (13), $\nu=4$, and from (11):

$$a_4 \approx -i\gamma e m^{-2} F_{4k} a_k + m^{-1}\partial a_k/\partial x_k.$$

If we exclude very strong electric fields, we may neglect in (13) $F_{k4}a_4$ against $F_{kl}a_l$ ($k, l=1, 2, 3$). In this approximation, (13) reduces to

$$\partial \mathbf{a}/\partial t = -(1+\gamma)(e/2m)[\mathbf{H}\times\mathbf{a}], \qquad (15)$$

indicating that the polarization vector $\mathbf{a}=(a_1, a_2, a_3)$ precesses around the direction of the magnetic field $\mathbf{H}$ with the angular velocity $(1+\gamma)e/2m$, corresponding to a Landé factor $g=1+\gamma$. In the special case of a circular polarization (e.g., $a_2=ia_1$, $a_3=0$), this provides for the well-known precession of the spin vector $i\mathbf{a}\times\mathbf{a}^*$; indeed, from (15), it follows that

$$\partial[\mathbf{a}\times\mathbf{a}^*]/\partial t = -(1+\gamma)(e/2m)[\mathbf{H}\times[\mathbf{a}\times\mathbf{a}^*]].$$

But (15) holds also if the polarization is, for instance, a linear one ($\mathbf{a}\times\mathbf{a}^*=0$).

Of course, the above equations can also be interpreted in terms of particles traveling on certain trajectories and carrying along a vector a_ν which may be considered as a function of the proper time s of the particle. In (13), then, $(\partial_\mu\varphi)\partial a_\nu/\partial x_\mu$ goes over into $(im\varphi)da_\nu/ds$.

The first obvious application of Eq. (13) or (15) will be to π-mesons traveling in a magnetic field (as, for instance, mesons produced in a target located in the field of a cyclotron). The polarization vector which initially, according to (4), may be parallel or perpendicular to the primary nucleon beam, will change its direction along the trajectory of the meson, the total angle of precession being proportional to the time integral of the magnetic field and to the Landé factor $g=(1+\gamma)$. If π-μ-disintegrations can be observed at various points of the trajectory, the anisotropic distribution of the μ-meson velocities should reveal this precession, and the Landé factor should be measurable.

If the disintegration is observed after the π-meson has passed through dense matter, it will be important to know how the polarization is affected by the electric fields in the material. For fast particles ($v>1/137$) this question can be settled by applying the Born approximation.[6] However, we are interested in low velocities also because positive π-mesons may spend the major part of their lifetime ($\sim 10^{-8}$ sec.) at thermal velocities before they disintegrate. We content ourselves with an upper limit estimate sufficient to show that the depolarization of positive mesons is weak at non-relativistic velocities.

[6] O. Laporte, Phys. Rev. **54**, 905 (1938); see also G. Wentzel, reference 3, §13.

IV. DEPOLARIZATION

Consider a π^+-meson as a classical particle passing through the electric field $\mathbf{E}$ of an atom which may be assumed to be a central field. We choose a rectangular coordinate system with the z axis perpendicular to the plane of motion and the x axis parallel to $\mathbf{v}_2-\mathbf{v}_1$, $\mathbf{v}_1$ and $\mathbf{v}_2$ denoting the initial and final velocities of the particle. The polarization vector is, in the rest system, subject to an effective magnetic field $\mathbf{E}\times\mathbf{v}$ which has the z direction; as to its magnitude, a simple geometrical argument shows that for a particle of positive charge e (repulsive force $e\mathbf{E}$):

$$|\mathbf{E}\times\mathbf{v}| \leqq E_x v \leqq E_x v_1. \qquad (16)$$

The polarization vector $\mathbf{a}$ precesses around the z axis, and its total angle of deflection is

$$\delta = (ge/2m)(\sin\alpha)\int dt\,|\mathbf{E}\times\mathbf{v}|$$

(α=angle of $\mathbf{a}$ with the z axis). Inserting (16), and noting that

$$e\int dt E_x = m(\mathbf{v}_2-\mathbf{v}_1)_x = m\,|\mathbf{v}_2-\mathbf{v}_1|,$$

we obtain

$$\delta \leqq (g/2)(\sin\alpha)v_1\,|\mathbf{v}_2-\mathbf{v}_1|,$$

or introducing the scattering angle ϑ by

$$|\mathbf{v}_2-\mathbf{v}_1| = 2v_1\sin\vartheta/2:$$

$$\delta \leqq g(\sin\alpha)v_1^2\sin\vartheta/2. \qquad (17)$$

On account of the random directional distribution, the probable deflection Δ of the polarization vector after many atomic collisions is given by

$$\Delta^2 = \sum\delta^2.$$

In a time interval dt, Δ^2 changes by

$$d(\Delta^2) = Nvdt\int_0^{2\pi} d\alpha\int_0^\infty d\rho\rho\delta^2, \qquad (18)$$

where N denotes the number of atoms per unit volume. Inserting (17), the scattering angle ϑ is to be regarded as a function of the impact parameter ρ. If v_1 is still large enough that the particle can penetrate deeply into the atoms, we may use the Rutherford formula

$$\tan\vartheta/2 = \rho_1/\rho, \quad \rho_1 = Ze^2/mv_1^2,$$

where Z=effective nuclear charge, and integrate in

(18) up to the atomic radius R:

$$d(\Delta^2) < Nvdt \cdot g^2(\pi/2)(Ze^2/m)^2 \log(1+R^2/\rho_1^2). \quad (19)^7$$

While traversing the matter, the meson is slowed down according to the well-known law

$$-dv = Nvdt \cdot (4\pi Ze^4/m_e m v^3) \log q, \quad (20)$$

where m_e denotes the electronic mass (m always means the mass of the π-meson); $\log q \sim 1$ for meson velocities substantially larger than the velocity of valence electrons. In this velocity range

$$d(\Delta^2) \lesssim |dv| v^3 Z m_e/m. \quad (21)$$

Integrated over a time interval during which v decreases from an initial value v_i to a lower value:

$$\Delta^2 \lesssim v_i^4 Z m_e/m. \quad (22)$$

This upper limit is certainly very small for non-relativistic initial velocities ($v_i \ll 1$).

For the lowest velocities where (20) no longer holds, it is sufficient to remember that according to (17)

$$\delta^2 \lesssim v^4$$

for positive mesons. Owing to this very small value, Δ^2 can hardly grow to a value larger than (22), even during a lifetime as large as 10^{-8} sec., spent in dense matter.

This estimate seems to prove that for positive vector-mesons of at most some Mev energy, no appreciable depolarization is to be expected.

Since, according to Section I, slow π-mesons are most likely to be strongly polarized, one may hope that the photographic registration of π-μ-disintegrations will reveal the polarization effects as discussed in Section II. In this connection it should be noted that if the meson at the end of its range in the photographic emulsion is still subject to a magnetic field, the polarization vector will go on precessing until the disintegration occurs, and since the individual lifetime may be shorter or longer, with an uncertainty of about 10^{-8} sec., the polarization effect will be blurred out in a too strong magnetic field. In order to keep the polarization well defined, the magnetic field strength should be kept below about 100 gauss, in the region of observation.

Note added in proof.—As Dr. I. I. Rabi pointed out, there is the possibility that the positive meson, before decaying, captures an electron from the surrounding matter such that the electron is bound in a hydrogen-like orbit; then the electron's magnetic field might cause a considerable depolarization of the meson, leading to a weaker anisotropy in the angular distribution of the μ-mesons. For instance, if the electron is bound in an s-state (external magnetic fields being absent or weak) the distribution will be, instead of (9),

$$\text{const. } d\Omega\{1 \mp v_\mu[(6\cos^2\theta - 5)/9 + (1+\epsilon^2\tau^2)^{-1}4(3\cos^2\theta - 1)/9]\},$$

where ϵ is the hyperfine structure splitting ($\Delta E/\hbar$) of the s level due to the magnetic moment of the π-meson, and τ the mean lifetime of the hydrogen-like state. For the ground state: $\epsilon \sim 10^{10}$ sec.$^{-1}$ (with $g \sim 1$), so that with a lifetime $\tau \sim 10^{-8}$ sec. the second term in the square bracket would be negligible, and the anisotropy would be reduced to about one-third, supposing that the capture process is a frequent occurrence. But actually its probability may be far below unity, and also the lifetime τ may be considerably shortened by chemical forces acting on the "pseudohydrogen atom" and tending to restore a diamagnetic state of the electrons. In either case, the larger anisotropy (9) is to be expected.

[7] As to the order of magnitude, (19) agrees with the cruder estimate (suggested to me by Dr. E. Teller):

$$\delta \sim (e/m)(Zev/\rho^2)(\rho/v),$$

where the last factor (ρ/v) is the collision time; hence

$$\int d\rho\rho\delta^2 \sim (Ze^2/m)^2 \int d\rho/\rho \sim (Ze^2/m)^2.$$

This, however, is an overestimate in the case of slow positive particles ($mv^2 < Ze^2/R$, see below). On the other hand, for higher velocities ($v > Z/137$), the classical particle picture is no longer reliable, but the Born approximation confirms (19) as an upper limit estimate provided that $v \ll 1$. The factor g^2 in (19) appears to be replaced by $\gamma^2 = (g-1)^2$, indicating that for $\gamma = 0$, and $Z/137 < v \ll 1$, the depolarization is even weaker than one would expect from (19).

Nitrogen 12*

LUIS W. ALVAREZ
Radiation Laboratory, University of California, Berkeley, California
(Received February 14, 1949)

N^{12} is shown to have a half-life of 12.5±1 milliseconds, and a positron upper limit of 16.6±0.2 Mev. It is produced by the reaction $C^{12}(p,n)N^{13}$, and has a threshold proton energy of 20.0 Mev. This indicates that N^{12} is within about 200 kev of being unstable against proton emission. The mass of N^{12} is 12.0228±0.00015, and the beta-transition is allowed.

1. INTRODUCTION

A RADIOACTIVE substance with a very short half-life was observed when high energy protons from a linear accelerator were incident on carbon. This activity has been studied in some detail and has been shown to be due to N^{12}. It is a rather interesting substance, in that it has the shortest lifetime of any known beta-emitter, and its positrons are more than three times as energetic as those from any other previously known radioactive isotope. The mass of N^{12} has been investigated theoretically by Barkas,[1] who concluded that its stability against proton emission is borderline. N^{12} is the third identified member of the new radioactive series with $A=2(Z-1)$. C^{10} and O^{14} have been observed by Sherr, Muether, and White.[2]

All of the radioactive measurements on N^{12} were made with the carbon target in its bombarded position. The normal time between beam pulses on the linear accelerator is 67 milliseconds, which is 5.3 half-lives. Therefore, the activity decays almost to background between pulses, and fifteen new samples of N^{12} are made each second. After the first experiment with a single counter, all later work was done with a pair of trays of Geiger counters, which were connected in coincidence. The counting circuit was sensitive for only 1/120 second, almost immediately after the proton beam was turned off. This "gating" of the circuit helped to reduce the background, and, in addition, a 1 mm thick piece of copper was placed between the counter trays. This absorber eliminated γ-ray coincidences from the C^{11}, which is also formed in the carbon target by high energy protons.[3] The background was always negligible, and, in fact, was largely due to cosmic rays. N^{12} samples with an activity of the order of one millicurie may be produced with the full beam current (1μ amp. peak; 4×10^{-9} amp. average), but all measurements were done at greatly reduced beam intensities, to avoid saturation of the counters.

2. HALF-LIFE MEASUREMENT

The half-life was measured with the aid of the gate circuit previously described. The repetition rate of the linear accelerator was cut from 15 cycles per second to 7.5 cycles per second, in order that the decay curve could be carried out to greater times. The width of the gate, or sensitive time of the counting circuit, was kept fixed at 0.008 second, and its delay time after the end of the proton pulse was varied by steps of 1/60 second, as measured on an oscilloscope. The number of positrons recorded through the gate for a given number of incident protons was measured as a function of the gate delay. The integration of the proton current was carried out by counting the C^{11} activity induced in a 0.001″ polystyrene foil, through which the protons passed before striking the carbon target.

The half-life was measured several times in a period of several weeks, with different experimental arrangements, and the various values agreed within experimental error. Great care had to be taken to avoid overloading of the counters since, although the average counting rates appear to be

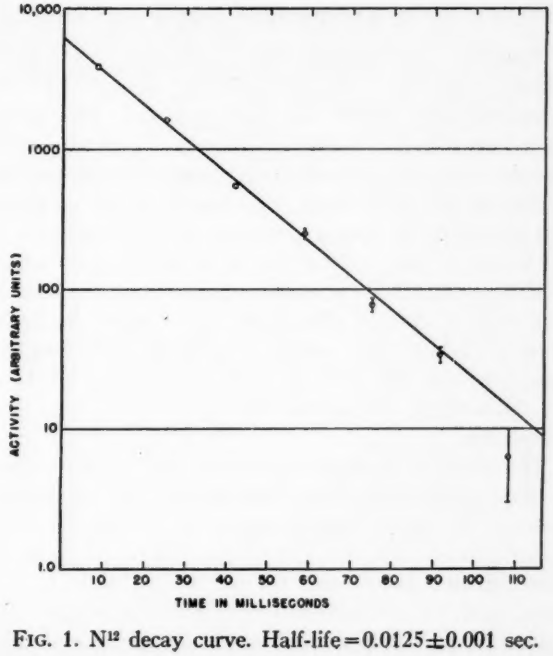

FIG. 1. N^{12} decay curve. Half-life = 0.0125±0.001 sec.

* This work was done under the auspices of the AEC.

[1] W. H. Barkas, Phys. Rev. **55**, 691 (1939).

[2] R. Sherr, H. R. Muether, and M. G. White, Phys. Rev. **74**, 1239A (1948) and Phys. Rev. **75**, 282 (1949).

[3] W. W. Chupp and E. M. McMillan, Phys. Rev. **72**, 873 (1947); E. M. McMillan and R. D. Miller, Phys. Rev. **73**, 80 (1948); W. K. H. Panofsky and R. Phillips, Phys. Rev. **74**, 1732 (1948).

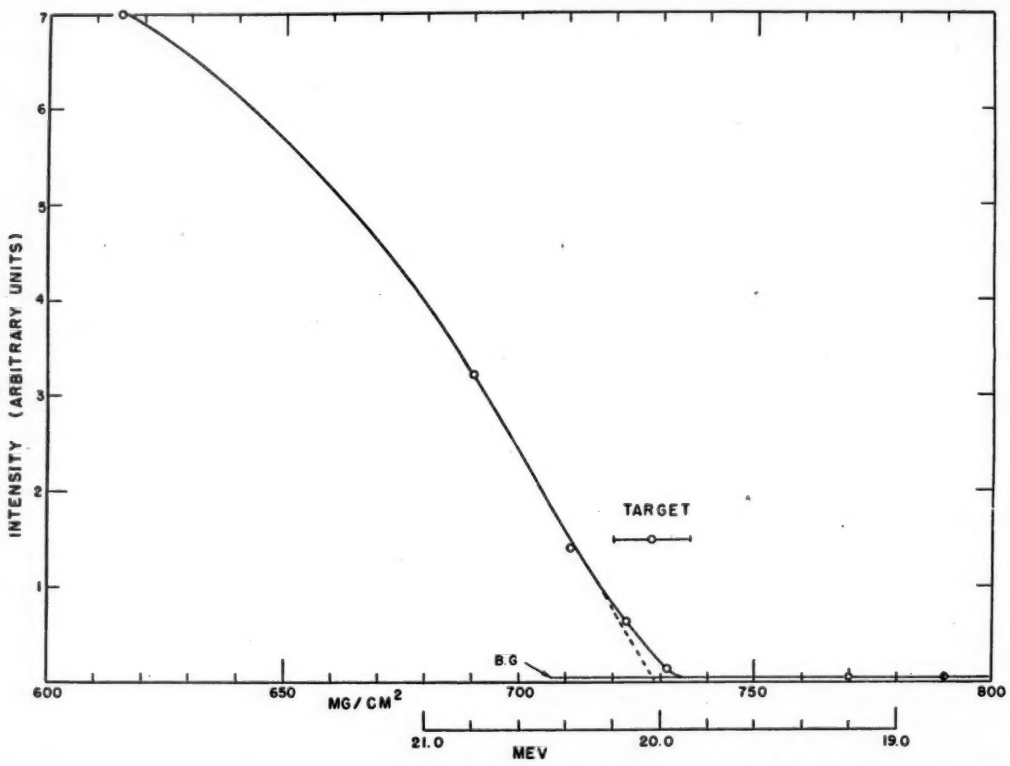

FIG. 2. N^{12} thin target excitation curve. Target 17 mg/cm² polystyrene. Initial proton energy = 32 Mev. $C^{13}(p,n)N^{12}$. $N^{12} \rightarrow C^{12} + e^+$.

relatively low, the instantaneous rates are very high because of the intermittant character of the operations. Figure 1 shows a typical decay curve over a factor of approximately 1000 in intensity, which yields a value of 0.0125 ± 0.001 second for the half-life.

3. EXCITATION CURVE

Panofsky and Phillips have determined the excitation curve for the production of C^{11} by the bombardment of C^{12} by fast protons. The theoretical threshold of the $C^{12}(p,pn)C^{11}$ reaction may be calculated from the known masses of the reacting nuclei, and is 20.2 Mev. The fact that C^{11} activity was observed at lower energies was interpreted as evidence for the $C^{12}(p,d)C^{11}$ reaction. It may easily be shown that if N^{12} is stable against proton emission to form C^{11}, its p,n threshold on C^{12} must be lower than 20.2 Mev, the (p,pn) threshold. The binding energy of the last proton in N^{12} is equal to 12/13 of the difference between the p,pn, and the p,n thresholds.

The first excitation curves for the 12 millisecond period appeared to have thresholds in the neighborhood of 21 Mev. Thick targets were used in these experiments, however, and the extrapolations to zero activity were more difficult than if thin targets were used. Since the reasonable identification of the activity as N^{12} depended critically on the precise value of the proton energy threshold, a number of thin target excitation curves were measured. The data for Fig. 2 were taken with a target of polystyrene 0.005″ thick. The aluminum absorbers were weighed, and the tabulated values of the absorber mass per unit area include the aluminum window of the accelerator, the air path between the window and target, and one-half the thickness of the target. The range energy curve is from the work of Smith.[4] There are a number of reasons to believe that it gives the proper energies in the 20–30 Mev region. Immediately after several of the determinations of the proton threshold, calibrated nuclear emulsion plates were exposed to the protons from the linear accelerator. The protons were found to have a range corresponding to 32.0 ± 0.1 Mev, which is the energy one calculates from the dimensions and frequency of the accelerator. Dr. Panofsky has measured the lengths of scattered proton tracks in the same plates, where the original protons had the full accelerator energy and were scattered from protons at known angles. This is an excellent way of extending the range-energy curve for nuclear emulsion plates from the lower energy region, where it is known accurately, to the range of 32 Mev. One makes use of the relationship,

$$E_\theta = E_0 \cos^2\theta.$$

[4] J. H. Smith, Phys. Rev. 71, 32 (1947).

In addition to these checks of the range-energy curve, one may work differentially from the measured threshold of the $C^{12}(p,d)C^{11}$ reaction, correcting for the Gamow factor of the escaping deuteron. All methods of determining the energy of a proton in the 20 Mev range give results which check to better than ± 100 kev.

The threshold of the $C^{12}(p,n)N^{12}$ reaction is at 20.0 Mev. If one assumes that the excitation curve near the threshold for an infinitely thin target is a straight line meeting the horizontal axis at a finite angle, then the curve for a target of finite thickness should extrapolate to the axis at "the center of the target." It should be curved over a range of absorber thickness equal to that of the target. Within the accuracy of the data in Fig. 2, that is just the appearance of the excitation curve. The effects of straggling, and of the initial energy inhomogeneity of the 32 Mev beam do not show in the curve. There is at present no method available in our laboratory sensitive enough to detect the energy spread in the 32 Mev beam. From this work, and that of Panofsky and Phillips, it is known that the energy spread is less than 100 kev, or less than 3×10^{-3}.

The excitation curve was found to level off at a value of 10 arbitrary units for energies above about 24 Mev. No physical significance should be attached to this observation, because recoil of the N^{12} from the thin target foil would be expected in this range. With the stacked foil technique, this effect is not important, but in this case, no compensating factors offset the recoil effect. In one run with a much thicker target, the excitation curve was observed to rise continuously from 20 to 32 Mev as it should if the recoil hypothesis is correct.

4. ABSORPTION DATA

The absorption of the N^{12} positrons is shown in Fig. 3. The intensity was reduced by a factor of about 10^3, and the end point is of the so-called inspection type, which is generally more reliable than end points based on comparisons with known spectra. Any comparison with other positron emitters would involve rather large extrapolations, and the only convenient high energy negative electron emitter which may be produced by the accelerator is Li^8, from the $Be^9(p,2p)$ reaction. Since this isotope has a complex spectrum, it would not be suitable for use with the Feather comparison method. The upper limit is calculated from Feather's formula, as corrected by Glendenin and Coryell,[5]

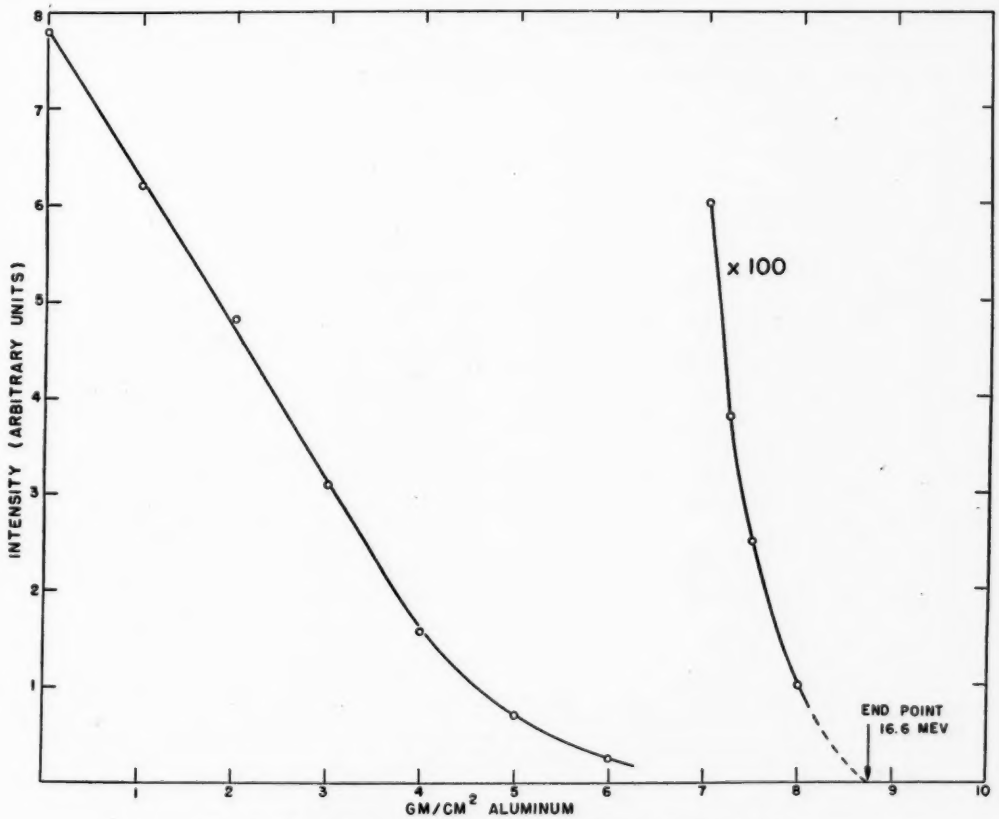

FIG. 3. Absorption of N^{12} positrons (background subtracted).

[5] L. E. Glendenin and C. D. Coryell, MDDC 19 (1946).

and has the value 16.6 Mev. This is precisely the upper limit one calculates from the atomic masses, assuming a p,n threshold of 20.0 Mev.

To show that the electronic component consisted of positrons, a search was made for annihilation radiation. A γ-ray was found which decayed with a period of approximately 10^{-2} second. That this γ-ray was not of nuclear origin was shown by surrounding a bare source of N^{12} with a heavy copper cylinder. Lead diaphragms were placed so that the counters could "see" only the region near the N^{12} source. When the cylinder was placed around the N^{12} sample, the γ-ray counting rate increased, which showed that formerly, the positrons were annihilated at more distant points, from which the annihilation quanta could not reach the counters.

5. IDENTIFICATION OF THE ACTIVITY

In the early stages of the work, before accurate half-life and threshold values were available, it was thought that the activity might be the 0.022 second period of B^{12}, formed in the reaction $C^{13}(p,2p)B^{12}$. Bombardment of samples enriched in C^{13} showed that the activity definitely arose from the C^{12}.**

The identification of the activity comes from the following energetic evidence:

(a) The masses of N^{12}, as computed from the proton threshold and the positron endpoint are the same to within the error of the measurements, or about ± 0.0002 mass unit.

(b) It may be shown by a series of detailed calculations that on energetic ground, *all* isotopes with Z less than 8, and A less than 14, may be ruled out as being responsible for the 0.0125 second activity. From the positron energy, one may compute the mass of any supposed responsible isotope, which decays into a known isotope. Then, using the observed proton threshold, the mass of the excited N^{13} atom is calculated. It has been shown that the only two nuclei which come within five Mev of satisfying the energetic requirements are Li^4 and B^8, which are each off by about 4 Mev. (These nuclei would be formed in $(p,\alpha n)$ or $(p,2\alpha n)$ reactions.) In all cases, there is not enough energy available to make the reactions go. It is not just that the numbers do not agree perfectly as they do in the N^{12} calculation; the reactions are energetically forbidden. For all other isotopes, which lie further from the stability curve, it is possible to show that they are even more easily disposed of on energetic grounds.

** I am indebted to Dr. J. W. Otvos of the Shell Development Company for the loan of the enriched carbon samples.

6. DISCUSSION

The mass of N^{12} is 12.0228 ± 0.00015 M.U., based on $C^{12} = 12.0038$. The beta-transition from N^{12} to C^{12} is allowed. As calculated from the formula given by Konopinski,[6] the ft. value for the transition is 1.6×10^4, as compared with 1.4×10^4 for B^{12}, using the latest values for the upper limit of B^{12}.[7]

According to Professor E. Teller,[8] the existence of N^{12} may be of some importance in theories of the evolution of the light elements.

N^{12} may be the most nearly ideal radioactive isotope for testing the neutrino theory. The maximum recoil energy of a C^{12} nucleus from the reaction of a neutrino is 13,200 electron volts. Such recoils should have a range of about 2 cm in a cloud chamber operated with pure water vapor at a few degrees centigrade. The N^{12} could be deposited on a charged wire in an atmosphere of some hydrocarbon and then rapidly transported through a small hole into the low pressure cloud chamber. The direction of the recoil would be evident, and its energy could be measured by drop counting techniques. The drop counting technique could be calibrated by O^{16} recoils from neutrons incident on the chamber. The direction and energy of the positron could be photographed in an ordinary cloud chamber plus magnetic field, placed adjacent to the small, low pressure recoil chamber. If the experiment could be done, one would have the direction and energy of recoil and electron, and could compute from momentum consideration, the direction and energy of the neutrino. This computed energy could then be compared with the energy calculated from the positron energy and the upper limit. If the two values always agreed, one would gain still more confidence in the neutrino theory.

ACKNOWLEDGMENTS

I am indebted to Mr. Donald Cone for constructing the electronic gate circuit, to Dr. Hugh Bradner for help with some of the measurements, and to the linear accelerator crew for the bombardments.

[6] E. J. Konopinski, Rev. Mod. Phys. **15**, 209 (1943).
[7] W. F. Harnyak, C. B. Dougherty, and T. Lauritsen, Phys. Rev. **74**, 1727 (1948).
[8] Private communication.

Angular Distribution of 14-Mev Neutrons Scattered by Protons*

H. H. BARSCHALL AND R. F. TASCHEK
University of California, Los Alamos Scientific Laboratory, Los Alamos, New Mexico
(Received February 15, 1949)

By bombarding a tritium target with 200-kev deuterons, 14-Mev neutrons were produced. Proton recoils originating in a thin polythene radiator could pass through three proportional counters between which coincidences were observed. By rotating the foil and the counter about the center of the foil the angular distribution of the recoiling protons could be measured. Protons corresponding to neutrons scattered through 90°, 120°, 150°, and 180° in the CM system were observed. Within the statistical accuracy of about 6 percent at each angle the angular distribution of the scattered neutrons appeared isotropic.

INTRODUCTION

An important source of information regarding the nature of the interaction between neutrons and protons is the measurement of the angular distribution of fast neutrons scattered by protons.[1] All recent experiments on neutrons of less than 10-Mev energy are consistent with the assumption of spherically symmetric scattering predicted by most theories.[2] Appreciable deviations from spherical symmetry would be expected on the basis of several of the suggested types of neutron-proton forces for neutrons above 10-Mev energy, and a choice between the various proposed forces would be facilitated by an accurate knowledge of the angular distribution.

Previous measurements[3–5] of the angular distribution of neutrons of energies between 10 and 15 Mev have given results which were not in good agreement. The most recently published results are those of Laughlin and Kruger.[6] These authors observed the scattering of neutrons between 12 and 13 Mev in a cloud chamber and found that the ratio of the differential cross sections for neutron scattering in the backward direction to that for scattering in a direction perpendicular to the incident neutrons was equal to or slightly greater than unity.

The principal difficulty in measuring the scattering of fast neutrons by protons has been that an intense source of monoergic fast neutrons has not been available. The deuterium-tritium reaction, the use of which has recently become possible, furnishes a very convenient source of neutrons for these experiments. It appeared worth while, therefore, to obtain additional data on the angular distribution of the neutron-proton scattering using this source.

APPARATUS

Neutrons were obtained from the reaction

$$T+D\rightarrow He^4+n+17.3 \text{ Mev}. \qquad (1)$$

Deuterium ions were accelerated by a Cockcroft-Walton set to an energy of 200 kev. The ion beam was magnetically analyzed, and the monatomic ions were used to bombard a thick target consisting of a zirconium foil in which tritium had been absorbed.[7] The neutrons leaving the target at right angles to the incident deuterons were used in the present experiments; they have an energy of 14 Mev with a spread of about 120 kev. In order to monitor the neutron intensity, α-particles from reaction (1) were counted in a proportional counter. All neutron counting rates will be referred to a fixed number of α-particle counts. Integration of the deuteron current incident on the target could not be used to measure the neutron intensity since the distribution

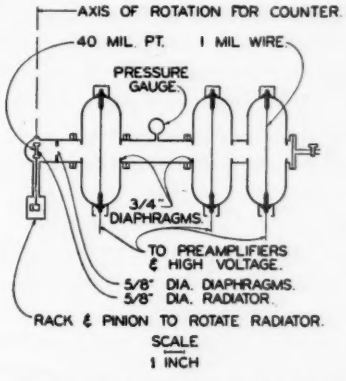

FIG. 1. Triple coincidence counter for detection of recoiling protons.

* This paper is based on work performed at Los Alamos Scientific Laboratory of the University of California under government contract W-7405-Eng-36.

[1] W. Pauli, *Meson Theory of Nuclear Forces* (Interscience Publishers, Inc., New York, 1946), p. 55.

[2] A summary and discussion of the experimental results may be found in L. Rosenfeld, *Nuclear Forces* (Interscience Publishers, Inc., New York, 1948), Vol. I, p. 123.

[3] E. Amaldi, D. Bocciarelli, B. Ferretti, and G. C. Trabacchi, Naturwiss. **30**, 582 (1942).

[4] F. C. Champion and C. F. Powell, Proc. Roy. Soc. **A183**, 64 (1944).

[5] C. F. Powell and G. P. S. Occhialini, *Fundamental Particles* (The Physical Society, London, 1947), p. 150.

[6] J. S. Laughlin and P. G. Kruger, Phys. Rev. **73**, 197 (1948).

[7] F. M. Penning and J. H. A. Moubis, Physica **4**, 1190 (1937). Graves, Rodriguez, Goldblatt, and Meyer, private communication.

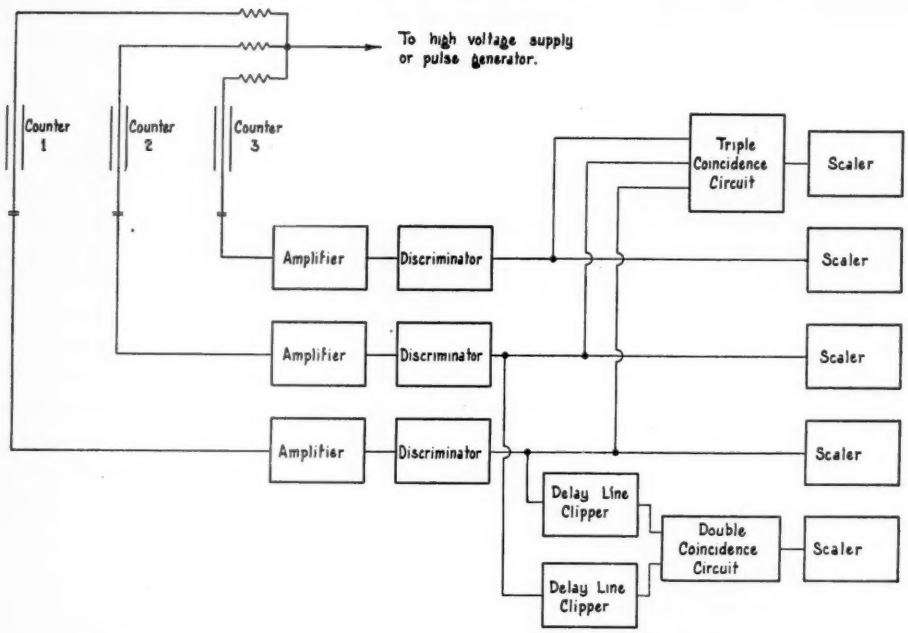

FIG. 2. Block diagram of circuits used to detect protons.

of tritium in the target became quite non-uniform after some bombardment.

The interaction of the neutrons with protons was studied by observing proton recoils originating in a foil of polythene. This foil was located at a distance of 18 cm from the target, it had a thickness of 9.8 mg/cm² and a diameter of $\frac{5}{8}$ in., and was backed by a thick layer of platinum. The radiator subtended an angle of 5° at the neutron source.

The recoiling protons were detected in the counter system shown in Fig. 1. They were collimated first by a platinum diaphragm, $\frac{5}{8}''$ in diameter, and then by five apertures, $\frac{3}{4}''$ in diameter, so that only those protons which left the radiator within an angle of approximately 2° from the normal to the radiator could pass through the counting system.

To detect the protons three proportional counters were used, each consisting of a brass cylinder, 4.8 cm in diameter, with a 1-mil tungsten central wire. The counters were filled with a mixture of tank argon and carbon dioxide. Under the conditions of the present experiment a recoiling proton loses less energy in one counter than the maximum recoil energy of a nucleus of the filling gas. Therefore, protons could be identified only by observing coincidences between counters. In addition to the coincidences produced by recoiling protons originating in the radiator, coincidence counts may also be due to accidental coincidences of the many gas recoils, to disintegrations taking place in the walls or the gas of the counter, or to the recoil of light nuclei which might be present in the various parts of the counter. To determine this background the polythene foil could be rotated through 180° so as to expose to the counter the platinum backing, rather than the hydrogenous foil, by the rack and pinion mechanism shown in Fig. 1.

For calibration purposes, each counter was provided with a side tube which contained a plutonium α-particle source. By means of a magnet this source could be moved to the edge of the active volume of the counter or sufficiently far away from it so that the α-particles would not enter the counter.

The electronic circuits used with the counter are shown schematically in Fig. 2. High voltage for the three proportional counters was obtained from a common battery pack. The pulses from each counter were amplified by means of a Los Alamos type 100 amplifier, which has a rise time of 0.5 μsec. and was used with a clipping time of 1.5 μsec. The output of each amplifier was fed into a discriminator which produced square pulses of fixed height. These were counted directly by means of scales-of-64 and recorders, and at the same time they were fed into coincidence circuits. Two circuits were used, a double coincidence circuit which recorded coincidences between the two counters closest to the radiator, and a triple coincidence circuit which detected coincidences between all three counters. In view of the fact that the counting rates recorded from the individual counters were about a thousand times those produced by the protons, a good resolving power was required for the double coincidences. For this purpose the square pulses from the discriminator were clipped by delay lines after 0.5 μsec. The over-all resolving power of the counting system for double coincidences was measured to be 0.8 μsec. by observing accidental coincidences produced by the Pu α-particle sources in the counters. The pulses fed into the triple coincidence circuit

were clipped by an RC circuit with a time constant of 1 μsec.; the over-all resolving power of the triple coincidence counting system was measured to be 1.6 μsec. For the proper operation of the coincidence circuits it is essential that the pulses from the amplifier all have approximately the same rise time, since the height of the pulses is not the same in the counters because of the variation of ionization density with range. It was found that if the counters were filled with argon the variation of rise time caused difficulties. When, however, CO_2 was added the drift velocity of the electrons was sufficiently great to make the rise time of the amplifier determine the rise time of the output pulses.

PROCEDURE

To determine the angular distribution of the recoiling protons the whole counter including the radiator could be rotated about an axis in the plane of the foil through its center. In this way the effect of neutrons scattered through different angles could be studied without change in the geometry of the detector. Measurements were carried out for protons recoiling at 0°, 15°, 30°, and 45° with respect to the incident neutrons.

As the counter is rotated the range and ionization density of the recoiling protons change considerably so that the stopping power of the gas and the discriminator biases have to be chosen with some care. The protons emitted in the direction of the incident neutrons have a maximum range of 210 cm in air under normal conditions while the protons recoiling at 45° have a minimum range of 35 cm. If the gas pressure in the counter is chosen such that the protons of shortest range pass through all three counters, the protons of longest range lose only

TABLE I. Experimental results.

Proton scattering angle (lab)	Neutron scattering angle (CM)	Argon pressure (atmos.)		Double coincidences rad. in		Double coincidences rad. out	Triple coincidences rad. in		Triple coincidences rad. out
0°	180°	1.8	Total counts	1059		169	500		25
			Total α's/6400	132		100	132		100
			Lab net		6.33			3.53	
			CM net		1.58			0.882	
15°	150°	1.8	Total counts	607		73	296		15
			Total α's/6400	77		40	77		40
			Lab net		6.05			3.47	
			CM net		1.57			0.899	
30°	120°	1.8	Total counts	984		186	410		21
			Total α's/6400	127		92	127		92
			Lab net		5.75			3.01	
			CM net		1.66			0.868	
30°	120°	1.0	Total counts	690		99	309		13
			Total α's/6400	95		52	95		52
			Lab net		5.34			3.00	
			CM net		1.54			0.866	
45°	90°	1.0	Total counts	1629		351	661		49
			Total α's/6400	249		153	249		153
			Lab net		4.25			2.33	
			CM net		1.50			0.825	

TABLE II. Scattered neutron intensity in center-of-mass system referred to intensity at 180°.

	180°	150°	120°	90°
Double coincidences	1.00±5%	1.00±7%	1.02±4%	0.95±5%
Triple coincidences	1.00±5%	1.02±7%	0.98±6%	0.94±5%

180 kev in the first counter, which is comparable to the energy lost by β-particles from activities induced by the fast neutrons in the counter walls. Since this makes reliable detection of the protons difficult, two different gas pressures were used in the experiments. Protons recoiling at 0° and 15° were observed with a counter filling of 1.8 atmos. of argon, while for protons recoiling at 45°, 1 atmos. of argon was used. Measurements at 30° were carried out at both pressures.

The discriminator biases were set in the following manner. A generator of artificial pulses was calibrated in terms of energy by comparing the height of the artificial pulses with those from the Pu α-particles. The minimum energy lost by protons in each counter could be calculated. Using the pulse generator, the corresponding bias settings of the discriminators could be determined. The biases were actually set at approximately half this value to make sure that all the pulses due to protons would be counted.

In order to check the setting of the biases, the coincidence counting rate above background was measured at a fixed angle as a function of the bias of each discriminator. It was found that the counting rates were independent of bias over a wide range of biases. The previously described procedure for setting the biases made it possible to select pulses corresponding to the same energy loss even if changes in gas amplification or amplifier gain occurred.

The counting rates observed for double and triple coincidences would be expected to be in the ratio of the solid angles subtended at the radiator by the openings of the second and third counter, respectively. The two methods of counting were used only to afford a check of the proper operation of the counter and of the coincidence counting circuits.

RESULTS

The experimental results are summarized in Table I. For each angle at which observations were carried out, the actual numbers of coincidence counts are recorded, both for experiments with the polythene foil facing the counter and for the background. With each number of coincidences the corresponding number of α-particle monitor counts is given in multiples of 6400. The lines entitled "Lab net" show the coincidence counts divided by the monitor counts minus the corresponding ratio for the background. The following line gives the

same number converted to the center of mass system of reference.

For a proton scattering angle of 30° the results obtained at two different pressures are shown. The agreement is as good as can be expected from the number of counts observed. If recoiling protons of lower energy were present, one would obtain a higher number at the lower pressure. Since the observed variation is in the opposite direction, it is unlikely that it is real. For the further evaluation the average of all measurements taken at 30° was used.

In Table II the relative intensity of scattered neutrons in the center-of-mass system is given in terms of the intensity of neutrons scattered through 180°. The error shown with each number is the standard statistical error based on the number of counts observed. The agreement between the results for double and triple coincidences indicates that the counters were working properly. It should be pointed out, however, that the two sets of results are not independent of each other. The largest deviation shown in Table II from the intensity observed for neutrons scattered through 180° is 6 percent which is within the statistical error. Therefore, the results of the present experiments indicate that the scattering of 14-Mev neutrons by protons is isotropic in the center of mass system within 10 percent between scattering angles of 90° and 180°. The resolving power in angle is about ±9° in the center of mass system. It was not felt to be worth while to improve the statistical accuracy over that shown in Table II since systematic errors of the order of 5 percent might be present which could not be estimated quantitatively. Such errors might be introduced by the scattering of neutrons in the counter itself, by neutrons scattered by the floor, and by the scattering of recoil protons by the diaphragms and the gas in the counter.

A comparison of the present results with previous investigations is made difficult by the fact that the measurements were carried out at different neutron energies. The measurements of Powell and Occhialini[5] and those of Laughlin and Kruger[6] for neutrons of energy between 12 and 13 Mev agree with the present results within the statistical errors of the three sets of data.

The results of the present experiment refer to neutrons scattered backward. In principle, it should be possible to deduce information concerning the scattering of neutrons into the forward hemisphere by combining the present data with measurements of the total cross section of hydrogen.[8,9] The neutron flux per unit solid angle from the $T^3(d,n)He^4$ reaction at the angle used is known from the alpha-particle count observed simultaneously, under the reasonable assumption that the angular distribution in the center of mass system is spherically symmetric. From this neutron flux and counting rate, the known number of hydrogen atoms in the polythene foil, and the geometry, the differential cross section for 0° in the laboratory system was found to be 0.20×10^{-24} cm² per unit solid angle after an 18 percent correction for flux asymmetry was applied. This asymmetry in neutron intensity around the target was mapped with threshold detectors and could be rather well accounted for by inelastic scattering alone. Other experience in this laboratory has shown that 14-Mev neutrons are nearly always degraded in a single inelastic scattering process to an energy at which the coincidence counter could not detect them. The direction of the counter coincided with material of such an amount that 14 percent of the 18 percent could be accounted for by the known inelastic cross sections of the materials, the remainder probably arising from good geometry elastic scattering. The neutron flux was presumed correctly measured by the threshold detectors in a direction where only a $\frac{1}{16}$-in. brass wall lies between source and detector.

The above cross section gives 0.050 barn per unit solid angle for the 0° center of mass value and, if spherical symmetry is assumed, a total cross section of 0.62×10^{-24} cm². This latter value is to be compared with an observed value[8,9] of 0.69×10^{-24} cm². Within the rather large experimental errors of both measurements the agreement is good.

ACKNOWLEDGMENTS

The counter used in the present experiments was originally designed and tested by Professor R. Sherr, and further work on it was carried out by Dr. J. H. Manley. The cooperation of Drs. J. H. Coon, E. R. Graves, and R. N. Little in operating the accelerator is gratefully acknowledged. The authors wish to thank Professor C. L. Critchfield for valuable suggestions, and Mr. H. T. Gittings for his help in improving the electronic circuits.

[8] E. O. Salant and N. F. Ramsey, Phys. Rev. **57**, 1075 (1940).

[9] M. Ageno, E. Amaldi, D. Bocciarelli, and G. C. Trabacchi, Phys. Rev. **71**, 20 (1947).

Effect of Neutron Bombardment on Order in the Alloy Cu_3Au

SIDNEY SIEGEL*
Oak Ridge National Laboratory, Oak Ridge, Tennessee
(Received February 18, 1949)

Samples of the alloy Cu_3Au in the ordered and disordered states have been exposed in a nuclear reactor, subject to an integrated fast neutron flux up to 3.3×10^{-19} neutron/cm². The electrical resistivity, and presumably the disorder, in the initially ordered samples increases, while little change is observed in the initially disordered samples.

IN a nuclear chain reactor under operating conditions, there are present nuclear radiations of several kinds, neutrons, γ-rays, β-particles. In a reactor designed to operate on fissions produced by neutrons of thermal energy, the energy spectrum of the neutrons extends from fission neutron energies, of the order of several Mev, down to thermal energy, about 0.03 ev. The more energetic neutrons, in elastic collisions with nuclei of substances within the reactor, impart to these a considerable fraction of their kinetic energy, on the average the amount ΔE, where

$$\Delta E = E_0(2A/(A+1)^2), \qquad (1)$$

E_0 being the initial neutron energy, A the atomic weight of the struck nucleus. For an initial energy $E_0=2$ Mev, on the average a copper atom receives 67,000 ev, a gold atom 20,000 ev of kinetic energy as a result of such an elastic collision.

This energy is sufficient to knock the atom out of its normal lattice site, leaving behind it a lattice vacancy. The recoil atom loses its energy primarily by excitation and ionization of the other atoms it encounters along its trajectory through the solid, and to a smaller extent by displacing in turn other atoms from the lattice, or by exciting localized lattice vibrations of a mean energy corresponding to a temperature higher than the average temperature of the lattice.

While the principal process involved for fast neutrons is elastic scattering, for slow neutrons capture may be the most probable process. Thus, the cross-section σ_c for capture of thermal neutrons by gold is 95×10^{-24} cm², while the scattering cross-section σ_s is 6.5×10^{-24} cm². Capture of a neutron produces a radio-isotope, here Au^{198} which decays with a half-life of 2.7 days to Hg^{198}, leaving a foreign atom in the lattice.

Thus, the irradiation of a solid by the neutron flux present in a reactor can produce displaced atoms, lattice vacancies, localized thermal lattice vibration, and foreign atoms. These products can affect the macroscopic properties of the solid.

In a simple metal the displaced atoms will not all remain interstitially stuck in the lattice, for vacancies already existing, or produced by the neutron bombardment, will diffuse into the neighborhood of a stuck atom, and the latter will fall into a lattice position equivalent to its original one. The equilibrium number of displaced atoms will depend on the neutron flux, on the rate of vacancy diffusion in the solid, and may be too small to produce significant changes in macroscopic properties. In an order-disorder alloy, however, the possibility exists for observing effects produced by the displacement of atoms, and of lattice vibrations of excessive mean energy, even after the displaced atoms have gone back to lattice sites, for the degree of order of the lattice may have been changed. This change in order will be substantially permanent if the neutron exposure is carried out at a temperature at which no change in order occurs normally, due to conventional thermal annealing. An example of such an alloy is Cu_3Au, which can be permanently kept in any state of order by appropriate heat treatment if the temperature is not subsequently raised above about 200°C.

Samples of the alloy Cu_3Au were prepared in the form of rods 0.3 cm in diameter, 7 cm long. Ordered samples were prepared by slow cooling

TABLE I. Resistivity of samples before and after irradiation.

Original resistivity			Final resistivity	
Ordered samples	Disordered samples	nvt above 50 kev	Initially ordered samples	Initially disordered samples
4.60×10^{-6} ohm cm	11.20×10^{-6} ohm cm	0.4×10^{19} n/cm²	5.71×10^{-6} ohm cm	11.25
4.60×10^{-6} ohm cm	11.20×10^{-6} ohm cm	0.6	6.25	11.25
4.60×10^{-6} ohm cm	11.20×10^{-6} ohm cm	1.0	7.54	11.17
4.60×10^{-6} ohm cm	11.20×10^{-6} ohm cm	1.5	8.36	11.21
4.60×10^{-6} ohm cm	11.20×10^{-6} ohm cm	3.3	10.10	11.30

* Present address: Atomic Power Division, Westinghouse Electric Corporation, Pittsburgh, Pennsylvania.

from 400°C during about 50 hours. These samples have an electrical resistivity at 25°C of 4.6×10^{-6} cm. The disordered samples were prepared by quenching in water from 550°C. These have an electrical resistivity of 11.2×10^{-6} cm. The electrical resistivity was used as a measure of the degree of order in these experiments.

The samples were exposed in a chain reactor for various periods in a position where the integrated flux of neutrons of energy higher than 50 kev, times the time of exposure, had the values nvt tabulated below. In each case an initially well-ordered and initially disordered sample were exposed.

During the exposure the temperature of the samples was near 40°C. After exposure the samples are strongly radioactive, and the measurements of electrical resistance must be carried out with remotely controlled devices behind suitable radiation shields. The sample is inserted into a fixture in which current and potential leads are clamped to it by hydraulic pressure acting through a sylphon bellows. The entire fixture is lowered into an oil bath thermostatically controlled at 25°C. The potential drop across a known length of the sample is measured with a Leeds & Northrup Type K2 potentiometer, the current through the sample being determined with the same instrument from the potential drop across a standard 0.001-ohm resistance. The accuracy of the resistance measurements is ±0.2 percent.

The values of the resistivity of these samples before exposure, the integrated neutron flux, and the final resistivity values are given in Table I.

It is evident that the electrical resistance, and presumably the degree of disorder, of the initially well-ordered samples increases with neutron exposure. The electrical resistance of the initially disordered samples increases by less than 1 percent, and this increase of resistance can be accounted for by the formation, through neutron capture, of Hg^{198}, an impurity which raises the resistance of gold.[1]

The samples are so strongly radioactive shortly after exposure that conventional x-ray diffraction study of degree of order through superlattice lines is difficult. However, after the samples had decayed for many months, x-ray evidence confirmed the fact that the initially ordered samples had become disordered.

The calculations of Seitz[2] permit an estimate to be made of the fraction of displaced atoms produced in the integrated flux given in Table I. This fraction is only a few percent, and appears too small to account for the nearly complete disordering of the last sample. However, in addition to atomic displacements, elastic collisions can produce lattice vibrations of greater than thermal energy along the track of the recoil atoms, and reasonable estimates show that the excessive temperature along the recoil tracks may reach values of the order of 1500°K for short periods of the order of 10^{-10} second. These temperature spikes thus produce the effect of highly localized quenches from high temperature, and disorder the lattice in this way. The energy dissipated in exciting elastic vibrations of this type during the exposure appears to be sufficient to account for the disordering observed.

This work was performed under AEC Contract No. W-35-058-eng. 71 at Oak Ridge National Laboratory. Miss Mildred Valentine assisted in obtaining the data.

[1] J. O. Linde, Ann. d. Physik **10**, 52 (1931).
[2] Frederick Seitz, Trans. Faraday Soc. April, 1949 (in press).

The Half-Life of Radiocarbon (C^{14})

ANTOINETTE G. ENGELKEMEIR, W. H. HAMILL,* MARK G. INGHRAM, AND W. F. LIBBY**
Agonne National Laboratory, Chicago, Illinois
(Received March 4, 1949)

The half-life of C^{14} has been found to be 5720±47 years by means of the use of mass spectrometrically analyzed $C^{14}O_2$ as a part of the counter gas in brass wall Geiger counters. Some of the problems of absolute β-counting with internal counters have been investigated, particularly the coincidence and end corrections.

I. INTRODUCTION

THE half-life of radiocarbon (C^{14}) has been measured several times.[1–7] The discrepancies in the results and the increasing importance of radiocarbon seemed to call for a further measurement of the half-life. The use of the gas counting technique as a method of accurate, absolute measurement for radioactivities also appeared to be worth investigation. It was further realized that since most of the measurements available at the time this research was begun used solid counting techniques, the use of an entirely different procedure would lend additional weight to any agreement with the earlier results. Finally, it was thought likely that the gas counting procedure was capable of somewhat higher accuracy than the solid counting method.

Previously published results are tabulated in Table I, together with the methods of measuring the number of C^{14} atoms in the sample used and the methods of measuring the radioactivity of the sample.

Since the first three values depend upon more uncertain methods of determining the isotopic composition of the samples, they are not comparable to the later values; but it is clear that the more recent results scatter somewhat more than the estimated errors given by the authors. The agreement, however, is sufficiently good as to suggest that the true value lies near the mean of these values. The error in this mean is difficult to estimate, but it might be permissible to take it from the observed deviations from the mean. The result of such calculations is 5687±100 years. The difficulty in accepting such a mean is the possibility of systematic errors, especially since most of the measurements used solid counting techniques. It is true, however, that the different researches used different detailed procedures and different considerations for such corrections as back scattering, self-absorption, geometrical efficiency, and counter efficiency. It is interesting, therefore, that this mean lies close to the result of the present research, 5720±47 years.

The general method used in this research was the following. A sample of barium carbonate obtained from the Isotopes Division in Oak Ridge was converted to carbon dioxide, the isotopic abundance of C^{14} determined, and an accurate dilution of several thousand fold performed. After mixing, carefully measured portions of the diluted sample were counted. The counting was done with brass-walled counters of different diameters and lengths filled with an argon-alcohol mixture to which the samples of CO_2 were added. The samples varied

TABLE I. Summary of the previously published values for the half-life of radiocarbon.

Half-life (years)	Method for isotopic composition of sample	Method for radioactivity of sample	Reference
10^3-10^5	Estimated bombardment yield	Solid carbonate counting: $CaCO_3$ in screen wall counter	1
26,000 ±13,000	Estimated bombardment yield	Gas counting: CO_2 in counter	2
21,000 ±4000	Estimated bombardment yield	a. Solid sample counting: sample with thin window counter b. Gas counting: CO_2 in counter	3
4700±470	Mass spectrometer (1.71%)	Solid carbonate counting: $BaCO_3$ with thin window counter	4
5300±800	Mass spectrometer (3.23 and 3.35%)	Solid carbonate counting: $BaCO_3$ in low absorption counter	5a
5100±200	Mass spectrometer (3.23 and 3.35%)	Solid carbonate counting: $BaCO_3$ in low absorption counter	5b
6400±200 or 6100 ±200	Mass spectrometer	Gas counting: (Miller technique[a,b])	6
7200±500	Mass spectrometer	Solid carbonate counting: $BaCO_3$ with thin window counter	7

[a] W. W. Miller, Science **105**, 123 (1947).
[b] S. C. Brown and W. W. Miller, Rev. Sci. Inst. **18**, 496 (1947)

* On leave from the Department of Chemistry, University of Notre Dame, Notre Dame, Indiana.
** Institute for Nuclear Studies, University of Chicago, Chicago, Illinois.
[1] S. Ruben and M. D. Kamen, Phys. Rev. **59**, 349 (1941).
[2] M. D. Kamen, Manhattan Project Literature, A-316.
[3] A. S. Langsdorf, Jr., and R. L. Purbrick, Manhattan Project Literature, CP-G-3272.
[4] Reid, Dunning, Weinhouse, and Grosse, Phys. Rev. **70**, 431 (1946).
[5a] L. D. Norris and M. G. Inghram, Phys. Rev. **70**, 772 (1946).
[5b] L. D. Norris and M. G. Inghram, Phys. Rev. **73**, 350 (1948).
[6] Hawkings, Hunter, Mann, and Stevens, Phys. Rev. **74**, 696 (1948).
[7] L. Yaffe and Jean Grunlund, Phys. Rev. **74**, 696 (1948).

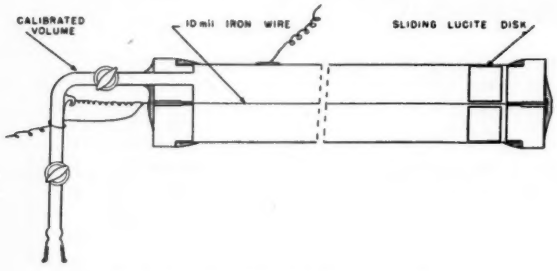

FIG. 1. Counter with Lucite ends.

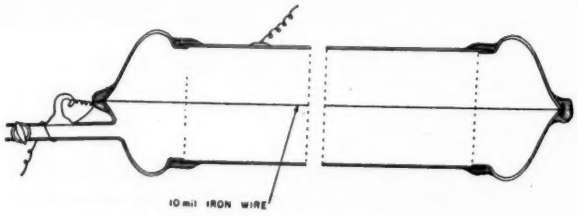

FIG. 2. Counter with glass ends.

from 0.01 to 0.1 cc S.T.P. End corrections were determined by comparing the results per unit volume of active gas from counters of the same diameter but of different lengths; a possible small variation in end correction was observed for counters of different diameters. It was assumed on the basis of previous experience reported in the literature and the basis of the absence of any appreciable variation with radius, that the counters were 100 percent efficient except for the end correction. Several CO_2 master samples were used, varying in composition from 1.24 to 6.14 atomic percent C^{14}. There was no systematic variation attributable to either the master samples or the various methods of introducing the CO_2 into the counters.

II. PREPARATION AND ISOTOPIC ANALYSIS OF THE MASTER SAMPLES; PREPARATION OF THE WORKING SAMPLES

Two methods were used for the evolution of CO_2 from the barium carbonate. The first method utilized the reaction of acid with the carbonate. About 10 mg of the Oak Ridge barium carbonate were placed in the bottom of a tube to which a ground joint had been sealed. The tube was immersed in liquid nitrogen and one or two cubic centimeters of concentrated sulfuric acid pipetted down the side of the tube so that the acid froze before coming into contact with the carbonate. While still immersed in liquid nitrogen the tube was connected to the vacuum line and thoroughly evacuated. The pump was then turned off and the tube allowed to warm to room temperature with consequent evolution of the CO_2. The gas was condensed into a 50-cc bulb to which two sample tubes with break-off seals had been attached. The sample was allowed to stand in the bulb to ensure equilibrium with any CO_2 adsorbed on the glass walls or in the grease on the stopcock. After an hour or two one of the sample tubes was sealed off and analyzed on the mass spectrometer. The dilution was then made and the second tube sealed off to bracket the composition of the gas actually used in the dilution. It was found that the two compositions agreed within the error of the mass spectrometric analysis.

TABLE II. The compositions and dilution factors for the radioactive carbon dioxide samples measured. Column 2 gives the isotopic composition of the master sample and column 3 the factor by which the master was diluted. Column 4 is the ratio of column 3 to column 2.

Designation	Isotopic composition of master (atomic percent C^{14})	Dilution factor	Ratio stable to C^{14} atoms
Ia	1.28±0.01	1592	124370
Ib	1.28±0.01	6410	500780
Ic	1.28±0.01	1670	130470
Aa	3.28±0.03	22750	693600
A	3.28±0.03	7410	225900
IIa	2.55±0.03	3722	145960
IIb	2.55±0.03	4410	172940
Fa	2.55±0.03	803.4	31505
$\alpha 1$	6.144±0.042	6215	10160
$\alpha 2$	6.131±0.038	7521	122670

The second method of evolving CO_2 from barium carbonate, suggested by Dr. W. W. Miller in a private conversation, was the metathesis of the carbonate with lead chloride. The Oak Ridge barium carbonate was mixed with dry lead chloride powder in a mortar and transferred to a tube on the vacuum line. The tube was evacuated and the pumping continued during the initial stages of heating in order to outgas the mixture. The pump was shut off when the temperature reached 100°C. CO_2 was evolved as the temperature was raised, the evolution appearing complete and quantitative at 350°C. In terms of the metathetic reaction

$$BaCO_3+PbCl_2=BaCl_2+PbO+CO_2, \quad (1)$$

a 100 percent excess of $PbCl_2$ was used. A typical result by this procedure was that a sample of barium carbonate labeled 5.9 percent C^{14} by the Oak Ridge Isotopes Division yielded CO_2 of 6.144 ±0.042 percent composition, indicating no appreciable dilution. By contrast, the acid evolution method gave samples varying from 1.24 to 3.28 percent from barium carbonate labeled 3 percent, the variation presumably being due to the introduction of inert CO_2, either in the acid or from the freezing of the acid in air.

The dilution was performed by allowing part of the master sample to expand from its storage bulb through the vacuum line into a McLeod gauge. A 0.3281-cc bulb had been sealed to the capillary of

the McLeod, and the active CO_2 was forced into this bulb by raising the mercury. The vacuum line was thoroughly evacuated and the pressure of the CO_2 in the bulb measured. The vacuum line was flushed with inert CO_2, and a pressure of CO_2 allowed to build up, sufficient that, as the mercury was lowered, inert CO_2 was forced through the mercury into the McLeod to a pressure of 40 or 50 cm. The vacuum line was evacuated and the total pressure in the 503.1-cc McLeod volume measured. Care was exercised throughout the operation to keep the mercury level in the McLeod above the side arm to prevent the active sample from diffusing into the line. The gas was allowed to stand for a time to insure diffusive mixing although the bubbling attendant, upon the transfer of the inert CO_2 through the mercury, was sufficiently vigorous as to have assured fairly complete mixing. The sample was then transferred by condensing with liquid nitrogen into a trap sealed to a 500-cc storage bulb with a stopcock.

Each master sample was usually used to make more than one working sample. Table II summarizes the data on the masters and working samples.

The technique used for the isotopic analysis was identical with that described by Norris and Inghram.[5b] It is considered that the accuracy of the measurement is not less than 0.6 percent, the principal error being uncertainty about the relative ionization probabilities of $C^{12}O_2$ *versus* $C^{14}O_2$. The precaution of using molecular flow conditions between the sample tube and the ion chamber eliminates any correction for fractionation of the gas during flow into the mass spectrometer source. The instrument was that used by Norris and Inghram.

III. ABSOLUTE GAS COUNTING

A. Counter Construction and Operation

As mentioned in the Introduction, an argon-alcohol mixture was selected for the counter gas because of previous experience with the mixture and the extensive information as to its high efficiency.[8] The standard pressures employed were 1.2 cm alcohol and 7 cm argon. Two types of counters were used. The principal type, shown in Fig. 1, consisted of a brass cylinder with flat Lucite plugs waxed into the ends. Both De Khotinsky and Apiezon "W" waxes were used. The central electrode, 0.22-mm diameter, was iron wire carefully cleaned with fine emery before being put into the counter. The Lucite plugs were turned on a lathe and were $\frac{3}{4}''$ thick, extending $\frac{3}{8}''$ into the counter. For about half the data, a movable Lucite disk, slightly smaller in diameter than the counter and $\frac{3}{4}''$ thick with a $\frac{1}{8}''$ hole through the center, had been placed in the counter to facilitate mixing the gases. In later measurements this disk was omitted. The second type of counter, used for a few early measurements, was a brass tube with glass ends, as shown in Fig. 2. Its use was discontinued because the end correction was so much larger than that for counters with flat ends.

It was found that the presence of small partial pressures of inert CO_2 in the standard argon-alcohol filling had very little effect on counter operation. Figure 3 shows plateau curves for the addition of various amounts of CO_2. The evidence clearly indicates that pressures of CO_2 up to 7 mm are tolerable; and that the pressure range in this research, namely, 0.01 to 0.5 mm, was completely safe. The precaution was always taken to record the response to an external standard (a piece of an old copper cyclotron-target). It was observed that whereas CO_2 at these pressures had no effect on the observed rate, considerable care had to be taken to guard against certain slightly volatile materials which reduced counter efficiency. Apparently these materials arose in the wax or in the Lucite, and extensive pumping was required for their removal. In the two and a half years spent on this research, this happened only 5 or 6 times in several hundred counter fillings. With the exception of these few runs, the counters always responded properly to the standard regardless of whether or not there was an active filling in the counter.

Memory effects were quite serious during the first weeks, especially with newly built counters. The background after evacuation and refilling with argon-alcohol was several percent higher, following the counting of an active CO_2 sample, than before. The initial background rate was restored by acid washing the counter, but heating to temperatures of 50–60°C for 12 to 14 hours in the presence of inert CO_2 did little good. Treatment with water

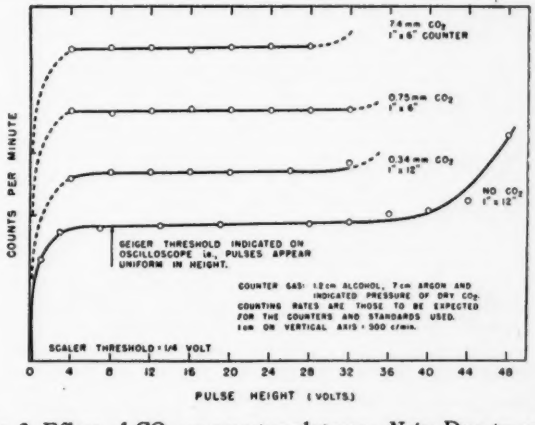

FIG. 3. Effect of CO_2 on counter plateaus. *Note:* Due to scale down, bottom right-hand line should read ". . . 1 cm on vertical axis = 1500 c/min.

[8] K. Greisen and N. Nereson, Phys. Rev. **62**, 316 (1942).

TABLE III. Physical characteristics of the counters.

	Diameter × length (inches)	Volume between ends (cc)	Dead volume (percent of total external to brass cylinder)
A.	1×6	48	34.3
	1×12	106	16.4
	2×12	484	24.5
	2×24	1065	13.1

	Diameter × length (inches)	Volume between ends (cc)	Total volume (cc)	Dead volume (percent)
B.	1×6	75.8	76.5	0.92
	1×12	153.8	155.1	0.79
	1.5×9	263.0	265.5	0.57
	1.5×18	521.0	522.6	0.31
	1.5×27	778.3	780.1	0.23
	2×12	614.0	615.7	0.18
	2×24	1232.0	1233.0	0.09

vapor and CO_2 was fairly effective in reducing the background even at room temperature. The explanation probably is the formation of a chemical compound on the surface of the brass. The preparation of the cylinder before the counter was assembled included washing in dilute nitric acid and rinsing in distilled water. Presumably this left a surface oxide film relatively free of carbonate. Subsequent exposure to CO_2 would encourage the formation of zinc and copper carbonates. These being relatively stable compounds, particularly the zinc carbonate, only very high temperatures, acid washing, or exchange with CO_2 could be expected to effect their removal. Since this notion explained the observations, it was concluded that an efficient pretreatment ought to be exposure of the newly constructed counter to inert CO_2 until the layers were saturated. CO_2 at 1 atmosphere was allowed to stand in the counter for twenty-four hours at room temperature. This pre-treatment proved to be completely effective provided no appreciable amounts of moisture were allowed to enter the counter, and for all practical purposes, the difficulty was solved. This procedure should serve for ion chambers and other instruments constructed of brass, and the notion applies more or less generally to other detection devices constructed of metal and operating with CO_2.

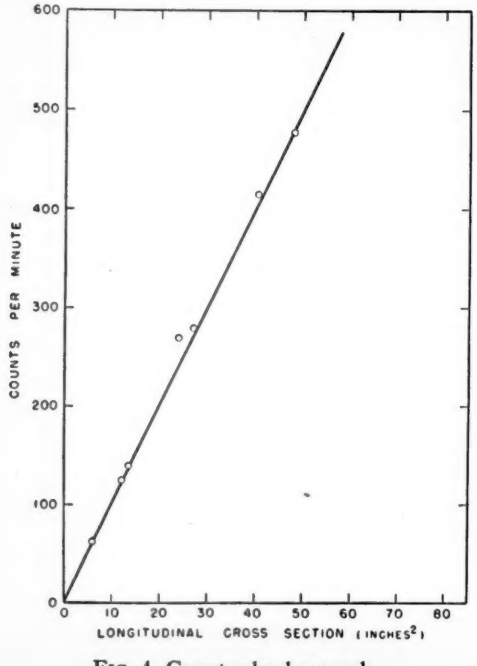

FIG. 4. Counter backgrounds.

The counter was operated on a scale of 64 with a commercial unit sold by Instrument Development Laboratories (Model 161). It was found necessary to modify this unit for the larger counters by the insertion of a 3-megohm variable resistor in the first multivibrator circuit of the set. Prior to this change, somewhat disconcerting behavior was observed with the larger counters, namely, that pulses were doubly recorded when the pulse height exceeded a certain value and that consequently the counting rate doubled about half-way along the plateau. Counters 2″ in diameter and larger invariably showed this doubling, whereas it was never observed with 1″ counters even though these were made as long as twelve inches. The small alteration mentioned, however, was the only one necessary to use the commercial unit with even the largest counters.

The central wire was connected directly to the input lead and the counter wall grounded through a standard cathode-ray oscilloscope. This enabled the operator to determine the true pulse shape and not its first derivative, and proved convenient in setting the operating voltage so that reproducible pulse heights were obtained. It was observed that the middle of the plateau usually corresponded to a given pulse height; this served as a check on the counter behavior. There was also a linear relationship between pulse height and voltage, a change of 2 volts in the pulse height corresponding to a ten-volt change in the operating voltage.

The counters were shielded with $1\frac{1}{2}$″ of lead at the sides, ends and bottom. The top was left unshielded for convenience. Table III gives the dimensions of the counters used, Part A, the "glass counters" and Part B, the "Lucite counters" used throughout most of the work.

It was observed, particularly with the Lucite counters, that the background rate was a linear function of the longitudinal cross-sectional area of the counters. Table IV gives the data for the Lucite counters when shielded as described and lying in a horizontal position.

These data are plotted in Fig. 4. It is clear that linearity is fairly well established and that the slope of the line is in agreement with numerous

TABLE IV. Background *vs.* area for lucite counters.

Counter dimensions (inches)	Background (c/min.)	Ratio of bkgd./area (c/min./in.²)
1×6	64	10.7
1×12	125	10.4
1.5×9	137	10.1
1.5×18	285	10.6
1.5×27	415	10.2
2×12	275	11.5
2×24	480	10.0

TABLE V. Resolving times for the lucite counters.

Counter dimensions (inches)	Resolving time τ (microminutes)
1×6	3.86±0.2
1×12	4.20±0.15
1.5×9	5.61±0.5
1.5×18	5.81±0.2
1.5×27	5.50±0.3
2×12	6.93±0.15
2×24	7.04±0.14

reports in the literature on backgrounds under similar conditions. It should be remarked that the addition of $1\frac{1}{2}''$ of lead above the counter reduces the slope approximately 30 percent, so that a rough rule for the background at sea level of a counter shielded in all directions by $1\frac{1}{2}''$ of lead is 7 c/min./in.²

B. Coincidence Correction

The coincidence corrections were determined by the use of carefully paired Cs^{137} sources mounted on thin copper disks. The formulas used were

$$y_1 = x_1 \exp \tau y_1, \tag{2}$$

$$y_2 = x_2 \exp \tau y_2, \tag{3}$$

$$y_1 + y_2 = x_{1,2} \exp \tau (y_1 + y_2), \tag{4}$$

where the y's are the true rates, the x's the observed rates, and τ the resolving time of the counter. The exponential form of the coincidence correction law was used rather than the linear form, although calculations with the linear form showed little difference in the correction obtained. In the case that $x_1 = x_2 = x$, then y_1 will be equal to y_2, (y), and a general simplification results. In fact, since from (2), (3), and (4),

$$y_1 y_2/(y_1 + y_2) = x_1 x_2 / x_{1,2},$$

substitution gives

$$y = 2x^2/x_{1,2} \tag{5}$$

which, when replaced in Eq. (2) or (3), gives a useful expression for τ.

$$\tau = (x_{1,2}/2x^2) \ln(2x/x_{1,2}). \tag{6}$$

In using this method it must be realized that the background is measured as a part of both x_1 and x_2, and that it enters only once in the measurement of $x_{1,2}$. This correction has been made throughout this work.

The values obtained for τ for the Lucite counters are listed in Table V.

The apparent conclusion to be drawn from these data is that the value of τ is a function of counter diameter alone. This appears reasonable on all bases previously considered.[9]

The values of τ tabulated above agree within experimental error with those obtained by means

TABLE VI. Half-life data for glass counters.

Sample	Vol. $C^{14}O_2$ used (μ cc S.T.P.)	Specific activity (c/min./μ cc)
A. 2″×24″ counter (net vol. = 1065 cc between cap ends, total vol. = 1225 cc)		
Ic	1.57	5150±600
Ia	0.508	5570±250
Ia	0.671	5620±250
Ia	1.163	4880±250
A	1.463	4540±400
B. 2″×12″ counter (net vol. = 484 cc, total vol. = 649 cc)		
Aa	0.870	4200±150
Ic	1.39	4680±300
Ic	0.189	5380±250
Ib	0.183	5560±250
Ia	0.446	5280±250
	Average	4960±150
C. 1″×12″ counter (net vol. = 106 cc, total vol. = 127 cc)		
Ic	1.28	4840±250
Ic	0.427	4520±250
Ib	0.180	4900±300
	Average	4710±200
D. 1″×6″ counter (net vol. = 48 cc, total vol. = 73 cc)		
Ib	0.165	3480±250
Ib	0.393	3970±250
Ic	0.278	3850±200
Ic	0.485	3740±200
Ib	0.138	4360±250
	Average	3860±150

E. Calculated half-life

1. 2″ counters

Geom. end correction: $24'' \frac{1225}{1065} \times 5120 = 5900 \pm 150$

$12'' \quad = 6650 \pm 200$

Formula end correction: $\frac{1225 \cdot 5120 - 649 \cdot 4960}{1225 - 649} = 5330 \pm 600$

Half-life

Geom. end correction: 24″ 6010 years±150

12″ 5320 years±200

Formula 6600 years±600

Average (geom.) 5665±300

2. 1″ Counters

Half-life

Geom. end correction: 12″ 6230±300

6″ 6030±300

Formula end correction: 6030±900

Average (geom.) 6130±300

[9] S. A. Korff, *Electron and Nuclear Counters* (D. Van Nostrand Company, Inc., 1946), Chapter 4.

TABLE VII. Half-life data for Lucite counters, 1″×6″ counter.

Sample	Vol. of $C^{14}O_2$ (μ cc S.T.P.)	Specific activity (c/min./μ cc S.T.P.)	Date
IIb	0.4259	5631±50	12/12/46
IIa	0.5592	5575±50	12/13/46
IIb*†	0.4153	5730±285	2/19/48
IIa*†	0.5456	5768±60	3/19/48
IIb*†	0.3914	5778±100	6/30/48
IIb‡†	0.2567	5700±60	7/22/48
IIb‡†	0.1422	5905±90	7/27/48
(IIa‡†§	0.2540	5504±60	8/4/48)
(IIa‡†§	0.3162	5298±110	8/5/48)
(IIa‡†§	0.2989	5597±60	8/9/48)
(IIa‡†§	0.2049	5778±110	8/10/48)
Average (corrected for dead volume) 5780±36			
1″×12″ counter			
IIa	0.7952	5838±50	12/4/46
IIb	0.7320	5881±50	12/4/46
IIb	0.5156	5737±50	12/12/46
IIa	0.5935	5580±50	12/12/46
IIb*†	0.3741	5888±230	2/19/48
IIa*†	0.4934	6196±60	3/19/48
IIb*†	0.3561	6017±60	6/30/48
IIb‡†	0.3134	5910±60	7/21/48
IIb‡†	0.4035	5988±60	7/22/48
IIb‡†	0.2234	5918±110	7/28/48
(IIa‡†§	0.3981	5683±85	8/4/48)
(IIa‡†§	0.3376	5694±60	8/5/48)
(IIa‡†§	0.4730	5792±90	8/9/48)
(IIa‡†§	0.4158	5688±110	8/10/48)
Average (corrected for dead volume) 5941±50			
1½″×9″ counter			
IIb*	0.7126	6170±50	1/23/48
IIb*†	0.7228	5993±300	2/19/48
IIb*†	0.7730	5910±150	3/9/48
IIa*†	0.9109	6143±300	3/23/48
IIb*†	0.9131	5911±300	6/25/48
IIb*†	0.7221	5980±110	6/30/48
IIb‡†	0.4588	5832±60	7/22/48
IIb‡†	0.1684	5553±220	7/29/48
(IIa‡†§	0.7281	5732±120	8/5/48)
(IIa‡†§	0.6128	5551±190	8/10/48)
α1‡†	0.3163	6045±100	10/27/48
α1‡†	0.1912	6060±100	11/1/48
α2‡†	0.5673	5961±60	11/8/48
α2‡†	0.6250	5763±100	11/11/48
α2‡†	0.5247	5808±60	11/12/48
Average (corrected for dead volume) 5975±45			
1½″×18″ counter			
IIb*†	0.5150	6335±600	3/9/48
IIa*†	0.6069	6144±110	3/23/48
IIb*†	0.4391	6154±90	5/7/48
IIa*†	0.4820	6133±60	5/13/48
IIb*†	0.9829	5561±160	6/25/48
Fa*†	0.9362	5739±150	5/27/48
IIb‡†	0.8269	6133±90	7/21/48
IIb‡†	0.8699	6169±120	7/23/48
IIb‡†	0.2964	6366±190	7/29/48
(IIa‡†§	0.5825	5843±60	8/5/48)
(IIa‡†§	0.9132	5866±150	8/10/48)
α1‡†	0.6053	6073±60	10/21/48
α1‡†	0.5960	5904±110	10/22/48
α1‡†	0.6259	5992±110	10/27/48
α2‡†	0.7372	6118±120	11/24/48
Average (corrected for dead volume) 6082±59			
1½″×27″ counter			
IIb*†	0.4352	6326±120	3/9/48
IIa*†	0.5143	6125±60	3/23/48
IIb*†	0.3720	6071±120	5/7/48
IIa*†	0.4080	6289±250	5/13/48
Fa*†	0.5286	5802±60	5/27/48
IIb*†	0.5549	6103±120	6/25/48
IIb‡†	0.7608	6103±120	7/23/48
IIb‡†	0.4430	6022±120	7/29/48
α1‡†	0.5654	6078±120	11/1/48
α2‡†	1.121	6188±120	11/8/48
α2‡†	0.7540	6008±60	11/11/48
α2‡†	1.032	6165±120	11/24/48
Average (corrected for dead volume) 6121±38			
2″×12″ counter			
IIa	0.4500	5760±50	12/3/46
IIa	0.9500	5736±50	12/4/46
IIb	0.6740	5501±50	12/4/46
IIa	0.3600	5627±60	5/29/47
IIb	0.3440	6118±50	5/30/47
IIa	0.2575	5887±500	6/3/47
IIa	0.1930	5815±100	6/3/47
IIa*	0.3560	6130±45	6/5/47
IIa*	0.7190	5920±40	6/5/47
IIa*	0.4150	6185±50	6/11/47
IIa*	2.4800	6125±100	6/11/47
IIa*	0.6380	6175±100	6/11/47
IIb*†	0.7599	5921±150	2/26/48
IIa*†	0.7864	6231±180	3/2/48
Fa*†	4.2610	5894±500	3/1/48
IIa*†	1.0004	6275±400	3/19/48
IIb*†	1.2446	5888±120	5/3/48
IIa*†	0.7004	6180±300	6/11/48
Fa*†	1.0600	5770±150	6/26/48
IIb*†	1.2380	5977±250	6/24/48
IIb*†	1.1600	6015±180	6/25/48
IIb‡†	0.5191	6013±80	7/22/48
(IIa‡†§	0.7506	5922±120	8/4/48)
(IIa‡†§	0.8856	5865±200	8/9/48)
α1*†	1.2699	6008±240	10/7/48
α2*†	1.0526	6218±190	10/13/48
α1‡†	0.7096	6002±40	10/18/48
α1‡†	0.6276	5998±60	10/20/48
Average (corrected for dead volume) 5987±38			
2″×24″ counter			
IIa	0.8329	6244±50	12/6/46
IIb	0.7946	6245±80	12/6/46
IIb	0.8170	5944±60	12/6/46
IIb	0.2650	6166±120	12/6/46
IIb	0.1780	6121±120	By Pumping
IIb	0.1140	6772±500	12/11/46
IIa	0.3230	6143±90	5/22/47
IIb*	1.0070	6134±50	1/23/48
IIb*†	1.0770	6256±370	2/26/48
Fa*†	6.0390	6224±600	3/1/48
IIa*†	1.1146	6442±130	3/2/48
IIa*†	0.8295	6386±190	3/19/48
IIb*†	1.1087	6163±120	5/3/48
IIa*†	0.6274	6320±90	5/11/48
Fa*†	0.9499	5927±100	5/26/48
IIb*†	0.8396	5886±90	6/24/48
IIb*†	0.7864	6045±60	6/25/48
IIa*†	0.4223	5984±60	6/29/48
IIb‡†	0.5841	5986±60	7/21/48
IIb‡†	0.7220	5980±150	7/28/48
IIb‡†	1.0163	5938±120	7/26/48
α1*†	0.8698	6027±120	10/7/48
α2*†	0.7218	6191±120	10/13/48
α1‡†	0.6290	6090±60	10/18/48
α1‡†	0.7765	6060±60	11/19/48
Average (corrected for dead volume) 6126±30			

* New std. vol. introduction technique.
† Pot. in IDL.
‡ Premixing technique.
§ Doubtful premix dilution value, omitted in calculating half-life.

of a single sweep cathode-ray oscilloscope whereon the resolving time was observed visually. They agree also with values obtained by following the decay of 54-minute In through several half-lives, as well as with values reported in the literature for counters with argon-alcohol fillings.

The register appeared to record faithfully for rates up to 40,000 c/min. It was assumed, therefore, that its characteristics did not affect the resolving time determinations in which the maximum rates did not exceed 30,000 c/min., nor did they affect the coincidence loss during the half-life measurements, since most of the measurements were made at rates well below 10,000 c/min. Furthermore, because the rates were less than 10,000 c/min., the coincidence corrections were never more than a few percent.

C. Sample Introduction

The problem of introducing the CO_2 samples into the counters was one of the most serious encountered. The method first used involved measuring the pressure of CO_2 in a 0.982-cc bulb and condensing this CO_2 with liquid nitrogen into a glass U-trap between the counter and the vacuum line. The stopcock between the trap and the line was closed and the CO_2 allowed to sublime into the counter. The residual active CO_2 was swept into the counter in the course of introducing the alcohol and argon. Since incomplete transfer was suspected, a second method was devised. A second stopcock was sealed to the counter filling tube (see Fig. 1), and the volume between stopcocks calibrated. With the stopcock towards the vacuum line open and the stopcock adjacent to the counter closed, active CO_2 was introduced into the vacuum line and the pressure and temperature measured. The calibrated volume was closed off from the line and the stopcock to the counter opened. The line was evacuated, and the alcohol and argon were let into the counter. This method seemed to be quite satisfactory except for the possibility that grease from the stopcock might change the volume by $\frac{1}{2}$ to 1 percent. A third procedure consisted of introducing a known amount of CO_2 into a liter bulb, adding approximately a liter of argon and measuring the total pressure. Since the volume of the bulb was known, it was then possible to calculate the CO_2/argon ratio. After standing several hours to insure diffusive mixing, the gas was ready for filling counters. The counters, the volumes of which were known, were first filled with alcohol at its vapor pressure at 0°C; the CO_2-argon mixture was added and the pressure of the alcohol plus the mixture measured. When necessary, additional argon was used to bring the total pressure to 8.2 cm. The data from all three methods agreed well on the average, although the scatter seemed to be greatest in the first and least in the third.

TABLE VIII. End correction calculations.

Sample	Counter	Specific activity (corrected for dead volume)		Calc. end correction (percent)
		A. Premix data		
IIa	1″×6″	5599±72		6.2±3.2
	1″×12″	5772±52		3.0±1.6
	1½″×9″	5719±172		5.2±5.4
	1½″×18″	5867±117		2.5±2.6
IIb	1″×6″	5816±70		6.1±3.2
	1″×12″	5992±60		2.9±1.5
	1½″×9″	5862±115	(1½×18)	11.6±6.9
			(1½×27)	5.4±5.1
	1½″×18″	6196±99	(1½×9)	5.4±3.2
			(1½×27)	−5.9±7.6
	1½″×27″	6075±120	(1½×9)	1.8±1.7
			(1½×18)	−4.0±5.2
	2″×12″	5941±100		2.1±4.0
	2″×24″	6004±90		1.0±2.0
α1	1½″×9″	6108±92	(18)	−2.2±3.8
			(27)	−0.39±3.4
	1½″×18″	6042±66	(9)	−1.1±1.9
			(27)	2.5±7.0
	1½″×27″	6092±120	(9)	−0.13±1.1
			(18)	1.6±4.5
	2″×12″	6011±100		2.1±3.9
	2″×24″	6075±60		1.1±2.0
α2	1½″×9″	5914±53	(18)	7.5±4.4
			(27)	4.2±2.3
	1½″×18″	6137±122	(9)	3.6±2.1
			(27)	−2.8±7.0
	1½″×27″	6080±73	(9)	1.4±0.8
			(18)	−1.9±4.6
Counter		Average specific activity (corrected for dead volume)		Calc. end correction (percent)
		B. Standard volume data		
1″×6″		5749±36		8.5±2.7
1″×12″		5793±60		4.1±1.3
1½″×9″		6050±42	(18)	2.3±3.0
			(27)	3.7±1.2
1½″×18″		6120±88	(9)	1.1±1.5
			(27)	3.8±4.5
1½″×27″		6199±46	(9)	1.2±0.4
			(18)	2.5±3.0
2″×12″		6068±34		3.0±1.4
2″×24″		6158±30		1.5±0.7
		C. Total half-life data		
1″×6″		5780±35		6.9±2.1
1″×12″		5978±50		3.3±1.0
1½″×9″		5975±45	(18)	5.0±1.7
			(27)	4.3±1.3
1½″×18″		6124±47	(9)	2.4±0.8
			(27)	1.2±2.8
1½″×27″		6148±29	(9)	1.4±0.4
			(18)	0.8±1.8
2″×12″		6006±34		3.9±1.25
2″×24″		6126±30		1.9±0.6

D. End Correction

The problem of determining the inefficiency of the counters, due to inhomogeneous and weakening fields near the counter ends, was handled by comparing the observed rates per unit volume of radioactive CO_2 for counters of the same diameter but

TABLE IX. End corrections.

Counter diameter	$D/L=1/6$	$D/L=1/12$	$D/L=1/18$
A. Premix data			
1″	6.2±1.5	3.0±0.8	——
1½″	4.2±1.5	2.2±1.3	1.2±0.5
2″	2.1±2.0	1.1±1.0	——
B. Std. vol. data			
1″	8.5±2.7	4.1±1.3	——
1½″	3.2±1.5	2.0±2.0	1.4±0.5
2″	3.0±1.4	1.5±0.7	——
C. Total data			
1″	6.9±2.1	3.3±1.0	——
1½″	4.5±1.5	2.3±1.0	1.3±0.7
2″	3.9±1.3	1.9±0.6	
Average (independent of diameter)	4.7±0.6	2.3±0.5	1.3±0.4
K	0.269	0.270	0.231
Average (by diameter)			
1″	7.2±2.0	3.5±1.0	——
1½″	4.0±1.2	2.3±1.0	1.3±0.4
2″	3.0±1.2	1.5±0.6	——

of different lengths. If the observed rates are called R and r for counters of length L and l, respectively, and the count rate per unit volume for 100 percent efficiency is called ρ, then

$$\rho(L-l)=RL-rl, \tag{7}$$

or

$$(\rho-R)/R=(l/(L-l))(1-r/R) \tag{8}$$

for the end correction for the longer counter, and

$$(\rho-r)/r=L/(L-l)((R-r)/r) \tag{9}$$

for the end correction for the shorter counter. The accurate determination of the end corrections was attempted only for the Lucite counters. For the glass counters, the formulas were used, and the results were in agreement with the assumption that the active volume ended at the beginning of the glass inserts. The corrections, however, were so large that the use of these counters was discontinued.

The data for the Lucite counters seem to indicate that the end correction is primarily dependent upon the ratio of length to diameter rather than upon the actual size. There is, however, some evidence for a slight variation in end correction from diameter to diameter, and the corrections were applied in both ways. Since the difference in the final results was small, the two were averaged. It is believed that the error in the end correction was the largest single error in the determination of the half-life. Since the magnitude of the end correction is small, the maximum correction being 7 percent, this error is less than 1 percent in its effect on the final result.

It is quite conceivable that a short-range radiation such as tritium or certain K capture gases will show a different end correction than C^{14}. It is

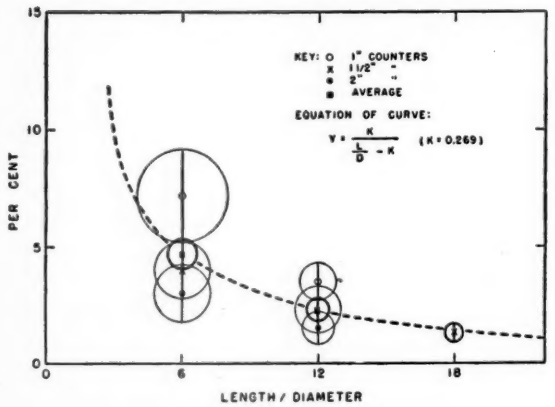

FIG. 5. End corrections.

TABLE X. Summary of half-life data by sample and counter; independence of master sample.

Counter	Sample	No. runs	Average specific activity (corrected for dead volume)	Corrected specific activity *a	Corrected specific activity *b
1″×6″	IIa	1	5821	6094	6240
	IIb	4	5831	6105	6250
1″×12″	IIa	3	5917	6053	6124
	IIb	7	5953	6090	6161
1½″×9″	IIa	1	6178	6468	6425
	IIb	7	5941	6220	6179
	α1	2	6108	6395	6352
	α2	3	5898	6175	6134
1½″×18″	IIa	2	6157	6299	6299
	IIb	6	6138	6279	6279
	Fa	1	5757	5889	5889
	α1	3	6009	6147	6147
	α2	1	6137	6278	6278
1½″×27″	IIa	2	6221	6314	6302
	IIb	5	6139	6231	6219
	Fa	1	5815	5902	5890
	α1	1	6092	6183	6171
	α2	3	6134	6226	6214
2″×12″	IIa	13	6015	6298	6195
	IIb	7	5930	6209	6108
	Fa	2	5842	6116	6017
	α1	3	6016	6299	6196
	α2	1	6229	6522	6416
2″×24″	IIa	6	6259	6403	6353
	IIb	12	6077	6217	6168
	Fa	2	6081	6221	6172
	α1	3	6064	6203	6155
	α2	1	6196	6338	6289
Average, all counters	IIa	28		6276±37	6278±24
	IIb	48		6193±17	6195±15
	Fa	6		6032±49	5992±42
	α1	12		6245±28	6204±24
	α2	9		6308±37	6266±30
Average				6213±30	6187±31
Half-life				5700±28	5724±29

*a Average end corrections, independent of diameter.
*b Average end corrections, by diameters.

TABLE XI. Summary of half-life data by counters (total averages, disregarding sample differences).

Diam./ length	Counter	Average specific activity	Corrected specific activity *a	*b
1/6	1″×6″	5780±25	6052	6196
	1½″×9″	5975±31	6256	6214
	2″×12″	5976±30	6257	6155
1/12	1″×12″	5941±35	6078	6149
	1½″×18″	6082±41	6222	6222
	2″×24″	6126±21	6267	6218
1/18	1½″×27″	6121±26	6213	6201
	Average (103 runs)		6192±22	6193±10
	Half-life		5719±20	5719±10

*a Average end corrections, independent of diameter.
*b Average end corrections, by diameters.

TABLE XII. Summary of half-life values; precision and best value.

A. Individual values		
1. Glass counters		
1″		6130±300 years
2″		5665±300 years
	Average	5898±200 years
2. Lucite counters		
a. Average by samples		5700±42 years
b. Average by samples (diameter dependent end correction)		5724±57 years
c. Total average (independent of sample)		5719±40 years
	Average	5712±46 years
B. Best value (average by inverse square of errors)		5720±47 years (mean solar)

intended to measure this effect to determine any difference.

Note added in proof.—Measurements with A^{37} (34.1d; K capture) which give 2.8 kev pulses of Auger electrons have given no evidence of dependence of the correction on diameter and the corrections found agree within a small error with those reported here for C^{14} (dotted curve in Fig. 5). These results will be published later elsewhere.

IV. EXPERIMENTAL DATA AND RESULTS

Table VI presents the data obtained in the fall of 1946 with the glass counters described earlier. Part E of the table summarizes the half-life calculations from these data. A geometrical end correction was used rather than the formula end correction discussed in the previous section, because the errors in the individual rates were too large for the differences to be significant.

Table VII is a similar summary of the data from the Lucite counters. Specific activities are calculated from the observed rates after correcting for coincidence losses and background. The dead volume correction for each counter is made for the average specific activity. The data from sample IIa premixing are omitted in the average because of an error in the preparation of the CO_2-argon mixture.

Table VIII contains data used in calculating end corrections, Part A, data from the premix method of introducing CO_2; Part B, data from the calibrated volume method, and Part C, total averages. The premix data for sample IIa are included in the end correction calculations because an error in the dilution does not affect the end correction.

Table IX is a summary of the calculated end corrections.

The average end corrections are plotted as a function of length to diameter ratio in Fig. 5, and smooth curve drawn for the end correction independent of any diameter effect. The theoretical equation for the curve is given with the value for the constant K derived from the data. This equation is derived easily on the assumption that the correction depends only on the ratio of length to diameter.

The average specific activity obtained for each working sample with each counter is listed in Table X. The corrected specific activity is calculated for each value with (1) end corrections as a function of length/diameter only and (2) end corrections varying by diameter.

Table XI is a summary of the average specific activities independent of sample. End corrections are made in two ways, as above.

Table XII summarizes all the results, together with the standard deviation of the mean. The final result, 5720±47 mean solar years, is obtained by weighting individual results according to the inverse square of their errors.

V. DISCUSSION

The published values for the half-life of radiocarbon (see Table I) exhibit a scatter somewhat beyond the errors estimated by the authors, and apparently random. The mean of the last 5 values in the table, when weighted according to the errors quoted by the authors in each case, is 5687±100 years. It is difficult to know what significance the standard deviation ±100 years has in this calculation. The agreement between the result of the present research, 5720±47, and the mean 5687 ±100, should not be overstressed since the validity of such an average is uncertain. It is interesting, however, that some accord does exist, and may add to confidence in a value close to this point.

The precision quoted for the present result (47 years) is the standard deviation of the mean; statistical deviations of the observed specific activities, the errors in the coincidence and end corrections, the error in the spectrometric analyses, and dilution errors were considered in computing this error. The "safe error" may be considered to be about twice this, or, in round numbers, ±100 years.

The Disintegration Scheme of Cerium (141)*

C. E. MANDEVILLE AND E. SHAPIRO
Bartol Research Foundation of the Franklin Institute, Swarthmore, Pennsylvania
(Received March 11, 1949)

The beta-rays of Ce^{141} have a maximum energy of 0.44 Mev. An absorption curve in lead of the gamma-radiation yields a quantum energy of 0.13 Mev. This gamma-ray is coincident in time with the beta-ray spectrum. Beta-beta-coincidences are present in the disintegration of Ce^{141}, showing that the gamma-ray is to some extent converted. The beta-rays of Pr^{143} have a maximum energy of 0.835 Mev.

INTRODUCTION

THE isotopic assignments of the 30-day cerium and the 13-day praseodymium were first established by Pool and Kurbatov.[1] The radiations were given by them as 0.65-Mev beta-rays and 0.2-Mev gamma-rays for Ce^{141} and 0.95-Mev beta-rays for Pr^{143}. Subsequent investigations[2] by the Ohio State group yielded 0.66-Mev beta-rays and 0.2-Mev gamma-rays as the radiations of Ce^{141} and 0.83-Mev beta-rays for Pr^{143}. Classified measurements[3] give 0.60-Mev beta-rays and 0.21-Mev gamma-rays from Ce^{141} and 0.95-Mev beta-rays from Pr^{143}. Bothe[4] reports 0.4 Mev as the maximum energy of the beta-rays of Ce^{141} and Marinsky and Glendenin[5] give 1.0 Mev as the end point of the beta-rays of Pr^{143}.

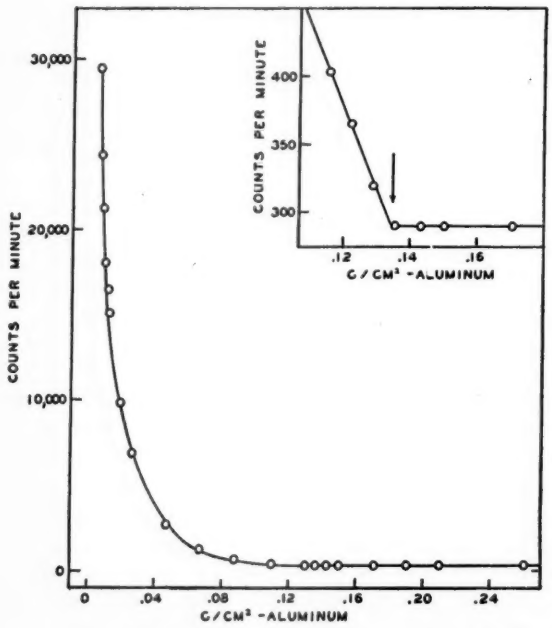

FIG. 1. Absorption in aluminum of the beta-rays of Ce^{141}. The end point corresponds to a maximum energy of 0.44 Mev.

For the purposes of this investigation, CeO_2 was irradiated by slow neutrons in the Oak Ridge pile. The irradiated material was aged for two months before measurements were commenced. This period of time was sufficient to allow for the disappearance of Ce^{143}, the 33-hour parent of Pr^{143}.

150 mg of pile irradiated ceric oxide and 25 mg of inactive praseodymium oxide were dissolved by prolonged heating with concentrated sulfuric acid at 250°C. Cerium was separated from praseodymium by precipitation of ceric iodate following the procedure of Scott.[6] Inactive cerous nitrate was added to the filtrate from the ceric iodate precipitation and ceric iodate was precipitated to remove all active cerium from the praseodymium fraction. The praseodymium was precipitated and counted as the hydroxide. Gamma-ray absorption data re-

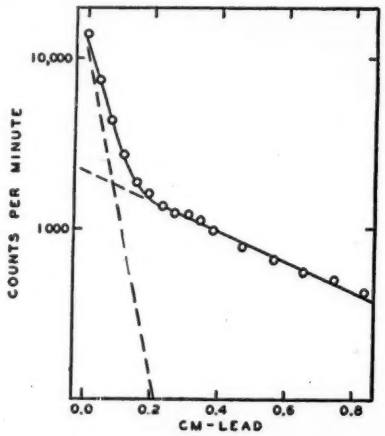

FIG. 2. Absorption in lead of the quantum radiations of Ce^{141}. The curve is resolved into two components having energies of 0.13 Mev and 0.42 Mev. The intensity of the harder gamma-ray decreased with successive chemical separations, showing that it must be associated with an impurity.

* Assisted by the Joint Program of the ONR and the AEC.
[1] M. L. Pool and J. D. Kurbatov, Phys. Rev. **63**, 463 (1943).
[2] M. L. Pool and N. L. Krisberg, Phys. Rev. **73**, 1035 (1948).
[3] W. H. Burgus, Plutonium Project Report CC-680, 13 (1943), quoted by G. T. Seaborg and I. Perlman, Rev. Mod. Phys. **20**, 585 (1948).
[4] W. Bothe, Zeits. f. Naturforschung **1**, 179 (1946).
[5] J. Marinsky and L. E. Glendenin, Plutonium Project Report CC-2829 (1945), quoted by G. T. Seaborg and I. Perlman, Rev. Mod. Phys. **20**, 585 (1948).
[6] W. W. Scott, *Standard Methods of Chemical Analysis* (D. Van Nostrand Company, Inc., New York, 1939), fifth edition, pp. 252, 253.

vealed the presence of a relatively hard gamma (0.42 Mev) not previously reported to be associated with Ce^{141}. Consequently, the ceric iodate was dissolved in a hot dilute hydrochloric acid solution through which sulfur dioxide was bubbled. When solution was complete, cerium hydroxide was precipitated, filtered, washed with hot water, and dissolved in sulfuric acid. Sodium cerium sulfate was precipitated, filtered, and washed. This salt was converted to cerium hydroxide which was treated as before and then precipitated as potassium cerium sulfate, which was in turn converted to cerium hydroxide in which form observations were made.

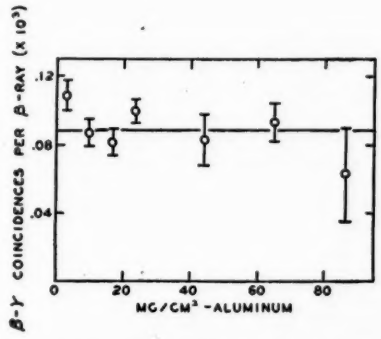

FIG. 3. Beta-gamma-coincidence rate of Ce^{141} as a function of the surface density of aluminum placed before the beta-ray counter.

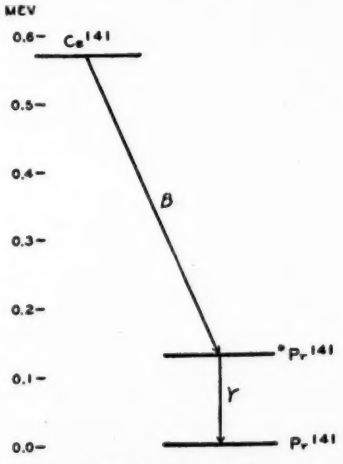

FIG. 4. Proposed disintegration diagram for Ce^{141}.

Ce^{141}

The aluminum absorption curve of the beta-rays of Ce^{141} is shown in Fig. 1 where the end point is seen to occur at 135 mg/cm², 0.44 Mev as indicated by Glendenin's curve.[7] This value is in good agreement with Bothe's measurement[4] but is considerably lower than the several American reports.[1–3] The absorption of the gamma-rays of Ce^{141} in lead

[7] L. E. Glendenin, Nucleonics 2, No. 1, 12 (1948).

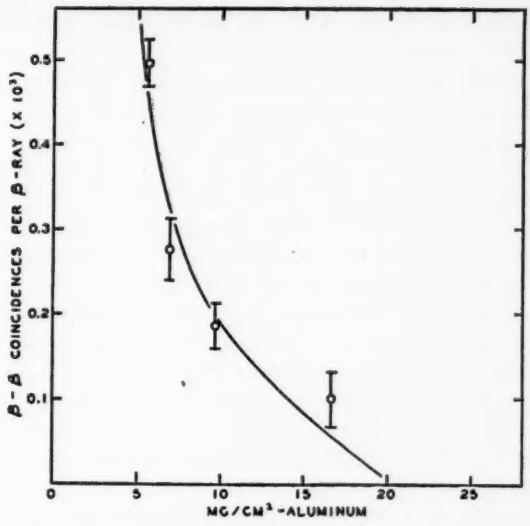

FIG. 5. Beta-beta-coincidences in Ce^{141} as a function of the surface density of aluminum placed before both beta-ray counters.

is shown in Fig. 2 where it is immediately clear that the radiation is complex. The linear absorption coefficient of the softer component is 26.6 cm^{-1}, corresponding to a quantum energy of about 0.13 Mev. This value is considerably lower than the earlier estimates. The energy of the second component is 0.42 Mev. This harder gamma-ray is associated with an impurity as yet not positively identified. In the particular curve of Fig. 2, the intensity of the hard gamma-ray relative to that of the 0.13-Mev quantum is 0.06. This estimate of relative intensity is corrected for the fact that the detection efficiency of the counter varies with quantum energy. When the source was subjected to further chemical separation, this intensity was re-

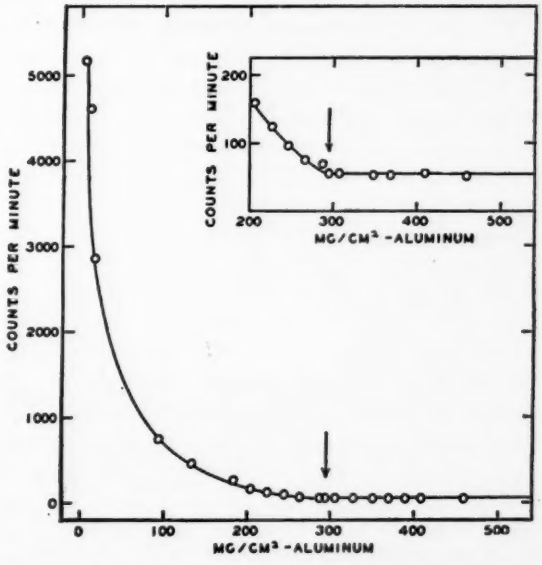

FIG. 6. Absorption in aluminum of the beta-rays of Pr^{143}.

duced to 0.02. For a given sample of material, the relative intensities were found to remain constant over a period of two months so that the impurity must also have a half-period of about 30 days.

The beta-gamma-coincidence rate of Ce^{141} is shown in Fig. 3 as a function of the surface density of aluminum placed before the beta-ray counter. The constancy of the beta-gamma-coincidence rate shows that the beta-ray spectrum is simple. The absolute magnitude of the coincidence rate is such as to suggest that each beta-ray is followed by a 0.13-Mev quantum. The proposed disintegration scheme for Ce^{141} is shown in Fig. 4.

Beta-beta-coincidences were found in the disintegration of Ce^{141} and are shown in Fig. 5 as a function of the surface density of aluminum placed before both of the beta-ray counters. The coincidence rate is seen to approach zero in the vicinity of 20 mg/cm², showing that the 0.13-Mev quantum is to some extent converted.**

** A small gamma-gamma-coincidence rate, (0.03, 0.01 $\times 10^{-3}$) coincidence per gamma-ray, was noted in the disintegration of Ce^{141}. Since considerable evidence [see Siegbahn and Hedgran, Phys. Rev. **75**, 523 (1949)] has been accumulated to show that such small coincidence rates are sometimes spurious, the observed effect cannot be regarded as genuine. Any geometry dependent effects such as scattering, would be enhanced by the presence of the hard gamma-ray of the impurity.

Pr^{143}

The beta-rays of Pr^{143} were absorbed in aluminum as shown in Fig. 6. The visual end point occurs at 294 mg/cm², 0.835 Mev as calculated by Feather's equation.[8] Best agreement is found with the more recent data of the Ohio State group.[2]

Note added in proof—The spectrometric measurements of L. R. Shepherd [Research **1**, No. 14, 671 (1948)] have just come to the attention of the writers. His data indicate that 70 percent of the disintegrations proceed by way of the disintegration scheme of the present paper and that the remaining disintegrations occur with beta-emission to the ground state of Tr^{141}. The maximum beta-ray energy reported by Shepherd is 0.56 Mev, corresponding to an absorption limit of 200 mg/cm². This end point is not apparent on the absorption curve of Fig. 1 of the present paper.

[8] N. Feather, Proc. Camb. Phil. Soc. **34**, 599 (1938).

PHYSICAL REVIEW VOLUME 75, NUMBER 12 JUNE 15, 1949

Energy Levels in Ca^{41} and the Mass Difference between A^{40} and Ca^{40} *

VANCE L. SAILOR
*Sloane Physics Laboratory, Yale University,** New Haven, Connecticut*

(Received February 28, 1949)

The reaction $Ca^{40}(d,p)Ca^{41}$ was studied and Q-values of 6.17, 4.22, 3.76, 2.31 Mev were found. Four additional Q-values 3.2, 2.9, 2.7, 2.5 Mev are probable. The mass increment $(A^{41}-A^{40})-(Ca^{41}-Ca^{40})=2.54\pm0.03$ mMU was obtained by comparing the end groups of the two reactions $A^{40}(d,p)A^{41}$ and $Ca^{40}(d,p)Ca^{41}$. These data combined with data from two other nuclear reactions give the mass difference $Ca^{40}-A^{40}=0.27\pm0.21$ mMU, indicating that A^{40} is slightly more stable than Ca^{40}. This mass difference is compared with data on the radioactive decay of K^{40}, showing that the assignment of the 1.55-Mev γ-ray to $K^{40}\rightarrow A^{40}$ K-capture process is reasonable.

I. INTRODUCTION

THE mass differences between the three important isobars A^{40}, K^{40}, and Ca^{40} are uncertain. Since Ca^{40} is a closed shell nucleus, it might be expected to be more stable[1] than A^{40}. On the other hand, some experimental evidence[2] seems to contradict this conclusion. If the 1.55-Mev γ-ray accompanying the radioactive decay of K^{40} is assigned to the K-capture process, then A^{40} appears to be more stable than Ca^{40}.

It is possible to obtain the mass difference between A^{40} and Ca^{40} by using the four nuclear reactions: $A^{40}(d,p)A^{41}$, $A^{41}\rightarrow K^{41}+\beta^-$, $K^{41}(p,n)Ca^{41}$ (threshold), and $Ca^{40}(d,p)Ca^{41}$. All four of these reactions have been investigated previously.[3-6]

In order to reduce the uncertainties in two of the above reactions, two studies have been made: (1) the $Ca^{40}(d,p)Ca^{41}$ reaction has been reinvestigated using thin targets, and (2) a direct comparison was made between the end groups of the two reactions $A^{40}(d,p)A^{41}$ and $Ca^{40}(d,p)Ca^{41}$. This was done so that the mass difference $(A^{41}-A^{40})-(Ca^{41}-Ca^{40})$ could be obtained with the uncertainties of beam energy and counter depth eliminated.

II. PROTON ENERGIES FROM $Ca^{40}(d,p)Ca^{41}$

Thin targets were used for the investigation of the proton spectrum from the $Ca^{40}(d,p)Ca^{41}$ reaction. These targets consisted of approximately 0.35 mg/cm² of calcium metal evaporated on gold foil.

* Part of a dissertation presented to the Graduate School of Yale University in partial fulfillment of requirements for the degree of Doctor of Philosophy.

** Assisted by the Joint Program of the ONR and AEC.

[1] L. B. Borst and J. J. Floyd, Phys. Rev. **74**, 989 (1948).

[2] O. Hirzel and H. Wäffler, Phys. Rev. **74**, 1553 (1948).

[3] E. C. Pollard and P. W. Davison, Phys. Rev. **73**, 1241 (1948). Also more complete work on $A^{40}(d,p)A^{41}$ by P. W. Davison, J. O. Buchanan, and E. C. Pollard is in the course of publication.

[4] Bleuler, Bollman, and Zünti, Helv. Phys. Acta **19**, 419 (1946).

[5] H. T. Richards and R. V. Smith, Phys. Rev. **74**, 1257 (1948).

[6] William L. Davidson, Jr., Phys. Rev. **56**, 1061 (1939).

The surface of the target forms CaO on exposure to air. The proton groups from this oxygen can be used as a standard for appraising the accuracy of the Q-values obtained from the calcium.

The procedure for observing the proton yield has been described in detail in previous papers.[7,8] Figure 1 is a schematic diagram of the apparatus. The target was bombarded by 3.90-Mev deuterons from the cyclotron. The target was supported on a C-shaped holder so that the beam strikes only the target. The protons resulting from the reaction were observed at ninety degrees with respect to the incident beam. The yield was determined as a function of the thickness of aluminum plus air between the target and the counter. A proportional counter was used for detection of the protons. A counting level was chosen such that only the largest pulses were recorded, i.e., only those protons near the end of their range and giving maximum specific ionization. The observed yield is shown in Fig. 2.

The spectrum shows four groups which are clearly resolved. In addition, a graphical analysis of the range 40 to 55 cm shows 4 additional poorly resolved groups. The two oxygen groups arising from the CaO layer of the target surface are shown as the dashed curve in Fig. 2. These have been reduced to one-tenth their true size.

To obtain the energy corresponding to each proton group, the extrapolated range is found from Fig. 2. A small correction must be added to the observed range to correct for the variation of the stopping power of Al with proton energy. The corrected range is then converted to energy using Cornell University 1937 range-energy curves.

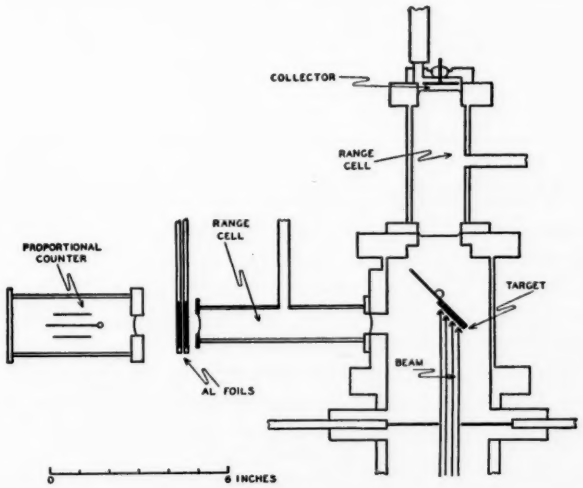

FIG. 1. Schematic diagram of bombardment chamber. The target is mounted on a Wilson seal and may be turned aside. The range cell behind the target is for measuring the energy of the deuteron beam. The range cell at right angles to the beam measures the range of the protons. An automatic foil changer between range cell and counter makes large changes of absorption possible.

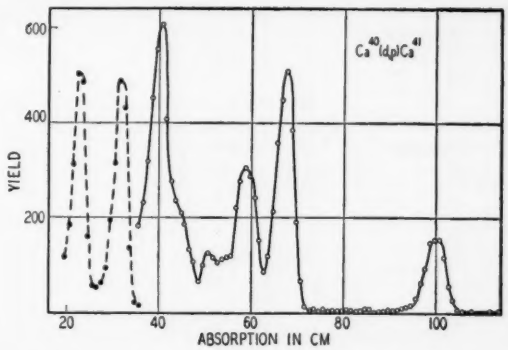

FIG. 2. The proton yield from $Ca^{40}(d,p)Ca^{41}$. Relative yield in arbitrary units is plotted against the total absorption in centimeters air equivalent. The dashed curve is the yield from oxygen in the form of CaO on target surface. It is reduced to one-tenth of its actual yield relative to the calcium.

The beam energy was measured by means of the range cell behind the target (Fig. 1). This was done by turning the target aside and measuring the beam-galvanometer current as a function of the air pressure in the range cell. The extrapolated energy of the deuteron beam was 3.90 ± 0.02 Mev and its half-width was 0.10 Mev. The Q-values were calculated using the extrapolated beam energy and extrapolated proton energy. It was found that the correction resulting from the calculation of the Q-values, using mean beam energy and mean proton energy, was much smaller than the probable errors.

The results are summarized in Table I. The Q-values are in fair agreement with those obtained by Davidson[6] (6.30 and 4.51 Mev), considering that Davidson used a thick target.

The values in Table I in italics are the groups obtained by a graphical analysis of the curve and are less certain than the other groups listed.

Since Ca^{40} is 96.96 percent abundant, it is probable that all of these Q-values should be assigned to the reaction $Ca^{40}(d,p)Ca^{41}$. Any other isotope of calcium would have to have a cross section more than 50 times greater than Ca^{40} to give a comparable yield.

A careful search was made over the range 110 to 200 cm for additional groups, but none were found. It is assumed, therefore, that the Q-value of 6.17 Mev corresponds to the formation of Ca^{41} in the ground state. The mass difference calculated from this Q-value is $Ca^{41}-Ca^{40}=0.99997\pm0.00005$ MU.

A plot of the excitation of the levels is shown in Fig. 3. The thickness of each line in this diagram is proportional to the relative intensity of the group. The spacing of the levels is striking in that the interval between the ground and the first excited

[7] A. B. Martin, Phys. Rev. **72**, 378 (1947).
[8] Pollard, Sailor, and Wyly, Phys. Rev. **75**, 725 (1949).

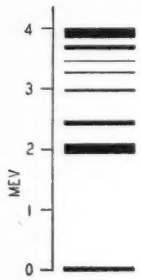

FIG. 3. Energy level diagram for Ca^{41} obtained from $Ca^{40}(d,p)Ca^{41}$. The thickness of each line corresponds to the relative yield of the proton group.

state is unusually large. The spacing between the higher excited states decreases rapidly.

III. COMPARISON OF Q_0 FOR A^{41} AND Ca^{41}

The $A^{40}(d,p)A^{41}$ reaction has been carefully observed and previously reported by Pollard and Davison.[3] However, for the purpose of calculating the mass difference $Ca^{40}-A^{40}$, a comparison of the end groups from the argon and the calcium reactions is needed. Using the same bombardment chamber and taking the measurements in immediate sequence would greatly reduce the error limits in the mass difference $(A^{41}-A^{40})-(Ca^{41}-Ca^{40})$. Such a comparison would eliminate the uncertainty in the beam energy which is ± 0.02 Mev. Also other small uncertainties would be removed such as the effective counter depth, the thickness of the aluminum windows, and the energy loss of the deuterons and protons in the argon-filled bombardment chamber.

To compare the end groups of the two reactions, a gas bombardment chamber was filled with argon and the proton spectrum of argon was observed. The proton group corresponding to the ground state of A^{41} was located. This had previously been identified[3] with reasonable certainty. A calcium target was then introduced into the bombardment chamber, the chamber was refilled with argon to the same pressure as before, and the end group from calcium was observed.

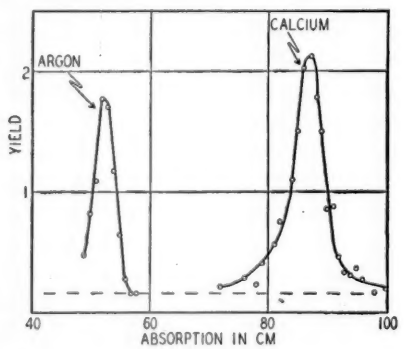

FIG. 4. The end groups from $A^{40}(d,p)A^{41}$ and $Ca^{40}(d,p)Ca^{41}$. These were taken in immediate sequence using the same bombardment chamber, counter setting, and geometric arrangement. The dashed line shows the average neutron background.

The results are plotted in Fig. 4. The difference in the energies of the protons corresponding to the ground state in the two reactions is obtained as shown in Table II.

The mass difference is calculated as follows:

$$\begin{aligned}(A^{41}-A^{40})-(Ca^{41}-Ca^{40}) &= -(Q_0{}^{A}-Q_0{}^{Ca})\ \text{Mev}\\ &= -42/41(E_p{}^{A}-E_p{}^{Ca})\ \text{Mev}\\ &= -42/41(1.074)(E_p{}^{A}-E_p{}^{Ca})\ \text{mMU}\\ &= 2.54\pm 0.03\ \text{mMU}. \qquad (1)\end{aligned}$$

TABLE I. Q-values for $Ca^{40}(d,p)Ca^{41}$ and $O^{16}(d,p)O^{17}$ obtained from Fig. 2, after applying aluminum correction to the observed extrapolated ranges, and using the Cornell 1937 range-energy curves to obtain the proton energy. The energy of the deuteron beam was 3.90 Mev.

	Q	Excitation
	$Ca^{40}(d,p)Ca^{41}$	
Q_0	6.17 ± 0.05 Mev	0.0 Mev
Q_1	4.22 ± 0.05	1.95
Q_2	3.76 ± 0.05	2.41
Q_3	*3.2 ±0.1*	*3.0*
Q_4	*2.9 ±0.1*	*3.3*
Q_5	*2.7 ±0.1*	*3.5*
Q_6	*2.5 ±0.1*	*3.7*
Q_7	2.31 ± 0.05	3.86
	$O^{16}(d,p)O^{17}$	
Q_0	1.95	0.0
Q_1	1.06	0.89

TABLE II. Comparison of the end groups of protons from the two reactions $Ca^{40}(d,p)Ca^{41}$ and $A^{40}(d,p)A^{41}$. The observed extrapolated ranges were obtained from Fig. 4.

	Observed range	Aluminum correction	Corrected range	Proton energy
$Q_0{}^{Ca}$	92.4 cm	3.2 cm	95.6 cm	9.02 ± 0.02 Mev
$Q_0{}^{A}$	55.7	1.2	56.9	6.71 ± 0.02

It should be noticed that the deuteron beam must enter the gas target through an aluminum foil and, therefore, is reduced in energy from 3.90 Mev to 3.26 Mev. This explains why the observed range of the calcium protons is less in this case than in Fig. 2 where full beam energy was used.

As a check of the consistency of these results, $Q_0{}^{A}$ for argon can be computed using $Q_0{}^{Ca}$ for calcium obtained in Section II of this paper:

$$Q_0{}^{Ca}-Q_0{}^{A}=2.37\ \text{Mev},$$
$$Q_0{}^{A}=6.17-2.37=3.80\pm 0.06\ \text{Mev}.$$

This agrees closely to the value $Q_0{}^{A}=3.82\pm 0.05$ Mev reported by Pollard and Davison.[3]

IV. THE MASS DIFFERENCE ($Ca^{40}-A^{40}$)

If the value found in Eq. (1) is combined with the values found by Richards[5] and Bleuler,[4] the

TABLE III. Mass differences and the nuclear reactions from which they were computed, using $H^1=1.008128$, $D^2=2.014718$, $n=1.00897$ mass units.

Nuclei	Calculated mass difference	Reaction	Data used in calculation	Reference
$Ca^{41}-Ca^{40}$	0.99997±5	$Ca^{40}(d,p)Ca^{41}$	$Q_0^{Ca}=6.17\pm0.05$ Mev	This paper
$(A^{41}-A^{40})-(Ca^{41}-Ca^{40})$	0.00254±3	Comparison of end groups of $Ca^{40}(d,p)Ca^{41}$ and $A^{40}(d,p)A^{41}$	$Q_0^{Ca}-Q_0^{A}=2.37\pm0.03$ Mev	This paper
$A^{41}-A^{40}$	1.00249±5	$A^{40}(d,p)A^{41}$	$Q_0^{A}=3.82\pm0.05$ Mev	3
$Ca^{41}-K^{41}$	0.00047±7	$K^{41}(p,n)Ca^{41}$	$E_{thresh}=1.25\pm0.06$ Mev	5
$A^{41}-K^{41}$	0.00274±20	$A^{41}\rightarrow K^{41}+\beta^-$	$\beta^-_{max}=2.55\pm0.2$ Mev	4
$K^{40}-A^{40}$	0.0017	$A^{40}(p,n)K^{40}$	$E_{thresh}=2.4$ Mev	11
$K^{40}-A^{40}$	0.00167±10	$K^{40}\rightarrow A^{40}+\gamma$, K-capture	$\gamma=1.55\pm0.1$ Mev	10
$K^{40}-Ca^{40}$	0.00145±5	$K^{40}\rightarrow Ca^{40}+\beta^-$	$\beta^-_{max}=1.35\pm0.05$ Mev	9

difference in mass between A^{40} and Ca^{40} can be calculated. The data used in this calculation are summarized in Table III.

$$(Ca^{40}-A^{40})=[(A^{41}-A^{40})-(Ca^{41}-Ca^{40})]+(Ca^{41}-K^{41})-(A^{41}-K^{41}),$$
$$(Ca^{40}-A^{40})=2.54+0.47-2.74 \text{ mMU}$$
$$=0.27\pm0.21 \text{ mMU},$$

where the r.m.s. error has been taken. These data indicate that Ca^{40} is slightly heavier than A^{40}.

$Ca^{40}-A^{40}$ can also be obtained from the energy of radioactive decay of K^{40} by β^--emission[9] and K-capture:[10]

$$(Ca^{40}-A^{40})=(K^{40}-A^{40})-(K^{40}-Ca^{40}),$$
$$(Ca^{40}-A^{40})=1.67-1.45$$
$$=0.22\pm0.11 \text{ mMU (Table III)}.$$

There is excellent agreement between the two methods of calculating this mass difference.

If the 1.55-Mev γ-ray observed by Hirzel[10] is due to K-capture, then $K^{40}-A^{40}=1.67$ mMU. This agrees closely to the threshold energy for $A^{40}(p,n)K^{40}$ found by Richards,[11] which gives $K^{40}-A^{40}=1.7$ mMU. It appears that this threshold corresponds to the production of K^{40} in the ground state rather than in an excited state as was postulated.[11] The assumption that the threshold is for an excited state of K^{40} would make the agreement of these various mass differences worse. This disagreement would be large if the excited state of K^{40} lay several tenths of a Mev above the ground state. (The first excited state of K^{40} found from the reaction $K^{39}(d,p)K^{40}$ was 0.84 Mev above the ground state.[12])

V. ACKNOWLEDGMENT

The author would like to express his appreciation to Professor E. C. Pollard who assisted with many helpful discussions.

[9] Dželepow, Kopjova, and Vorobjov, Phys. Rev. **69**, 538 (1946).
[10] O. Hirzel and H. Wäffler, Helv. Phys. Acta **19**, 216 (1946).
[11] H. T. Richards and R. V. Smith, Phys. Rev. **74**, 1870 (1948).
[12] Vance L. Sailor, unpublished work.

The Absorption Spectrum of Atomic Sodium

E. R. THACKERAY*
University of Wisconsin, Madison, Wisconsin
(Received February 14, 1949)

Using a long optical path attained by the method of Kratz and Mack, the wave-lengths of the principal series of sodium in absorption have been measured to $n=73$, and observed to $n=79$. The members to $n=9$ have been resolved. The series limit has been computed to be 41449.65 ± 0.02 cm^{-1} from the center of gravity or 41449.69 ± 0.02 cm^{-1} from the lower hyperfine structure component, of the $3s\,^2S_{1/2}$ term. Forbidden $3s\,^2S_{1/2}-nd\,^2D_{3/2,5/2}$ were found up to $n=13$. A critically compiled table to all known levels, including $np\,^2P_{1/2,3/2}$ to $n=73$ and $nd\,^2D_{3/2,5/2}$ to $n=13$, is given. The pressure shift from a foreign gas is less than reported by some earlier observers.

EXPERIMENTAL

THE absorption spectrum of atomic sodium consists chiefly of the principal series, i.e., of transitions from the ground $3s\,^2S_{\frac{1}{2}}$ to the excited $np\,^2P_{\frac{1}{2},3/2}$ levels. Forbidden $3s\,^2S_{\frac{1}{2}}-nd\,^2D_{3/2,5/2}$ transitions occur with much lower intensity. In 1916 Wood and Fortrat[1] measured the principal series to $n=59$, resolving the first seven members. If their results are fitted to a Ritz formula the last three members show a marked discrepancy and the doublet separation of the last member resolved appears much too large. The present work has to do with the extension of the principal series and the forbidden $3s-nd$ series, and new measurements on the doublet separations.

In order to obtain absorption in a vapor at the low temperature and the low vapor pressure required to obtain sharp lines, it is necessary to have a long optical path. This was accomplished in this investigation by the use of the method and apparatus developed by H. R. Kratz and J. E. Mack,[2] in which the long optical path is achieved by repeated traversals between a concave spherical mirror and a totally reflecting prism. The absorption tube was maintained at a constant temperature to within ±0.5°C by means of a balanced Wheatstone bridge circuit.[3] The furnace windings of the tube acted as one arm of the bridge. The galvanometer was replaced by a sensitive Weston 534 relay, which in turn was connected by means of a lock-in circuit of two Weston 712 relays to a power relay which controlled the heating circuit.

The sodium used was of ordinary chemical grade. It was placed at the center of the tube in an iron boat after a cleansing in water-free benzene. After the insertion of the sodium the tube was evacuated for 6 or 8 hours and then filled with helium to a pressure of about 1 or 2 mm.

The source of continuous radiation was a General Electric AH-6 mercury arc lamp. Chiefly because of the low reflectivity of the aluminum surface of the concave spherical mirror in the wave-length region in which most of the members of the principal series were found, the number of traversals was limited to six, yielding an absorption path of about 23 meters.

The spectrograms were made with a 21 foot, 15000 lines/inch grating 6-inches wide, in a Rowland mounting. Out to 2600A the third order, with a dispersion of about 0.88A/mm, was used, and beyond that, the fourth order, with a dispersion of 0.66A/mm. Suitable filters of bromine and chlorine vapor were used to prevent the overlapping of orders.

For the lower series members Eastman 103-O spectroscopic plates were used and exposure times ranged from 20 minutes to 1 hour. Beyond 2852A, the faintness of the continuum made it advisable to use 103a-O plates, with exposures of 10 to 20 hours. The wave-lengths of the absorption lines were found by comparing them with secondary standard and recommended iron lines[4] from a Pfund arc.[5] Except where the contrary is stated, each line was measured on at least two different plates. The last eight members of the principal series were measured on only the best plate.

A different temperature was used for the optimum sharpness of each doublet resolved. For the higher series members many lines were found satisfactorily sharp on a single plate. The temperature, t, and the corresponding vapor pressure,[6] p, of sodium were as follows:

	t	p
Resolved doublets	130°C to 182°C	10^{-6} to $4.5\cdot10^{-5}$ mm Hg
High series members	326°C	$3.5\cdot10^{-2}$ mm Hg
Forbidden lines, $3s-nd$	218°C to 330°C	$3\cdot10^{-4}$ to $3\cdot10^{-2}$ mm Hg

* Now at Regina College, Regina, Saskatchewan, Canada.
[1] R. W. Wood and R. Fortrat, Astrophys. J. **43**, 73 (1916).
[2] H. R. Kratz and J. E. Mack, J. Opt. Soc. Am. **32**, 457 (1942); H. R. Kratz, Phys. Rev. **75**, 1844 (1949).
[3] H. S. Roberts, J. Wash. Acad. Sci. **11**, 401 (1921).
[4] Commission des Etalons de Longueur D'onde et des Tables de Spectres Solaires. Trans. Int. Astron. Union **6**, 79 (1939).
[5] Commission des Etalons de Longueur D'onde et des Tables de Spectra Solaires. Trans. Int. Astron. Union **2**, 41 (1925).
[6] R. W. Ditchburn and J. C. Gilmour, Rev. Mod. Phys. **13**, 310 (1941).

Table I. Principal series of sodium in absorption.

n	λ (air) Angstrom units $3s\ ^2S_{1/2}-np\ ^2P_{1/2}$	λ (air) Angstrom units $3s\ ^2S_{1/2}-np\ ^2P_{3/2}$	ν (vacuum) cm^{-1} $3s\ ^2S_{1/2}-np\ ^2P_{1/2}$	ν (vacuum) cm^{-1} $3s\ ^2S_{1/2}-np\ ^2P_{3/2}$
4	3302.987	3302.375	30266.94	30272.55
5	2853.023	2852.816	35040.27	35042.79
6	2680.421	2680.331	37296.51	37297.76
7	——	——	——	——
8	——	——	——	——
9	2512.149[b]	2512.121[b]	39794.53	39795.00
10	2490.701±		40137.23	
11	2475.532		40383.16	
12	2464.371		40566.03	
13	2455.916		40705.68	
14	2449.369		40814.47	
15	2444.180		40901.11	
16	2440.001		40971.16	
17	2436.580		41028.68	
18	2433.751		41076.37	
19	2431.388		41116.28	
20	2429.373		41150.39	
21	2427.672		41179.22	
22	2426.195		41204.28	
23	2424.918		41225.88	
24	2423.813		41244.77	
25	2422.835		41261.42	
26	2421.973		41276.11	
27	2421.207		41289.16	
28	2420.528		41300.74	
29	2419.922		41311.09	
30	2419.380		41320.34	
31	2418.881		41328.87	
32	2418.434		41336.50	
33	2418.025		41343.49	
34	2417.662		41349.70	
35	2417.323		41355.50	
36	2417.012		41360.82	
37	2416.729		41365.66	
38	2416.469		41370.11	
39	2416.226		41374.27	
40	2416.006		41378.04	
41	2415.801		41381.55	
42	2415.609		41384.84	
43	2415.430		41387.91	
44	2415.265		41390.73	
45	2415.113		41393.34	

TABLE I.—*Continued.*

n	λ (air) Angstrom units $3s\ ^2S_{1/2}-np\ ^2P_{1/2}$	λ (air) Angstrom units $3s\ ^2S_{1/2}-np\ ^2P_{3/2}$	ν (vacuum) cm^{-1} $3s\ ^2S_{1/2}-np\ ^2P_{1/2}$	ν (vacuum) cm^{-1} $3s\ ^2S_{1/2}-np\ ^2P_{3/2}$
46	2414.971		41395.77	
47	2414.835		41398.10	
48	2414.708		41400.28	
49	2414.593		41402.25	
50	2414.481		41404.18	
51	2414.373		41406.03	
52	2414.276		41407.69	
53	2414.182		41409.30	
54	2414.094		41410.81	
55	2414.013		41412.20	
56	2413.932		41413.59	
57	2413.856		41414.89	
58	2413.788		41416.06	
59	2413.722		41417.18	
60	2413.660		41418.26	
61	2413.599		41419.30	
62	2413.539		41420.33	
63	2413.485		41421.26	
64	2413.434		41422.13	
65	2413.382		41423.03	
66	2413.337[b]		41423.80	
67	2413.291[b]		41424.59	
68	2413.248[b]		41425.32	
69	2413.208[b]		41426.01	
70	2413.170[b]		41426.66	
71	2413.136[b]		41427.25	
72	2413.102[b]		41427.83	
73	2413.069[b]		41428.40	
74	(2413.035)		(41428.98)	
75	(2413.003)		(41429.53)	
76	(2412.971)		(41430.07)	
77	(2412.942)		(41430.58)	
78	(2412.913)		(41431.07)	
79	(2412.885)		(41431.55)	
∞	(2411.832)		(41449.65±0.02)	

[b] Measurement from one plate only.
± For the unresolved 10p line, the readings on two plates differed by 0.007A.
( ) Extrapolated limit, or interpolated value of observed but unmeasured line.

The maximum variations of the temperature and pressure in the grating room for long exposures were 0.3°C and 6 mm, respectively. These variations, together with the line width, appear to have been the limiting factor in the number of members resolved near the series limit.

In the course of an exposure of 10 hours or longer, the pressure of the foreign gas increased as much as 55 mm at the higher operating temperatures. Since pumping was not feasible during an exposure the pressure was observed and found to range from about 6 to 55 mm for the different plates. The nature of the foreign gas was not investigated.

TABLE II. Forbidden transitions $3s\ ^2S_{\frac{1}{2}}-nd\ ^2D$ in sodium.

n	λ (air) Angstrom units $3s\ ^2S_{1/2}-nd\ ^2D$	ν (vacuum) cm^{-1} $3s\ ^2S_{1/2}-nd\ ^2D$
3	3426.858	29172.92
4	2893.619	34548.70
5	2699.217[b]	37036.81
6		
7		
8	2516.296	39729.00
9	2493.600	40090.57
10	2477.617	40349.17
11	2465.932	40540.35
12	2457.11±	40685.9
13	2450.31[b]	40798.8

[b] Measurement from one plate only. The $3s-5d$ and $3s-13d$ lines were faint.
± The readings on two plates differed by 0.02A.

TABLE III. Energy levels of neutral sodium, NaI (cm^{-1}).

n	$ns^2S_{1/2}$	$np^2P_{1/2}$	$np^2P_{3/2}$	$\Delta\nu(^2P)$	$nd^2D_{3/2}$	$nd^2D_{5/2}$	$\Delta\nu(^2D)$	$nf^2F_{5/2,7/2}$
3	41449.6500ah	24493.4672hm	24476.2709hm	17.1963hm	12276.746m	12276.795m	−0.0494m	
4	15709.78m	11182.77g	11177.14g	5.63g	6900.861m	6900.896m	−0.0346m	6861.0p
5	8248.954m	6409.38	6406.86	2.52	4412.845m	4412.869m	−0.0230m	4392.0r
6	5077.004m	4153.14	4151.89	1.25	3062.350m	3062.363m	−0.0124m	3049.5r
7	3437.576m	(2909.25)	(2908.51)	(0.74)	2248.688m			2240.4r
8	(2481.03)d	(2151.11)	(2150.64)	(0.47)	1720.65			1715.6r
9	(1874.67)d	1655.12b	1654.65b	0.47	1359.08			1356.4r
10	(1466.24)d	1312.42±			1100.48			(1097.9)s
11	(1178.096)z	1066.49			909.30			(907.3)s
12	(967.246)z	883.62			763.8			
13	(808.327)z	743.97			650.8b			
14	(685.586)z	635.18			(561.15)z			
15		548.54			(488.75)z			
16		478.49						
17		420.97						
18		373.28						
19		333.37						
20		299.26						
21		270.43						
22		245.37						
23		223.77						
24		204.88						
25		188.23						
26		173.54						
27		160.49						
28		148.91						
29		138.56						
30		129.31						
31		120.78						
32		113.15						
33		106.16						
34		99.95						
35		94.15						
36		88.83						
37		83.99						
38		79.54						
39		75.38						
40		71.61						
41		68.10						
42		64.81						
43		61.74						
44		58.92						
45		56.31						
46		53.88						
47		51.55						
48		49.37						
49		47.40						
50		45.47						
51		43.62						
52		41.96						
53		40.35						
54		38.84						
55		37.45						
56		36.06						
57		34.76						
58		33.59						
59		32.47						
60		31.39						
61		30.35						
62		29.32						
63		28.39						
64		27.52						
65		26.62						
66		25.85b						
67		25.06b						
68		24.33b						
69		23.64b						
70		22.99b						
71		22.40b						
72		21.82b						
73		21.25b						
74		(20.67)						
75		(20.12)						
76		(19.58)						
77		(19.07)						
78		(18.58)						
79		(18.10)						

a In this number, the last two digits (zeros), which have no significance for the absolute value of the term, have been arbitrarily added for convenience in expressing certain accurately known differences. The probable error in the value of the term, estimated from the series limit, is about ±0.02 cm^{-1}. In the term values given elsewhere to 2 digits after the decimal point (except 10p), the uncertainty is about ±0.04 cm^{-1}. These estimates depend upon our acceptance of Kayser's values for the index of air; i.e., the terms ought to be recalculated when new values are available for the refractive index of air.

b Measurement for one plate only.

d Experimental values of Datta[1] corrected for the ground state are:
$8s = 2481.28$
$9s = 1875.14$
$10s = 1466.6$

g Mean between this work and unpublished values from the infra-red solar absorption transition $4s - 4p$, kindly supplied by L. Goldberg. The separate values are:
$4p^2\,P_{1/2}$—This work, 11182.71; Goldberg (22083.9A), 11182.83.
$4p^2\,P_{3/2}$—This work, 11177.10; Goldberg (22056.4A), 11177.19.

h Center of gravity of hyperfine structure. The following is a critical estimate of the hyperfine structure of sodium, kindly supplied by Hack Arroe. $\Delta\nu(3s^2S_{1/2})$ is from the radiofrequency measurements of Millman and Kusch.[2] The values assigned to $\Delta\nu(3p^2P_{1/2})$ and $\Delta\nu(3p^2P_{3/2})$ agree with the experimental results of Meissner and Puft (reference 9), Jackson and Kuhn,[3] and Arroe[4] within the limits of experimental error.

$3s^2S_{1/2^1} = 41449.6869$
$3s^2S_{1/2^2} = 41449.6278$
$\Delta\nu(3s^2S_{1/2}) = 0.059103 \pm 0.000002$

$3p^2P_{1/2^1} = 24493.4706$
$3p^2P_{1/2^2} = 24493.4652$
$\Delta\nu(3p^2P_{1/2}) = 0.0054 \pm 0.0002$

$3p^2P_{3/2^{0\text{ to }3}} = 24476.2729$ to 24476.2697
$\Delta\nu(3p^2P_{3/2}, \text{total}) = 0.0032 \pm 0.0002$

m Meissner and Luft, reference 9, interferometric values, corrected for the ground state found in this work. This work, which yields less accurate differences, would independently give the following center-of-gravity values:
$3d = 12276.73$
$4d = 6900.95$
$5d = 4412.84$

p Experimental value of Paschen[5] corrected for the ground state.

r Experimental value of Rood and Sawyer[6] corrected for the ground state.

s Experimental values of Rood and Sawyer[6] yield
$10f = 1098.7$
$11f = 911.0$

z Experimental values of Zickendraht[7] corrected for the ground state are:
$11s = 1176.2$
$12s = 966.8$
$13s = 805.1$
$14s = 680.1$
$14d = 559.7$
$15d = 491.0$

± This value is uncertain by about ±0.06.

( ) Interpolated value supplied by J. E. Mack.

[1] S. Datta, Proc. Roy. Soc. London, A, **99**, 69 (1921).
[2] S. Millman and P. Kusch, Phys. Rev. **58**, 438 (1940).
[3] D. A. Jackson and H. Kuhn, Proc. Roy. Soc. London, A, **167** (1938).
[4] Hack Arroe, The Gold Medal Thesis in Physics, 1945, University of Copenhagen.
[5] F. Paschen, Ann. d. Physik, **27**, 537 (1908).
[6] P. Rood and R. A. Saywer, Astrophys. J., **87**, 68 (1938).
[7] H. Zickendraht, Ann. d. Physik, **31**, 233 (1910).

RESULTS

The wave-lengths of the principal series and of the forbidden $3s\ ^2S_{\frac{1}{2}}-nd\ ^2D_{3/2,\,5/2}$ transitions, referred to air at 15°C and 760 mm, are recorded in Tables I and II, respectively. These wave-lengths have been reduced to vacuum wave numbers by use of the corrections given in Kayser's "Tabelle der Schwingungszahlen." The wave-lengths as measured on different plates agree in almost all cases to 0.003A, and all agree to within 0.005A with two exceptions marked ± in the tables. In the $3s-10p$ line evidently the unresolved doublet separation was enough to make the reading unreliable. The random error in the wave numbers does not exceed about ±0.04 cm^{-1}, except where indicated. The ± estimates on the wave numbers do not take into account the uncertainty in the dispersion of air.

In Table III the values of the S, P, D and F levels are recorded. For completeness the values of other observers are included for levels unobserved in this work or measured more accurately by others. The limit of the principal series, computed in collaboration with Mr. J. G. Hirschberg, Jr., by the method of Shenstone and Russell,[7] was found to be 41449.65±0.02 cm^{-1} from the center of gravity of the ground term or 41449.69±0.02 cm^{-1} from the lower hyperfine structure level $3s\ ^2S_{\frac{1}{2}}$,[1] the ionization potential is thus 5.138±0.001 volts, the uncertainty in the ionization potential lying principally in the value of the electron volt.[8] The smallness of the uncertainty as to the length of the series may be credited to the closeness of the approach to the series limit. Other low levels, including the separations of the $3p\ ^2P$ and the $nd\ ^2D$ terms up to $6d$, are from the definitive work of Meissner and Luft,[9] corrected to the ground level value found in this work. Values for the hyperfine structure of the $3s\ ^2S_{\frac{1}{2}}$ and $3p\ ^2P_{\frac{1}{2},3/2}$ levels were kindly supplied by Mr. Hack Arroe.

The $3s-7p$ and $3s-8p$ lines were not observed, for they fell in a gap in the continuum. The $7p$ and $8p$ term values have been computed by use of a Ritz formula.

A microphotometer traced of the higher members of the principal series of sodium is shown in Fig. 1. It shows the presence of lines to $n=79$, or approximately 1 angstrom unit from the series limit. [*Note added in Proof:* New microphotometer traces clearly show the presence of lines to $n=82$.] Although the present work does not include any intensity measurements, it can be stated that microphotometer traces traversing the series limit do not show the sudden change in absorption at the series limit that has been reported by some, but not all, previous observers.[10–13] Our failure to find the discontinuity may have been a result of our careful limitation of the pressure to avoid unnecessary line breadth.

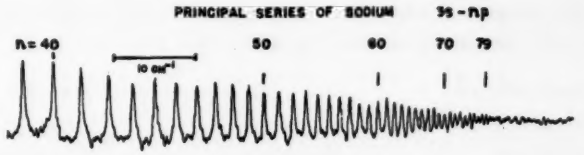

FIG. 1. A microphotometer trace of the higher members of the principal series of sodium showing the presence of lines to $n=79$.

DISCUSSION OF RESULTS

The principal series has been measured for values of n to 73 and observed to 79. This is 14 to 20 members beyond the observations of Wood and Fortrat. The wave-lengths found are in general slightly shorter than those of Wood and Fortrat. The energy levels found, as measured from the series limit, are both larger and smaller.

The number of doublets resolved was not increased but the separation of 0.028A found for $n=9$ was much smaller than that of Wood and Fortrat, who reported 0.082A. Although there was some difficulty in resolving this doublet, there is no doubt that the separation obtained here is much nearer the true one than is that of Wood and Fortrat: the over-all width of the line pair measured only 0.06A. A calculation, assuming an n_{eff}^{-3} law of $\Delta\nu$, yields 0.019A. When the possible experimental error is considered in the measurement of the barely resolved components, the observed value is in fair agreement.

The forbidden $3s\ ^2S_{\frac{1}{2}}-nd\ ^2D_{3/2,\,5/2}$ transitions were found up to $n=13$, since the absorption occurred in a field-free region, it ought undoubtedly to be attributed principally to electric quadrupole absorption. These $3s-nd$ transitions to $n=20$ have been previously observed in the presence of an electric field by Ny Tsi-Ze and Weng Wen-Po.[14] The expected pressure shift,[15] due to foreign gas, was not found. A shift of the order of magnitude found in the sodium D lines by Kleman and Lindholm[16] would have been too small for detection at

[7] A. G. Shenstone and H. N. Russell, Phys. Rev. **39**, 415 (1932).
[8] J. W. DuMond and E. R. Cohen, Rev. Mod. Phys. **20**, 82 (1948).
[9] K. W. Meissner and K. F. Luft, Ann. d. Physik **31**, 233 (1937).
[10] R. W. Wood, Phil. Mag. **16**, 945 (1908).
[11] G. R. Harrison, Phys. Rev. **25**, 768 (1925).
[12] H. Bartels, Zeits. f. Physik **105**, 704 (1937).
[13] R. W. Ditchburn, Zeits. f. Physik **107**, 719 (1937).
[14] Ny Tsi-Ze and Weng Wen-Po, J. Phys. et le Radium **7**, 193 (1936).
[15] S. Tolansky, *High Resolution Spectroscopy* (Pitman Publishing Corp., Chicago, 1947).
[16] B. Kleman and E. Lindholm, Arkiv Mat., Astro. Och. Fys. 32B, No. 10 (1945).

the pressures used in this work. Measurements at three pressures on lines $3s-31p$ and $3s-32p$ yield:

Total pressure	$\lambda(n=31)$	$\lambda(n=32)$
18 mm	2418.881A	2418.435A
28 mm	2418.878A	2418.432A
43 mm	2418.883A	2418.435A

For larger values of n there was a small statistical trend towards longer wave-lengths for increased pressure, but in all these cases the observed fluctuation is within the errors of measurement, and we find a pressure shift of zero within ± 0.006 cm^{-1}/mm Hg.

ACKNOWLEDGMENTS

The author wishes to express his gratitude to Professor J. E. Mack for his constant assistance and encouragement, to Mr. Hack Arroe for the critical estimate on the hyperfine structure, and to the University of Wisconsin for the opportunity of carrying out the investigation and for their grants of an honorary scholarship and the Charles E. Mendenhall fellowship.

PHYSICAL REVIEW VOLUME 75, NUMBER 12 JUNE 15, 1949

The Principal Series of Potassium, Rubidium, and Cesium in Absorption*

H. R. KRATZ**
University of Wisconsin, Madison, Wisconsin
(Received February 14, 1949)

The principal series of potassium, rubidium, and cesium in absorption have been measured. The doublet fine-structure has been resolved out to $17p$ in potassium, to $26p$ in rubidium, and to $21p$ in cesium; the doublet fine-structure interval varies in each spectrum inversely as the cube of the effective principal quantum number. In cesium, the doublet intensity ratio, instead of having a maximum, increases with increasing n as far as it can be followed. Higher series members, with their doublet fine-structure unresolved, have been measured to $79p$ in potassium, to $77p$ in rubidium, and to $73p$ in cesium. The series limits, calculated from the lowest hyperfine structure levels, are: K^{39} $4s\ ^2S_{\frac{1}{2}}{}^1-\infty=35009.83$ cm^{-1}, Rb^{85} $5s\ ^2S_{\frac{1}{2}}{}^2-\infty=33691.02$ cm^{-1}, Cs $6s\ ^2S_{\frac{1}{2}}{}^3=31406.71$ cm^{-1}. The hyperfine structure of the ground level $6s\ ^2S_{\frac{1}{2}}$ has been resolved in each member of the principal series of cesium.

INTRODUCTION

THE absorption spectra of the alkali metal atoms consist mainly of the principal series, corresponding to transitions from the normal $^2S_{\frac{1}{2}}$ level to the excited $np\ ^2P_{1/2,3/2}$ levels.[1] The doublet interval $np\ ^2P_{1/2}-np\ ^2P_{3/2}$ increases with increasing atomic number and decreases with increasing principal quantum number n.

A considerable amount of work had previously been done on the absorption spectra of the alkali metal atoms, but since the early days of investigations of complex spectra, work on these simple spectra had been almost abandoned. The most extensive of the early work on the spectra of the alkali metal atoms is that of Wood and Fortrat[2] on sodium, in which they measured the doublet separations of the first seven members of the principal series and the higher members of the series, with the doublet structure unresolved, out to the 59th member.[3] Only the first member of the principal series of lithium has been resolved,[4] and 41 members measured.[5,6] Previous to this investigation, five members of the principal series of potassium,[7] six members of rubidium,[6] and nine members of cesium[6] had been resolved. Because of uncertainties in some of these wave-length measurements, and the relatively small numbers of doublets resolved, it seemed desirable to determine accurately the wave-lengths of the principal series as observed in absorption. In particular, it was the purpose of this investigation to measure the doublet separations of as many members of the principal series of potassium, rubidium, and cesium as possible, in order to determine accurately the variation of the doublet interval with the principal quantum number. The higher members of the principal series

* The experimental part of this paper was completed in 1942, having been begun at Wisconsin and continued at Princeton University. The cesium plates were measured after the war while the author was at Los Alamos.

** Now at the Research Laboratory, General Electric Company, Schenectady, New York.

[1] Lines corresponding to forbidden transitions to $nd\ ^2D_{3/2,5/2}$, $nf\ ^2F_{5/2,7/2}$ and levels of even higher l were also observed on the same plates as the principal series. Measurements of these lines will be reported in a forthcoming paper by J. E. Mack.

[2] R. W. Wood and R. Fortrat, Astrophys. J. **43**, 73 (1916).

[3] Additional work on the absorption spectrum of sodium, carrying the measurements to $73p$, is reported by E. R. Thackeray, Phys. Rev. **75**, 1840 (1949).

[4] N. A. Kent, Astrophys. J. **40**, 337 (1914).

[5] Huppers, Zeits. f. Wiss. Phot. **13**, 46 (1914).

[6] P. V. Bevan, Proc. Roy. Soc. London **A83**, 421 (1910).

[7] S. Datta, Proc. Roy. Soc. London **A99**, 69 (1921).

of these spectra, with their doublet structure unresolved, were also measured.

EXPERIMENTAL

From considerations of the various causes of spectral line breadth, it can be seen to be necessary in order to produce absorption lines sharp enough for the resolution of close doublets, that: (a) the temperature and pressure of the absorbing vapor be sufficiently low, and (b) the pressure of any foreign gas be low. In order to have the pressure of the absorbing vapor low, and at the same time have the number of atoms in the optical path necessary to produce absorption, a long optical path within the absorbing vapor is required.

In this investigation, a long optical path was produced by repeated traversals of the length of a tube containing the alkali metal vapors.[8] The light beam was reflected at one end of the tube by a totally reflecting prism and at the other end by a spherical mirror whose radius of curvature was equal to the distance between the prism and the mirror. The absorption tube was a steel tube 13½-feet long and 3 inches in diameter; each end of the tube was cooled by a water jacket. The optical parts were located beyond the water jackets at either end of this tube. The section of tube between the water jackets was heated by a d.c. current flowing in a winding of nickel ribbon. The temperature of this section of the tube was maintained constant to within ±0.1°C by means of a balanced Wheatstone bridge circuit,[9] the nickel windings on the tube serving as one arm of the bridge circuit. The circuit was adjustable to any temperature between 100° and 500°C. The entire apparatus was mounted on a 2½×4-inch steel I-beam to supply the rigidity necessary for accurate adjustment of the optical system. The optical system was designed for a total of twelve traversals of the absorption tube, but it was possible to adjust the system so that the twenty-traversal beam could be seen. Most of the absorption spectra were taken with from six to twelve traversals, giving an absorption path length of 24 to 48 meters. The light source was a General Electric, Type AH-6 water-cooled high-pressure mercury arc with a quartz water jacket. It had a fairly strong continuum throughout the wave-length region investigated. The alkali metals were prepared in a vacuum by reducing their chlorides with calcium metal.[10]

The procedure for filling the absorption tube with an alkali metal vapor was as follows: A bulb of the alkali metal was placed near the center of the tube,

TABLE I. Principal series of potassium.

	λ(air)		ν(vacuum)		
n	$4s\,^2S_{1/2}-np\,^2P_{1/2}$	$4s\,^2S_{1/2}-np\,^2P_{3/2}$	$4s\,^2S_{1/2}-np\,^2P_{1/2}$	$4s\,^2S_{1/2}-np\,^2P_{3/2}$	$\Delta\nu_p$
4	7698.979*	7664.907*	12985.17	13042.89	57.72
5	4047.208	4044.136	24701.44	24720.20	18.76
6	3447.376	3446.376	28999.29	29007.70	8.41
7	3217.615	3217.151	31069.98	31074.46	4.48
8	3102.051	3101.791	32227.42	32230.12	2.70
9	3034.911	3034.751	32940.34	32942.08	1.74
10	2992.215	2992.108	33410.34	33411.54	1.20
11	2963.277	2963.203	33736.60	33737.44	0.84
12	2942.713	2942.661	33972.34	33972.94	0.60
13	2927.562	2927.521	34148.15	34148.63	0.48
14	2916.065	2916.033	34282.77	34283.15	0.38
15	2907.129	2907.103	34388.16	34388.46	0.30
16	2900.042	2900.021	34472.18	34472.43	0.25
17	2894.329	2894.311	34540.23	34540.44	0.21
18	2889.640		34596.27		
19	2885.760		34642.78		
20	2882.510		34681.84		
21	2879.758		34714.98		
22	2877.405		34743.37		
23	2875.384		34767.78		
24	2873.628*		34789.03		
25	2872.093		34807.62		
26	2870.756		34823.83		
27	2869.564±		34838.30		
28	2868.509		34851.11		
29	2867.570*		34862.52		
30	2866.733		34872.70		
31	2865.974		34881.94		
32	2865.295		34890.20		
33	2864.675		34897.75		
34	2864.115		34904.57		
35	2863.605		34910.79		
36	2863.136		34916.51		
37	2862.711		34921.69		
38	2862.319		34926.47		
39	2861.956		34930.91		
40	2861.623		34934.97		
41	2861.316		34938.72		
42	2861.031		34942.20		
43	2860.765		34945.45		
44	2860.517		34948.48		
45	2860.289		34951.26		
46	2860.077		34953.85		
47	2859.875		34956.32		
48	2859.688		34958.61		
49	2859.514		34960.73		
50	2859.342		34962.83		
51	2859.192		34964.67		
52	2859.046		34966.45		
53	2858.912		34968.09		
54	2858.781		34969.69		
55	2858.660		34971.17		
56	2858.546		34972.57		
57	2858.439		34973.88		
58	2858.335		34975.15		
59	2858.236		34976.36		
60	2858.143		34977.50		
61	2858.052		34978.62		
62	2857.972		34979.60		
63	2857.886		34980.65		
64	2857.810		34981.58		
65	2857.738		34982.47		
66	2857.672		34983.27		
67	2857.604		34984.10		
68	2857.545		34984.83		
69	2857.484		34985.57		
70	2857.429		34986.25		
71	2857.371		34986.96		
72	2857.324		34987.53		
73	2857.270		34988.19		
74	2857.216		34988.85		
75	2857.17		34989.4		
76	2857.13		34989.9		
77	2857.08		34990.5		
78	2857.05		34990.8		
79	2857.02		34991.2		
∞	2855.505		35009.82 ±0.03		

* Wave-lengths for $n=4$ are from the vacuum arc measurements of C. W. Hetzler, R. W. Boreman, and K. Burns, Phys. Rev. **48**, 656 (1935).
± Measurement relatively uncertain (see text).

[8] H. R. Kratz and J. E. Mack, J. Opt. Soc. Am. **32**, 457 (1942).
[9] H. S. Roberts, J. Opt. Soc. Am. **6**, 965 (1922).
[10] J. Strong, *Procedures in Experimental Physics* (Prentice Hall, Inc., New York, 1938), p. 531.

TABLE II. Principal series of rubidium.

	λ(air)		ν(vacuum)		
n	$5s\ ^2S_{1/2}$ $-np\ ^2P_{1/2}$	$5s\ ^2S_{1/2}$ $-np\ ^2P_{3/2}$	$5s\ ^2S_{1/2}$ $-np\ ^2P_{1/2}$	$5s\ ^2S_{1/2}$ $-np\ ^2P_{3/2}$	$\Delta\nu_p$
5	7947.60*	7800.227*	12578.96	12816.62	237.66
6	4215.524	4201.792	23715.19	23792.69	77.50
7	3591.572	3587.050	27835.05	27870.14	35.09
8	3350.812±	3348.696±	29834.96	29853.82	18.86
9	3229.156	3227.979	30958.94	30970.22	11.28
10	3158.259	3157.530	31653.88	31661.19	7.31
11	3113.047	3112.566	32113.58	32118.55	4.97
12	3082.340	3082.003	32433.50	32437.04	3.54
13	3060.491	3060.247	32665.03	32667.63	2.60
14	3044.368	3044.182	32838.02	32840.02	2.00
15	3032.120	3031.979	32970.66	32972.19	1.53
16	3022.591	3022.478	33074.59	33075.83	1.24
17	3015.029	3014.938	33157.54	33158.54	1.00
18	3008.923	3008.847	33224.83	33225.67	0.84
19	3003.923	3003.862	33280.13	33280.81	0.68
20	2999.776	2999.725	33326.13	33326.70	0.57
21	2996.299	2996.256	33364.81	33365.29	0.48
22	2993.352	2993.313	33397.66	33398.09	0.43
23	2990.835	2990.800	33425.76	33426.15	0.39
24	2988.665	2988.634	33450.03	33450.38	0.35
25	2986.782	2986.754	33471.11	33471.43	0.32
26	2985.140	2985.117	33489.53	33489.79	0.26
27	2983.679		33505.92		
28	2982.406		33520.22		
29	2981.278		33532.91		
30	2980.269		33544.26		
31	2979.362		33554.47		
32	2978.554		33563.57		
33	2977.819		33571.85		
34	2977.156		33579.34		
35	2976.555		33586.11		
36	2976.006		33592.31		
37	2975.505		33597.96		
38	2975.046		33603.14		
39	2974.620		33607.96		
40	2974.232		33612.34		
41	2973.874		33616.38		
42	2973.541		33620.15		
43	2973.236		33623.61		
44	2972.951		33626.83		
45	2972.688		33629.80		
46	2972.441		33632.60		
47	2972.210		33635.21		
48	2971.996		33637.63		
49	2971.796		33639.89		
50	2971.609		33642.01		
51	2971.431		33644.02		
52	2971.264		33645.96		
53	2971.105		33647.72		
54	2970.962		33649.33		
55	2970.819		33650.95		
56	2970.690		33652.41		
57	2970.568		33653.80		
58	2970.452		33655.11		
59	2970.339		33656.39		
60	2970.237		33657.55		
61	2970.136		33658.69		
62	2970.038		33659.80		
63	2969.948		33660.82		
64	2969.861		33661.81		
65	2969.779		33662.73		
66	2969.700		33663.63		
67	2969.625		33664.48		
68	2969.554		33665.28		
69	2969.487		33666.04		
70	2969.422		33666.78		
71	2969.359		33667.49		
72	2969.305		33668.11		
73	2969.245		33668.79		
74	2969.195		33669.36		
75	2969.138		33670.01		
76	2969.085		33670.61		
77	2969.045		33671.07		
∞	2967.226		33690.96 ±0.03		

* Wave-lengths for $n=5$ are from the vacuum arc measurements of C. W. Hetzler, R. W. Boreman, and K. Burns, Phys. Rev. **48**, 656 (1935).
± Measurement relatively uncertain (see text).

and the tube was evacuated and then filled to a pressure of 10 mm Hg with helium which had been dried by passing through a liquid air trap. The helium was introduced to prevent the alkali metal vapors from distilling too rapidly to the water jackets and to prevent the vapors from condensing on the optical parts. After the tube was filled with helium, the bulb of alkali metal was broken and the tube heated at the required temperature for a time sufficient to allow the section of tube between the water jackets to become completely filled with vapor.

The preliminary exposures to determine the optimum temperature of the absorption tube for different members of a series were taken with a Hilger E-1 quartz prism spectrograph. The plates on which the final measurements were made were taken with the 21-foot grating spectrograph at Princeton. This spectrograph had a nominal resolving power of approximately 300,000 in the second order. All the plates on which measurements were made were taken in the second order of the grating except those of wave-length greater than 4000A, for which the first order was used. The exposures at wave-lengths less than 3100A were taken on Eastman 33 spectrographic plates, and because of the shorter exposures required for longer wave-lengths, most of those at wave-lengths greater than 3100A were taken on Eastman Spectrum Analysis plates. The exposure times varied from two minutes, for the second member of the cesium series, to eight hours, for the higher members of the potassium series. Most of the exposure times, however, were between two and five hours.

The temperatures t, and the corresponding vapor pressures p,[11] that were required for resolving the doublet structure of the low members of the series and recording the unresolved higher members of the series are:

	Resolved Doublets	High Series Members
Potassium	$t=116°$ to 243°C $p=6\cdot10^{-5}$ to $4\cdot10^{-2}$ mm Hg	$t=303$°C $p=3\cdot10^{-1}$ mm Hg
Rubidium	$t=52°$ to 158°C $p=5\cdot10^{-6}$ to $6\cdot10^{-3}$ mm Hg	$t=270$°C $p=5\cdot10^{-1}$ mm Hg
Cesium	$t=37°$ to 248°C $p=4\cdot10^{-6}$ to $4\cdot10^{-1}$ mm Hg	$t=260$°C $p=6\cdot10^{-1}$ mm Hg

A different temperature, and hence a separate exposure, was required for nearly every resolved doublet in order to produce absorption lines of optimum sharpness. The relatively high vapor pressure of $4\cdot10^{-1}$ mm that was used for the highest series member of cesium whose doublet structure was resolved, was necessary because of the large intensity ratio of about 25:1 that exists between

[11] R. W. Ditchburn and J. C. Gilmour, Rev. Mod. Phys. **13**, 310 (1941).

TABLE III. Principal series of cesium.

		$6s\ ^2S_{\frac{1}{2}}(F=3)-np\ ^2P_J$			$6s\ ^2S_{\frac{1}{2}}(F=4)-np\ ^2P_J$			
n	J	λ(air)	ν(vacuum)	$\Delta\nu_p$	λ(air)	ν(vacuum)	$\Delta\nu_p$	hfs $\Delta\nu$
6	1/2	8943.50*	11178.24	554.11	*			
	3/2	8521.10*	11732.35		*			
7	1/2	4593.114[ab]	21765.65	181.01	4593.193[ab]	21765.27	181.06	0.38
	3/2	4555.228[ab]	21946.66		4555.298[ab]	21946.33		0.33
8	1/2	3888.570[b]	25709.14	82.64	3888.613[b]	25708.85	82.63	0.29
	3/2	3876.109[b]	25791.78		3876.155[b]	25791.48		0.30
9	1/2	3617.271[b]	27637.29	44.67	3617.313[b]	27636.98	44.65	0.31
	3/2	3611.435[b]	27681.96		3611.478[b]	27681.63		0.33
10	1/2	3480.042[b]	28727.09	26.84	3480.080[b]	28726.77	26.87	0.32
	3/2	3476.794[b]	28753.93		3476.830[b]	28753.64		0.29
11	1/2	3399.963	29403.68	17.42	3399.999	29403.37	17.43	0.31
	3/2	3397.949	29421.10		3397.984	29420.80		0.30
12	1/2	3348.805	29852.85	11.87	3348.840	29852.54	11.86	0.31
	3/2	3347.474	29864.72		3347.510	29864.40		0.32
13	1/2	3314.040	30166.00	8.51	3314.074	30165.69	8.51	0.31
	3/2	3313.105	30174.51		3313.139	30174.20		0.31
14	1/2	3289.270	30393.16	6.33	3289.305	30392.84	6.33	0.32
	3/2	3288.585	30399.49		3288.620	30399.17		0.32
15	1/2	3270.962	30563.27	4.71	3270.995	30562.96	4.70	0.31
	3/2	3270.458	30567.98		3270.492	30567.66		0.32
16	1/2	3257.055	30693.76	3.76	3257.090	30693.43	3.76	0.33
	3/2	3256.656	30697.52		3256.691	30697.19		0.33
17	1/2	3246.220	30796.20	2.95	3246.255	30795.87	2.95	0.33
	3/2	3245.909	30799.15		3245.944	30798.82		0.33
18	1/2	3237.612	30878.07	2.34	3237.648	30877.73	2.37	0.34
	3/2	3237.367	30880.41		3237.400	30880.10		0.31
19	1/2	3230.663	30944.49	1.94	3230.699*	30944.15	1.96	0.34
	3/2	3230.460	30946.43		3230.494	30946.11		0.32
20	1/2	3224.967	30999.15	1.59	3225.000*	30998.83	1.58	0.32
	3/2	3224.801	31000.74		3224.836	31000.41		0.33
21	1/2	3220.242	31044.63	1.37	3220.276	31044.30	1.37	0.33
	3/2	3220.100	31046.00		3220.134	31045.67		0.33
22	1/2, 3/2	3216.155	31084.08		3216.188	31083.76		0.32
23		3212.814	31116.40		3212.849	31116.06		0.34
24		3209.954	31144.13		3209.984	31143.84		0.29
25		3207.491	31168.04		3207.524	31167.72		0.32
26		3205.349	31188.87		3205.380	31188.57		0.30
27		3203.480	31207.07		3203.512	31206.76		0.31
28		3201.836	31223.09		3201.870	31222.76		0.32
29		3200.385	31237.24		3200.418	31236.92		0.32
30		3199.097	31249.81		3199.131	31249.48		0.33
31		3197.948	31261.05		3197.983	31260.71		0.34
32		3196.917	31271.13		3196.949	31270.81		0.32
33		3195.993	31280.17		3196.028	31279.82		0.35
34		3195.157	31288.36		3195.189	31288.04		0.32
35		3194.401	31295.76		3194.434	31295.44		0.32
36		3193.712	31302.51		3193.743	31302.21		0.30
37		3193.090	31308.61		3193.123	31308.28		0.33
38		3192.518	31314.21		3192.550*	31313.90		0.31
39		3191.990	31319.39		3192.024	31319.06		0.33
40		3191.510	31324.11		3191.543	31323.79		0.32

the components of this doublet. This high vapor pressure was required to bring out the weaker component of the doublet. At this pressure, however, the stronger component was very broad; it was this broadening of the stronger component that limited the number of cesium doublets that could be resolved. It was, therefore, necessary in the case of cesium to measure the components of some doublets separately on different plates taken at different temperatures.

The wave-lengths of the absorption lines were measured by comparing them with secondary and tertiary iron standards. A standard Pfund arc in air as specified by the International Astronomical Union[12] was used as the source of iron lines, the iron spectra being placed so that they partly overlapped the continuum of the absorption spectra. Each of the resolved doublets was measured on at least two plates except where the contrary is indicated, but several of the high series members

[12] Trans. Int. Astron. Union 2, 18 (1925).

TABLE III—(*Cont.*).

n	J	$6s\ ^2S_{\frac{1}{2}}(F=3)-np\ ^2P_J$ λ(air)	ν(vacuum)	$\Delta\nu_p$	$6s\ ^2S_{\frac{1}{2}}(F=4)-np\ ^2P_J$ λ(air)	ν(vacuum)	$\Delta\nu_p$	hfs $\Delta\nu$
41		3191.066	31328.47		3191.096	31328.17		0.30
42		3190.658	31332.47		3190.690	31332.16		0.31
43		3190.279	31336.19		3190.309	31335.90		0.29
44		3189.925	31339.67		3189.957	31339.36		0.31
45		3189.602	31342.84		3189.634	31342.53		0.31
46		3189.301	31345.80		3189.334*	31345.48		0.32
47		3189.018*	31348.58		3189.052	31348.25		0.33
48		3188.754	31351.18		3188.786	31350.86		0.32
49		3188.510	31353.57		3188.543	31353.25		0.32
50		3188.279*	31355.85		3188.313	31355.51		0.34
51		3188.064	31357.96		3188.096	31357.64		0.32
52		3187.862	31359.95		3187.894	31359.63		0.32
53		3187.673	31361.80		3187.704	31361.50		0.30
54		3187.490	31363.60		3187.521	31363.30		0.30
55		3187.325	31365.23		3187.357	31364.91		0.32
56		3187.167	31366.78		3187.199	31366.47		0.31
57		3187.013	31368.31		3187.045	31367.99		0.32
58		3186.872	31369.69		3186.904	31369.38		0.31
59		3186.743	31370.96		3186.773	31370.67		0.29
60		3186.611	31372.26		3186.642	31371.96		0.30
61		3186.493	31373.43		3186.523	31373.13		0.30
62		3186.378	31374.56		3186.409	31374.25		0.31
63		3186.270	31375.62		3186.301	31375.31		0.31
64		3186.168	31376.62		3186.200	31376.31		0.31
65		3186.070	31377.59		3186.100	31377.29		0.30
66		3185.971	31378.56		3186.004	31378.24		0.32
67		3185.880	31379.46		3185.913	31379.13		0.33
68		3185.796	31380.29		3185.829	31379.96		0.33
69		3185.715	31381.08		3185.749	31380.74		0.34
70		3185.635	31381.87		3185.669	31381.54		0.33
71		3185.554	31382.67		3185.586	31382.36		0.31
72		3185.492	31383.28		3185.522	31382.99		0.29
73		3185.455	31383.65					
—		—	—		—	—		
∞		3183.115	31406.71		3183.146	31406.40		

* Wave-lengths for $n=6$ are from W. F. Meggers, Nat. Bur. Stand. J. Res. **10**, 669 (1933). The hyperfine structure was unresolved, so these values are for a mean of the $F=3$ and $F=4$ levels.

[a] The $6s-7p$ lines were not as sharp and could not be measured as accurately as the other lines. This may have been caused by structure in the $7p\ ^2P_{1/2,3/2}$ levels, although Granath and Stranathan, Phys. Rev. **48**, 725 (1935) report a value for the hyperfine structure interval of the $7p\ ^2P_{\frac{1}{2}}$ level of only 0.0033 cm^{-1}.

[b] Measured on one plate only.

± Measurement relatively uncertain (see text).

of potassium and rubidium were measured on only one plate.

RESULTS AND DISCUSSION

The wave-lengths of the principal series of potassium, rubidium, and cesium that were measured, and their reduction to wave-numbers, are given in Tables I, II, and III respectively. The wave-lengths are referred to air at 15°C and 760 mm pressure; the wave-numbers are reduced to vacuum by the use of the vacuum corrections given in Kayser's "Tabelle der Schwingungszahlen." Nearly all the wave-lengths that were measured on two or more plates agree to within ±0.003A, and all agree to within ±0.005A except those marked ± in the tables, which agree only to within ±0.006A. The doublet separations of 14 members of the principal series of potassium, 22 members of the rubidium series, and 16 members of the cesium series were measured. The higher members of the principal series, with their doublet fine-structure unresolved, were measured to the 76th member in potassium, the 73d member in rubidium, and the 68th member in cesium.

The series limits shown in Table IV, kindly calculated by J. G. Hirschberg and J. E. Mack, are from 2 to 4 cm^{-1} higher than those previously accepted. The values may be changed, within the limits of uncertainty listed, in a later investigation.

As shown in Table III, each component of the cesium fine-structure doublets is itself doubled by hyperfine structure. This structure results from the hyperfine structure of the ground level, $6s\ ^2S_{\frac{1}{2}}$; the hyperfine structure of the $np\ ^2P_{1/2,3/2}$ levels is too small to resolve. The hyperfine structure interval for each member of the series is recorded in

Table III, the values being generally in good agreement with the values 0.307 cm^{-1} reported by Granath and Stranathan[13] and 0.30665 cm^{-1} derived from a microwave experiment.[14] This hyperfine structure limited to 68 the number of higher series members that could be measured; beyond the 68th member the $F=3$ component of one member overlapped the $F=4$ component of the next higher member.

The doublet fine-structure in the spectra of the alkali metal atoms results from the electron spin-orbit interaction. Calculations of the spin-orbit interaction energy by quantum mechanical methods have been made by Pauli,[15] Darwin,[16] Dirac,[17] Gordon,[18] and others. These calculations lead to the following expression for the doublet fine-structure interval, if the screening effect of the electrons in the atomic core is neglected:

$$\Delta\nu=\frac{R\alpha^2Z^4}{n^3l(l+1)}\ \text{cm}^{-1} \qquad (1)$$

where R=Rydberg constant, α=fine structure constant, Z=atomic number, n=principal quantum number, and l=orbital angular momentum quantum number.

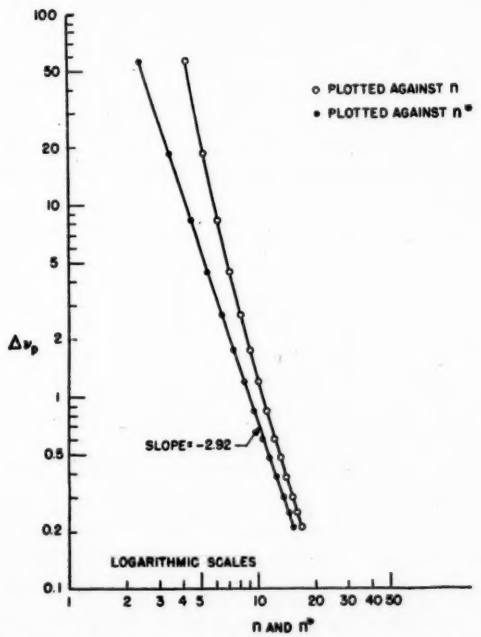

FIG. 1. Variation of $\Delta\nu_p$ with n and n^* in the principal series of potassium.

TABLE IV. Series limits and ionization potentials.

	K	Rb	Cs
n (ground level)	4	5	6
Centroid of ns hfs pattern:			
$ns\ ^2S_{\frac{1}{2}}-\infty$ (cm^{-1})	35009.82 ±0.03	33690.96 ±0.03	31406.54 ±0.03
Predominant isotope	39	85	133
F (lowest sublevel)	1	2	3
$ns\ ^2S_{\frac{1}{2}}{}^F-\infty$ (cm^{-1})	35009.83 ±0.03	33691.02 ±0.03	31406.71 ±0.03
Ionization potential (volts) basis: 8068.2 cm^{-1}=1 volt	4.3392	4.1758	3.8926
Fowler report (1922)	35005.88	33689.1	31404.6
Edlén [Zeits. f. Physik **98**, 445 (1933)]	35009.08		
MMHO (see note at end of this paper)			31406.32

For principal series doublets, Eq. (1) reduces to

$$\Delta\nu_p=np\ ^2P_{1/2}-np\ ^2P_{3/2}=R\alpha^2Z^4/2n^3. \qquad (2)$$

In view of the influence of the screening upon the roles of Z and n, this expression could not be expected to predict accurately the magnitudes of the doublet fine-structure intervals. In the modified

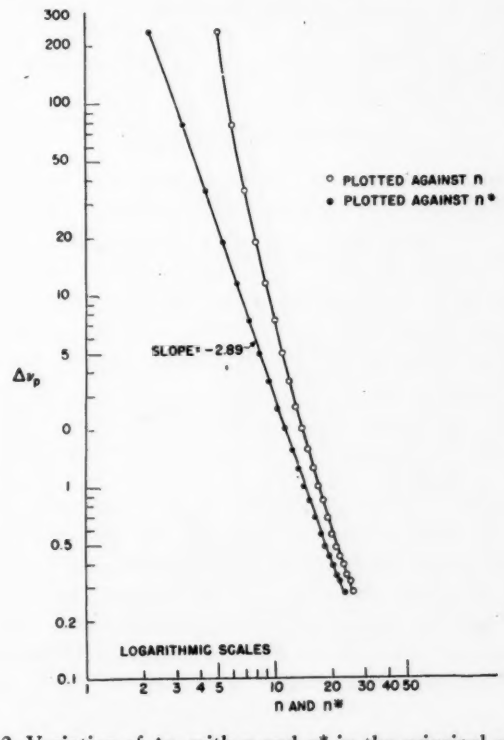

FIG. 2. Variation of $\Delta\nu_p$ with n and n^* in the principal series of rubidium.

[13] L. P. Granath and R. K. Stranathan, Phys. Rev. **48**, 725 (1935).
[14] S. Millman and P. Kusch, Phys. Rev. **60**, 91 (1941).
[15] W. Pauli, Zeits. f. Physik **43**, 601 (1929).
[16] C. G. Darwin, Proc. Roy. Soc. London **A116**, 227 (1927); **A118**, 654 (1928).
[17] P. A. M. Dirac, Proc. Roy. Soc. London **A117**, 610 (1927); **A118**, 351 (1928).
[18] W. Gordon, Zeits. f. Physik **48**, 11 (1929).

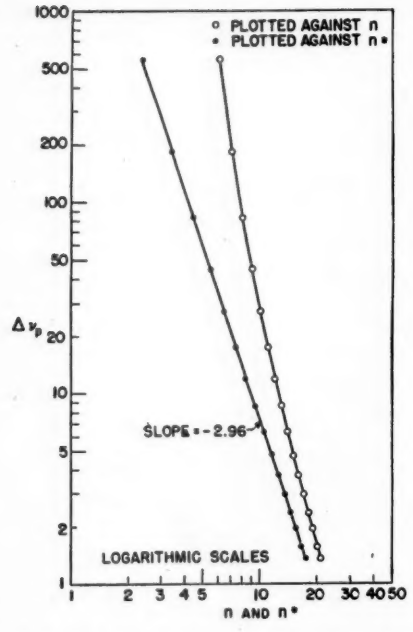

FIG. 3. Variation of $\Delta\nu_p$ with n and n^* in the principal series of cesium.

expressions

$$\Delta\nu_p=\frac{R\alpha^2Z^4_{\text{eff}}}{2n^3_{\text{eff}}} \quad \text{or} \quad \frac{R\alpha^2Z_{\text{outer}}{}^2Z_{\text{inner}}{}^2}{2n^3_{\text{eff}}} \tag{3}$$

where Z_{eff} and n_{eff} stand for Z and n respectively, corrected for the core effect, the accurate calculation of Z_{eff} and n_{eff} presents difficulties.

Let us assume Z_{eff}, or Z_{outer} and Z_{inner}, to be independent of n, and n_{eff} to be the same as n^* in the Rydberg expression

$$n^*=[R/(\text{term value})]^{\frac{1}{2}}. \tag{4}$$

If these assumptions are valid, we get by taking the logarithm of each side of Eq. (3)

$$\log\Delta\nu_p=\text{constant}-3\log n^*. \tag{5}$$

This is the equation of a straight line with a slope of -3. Plots of $\Delta\nu_p$ against n^* and n on logarithmic scales are given in Figs. 1, 2, and 3 for potassium, rubidium, and cesium respectively. In each case the plot against n^* is a straight line with a slope of almost exactly -3, whereas the plot against n is not a straight line.

Sambursky[19] has made quantitative measurements of the intensity ratios in the first eight members of the principal series of cesium. He found the intensity ratio to increase from 2 in the first member to 25 in the fifth member, and then to decrease to 4.5 in the eighth member. Although no quantitative measurements of these intensity ratios were made in this investigation, an inspection of the cesium plates shows, not the decrease observed by Sambursky, but rather an increase in the ratios, perhaps to an asymptotic value, with increasing principal quantum number. It was the large intensity ratios of the cesium doublets which limited to 16 the number that could be resolved.

[19] S. Sambursky, Zeits. f. Physik **49**, 731 (1928).

ACKNOWLEDGMENTS

It is a pleasure for the author to acknowledge his appreciation to Professor J. E. Mack, under whose direction this work was done, for his constant encouragement and considerable assistance. The author is also indebted to Princeton University, where the latter part of the experimental work was done, for cooperation during his stay there.

Note added February 16, 1949: Dr. McNally has kindly sent me, through Professor Mack, the galley proof of the paper by J. R. McNally, J. P. Molnar, W. J. Hitchcock, and N. F. Oliver, J. Opt. Soc. Am. **39**, 57 (1949), on cesium. The results of that investigation are qualitatively in agreement with those in this paper. The principal difference, aside from their failure to resolve the hyperfine structure, is a general discrepancy of between 0.1 and 0.2 cm^{-1} in wave number. This discrepancy can probably be attributed to the higher cesium pressure necessary in their investigation as a consequence of their shorter path length. Dr. McNally remarks that the line breadths are of the order of the expected hyperfine structure, and I agree with him that, in the face of the theoretical resolution of more than 10^5 in their grating, their lack of actual resolution must probably be accounted for by a combination of instrumental and source broadening. Their lines lie consistently to the red of mine by an amount shown in the following table, which gives the average of the quantity ν(Kratz, $J=3/2$ or unresolved fine structure, hfs centroid) $-\nu$(MMHO) for principal quantum numbers taken in groups of five:

$n=11$ to 15	0.18 cm^{-1}
16 to 20	0.15
21 to 25	0.18
26 to 30	0.19
31 to 35	0.18
36 to 40	0.15
41 to 45	0.16
46 to 50	0.12
51 to 55	0.13
56 to 60	0.1
61 to 62	0.1

In this Table I have neglected their value for the $26p$ line; I was able to obtain the values given in Table III for the $26p$ and $32p$ lines, in spite of the Fe lines at 3205.400 and 3196.930A, only by reading them relative to neighboring lines in the series, in a strip free of iron lines.

Possibly the trend toward agreement with increasing n results from my use of plates with a Cs pressure of almost 1 mm for the highest members of the series. Unfortunately, the pressure used in the other investigation is not reported. In view of that trend, however, the discrepancy of 0.22 cm^{-1} in the series limits is not easy to account for wholly in terms of pressure shift. Mack and Hirschberg assign an uncertainty of 0.03 cm^{-1} to their series limit value (neglecting any possible error in Kayser's values for the index of air) and state that a change as great as 0.05 cm^{-1} from the value given in Table IV would cause an egregious trend in the quantum defects.

PHYSICAL REVIEW VOLUME 75, NUMBER 12 JUNE 15, 1949

Theory of Plasma Oscillations. A. Origin of Medium-Like Behavior

D. BOHM AND E. P. GROSS*
Department of Physics, Princeton University, Princeton, New Jersey
(Received January 13, 1949)

A theory of electron oscillations of an unbounded plasma of uniform ion density is developed, taking into account the effects of random thermal motions, but neglecting collisions.

The first problem considered is that of finding the frequencies at which a plasma can undergo organized steady-state oscillations of small enough amplitude so that a linear approximation applies. It is found that long wave-length oscillations of plasmas with a Maxwell distribution of electron velocities are characterized by the steady-state dispersion relation $\omega^2=\omega_P^2+(3\kappa T/m)(2\pi/\lambda)^2$. Here ω_P is the plasma frequency, T the absolute temperature of the electron gas, λ the wave-length, and ω the angular frequency of oscillation. It is also shown that organized oscillations of wave-lengths smaller than the Debye length for the electron gas are not possible.

The theory is then extended to describe the processes by which oscillations are set up. It is found that, for a given wave-length, a plasma can oscillate with arbitrary frequency, but that those frequencies not given by the steady-state dispersion relation describe motions in which, after some time, there is no contribution to macroscopic averages. These additional frequencies lead asymptotically only to microscopic fluctuations of the charge density about the organized oscillation of the plasma. In this way, one can describe the manner in which the system develops organized behavior.

The treatment is then applied to large steady-state oscillations for which the equations are non-linear. One obtains solutions in which particles close to the wave velocity are trapped in the trough of the potential, oscillating back and forth about a mean velocity equal to that of the wave. One can also obtain non-linear traveling pulse solutions in which a group of particles, moving as a pulse, creates a reaction on the surrounding charge, which traps the particles and holds them together.

I. INTRODUCTION

A GAS containing a suitably high density of free positive and negative charges is known as a plasma. As a result of the electrical interactions between the charges, a plasma displays certain forms of ordered behavior which make a description of the system regarded as a whole more appropriate than one in which the individual particles are treated separately. The ordering processes characteristics of a plasma result in a tendency to remain approximately field-free and electrically neutral. If electric fields are introduced, either by an external disturbance or by incomplete space-charge neutralization, the highly mobile free charges automatically respond to the forces in such a way as to shield out the fields. One can therefore regard a plasma as a medium which tends to remain near a field-free and neutral equilibrium state, resisting efforts to produce deviations from this state, just as a liquid tends to remain near an equilibrium state of definite volume, resisting efforts to produce changes in this volume.

In order that the concept of a medium be generally applicable, it is necessary that the dynamic behavior as well as the static behavior show characteristic organized properties. Let us return to our example of the liquid. When a given volume contains an excess of molecules the resulting pressure gradient creates a net flux of particles out of the region, but after a uniform density is reached, the particles still have a net outwardly directed momentum. This eventually results in a deficiency of molecules in the volume so that the motion is reversed; systematic oscillations about the equilibrium state will occur, and as a result, sound waves will be transmitted through the liquid. Because the particles are locked together by interatomic forces so that the system responds more or less as a unit, one does not have to take into account the details of individual particle motions.

The behavior of a medium near its equilibrium state can be described with the aid of a dispersion relation defining the angular frequency, ω, as a function of the wave number,[a] $k=2\pi/\lambda$. Because of the linearity of the equations of motion for small displacements, one can Fourier-analyze the motion, and thus regard an arbitrary displacement as a superposition of waves. From the value of the displacement and of its rate of change at every point in space at a given time, combined with the dispersion relation, one can then calculate the subsequent behavior of the medium. For sound waves in a liquid, for example, the angular frequency is $\omega=\pm kv_s$, where v_s is the speed of sound, which is independent of wave-length. The group velocity, $v_g=\partial\omega/\partial k$, then yields the speed at which energy is transmitted through the system. For a liquid one obtains $v_g=\pm v_s$, a well-known result.

In a plasma a similar medium-like organization of the particle motions is made possible by the electrical forces. If, for example, a given region contains an excess of electrons, they repel each other and therefore begin to move out. By the time neutrality has been established the electrons have gained momentum so that they keep on going and create a deficiency of negative charge which at-

* Now at Harvard University, Cambridge, Massachusetts.

[a] There may be one or more values of ω for each k; e.g., in a crystal, there may be one frequency corresponding to ordinary sound waves and a higher frequency corresponding to excitation of intra-molecular vibrations with the same k.

tracts the electrons back in. In time the motion is reversed, and a systematic oscillation of the charged region is set up. For the case in which the random thermal motions of the charges are slow enough to be neglected, Langmuir and Tonks[1] have studied these oscillations and have shown that their angular frequency is given by

$$\omega_P = ((4\pi n_0 \epsilon^2)/m)^{\frac{1}{2}}, \tag{1}$$

where n_0 is the density of charged particles, and m is their mass. For a typical density of 10^{12} electrons per cm^3, the plasma frequency is about 10^{10} c.p.s. This equation is modified somewhat by the effects of random thermal motions in a way which will be discussed further ahead.

These oscillations are irrotational and therefore do not radiate. Transverse plasma oscillations are, however, also possible, but we shall not study them here because a reasonably complete theory[2] already exists for them. Because the ions are so much heavier than the electrons, their motions will be so small that we can neglect them altogether and assume they remain at rest. The positive ions can also oscillate, but at a much lower frequency.[3] In this paper, however, we shall consider only electron oscillations. For wave-lengths much greater than interionic spacing, it is a good approximation to regard the charge of the positive ions as uniformly smeared over the region.

For a plasma we observe that ω is independent of k, so that the group velocity is zero. This means that in this approximation plasma oscillations are not transmitted through the system at all. Consider, for example, an arbitrary disturbance, which at $t=0$ is localized in a definite region of space. The displacement $\xi(\mathbf{x}, t)$ can be expressed at $t=0$ as a Fourier integral, $\xi(\mathbf{x}, 0) = \int \mathbf{f}(\mathbf{k}) \exp i\mathbf{k}\cdot\mathbf{x} d\mathbf{k}$. The behavior as a function of time can be found by inserting the proper frequency $\omega(\mathbf{k})$, and we obtain $\xi(\mathbf{x}, t) = \int \mathbf{f}(\mathbf{k}) \exp i(\mathbf{k}\cdot\mathbf{x} - \omega t) d\mathbf{k}$. Since ω is independent of $\mathbf{k}$, $\exp -i\omega t$ can be taken out of the integral so that the disturbance remains localized, regardless of the size or shape of the region.[b] Such an oscillation is reminiscent of the behavior of a very thin jelly; hence, the name plasma oscillation.

The dispersion relation (1) does not take into account the effect of random thermal motions of the electrons. In Paper A we extend the theory to include random motions, showing when and how an ionized gas exhibits medium-like properties. This problem has a general interest because the plasma is the only system which is simple enough so that the origin of medium-like behavior can be traced out in detail with the aid of kinetic theory. In addition to giving a complete discussion of the case of small potentials, for which the equations are linear, we also obtain exact non-linear solutions for several cases where the linear approximation fails. In Paper B we discuss the conditions under which plasma oscillations can be excited and damped. In Paper C we discuss the effects of spatial boundaries. These are particularly important in plasmas occurring in discharge tubes where the extent is limited by the walls of the tube.

II. MICROSCOPIC PROCESSES LEADING TO MEDIUM-LIKE BEHAVIOR

In any medium each particle moves in a field of force which is the sum of the forces due to all the other particles, plus those arising from externally imposed fields, if any. In general, this problem is too complex to be solved, because as a given particle collides with other particles, it experiences a rapidly fluctuating force, which is very difficult to take into account. In order to simplify this problem, one must take some sort of average of the field, and one must therefore consider aggregates large enough to contain many particles at once. If a disturbance is to be discussed in terms of oscillations of a medium, it is therefore necessary, at the very least, that the wave-length be considerably larger than the inter-particle distance $n_0^{-\frac{1}{3}}$.

Further conditions must be satisfied, however, before the motion predicted by the average forces is a good approximation to the motion produced by the actual forces. In general, such a simplification is possible in either of two limiting conditions: (a) the forces have a short range and the density is so high that many collisions occur during the period of an oscillation, (b) the forces have a long range and the speed of the particles is so low that the mean distance between most of the interacting particles does not change appreciably during the period of an oscillation. The former occurs with sound waves in a gas or a liquid, the latter in a plasma.

If condition (a) is satisfied, each particle experiences so many small impulses in a short time that its mean motion is determined very accurately by a short-time average momentum transfer. It is in this way that organized medium-like behavior is produced. If, for example, the density in a given region is not uniform, so that in macroscopic terms there is a pressure gradient, each particle will be struck more often from the denser side than from the rarer, and will therefore tend to accelerate in such a way as to leave the denser region. This is the process responsible for the tendency of a liquid or a gas to maintain its static property of constant density.

There are further processes, however, which cause the particle motions to interlock to a much higher

[1] I. Langmuir and L. Tonks, Phys. Rev. **33**, 195 (1929).
[2] H. R. Mimno, Rev. Mod. Phys. **9**, 1 (1937); H. Lassen, Ann d. Physik 1, 415–28 (1947); H. Margenau, Phys. Rev. **73**, 297 (1948).
[3] R. Rompe and H. Steenbeck—Ergeb. d. exakt. Naturwiss. Bd **18**, 303 (1939).
[b] Actually one must take into account the fact that $\omega = \pm\omega_p$ and that both initial displacement and velocity must be specified. The above analysis can easily be carried through with this correction.

degree than that necessary simply to produce a tendency towards uniform density. If, for example, a particle moves faster than the mean velocity of the surrounding particles, it will be struck more often from the forward than from the backward directions, so that it tends to slow down to the mean velocity. If the particle is slower than the surrounding particles, it will in a similar way tend to speed up to the mean velocity. Thus, the collision processes interlock the time average velocity of each particle to the average flow velocity prevailing at each point. This high degree of interlocking makes the hydrodynamic equations, in terms of the velocity and density prevailing at each point, a good approximation to the actual motion.

Let us now contrast with the above, the type of interlocking process which occurs when condition (b) is satisfied. The forces then have such a long range that each particle is continually colliding with many particles at once, but with small momentum transfers for each collision. Here, it is necessary to trace the actual orbit of the particle resulting from the forces, rather than to regard the interaction as a sudden process, completed in a time too short for any significant average motion to occur. In fact, each particle moves almost freely, except that it experiences a gradual change of velocity caused by the cumulative and simultaneous forces produced by all of the other particles. Under these conditions one can simplify the problem by taking a space average of the potential, in the sense that one smooths out the fluctuations resulting from the point character of the charges. This method is more or less analogous to the Hartree self-consistent field method, used in quantum theory, and was first applied to the plasma by Vlasov.[4] He applied this method also to the short range forces, but this is not permissible because the smoothed-out average field, neglecting the large fluctuations which occur in collision, is then a poor approximation to the actual field.

The use of the smoothed-out average field neglects those few Coulomb collisions which occur at short range, and which involve large momentum transfers delivered during a time which is short compared with the period of a plasma oscillation. Collisions between electrons and gas molecules are of the same kind. At the low pressures typical of gaseous discharges, the mean time between such close collisions is much longer than the period of a plasma oscillation. When a collision does occur, however, its effect is to destroy the ordered component of the motion, since the time of collision is independent of the state of the average field. In Paper B this problem is treated in detail, and it is shown that in most plasmas collisions lead to a small damping of oscillations which can usually be neglected without much error. In this paper we shall therefore ignore collisions altogether.

[4] A. Vlasov—J. Phys. U.S.S.R. 9, 25, 130 (1945).

III. THE DISPERSION RELATION

We shall now solve for the organized motion of the particles in a plasma. It is sufficient to seek solutions in which the potential varies trigonometrically in space and time, i.e., $\varphi = Re\, \varphi_0 \exp i(\mathbf{k}\cdot\mathbf{x} - \omega t)$. In any small disturbance in which the plasma acts as a medium, the potential can be represented as the sum of waves of this kind, but ω must satisfy the dispersion relation which we shall now obtain.

One can simplify the problem considerably by going to the coordinate system in which the wave is at rest; such a coordinate system moves with the velocity $\mathbf{V}_W = \omega\mathbf{k}/k^2$, and in this system, the potential is equal to $\varphi = \varphi_0 \exp i(\mathbf{k}\cdot\mathbf{x})$. It consists simply of a static potential wave. In general, particles which are far from the wave velocity will move across this wave, suffering small periodic changes of velocity as they go from crest to trough and on to the next trough. Particles which are close to the wave velocity, however, may be unable to go over the crest of a wave, and can thus be trapped, so that they oscillate back and forth inside a single trough.

Since the potential is static in the wave system, one can integrate the equations of motions by means of conservation of energy. Let us take the x axis in the $\mathbf{k}$ direction. If $\mathbf{U}_{0x}$ is the x component of the velocity in the wave system[6] at the point where $\varphi = 0$, one obtains for the velocity, $\mathbf{U}_x$, at any other point

$$U_x^2 = U_{0x}^2 + (2\epsilon\varphi/m). \tag{2}$$

(Note that ϵ is positive by definition, and that we are dealing with electrons.)

The condition for trapping is then obtained by setting $U_x = 0$ where $\varphi = \varphi_{\min.}$ The result is, for a trapped particle,

$$U_{0x}^2 < -(2\epsilon\varphi_{\min.}/m). \tag{3}$$

In order to obtain solutions which are static in the wave system, and therefore oscillations in the laboratory system which have reached a steady state, we shall have to wait long enough for the number of particles of any given velocity to become constant at each point in space. It will be necessary to take as given, the final distribution of velocities at some specified point. For the untrapped particles, it is convenient to choose this point at $\varphi = 0$ (where $\mathbf{V} = \mathbf{V}_0$). We suppose that the velocity distribution

[6] In general, velocities in the laboratory system will be denoted by $\mathbf{V}$, those in the wave system by $\mathbf{U}$.

function for these particles is given by

$$dN_0 = n_0 f(\mathbf{V}_0) d\mathbf{V}_0 = n_0 f(\mathbf{U}_0 + \mathbf{V}_W) d\mathbf{U}_0,$$

where f is normalized to unity. In most plasmas, $f(\mathbf{V}_0)$ will be close to a Maxwellian function. We shall see that the wave velocity, $\mathbf{V}_W$, is usually far above the mean thermal speeds. This means that for most particles, $\mathbf{U}_x = \mathbf{V}_x - \mathbf{V}_W$, will be very large, so that for moderate potentials, very few particles are trapped. These few trapped particles make only a small change in the final result; hence, it is permissible to neglect them. We shall therefore assume in this section that $f(\mathbf{V}_0) = 0$ over a small region in the neighborhood of $\mathbf{V}_0 = \mathbf{V}_W$. In the next section, however, we shall study in detail the effects of the trapped particles.

Because of the average potential, $\varphi(\mathbf{x})$, each particle undergoes a periodic change of velocity and a corresponding change of its contribution to the density. To obtain the particle density at any point $\mathbf{x}$, we note that if the particle distribution has reached a steady state in the wave system, the contribution of a given particle to the density is inversely proportional to its speed. Thus, one obtains

$$dN = \frac{n_0 f(\mathbf{V}_0) |\mathbf{U}_{0x}| d\mathbf{U}_0}{|\mathbf{U}_x|} = \frac{n_0 f(\mathbf{V}_0) d\mathbf{U}_0}{\left(1 + \frac{2\epsilon\varphi(\mathbf{x})}{m U_{0x}^2}\right)^{\frac{1}{2}}}. \quad (4)$$

The total electron density is found by integrating over-all $\mathbf{U}_0$. The positive ion density does not change appreciably; hence, it remains equal to the mean density, n_0. The total charge density is then

$$\rho(\mathbf{x}) = +n_0\epsilon - n_0\epsilon \int \frac{f(\mathbf{V}_0) d\mathbf{U}_0}{\left(1 + \frac{2\epsilon\varphi(\mathbf{x})}{m U_{0x}^2}\right)^{\frac{1}{2}}}. \quad (5)$$

This charge density results from the action of the assumed average potential, $\varphi(\mathbf{x})$. In order that $\varphi(\mathbf{x})$ be a solution it is necessary that the potential generated by the charge $\rho(\mathbf{x})$ be equal to the potential causing the charge; or, according to Poisson's equation, that

$$-\nabla^2\varphi = +4\pi\rho = 4\pi\epsilon n_0 - 4\pi\epsilon n_0 \int \frac{f(\mathbf{V}_0) d\mathbf{V}_0}{\left(1 + \frac{2\epsilon\varphi(\mathbf{x})}{m U_{0x}^2}\right)^{\frac{1}{2}}}. \quad (6)$$

The above is a non-linear integro-differential equation, defining $\varphi(\mathbf{x})$. In general, $\varphi(\mathbf{x})$ may not be trigonometric in form, but the assumption that φ is static in the wave system restricts us to solutions in which all quantities are functions only of $(\mathbf{x} - \mathbf{V}_W t)$; i.e., to travelling wave solutions.

For small values of $2\epsilon\varphi/mU_{0x}^2$, one can expand the square root, obtaining the linear approximation

$$-\nabla^2\varphi = \frac{4\pi n_0\epsilon^2}{m}\varphi \int \frac{f(\mathbf{V}_0) d\mathbf{V}_0}{U_{0x}^2} = \frac{4\pi n_0\epsilon^2}{m}\varphi \int \frac{f(\mathbf{V}_0) d\mathbf{V}_0}{(\mathbf{V}_{0x} - \mathbf{V}_W)^2}. \quad (7)$$

In the above, it is essential that $f(\mathbf{V}_0)$ vanish in a range near $\mathbf{V} = \mathbf{V}_W$; otherwise, the expansion is not permissible. This is equivalent to neglecting the trapped particles.

To obtain the dispersion relation we write $\mathbf{V}_W = \omega/k$, and $\nabla^2\varphi = -k^2\varphi$. The result is

$$k^2\varphi = \frac{4\pi n_0\epsilon^2}{m} k^2\varphi \int \frac{f(\mathbf{V}_0) d\mathbf{V}_0}{(\omega - \mathbf{k}\cdot\mathbf{V}_0)^2}.$$

There are two conditions yielding a solution

$$k^2\varphi = 0 \quad (8)$$

or

$$1 = \frac{4\pi n_0\epsilon^2}{m} \int \frac{f(\mathbf{V}_0) d\mathbf{V}_0}{(\omega - \mathbf{k}\cdot\mathbf{V}_0)^2}. \quad (9)$$

The first condition is equivalent to $\nabla^2\varphi = 0$. In other words, any solution of Laplace's equation yields a solution of the plasma equations. To obtain a non-zero solution of this kind, however, one must have bounding electrodes on which the charge does not vanish. This type of solution will be discussed further in Paper C. For the present, however, we consider only condition (9), which is an integral equation defining ω as a function of $\mathbf{k}$; this constitutes the dispersion relation. In the linear approximation, this result reduces to a relation first obtained by Vlasov[4] by a different method.

Under the assumption that $\mathbf{V}_W$ is so large that very few particles are present for $|\mathbf{V}_{0x}| > |\mathbf{V}_W|$, the above result can be simplified by expansion in a series of powers of $\mathbf{k}\cdot\mathbf{V}_0/\omega$. Since it turns out that ω is usually somewhat larger than the plasma frequency without random motion (Eq. (1)) it is clear that this expansion is good for small k, i.e., long waves. One can then neglect the small contributions of those particles in the regions for which the expansion does not converge, and one obtains

$$1 = \frac{4\pi n_0\epsilon^2}{m\omega^2} \int \left[1 + 2\frac{\mathbf{k}\cdot\mathbf{V}_0}{\omega} + 3\frac{(\mathbf{k}\cdot\mathbf{V}_0)^2}{\omega^2} + \cdots\right] f(\mathbf{V}_0) d\mathbf{V}_0. \quad (10)$$

By definition, $\int f(\mathbf{V}_0) d\mathbf{V}_0 = 1$; $\int f(\mathbf{V}_0)(\mathbf{k}\cdot\mathbf{V}_0) d\mathbf{V}_0$

$=k\bar{V}_k$ where $\bar{V}_k$ is the mean plasma velocity in the k direction, and $\int f(\mathbf{V}_0)(\mathbf{k}\cdot\mathbf{V}_0)^2 d\mathbf{V}_0 = k^2\bar{V}_k^2$, where $\bar{V}_k^2$ is the mean square velocity in the $\mathbf{k}$ direction. For an isotropic distribution one obtains $\bar{V}_k^2 = \frac{1}{3}\bar{V}^2$, and $\bar{V}_k$ vanishes. Solving for ω up to second order in k, one obtains

$$\omega^2 \cong (4\pi n_0\epsilon^2/m) + k^2\bar{V}^2 = \omega_P^2 + (3\kappa T/m)k^2. \quad (11)$$

As k approaches zero, the above becomes equivalent to Eq. (1), obtained with the neglect of thermal motions. We see that, for small k at least, plasma oscillations are possible for any distribution function which falls off rapidly enough to make the integrals converge. In this approximation the form of the dispersion relation is also independent of the precise form of $f(\mathbf{V}_0)$.

J. J. Thomson and G. P. Thomson[5] have obtained a similar relation using a macroscopic transport treatment, but their result is not exactly the same. Instead it is $\omega^2 = \omega_P^2 + (\kappa T/m)k^2$. The macroscopic theory, however, makes arbitrary assumptions about the distribution function which are not quite correct, and which lead to an error of a factor of 3 in the latter term.

IV. DESCRIPTION OF ORDERED MOTION

Let us now consider in detail the processes by which ordered plasma oscillations are maintained. We first observe that except for the particles near the wave velocity, which we are not now considering, each particle experiences only a small perturbation in its velocity and in its contribution to the density. Despite the random motion, however, the contributions of all particles are coherent because they are all in phase with the average force which produces them. Because of the long range of the Coulomb force, the small perturbations in density suffered by the individual particles can still produce a large cumulative contribution to the net potential. The ordering is unlike the ordering of motion in a liquid where the velocity in each particle is interlocked with the local average. In a plasma, the local average velocity is of no significance because it does not directly control any forces; the local average density is not even what is important. Hence, the motion of a plasma shows only long range organization, while locally it is almost indistinguishable from a perfect gas.

The oscillations obtained so far describe only the behavior after the distribution has become constant in the wave system; the process by which it approaches constancy will be discussed later.

It is instructive to view the motion of the particles in the laboratory system. From Eq. (2), one obtains to a first approximation

$$U_x = U_{0x} + \frac{\epsilon\varphi}{mU_{0x}}; \quad V_x = V_{0x} + \frac{\epsilon\varphi_0 \exp i(kx-\omega t)}{m(V_0 - V_W)}. \quad (12)$$

Thus, each particle suffers a wave-like perturbation in its velocity, which is larger for particles moving in the direction of the wave than for those moving in the opposite direction. The reason is that particles moving in the direction of the wave stay in phase longer and, therefore, experience a larger change of momentum in any given direction before the electric field, which imparts the momentum, is reversed. Particles going with the speed of the wave would stay in phase with the wave indefinitely, and thus the change of momentum, $\Delta p = \epsilon\int E dt$, would grow indefinitely with time. This is the description in the laboratory system of the reason for the infinity in Eq. (12) at $\mathbf{V}_0 = \mathbf{V}_W$ (in the linear approximation).

It is clear that random thermal actions make the localization of an oscillation impossible, because these motions carry the disturbance from one region to another. The average effect is not, however, isotropic, as one might first suppose. Because the particles moving in the direction of the wave experience a larger change of density, there will be a net tendency to carry the disturbance in the direction of the wave. This can be demonstrated by calculating the group velocity

$$\mathbf{V}_g = \partial\omega/\partial\mathbf{k} = (3\kappa T/m)(\mathbf{k}/\omega). \quad (13)$$

This equation shows that for long wave-lengths and low temperatures, the energy transport is small, so that almost complete localization is possible.

It is noteworthy that in plasma oscillations energy is transported by random thermal drift, which bodily carries the excitation from one region of space to another. This is in contrast to the process of transfer in a liquid or in a gas, where the energy transfer is mainly by direct impacts of molecules which are very frequent during a period of an oscillation. This means that in plasmas of low density such as we have been considering, the hydrodynamic description in terms of a fluid with a definite velocity at each point, in which the force on a particle is determined by the pressure gradient, is inappropriate. Thus, the treatment of Linder,[6] which is along these general lines, can be applied only to plasmas of very much higher density than are commonly met with in applications.[d]

[5] J. J. Thomson and G. P. Thomson, *Conduction of Electricity in Gases* (Cambridge University Press, London, 1933), third edition, Vol. 2, p. 353.

[6] E. G. Linder, Phys. Rev. **49**, 753 (1936).

[d] Linder also assumes that the oscillations are isothermal. This assumption requires more study, even at plasma densities so high that formulation in terms of a pressure gradient is permissible.

V. ORIGIN OF MEDIUM-LIKE BEHAVIOR

In this section we shall investigate the non-steady-state solutions for plasma motion, and show that the steady-state oscillations, obtained in the previous work, describe the limiting behavior of the plasma, which is approached after a suitable period of time. The corresponding non-steady-state solutions in a liquid would, for example, involve a description of the details of the collision processes responsible for interlocking the time average of the individual particle velocities to the local average velocity.

In order to obtain a steady state of plasma oscillation with a given $\mathbf{k}$, it is necessary that the initial perturbations in velocity and density match those demanded by Eqs. (12) and (4). If the actual initial conditions are different we shall see that waves of a given $\mathbf{k}$ are not restricted to frequencies given by the dispersion relation, Eq. (9), but can exist with arbitrary frequency. In time, however, oscillations with frequencies not given by the dispersion relation tend to get out of phase with each other, and only the organized plasma oscillations, for which the frequency is given by the dispersion relation, continue to contribute to macroscopic averages such as the mean potential. The other frequencies then correspond to the excitation of random microscopic motions, which are essentially a form of heat energy. One can therefore regard the plasma oscillations as a dynamically stable limiting form of motion, about which small deviations corresponding to random or disorganized particle motions occur. Hence, for calculating macroscopic averages, one can ignore all frequencies of oscillation other than the plasma frequency; and regard the system as a medium constrained to oscillate only with the plasma frequency, and with the perturbations of the individual particle velocities apparently interlocked in such a way that Eq. (12) holds.

We shall, for simplicity, consider a one-dimensional plasma. If there are N particles in this system, there are N degrees of freedom, which may be taken as the initial coordinates of each particle. We shall find it convenient to group particles of the same initial velocity together, and to regard each of these groups as the origin of a beam. The continuity of the range of velocities leads to formal difficulties which can be avoided, as is commonly done in other problems, by considering only a discrete set of velocities, V_i, which are separated by an interval, λ, so small that no important physical quantity changes in the step from one velocity to the next. We shall further assume that the system contains so many particles that the fluctuations in each beam due to the particle nature of the charges can be neglected.

One can then specify the state of this system by giving at each point in space the initial charge density in each beam, $\lambda n_i(x, 0)$. For our purpose it is more convenient to Fourier-analyze this function, writing

$$n_i(x, 0) = n_{0i} + \int \delta n_{ki} e^{ikx} dk, \tag{14}$$

where λn_{0i} is the mean density, and $\lambda \delta n_{ki}$ yields the variation about this mean. To avoid problems introduced by continuity, we also restrict k to a set of discrete, but closely spaced, values, separated by Δk. The total initial density can then be written

$$N(x, 0) = \lambda \sum_i (n_{0i} + \Delta k \sum_k \delta n_{ki} e^{ikx}), \tag{15}$$

and in the limit, as λ and Δk approach zero, the sums become integrals, so that we get

$$N(x, 0) = \int n_0(V_0) dV_0 + \int\int \delta n_k(V_0) e^{ikx} dV_0 dk.$$

By suitably specifying δn_{ki}, one can produce an arbitrary initial distribution of charge. To take into account the fact that each beam is made up of a finite number of particles, however, one should limit the maximum k so that the number of degrees of freedom is equal to the number of particles in the beam. We shall assume here that there are enough particles so that we can describe in this way waves of as short a length as interest us.[e]

Our program will be to treat first a perfect gas of non-interacting particles, and then to show how these results are modified by the introduction of Coulomb forces.

In the perfect gas, each particle moves at a constant velocity equal to its initial value, V_{0i}. Its position is therefore given by $x = x_0 + V_{0i}t$. To obtain the density at any other time, we simply replace x in Eq. (15) by $x - tV_{0i}$; this means that each group of particles carries its own perturbation in density bodily with its own velocity. We get

$$N(x, t) = \lambda \sum_i (n_{0i} + \Delta k \sum_k \delta n_{ki} e^{ikx} \cdot e^{-ikV_{0i}t}). \tag{16}$$

It is instructive to consider first a special case in which all of the δn_{ki} are zero except one, which we denote as δn_{kj}. We then get for the variable portion of the density,

$$\delta N_{kj}(x, t) = \lambda \delta n_{kj} \exp i(kx - kV_{0j}t). \tag{17}$$

This shows that if one starts out with a trigonometric spatial variation of density of particles of a given velocity, one obtains a wave with a definite angular frequency, $\omega = kV_{0j}$. This is because the wave is

[e] We are interested here in only giving a schematic description, which will apply rigorously to adequately high densities, but is intended more generally to give a qualitative picture of the processes by which medium-like behavior is set up.

being carried only by the motion of the particles. The frequency of this wave is determined by the Doppler shift.

One can now build up an arbitrary initial distribution from waves of this kind, simply by adding with suitable coefficients terms coming from different values of k and j. Each different wave can be regarded formally as a normal mode, from which one builds up arbitrary solutions. One obtains essentially a double Fourier series for $N(x, t)$. This is in contrast to the results obtained for steady-state plasma oscillations (Eq. (9)) as well as those of any other medium, where for each k there are, in general, at most a limited small number of allowable values of ω.

In order to obtain a definite frequency in a perfect gas, however, it is, as we have seen, necessary to vary the density of only one beam of particles. As λ approaches zero, there will be fewer and fewer particles in each beam, hence, only a negligible variation in charge density having a definite frequency can be obtained in this way.[f] To obtain appreciable variations, one must sum over particles of many velocities. In order to illustrate the effects of this, let us assume that all particles in the range $V_{0i}-(\delta/2)$ to $V_{0i}+(\delta/2)$ have been given the same trigonometric variations in density, $\delta n_k e^{ikx}$.

From Eq. (16), one obtains the total variation in density,

$$\delta N(x, t)=\lambda\Delta k \sum_{V_{0i}-(\delta/2)}^{V_{0i}+(\delta/2)} \delta n_k e^{i(kx-kV_{0j}t)}. \qquad (18)$$

For small λ, this may be approximated by the integral,

$$\delta N(x, t)=\delta n_k e^{ikx}\Delta k \int_{V_0=V_{0i}-(\delta/2)}^{V_0=V_{0i}+(\delta/2)} e^{-ikV_0 t}dV_0$$

$$=-2\Delta k \frac{\delta n_k e^{ik(x-V_{0i}t)}\sin(k\delta t/2)}{kt}.$$

We see that as t gets large, $\delta N(x, t)$ approaches zero. This means that a wave-like disturbance involving a range, r, of particle velocities dies out in a time of order $t=2/kr$. The reason is that the waves, associated with particles of different velocity, get out of phase with each other. (One can obtain similar results with almost any distribution, which falls off with increasing velocity. For example, a Gaussian initial distribution,

$$\delta n_k(V_0)=(2/\sigma\sqrt{\pi})\exp -V_0^2/\sigma^2,$$

leads to

$$\delta N_k(x, t)=\exp ikx \exp -k^2\sigma^2 t^2/4\cdot(\Delta k).$$

The physical process responsible for the decay of these waves is essentially the random diffusion of particles of different velocities, which tends to carry particles away from regions where they are initially in excess and into regions in which they are initially deficient. Thus, we see that in a perfect gas, there can be no medium-like oscillations.[g]

VI. EFFECTS OF ELECTRICAL FORCES

The effect of electrical forces is, as we have seen in Section III, to couple the motions of particles of different velocity, and thus to make possible organized oscillations. In this section we shall trace out in detail how the normal modes of the perfect gas, consisting of waves carried along by the motion of each group of particles, go over into organized plasma oscillations.

Let us begin with the equation of motion for each particle,

$$m(dV/dt)=\epsilon\nabla\varphi. \qquad (19)$$

Suppose that in the absence of an oscillation, the velocity of a particle is V_{0i}, and that, more generally, the velocity is $V_i=V_{0i}+\delta V_i(x, t)$, where we note that the small perturbation, δV_i depends, in general, on the position and time. One can therefore write $dV/dt=(\partial V/\partial t)+V(\partial V/\partial x)$, and with the neglect of the second order term, $\delta V_i(\partial\delta V_i/\partial x)$, one obtains

$$(\partial\delta V_i/\partial t)+V_{0i}(\partial\delta V_i/\partial x)=(\epsilon/m)(\partial\varphi/\partial x). \qquad (20)$$

The charge density is obtained from the equation of continuity, applied to each beam,

$$(\partial n_i/\partial t)+(\partial/\partial x)(n_i V_i)=0. \qquad (21)$$

For a small oscillation, the density takes the form

$$n_i=n_{0i}+\delta n_i(x, t), \qquad (22)$$

and in the linear approximation, Eq. (21) becomes

$$(\partial/\partial t)\delta n_i+V_{0i}(\partial\delta n_i/\partial x)=-n_{0i}(\partial\delta V_i/\partial x). \qquad (23)$$

For a trigonometric perturbation, where δV_i and δn_i are proportional to $\exp ikx$, one obtains

$$(\partial/\partial t)\delta V_i+ikV_{0i}\delta V_i=(i\epsilon/m)k\varphi,$$

$$(\partial/\partial t)\delta n_i+ikV_{0i}\delta n_i=-ikn_{0i}\delta V_i. \qquad (24)$$

The most general initial conditions on the above equations are that, at $t=0$, $\delta V_i=\delta V_{0i}$ and $\delta n_i=\delta n_{0i}$.

[f] It can be seen that the possibility of obtaining waves of arbitrary frequency comes from splitting the distribution into beams of discrete velocities. This step is a way of taking into account some of the fluctuations resulting from the particle nature of the elementary charges.

[g] Sound waves in a real gas are made possible by collisions, which are caused by short range interactions of particles, as a result of which the gas ceases to be perfect.

The solutions satisfying these conditions are

$$\delta V_i=\frac{ik\epsilon}{m}e^{-ikV_{0i}t}\int_0^t e^{ikV_{0i}\tau}\varphi(\tau)d\tau+\delta V_{0i}e^{-ikV_{0i}t},$$

$$\delta n_i=-ikn_{0i}e^{-ikV_{0i}t}\int_0^t e^{ikV_{0i}\tau}\delta V_i(\tau)d\tau+\delta n_{0i}e^{-ikV_{0i}t}$$

$$=\frac{k^2n_{0i}\epsilon}{m}e^{-ikV_{0i}t}\int_0^t e^{ikV_{0i}\tau}(t-\tau)\varphi(\tau)d\tau+\delta n_{0i}e^{-ikV_{0i}t}-ikn_{0i}\delta V_{0i}te^{-ikV_{0i}t}. \quad (25)$$

The equation determing φ is obtained from Poisson's equation

$$\nabla^2\varphi=-k^2\varphi=4\pi\epsilon\lambda\sum_i\delta n_i$$

$$=4\pi\epsilon\lambda\sum_i\Big[k^2n_{0i}(\epsilon/m)e^{-ikV_{0i}t}\times\int_0^t e^{ikV_{0i}\tau}(t-\tau)\varphi(\tau)d\tau+\delta n_{0i}e^{-ikV_{0i}t}-ikn_{0i}\delta V_{0i}te^{-ikV_{0i}t}\Big]. \quad (26)$$

In the limit as λ goes to zero, this becomes an integral equation defining φ as a function of the time. It can be solved with the aid of a Laplace transform, as was done first by Landau.[7] We shall adopt, however, the method of obtaining the normal coordinates, and subsequently expanding an arbitrary solution as a sum of normal modes, because in this way, the physical processes responsible for the origin of medium-like behavior can be made more evident.

We begin, therefore, by seeking solutions in which $\varphi=\varphi_0\exp-i\omega t$. One then obtains from Eqs. (25)

$$\delta V_i=\frac{k\epsilon}{m}\frac{\varphi_0e^{-i\omega t}}{(kV_{0i}-\omega)}(1-e^{i(\omega-kV_{0i})t})+\delta V_{0i}e^{-ikV_{0i}t},$$

$$\delta n_i=\frac{i\epsilon kn_{0i}\varphi_0}{m}e^{-i\omega t}\frac{\partial}{\partial V_{0i}}\times\left(\frac{1-e^{i(\omega-kV_{0i})t}}{(kV_{0i}-\omega)}\right)-ikn_{0i}\delta V_{0i}te^{-ikV_{0i}t}+\delta n_{0i}e^{-ikV_{0i}t}. \quad (27)$$

The above equations show that, in general, the response of a particle of velocity V_{0i} to the potential, $\varphi_0\exp-i\omega t$, is not only to produce a component of charge density which has the "forcing frequency," ω, but also other components having the frequency, kV_{0i}, which result from the "free oscillation" terms. In order that δn_i vary only with the frequency, ω, one must choose the following boundary conditions:

$$\delta V_{0i}=(k\epsilon/m)(\varphi_0/kV_{0i}-\omega),$$

$$\delta n_{0i}=(k^2\epsilon/m)n_{0i}[\varphi_0/(kV_{0i}-\omega)^2]+g_\omega\delta(\omega-kV_{0i}), \quad (28)$$

where $\delta(\omega-kV_{0i})=0$ unless $V_{0i}=\omega/k$, in which case it is unity and gives an arbitrary constant.[h] The term $g_\omega\delta(\omega-kV_{0i})$ represents an initial trigonometric perturbation in the density of particles of a definite velocity, V_{0i}. As in the perfect gas, this leads to a wave of definite frequency, $\omega=kV_{0i}$. The remaining terms represent the response of the rest of the plasma to the total potential. Note that this response is the same as that given in Eq. (12), as it should be, since in both cases one is solving for the steady-state solution in the linear approximation.

We then obtain for the velocity and density perturbation of each particle

$$\delta V_i=\frac{k\epsilon}{m}\frac{\varphi_0e^{-i\omega t}}{(kV_{0i}-\omega)},$$

$$\delta n_i=\left[\frac{k^2\epsilon n_{0i}\varphi_0}{m(kV_{0i}-\omega)^2}+g_\omega\delta(\omega-kV_{0i})\right]e^{-i\omega t}. \quad (29)$$

At this point we encounter the difficulty that, according to the above formula, the response of the particles to the potential becomes infinite at the wave velocity, $V_{0i}=\omega/k$. This is because, as shown in Sections (III) and (VII), the linear approximation breaks down when $|V_0-\omega/k|^2<(2\epsilon\varphi_0/m)$. We shall see in the next section that the actual response of these particles, in the exact non-linear treatment, is finite and not usually very important, except when there are many particles near the wave velocity. In order to keep the procedure of expanding the oscillations as a sum of normal modes, however, we shall find it desirable, if possible, to retain the linear approximation. From Eq. (27), one sees that over a finite time, t, the response of δV_i and δn_i to the potential always remains finite, even at the wave velocity. Since this response is proportional to φ_0, one concludes that over any finite time, t, however long, it will always be possible to choose a φ_0 so small that the linear approximation is good for all particles. The time, t, can still be chosen long enough so that plasma oscillations can go through many cycles. Although this procedure

[7] L. Landau, J. Phys. U.S.S.R. 10, 25 (1946).

[h] It will turn out that, for all of the permissible frequencies of oscillation, ω/k will be equal to the velocity of some one of the groups of particles.

may restrict us to rather small potentials, it should still give a qualitatively correct description of what happens with moderately large φ_0, since only a few particles near the wave velocity need then be treated in a non-linear way.

Let us separate the range of velocities into two regions. In Region I, $|V_0-\omega/k|>\alpha(2\epsilon\varphi_0/m)^{\frac{1}{2}}$, where α is a number of the order of 10 or more, while in Region II, $|V_0-\omega/k|<\alpha(2\epsilon\varphi_0/m)^{\frac{1}{2}}$. In Region I, where the linear approximation applies, we adopt the boundary conditions leading to a steady state, Eqs. (28). In Region II, we cannot adopt these boundary conditions, because they imply an infinite perturbation in the velocity and density. We shall see, however, that if we adopt instead the conditions, $\delta V_{0i}=0$, and $\delta n_{0i}=g_\omega\delta(\omega-kV_{0i})$, then over a finite period of time, however long, it is always possible to choose φ_0 so small that the response of these particles to the potential can be neglected altogether. To show this, we note first that the number of particles in Region II is proportional to the range of velocities for which the linear approximation fails, which is $\alpha(2\epsilon\varphi_0/m^{\frac{1}{2}})$. Since, for a finite time, the response of each group of particles is proportional to φ_0, the total charge density contributed by the response of particles in Region II is proportional to $\varphi_0^{\frac{1}{2}}$. It is always possible, by choosing φ_0 small enough, to make this negligible in comparison with the response of the particles in Region I, which is proportional to φ_0, since the number of particles in this region is practically independent of φ_0.

To complete the calculation, one must now satisfy Poisson's equation, which now takes the form,

$$k^2\left(1-4\pi\lambda\sum\nolimits_{\mathrm{I}}\frac{\epsilon^2}{m}\frac{n_{0i}}{(\omega-kV_{0i})^2}\right)\varphi_0=4\pi\epsilon g_\omega, \quad (30)$$

where the summation is carried out only over Region I. As λ goes to zero, the sum may be replaced by an integral, and one obtains

$$k^2\left(1-\frac{4\pi\epsilon^2}{m}\int_{\mathrm{I}}\frac{n_0 f(V_0)dV_0}{(\omega-kV_0)^2}\right)\varphi_0=4\pi\epsilon g_\omega, \quad (31)$$

where $\omega=kV_{0j}$ for some j. Note that when the expression on the left hand side is zero, ω is equal to the "plasma frequency," from the dispersion relation (9).

From the above equation, one concludes that an oscillation of definite frequency, ω_j can be set up by starting the particles in Region I according to Eq. (28), with ω set equal to ω_j, while in Region II, one takes the initial conditions, $\delta V_{0i}=0$, $\delta n_{0i}=g_\omega\delta(\omega-kV_{0i})$. Each one of these oscillations is a normal mode, and since one obtains an oscillation only when ω_j/k is equal to the velocity of some beam, one concludes that there are as many oscillations of this kind as there are beams of particles. One obtains, therefore, just as many normal modes as were obtained for the perfect gas.

Let us now investigate the general character of the oscillations. The second term on the left hand side of Eq. (31) represents the response of all particles to the total potential. In general, this response modifies the potential resulting from the $g_\omega\delta(\omega-kV_{0j})$ term, which latter represents the effects of particles at the wave velocity. When ω is far from the "plasma frequency," however, the coefficient of φ_0 remains large, so that the potential is of the same order of magnitude as $\varphi_0=(4\pi\epsilon g_\omega)/k^2$. Since there are very few particles near the wave velocity, the maximum potential that can be obtained from such an oscillation is very small. The general character of the wave is not very different from that of the waves in a perfect gas, since an oscillation is possible only if it is supported by inhomogeneities in density of particles at the wave velocity. Although the potential is somewhat modified by the response of the other particles, there is no real organization of the motion.

As ω approaches the plasma frequency, however, there is a qualitative change in the nature of the motion, resulting from the fact that the potential associated with a given value of g_ω becomes larger and larger. This means, for one thing, that the maximum potential attainable with waves of a definite frequency increases. When ω is equal to the plasma frequency, one obtains waves with g_ω set equal to zero. This means that the oscillations are no longer supported by periodic pulses of particles at the wave velocity, but that, instead, the charge density is made up of the cumulative and coherent contributions of all particles to the total potential. The motion therefore shows a considerable degree of organization. The amplitude of an oscillation at the plasma frequency is not limited by the number of particles at the wave velocity, since the latter play no role at all in maintaining the motion. Thus, even in the linear approximation, large potentials may be built up at the plasma frequency made possible by the fact that all particles act in unison with long range forces.

In order to obtain a single frequency, it is necessary, as we have seen, that all particles be started out with exactly the right phase relations. With most mechanisms of excitation, however, it will be very unlikely that exactly these initial conditions will be produced. More generally, one can expect that a whole range of frequencies will be excited. As in the perfect gas, it will be impossible to excite to any high degree these normal modes involving mostly a few particles near the wave velocity, and if these modes have any appreciable energy, there will be a corresponding range of frequencies, which

eventually get out of phase with each other and produce no macroscopically observable results. The plasma frequency, however, can be highly excited, and its oscillations produce a potential which persists indefinitely. Thus, in the long run, only the plasma oscillations will be observable. This means that a system starting in an arbitrary way will eventually seem to have all of the particles interlocked with the velocity perturbations (Eq. (12)) characteristic of organized plasma oscillation. Thus, the complexities introduced by the degree of freedom in which oscillations are carried mainly by particles at the wave velocity can be ignored, because they produce no macroscopically observable effects. In this way, the system takes on the behavior of a medium.[i]

The above conclusions apply only to plasmas in which there are no large number of particles with a common, sharply defined velocity. If the latter are present, their macroscopically observable charge density does not cancel out after a long time. In other words, pulses of charge in a beam of well-defined velocity can persist for a long time. Hence, such beams continue to contribute to the total number of degrees of freedom, and are best described as separate plasmas, interpenetrating the original plasma, and interacting strongly with it. We shall have occasion to consider the effects of such beams in Paper B.

VII. MINIMUM WAVE-LENGTH FOR PLASMA OSCILLATIONS

Thus far we have studied the dispersion relation in detail only for the case of small k. To extend the investigation to arbitrary k, we rewrite Eq. (9) as follows: (we take the x axis in $\mathbf{k}$ direction and integrate over v_y, v_z.)

$$k^2=\omega_P^2\int\frac{g(V_x)dV_x}{(V_x-\omega/k)^2}=F(\omega/k);$$
$$g(V_x)=\int\int f(\mathbf{V})dV_ydV_z, \tag{32}$$

where a small range of velocities near $V_x=\omega/k$ is excluded. $f(\mathbf{V})$ may be taken as the Maxwellian distribution with mean speed $\bar{V}$.

For large ω/k, F is approximately equal to $\omega_P^2/(\omega/k)^2$. Because $f(\omega/k)$ is so small, F has a value practically independent of the range near the wave velocity which has been cut out. As ω/k approaches zero, F reaches a maximum, the value of which depends fairly strongly on the range which has been cut out. It is clear, therefore, that there is a maximum k, for which ordered plasma oscillations are possible. (There is, of course, no maximum if we seek oscillations which are, as shown in Eq. (31), supported mainly by the few particles near the wave velocity.)

One can easily show that for oscillations in which ω/k is of the order of $\bar{V}$ or less, most of the response to the potential will come from particles as near the wave velocity as one can get before reaching the cut out region. (See, for example, Eq. (31), noting that if $f(\omega/k)$ is large, the main contribution to the integral comes from near $V_x=\omega/k$.) Hence, the degree of organization is very rudimentary in this region, and the motion is difficult to distinguish from disorganized free particle motion. A rough dividing velocity, above which the contribution of particles near the wave velocity becomes small, occurs where $\omega/k=\bar{V}$. Beyond this point, the frequency also depends only weakly on how large a range of velocities is cut out.

With $\bar{V}\approx(8\kappa T/\pi m)^{\frac{1}{2}}$, one obtains for the critical wave-length $\lambda_c=2\pi/k=2\pi(\bar{V}/\omega)$. From Eq. (11), one can show that when

$$\omega/k=\bar{V},\quad \omega^2\approx 2\omega_P^2=(8\pi n_0\epsilon^2/m)$$

and

$$\lambda_c=2\pi(\kappa T/\pi^2 n_0\epsilon^2)^{\frac{1}{2}}.$$

A similar limiting wave-length was obtained by Debye,[8] who showed that static disturbances could not be shielded out in a distance less than $(\kappa T/4\pi n_0\epsilon^2)^{\frac{1}{2}}$. Since shielding is the characteristic static property of a plasma, considered as a medium, one concludes that both statically and dynamically, aggregates smaller than a Debye length cease to act like an organized medium.[j]

Langmuir[9] has given a simple qualitative picture of why the Debye length should be the minimum wave-length for a plasma oscillation. A particle, moving much slower than the wave, experiences almost the same force as a particle at rest; hence, its contribution to the charge density is nearly the same as with the neglect of thermal motion. A particle moving much faster than the wave covers many wave-lengths during the period of a plasma oscillation, so that the average force on it tends to cancel. It therefore does not take part very strongly in the organized motion. When the wave velocity is so low that most particles are as fast as the wave or faster, organized oscillation becomes impossible.

[i] Landau (see reference 7), using a Laplace transform, has obtained essentially the same result as ours: i.e., no matter what are the initial conditions, the system oscillates asymptotically with the plasma frequency. Our method differs primarily in that it uses a discrete but closely spaced set of velocities, with the aid of which the particle nature of the charge is taken into account schematically in a more convenient way than can be done with a continuous distribution of velocities.

[8] P. Debye and E. Hückel, Physik. Zeits. **24**, 185 (1923).

[j] This limitation has also been discussed by Vlasov (see reference 4), and Landau (see reference 7).

[9] I. Langmuir, Proc. Nat. Acad. Sci. **14**, 627 (1928).

VIII. EXACT NON-LINEAR TRAVELING WAVE SOLUTIONS

In a steady state of oscillation,[k] the condition for breakdown of the linear approximation is that, in the wave system of coordinates, there exist many particles for which the kinetic energy is comparable with the potential, or for which

$$\epsilon\varphi \cong (m/2)U_0^2 = m/2(V_0 - V_W)^2. \tag{33}$$

In the neighborhood of the wave velocity the expansion (10) breaks down, and the equation for φ is no longer linear. We shall indicate here the general lines on which an exact traveling wave solution, $\varphi = \varphi(x - V_W t)$, can be obtained, and shall also give the solutions for a few cases. For convenience, we shall restrict ourselves to the one-dimensional case. Although the restriction to traveling waves considerably decreases the generality of the treatment, one can still solve a wide variety of problems in this way. For example, if one has a standing wave resulting from reflections off boundaries, one can express the potential as the sum of two waves running in opposite directions, $\varphi = F(x - V_W t) + F(x + V_W t)$. Since the non-linearity is usually important only for particles close to the wave velocity, it is a good approximation to solve exactly for each running wave separately, and then to add the two solutions. This is because the wave running in the negative direction has only a slight influence on particles trapped in the wave running in the positive direction, and vice versa.

Since only a small fraction of the untrapped particles are usually near the wave velocity, and since, as we shall see, the non-linear effects introduced by their coming near the wave velocity are not qualitatively new, we shall assume that the distribution of untrapped particles is such that their density is given adequately by the linear approximation, where it is understood that $f(V_0)$ is to be taken zero in a region surrounding $V = V_W$, and broad enough to exclude the velocities for which the linear approximation fails.

The trapped particles, however, we shall treat rigorously, because they lead to qualitatively new effects. It is convenient to specify the velocity distribution of trapped particles in terms of the velocity U_1, with which they pass through the bottom of the potential trough. We denote the potential at this point by $\varphi = \varphi_1$; note that it is a *maximum* here, because we are dealing with electrons. The distribution of trapped particles at this point we denote by $dN_1 = g(U_1)dU_1$. To compute the distribution of trapped particles at any other point, x, we note that, in the steady state, the density is inversely proportional to the velocity. We obtain

$$dN_1 = \frac{g(U_1)\,|U_1|\,dU_1}{(U_1^2 + (2\epsilon/m)(\varphi(x) - \varphi_1))^{\frac{1}{2}}}. \tag{34}$$

We must take into account the fact, however, that particles with velocities less than $U_1^2 = (2\epsilon/m) \times (\varphi_1 - \varphi(x))$ will never reach the point, x. If φ_2 is the potential at the top of the trough, we note also that particles with velocities greater than $U_1^2 = (2\epsilon/m)(\varphi_1 - \varphi_2)$ cannot be trapped. The upper limit on U_1 is therefore always $U_1 = ((2\epsilon/m)(\varphi_1 - \varphi_2))^{\frac{1}{2}}$. The total density of trapped particles at the point, x, is then

$$N_1 = \int_{((2\epsilon/m)(\varphi_1 - \varphi(x)))^{\frac{1}{2}}}^{((2\epsilon/m)(\varphi_1 - \varphi_2))^{\frac{1}{2}}} \frac{g(U_1)dU_1\,|U_1|}{(U_1^2 + (2\epsilon/m)(\varphi(x) - \varphi_1))^{\frac{1}{2}}}. \tag{35}$$

This can be given a more convenient form with the substitution

$$\xi^2 = U_1^2 - (2\epsilon/m)(\varphi_1 - \varphi(x)); \quad \xi d\xi = U_1 dU_1. \tag{36}$$

We get

$$N_1 = \int_0^{((2\epsilon/m)(\varphi(x) - \varphi_2))^{\frac{1}{2}}} \times g((\xi^2 - (2\epsilon/m)(\varphi(x) - \varphi_1))^{\frac{1}{2}})d\xi. \tag{37}$$

The equation defining φ can be obtained from Poisson's equation, using the linear approximation (7), for the contribution of the untrapped particles to the charge density,

$$\nabla^2\varphi = 4\pi\epsilon\left[n_0 - n_+ - n_0\frac{\epsilon\varphi(x)}{m}\int \frac{f(V_0)dV_0}{(V_0 - V_W)^2} + \int_0^{((2\epsilon/m)(\varphi - \varphi_2))^{\frac{1}{2}}} g((\xi^2 - (2\epsilon/m)(\varphi - \varphi_1))^{\frac{1}{2}})d\xi\right], \tag{38}$$

where n_0 is the mean density of untrapped particles, and n_+ is the density of positive ions.

To solve this equation for φ, one must first know $g(U_1)$. This function depends on the processes which cause particles to be trapped in the wave. In actual plasmas, the two most important processes of this kind are (a) collisions, (b) processes by which electrons enter the plasma, such as ionization, or injection from a hot cathode.

In the present work, we have assumed that collisions are so infrequent that their effects on particle motions can be neglected. Yet, they will still be important in determining $f(V_0)$ and $g(U_1)$. For example, they will tend to throw particles into the range of trapped velocities, with a more or less uniform distribution, and they will also tend to throw them back out. The net distribution function $g(U_1)$ is the result of the balance of the rate at which

[k] In this section, we restrict ourselves to steady-state oscillations, and do not solve the initial value problem considered in the section on the origin of medium-like behavior.

particles enter the trapped region and that at which they leave. The precise form of $g(U_1)$ is, however, very hard to predict, but one can easily see what are its main qualitative features. In general, one expects to find more particles with small velocities, U_1, than with values of U_1 so large that the particle is barely trapped. This is because particles enter the trapped region with a more or less uniform distribution in velocity, but leave more easily if barely trapped, since a comparatively small collision is then sufficient to throw them out of the trapped region. We shall take here for a typical function of this type

$$g(U_1)=a((2\epsilon/m)(\varphi_1-\varphi_2)-U_1^2)^{\frac{1}{2}}. \quad (39)$$

This function has $g(U_1)=0$, for the critical value of U_1 which leads to escape (see Eq. (33)), and $g(U_1)$ is a maximum for the most thoroughly trapped particles ($U_1=0$). This distribution in taken primarily because it is a plausible one leading to very simple mathematical results. We have, however, carried out calculations with other functions, and have obtained similar results which are considerably more complicated in mathematical form. The contribution of the trapped particles to the density is then

$$N_1(x)=a\int_0^{((2\epsilon/m)(\varphi(x)-\varphi_2))^{\frac{1}{2}}} \times((2\epsilon/m)(\varphi(x)-\varphi_2)-\xi^2)^{\frac{1}{2}}d\xi. \quad (40)$$

With the substitution, $\xi=((2\epsilon/m)(\varphi(x)-\varphi_2))^{\frac{1}{2}}\zeta$, the above becomes

$$N_1(x)=\frac{2a\epsilon}{m}(\varphi(x)-\varphi_2)\int_0^1(1-\zeta^2)^{\frac{1}{2}}d\zeta =\frac{\pi a\epsilon}{2m}(\varphi(x)-\varphi_2). \quad (41)$$

The number "a" can be evaluated in terms of n_1, the total number of trapped particles.

$$n_1=\int_0^{((2\epsilon/m)(\varphi_1-\varphi_2))^{\frac{1}{2}}} g(U_1)dU_1 =a\int_0^{((2\epsilon/m)(\varphi_1-\varphi_2))^{\frac{1}{2}}}((2\epsilon/m)(\varphi_1-\varphi_2)-U_1^2)^{\frac{1}{2}}dU_1,$$

or

$$a=\frac{2n_1m}{\pi\epsilon(\varphi_1-\varphi_2)},$$

and

$$N_1(x)=n_1\frac{(\varphi(x)-\varphi_2)}{(\varphi_1-\varphi_2)}. \quad (42)$$

This expression is especially simple in that it is linear in $\varphi(x)$, (but not in the amplitude φ_2). The simplicity results from the special choice of $g(U_1)$; other choices lead to functions, $N_1(x)$, which are not linear in $\varphi(x)$, but which nevertheless yield qualitatively similar results for the potential. Poisson's equation becomes

$$\nabla^2\varphi=\left[\frac{-4\pi n_0\epsilon^2}{m} \times\int\frac{f(V_0)dV_0}{(V_0-V_W)^2}+\frac{4\pi n_1\epsilon}{\varphi_1-\varphi_2}\right]\varphi +\left(n_0-n_+-\frac{n_1\varphi_2}{\varphi_1-\varphi_2}\right)4\pi\epsilon. \quad (43)$$

In order that the average field vanish over very long distances, it is necessary that

$$n_+=n_0-(n_1\varphi_2/\varphi_1-\varphi_2).$$

This relation will be brought about automatically as a result of the processes which insure over-all static neutralization.

The solutions of the remaining equation are of the form

$$\varphi=A\cos(kx+\alpha)=(\varphi_1-\varphi_2/2)\cos(kx+\alpha), \quad (44)$$

where

$$k^2-\omega_P^2\int\frac{f(V_0)dV_0}{(V_0-V_W)^2}=-\frac{4\pi\epsilon n_1}{\varphi_1-\varphi_2}, \quad (45)$$

and we have replaced $\varphi_1-\varphi_2$ by $2A$. For the case that $f(V_0)$ is negligible for $V_0>V_W$, one can expand the denominator of the integrand in the above equation, obtaining (for $\bar{V}=0$)

$$\omega_P^2/V_W^2(1+3\bar{V}^2/V_W^2+\cdots) =k^2+(4\pi\epsilon n_1/\varphi_1-\varphi_2). \quad (46)$$

This is an equation defining V_W in terms of k and the wave amplitude, $\varphi_1-\varphi_2$. The effect of increasing the number of trapped particles n_1 is to reduce the wave velocity. To obtain the frequency, we write $V_W=\omega/k$. For the special case of no thermal motion ($\bar{V}^2=0$), we get

$$\omega^2=\frac{\omega_P^2k^2}{k^2+(4\pi\epsilon n_1/\varphi_1-\varphi_2)}. \quad (47)$$

By comparison with (1), we see that the effect of increasing n_1 is always to lower the frequency of oscillation. This is exactly the opposite of what happens when one increases the density of untrapped particles, for this raises the frequency of

plasma oscillation. The physical reason why trapped electrons lower the frequency is that they tend to concentrate in regions of positive potential, hence shield out the forces which are causing the space charge to oscillate. The untrapped electrons, on the other hand, move faster through regions of positive potential, hence tend to make the region more positive still, and increase the forces tending to cause oscillation.

It is interesting to note that for very long wavelengths ($k\rightarrow 0$), the frequency approaches

$$\omega^2=\frac{\omega_P{}^2k^2}{4\pi n_1\epsilon}(\varphi_1-\varphi_2)=\frac{n_0}{n_1}\frac{\epsilon}{m}(\varphi_1-\varphi_2)k^2. \quad (48)$$

The dispersion relation here resembles that of sound waves in a gas except that the speed of the waves, $V_W=\omega/k$, is proportional to the square root of the amplitude. It should be noted that the type of plasma oscillation represented by these waves is very different from those described by Eq. (11). The low frequency waves appear only in the non-linear approximation, and are made possible by the contributions of particles near the wave velocity. These waves are, in fact, of exactly the same type as the oscillations supplied mainly by particles near the wave velocity, obtained in Section VI except that here, of course, the treatment is non-linear.

IX. TRAVELING PULSE SOLUTIONS

One can use the results of the last section to obtain an interesting new type of solution, in which a group of particles is trapped in a potential pulse traveling through the rest of the plasma at constant velocity. In order to see qualitatively how the particles are trapped, let us go to the coordinate system in which the pulse is at rest, while the plasma electrons move past at high speed. In the region where the potential is positive, the plasma electrons speed up, thus contributing less to the density, and tending to create an excess of positive charge. This excess of positive charge in turn produces the positive potential, which we assumed to begin with, and also traps a certain amount of negative charge, overcoming the tendency of the latter to blow up by mutual repulsion of its parts.

On either side of the pulse, which we take to be symmetric about $x=0$, and to be within the limits, $x=\pm\beta$, the plasma electrons are present with the same density as that of the positive ions (n_+). It is consistent then, to assume no field in this region. Since the positive ions have no time to respond as the pulse moves past, their density inside the pulse is the same as outside.

In order to show that pulses of this kind can exist, one must now seek solutions of Eq. (38) for the intermediate region which satisfy the following conditions, which permit one to fit the pulse solution continuously to the constant solutions outside the pulse.[1]

1. The density of untrapped electrons at the edge of the pulse must remain continuous. Thus, the density must be $N(\pm\beta)=n_+$.
2. The electric field is zero at $x=\pm\beta$.

For simplicity, we shall neglect thermal motions of the untrapped electrons, which do not alter the qualitative results in any important way. To do this, write $f(V_0)=\delta(V_0)$. Using the linear approximation (7), we obtain for the density of untrapped electrons.

$$N(x)=n_0\{1+(\epsilon/m)[\varphi(x)/V_W{}^2]\}.$$

The first condition becomes

$$n_+=n_0(1+\epsilon\varphi(\pm\beta)/mV_W{}^2).$$

The equation determining $\varphi(x)$ inside the pulse is

$$\nabla^2\varphi=-\left(\omega_P{}^2/V_W{}^2-\frac{4\pi n_1\epsilon}{\varphi_1-\varphi_2}\right)\varphi$$
$$-4\pi\epsilon\left(n_+-n_0+\frac{n_1\varphi_1}{\varphi_1-\varphi_2}\right). \quad (49)$$

The most general solution, symmetric about $x=0$, is

$$\varphi=A\cos kx-2\pi\epsilon\left(n_+-n_0+\frac{n_1\varphi_1}{\varphi_1-\varphi_2}\right)x^2, \quad (50)$$

where k is given by Eq. (47). We must satisfy the definitions that at $x=0$, $\varphi=\varphi_1$ and at $x=\pm\beta$, $\varphi=\varphi_2$ (i.e., $x=\pm\beta$ is the last point at which particles can be trapped). These conditions yield

$$\varphi_1=A,$$
$$\varphi_2=A\cos ka-2\pi\epsilon\beta^2(n_+-n_0+n_1\varphi_1/\varphi_1-\varphi_2). \quad (51)$$

The condition that $\partial\varphi/\partial x$ vanishes at $x=\pm\beta$ is

$$0=-kA\sin k\beta-4\pi\epsilon\beta(n_+-n_0+n_1\varphi_1/\varphi_1-\varphi_2). \quad (52)$$

The condition (1) on $N(x)$ yields

$$n_+=n_0(1+\epsilon\varphi_2/mV_W{}^2). \quad (53)$$

These conditions reduce to

$$\varphi_2=\varphi_1\cos k\beta-2\pi\epsilon\beta^2\left(\frac{n_0\epsilon\varphi_2}{mV_W{}^2}+\frac{n_1\varphi_1}{\varphi_1-\varphi_2}\right),$$
$$0=-k\varphi_1\sin k\beta-4\pi\epsilon\beta\left(\frac{n_0\epsilon\varphi_2}{mV_W{}^2}+\frac{n_1\varphi_1}{\varphi_1-\varphi_2}\right). \quad (54)$$

[1] In this work we do not attempt to follow the processes by which such a pulse solution can be set up. We merely wish to show that in the steady state, such solutions can exist.

Division of the first of these equations by the second yields

$$\varphi_2=\varphi_1\cos k\beta+\frac{\beta k}{2}\varphi_1\sin ka$$

$$=\varphi_1\left(\cos k\beta+\frac{k\beta}{2}\sin k\beta\right). \quad (55)$$

Insertion into Eq. (52) yields

$$0=-k\varphi_1\sin k\beta$$

$$-4\pi\epsilon\beta\left(\frac{n_0\epsilon}{mV_W{}^2}\left(\cos k\beta+\frac{k\beta}{2}\sin k\beta\right)\right)\varphi_1$$

$$-4\pi\epsilon\beta n_1\Big/1-\cos k\beta-\frac{k\beta}{2}\sin k\beta, \quad (56)$$

or

$$\varphi_1\left(k\sin k\beta+\frac{4\pi\epsilon^2}{m}\frac{\beta n_0}{V_W{}^2}\times\left(\cos k\beta+\frac{k\beta}{2}\sin k\beta\right)\right)$$

$$=\frac{-4\pi\epsilon\beta n_1}{1-\cos k\beta-\frac{k\beta}{2}\sin k\beta}.$$

We can solve for φ_1 from the above, then for φ_2 from (55), and finally for n_+-n_0 from (53). This provides a pulse solution, in which V_W, the wave velocity, and n_1, the number of trapped particles, may be specified arbitrarily.

PHYSICAL REVIEW VOLUME 75, NUMBER 12 JUNE 15, 1949

Theory of Plasma Oscillations. B. Excitation and Damping of Oscillations

D. BOHM AND E. P. GROSS*
Department of Physics, Princeton University, Princeton, New Jersey
(Received January 27, 1949)

The theory of electron oscillations of an unbounded plasma is extended to take into account the effects of collisions and special groups of particles having well-defined ranges of velocities. It is found that as a result of collisions a wave tends to be damped in a time of the order of the mean time between collisions. If beams of sharply defined velocity or groups of particles far above mean thermal speeds are present, however, they introduce a tendency toward instability so that small oscillations grow until limited by effects not taken into account in the linear approximation. An estimate is made of the steady-state amplitude for plasma oscillations in which excitation occurs because of a peak at high velocities in the electron velocity distribution, and in which the main damping arises from collisions. It is also found that in variable density plasmas, waves moving in the direction of decreasing plasma density show even stronger instability.

In absence of plasma oscillations, any beam of well-defined velocity is scattered by the individual plasma electrons acting at random, but, when all particles act in unison in the form of a plasma oscillation, the scattering can become much greater. Because of the instability of the plasma when special beams are present, the beams are scattered by the oscillations which they produce. It is suggested that this type of instability can explain the results of Langmuir, which show that beams of electrons traversing a plasma are scattered much more rapidly than can be accounted for by random collisions alone. It is also suggested that this type of instability may be responsible for radio noises received from the sun's atmosphere and from interstellar space.

I. INTRODUCTION

IN the preceding paper (referred to as A), we gave a theory of oscillations of an unbounded plasma, neglecting collisions, and treating in detail only ion gases with a continuous distribution of velocities, which decreases monotonically with increasing velocity. In this paper, we extend the theory to include effects of collisions and more general velocity distributions, showing how these can bring about excitation and damping of plasma oscillations.

II. EFFECTS OF COLLISIONS

A collision may be said to occur whenever two particles come so close together that a sudden transfer of momentum takes place, which is so rapid that for macroscopic phenomena, such as wave motion, it may be regarded as instantaneous. These momentum transfers occur at random relative to the phase of organized wave motion; hence, their general effect is to disrupt it and to cause damping. Because of persistence of velocity, not all of the organized motion will be lost, but in a close collision of an electron with a heavy object, such as a neutral atom or an ion, the persistence of velocity is not very important, and one can, in a rough quantitative treatment such as this, neglect it altogether. We therefore take a simplified model of these collision processes, and assume that particles emerge from a collision with no relation to their previous velocity, but with a velocity distri-

* Now at Harvard University, Cambridge, Massachusetts.

bution, $f(\mathbf{V}_0)$, which is the same as that prevailing in the absence of plasma oscillations (usually very nearly Maxwellian). Between collisions, the particle moves in the average field of all the other particles, gaining an ordered component to its motion, which is lost in the next collision. As a result, there is a continual process of degradation of ordered energy by collisions. The description is completely analogous to the Lorentz theory of collision broadening of spectral lines.

Although this method provides a good representation of short range collisions, such as those between electrons and neutral molecules, it is not so good for Coulomb collisions, in which, because of the long range of the forces, there is a preponderance of distant impacts involving small momentum transfers and a great deal of persistence of velocities. As shown in A (Section II), the very distant collisions are best treated in terms of the smeared-out average field. A rough distinction between collision forces and the ordered average component of the force can be obtained by saying that momentum transfers occurring in less than a period of oscillation do not contribute to the ordered motion, but instead, tend to disrupt it. This provides an upper limit on the impact parameter, P, for collisions. To compute this limit, we note that the time of collision is of the order of P/V. Setting this equal to the period of a plasma oscillation, we get $P/V\sim\cdot 2\pi/(4\pi n_0\epsilon^2/m)^{\frac{1}{2}}$. With $V\sim(\kappa T/m)^{\frac{1}{2}}$, one obtains $P\sim 2\pi(\kappa T/4\pi n_0\epsilon^2)^{\frac{1}{2}}$. This is just 2π times the Debye length which is the characteristic shielding radius for the plasma (see A, Section VII).

The Debye length is usually much larger than an atomic radius; hence, there are a great many electron-ion collisions of range so long that the momentum transfer is very small. One can account for these collisions roughly by adding in a mean free path for electron-ion collisions. It is well known[1] that this mean free path depends on the logarithm of the maximum collision parameter, which should be taken equal to a Debye length. Because of the logarithmic dependence, the ambiguity introduced by the arbitrary separation of collisions from the ordered component of the force at this length will be unimportant.

In electron-electron collisions, one deduces from the conservation of momentum that the total current is not changed in a collision process. It can be shown, by an extension of our treatment, which is not, however, included in this paper, that for wavelengths appreciably longer than a Debye length, an electron-electron collision leaves the ordered component of the motion unaltered, to a very high degree of approximation. Hence, one can ignore the damping due to electron-electron collisions. At very high plasma densities, such collisions will, however, make possible the transmission of sound waves, by the same mechanism as occurs in a non-ionized gas.

It is instructive to estimate the various mean-free paths for typical cases. At a pressure of 5×10^{-3} mm, the free path for electron-gas collisions is about 10 cm, while that for electron-ion collisions (ion density $\sim10^{11}/\text{cm}^3$) is about $4E^2$ cm, where E is the mean electronic energy in electron volts. At a typical electronic temperature of 3 ev, this is about 36 cm. Since the mean electronic speed is of the order of 10^8 cm/sec., the inter-collision time is about 10^{-7} sec., which is about 1000 times the period of a plasma oscillation, 10^{-10} sec. Hence, the effect of collisions will be small, and the approximation of paper A, neglecting them, is justified.

The lowest density plasmas that are known probably occur in the gas clouds of interstellar space, where the ion density is of the order of 1 per cm^3, the plasma frequency is about 10^4 c.p.s., and the mean free path about 10^{12} cm. The electronic temperature is of the order of a few ev, and the time between collisions is about 10^4 sec. Hence, the neglect of collisions is a good approximation here also.

In an actual plasma, the system is seldom in thermodynamic equilibrium, because ions and electrons are continually being generated by processes such as photo-ionization, ionization by impact, and direct injection from a cathode, while they leave by recombination, either in the body of the plasma or at the walls. The generation of electrons can alter the velocity distribution function, $f(\mathbf{V}_0)$ in such a way that peaks occur at high velocity. Injection from a cathode will introduce a beam of sharply defined velocity.

The electrons are usually liberated with more than the mean thermal energies, but they tend to lose their excess, either by collision with individual particles, or, as we shall see, by interaction with organized plasma oscillations which result from the instability of the plasma. Thus, a plasma is continually degrading a stream of energy into heat.

III. MATHEMATICAL TREATMENT

We shall use a method here in which the motion of each particle is traced from the time at which it makes its last collision to the present. To do this, we label each particle according to the position and velocity $(\mathbf{x}_0, \mathbf{V}_0)$, which it had when it emerged from its last collision, at the time t_0. We assume that in the process of collision the particles lose all trace of any previous ordering in velocities. This means that one can write the distribution of particles emerging from collisions in unit time as a product of terms involving, respectively, the

[1] S. Chandrasekhar, *Principles of Stellar Dynamics* (University of Chicago Press, Chicago, 1942), p. 75.

spatial and velocity dependences, as follows:

$$dN=\frac{N(\mathbf{x}_0, t_0)}{\langle\tau\rangle_{Av}}f(\mathbf{V}_0)d\mathbf{V}_0d\mathbf{x}_0, \tag{1}$$

where $N(\mathbf{x}_0, t_0)$ is the total density of particles existing at the point $\mathbf{x}_0, t_0$, and $f(\mathbf{V}_0)$ is the velocity distribution with which the particles come off after collision. $f(\mathbf{V}_0)$ is normalized so that $\int f(\mathbf{V}_0)d\mathbf{V}_0=1$. If any particles are being liberated by ionization or injection, these should be included in $f(\mathbf{V}_0)$, and for these particles $\mathbf{x}_0$, $\mathbf{V}_0$ refer to the position and velocity with which the particles entered the plasma.[a] $\langle\tau\rangle_{Av}$ is the velocity average of the mean time between collisions.

We first seek wave-like solutions of the form

$$\varphi=\varphi_0\exp i(\mathbf{k}\cdot\mathbf{x}-\omega t),$$
$$N(\mathbf{x}, t)=n_0+\delta N_0\exp i(\mathbf{k}\cdot\mathbf{x}-\omega t),$$

where n_0 is the equilibrium density of particles. As in A, we shall obtain the dispersion relation, defining ω as a function of $\mathbf{k}$.

In the presence of the average electric field, each electron changes its velocity according to the equation of motion

$$m(d\mathbf{V}/dt)=\epsilon\nabla\varphi=i\epsilon\mathbf{k}\varphi_0\exp i(\mathbf{k}\cdot\mathbf{x}-\omega t).$$

To solve for the velocity change, one must know $\mathbf{x}$ as a function of t. Because φ_0 is small, however, the velocity must remain close to its initial value, $\mathbf{V}_0$, so that to a first approximation, $\mathbf{x}=\mathbf{x}_0+\mathbf{V}_0(t-t_0)$. This approximation is adequate to insert in the right-hand side of the above equation, as the latter is already proportional to the first order term φ_0. The result is

$$m(d\mathbf{V}/dt)\cong i\epsilon\mathbf{k}\varphi_0\exp i(\mathbf{k}\cdot\mathbf{x}_0-\omega t_0)\times\exp i(\mathbf{k}\cdot\mathbf{V}_0-\omega)(t-t_0). \tag{2}$$

Integration, with the boundary condition that $\mathbf{V}=\mathbf{V}_0$ at $t=t_0$, yields

$$\mathbf{V}\cong\mathbf{V}_0-\frac{\epsilon\mathbf{k}\varphi_0}{m}\frac{\exp i(\mathbf{k}\cdot\mathbf{x}_0-\omega t_0)}{(\omega-\mathbf{k}\cdot\mathbf{V}_0)}\times(\exp i(\mathbf{k}\cdot\mathbf{V}_0-\omega)(t-t_0)-1).$$

In the subsequent work, we shall need to express $\mathbf{V}_0$ as a function of $\mathbf{V}$. To first order, one easily sees that this result is

$$\mathbf{V}_0=\mathbf{V}+\frac{\epsilon\mathbf{k}\varphi_0}{m}\frac{\exp i(\mathbf{k}\cdot\mathbf{x}_0-\omega t_0)}{(\omega-\mathbf{k}\cdot\mathbf{V})}\times(\exp i(\mathbf{k}\cdot\mathbf{V}-\omega)(t-t_0)-1)=\mathbf{V}-\delta\mathbf{V}, \tag{3}$$

[a] This schematic description is a way of treating the effects on plasma oscillations of collisions and high velocity particles without simultaneously entering into a detailed discussion of the mechanisms by which the steady-state distribution is maintained.

where we have replaced $\mathbf{V}_0$ by $\mathbf{V}$ in all first-order terms. One can find $\mathbf{x}$ in terms of $\mathbf{x}_0$ by integration of (3), but we shall not do so here, because the result is not needed in an explicit form.

Let us now consider all of the particles passing through the point $\mathbf{x}$, at the time, t. The probability that such particles suffered their last collisions between $\mathbf{x}_0$ and $\mathbf{x}_0+d\mathbf{x}_0$ will be denoted by $P(\mathbf{x}, \mathbf{x}_0, \mathbf{V}_0, t)d\mathbf{x}_0$. To a first approximation, it is equal to $(1/l)\exp-|\mathbf{x}-\mathbf{x}_0|/l)$, where l is the mean free path. If the mean free path depends on the velocity, the expression is more complicated because the particle velocity changes as the particle moves under the action of the field. Since the motion is determined in terms of $\mathbf{x}, \mathbf{x}_0, \mathbf{V}_0, t$, the accurate expression for this probability is, at most a function of these. If there were no collisions, the number of particles starting between $\mathbf{x}_0$ and $\mathbf{x}_0+d\mathbf{x}_0$ with velocities between $\mathbf{V}_0$ and $\mathbf{V}_0+d\mathbf{V}_0$ would be given by Eq. (1) as

$$\delta N=N(\mathbf{x}_0, t_0)f(\mathbf{V}_0)d\mathbf{x}_0d\mathbf{V}_0. \tag{4}$$

One now applies Liouville's theorem, which states that the density of particles in phase space remains constant if one follows a moving particle for which the equations of motion can be derived from a Hamiltonian function. Hence, for a volume element which follows a particle, we can write $d\mathbf{x}d\mathbf{V}=d\mathbf{x}_0d\mathbf{V}_0$. Since the number of particles in this element does not change, we obtain from Eq. (4),

$$\delta N=N(\mathbf{x}_0, t_0)f(\mathbf{V}-\delta\mathbf{V})d\mathbf{x}d\mathbf{V}. \tag{5}$$

By dividing by $d\mathbf{x}$, one obtains the contribution to the density at the point $\mathbf{x}$, resulting from particles starting at the point $\mathbf{x}_0$, with the velocity $\mathbf{V}_0=\mathbf{V}-\delta\mathbf{V}$,

$$\rho(\mathbf{x}, \mathbf{x}_0, \mathbf{V}-\delta\mathbf{V}, t)d\mathbf{V}=N(\mathbf{x}_0, t_0)f(\mathbf{V}-\delta\mathbf{V})d\mathbf{V}. \tag{6}$$

To obtain the average density, one must multiply the above by the probability that the particle starts between $\mathbf{x}_0$ and $\mathbf{x}_0+d\mathbf{x}_0$, and integrate over $\mathbf{x}_0$ and $\mathbf{V}$. The result is

$$N(\mathbf{x}, t)=\int\int N(\mathbf{x}_0, t_0)f(\mathbf{V}-\delta\mathbf{V})\times P(\mathbf{x}, \mathbf{x}_0, \mathbf{V}-\delta\mathbf{V}, t)d\mathbf{x}_0d\mathbf{V}. \tag{7}$$

Let us now expand $f(\mathbf{V}-\delta\mathbf{V})$ and $P(\mathbf{x}, \mathbf{x}_0, \mathbf{V}-\delta\mathbf{V}, t)$ as a series of powers of $\delta\mathbf{V}$. We also write

$$N(\mathbf{x}_0, t_0)=n_0+\delta N_0\exp i(\mathbf{k}\cdot\mathbf{x}_0-\omega t_0)=n_0+\delta N(\mathbf{x}_0, t_0).$$

With the retention of first-order terms, we get

$$N(\mathbf{x}, t)=\int\int[P(\mathbf{x}, \mathbf{x}_0, \mathbf{V}, t)(n_0f(\mathbf{V})+\delta N(\mathbf{x}_0, t_0)f(\mathbf{V}))-n_0\delta\mathbf{V}\cdot\nabla_V(fP)]d\mathbf{x}_0d\mathbf{V}. \tag{8}$$

From Eqs. (8), and from the fact that $\int Pd\mathbf{x}_0=1$,

we see that integration of the first term over $d\mathbf{x}_0 d\mathbf{V}$ in the integrand yields n_0. The third term may be simplified by noting from Eq. (3) that $\delta\mathbf{V}$ is in the $\mathbf{k}$ direction, so that $\delta\mathbf{V}\cdot\nabla_V$ can be written as $\delta V_k(\partial/\partial V_k)$ where V_k is the component of $\mathbf{V}$ in the $\mathbf{k}$ direction. One can now integrate this expression by parts over V_k, noting that the integrated parts vanish because $f(\mathbf{V})$ vanishes at infinity. We then obtain

$$N(\mathbf{x},t)=n_0+\int\int f(\mathbf{V})P\Big[\delta N(\mathbf{x}_0,t_0) - \frac{\epsilon\mathbf{k}\varphi_0 n_0}{m}\exp i(\mathbf{k}\cdot\mathbf{x}_0-\omega t_0)\frac{\partial}{\partial V_k} \times\left(\frac{\exp i(\mathbf{k}\cdot\mathbf{V}-\omega)(t-t_0)-1}{(\omega-\mathbf{k}\cdot\mathbf{V})}\right)\Big].$$

Since P now multiplies only first-order terms, we can evaluate it by its first approximation, $(1/l)\,(\exp-|\mathbf{x}-\mathbf{x}_0|/l)$. To first order, one can also replace $\mathbf{x}-\mathbf{x}_0$ by $\mathbf{V}(t-t_0)$. We also set $l/V=\tau(V)$ = mean time between collisions. We get

$$N(\mathbf{x},t)=n_0+\exp i(\mathbf{k}\cdot\mathbf{x}-\omega t) \times\int\int_{t-t_0=-\infty}^{0} d\mathbf{V}\frac{dt_0}{\tau}\exp-(t-t_0)/\tau f(\mathbf{V}) \times\Big[\delta N_0\exp i(\omega-\mathbf{k}\cdot\mathbf{V})(t-t_0)-\frac{n_0\epsilon\varphi_0}{mV}k^2 \times\exp i(\omega-\mathbf{k}\cdot\mathbf{V})(t-t_0)\frac{\partial}{\partial k} \times\left(\frac{\exp-i(\omega-\mathbf{k}\cdot\mathbf{V})(t-t_0)-1}{\omega-\mathbf{k}\cdot\mathbf{V}}\right)\Big]. \quad (9)$$

The result of carrying out the integration over t_0 is

$$N(\mathbf{x},t)=n_0+\delta N_0\exp i(\mathbf{k}\cdot\mathbf{x}-\omega t)\int_{-\infty}^{+\infty}d\mathbf{V}_0 f(\mathbf{V}_0) \times\left\{\frac{n_0\epsilon k^2\varphi_0}{m(\omega-\mathbf{k}\cdot\mathbf{V}_0+i/\tau)^2}+\frac{i\delta N_0}{\tau(\omega-\mathbf{k}\cdot\mathbf{V}_0+i/\tau)}\right\}. \quad (10)$$

According to Poisson's equation, $-k^2\varphi_0=-4\pi\epsilon\delta N_0$. Eliminating δN_0 between these two equations gives the following dispersion relation

$$1=\int f(\mathbf{V}_0)d\mathbf{V}_0\left[\frac{4\pi n_0\epsilon^2}{m}\frac{1}{(\omega-\mathbf{k}\cdot\mathbf{V}_0+i/\tau)^2} +i/\tau\frac{1}{(\omega-\mathbf{k}\cdot\mathbf{V}_0+i/\tau)}\right]. \quad (11)$$

We note that as the collision time, τ, becomes infinite, this reduces to Eq. (9) of paper A obtained with the neglect of collisions.[b] We shall concern ourselves with situations in which the collision time is much larger than the period of the plasma oscillations. For collision times comparable with a period of oscillation, the use of an average field to describe the forces on plasma particles becomes a bad approximation and our treatment breaks down.[c] This means that we will neglect powers of the quantity $1/\omega_P\tau$ higher than the first. At long wave-lengths, $\mathbf{k}\cdot\mathbf{V}_0/\omega$ is small compared to unity for all $\mathbf{V}_0$ for which $f(\mathbf{V}_0)$ is appreciable. Expanding in powers of $\mathbf{k}\cdot\mathbf{V}_0/\omega$ as in paper A, Eq. (10), we obtain

$$\omega^2=\omega_P^2\int f(\mathbf{V}_0)d\mathbf{V}_0\left[1+\frac{2\mathbf{k}\cdot\mathbf{V}_0}{\omega} +3\left(\frac{\mathbf{k}\cdot\mathbf{V}_0}{\omega}\right)^2+\cdots\right]-\frac{i}{\omega\tau}[2\omega_P^2-\omega^2].$$

With the same assumptions for the distribution function as in A, we find as the dispersion relation for small k,

$$\omega^2=\omega_P^2+(3\kappa T/m)k^2-(i\omega_P/\tau)$$

or

$$\omega=(\omega_P^2+(3\kappa T/m)k^2)^{\frac{1}{2}}-(i/2\tau). \quad (12)$$

This shows that the effect of collisions is to damp the wave. The time necessary for the intensity to fall to $1/e$ of its initial intensity is just the collision time, τ.[d] This result is reasonable because each electron was assumed to lose all ordered motion on collision. As a result, the time needed to dissipate most of the ordered energy is just the mean time between collisions. It should be noted that unless there are specific excitation processes such as those described further ahead in this paper, plasma oscillations cannot persist.

IV. VALIDITY OF LINEAR APPROXIMATION

As shown in paper A, Section III, in the absence of collisions the linear approximation always breaks

[b] Note that Eq. (11) approaches the dispersion relation corresponding to organized motions. The non-medium-like oscillations considered in paper A, Section (VI), are produced mostly by a few particles near the wave velocity. In the collision treatment that we have just given, the density distribution is assumed at all times to be a continuous function of the velocity, so that there can be no waves in which most of the oscillation is carried by a few particles near a special velocity. In order to obtain waves of the latter type, one would have to start out with a density distribution in which a few particles of some definite velocity had a large trigonometric perturbation in density, much greater than that of particles of any other velocity. As shown in A (Section VI), such oscillations can have at most a very small amplitude.

[c] Our treatment is too rough to be able to lead to sound waves in the limit of short free path.

[d] If τ is a function of velocity, the above refers to a suitable average over velocities.

down for particles close to the wave velocity, because these are trapped in the trough of the potential, oscillating back and forth many times. It is easily seen that the effect of collisions is to improve the linear approximation for particles near the wave velocity. From Eq. (3), one sees that each particle suffers an oscillatory change of velocity, and that particles very close to the wave velocity (where $\omega=\mathbf{k}\cdot\mathbf{V}_0$) will in a long time suffer very large changes of velocity, so that the assumption that $\delta\mathbf{V}$ is small, tends to break down. If particles collide before they have time to do this, however, the linear approximation will be valid even for particles near the wave velocity. In the coordinate system in which the wave is at rest, the description of this effect is that the time between collisions is much less than the period of oscillation of a particle in the potential trough.

In order that the linear approximation be valid, it is necessary that for each group of particles of a given velocity, the charge density resulting from the response to the average potential be much less than the unperturbed initial density after collision, $n_0 f(\mathbf{V}_0)$. According to Eq. (10), the density resulting from the response to the potential is

$$f(\mathbf{V}_0)\left\{\frac{\epsilon\varphi_0 k^2 n_0}{m(\omega-\mathbf{k}\cdot\mathbf{V}_0+i/\tau)^2}+i\frac{\delta N_0}{\tau(\omega-\mathbf{k}\cdot\mathbf{V}_0+i/\tau)}\right\}.$$

It is clear that the most unfavorable values for the validity of the linear approximation is $\omega-\mathbf{k}\cdot\mathbf{V}_0=0$. At this point, the first term in the above expression is usually larger than the second in the ratio $\tau^2\omega_P^2$, and $\omega_P\tau$ is usually much greater than unity. Hence, our criterion becomes[e]

$$\frac{\epsilon\varphi_0}{m}k^2\tau^2\ll 1. \tag{13}$$

Thus, in accordance with our qualitative picture, a short collision time improves the linear approximation.

V. EXCITATION OF PLASMA OSCILLATIONS AS A RESULT OF INSTABILITY

We shall now study some of the processes which can lead to excitation of plasma oscillations, and which can overcome the collision damping. The first of these processes involves the effects of particles near the wave velocity $\mathbf{V}_W=(\omega/k^2)\mathbf{k}$. In Eq. (12) we expanded the dispersion relation, under the assumption that there were so few particles near the wave velocity that their effects could be neglected. If there are an appreciable number of such particles, this expansion is not permissible, and we shall see by a more accurate treatment that either excitation or further damping may be brought about.

If τ is large, the integrand in Eq. (11) has a very high and narrow peak centering at $\mathbf{V}_0=(\omega/k^2)\mathbf{k}$. For small k, this peak occurs at such a high value of $\mathbf{V}_0$ that $f(\mathbf{V}_0)$ is fairly small. It is convenient to divide the domain of integration over $\mathbf{V}_0$ into two regions, with the division line at a value of $\mathbf{V}_0$ large enough so that $f(\mathbf{V}_0)$ is already fairly small, but such that $|1/(\omega-\mathbf{k}\cdot\mathbf{V}_0+i/\tau)|^2$ is also fairly small. The contribution of the first region to the integral can then be obtained by expansion; in fact, the result is identical with that given Eq. (12). The contribution of the second region is now written down explicitly.[f]

$$S=\int_{V_1}^{\infty}\frac{f(V_0)\omega_P^2 dV_0}{(\omega-kV_0+i/\tau)^2}+\frac{i}{\tau}\int_{V_1}^{\infty}\frac{f(V_0)dV_0}{(\omega-kV_0+i/\tau)}. \tag{14}$$

Since the frequency must, in general, be complex, we write $\omega=\omega_0+i\lambda$. We then get

$$S=\int_{V_1}^{\infty}f(V_0)dV_0\left[\omega_P^2\frac{\left((\omega_0-kV_0)^2-\left(\frac{1}{\tau}+\lambda\right)^2-2i(\omega_0-kV_0)\left(\frac{1}{\tau}+\lambda\right)\right)}{\left((\omega_0-kV_0)^2+\left(\frac{1}{\tau}+\lambda\right)^2\right)^2}+\frac{\frac{i}{\tau}(\omega_0-kV_0)+\frac{1}{\tau}\left(\frac{1}{\tau}+\lambda\right)}{(\omega_0-kV_0)^2+\left(\frac{1}{\tau}+\lambda\right)^2}\right]. \tag{15}$$

The dispersion relation is obtained by adding to S, the contribution of the low velocity region, obtained from Eq. (12). We get (for small k, large τ) where ω is close to ω_P,

$$1\cong\frac{\omega_P^2}{\omega^2}\left(1+\frac{3k^2\kappa T}{m\omega_P^2}\right)-\frac{i}{\omega_P\tau}+S. \tag{16}$$

One must satify both real and imaginary parts of the above equation. With $\omega=\omega_0+i\lambda$, the imaginary

[e] For a typical plasma in a discharge tube $\lambda\approx 0.1$ cm, $m\omega_P^2/k^2\approx 20$ ev, $l\sim 10$ cm, so $\tau=l/V\sim 10^{-7}$ sec and one obtains $\epsilon\varphi_{\max}\approx m(\omega_P^2/k^2)\cdot(1/\omega_P^2\tau^2)\sim 2\cdot 10^{-5}$ ev. In the interstellar plasma $l\approx 10^{13}$ cm. With $\lambda=10^5$ cm we have $\epsilon\varphi_{\max}\sim 10^{-17}$ ev. We see that near the wave velocity the linear approximation breaks down badly. The effects of particles near the wave velocity on observable plasma oscillations must be studied by the non-linear treatment given in A.

[f] In this work, we restrict ourselves to the one-dimensional case.

part yields

$$0=-\frac{2i\lambda\omega_0\omega_P^2}{(\omega_0^2+\lambda^2)^2}\left(1+\frac{3k^2\kappa T}{m\omega_P^2}\right)-\frac{i}{\omega_P\tau}-i\int_{V_1}^{\infty}f(V_0)dV_0\left[\frac{2(\omega_0-kV_0)\left(\frac{1}{\tau}+\lambda\right)\omega_P^2}{\left((\omega_0-kV_0)^2+\left(\frac{1}{\tau}+\lambda\right)^2\right)^2}-\frac{\frac{1}{\tau}(\omega_0-kV_0)}{(\omega_0-kV_0)^2+\left(\frac{1}{\tau}+\lambda\right)^2}\right]. \tag{17}$$

The real part yields

$$1=\frac{\omega_P^2(\omega_0^2-\lambda^2)}{(\omega_0^2+\lambda^2)^2}\left(1+\frac{3k^2\kappa T}{m\omega_P^2}\right)+\int_{V1}^{\infty}f(V_0)dV_0\left[\frac{\omega_P^2\left((\omega_0-kV_0)^2-\left(\frac{1}{\tau}+\lambda\right)^2\right)}{\left((\omega_0-kV_0)^2+\left(\frac{1}{\tau}+\lambda\right)^2\right)^2}+\frac{\frac{1}{\tau}\left(\frac{1}{\tau}+\lambda\right)}{(\omega_0-kV_0)^2+\left(\frac{1}{\tau}+\lambda\right)^2}\right]. \tag{18}$$

We observe that if $f(V_0)$ is small near the wave velocity, neither the real nor the imaginary part of the frequency will be greatly altered by the integral from V_1, to ∞. Equation (18) will describe mainly a small shift in the real part of the frequency, in which we are not interested, here.[8] Let us then study Eq. (17), from which one can estimate the imaginary part of the frequency. Since the main contribution to the integral comes from a small region near $V_0=\omega/k$, one can expand $f(V_0)=f(\omega_0/k)+(V_0-\omega_0/k)f'(\omega_0/k)+\cdots$. If $\omega_P\tau$ is large, the second term in the integral appearing in Eq. (17) can be shown to be very small compared with the first; hence, we neglect it. The integral then becomes

$$-2\left(\frac{1}{\tau}+\lambda\right)\omega_P^2k\int_{V_1}^{\infty}\frac{\left[f\left(\frac{\omega_0}{k}\right)\left(V_0-\frac{\omega_0}{k}\right)+f'\left(\frac{\omega_0}{k}\right)\left(V_0-\frac{\omega_0}{k}\right)^2+\ldots\right]}{\left((\omega_0-kV_0)^2+\left(\frac{1}{\tau}+\lambda\right)^2\right)^2}dV_0.$$

If V_1 is far away from ω_0/k, the range of integration can, with small error, be extended to infinity. The first integral is then zero, because the integrand is an odd function of $V_0-(\omega_0/k)$. The second integral becomes $-2f'(\omega_0/k)(\omega_P^2/k^2)\cdot\pi/2$.

Noting that for small k and large τ, ω is close to ω_P, we obtain the following approximation to λ

$$\lambda\cong-\frac{1}{2\tau}+\frac{\omega_P^3}{k^2}\cdot\frac{\pi}{2}f'(\omega_0/k). \tag{19}$$

The term involving $1/2\tau$ leads to damping; it has already been obtained in Eq. (12). The second term, however, can lead either to further damping, if $f'(\omega_0/k)$ is negative, or to excitation, if it is positive. In a Maxwellian-like distribution, where f decreases monotonically with the velocity, $f'(\omega_0/k)$ is usually so small that the additional damping is negligible in comparison with that due to collisions. In a Maxwellian distribution, for example, one can write $f=(m/2\pi\kappa T)^{\frac{1}{2}}\exp-mV^2/2\kappa T$, obtaining

$$\lambda\cong-\frac{1}{2\tau}-\frac{\pi}{2}\frac{\omega_0}{(2\pi)^{\frac{1}{2}}}\frac{\omega_P^3}{k^3}\left(\frac{m}{\kappa T}\right)^{\frac{1}{2}}\exp-m\omega^2/2\kappa Tk^2.$$

For a typical value of $\omega_P=10^{10}$ c.p.s., $\kappa T\sim1$ ev, and a wave-length of 1 cm, the additional damping rate is $\cong10^{-26}$/sec., which is very small in comparison with 10^{-7} per second, resulting from collisions. For large k, however, the damping is very large; in fact, as one approaches the Debye wave-length, the damping time becomes less than the period of a plasma oscillation. This shows that when collisions are taken into account, one obtains an additional reason why organized oscillations shorter than a Debye length cannot occur; beyond those reasons given in A, Section (VII). The significance of this point will be discussed further ahead.

In order to obtain excitation, one must have a region above mean thermal speeds where $f'(\omega_0/k)$ is positive; this requires a peak in the distribution function at high velocities, or in other words, a special group of high energy particles. The reason

[8] If $f(V_0)$ is large near the wave velocity, then the shift may be large. We consider such cases later, in connection with teams of well-defined velocity.

why particles near the wave velocity can excite or damp plasma oscillations can be understood in terms of the transfer of energy from particles to waves. Let us recall that particles near the wave velocity can interact very strongly with the wave, because they stay in a force of the same phase for a very long time. It will be shown that particles which emerge from collision with a speed greater than that of the wave tend, on the average, to lose energy to the wave by the time they make their next collision, while particles starting out a little slower gain energy. If $(\partial f/\partial V)(\omega_0/k)$ is positive, this means that there are more faster than slower particles, so that the wave tends to be built up at the expense of the kinetic energy of the particles, while a negative $f'(\omega_0/k)$ produces the opposite tendency. In order to build up the wave in this way, it is necessary, then, that there be a group of particles of higher than average velocity, so that $f'(V_0)$ can be positive for a velocity, ω/k, at which a plasma oscillation can exist.[h] If there were no oscillation, this energy would be degraded by collision, but the plasma wave provides a means of intercepting this stream of energy before it is degraded, and transforming it into electrical energy.

Let us first calculate the energy transfer in the linear approximation. If V_0 is the velocity with which a particle emerges from the collision at the point x_0, and the time t_0, and δV is the change of velocity suffered by the particle before it undergoes another collision at the time, t, and the point, x, the kinetic energy lost by the particle to the wave is

$$\Delta E=\frac{m}{2}(V_0^2-(V_0+\delta V)^2)$$
$$=-mV_0\delta V-m\frac{(\delta V)^2}{2}. \quad (20)$$

According to Eq. (3), δV is to the first order, proportional to $\exp i(kx_0-\omega t_0)$; hence, its average will vanish when taken over all possible starting positions, x_0, leaving only second-order contributions. δV must therefore be obtained by solving the equations of motion to second order. Let us denote this solution as $\delta V=\delta V_1+\delta V_2$, where δV_1 is the first-order solution, given in Eq. (3), and δV_2 is the second-order correction. One must average ΔE over x_0 with the weighting factor

$$N(x_0, t_0)=n_0+Re\ \delta N_0 \exp i(kx_0-\omega t_0)=n_0+\delta N.$$

Since ΔE is already of first order, N need only be expressed to first order, in order to obtain a result correct to second order. The mean energy transfer per unit volume per second per unit velocity is then

$$\langle dW_1/dt\rangle_{Av}=-mf(V_0)/\tau\langle(n_0+\delta N)(V_0(\delta V_1+\delta V_2)$$
$$+1/2(\delta V_1+\delta V_2)^2\rangle_{Av} \quad (21)$$

and to second order, noting that $\langle\delta V_1\rangle_{Av}$ vanishes, we get

$$\langle dW_1/dt\rangle_{Av}=-(mf/\tau)[n_0V_0\langle\delta V_2\rangle_{Av}$$
$$+V_0\langle\delta N\delta V_1\rangle_{Av}+1/2n_0\langle(\delta V_1)^2\rangle_{Av}]. \quad (22)$$

After averaging over x_0, $\langle dW_1/dt\rangle_{Av}$ must be multiplied by the probability that the particles go for a time, without collision, which is

$$(t-t_0)\exp-(t-t_0)/\tau,$$

and integrating over t_0. These calculations are carried out in the appendix. The result is, for sufficiently long collision times,

$$\langle dW_1/dt\rangle_{Av}=\frac{f(V_0)}{\tau}\frac{\epsilon^2\varphi_0^2k^4}{m}\frac{n_0V_0(V_0-\omega/k)}{[(\omega-kV_0)^2+1/\tau^2]^2}. \quad (23)$$

For large τ and V_0 close to ω/k, the energy transfer becomes large, and it is clear that for $V_0>\omega/k$, it is positive, while for $V_0<\omega/k$ it is negative.[i]

For large φ_0 or large τ, the energy transfer implied by the linear approximation may be much larger than the energy available. In this case, one must go to a non-linear treatment. In A (Section III), we already saw that particles near the wave velocity are trapped and oscillate in the trough of the potential, so that after a long time, their gains and losses of energy tend to balance, thus preventing the indefinitely large transfer predicted for large τ, by the linear theory. Yet, in the non-linear limit, the same qualitative result holds. To see this, we note that particles, emerging from their last collision faster than the wave, will, when the potential is large or the mean free path long, end up by oscillating about a mean velocity equal to that of the wave, and hence, lose energy on the average, while particles starting slower than the wave will do the opposite. The non-linear effects merely set a limit to the amount of energy that a given particle can deliver.

In paper A, where it was assumed that no collisions took place, no excitation or damping by particles near the wave velocity was obtained in the exact non-linear treatment. The reason is that in A, the assumption was made that each particle had come to equilibrium with the wave, so that over a long period of time, transfer of energy between

[h] In A, Section VII, it was shown that organized oscillations cannot exist when ω/k is below mean thermal velocities.

[i] In studying the excitation of plasma waves, we have adopted the procedure of regarding the particles near the wave velocity, as a separate system, interacting with the rest of the wave. To justify this, we use the results of A, (Section VI), where it was shown that for organized plasma oscillations, the contribution to the charge density of particles near the wave velocity was negligible. Hence, it is permissible as a first approximation to discuss the wave motion, independently of these special particles, and then to bring in the interaction between these special particles and the rest of the wave. For the non-plasmatic oscillations, also treated in A, (Section VI), this procedure would be impossible, because the oscillation is supported mainly by particles near the wave velocity.

particle and wave averaged out to zero. But in the collision treatment, particles are assumed to emerge with no particular phase relation to the wave; in obtaining such a phase relation as a result of the forces, the particles either lose or gain energy, depending on whether they are faster than the wave or slower, and thus can excite or damp the wave. Landau[2] has given a treatment neglecting collisions in which the particles are assumed to start out at $t=0$ with no particular phase relation to the wave; he obtains the same type of excitation and damping due to particles close to the wave velocity, that we have obtained here. As one approaches the Debye length, where there are many particles near the wave velocity, it becomes necessary to bring so many particles into phase with the wave that heavy damping results.

To estimate the amplitude to expect when the linear approximation breaks down, we see that if $f'(\omega_0/k)$ is positive, and large enough to overcome collision damping, the wave amplitude will grow until the energy dissipated by collisions is equal to that made available by the fast particles as they are slowed down to the wave velocity. Only particles which can be trapped will exchange appreciable amounts of energy with the wave over a long period of time. According to A (Section III), the range of trapped velocities is $(V_0-\omega/k)^2\leqq 2\epsilon\varphi_0/m$. Since the particle ends up with an average velocity equal to that of the wave, $V_W=\omega/k$, the average energy gained by the particle over a long time will be

$$\Delta E=\frac{m}{2}\left(V_0^2-\frac{\omega^2}{k^2}\right)=\frac{m}{2}\left(V_0-\frac{\omega}{k}\right)\left(V_0+\frac{\omega}{k}\right).$$

If φ is not too large, V_0 will be close to ω/k, so that to a first approximation, the above becomes

$$\Delta E=m(\omega/k)(V_0-\omega/k). \tag{24}$$

If $R(V_0)dV_0$ is the mean number of particles entering the range dV_0 per cm^3 per second, then the mean rate at which the particles gain energy is

$$\frac{dW_1}{dt}=\int_{-(2\epsilon\varphi_0/m)^{\frac{1}{2}}}^{+(2\epsilon\varphi_0/m)^{\frac{1}{2}}} \times m\frac{\omega}{k}\left(V_0-\frac{\omega}{k}\right)R(V_0)d\left(V_0-\frac{\omega}{k}\right), \tag{25}$$

where the integration is carried out over the trapped range of velocities. If the gas is in a steady state, the number of particles entering a given velocity range is also equal to the number leaving as a result of collision. Thus, we obtain

$$R(V_0)dV_0=\frac{n_0f(V_0)}{\tau_f}dV_0, \tag{26}$$

where τ_f is the mean time between collisions for fast particles. We then get

$$\frac{dW_1}{dt}\cong\int_{-(2\epsilon\varphi_0/m)^{\frac{1}{2}}}^{+(2\epsilon\varphi_0/m)^{\frac{1}{2}}} \times m\frac{\omega}{k}\left(V_0-\frac{\omega}{k}\right)\frac{n_0f(V_0)}{\tau_f}d(V_0-\omega/k).$$

If the range of velocities is not too broad, $f(V_0)$ can be approximated by expansion as a series of $V_0-\omega/k$. The result is

$$\frac{dW_1}{dt}\cong m\frac{\omega}{k}\frac{n_0}{\tau_f}\cdot\frac{2}{3}\left(\frac{2\epsilon\varphi_0}{m}\right)^{\frac{3}{2}}f'\left(\frac{\omega}{k}\right). \tag{27}$$

To obtain the rate at which the wave dissipates energy by collision, we use the result (Eq. (12)) that the wave dies out to $1/e$ of its value in a time $1/\tau_s$. From this, one concludes that $dW_2/dt=-W/\tau_s$ is the rate of loss of energy, where W is the energy density in the wave, and τ_s is the mean time between collisions for slow particles. Since the total energy of any harmonic oscillation is always twice the mean potential energy, we get $W=\langle E^2\rangle_{\text{Av}}/4\pi=k^2\varphi_0^2/8\pi$ where E is the electric field.

Setting $(dW/dt)+(dW_2/dt)=0$ for a steady state, we obtain

$$\epsilon\varphi_0=\frac{m}{2}\left(\frac{\omega}{k}\right)^2\left(\frac{16}{3}\frac{\omega_P^2}{k^2}\frac{\tau_s}{\tau_f}f'\left(\frac{\omega}{k}\right)\right)^2. \tag{28}$$

In order to get appreciable amplitudes, one needs a region in which f is increasing rapidly with increasing velocity; this is possible only if there is a group of high energy particles. In a typical case, one may take $\omega_P/k\approx 10V_{th}$, and consider a beam of high energy particles containing 0.01 of the total number, and with a velocity spread of the order of mean thermal velocities. Take $\tau_f/\tau_s\approx 100$. Then $(\omega_P^2/k^2)f'(\omega/k)\sim 1$. With thermal energies of the order of 1 ev, one obtains $\epsilon\varphi_0\sim 0.3$ ev.

It is of interest to estimate how much energy a wave of a given potential can exchange with a particle. The maximum value of this quantity can be obtained from Eq. (24) by setting $|V_0-(\omega/k)|=(2\epsilon\varphi_0/m)^{\frac{1}{2}}$. One gets

$$\Delta W_{\max}\approx m\frac{\omega}{k}\left(\frac{2\epsilon\varphi_0}{m}\right)^{\frac{1}{2}}=2\epsilon\varphi_0\left(\frac{m}{2}\frac{(\omega/k)^2}{\epsilon\varphi_0}\right)^{\frac{1}{2}}. \tag{29}$$

One sees that for small $\epsilon\varphi$, the possible energy transfer is much larger than $\epsilon\varphi$ itself. This is because a particle moving at the speed of the wave feels a force of the same sign for a very long time. For example, consider a wave with $\epsilon\varphi_0=0.1$ ev, and wave-length 0.1 cm, so that $k=2\pi/\lambda=20\pi$ cm^{-1}. The maximum electric field is $E=|k\varphi_0|=2\pi$ v

[2] L. Landau, J. Phys., U.S.S.R., 10, 25 (1946).

per cm, so that if the particle moves with the wave for 1 cm, it can deliver 2π v, although no potentials larger than 0.1 v exist; hence, relatively small wave potentials may provide a very effective means of exchanging energy with particles.

VI. PLASMAS OF VARYING DENSITY

If the plasma density varies slowly with position, as, for example, it might do in the neighborhood of a wall, where ions and electrons are being lost by recombination, then there are much more powerful mechanisms for excitation of plasma oscillations. Let us refer to Eq. (12) for the plasma frequency, but express k as a function of ω. We get

$$(3\kappa T/m)k^2=\omega^2-\omega_P{}^2=\omega^2-(4\pi\epsilon^2/m)n_0(x). \quad (30)$$

Suppose that we have a plasma oscillation of a definite frequency, which is moving in a direction in which $n_0(x)$ is decreasing. The wave-length, $\lambda=2\pi/k$, then decreases in the direction of motion of the wave; and the phase velocity, $V_{Ph}=\omega/k$, also decreases.

Consider now a particle which enters the velocity range in which it can be trapped so that it oscillates back and forth about the potential trough. If the wave velocity decreases slowly enough, the particle will respond adiabatically as it moves with the wave, and it will continue to be trapped, oscillating about slower and slower speeds, and giving up more and more energy. When the wave velocity decreases to mean thermal speeds, however, wave motion becomes impossible (see A (Section VII)) so that this mechanism can operate only on particles considerably faster than the mean thermal speed, but where it does operate, practically the entire energy of the particle can be given up.

If the wave moves in the direction of increasing density, its phase velocity increases, and trapped particles can be accelerated. We have suggested this as a possible cause of acceleration of cosmic-ray particles.[3]

To estimate the wave amplitudes that might be produced in this way, we set the rate of loss of energy by particles to the wave equal to

$$\frac{dW_1}{dt}\cong\int_{-(2\epsilon\varphi_0/m)^{\frac{1}{2}}}^{+(2\epsilon\varphi_0/m)^{\frac{1}{2}}}\frac{m}{2}\left(\frac{\omega}{k}\right)^2R(V_0)d\left(V_0-\frac{\omega}{k}\right). \quad (31)$$

This expression implies that every trapped particle liberates all of its kinetic energy. $R(V_0)$ is evaluated in Eq. (26). Here, for small φ_0 we need retain only the first term in the power series. The result is

$$\frac{dW_1}{dt}=\frac{n_0}{\tau_f}m\left(\frac{\omega}{k}\right)^2f\left(\frac{\omega}{k}\right)\left(\frac{2\epsilon\varphi_0}{m}\right)^{\frac{1}{2}}. \quad (32)$$

[3] D. Bohm and E. P. Gross, Phys. Rev. **74**, 624 (1948).

The rate of loss of energy by collisions is still given by $dW_2/dt=-W/\tau_s$. Setting $dW_1/dt+dW_2/dt=0$, we obtain

$$\frac{\epsilon\varphi_0}{m}=2\left[\frac{\tau_s}{\tau_f}\frac{\omega_P{}^2}{k^2}\left(\frac{\omega}{k}\right)^2f\left(\frac{\omega}{k}\right)\right]^{\frac{1}{3}}. \quad (33)$$

The ratio, σ, of this potential to that obtained in Eq. (28), is

$$\sigma=\frac{9}{2}\left[\frac{\tau_s}{\tau_f}\frac{\omega_P{}^2}{k^2}\frac{\omega}{k}\right]^{-4/3}\frac{\left[\frac{\omega}{k}f\left(\frac{\omega}{k}\right)\right]^{\frac{1}{3}}}{[f'(\omega/k)]^2}. \quad (34)$$

One readily sees that for small f and f', σ can become very large. In this mechanism, the energy for excitation of the wave comes from a non-equilibrium property of a plasma of non-uniform density. There is a continual diffusion of particles from regions of high to low density, and this dissipates free energy. The wave can intercept this stream of energy, and transform part of it into energy of ordered motion.

VII. INSTABILITY OF BEAMS OF WELL-DEFINED VELOCITY

The treatment of instability given thus far applies only to a continuous and differentiable velocity distribution. Let us now consider a plasma in which there may be groups of particles within a narrow range of velocities, so that the expansion of Eq. (18) is no longer permissible.

The first problem that we shall consider here is that of a one-dimensional plasma consisting of two beams of the same speed, but moving in opposite directions through a plasma positive ion background with charge density compensating that of the beams in the absence of oscillations. Although this problem is somewhat abstract, it demonstrates in a simple way the most important effects of a sharply defined distribution function. Let $f(V_0)$ have the following values: $f(V_0)=1/2\delta$ when $|V_0|$ lies between $|V_0|=a$, and $|V_0|=a-\delta$; $f(V_0)=0$ for all other values of V_0. This means that each beam has a velocity spread of width, δ. This system has a zero mean velocity.

We assume a very long free path, so that collisions can be neglected, and the treatment given in paper A can be used. According to A (Eq. (9)), the dispersion relation becomes

$$1=\frac{\omega_P{}^2}{2\delta}\left[\left(\int_{-a}^{-a+\delta}+\int_{a-\delta}^{a}\right)\frac{dV_0}{(\omega-kV_0)^2}\right]$$
$$=\frac{\omega_P{}^2}{2k\delta}\left[\frac{1}{\omega-ka}-\frac{1}{\omega-k(a-\delta)}-\frac{1}{\omega+ka}+\frac{1}{\omega+k(a-\delta)}\right] \quad (35)$$

or

$$\frac{\omega_P^2(\omega^2+k^2a(a-\delta))}{(\omega^2-k^2a^2)(\omega^2-k^2(a-\delta)^2)}=1.$$

This is a second-order equation for ω^2, the roots are

$$\omega^2=\frac{\omega_P^2+k^2(a^2+(a-\delta)^2)}{2}$$
$$\pm\tfrac{1}{2}[(\omega_P^2+k^2(a^2+(a-\delta)^2))^2$$
$$-4k^2a(a-\delta)(k^2a(a-\delta)-\omega_P^2)]^{\frac{1}{2}}. \quad (36)$$

We shall restrict ourselves here to the case of small k. One root is (for small k):

$$\omega^2\cong\omega_P^2+k^2[a^2+(a-\delta)^2+a(a-\delta)]. \quad (37)$$

This root corresponds to the usual plasma frequency, obtained in A (Eq. (11)). The other root is

$$\omega^2\cong-k^2a(a-\delta). \quad (38)$$

Unless $\delta=a$, this root corresponds to an imaginary frequency; hence, it represents an instability of the system. (When $\delta=a$, the two beams fuse, and this root approaches $\omega=0$. It is readily verified that the root corresponding to the negative sign of the square root is always imaginary, as long as $k^2<\omega_P^2/a(a-\delta)$.

The physical reason for the instability of this system is as follows: A very small perturbation away from zero field at a given point causes a velocity modulation of each beam. In time, this produces a bunching of space charge, in the direction of motion of each beam, which creates a much larger potential than that due to the original perturbation. The fields due to any one beam modulate the other beam, which then feeds the disturbance back to the source in a highly amplified form. Thus, the perturbation builds up cumulatively, and instability results. If the beams have a spread of velocity, however, particles of different velocity tend to bunch in different places, so that the amplification of the original perturbation is less, and the instability is reduced. When the two beams fuse, the instability is removed altogether. We shall see that, in general, beams of well-defined velocity lead to instability which can be reduced or eliminated by a velocity spread.

Another illustrative problem arises if one sends a beam of fairly well-defined velocity into a main plasma having a continuous and more or less Maxwellian velocity distribution. In paper A, (Section VI), it was shown that a beam of sharply defined velocity adds another degree of freedom to the organized motion of a plasma; in fact, such a system is best described as being made up of two interpenetrating and interacting plasmas. One may therefore expect a corresponding increase in the number of possible frequencies of oscillation, in a manner which is analogous to the behavior of two coupled harmonic oscillators.

Let n_1 denote the density of the main plasma, n_2 that of the special beam. We take $\mathbf{V}_2$ as the mean velocity of the beam, and assume a uniform symmetric spread in velocity of $\boldsymbol{\delta}$ about $\mathbf{V}_2$. We seek solutions where all quantities vary as $\exp(\mathbf{k}\cdot\mathbf{x}-\omega t)$, but restrict outselves to waves long enough so that expansions in kV_0/ω are possible for the main plasma. We also assume infinite free path. We take the x axis of coordinates to be in the $\mathbf{V}_2$ direction. $\boldsymbol{\delta}$ is taken parallel to $\mathbf{V}_2$.

From Eq. (10) the change in density for the main plasma, resulting from the potential $\varphi=\varphi_0\exp(\mathbf{k}\cdot\mathbf{x}-\omega t)$ is

$$\delta N_1=-\frac{\epsilon n_1k^2}{m\omega^2}\left(1+\frac{(\mathbf{k}\cdot\mathbf{V}_0)^2}{\omega^2}\right)\varphi. \quad (39)$$

For the beam particles

$$\delta N_2=-\frac{\epsilon n_2k^2}{m}\frac{1}{2\delta}\varphi\int_{V_2-\delta}^{V_2+\delta}\frac{dV_x}{(\omega-k_xV_2)^2}. \quad (40)$$

From Poisson's equation we obtain the dispersion relation

$$1=\frac{\omega_1^2}{\omega^2}\left(1+\left\langle\left(\frac{\mathbf{k}\cdot\mathbf{V}_0}{\omega}\right)^2\right\rangle_{Av}\right)$$
$$+\frac{\omega_2^2}{(\omega-k_xV_2)^2-\delta^2k_x^2}, \quad (41)$$

where $\omega_1^2=4\pi n_1\epsilon^2/m$; $\omega_2^2=4\pi n_2\epsilon^2/m$. We shall consider here only the case of a weak beam where $n_2\ll n_1$ so that $\omega_2\ll\omega_1$.

The above equation has six roots, when $\langle(\mathbf{k}\cdot\mathbf{V}_0/\omega)^2\rangle_{Av}$ is not neglected. Even in the absence of a special beam, this term would introduce additional roots, which are brought in by the application of the expansion in powers of k^2 beyond the region of its validity. The only roots to be retained are, therefore, those which go continuously into the four obtained by neglecting this term.

Let us divide the discussion of the roots into three cases.

Case (a) $(k_xV_2)^2\gg\omega_1^2$.

One can obtain two of the roots by first noting that when $\omega_2=0$, the roots are

$$\omega\cong\pm\omega_1\left(1+\left\langle\left(\frac{\mathbf{k}\cdot\mathbf{V}_0}{\omega}\right)^2\right\rangle_{Av}\right)^{\frac{1}{2}}=\pm\omega_a.$$

For small ω_2 the solutions will be changed only

slightly. The result is

$$\omega \cong \pm\left[\omega_a^2+\frac{\omega_2^2}{\left(1-\frac{k_xV_2}{\pm\omega_1}\right)^2-\frac{\delta^2k_x^2}{\omega_1^2}}\right]^{\frac{1}{2}}. \quad (42)$$

We have assumed that both ω_1/k_xV_2 and $\langle(\mathbf{k}\cdot\mathbf{V}_0/\omega_1)^2\rangle_{Av}$ are small. These roots correspond to the normal modes in which the main plasma carries most of the energy, and the special group undergoes a small forced oscillation of velocity and density in the field of the main plasma.

To find the second type of root, we notice that if $\omega_1=0$, the solution would be

$$\omega=k_xV_2\pm(\omega_2^2+\delta^2k_x^2)^{\frac{1}{2}}=\omega_{b\pm}. \quad (43)$$

This represents an oscillation involving the special group of particles. The frequency is just the plasma frequency for the special group. For large k_xV_2 it is readily verified that the main plasma is only slightly perturbed by the fields due to the special group. We obtain

$$(\omega-k_xV_2)^2=\delta^2k^2+\frac{\omega_2^2}{1-\frac{\omega_1^2}{\omega_{b\pm}^2}\left(1+\left\langle\left(\frac{\mathbf{k}\cdot\mathbf{V}_0}{\omega_{b\pm}}\right)^2\right\rangle_{Av}\right)}. \quad (44)$$

Since $\omega_{b\pm}^2\gg\omega_1^2$, the above implies only a small frequency shift away from $\omega_{b\pm}$. This is, therefore, the normal mode in which the beam oscillates almost independently of the rest of the plasma. The frequency of oscillation may be, for this case, far above the natural frequency, ω_1, of the main plasma. Physically, this happens because the special group of particles has an oscillation with a very short wave-length, which together with the Doppler shift results in a frequency so high that the main plasma cannot respond appreciably.

The behavior of this system is very analogous to that of two weakly coupled harmonic oscillators. The case considered above corresponds to a situation in which the natural frequencies of each oscillator are very different. The normal modes then involve the excitation mainly of one oscillator to a time, while the other oscillator responds weakly.

Case (b) $k_xV_2\ll\omega_1$.

We can obtain the approximate solutions in a way similar to Case (a). One finds for the solution oscillating near the main plasma frequency

$$\omega^2\cong\omega_1^2+\langle(\mathbf{k}\cdot\mathbf{V}_0)^2\rangle_{Av}+\frac{\omega_2^2\omega_1^2}{(\omega_1-k_xV_2)^2-\delta^2k_x^2}. \quad (45)$$

To obtain the oscillation near the beam frequency, we write $\alpha=\omega-k_xV_2$. From Eq. (41) we then obtain

$$\alpha^2=k_x^2\delta^2+\frac{\omega_2^2}{1-\frac{\omega_1^2}{\omega^2}\left(1+\left\langle\left(\frac{\mathbf{k}\cdot\mathbf{V}_0}{\omega}\right)^2\right\rangle_{Av}\right)}. \quad (46)$$

We now assume $\alpha/k_xV_2\ll1$. The above equation yields, with the neglect of α on the right-hand side,

$$\alpha^2\cong k_x^2\delta^2-\left(\frac{k_xV_2}{\omega_1}\right)^2\frac{\omega_2^2}{\left(1+\left\langle\left(\frac{\mathbf{k}\cdot\mathbf{V}_0}{k_xV_2}\right)^2\right\rangle_{Av}\right)}. \quad (47)$$

Since $\omega_2/\omega_1\gg1$, and $k_x\delta\ll k_xV_2$, we see that α is indeed much less than k_xV_2.

The oscillation frequency[j] has not been changed much from k_xV_2, but there is a qualitatively new effect; namely, α can become imaginary, so that the system becomes unstable. We note that the spread of velocities, δ, opposes this instability; in fact, if $\delta^2>(\omega_2^2/\omega_1^2)V_2^2\cos^2\theta$, where θ is the angle between $\mathbf{k}$ and $\mathbf{V}_2$, the distribution is stable. This result is very analogous to that obtained with the plasma consisting of interpenetrating beams moving in opposite directions. In this case, the instability is due to amplification of a perturbation by bunching of the beam, with subsequent feedback through the main plasma.

Case (c) $k_xV_2\cong\omega_1$.

This corresponds to the resonant case for harmonic oscillators, because ω is close both to k_xV_2 and to ω_1. The interactions of the two systems will be greatest in this region. It is also in this region that the change from real to complex roots occurs, since, when $k_xV_2\gg\omega_1$, all the roots are real, while two of them are complex when $k_xV_2\ll\omega_1$. Furthermore $|Im\,\alpha|$ must have a maximum for some value of k_xV_2, because it rises steadily as k_xV_2 is increased, but must fall to zero again at the point of transition between real and complex roots. The maximum can be reached only in the region where k_xV_2/ω_1 is neither large nor small, hence, it must occur where $k_xV_2\cong\omega_1$. An order of magnitude estimate of this maximum can be obtained by setting $k_xV_2=\omega_1/2$ in Eq. (47). The result is

$$\alpha^2{}_{max}\cong k_x^2\delta^2-(\omega_2^2/4).$$

To prevent instability, the spread of velocities must be at least $\delta=\omega_2/2k_x$. This means that sharply defined beams cannot exist in equilibrium for any great length of time; they create the oscillations which scatter them.

[j] Note $kV_2\ll\omega_1$, so that we have oscillations far below the main plasma frequency. These can exist only by virtue of the beam charges.

VIII. CONCLUSION

Whenever a plasma contains beams of particles of well-defined velocity, or groups of particles for above mean thermal speeds, the system can become unstable, and small oscillations grow until they are limited by the appearance of non-linear effects. Collisions tend to damp the wave, and thus provide a stabilizing effect. In a sense, special groups of particles may be said to create the oscillations which scatter them since plasma electrons can scatter much more effectively when they move coherently than when they set at random. This effect must be taken into account in estimating the rate at which a Maxwellian distribution among the electrons tends to be established. With these results, one can explain the experiments of Langmuir[4] which showed that groups of fast electrons are scattered much more rapidly than can be accounted for by random collisions alone.

Thus far, we have studied only a few of the possible causes of instability. In Paper C, we shall treat the effects of boundary conditions, which are responsible for many important instabilities. A complete investigation, extending the treatment to include effects of variations of density and temperature, non-linear phenomena, positive ions, and magnetic fields remains to be carried out.

Plasmas occur not only in discharge tubes, but also in the ionosphere of the earth, the atmosphere of the sun, and interstellar gas and dust clouds. Since streams of fast particles are continually being emitted from below into the atmosphere of the sun, one may expect a great deal of instability, particularly because the plasma density decreases as one leaves the surface of the sun. Vlasov,[5] Martyn,[6] and Haeff[7] have suggested also that the motion of plasma particles in the magnetic fields of sunspots can cause oscillations, which may be able to account for the high intensity of radio waves that the sun is known to emit. When there is a magnetic field, transverse and longitudinal waves are coupled, so that all plasma oscillations can produce radio waves, which are certain to escape, because the plasma density decreases as one leaves the surface, so that the waves cannot be reflected back in.

It is not unlikely that the plasmas of interstellar space, are also highly unstable. For example, photo-ionization should be able to supply high energy electrons which can excite plasma waves by the mechanism described in this paper. There may also be a galactic magnetic field[8] which produces further instabilities. Any two ion gases with different average velocities will also be unstable if they collide and interpenetrate. Some of these mechanisms may perhaps explain the observed radio waves coming from interstellar space.

[4] I. Langmuir, Phys. Rev. **26**, 585 (1925).
[5] J. S. Shklovsky, Nature **159**, 752 (1947).
[6] D. F. Martyn, Nature **159**, 27 (1947).
[7] A. V. Haeff, Phys. Rev. **74**, 1532 (1948).
[8] L. Spitzer, Phys. Rev. **70**, 777 (1947).

IX. APPENDIX

The expression for the average transfer of kinetic energy from particle to wave is given in Eq. (23). The first step is to evaluate $\langle \delta V_2 \rangle_{Av}$, the average value of the second order correction to the velocity. To do this, we begin with the equation of motion

$$m\frac{dV}{dt} = Re\, i\epsilon k \varphi_0 e^{i(kx-\omega t)}. \tag{48}$$

Writing $x \cong x_0 + V_0(t-t_0) + \delta x_1$, where δx_1 is the first-order correction to x, we get the following expression for dV/dt, accurate to the second order

$$\frac{dV}{dt} \cong Re \frac{i\epsilon k \varphi_0}{m} e^{i(kx_0-\omega t_0)} e^{i(kV_0-\omega)(t-t_0)} e^{ik\, Re\, \delta x_1}. \tag{49}$$

Now, over a finite time, it is always possible to choose φ_0 so small that $k\delta x_1$ is also small; hence $\exp ik\, Re\, \delta x_1$ can be expanded, and we get

$$\frac{dV}{dt} = \frac{d}{dt}(\delta V_1) - Re \frac{\epsilon k^2 \varphi_0}{m} e^{i(kx_0-\omega t_0)} e^{i(kV_0-\omega)(t-t_0)} Re\, \delta x_1,$$

where δV_1 is the first-order correction to V, given in Eq. (3). To obtain δx_1, one integrates Eq. (3) for δV_1, obtaining

$$\delta x_1 = \int_{t_0}^{t} \delta V_1 dt = \frac{\epsilon k \varphi_0}{m} \int_{t_0}^{t} e^{i(kx_0-\omega t_0)} \times \left(\frac{e^{i(kV_0-\omega)(t-t_0)} - 1}{kV_0 - \omega} \right) dt. \tag{50}$$

We wish to average δV_2 over x_0, and then over $(t-t_0)$ with the weighting factor $\exp -(t-t_0)/\tau$. This can be accomplished by first averaging $d\delta V_2/dt$ over x_0 then integrating the latter to obtain δV_2, and then averaging the latter over t_0. To average over x_0, we use the theorem that if f and g are complex numbers proportional to $\exp ikx_0$, then $\langle Re\, f\, Re\, g \rangle_{Av} = \langle Re\, (f^* g/2) \rangle_{Av}$. We then get

$$\left\langle \frac{d}{dt} \delta V_2 \right\rangle_{Av} = -\frac{\epsilon^2 \varphi_0^2 k^3}{2m^2(kV_0-\omega)} \times Re \left[\frac{1 - e^{-i(kV_0-\omega)(t-t_0)}}{i(kV_0-\omega)} - (t-t_0) e^{-i(kV_0-\omega)(t-t_0)} \right]. \tag{51}$$

The next step is to average over $(t-t_0)$. To do this, we use the result that

$$\int_{t-t_0=0}^{\infty} \frac{e^{-(t-t_0)/\tau}}{\tau} \delta V_2(t-t_0)d(t-t_0) = \int_{t-t_0=0}^{\infty} e^{-(t-t_0)/\tau} \frac{d\delta V_2}{dt} d(t-t_0), \quad (52)$$

which can be obtained by integration by parts, and noting that $\delta V(t=t_0)$ vanishes by definition. Thus, we obtain for average over both x_0 and $t-t_0$,

$$\langle V_2\rangle_{Av} = -\frac{\epsilon^2\varphi_0^2k^3}{2m^2(kV_0-\omega)} \times Re\int_0^{\infty} d\eta e^{-\eta/\tau}\left[\frac{1-e^{-i(kV_0-\omega)\eta}}{i(kV_0-\omega)} - \eta e^{-i(kV_0-\omega)\eta}\right], \quad (53)$$

where we have replaced $(t-t_0)$ by η. This can be integrated to yield

$$\langle \delta V_2\rangle_{Av} = -\frac{\epsilon^2\varphi_0^2k^3}{m^2} \frac{(kV_0-\omega)}{[(\omega-kV_0)^2+1/\tau^2]^2}. \quad (54)$$

Let us now average the term δV_1^2 over x_0 (see Eq. (20)). From (3), we obtain

$$\langle \delta V_1^2\rangle_{Av} = \langle \tfrac{1}{2}|\delta V_1|^2\rangle_{Av} = \frac{\epsilon^2\varphi_0^2k^2}{m^2(\omega-kV_0)^2} \times(1-\cos(kV_0-\omega)(t-t_0)).$$

When this is multiplied by $\exp-(t-t_0)/\tau$, and integrated over $(t-t_0)$, we get

$$\langle \delta V_1^2\rangle_{Av} = \frac{\epsilon^2\varphi_0^2k^2}{m^2(\omega-kV_0)^2}\left[1-Re\,\frac{1}{1+i(\omega-kV_0)\tau}\right] = \frac{\epsilon^2\varphi_0^2k^2}{m^2} \frac{1}{(\omega-kV_0)^2+1/\tau^2}. \quad (55)$$

We now evaluate the term $\delta N(x_0, t_0)\delta V_1$. From Poisson's equation,

$$\nabla^2\varphi = +4\pi\epsilon\delta N$$

or

$$\delta N(x_0, t_0) = -\frac{k^2\varphi_0}{4\pi\epsilon} e^{i(kx_0-\omega t_0)}.$$

Averaging over x_0, we get

$$\langle \delta N\delta V_1\rangle_{Av} = -\frac{1}{2}\frac{k^3\varphi_0^2}{4\pi m(kV_0-\omega)} Re(e^{i(kV_0-\omega)(t-t_0)}-1).$$

Averaging over $(t-t_0)$ yields

$$\langle \delta N\delta V_1\rangle_{Av} = \frac{1}{2}\frac{k^3\varphi_0^2}{4\pi m}\frac{(kV_0-\omega)}{(kV_0-\omega)^2+1/\tau^2}. \quad (56)$$

The complete expression for ΔW is then, according to Eq. (22),

$$\langle dW_1/dt\rangle_{Av} = -\frac{mf(V_0)}{\tau} \times[n_0V_0\delta V_2 + V_0\delta N\delta V_1 + \tfrac{1}{2}n_0\delta V_1^2] = \frac{n_0f(V_0)}{\tau}\frac{\epsilon^2\varphi_0^2k^2}{m}\left[\frac{kV_0(kV_0-\omega)}{[(kV_0-\omega)^2+1/\tau^2]^2} - \frac{kV_0}{2\omega_P^2}\frac{(kV_0-\omega)}{(kV_0-\omega)^2+1/\tau^2} - \frac{1}{2}\frac{1}{(kV_0-\omega)^2+1/\tau^2}\right]. \quad (57)$$

For large values of τ, the first term is clearly the main one, and one obtains

$$\langle dW_1/dt\rangle_{Av} \cong \frac{n_0f(V_0)}{\tau}\frac{\epsilon^2\varphi_0^2k^4}{m}\frac{V_0(V_0-\omega/k)}{[(kV_0-\omega)^2+1/\tau^2]^2}. \quad (58)$$

Nuclear Shell Structure* **

EUGENE FEENBERG AND KENYON C. HAMMACK
Washington University, St. Louis, Missouri
(Received December 27, 1948)

The existence of closed shells in nuclei is indicated by the particular stability and abundance of nuclear systems with certain numbers of neutrons and of protons. An interesting correspondence exists between these numbers and the degeneracy of energy levels in the model of free particles in a simple rectangular potential well. The empirical relations suggest the addition of a central depression to the well for light nuclei (N or $Z \leqq 20$) and a central elevation (Elsasser's wine bottle potential) for heavy nuclei. The qualitative physical explanation of these modifications is that for light nuclei, the particle density, and thus the nuclear interaction energy, is greatest at the center of the nucleus; for heavy nuclei, the Coulomb repulsion between protons produces a particle density varying from a minimum at the center to a maximum near the boundary, and therefore a similarly varying interaction energy. In the free particle model, levels with small angular momentum and nodes within the nucleus are displaced upward by the central elevation and crossing of levels in the desired direction occurs, though not exactly as required to explain the complete empirical list of closed shell numbers. It is apparent that a single particle model of the nucleus is an insufficient approximation; however qualitative arguments based on configuration interaction enable one to formulate, with little ambiguity, a shell model in agreement with the empirical facts.

Experimentally known spins, magnetic moments and quadrupole moments of nuclei with a small number of particles outside of closed shells, or missing from closed shells, tend to corroborate the model. The agreement is particularly good for odd nuclei with one kind of nucleon forming a closed shell ±one particle (and still better if the even group of nucleons constitutes a closed shell). Under these conditions, the orbit of the odd particle, as given by the shell model, usually determines the state of the nucleus, which is checked for consistency with the known spins and moments. In some cases, the reasoning is reversed as a means of fixing the crossover points between energy levels in the theory.

Islands of isomerism appear in a table of odd nuclei arranged according to the odd member of the pair N, Z. Since isomerism occurs when large spin differences exist between the ground state and the excited state, the correlation of isomerism with the crossing or close spacing of energy levels in the shell model is readily seen. Possible paired configurations representing ground state and isomeric state are assigned to various isomeric transitions. Spins and moments (where known), and parity relationships given by Wiedenbeck's plot of half-life *vs.* energy, help to decide the preferred configurations and to clarify the details of the shell model.

Beta-decay transitions are classified empirically into allowed and forbidden categories on the basis of calculated ft values. The configurations of the parent and daughter nuclei, as given by the shell model, determine the parity and range of possible spin values for each. Using the Gamow-Teller selection rules, the consistency of the empirical allowed or forbidden classification with the possibilities of the shell model are investigated. In many cases the ambiguity of spin in the parent or daughter nucleus is lessened. The empirical transition classification breaks down in several cases, chiefly those in which transitions that are theoretically first forbidden ($\Delta I = \pm 2$, change in parity) have ft values that place them in the empirical second forbidden category, indicating a very small nuclear matrix element. An extensive table of allowed (unfavored) transitions shows no trend of ft with atomic mass over the range $19 \leqq A \leqq 140$.

I. INTRODUCTION

THE proton and neutron numbers 2, 8, 10, 20, 50, and 82 and the neutron number 126 are associated with particularly stable nuclear systems.[1–4] These numbers correlate in an interesting fashion with the degeneracy of the levels in the model of free particles in a potential well. Known results[5] for the oscillator potential and the rectangular well of infinite depth are listed in Tables I and II to facilitate the present discussion.

With a well of finite depth the levels are pushed closer together against the bottom of the well, but no crossovers occur.[6,7]

The two potentials possess the closed shell numbers $\Sigma\nu = 2$, 8, 20 and 40 in common. Neither shape of well yields the complete set of numbers $\Sigma\nu = 2$, 8, 10, 20 at the beginning of the empirical series. However there exist reasonable modifications of the potentials which put the $2s$ level below the $3d$ in agreement with the empirical order. In a light nucleus the inner region of constant particle density is lacking and the optimum single particle potential may be expected to resemble an inverted error

TABLE I. *Oscillator potential.* ϵ_{nl}-energy in arbitrary units measured from the bottom of the well. ν-degeneracy (statistical weight) of the level $(=2(2l+1))$.

Level	$1s$	$2p$	$2s+3d$	$3p+4f$	$3s+4d+5g$	$4p+5f+6h$
ϵ_{nl}	3	5	7	9	11	13
ν	2	6	12	20	30	42
$\Sigma\nu$	2	8	20	40	70	112

* Assisted by the joint program of the ONR and the AEC. This research was begun at the Brookhaven National Laboratory during the summer of 1948.

** Please see comments on this and the succeeding paper in a Letter to the Editor by Eugene Feenberg, Kenyon C. Hammack, and L. W. Nordheim, this issue.

[1] W. Elsasser, J. de phys. et rad. **5**, 625 (1934).
[2] Eugene Wigner, Phys. Rev. **51**, 947 (1937).
[3] William H. Barkas, Phys. Rev. **55**, 691 (1939).
[4] Maria G. Mayer, Phys. Rev. **74**, 235 (1948).
[5] H. A. Bethe and R. F. Bacher, Rev. Mod. Phys. **8**, 82 (1936). *Added in proof.*—The idea of a nuclear shell structure analogous to atomic shell structure was proposed by J. H. Bartlett, Nature **130**, 165 (1932). In this connection the early papers of W. D. Harkins (J. Frank. Inst. **194**, 645 (1923)) should be consulted.
[6] Henry Margenau, Phys. Rev. **46**, 613 (1934).
[7] L. Motz and E. Feenberg, Phys. Rev. **54**, 1055 (1938).

TABLE II. Rectangular potential of infinite depth and radius R. ϵ_{nl} in units $\hbar^2/MR^2 \sim 19.3/A^{2/3}$ (Mev) measured from the bottom of the well ($R \sim 1.47\times10^{-13}A^{1/3}$ cm).

Level	$1s$	$2p$	$3d$	$2s$	$4f$	$3p$	$5g$	$4d$	$6h$	$3s$	$5f$	$7i$	$4p$	$6g$
ϵ_{nl}	4.93	10.1	16.6	19.7	24.4	29.8	33.5	41.3	43.8	44.4	54.2	55.3	59.4	68.5
ν	2	6	10	2	14	6	18	10	22	2	14	26	6	18
$\Sigma\nu$	2	8	18	20	34	40	58	68	90	92	106	132	138	156
$\Sigma^{\mathrm{I}}\nu$				////////		////////	50		82					
$\Sigma^{\mathrm{II}}\nu$				////////		////////				////////	////////		////////	126
$\Sigma^{\mathrm{III}}\nu$						////////						126		
$\Sigma^{\mathrm{IV}}\nu$								////////		////////			126	

function. Such a function can be approximated, after a fashion, by a rectangular well with a central depression. It is clear that a narrow central depression pulls down the $2s$ level relative to the $3d$. Thus there is an adequate physical basis for the observed sequence of closed shells in light nuclei (N or $Z \leqq 20$). In somewhat heavier systems the optimum single particle potential begins to approximate to a rectangular well of finite depth paralleling the tendency for the particle density to become constant within the nucleus as the $4f$ shell fills up (because of the small magnitude of the $4f$ wave function in the central region). Elsasser[1] proposed omitting the $2s$, $3p$, and $3s$ levels. One would now add that the omission of $2s$ should not apply to light nuclei. The numbers 50 and 82 then occur among the possible values of $\Sigma\nu$ (fifth row of Table II). The number 126 occurs if the levels $2s$, $3p$, $3s$, $5f$, and $4p$ are omitted (sixth row of Table II) or if the $3p$ level only is omitted (seventh row of Table II) or if the $4d$ and $3s$ levels are omitted (last row of Table II).

Elsasser[1] also considers the possibility of a wine bottle shape of well to account for the displacement of the $2s$ and $3p$ levels above those which must be occupied to give the numbers 50 and 82. His numerical calculations show that a considerable displacement (although not enough) is produced by a central potential elevation of the form

$$(30\hbar^2/MR^2)\exp\{-25(r/R)^2\} \qquad (1)$$

rising from the floor of the well. This central elevation inverts the order of $2s$ and $4f$ and of $3p$ and $5g$ and brings $4d$ and $6h$ almost into coincidence. Clearly a displacement approaching or perhaps meeting the empirical requirements can be realized by increasing the range of the central elevation and simultaneously modifying the altitude.

Physical Basis for the Wine Bottle Potential

The explanation of the wine bottle potential is to be sought in the Coulomb repulsion between protons acting in opposition to the uniformizing tendency of the specifically nuclear forces. Because of the Coulomb force, the proton density within a heavy nucleus varies from a minimum value at the center to a maximum near the boundary. In addition a non-uniform proton density creates forces which distort the neutron distribution and tend to make the two particle densities vary in the same manner. This effect has been investigated independently by E. Wigner[7a] and one of the present writers.[8] A simple estimate yields the following results for the ratio of maximum to minimum particle density:

$$\{\rho_{\max}/\rho_{\min}\}_{\text{proton}} \sim 1+0.0022A,$$
$$\{\rho_{\max}/\rho_{\min}\}_{\text{neutron}} \sim 1+0.0010A. \qquad (2)$$

The existence of a central elevation growing rapidly with increasing atomic number follows at once from the behavior of the particle densities. A simple generalization of the theory leading to Eq. (2) should permit the numerical determination of the single particle potential within reasonable limits of uncertainty.

As the central elevation grows, levels with small angular momentum and nodes within the nucleus ($n>l+1$) move up on the energy diagram. In coordinate space, the corresponding wave functions are pushed out of the central region thus contributing to the decrease in particle density from which the central elevation arises. Simultaneously the filling of the $4f$, $5g$, and $6h$ orbits ($n=l+1$, no nodes within

[7a] Eugene Wigner, Bicentennial Symposium University of Pennsylvania (1940).

[8] Eugene Feenberg, Phys. Rev. **59**, 593 (1941); Richard D. Present, Phys. Rev. **72**, 1 (1947), has applied these results to explain the division of nuclear charge between light and heavy fragments in fission.

Equation (2) is based on the semi-empirical energy formula, in particular on the symmetry term $u_\tau(N-Z)^2/A$ with u_τ treated as a constant. However u_τ is not constant, but varies in an oscillatory manner (Eugene Feenberg, Rev. Mod. Phys. **19**, 239 (1947)). The inclusion of the first and second derivatives of u_τ with respect to A in the calculation of the non-uniform particle density should result in the addition of an oscillatory component to the right-hand member of Eq. (2). The writers hope to discuss the relation between these oscillatory effects and shell structure in a future paper.

the nucleus) reinforce the trend toward the formation of a semihollow nucleus.

Section V contains two numerical calculations on the behavior of energy levels in a wine bottle shape of potential well. The results show that the central elevation does indeed produce a notable relative shift of certain levels in the desired direction, but does not encourage the view that an exact reproduction of the empirical situation can be achieved in the single particle approximation. It is satisfactory that extremely simple models based on general physical ideas do go far in the desired direction.

For orientation one may consider the extreme limiting situation of a particle confined to a spherical shell with $R-\Delta R \leqq r \leqq R$ and $\Delta R \ll R$. The energy eigenvalues are

$$\epsilon_{nl}=\frac{\hbar^2\pi^2(n-l)^2}{2M(\Delta R)^2}+\frac{\hbar^2\pi^2}{2MR^2}\left(1+\frac{\Delta R}{R}\right)l(l+1). \quad (3)$$

In this case all states with nodes within the shell ($n>l+1$) are pushed far up on the energy diagram and the levels with $n=l+1$ occur in the order of increasing angular momentum.

The Shell Model

The shell model can now be formulated as follows:

(*a*) There exist closed shells of neutrons and protons having the structures

$$\begin{gathered}(1s)^2\\(1s)^2(2p)^6\\(1s)^2(2p)^6(2s)^2\\(1s)^2(2p)^6(2s)^2\,(3d)^{10}\\(1s)^2(2p)^6(3d)^{10}(4f)^{14}(5g)^{18}\\(1s)^2(2p)^6(3d)^{10}(4f)^{14}(5g)^{18}(6h)^{22}(4d)^{10}\begin{bmatrix}(4d)^{10}(6g)^{18}\\(4d)^{10}(5f)^{14}(2s)^2(3s)^2\\(5f)^{14}(3p)^6\,(4p)^6(2s)^2\end{bmatrix}\\(1s)^2(2p)^6(3d)^{10}(4f)^{14}(5g)^{18}(6h)^{22}(7i)^{26}.\end{gathered} \quad (4)$$

In the "82" and "126" structures, the order in which the "outer" shells are filled still requires discussion.

(*b*) Certain levels ($2s$, $3p$, $4d$ and others) drift upward with increasing N and Z.

(*c*) In odd nuclei (A odd) the shell structure of the odd group of particles is most pronounced and the predictions of the model most reliable when the even group of particles forms a closed shell.

Statements *a*, *b*, and *c* may be accepted as working hypotheses and utilized in the interpretation of spins, parities, magnetic moments, quadrupole moments, radioactivity, and isomerism. The model is particularly useful for studying systems containing one particle outside of closed shells or with one particle missing from a closed shell.

II. SPINS AND MOMENTS

The spins and magnetic moments of nuclei with a small number of particles outside of closed shells or missing from closed shells provide valuable corroborative evidence on the angular momentum of the single particle levels. Experimental results[9] and interpretations are collected in Table III(a).

The configuration $(3d)^1(3d)^2$ contains completely symmetrical states ^2I, ^2G, ^2F, ^2D, and ^2S; the absence of ^2P is a difficulty in the interpretation of the predominantly $^2P_{3/2}$ ground state of $_{11}Na^{23}$.

The interpretation of the $_7N^{15}$, $_9F^{19}$, $_{19}K^{39}$, and $_{19}K^{41}$ spins and moments in terms of shell structure is not new.[3,10,11] To account for the spin of $_{41}Cb^{93}$ it is supposed that the $3p$ and $4f$ levels fill up before any particle enters a $5g$ orbit; the first $5g$ proton then occurs at $Z=41$ and as the $5g$ shell fills up the $2s$ and $3p$ levels are pushed above the $5g$. Hypothesis *a* is therefore extended to include the closed shell structures

$$\begin{gathered}(1s)^2(2p)^6(3d)^{10}(4f)^{14}(3p)^6\\(1s)^2(2p)^6(3d)^{10}(4f)^{14}(3p)^6(2s)^2\\(1s)^2(2p)^6(3d)^{10}(4f)^{14}(2s)^2(3p)^6.\end{gathered} \quad (5)$$

The instability of all known nuclei containing 39 neutrons can be understood most simply in terms of an energetically favored closed shell at $N=40$ A similar situation exists at $N=19$ and 20, there being no stable systems with $N=19$. The magnetic moment of $_{39}Y^{89}$ favors the closing of a $3p$ shell at $Z=40$. If this interpretation is correct, the $2s$ and $3p$ levels have not yet crossed at $Z=39$ and only the third structure listed in Eq. (5) actually occurs. Independent evidence for the proposed shell structure is provided by the distribution of isomerism as a function of the odd member of the pair N, Z in

[9] H. H. Goldsmith and D. R. Inglis, *The Properties of Atomic Nuclei I* (Information and Publications Division, Brookhaven National Laboratory, Upton, New York, October 1, 1948), L. Rosenfeld, *Nuclear Forces II* (Interscience Publishers, New York, 1949), p. 393, R. Pound, Phys. Rev. **73**, 112 (1948).

[10] M. E. Rose and H. A. Bethe, Phys. Rev. **51**, 205 and 993 (1937).

[11] David R. Inglis, Phys. Rev. **53**, 470 (1938).

odd nuclei (next section). Table III(b) is helpful in locating the $2s$, $4f$ crossover.

Here the configurations are based on a $2s$, $4f$ crossover between $Z=31$ and 33. An earlier crossover would replace the $(4f)^{-3}$ configuration by $(4f)^{-1}$. However, the even group of neutrons in $_{31}Ga^{71}$ forms a closed "40" shell and should contribute no additional angular momentum. Thus a $(4f)^{-1}$ configuration at $Z=31$ is unlikely and the crossover should occur at $Z\geqq 31$. The existence of one or two nuclei with isomeric levels at $N=29$ (next section) suggests a crossover as close to $Z=29$ as possible consistent with other evidence. The jump from $(4f)^{-3}$ at $Z=31$ to $(4f)^{14}(2s)^1$ at $Z=33$ illustrates a characteristic feature of the shell model. A similar jump marks the closing of the $6h$ shell (Section III).

Note added in proof.—None of the immediate possibilities of the shell model fits $_{33}As^{75}$. Here the state contains approximately equal parts of $^2P_{3/2}$ and $^2D_{3/2}$. The shell model offers $(4f)^{14}(2s)^1$ (crossover at $Z=31$) or $(4f)^{-1}$ (crossover just beyond $Z=33$). In either case one or more units of additional angular momentum are required. Support for the latter assignment may be derived from the $_{27}Co^{61}(g)\rightarrow{}_{28}Ni^{61}(g)$ radioactivity (Parmley, Moyer, and Lilly, Phys. Rev. **75**, 619 (1949)) with $W_0=3.6$ mc^2 and half-life 6.3×10^3 sec. From $ft=2.6\times10^5$, the assignment to the allowed (unfavored) type of transition is unambiguous. Hence, the parities of both ground states are identical and consequently both are odd since the $(4f)^7$ configuration is assigned to $_{27}Co^{61}$ without ambiguity. In the absence of additional angular momentum supplied by the even group of particles the model requires a ^2F ground state for $_{28}Ni^{61}$.

Although the ground states of the bromine isotopes are predominantly $^2P_{3/2}$ there is a large admixture of $^2D_{3/2}$. An explanation may be sought in the proximity of the $(3p)^3$ configuration. The small positive quadrupole moments ($_{35}Br^{79}$: 0.28×10^{-24} cm^2, $_{35}Br^{81}$: 0.23×10^{-24} cm^2) are consistent with a large admixture of $^2D_{3/2}$.

Three nuclei fit satisfactorily with the closing of the $5g$ shell at $Z=50$ and the beginning of the $4d$ shell at $Z=51$. However, $_{51}Sb^{123}$ presents a difficulty since its spin suggests that an f or g shell begins to fill at $Z=51$. It is probable, of course, that the even group of neutrons supplies one or more units of orbital angular momentum. A similar situation with the addition of two neutrons changing the spin by one unit when N is even occurs at $Z=37$ and 77. More often the addition of two neutrons when N is even produces no change in spin and very little change in magnetic moment ($Z=1$, 17, 19, 29, 31, 47, 49, 55, 63, 75, and 81). The latter statement also holds for the addition of two protons ($N=65$) when Z is even.

The next item $_{56}Ba^{137}$ indicates the completion of the $4d$ shell at $N=82$. It appears that between $A=121$ and $A=137$ the $4d$ neutron level is displaced above the $6h$ and thus $4d$ orbits show up at $N=81$ as well as at $Z=51$. Since the $4d$ and $6h$ levels are quite close in the rectangular well the displacement required is not large and could be produced by a sufficiently rapid development of the central elevation with increasing atomic number.

The two thallium isotopes conform to the proposed shell structure only if the neutrons are permitted to contribute one or more units of orbital

TABLE III. (a) Nuclear spins and magnetic moments.*

Nucleus	Spin	Mag. moment	Configuration	Additional ang. moment	State
$_7N^{15}$	1/2	$\pm(?)0.280$	$(2p)^{-1}$	0	$^2P_{1/2}+(^2S_{1/2})$
$_9F^{19}$	1/2	2.63	$(2s)^{-1}$	0	$^2S_{1/2}+(^2P_{1/2})$
$_{11}Na^{22}$	3	1.8	$(3d)^1(3d)^1$	—	$^3D_3+^3G_3$
$_{11}Na^{23}$	3/2	2.22	$(3d)^1(3d)^2$	—	$(^2P_{1/2})+^2D_{3/2}$
$_{19}K^{39}$	3/2	0.39	$(3d)^{-1}$	0	$^2D_{3/2}+(^2P_{3/2})$
$_{19}K^{41}$	3/2	0.22	$(3d)^{-1}$	0	$^2D_{3/2}+(^2P_{3/2})$
$_{21}Sc^{45}$	7/2	4.8	$(4f)^1$	0	$^2F_{7/2}+(^2G_{7/2})$
$_{39}Y^{89}$	1/2(?)	<0.1	$(2s)^{-1}$	0	$^2S_{1/2}+(^2P_{1/2})$
$_{39}Y^{89}$	1/2(?)	<0.1	$(3p)^{-1}$	0	$^2P_{1/2}+(^2S_{1/2})$
$_{41}Cb^{93}$	9/2	5.3	$(5g)^1$	0	$^2G_{9/2}+(^2H_{9/2})$
$_{38}Sr^{87}$	9/2	-1.1	$(5g)^{-1}$	0	$^2G_{9/2}+(^2H_{9/2})$
$_{49}In^{113}$	9/2	5.5	$(5g)^{-1}$	0	$^2G_{9/2}+(^2H_{9/2})$
$_{49}In^{115}$	9/2	5.5	$(5g)^{-1}$	0	$^2G_{9/2}+(^2H_{9/2})$
$_{51}Sb^{121}$	5/2	3.7	$(4d)^1$	0	$^2D_{9/2}+(^2F_{9/2})$
$_{51}Sb^{123}$	7/2	2.8	$(4d)^1$	$\geqq1$	$^2F_{7/2}+^2G_{7/2}$
$_{56}Ba^{137}$	3/2	0.94	$(4d)^{-1}$	0	$^2D_{3/2}+(^2P_{3/2})$
$_{81}Tl^{203}$	1/2	1.61	$(4d)^{-1}$	$\geqq1$	$(^2S_{1/2})+(^2P_{1/2})$
$_{81}Tl^{205}$	1/2	1.63	$(4d)^{-1}$	$\geqq1$	$(^2S_{1/2})+(^2P_{1/2})$
$_{83}Bi^{209}$	9/2	3.45	?	?	$(^2G_{9/2})+(^2H_{9/2})$
$_{82}Pb^{207}$	1/2	0.6	$(4p)^{-1}$	0	$^2P_{1/2}+(^2S_{1/2})$

* The moments may be compared with the following formulas based on a definite value of orbital angular momentum and g_s (proton) $=5.58$, g_l (proton) $=1$, g_s (neutron) $=-3.82$ and g_l (neutron) $=0$:

I	μ odd proton	μ odd neutron
$l+1/2$	$I+2.29$	-1.91
$l-1/2$	$I-2.29\,I/(I+1)$	$1.91\,I/(I+1)$

The configuration symbol in Table III(a) usually denotes the orbit of the odd particle or hole; as a rule the configurations of the even groups are omitted. Both bracketed and unbracketed state symbols are usually required for the quantitative interpretation of the magnetic moments [T. Schmidt, Zeits. f. Physik **106**, 358 (1937); H. Margenau and E. Wigner, Phys. Rev. **58**, 103 (1939)] but only the latter occur in the shell model. The second reference contains a partial list of spins and moments and references to the experimental papers. The authors list four nuclei $_{21}Sc^{45}$, $_{49}In^{115}$, $_{38}Sr^{87}$, and $_{36}Kr^{83}$ as falling outside the limits derived from an assumption of uniformity at the opposite extreme from the shell model. It is interesting that three of the exceptional cases involve single particle or single hole configurations ($Z=21$, 49 and $N=49$)] but only the latter occur in the shell model. With one exception, the states in Table III(a) are predominantly of the unbracketed character (in accord with the shell model) whenever a single particle or hole determines the state. The exception is $_{83}Bi^{209}$ where the shell model fails to provide a suitable orbit for the odd particle. Also $_{82}Pb^{207}$ does not lend support to the model since the $4p$ orbit is only one among several possibilities.

TABLE III(b). Spins and moments at $Z=29$, 31, 33, and 35.

Nucleus	Spin	Mag. moment	Configuration	Additional ang. mom.	State*
$_{29}Cu^{63}$	3/2	2.23	$(4f)^{-5}$	—	$^2P_{3/2}+^2D_{3/2}$
$_{29}Cu^{65}$	3/2	2.38	$(4f)^{-5}$	—	$^2P_{3/2}+^2D_{3/2}$
$_{31}Ga^{69}$	3/2	2.02	$(4f)^{-3}$	—	$^2P_{3/2}+^2D_{3/2}$
$_{31}Ga^{71}$	3/2	2.56	$(4f)^{-3}$	0	$^2P_{3/2}+^2D_{3/2}$
$_{33}As^{75}$	3/2	1.5	$(4f)^{14}(2s)^1$	$\geqq1$	$^2P_{3/2}+^2D_{3/2}$
$_{35}Br^{79}$	3/2	2.11	$(2s)^2(3p)^1$	0	$^2P_{3/2}+(^2D_{3/2})$
$_{35}Br^{81}$	3/2	2.27	$(2s)^2(3p)^1$	0	$^2P_{3/2}+(^2D_{3/2})$

* $(4f)^{-3}$ contains one ^2P and two linearly independent ^2D states; $(4f)^{-5}$ contains four linearly independent ^2P and five linearly independent ^2D states; see Gibbs, Wilbur, and White, Phys. Rev. **29**, 790 (1927); Pauling and S. Goudsmit, *The Structure of Line Spectra* (McGraw-Hill Book Company, Inc., New York, 1930), p. 156.

angular momentum. In $_{83}Bi^{209}$ the neutrons form a closed shell of 126 particles, hence should contribute no angular momentum. The only available orbit for the eighty-third proton yielding spin 9/2 is $6g$. Granting, the remote possibility that the $2s$, $3p$, $3s$, $4p$, and even the $5f$ levels are all displaced above $6g$ by the large central elevation in heavy nuclei, it is not clear why $6g$ should lie lower than $7i$. The situation is not improved by the fact that the magnetic moment favors a predominantly $^2H_{9/2}$ state. In view of these difficulties the possibility of starting the $6g$ shell at $Z=83$ must be dismissed.

Note added in proof.—The absence of a distinction between neutron and proton shells may be the source of the difficulty. The possibility of a different structure for the proton shells beyond $Z=60$ deserves careful study.

Three possible structures for a shell of 126 particles are listed under hypothesis *a*. Of these the first puts $6g$ below $2s$, $3p$, $3s$, $5f$, and possibly also $4d$. The extent of level crossing is somewhat extreme. The second structure places $3p$ above $3s$. Here the difficulty is an extremely unlikely inversion or crossover. Not only is $3p$ below $3s$ in a rectangular well, but $3s$ rises more rapidly when perturbed by a central elevation. The third structure puts $4d$ and $3s$ above $4p$. Again the inversion is unlikely. The spin and magnetic moment of $_{82}Pb^{207}$ favor the third structure.

Considering the difficulties at $Z=83$ and $N=126$ it is possible that the validity of the shell model is so far reduced in heavy nuclei that only the stability of the actual closed shell remains to reveal the structure. With one particle more or one less nearly all trace of structure may be lost in the unpredictable interaction of a large number of configurations. However, a less drastic conclusion is indicated by the fact that the quadrupole moments of $_{49}In^{115}$ and of $_{83}Bi^{209}$ are, respectively, positive and negative (0.84×10^{-24} cm^2 and -0.4×10^{-24} cm^2) in agreement with expectations for a hole in a proton shell and for a proton outside of closed shells. The negative value for $_{83}Bi^{209}$ is particularly interesting because it is the only known negative quadrupole moment in a heavy nucleus ($A>127$).

Three nuclei with N or $Z=37$ require separate discussion because of the uncertainty in the order of the $2s$ and $3p$ levels just before the beginning of the $5g$ shell. Experimental information and alternative interpretations are collected in Table III(c).

Only $_{37}Rb^{87}$ fits the shell model without additional angular momentum if the $3p$ shell is filled before $2s$. The alternative $(3p)^{-3}$ configuration generates ^2P and ^2D levels belonging to the [21] irreducible representation of the symmetric group.[12] Again the agreement with $_{37}Rb^{87}$ is satisfactory, but the fit

TABLE III(c). Spins and moments at N or $Z=37$.

Nucleus	Spin	Mag. moment	Configuration	Additional ang. mom.	State
$_{30}Zn^{67}$	5/2	0.9	$(3p)^{-1}$	$\geqq1$	$(^2F_{5/2})+(^2D_{5/2})$
$_{30}Zn^{67}$	5/2	0.9	$(3p)^{-3}$	0	$^2D_{5/2}+(^2F_{5/2})$
$_{37}Rb^{85}$	5/2	1.35	$(3p)^{-1}$	$\geqq1$	$(^2F_{5/2})+(^2D_{5/2})$
$_{37}Rb^{85}$	5/2	1.35	$(3p)^{-3}$	0	$^2D_{5/2}+(^2F_{5/2})$
$_{37}Rb^{87}$	3/2	2.75	$(3p)^{-1}$	0	$^2P_{3/2}+(^2D_{3/2})$
$_{37}Rb^{87}$	3/2	2.75	$(3p)^{-3}$	0	$^2P_{3/2}+^2D_{3/2}$

with Zn^{67} and Rb^{85} is still poor (although improved) since the moments of these nuclei favor predominantly $^2F_{5/2}$ states. It may be argued that the shell model is unreliable at N or $Z=37$ and 39 because the $(3p)^{-1}$ and $(3p)^{-3}$ configurations have odd parity and are far removed from other odd configurations. On the other hand a large number of low configurations have even parity ($2s$, $5g$, and $4d$ orbits all even); hence, configuration interaction may produce a ground state of even parity and unpredictable spin. It is perhaps significant that $_{63}Eu^{153}$ departs from theory in exactly the same manner as $_{30}Zn^{67}$ and $_{37}Rb^{85}$. Here also strong configuration interaction may be invoked to account for the failure of the $(3p)^3$ configuration to determine the ground state. The reduced number of low even configurations when the neutrons form a stable closed shell is perhaps responsible for the success of the shell model at $_{37}Rb^{87}$ and $_{39}Y^{89}$.

Experimental information regarding spins, magnetic moments and quadrupole moments is lacking

TABLE IV. Correlation of isomerism with the odd member of the pair N, Z. $(A)-N$ and Z certain; $(B)-Z$ certain, N probable.

N or Z	Number of known stable and radioactive nuclei	Number of cases of isomerism
1–28	—	0
29	7–8	1(A)
31–37	22–26	0
39	6	3(A), 1(B)
41	4–6	1(A)
43	3–5	3(A), 1(B)
45	3	1(A), 1(B)
47	5	4(A), 1(BB)
49	9	5(A), 1(B)
51	8–9	1(BB)
53–61	29–39	0
63	5–6	1(A)
65	4	1(A)
67	3	1(A)
69	3	1(A), 1(B), 1(BB)
71	3	0
73	2–3	2(A), 1(BB)
75	4–5	2(A)
77	4	2(A)
79	5	2(A)
81	6–7	2(A)
83–97	36–38	0
99	2	1(A)

[12] E. Feenberg and M. Phillips, Phys. Rev. **51**, 597 (1937).

on the stable nuclei

$_8O^{17}$, $_{10}Ne^{21}$, $_{32}Ge^{73}$, $_{40}Zr^{91}$, $_{46}Pd^{105}$, and $_{60}Nd^{143}$.

These systems are particularly interesting from the point of view of the shell model. The predicted ground states are $^2S_{1/2}$, ^2D, ^2G, ^2D, and ^2D for the first five in the same order. No prediction is possible for $_{60}Nd^{143}$ but experimental information may help to clarify the confused situation at N and $Z=83$.

A discussion of the spins and moments of $(nd)^{\pm 3}$ configurations appears in the following section.

III. ISOMERISM IN ODD NUCLEI

A preliminary report on the topic of this section was published recently.[13] Isomerism throws light on shell structure because it occurs as a rule, only when the spin of the ground state is either quite small (1/2 or 3/2) or quite large (7/2, 9/2, or 11/2) permitting the possibility of a first excited state with spin differing by three or more units from that of the ground state.[14] If a particular shell structure predicts two closely spaced levels differing by three or four units in spin isomerism becomes a likely possibility. To test for a correlation between shell structure and isomerism all known nuclei, both stable and radioactive are classified with respect to the odd member of the pair N, Z. The known cases of isomerism are classified in the same manner.

Table IV[15–17] reveals a sharply defined island of isomerism extending from N or $Z=39$ to N or $Z=49$. At N or $Z=41$ and 49 the predicted spins and parities are 7/2 or 9/2 (even) while the experimental spin is 9/2 in four cases. For N or $Z=47$, the known spin values are 1/2 (two and 9/2(one). In the range $50<N$ or $Z<60$, the configuration $(4d)^{2n+1}$ might be expected to favor intermediate values of spin (3/2 and 5/2). Actually the tendency is again to extremes, 7/2 occuring four times, 5/2 twice, 3/2 not at all, and 1/2 with some uncertainty twice. Short-lived isomers might be expected in this region. So far none have been observed. In particular, DeBenedetti and McGowan (see reference b, Table V) obtained negative results from nine odd radioactive decay products on the range $51 \leqq Z \leqq 59$ in a search for isomeric transitions with half-lives between 10^{-6} and 10^{-3} sec.

From the large number of isomeric nuclei at N or $Z=39$, one may infer that one or the other of the paired configurations

$$(1s)^2(2p)^6(3d)^{10}(4f)^{14}(2p)^6\begin{bmatrix}(5g)^1\\(2s)^1\end{bmatrix}\begin{matrix}\text{even parity}\\\text{even parity}\end{matrix} \tag{6a}$$

$$(1s)^2(2p)^6(3d)^{10}(4f)^{14}(2s)^2\begin{bmatrix}(3p)^4(5g)^1\\(3p)^5\end{bmatrix}\begin{matrix}\text{even parity}\\\text{odd parity}\end{matrix} \tag{6b}$$

determines the ground state and first excited state of such systems. An occasional inversion of the spin order is not unlikely and would not prejudice the occurrence of isomerism.

The occurrence of an isomer at $N=29$ suggests that the $2s$ level overtakes the $4f$ before the completion of the $4f$ shell (see Table III (b)). Isomeric and ground states could then be generated by one or the other of the paired configurations.

$$(1s)^2(2p)^6(3d)^{10}\begin{bmatrix}(4f)^{10}(2s)^1\\(4f)^{11}\end{bmatrix}\begin{matrix}\text{even parity}\\\text{odd parity}\end{matrix} \tag{7a}$$

$$(1s)^2(2p)^6(3d)^{10}\begin{bmatrix}(2s)^1(4f)^{10}\\(2s)^2(4f)^9\end{bmatrix}\begin{matrix}\text{even parity}\\\text{odd parity.}\end{matrix} \tag{7b}$$

From the point of view of the shell model, the existence of additional isomers at N or $Z=29$ and 31 is a likely possibility.

In the interval 51–60 marking the filling of the $4d$ shell, a temporary halt in the decrease of the central particle density and the rise of the central elevation should occur, thus permitting the $4d$ shell to fill completely before the inversion of the $6h$ and $4d$ levels takes place. The reversed situation exists during the filling of the $5g$ shell, the central density falling rapidly as the number of particles in the shell is increased. The fact that there are no stable nuclei with N or $Z=61$ supports the conclusion that a closed $4d$ shell is formed at N or $Z=60$ and suggests a large spacing between the $4d$ and adjacent levels at that point. The spin value 5/2 of $_{59}Pr^{141}$ is also in agreement with the closing of the $4d$ shell at $Z=60$. Unfortunately the magnetic moment has not yet been measured. The shell model predicts $\mu>2.8$ nuclear magnetons.

A second island of isomerism stretches from N or $Z=63$ to N or $Z=81$ with some concentration (by a factor of two) on the upper half of the range. Included are systems with $N=63$, 65, 67, 69, N and

[13] E. Feenberg, Phys. Rev. **75**, 320 (1949).
[14] C. F. v. Weizsacker, Naturwiss. **24**, 813 (1936).

[15] H. N. Friedlander and I. Perlman, General Electric Nuclear Information Chart (April, 1948).
[16] E. Segrè, Nuclear Information Chart, Revised to April, 1948.
[17] G. T. Seaborg and I. Perlman, "Table of the isotopes," Rev. Mod. Phys. **20**, 585 (1948). Thanks are due to Professor Joseph W. Kennedy for the loan of a prepublication copy of this table. Additional references to the most recent publications occur throughout the text.

$Z=69$, 73, 75, 77, 79, and $Z=81$. The shell model provides an unforced interpretation of this distribution based on the upward drift of the $2s$, $3p$, and $4d$ levels. Already at N or $Z=50$, the $2s$ and $3p$ levels lie above $4d$. At N or $Z=82$ they lie above $6h$. It is natural to assume that one or both cross the $6h$ level between 50 and 82 giving rise to a range of N, Z values in which the paired configurations

$$[60\text{ shell}]\begin{bmatrix}(6h)^{2n}(2s)^1\\(6h)^{2n+1}\end{bmatrix}\begin{matrix}\text{even parity}\\\text{odd parity}\end{matrix}\qquad(8a)$$

$$[60\text{ shell}](3p)^6\begin{bmatrix}(6h)^{2n}(2s)^1\\(6h)^{2n+1}\end{bmatrix}\begin{matrix}\text{even parity}\\\text{odd parity}\end{matrix}\qquad(8b)$$

or

$$[60\text{ shell}]\begin{bmatrix}(6h)^{2n}(2p)^1\\(6h)^{2n+1}\end{bmatrix}\begin{matrix}\text{odd parity}\\\text{odd parity}\end{matrix}\qquad(9)$$

generate the ground and first excited states. Configurations containing $(2s)^2$ or $(3p)^5$ may also occur.

The nuclei $_{48}Cd^{111}$, $_{48}Cd^{113}$, $_{50}Sn^{115}$, $_{50}Sn^{117}$, $_{50}Sn^{119}$, and $_{54}Xe^{129}$ all have spin 1/2 and magnetic moments ranging from -0.65 to -0.90 nuclear magnetons. Thus the ground states are all predominantly $^2S_{1/2}$. We suggest that these states are generated by configurations containing a single $2s$ orbit in addition to an even number of $3p$ and $6h$ orbits; however it is not clear why the state of minimum angular momentum and even parity should be favored in so many cases.

The previously discussed crossover of the $4d$ and $6h$ levels also produces possibilities for the occurrence of isomerism correlated with the closely spaced paired configurations.

$$[50\text{ shell}]\begin{bmatrix}(4d)^9(6h)^{2n+2}\\(4d)^{10}(6h)^{2n+1}\end{bmatrix}\begin{matrix}\text{even parity}\\\text{odd parity}\end{matrix}\qquad(10a)$$

$$[50\text{ shell}]\begin{bmatrix}(6h)^{2n}(4d)^1\\(6h)^{2n+1}\end{bmatrix}\begin{matrix}\text{even parity}\\\text{odd parity}\end{matrix}\qquad(10b)$$

Linear combinations of configurations in (8) and (10) may on occasion determine the ground and first excited states.

If the $4d$, $6h$ crossover occurred before or at N or $Z=72$, the $6h$ shell would close there and the $4d$ shell begin anew at N or $Z=73$. However the spin value 7/2 of $_{71}Lu^{175}$ and $_{73}Ta^{181}$ suggests a later crossover, most likely at $Z=74$ in accord with the spins and magnetic moments of $_{75}Re^{187}$ and $_{75}Re^{189}$ (5/2 and 3.3 in both cases). On this latter view the proton configuration in $_{73}Ta^{181}$ is [50 shell] $\cdot(4d)^{10}(6h)^{13}$ and the spin 7/2 presents no difficulty (although, of course, it could not be predicted). Similarly the proton configuration at $Z=75$ is $[50\text{ shell}](6h)^{22}(4d)^3$. Accepting these configurations there are four odd nuclei in which three protons occupy d orbits. These are listed below:

Nucleus	Spin	Magnetic moment
$_{13}Al^{27}$	5/2	3.64
$_{53}I^{127}$	5/2	2.8
$_{75}Re^{185}$	5/2	3.3
$_{75}Re^{187}$	5/2	3.3

The shell model provides a choice of states, ^2H, ^2G, ^2F, ^2D, ^2D, and ^2P in the absence of additional angular momentum supplied by the even group of neutrons. Interaction within the configurations may be invoked to account for the experimental spins and moments ($^2D_{5/2}+{}^2F_{5/2}$). One nucleus with 75 neutrons has spin $\frac{1}{2}$ ($_{54}Xe^{129}$, correlated with Eq. (8)). It is possible that the $4d$, $6h$ crossover in the neutron group is delayed until near the completion of the 82 shell. An example of a neutron group containing three $4d$ neutrons is supplied by

TABLE V. Odd isomers; N or $Z\leqq 81$.

N or Z	Nucleus	Half-life	Energy (Mev)	ℓ
29	$_{22}Ti^{51}$			
39	$_{30}Zn^{69}$	13.8 hr.	0.44	5
39	$_{32}Ge^{71}$			
39	$_{39}Y^{87}(B)$	14 hr.	0.5	5
39	$_{39}Y^{91}$	50 min.	0.61	5
41	$_{41}Cb^{95}$	80–90 hr.	0.24	5
43	$_{34}Se^{77}$	17.5 sec.	0.15	4
43[a]	$_{43}Tc^{93}$			
43	$_{43}Tc^{95}(B)$			
43	$_{43}Tc^{97}$	90 days	0.10	5
43	$_{43}Tc^{99}$	6 hr.	0.14–0.18	5(?)
45	$_{32}Ge^{77}(B)$			
45	$_{45}Rh^{103}$	50 min.	0.04	4
47	$_{34}Se^{81}(BB)$	59 min.	0.10	4
47	$_{36}Kr^{83}$	113 min.	0.046	4
47	$_{38}Sr^{85}$	70 min.	0.17	4–5
47	$_{47}Ag^{107}$	40 sec.	0.093	4
47	$_{47}Ag^{109}$	40 sec.	0.087	4
49	$_{34}Se^{83}$	$\gg$67 sec.	0.26	5
49	$_{36}Kr^{85}(B)$			
49	$_{38}Sr^{87}$	2.7 hr.	0.37	5
49	$_{40}Zr^{89}$	4.5 min.		
49	$_{40}In^{113}$	105 min.	0.39	5
49	$_{49}In^{115}$	4.5 hr.	0.34	5
51	$_{42}Mo^{73}(BB)$			
63	$_{48}Cd^{111}$	48.7 min.	0.230, 0.145	4–5
65	$_{48}Cd^{113}$	2.3 min.		
67	$_{48}Cd^{115}$	>43 days[b]	0.2[b]	$\geqq$5
69	$_{52}Te^{121}$	1.2×10^7, 5×10^{-8} sec.	0.05, 0.23	5,3
69[c]	$_{69}Tm^{169}(B)$	1×10^{-6} sec.	0.2	3
69[c]	$_{69}Tm^{171}(BB)$	2.5×10^{-6} sec.	0.1	3
73[d]	$_{52}Te^{125}$	60 days	0.12	5
73	$_{54}Xe^{127}(BB)$	75 sec.	0.175, 0.125	4
73[c]	$_{73}Ta^{181}$	2×10^{-5} sec.	0.13	3
75	$_{52}Te^{127}$	90 days	0.086	5
75[c]	$_{75}Re^{187}$	0.65×10^{-6} sec.	0.13	3
77	$_{52}Te^{129}$	32 days	0.102	5
77	$_{56}Ba^{133}$	38 hr.	0.276	5
79	$_{52}Te^{131}$	30 hr.	0.177	5
79	$_{79}Au^{197}$	7.5 sec.	0.25	4
81	$_{54}Xe^{135}$	10 min.	0.52	5
81	$_{56}Ba^{137}$	2.5 min.	0.75	5

[a] D. N. Kundu and M. L. Pool, Phys. Rev. **74**, 1775 (1948).
[b] R. W. Hayward and A. C. Helmholz, Phys. Rev. **75**, 1469 (1949).
[c] S. DeBenedetti and F. K. McGowan, Phys. Rev. **74**, 728 (1948).
[d] Friedlander, Goldhaber, and Sharff-Goldhaber, Phys. Rev. **74**, 981 (1948).

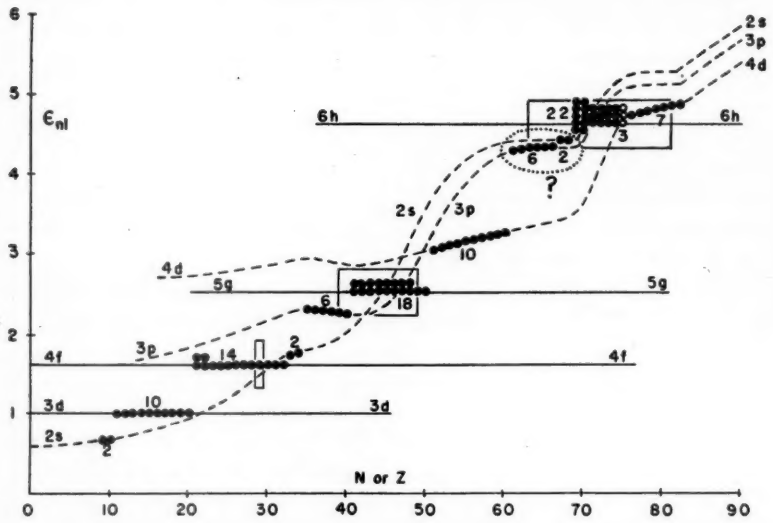

FIG. 1. Qualitative behavior of the single particle energy levels. Energy scale in arbitrary units. Solid dots denote the filling of the shells; the three open circles at N or $Z=75$ denote the three $4d$ particles that remain in the system when the $4d$ level crosses the $6h$ level. Boxes outline regions in which isomerism occurs in odd nuclei.

$_{42}Mo^{95}$. In this case the experimental spin determination yields $\frac{1}{2}$, but is uncertain. The analysis of radioactive transitions and isomerism at $A=95$ (next section) associates spin 5/2 and even parity with the ground state of $_{42}Mo^{95}$. A conclusive determination of the spin and magnetic moment of this nucleus would be helpful in the development of the shell model. The same statement may be applied to $_{12}Mg^{25}$.

Odd nuclei with three like particles missing from d orbits constitute another interesting group, among them:

Nucleus	Spin	Magnetic moment
$_{17}Cl^{35}$	3/2	0.82
$_{17}Cl^{37}$	3/2	0.68
$_{16}S^{33}$	3/2	—
$_{56}Ba^{135}$	3/2	0.84
$_{79}Au^{197}$	3/2	0.195

Those listed above are all in predominantly $^2D_{3/2}$ states excepting $_{16}S^{33}$ for which the magnetic moment is not known. Interaction within the $(nd)^{-3}$ configuration accounts for a $^2P_{3/2}$ admixture. Two other stable nuclei $_{44}Ru^{101}$ (spin and moment not known) and $_{57}La^{139}$ ($I=7/2$, $\mu=2.76$) belong in the $(4d)^{-3}$ group. No regularity is apparent in the group of odd nuclei containing half-filled d shells. Among the nuclei in the $(nd)^5$ group are two $_{15}P^{31}$ and $_{77}Ir^{191}$ with $I=\frac{1}{2}$. The first has $\mu=1.13$, hence is predominantly $^2P_{1/2}$ with a large admixture of $^2S_{1/2}$. A neighboring $(3d)^6(2s)^{-1}$ configuration may account for the $^2S_{1/2}$ admixture. From the spin of $_{77}Ir^{193}$ ($I=3/2$) and the ratio of magnetic moments $\mu^{191}/\mu^{193}=-0.92$ we conclude that $_{77}Ir^{191}$ is predominantly $^2P_{1/2}$. The fact that no nucleus in the $(nd)^5$ group is in a predominantly $^2S_{1/2}$ state may be correlated with the absence of $^2S_{1/2}$ states in the $(nd)^5$ manifold (references in Table III(b)).

It is a curious circumstance that all the known large positive quadrupole moments ($Q>2.5\times10^{-24}$ cm^2) occur in the narrow range of Z values (69–75) associated with the filling and termination of the $6h$ shell. What significance attaches to this coincidence is not clear. We note however that a configuration containing several orbits with large angular momentum generates a large number of linearly independent states with, for example, $I=5/2$. The largest eigenvalue of the quadrupole moment matrix in the subspace $I=5/2$ may then be much greater than the quadrupole moment produced by a single particle or hole.

Now it may be argued that the central particle density is so far reduced by the successive filling of the long $5g$ and $6h$ shells that a strong reaction occurs during the final filling of the $4d$ shell. The increasing central particle density and reduced (or reversed) rate of growth of the central elevation as more particles enter the 4d shell may maintain an approximate coincidence of the $4d$ and $6h$ levels between the crossover point and the completion of the "82" shell. Thus a condition may develop in which the lowest levels arising from the paired configuration,

$$[50\text{ shell}]\begin{bmatrix}(6h)^{21}(4d)^{2n+2} & \text{odd parity}\\ (6h)^{22}(4d)^{2n+1} & \text{even parity}\end{bmatrix} \quad (11)$$

stay close together over the entire range $Z=75$, 77, 79, and 81. Systems in which this occurs would have small spin ($\frac{1}{2}$, 3/2, 5/2 and rarely 7/2) in the ground state and large spin (possibly 9/2 or 11/2) in a close excited state.

Radiation transitions may be classified as electric $2^{\mathfrak{L}}$ or magnetic $2^{\mathfrak{L}-1}$ pole. Odd values of $\mathfrak{L}$ are associated with a parity change, even values with no change. The spin change is

$$\Delta I=\pm\mathfrak{L}\ \text{(electric } 2^{\mathfrak{L}}\text{ pole)},$$
$$\Delta I=\pm(\mathfrak{L}-1)\ \text{(electric } 2^{\mathfrak{L}}\text{ pole, magnetic } 2^{\mathfrak{L}-1}\text{ pole)}. \quad (12)$$

The theoretical relations between half-life, energy, and multipole order do not distinguish effectively between electric $2^{\mathfrak{L}}$ and magnetic $2^{\mathfrak{L}-1}$ poles.[18]

Wiedenbeck's plot of half-life against energy conforms to theoretical expectations sufficiently well to permit the identification of $\mathfrak{L}$ values. The known isomers fall under $\mathfrak{L}=3$, 4, and 5. Theoretical and experimental studies of internal conversion help to fix the multipole order and electric or magnetic character of the transition. A number of isomeric transitions have been studied sufficiently well to permit an unambiguous determination of both $\mathfrak{L}$ and ΔI.[19,20]

Table V lists all known odd isomers in the A and B classifications up to N or $Z=81$ and in the last column the $\mathfrak{L}$ values determined from Wiedenbeck's chart and the analysis of internal conversion.

Knowledge of the $\mathfrak{L}$ value in an isomeric transition reduces the ambiguity in the assignment of configurations to the ground and isomeric states. In particular at N or $Z=39$ the change in parity implied by $\mathfrak{L}=5$ removes Eq. 6(a) from the list of possibilities leaving only 6(b). Support for this conclusion is supplied by the spin and magnetic moment of ${}_{39}Y^{89}$. The states involved in the isomeric transitions are probably all included among the possibilities

$$\begin{aligned} &{}^2G_{9/2}\rightarrow{}^2P_{1/2}, \quad \Delta I=4,\\ &{}^2G_{11/2}\rightarrow{}^2P_{1/2}, \quad \Delta I=5,\\ &{}^2G_{11/2}\rightarrow{}^2P_{3/2}, \quad \Delta I=4. \end{aligned} \tag{13}$$

We conclude that the single particle levels occur in the order $2s$, $3p$, and $5g$ at N or $Z=39$, the spacing of the first pair being large and that of the second pair small.

At $Z=41$ there is again a change in parity and the low configurations are probably

$$(1s)^2(2p)^6(3d)^{10}(4f)^{14}(2s)^2\begin{bmatrix}(2p)^5(5g)^2\\(2p)^6(5g)^1\end{bmatrix}\begin{matrix}\text{odd parity}\\\text{even parity}\end{matrix} \tag{14}$$

giving rise to a ${}^2G$ ground state (compare with spin and moment of ${}_{41}Cb^{93}$]) and a ${}^2P$ excited state.

The crossovers occurring during the filling of the $5g$ shell introduce several possibilities for configurations involved in isomerism at N or $Z=43$, 45, 47, and 49. These configurations are

$$(1s)^2(2p)^6(3d)^{10}(4f)^{14}\begin{bmatrix}(3p)^5(5g)^{2n+2}\\(3p)^6(5g)^{2n+1}\end{bmatrix}\begin{matrix}\text{odd parity}\\\text{even parity,}\end{matrix} \tag{15a}$$

$$(1s)^2(2p)^6(3d)^{10}(4f)^{14}\begin{bmatrix}(5g)^{2n}(3p)^1\\(5g)^{2n+1}\end{bmatrix}\begin{matrix}\text{odd parity}\\\text{even parity,}\end{matrix} \tag{15b}$$

$$(1s)^2(2p)^6(3d)^{10}(4f)^{14}\begin{bmatrix}(2s)^1(5g)^{2n+2}\\(2s)^2(5g)^{2n+1}\end{bmatrix}\begin{matrix}\text{even parity}\\\text{even parity,}\end{matrix} \tag{15c}$$

$$(1s)^2(2p)^6(3d)^{10}(4f)^{14}\begin{bmatrix}(5g)^{2n}(2s)^1\\(5g)^{2n+1}\end{bmatrix}\begin{matrix}\text{even parity}\\\text{even parity.}\end{matrix} \tag{15d}$$

A modified version of (15a) and (15b) obtained by inserting a full $2s$ shell after $(4f)^{14}$ should also be included. Both $2s$ and $3p$ levels are required to cross $5g$ before the completion of the $5g$ shell at N or $Z=50$.

At N or $Z=49$ the configurations in (15b) probably produce the observed low states. These configurations imply a $2s$, $3p$ crossover before the completion of the $5g$ shell. A second crossover reversing the first may occur as the $4d$ shell fills up, since a retardation or reversal of trends should occur in that range. As noted earlier, the central particle density may increase or, at worst, decrease slowly during the filling of the $4d$ shell. The occurrence of $L=4$ in six isomeric transitions suggests a close competition between (15b) and (15d) and therefore a close spacing of $2s$ and $3p$ levels over most of the range involved ($41\leqq\cdot N$ or $Z\cdot\leqq 49$).

In the second island of isomerism ($63\leqq\cdot N$ or $Z\cdot\leqq 81$) $\mathfrak{L}=3$ occurs five times, $\mathfrak{L}=4$ two or three times and $\mathfrak{L}=5$ seven or eight times. The many isomeric transitions with change in parity ($\mathfrak{L}=3$ and 5) may be correlated with the configurations (8a), (8b), (10a), (10b), and (11). These all associate even parity with small spin ($1/2, 3/2, \cdots$) and odd parity with large spin ($\cdots 9/2, 11/2$). Two or three examples of isomerism with no parity change probably involve the configurations (9). Both isomeric and ground states have odd parity.

The isomerism of ${}_{56}Ba^{137}$ ($I=3/2$ in the ground state) provides experimental support for the configurations in Eq. (11). Here $\mathfrak{L}=5$[21] and $\Delta I=5$.[22]

[18] Marcellus L. Wiedenbeck, Phys. Rev. **69**, 567 (1946).
[19] A. C. Helmholz, Phys. Rev. **60**, 415 (1941).
[20] Bradt, Gugelot, Huber, Medicus, Preiswerk, Sherrer, and Steffen, Helv. Phys. Acta **XX**, 153 (1947).
[21] Townsend, Cleland, and Hughes, Phys. Rev. **74**, 499 (1948).
[22] A. C. G. Mitchell and C. L. Peacock, Phys. Rev. **75**, 197 (1949).

The ground state, generated by a $(4d)^{-1}$ configuration, has even parity. Thus the isomeric level has odd parity and $I=11/2$ or (more likely) 13/2. The larger value requires one or more units of orbital angular momentum supplied by the neutron group. Grave difficulties exist in the interpretation of the $_{55}Cs^{137}$ beta-decay. The absence of transitions to the ground state of the product nucleus is particularly puzzling.[22] A full discussion may be deferred until present uncertainty as to the spin and magnetic moment of $_{55}Cs^{137}$ has been removed (we are indebted to Professor G. Zacharias for the information that the unpublished assignment of $I=7/2$ to $_{55}Cs^{137}$ is provisional).

A second case in point is $_{56}Ba^{133}$ with $\mathfrak{L}=5$ for the isomeric transition. Assuming $I=3/2$ and even parity for the ground state (the configuration is $(4d)^5$; also $I=3/2$ for the isotopes of mass 135 and 137) the isomeric level has odd parity and $I=11/2$ or 13/2. A third example, $_{75}Re^{187}$, has $I=5/2$ in the ground state (the configuration is $(4d)^3$) and $\mathfrak{L}=3$ for the isomeric transition. Consequently the isomeric level has odd parity and spin 9/2 or 11/2.

Twenty examples of odd-odd isomers are known. Significant correlations with shell structure are difficult to establish primarily because there are few odd-odd nuclei for which both N and Z fall outside of the regions $29\pm?$, 39–49, and 63–81.

Figure 1 exhibits the qualitative behavior of the single particle levels as deduced from the analysis of stability relations, spins, magnetic moments, and isomerism. The order and spacing of the single particle levels at N or $Z=83$ suggests an interpretation of the predominantly $^2H_{9/2}$ ground state of $_{83}Bi^{209}$. Among the low configurations are several produced by promoting one or more particles from the $6h$ or $4d$ shells into $2s$ and $3p$ orbits. The list of low configurations with odd parity capable of generating $^2H_{9/2}$ and $^2G_{9/2}$ states includes

$$(6h)^{-1}(2s)^2,\ (6h)^{-1}(2p)^2,\ (4d)^{-2}(2s)^2(3p)^1,$$
$$(4d)^{-2}(3p)^3,\ (6h)^{-1}(4d)^{-1}(3p)^2(2s)^1.$$

It is possible that the coupling within this large group of closely spaced configurations depresses a predominantly $^2H_{9/2}$ state below the $^2S_{1/2}$ and $^2P_{1/2}$ and $^2P_{3/2}$ states associated with the $(2s)^1$ and $(3p)^1$ configurations.

IV. BETA-DECAY

The empirical classification of beta-spectra with respect to the allowed or forbidden character of the transition provides information on the spins and parities of parent and daughter nuclei. Caution is required in interpreting much of the experimental data because of the complicated and incompletely understood structure of many transitions. Relevant experimental information on light nuclei beyond the $1s$ and $2p$ shells appears in Table VI. Values of

TABLE VI. Shell structure of light radioactive and product nuclei.

Nucleus	ft	Type of transition#	Configuration	Spin	Parity
$_7N^{16}(g)$	—	—	$(2p)^{-1}(2s)^1$	0, 1†, 2†	odd
$_8O^{16}(e)$	1.6×10^4	allowed (unfavored)	$(2p)^{-1}(2s)^1$	1	odd
$_8O^{16}(g)$	5.2×10^6	1st forbidden	closed	0*	even
$_9F^{18}(g)$	—	—	$(2s)^1(2s)^1$	1	even
$_8O^{18}(g)$	6×10^3	allowed (favored)	closed	0	even
$_8O^{19}(g)$	—	—	$(3d)^1$	3/2†, 5/2	even
$_9F^{19}(e)$	2.0×10^4	allowed (unfavored)	$(3d)^1$	3/2, 5/2	even
$_9F^{19}(g)$	3.4×10^5	allowed (unfavored)	$(2s)^1$	1/2*	even
$_9F^{20}(g)$	—	—	$(2s)^1(3d)^1$	1, 2†, 3†	even
$_{10}Ne^{20}(e)$	8×10^4	allowed (unfavored)	$(2s)^{-1}(3d)^1$	2	even
$_{10}Ne^{20}(g)$	$\gg4\times10^5$	$\geqq$2nd forbidden	closed	0	even
$_{11}Ne^{22}(g)$	—	—	$(3d)^1(3d)^1$	0, 1, 2, 3*, 4, 5	even
$_{10}Ne^{22}(e)$	10^8	2nd (?) forbidden	—	—	—
$_{10}Ne^{22}(g)$	$\gg10^{10}$	highly forbidden	$(3d)^2$	0	even
$_{19}K^{38}(g)$	—	—	$(3d)^{-1}(3d)^{-1}$	0, 1, 2, 3†, 4, 5	even
$_{18}A^{38}(e)$	8×10^4	allowed (unfavored)	$(2s)^{-1}(3d)^{-1}$	2	even
$_{18}A^{38}(g)$	$\gg10^6$	highly forbidden	$(3d)^{-2}$	0	even
$_{19}K^{40}(g)$	—	—	$(3d)^{-1}(4f)^1$	0, 1, 2, 3, 4*, 5, 6	odd
$_{20}Ca^{40}(g)$	$\sim10^{15}$	$3d$ forbidden	closed	0	even
$_{18}A^{41}(g)$	—	—	$(3d)^{-2}(4f)^3$	1/2, 3/2, 5/2, 7/2†$\cdots$	odd
$_{19}K^{41}(e)$	1.0×10^5	allowed (unfavored)	$(4f)^1(3d)^{-2}(4f)^2$	$\cdots$5/2, 7/2$\cdots$	odd
$_{19}K^{41}(g)$	4×10^8	2nd (?) forbidden	$(3d)^{-1}(4f)^2$	3/2*	even

\# Empirical classification.
* Experimental value.
† Preferred theoretical possibility.
e—Excited state; g—ground state.

TABLE VII. Shell structure of intermediate radioactive, isomeric and product nuclei.

Nucleus	ft	Type of transition	Configuration	Spin	Parity
$_{30}Zn^{69}(m)$	—	—	$(3p)^{-2}(5g)^{1}$	7/2, 9/2†	even
$_{30}Zn^{69}(g)$	—	IT; $\mathfrak{L}=5$	$(3p)^{-1}$	1/2†, 3/2	odd
$_{31}Ga^{69}(g)$	5×10^{4}	allowed (unfavored)	—	3/2*	odd
$_{32}Ge^{71}(m)$	—	—	$(3p)^{-2}(5g)^{1}$	7/2, 9/2†	even
$_{32}Ge^{71}(g)$	—	IT; $\mathfrak{L}\geqq5$	$(3p)^{-1}$	1/2†, 3/2	odd
$_{31}Ga^{71}(g)$	8×10^{5}	allowed (unfavored)	—	3/2*	odd
$_{34}Se^{83}(m)$	—	—	$(5g)^{-2}(3p)^{1}$	1/2†, 3/2	odd
$_{35}Br^{83}(g)$	1.5×10^{5}	allowed (unfavored)	$(3p)^{1}$	1/2, 3/2	odd
$_{36}Kr^{83}(m)$	1.4×10^{5}	allowed (unfavored)	$(5g)^{-4}(3p)^{1}$	1/2, 3/2	odd
$_{36}Kr^{83}(g)$	—	IT; $\mathfrak{L}=4$	$(5g)^{-5}(3p)^{1}(2s)^{1}$	7/2, 9/2*···	odd
$_{34}Se^{83}(g)$	—	IT(n.o.); $\mathfrak{L}\geqq5$	$(5g)^{-1}$	7/2, 9/2†	even
$_{35}Br^{83}(e)$	1.2×10^{5}	allowed (unfavored)	?	?	odd
$_{39}Y^{87}(g)$	—	—	$(3p)^{-1}$	1/2†, 3/2	odd
$_{38}Sr^{87}(m)$	?	allowed (unfavored)	$(5g)^{-2}(3p)^{1}$	1/2†, 3/2	odd
$_{38}Sr^{87}(g)$	—	IT; $\mathfrak{L}=5$	$(5g)^{-1}$	7/2, 9/2*	even
$_{37}Rb^{87}(g)$	—	K(n.o.); allowed	$(3p)^{-3}$	1/2, 3/2*···	odd
$_{38}Sr^{87}(g)$	5×10^{16}	$3d$ forbidden	$(5g)^{-1}$	7/2, 9/2*	even
$_{38}Sr^{89}(g)$	—	—	$(4d)^{1}$	3/2, 5/2†	even
$_{39}Y^{89}(g)$	5×10^{8}	2nd (?) forbidden	$(3p)^{-1}$	1/2*(?), 3/2	odd
$_{40}Zr^{89}(m)$	—	—	$(5g)^{-1}$	7/2, 9/2†	even
$_{40}Zr^{89}(g)$	—	IT; $\mathfrak{L}=5$(?)	$(5g)^{-2}(3p)^{1}$	1/2†, 3/2	odd
$_{39}Y^{89}(g)$	6×10^{5}	allowed (unfavored)	$(3p)^{-1}$	1/2*(?), 3/2	odd
$_{38}Sr^{91}(g)$	—	—	$(4d)^{3}$	1/2, 3/2, 5/2†···	even
$_{39}Y^{91}(g)$	1.2×10^{8}	2nd (?) forbidden	$(3p)^{-1}$	1/2†, 3/2	odd
$_{40}Zr^{91}(g)$	5×10^{8}	2nd (?) forbidden	$(4d)^{1}$	3/2, 5/2†	even
$_{39}Y^{91}(e)$	5×10^{6}	1st forbidden	—	3/2, 5/2, 7/2	odd
$_{39}Y^{91}(m)$	—	γ; $\mathfrak{L}\leqq4$	$(3p)^{-2}(5g)^{1}$	7/2, 9/2†	even
$_{39}Y^{91}(g)$	—	IT; $\mathfrak{L}=5$	$(3p)^{-1}$	1/2†, 3/2	odd
$_{43}Tc^{99}(m)$	—	—	$(5g)^{2n}(2s)^{1}$	1/2	even
$_{43}Tc^{99}(m)$	—	—	$(5g)^{2n}(3p)^{1}$	1/2†, 3/2	odd
$_{43}Tc^{99}(g)$	—	γ; $\mathfrak{L}=4$ or 5	$(5g)^{2n+1}$	···9/2···	even
$_{44}Ru^{99}(g)$	10^{13}	highly forbidden	$(4d)^{5}$	1/2, 3/2†, 5/2···	even
$_{44}Ru^{103}(g)$	—	—	$(4d)^{-1}$	3/2, 5/2†	even
$_{45}Rh^{103}(e)$	1.3×10^{6}	1st forbidden (?)	—	—	odd(?)
$_{45}Rh^{103}(m)$	$\gg4\times10^{7}$	2nd forbidden	$(5g)^{2n}(2s)^{1}$	1/2	even
$_{45}Rh^{103}(g)$	$\gg4\times10^{7}$	2nd forbidden	$(5g)^{2n+1}$	···7/2, 9/2†	even
$_{48}Cd^{107}(g)$	—	—	$(4d)^{-1}$	3/2, 5/2†	even
$_{47}Ag^{107}(m)$	4.2×10^{4}	K capture, allowed (?)	$(5g)^{-5}(3p)^{1}(2s)^{1}$	7/2,† 9/2···	odd
$_{47}Ag^{107}(g)$	—	IT; $\mathfrak{L}=4$	$(5g)^{-4}(3p)^{1}$	1/2,* 3/2	odd
$_{46}Pd^{109}(g)$	—	—	—	—	—
$_{47}Ag^{109}(m)$	1.4×10^{6}	1st forbidden	$(5g)^{-5}(3p)^{1}(2s)^{1}$	···7/2†, 9/2	odd
$_{47}Ag^{109}(g)$	—	IT; $\mathfrak{L}=4$	$(5g)^{-4}(3p)^{1}$	1/2*, 3/2	odd
$_{48}Cd^{109}(g)$	—	—	$(6h)^{1}$	9/2†, 11/2	odd
$_{47}Ag^{109}(m)$	?	allowed (unfavored)	$(5g)^{-5}(3p)^{1}(2s)^{1}$	···7/2†, 9/2···	odd

† Preferred theoretical possibility.
* Experimental value.
e—Excited state; m—metastable state; g—ground state; n.o.—not observed.

f are taken from charts in the review article by Konopinski.[23] The empirical classification and the available theoretical calculations are followed in assessing the degree of forbiddenness of the transitions. The spin column contains the range of spin values permitted by the shell structure; experimental values are starred. Parity given in the last column is fixed uniquely by the shell structure. The discussion following the table is based on the Gamow-Teller selection rules as derived from tensor or axial-vector coupling:[23]

$\Delta I=0, \pm1$, no parity change, no $0\rightarrow0$ (allowed),
$\Delta I=0, \pm1, \pm2$, parity change (1st forbidden),
$\Delta I=0, \pm2, \pm3$, no parity change (2nd forbidden).

An additional selection rule due to Wigner[24] classifies the allowed transitions as favored (no change in supermultiplet, $ft\sim3000$) and unfavored

[23] Emil J. Konopinski, Rev. Mod. Phys. 15, 209 (1943).

[24] Eugene P. Wigner, Phys. Rev. 56, 519 (1939); L. W. Nordheim and F. L. Yost, Phys. Rev. 51, 942 (1937) present an informal, but, in essentials, equivalent statement of the distinction between favored and unfavored transitions.

(change in supermultiplet, but no change in parity, $ft \sim 10^5$). In simpler terms the transition is favored if the same space wave function occurs in both parent and daughter nuclei, while it may be allowed, but with a reduced value of the nuclear matrix element, if there is a substantial change in the space wave functions (change in symmetry or configuration). It is apparent from the empirical classification of transition types that the *ft* values of allowed (unfavored) and first forbidden transitions overlap, thus in extreme cases precluding positive identification of the transition types on the basis of these values alone. Very often the shell model provides the information needed to make the identification.

Discussion of Table VI

$_7N^{16}$: half-life 7.35 sec., β^- 3.8 Mev ($\sim$75 percent), 10.0 Mev ($\sim$25 percent), γ 6.2, 6.8 Mev. From the intensity ratio the "half-lives" of the separate components are 10 sec. (low energy transitions) and 30 sec. (high energy transitions). Both ^1P and ^3P levels occur among the low terms arising from the $(2p)^{-1}(2s)^1$ configuration in $_7N^{16}$. The same configuration and a lower supermultiplet yield a ^1P excited state for $_8O^{16}$.

$_9F^{18}$: half-life 6700 sec., β^+ 0.7 Mev. The transition is favored because both parent ($^3S_1$) and daughter ($^1S_0$) ground states belong to the same supermultiplet (and also the same configuration). A search for a gamma-ray (William J. Knox, Phys. Rev. **74**, 1192 (1948)) yielded a negative result.

$_8O^{19}$: half-life 27 sec., β^- 2.9 Mev ($\sim$70 percent), 4.5 Mev ($\sim$30 percent), γ 1.6 Mev; the half-lives of the separate components are 39 sec. (low energy transition) and 90 sec. (high energy transition). The high energy transition is particularly unfavored because the two ground states involved belong to different configurations ($(3d)^1$ and $(2s)^1$).

$_9F^{20}$: half-life 12 sec., β^- 5.0 Mev, γ 2.2 Mev. Both ^1D and ^3D levels occur among the low terms arising from the $(2s)^1(3d)^1$ configuration in $_9F^{20}$. The same configuration and a lower supermultiplet yield a $^1D_2$ excited state for $_{10}Ne^{20}$. It is also possible that the spectrum is complex; β^- 5.0 Mev to $_{10}Ne^{20}(g)$ and β^- 2.8 Mev to $_{10}Ne^{20}(e)$ followed by γ 2.2 Mev. In this case spin 1 would be preferred for $_9F^{20}(g)$ and the β^--transition to the ground state would be allowed (unfavored).

$_{11}Na^{22}$: half-life 10^8 sec., β^+ 0.56 Mev, γ 1.3 Mev. Again both singlets and triplets appear among the group of low levels in $_{11}Na^{22}$.

Empirically the transition to the ground state is highly forbidden whereas the quantum numbers of parent and daughter nuclei place it in the second forbidden category. However the matrix element involved does not appear in the more common 2nd forbidden transitions (presumably with $\Delta I = \pm 2$) and may be small enough to increase the empirical order of the transition.[23,25] This conjecture is confirmed by the $_4Be^{10} \rightarrow {}_5B^{10}$ transition (half-life 8×10^{13} sec., β^- 0.56 Mev, $ft \sim 5.6\times10^{13}$). Here the spins are 0 and 3 and both parities are even. Moreover the magnetic moments of $_5B^{10}$ and $_{11}Na^{22}$ are almost identical (1.8 nuclear magnetons implying a $^3D_3$ ground state in both systems). Consequently the nuclear matrix elements of the beta-decay theory should have about the same value in both 10- and 22-particle systems for the transitions between ground states. With $f \sim 56$ at $Z=10$ and β^+ 1.86 Mev the half-life of the transition to the ground state of $_{10}Ne^{22}$ is determined by the equation

$$56\, t_{22}\ (\text{ground state}) \sim 8\times10^{13}\times0.70 \text{ sec.},$$
$$t_{22}\ (\text{ground state}) \sim 10^{12} \text{ sec.} \qquad (16)$$

Thus only one transition out of ten thousand should go directly to the ground state, a small enough proportion to have escaped observation in spectrometer and early cloud-chamber studies.[26]

$_{19}K^{38}$: half-life 460 sec., β^+ 2.53 Mev, γ 2.15 Mev; almost certainly in cascade. For β^+ 2.53 Mev, $W_0 = 6.0$ mc^2 and $f \sim 165$ yielding $ft \sim 8\times10^4$. If the β^+-spectrum were complex with the gamma-transition following β^+ 0.38 Mev, the number of gamma's per positron could not exceed $6\times10^{-2}/165 \sim 4\times10^{-4}$ (the ratio of the *f* values at $W_0 = 1.75$ and 6.0 mc^2). A change in configuration is required to make the transition to $_{18}A^{38}(e)$ unfavored.

$_{19}K^{40}$: half-life $\sim 3\times10^{16}$ sec., β^- 1.35 Mev, γ 1.5 Mev (with *K* capture). The selection rules for the third forbidden transition include $\Delta I = \pm 4$ with change in parity. A summary of theoretical studies of this transition appears in reference 23.

$_{18}A^{41}$: half-life 6600 sec., β^- 1.18 Mev, 2.55 Mev (0.7 percent), γ 1.37 Mev; half-life of the transition to the ground state 10^6 sec. The transition to $_{19}K^{41}(e)$ requires a change in supermultiplet, but once more no change in configuration. The large *ft* value of the transition to the ground state implies a small nuclear matrix element for $\Delta I = \pm 2$ with change in parity.[25]

The special selection rule invoked in the discussion of the $_{18}A^{41}$ transition recurs in heavier systems. In several examples the empirical classification is 2nd forbidden while the shell model requires a change of parity and $\Delta I = \pm 2$ (1st forbidden by the G. T. selection rules derived from tensor coupling).

The extraordinary $_4Be^{10}$ decay provides an ex-

[25] N. Feather and H. O. W. Richardson, Proc. Phys. Soc. **61**, 452 (1948).

[26] K. H. Morganstern, at this laboratory, has observed a small number of long range positron tracks from the disintegration of a $_{11}Na^{22}$ source in a cloud chamber placed in a strong magnetic field.

ample of a transition [27-28] with no change in parity and $\Delta I = -3$. Here the selection rules classify the transition as second forbidden while the empirical classification is at least $3d$ forbidden. The same situation recurs[29] in the $_{11}Na^{22}(g)$ transition to $_{10}Ne^{22}(g)$. In view of these examples it is not astonishing to find a parallel situation for $\Delta I = \pm 2$ with change in parity.

Table VII exhibits the connection between the configurations suggested by the shell model, the selection rules for isomeric and radioactive transitions and the empirical evidence on such transitions. In several series of isomeric and radioactive transitions (notably at $A = 71$, 87, 89, and 91) the information on the nature and order of the transitions when combined with the selection rules almost completely determines the unknown spins and parities. Such cases provide a searching test of the shell model. The series at $A = 91$ is particularly interesting since no experimental spin values are available. Three series (at $A = 69$, 71, and 91) exhibit the same pattern of spins and parities for the ground and isomeric levels of the nuclei with N or $Z = 39$. A similar statement can be made for two series at $A = 83$ and 87 involving $N = 49$. The two indium isotopes $_{49}In^{113}$ and $_{49}In^{115}$, each with known spin 9/2 in the ground state and $\mathfrak{P} = 5$ characterizing the isomeric transition, belong with $_{34}Sc^{83}$ and $_{38}Sr^{87}$. In a fifth series at $A = 89$ the nucleus with $N = 49$ exhibits an exact inversion of the ground state-isomeric state spin and parity relations observed in $_{34}Se^{83}$, $_{38}Sr^{87}$, $_{49}In^{113}$, and $_{49}In^{115}$.

Discussion of Table VII

$_{30}Zn^{69}(m)$: half-life 5×10^4 sec., γ 0.44 Mev. Studies of internal conversion (reference 20) support the assignment $\mathfrak{P} = 5$ taken from Wiedenbeck's chart.

$_{30}Zn^{69}(g)$: half-life 3400 sec., β^- 1.0 Mev; an allowed (unfavored) transition to $_{31}Ga^{69}(g)$. The selection rules require spin 1/2 or 3/2 and odd parity for $_{30}Zn^{69}(g)$ in agreement with the shell model.

$_{32}Ge^{71}(m)$: half-life 10^6 sec., γ 0.6 Mev; closer to $\mathfrak{P} = 6$ than $\mathfrak{P} = 5$ on Wiedenbeck's chart. Bearing in mind the scattering of experimental points on the chart the assignment to $\mathfrak{P} = 5$ is not unreasonable.

$_{32}Ge^{71}(g)$: half-life 1.4×10^5 sec., β^- 1.2 Mev; an allowed (unfavored) transition to $_{31}Ga^{71}(g)$. The odd parity assigned to $_{31}Ga^{69}(g)$ and $_{31}Ga^{71}(g)$ is derived from the odd parity of configurations containing an odd number of $4f$ wave functions. The possibility of using even parity seems ruled out by the small ft value in the Zn^{69}, Ga^{69} transition.

[27] M. Goldhaber, Phys. Rev. **74**, 1194 (1948).
[28] Gordy, Ring, and Burg, Phys. Rev. **74**, 1191 (1948).
[29] Luther Davis, Phys. Rev. **74**, 1193 (1948).

TABLE VIII. Beta-decay with change in parity.

Emitter	Radiation	Half-life (sec.)	$Wo(mc^2)$	f	ft
$_{7}N^{16}$	β^-	7.35 (25%)	21.0	1.7×10^5	5.2×10^6
$_{17}Cl^{38}$	β^-	2300 (53%)	11.3	9.2×10^3	4.0×10^7
$_{18}A^{41}$	β^-	6600 (0.7%)	6.03	430	4.0×10^8
$_{19}K^{42}$	β^-	4.5×10^4 (75%)	8.06	1.8×10^3	1.1×10^8
$_{35}Br^{84}$	β^-	1800	11.4	1.8×10^4	3.2×10^7
$_{36}Kr^{88}$	β^-	1.1×10^4	5.9	720	7.9×10^6
$_{37}Rb^{88}$	β^-	1050	10.2	1.11×10^4	1.2×10^7
$_{38}Sr^{89}$	β^-(no γ)	4.8×10^6	4.0	103	4.9×10^8
$_{38}Sr^{90}$	β^-(no γ)	8×10^8	2.05	1.8	1.4×10^9
$_{38}Sr^{91}$	β^-	3.6×10^4 (60%)	7.3	2.1×10^3	1.3×10^8
$_{39}Y^{90}$	β^-(no γ)	2.2×10^5	5.4	500	1.1×10^8
$_{39}Y^{91}$	β^-(no γ)	5.2×10^6	4.01	105	5.4×10^8
$_{37}Rb^{87}$	β^-	2×10^{18}	1.26	0.025	5×10^{16}

$_{34}Se^{83}(m)$: half-life 67 sec., β^- 3.4 Mev; an allowed (unfavored) transition to $_{35}Br^{83}(g)$. The odd parity is required by the failure to observe an isomeric transition to $_{34}Se^{83}(g)$ (with γ 0.26 Mev), implying $\mathfrak{P} = 5$. Since $_{34}Se^{83}(g)$ is assigned even parity that of the isomeric level must be odd (assuming $\mathfrak{P} = 5$ since $\mathfrak{P} = 6$ seems unlikely).

$_{34}Se^{83}(g)$: half-life 1500 sec., β^- 1.5 Mev, γ 0.17, 0.37, 1.1 Mev, an allowed (unfavored) or 1st forbidden transition to $_{35}Br^{83}(e)$ followed by a cascade of three gamma-rays.

$_{35}Br^{83}(g)$: half-life 8600 sec., β^- 1.0 Mev; an allowed (unfavored) transition to $_{36}Kr^{83}(m)$.

$_{36}Kr^{83}(m)$: half-life 6800 sec., γ 0.029, 0.046 Mev; an isomeric transition with $\mathfrak{P} = 4$. The K/L conversion ratio of the 46-kev line requires $\Delta I = \pm 4$ (reference 20); in view of the known spin 9/2 of the ground state the isomeric level must have spin 1/2. The simplest possibility supplied by the shell model gives both levels even parity. However, the $(3g)^{-3}$ and $(3g)^{-4}(2s)^1$ configurations are rejected, and more complicated configurations involving the $3p$ orbit are accepted for two reasons: (a) the ft values of allowed and forbidden transitions should not overlap and (b) the properties of the odd silver isotopes associate the more complicated configurations with $Z = 47$, hence, also with $N = 47$.

$_{39}Y^{87}(g)$: half-life 2.9×10^5 sec., K capture to $_{38}Sr^{87}(m)$. The selection rules and the quantum numbers required by the shell model make this an allowed (unfavored) transition. Considering Eq. (33b) of reference 23 for f_k, this interpretation is indeed reasonable.

$_{38}Sr^{87}(m)$: half-life 9.7×10^3 sec., γ 0.38 Mev; near $\mathfrak{P} = 5$ on Wiedenbeck's chart. Since $_{38}Sr^{87}(g)$ has spin 9/2 (experimental) and even parity (shell model) the isomeric state must have odd parity and spin 1/2. K capture to $_{37}Rb^{87}(g)$ is energetically possible and also allowed (unfavored). From Eq. 33b, reference 23, $f_k \sim 0.03$. Consequently, $t_k \sim 10^6$ sec. and $_{38}Sr^{87}(m)$ should exhibit a branching decay: 1 percent K capture and 99 percent IT. The K capture has not yet been observed.

$_{37}Rb^{87}(g)$: half-life 2×10^{18} sec., β^- 0.14 Mev, γ?; spins of both parent and daughter nuclei have been measured. The change in parity required by the shell model makes the transition 3d forbidden.

$_{38}Sr^{89}(g)$: half-life 4.7×10^{6} sec., β^- 1.5 Mev, no γ; in the empirical classification a 2nd forbidden transition to $_{39}Y^{89}(g)$. The theoretical classification is 1st forbidden with maximum possible spin change ($\Delta I=\pm2$).

$_{40}Zr^{89}(m)$: half-life 270 sec., IT energy not known, but γ up to 1 Mev observed; $\mathfrak{L}=5$ indicated. The absence of transitions from $_{40}Zr^{89}(m)$ to $_{39}Y^{89}(g)$ associates large spin with the isomeric level and small spin with the ground level. An occasional reversal of the expected order is not unreasonable.

$_{40}Zr^{89}(g)$: half-life 2.9×10^{5} sec., β^+ 1.0 Mev; an allowed (unfavored) transition to $_{39}Y^{89}(g)$. With spin 1/2 and odd parity for $_{40}Zr^{89}(g)$ all requirements are met. In particular $\mathfrak{L}=5$ and $\Delta I=4$ in the isomeric transition from $_{40}Zr^{89}(m)$.

$_{38}Sr^{91}(g)$: half-life 3.6×10^{4} sec., β^- 3.2 Mev (60 percent), 1.3 Mev (40 percent), γ 1.3 Mev. Separate half-lives are 6×10^{4} sec. (ground state) and 9×10^{4} (excited state). In the empirical classification the transition types are 2nd forbidden to $_{39}Y^{91}(g)$: 1st forbidden to $_{39}Y^{91}(e)$ and 3d forbidden (at least) for the unobserved transition to $_{39}Y^{91}(m)$. The theoretical classification of the transition to $_{39}Y^{91}(g)$ is 1st forbidden with maximum possible spin change ($\Delta I=\pm2$).

$_{39}Y^{91}(e)$: γ 1.3 Mev to $_{39}Y^{91}(m)$, no observed delay, no observed direct transitions to $_{39}Y^{91}(g)$.

$_{39}Y^{91}(m)$: half-life 3000 sec., γ 0.61 Mev; an isomeric transition on Wiedenbeck's $\mathfrak{L}=5$ curve. The unobserved transition to $_{40}Zr^{91}(g)$ is only 2nd forbidden. With β^- 2.14 Mev for this transition the

TABLE IX. Beta-decay with no change in parity.

Emitter	Radiation	Half-life (sec.)	$Wo(mc^2)$	f	ft
$_0n^1$	β^-	>900#	2.5	1.6	$>1.4\times10^3$
$_1H^3$	β^-(no γ)	3.8×10^8	1.038*	2.9×10^{-6}†	1.1×10^3
$_4Be^7$	K-capture	3.7×10^6 (90%)	0.70	4.5×10^{-4}	1.8×10^3
$_6C^{11}$	β^+(no γ)	1200	2.95	4.1	4.9×10^3
$_7N^{13}$	β^+(no γ)	600	3.44	10.3	6.2×10^3
$_8O^{15}$	β^+	126	4.4	41	5.1×10^3
$_9F^{17}$	β^+	70	5.1	92	6.4×10^3
$_{10}Ne^{19}$	β^+	20.3	5.35	115	2.3×10^3
$_{12}Mg^{23}$	β^+	11.6	6.56	320	3.7×10^3
$_{14}Si^{27}$	β^+	4.9	8.2	890	4.4×10^3
$_{15}P^{29}$	β^+	4.6	8.2	860	4.0×10^3
$_{16}S^{31}$	β^+	2.6	8.6	1.1×10^3	2.9×10^3
$_{17}Cl^{33}$	β^+	2.4	9.14	1.4×10^3	3.4×10^3
$_{18}A^{35}$	β^+	1.88	9.7	1.9×10^3	3.6×10^3
$_{21}Sc^{41}$	β^+	0.87	10.74	3×10^3	2.6×10^3
$_2He^6$	β^-	0.89	7.9	1.0×10^3	0.9×10^3
$_{13}Al^{26}$	β^+	6	6.9(?)	400	2.4×10^3
$_4Be^{10}$	β^-	8×10^{13}	2.10	0.6	5×10^{13}
$_6C^{14}$	β^-	1.5×10^4	1.30	0.005	8×10^8
$_{15}P^{30}$	β^+	153	7.9(?)	710	1.1×10^5
$_8O^{19}$	β^-	29.5 (30%)	9.9	3.9×10^3	3.8×10^5
$_{10}Ne^{23}$	β^-	40	9.1	2.6×10^3	1.1×10^5
$_{12}Al^{29}$	β^-	400	5.9	340	1.4×10^5
$_{14}Si^{31}$	β^-(no γ)	1.02×10^4	4.6	98	10×10^5
$_{16}S^{35}$	β^-	7.5×10^6	1.33	0.023	1.8×10^5
$_{20}Ca^{45}$	β^-(no γ)	1.3×10^7	1.49	0.08	10×10^5
$_{22}Ti^{45}$	β^+	1.1×10^4	3.4	6.8	0.74×10^5
$_{25}Mn^{51}$	β^+	2.8×10^3	5.0	58	1.6×10^5
$_{27}Co^{61}$	β^-	6.3×10^3	3.6	42	2.6×10^5
$_{28}Ni^{57}$	β^+	1.3×10^5	2.33	0.46	0.60×10^5
$_{29}Cu^{64}$	β^-	4.6×10^4 (31%)	2.13	1.87	2.4×10^5
$_{29}Cu^{64}$	β^+	4.6×10^4 (15%)	2.30	0.39	1.2×10^5
$_{30}Zn^{69}$	β^-	3.4×10^3	3.0	15	0.51×10^5
$_{31}Ga^{68}$	β^+	4.1×10^3	4.8	42	1.7×10^5
$_{32}Ge^{71}$	β^+	1.4×10^5	3.4	5.6	7.8×10^5
$_{40}Zr^{89}$	β^+(no γ)	2.9×10^5	3.0	2.0	5.8×10^5
$_{46}Pd^{112}$	β^-(no γ)	7.6×10^4	1.4	0.14	0.11×10^5
$_{47}Ag^{106}$	β^+	1470	5.0	41	0.60×10^5
$_{49}In^{114}$	β^-	72	4.9	460	0.33×10^5
$_{50}Sn^{121}$	β^-(no γ)	9.7×10^4	1.8	1.3	1.3×10^5
$_{52}Te^{127}$	β^-(no γ)	3.3×10^4	2.5	13	4.3×10^5
$_{53}I^{128}$	β^-	1500 (93%)	5.0	600	9.6×10^5
$_{59}Pr^{140}$	β^+	210	5.8	83	0.17×10^5

Snell and Milker, Phys. Rev. **74**, 1217 (1948).
* Hanna, Pontecorvo, and Kirkwood, Phys. Rev. **75**, 983 (1949).
† E. J. Konopinski, private communication.

f value is 400. Assuming $ft \sim 4\times10^8$, $t \sim 10^6$ sec. Hence, the intensity of the β^--transition relative to the isomeric transition may be as large as 0.3 percent. A somewhat smaller intensity (by a factor of 10) would not be unreasonable.

$_{39}Y^{91}(g)$: half-life 5.2×10^6 sec., β^- 1.53 Mev; in the empirical classification a 2nd forbidden transition to $_{40}Zr^{91}(g)$. The theoretical classification is 1st forbidden with maximum possible spin change ($\Delta I = \pm 2$).

Three examples of transitions in the empirical 2nd forbidden classification occur in Table VII. If $_{39}Y^{89}(g)$ and $_{39}Y^{91}(g)$ were assigned even parity the transitions could be interpreted theoretically as 2nd forbidden. However, even parity for the ground state at $Z=39$ requires the substitution of a $2s$ orbit for $3p$ and yields a ^2S state for $_{39}Y^{89,91}(g)$. The magnetic moment of $_{39}Y^{89}(g)$ is in much better accord with a ^2P state. Also, the parity change in the isomeric transition $_{39}Y^{91}(m)$ to $_{39}Y^{91}(g)$ is hardly consistent with the available low configurations if the ground state has even parity; $(3p)^{-3}(2s)^1(5g)^1$ would do for the isomeric state, but does not look plausible.

An interesting series of radioactive and isomeric transitions occurs at $A=95$ beginning with $_{40}Zr^{95}(g)$, continuing through $_{41}Cb^{95}(e)$, $_{41}Cb^{95}(m)$, $_{41}Cb^{95}(g)$, $_{42}Mo^{95}(e)$, and terminating at $_{42}Mo^{95}(g)$. Wiedenbeck's chart yields $\mathfrak{L}=5$ for the isomeric transition in $_{41}Cb^{95}$. Excluding the possibility of a spin value exceeding 11/2 one of the states involved in the isomeric transition has spin 1/2 or 3/2. Inconclusive measurements yield 1/2 for the spin of $_{42}Mo^{95}(g)$. It is apparent that this value is incompatible with the absence of direct transitions from $_{41}Cb^{95}(m)$ or (g) to $_{42}Mo^{95}(g)$.

$_{43}Tc^{99}(m)$: half-life 2×10^4 sec., γ 0.136 Mev; between $\mathfrak{L}=4$ and $\mathfrak{L}=5$ on Wiedenbeck's chart, $\mathfrak{L}=5$ preferred.

$_{43}Tc^{99}(g)$: half-life 10^{13} sec., β^- 0.32 Mev: not 4th forbidden (compare K^{40}) probably another example of the special selection rule $\Delta I = \pm 3$, no change in parity (compare 10 and 22 particle systems). The special selection rule and the low configurations for 43 and 45 particles fix the spin at 9/2 for $_{43}Tc^{99}(g)$ and 3/2 for $_{44}Ru^{99}(g)$. Both parities are even.

$_{44}Ru^{99}$: $a \rightarrow \beta^-$ 0.46-Mev transition from $_{43}Tc^{99}(m)$ to $_{44}Ru^{99}(g)$ is either 1st forbidden or allowed (unfavored). With $f \sim 1.4$ the half-life for the direct transition is certainly less than 10^7 sec. The ratio of β^- to isomeric transitions is therefore certainly greater than 2×10^{-3}, but as yet, only the isomeric transition has been observed.

$_{44}Ru^{103}$: half-life 3.5×10^6 sec., β^- 0.3 Mev, 0.8 Mev (weak), γ 0.56 Mev; 1st forbidden or allowed (unfavored) to $_{45}Rh^{103}(e)$ followed by gamma-transition to $_{45}Rh^{103}(m)$ and possibly also to $_{45}Rh^{103}(g)$; 2nd forbidden β^--transition to $_{45}Rh^{103}(m)$ and probably also to $_{45}Rh^{103}(g)$.

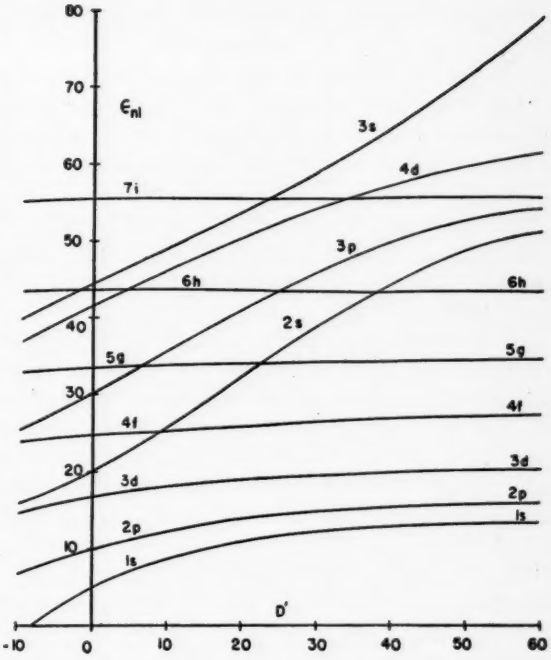

FIG. 2. Behavior of energy levels with increase of potential elevation D' in well of infinite depth and radius R. The elevation covers the range $0 \leqq r \leqq R/2$. ϵ_{nl} and D' in units $\hbar^2/MR^2$.

$_{45}Rh^{103}(m)$: half-life 3×10^3 sec., γ 0.04 Mev; $\mathfrak{L}=4$ from Wiedenbeck's chart.

$_{46}Pd^{103}(g)$: half-life 1.5×10^6 sec., K capture (no γ) to $_{45}Rh^{103}(m)$; allowed (unfavored) excluding the unlikely possibility that the energy release is large ($W_0 \gg 1$).

$_{48}Cd^{107}(g)$: half-life 2.4×10^4 sec., K capture, and β^+ 0.32 Mev (0.3 percent) to metastable state of $_{47}Ag^{107}$. With $W_0 \sim 1.63$ the f values are $f_k \sim 1.75$ and $f(\beta^+) \sim 5\times10^{-3}$. The ratio is 1/350 in agreement with the observed branching ratio. The small value of ft places the transition in the allowed (unfavored) classification.

$_{48}Ag^{107}(m)$: half-life 40 sec., γ 0.094 Mev, an isomeric transition with $\mathfrak{L}=4$ (Wiedenbeck's chart), and $\Delta I = 3$ (internal conversion and K/L ratios, reference 20). The spin (1/2) and magnetic moment (−0.10) of $_{47}Ag^{107}(g)$ show that the ground state is predominantly ^2P. This result excludes the simpler possibilities of the shell model and requires the introduction of a ^2P orbit into both ground and metastable state configurations. The spin of the metastable state is therefore 7/2 (or possibly 9/2) and the parity is odd. A spin value 5/2, 7/2, 9/2, or 11/2 and odd parity are required by the selection rules for $_{48}Cd^{107}$. The only reasonable configuration for $N=59$ is $(4d)^{-1}$ yielding a $^2D_{5/2}$ state of even parity. This discrepancy in parity is a serious difficulty for the shell model.

$_{46}Pd^{109}(g)$: half-life 4.7×10^4 sec., β^- 1.0 Mev to $_{47}Ag^{109}(m)$, probably 1st forbidden.

$_{47}Ag^{109}(m)$: half-life 40 sec., γ 0.087 Mev. The discussion parallels that for $_{47}Ag^{107}(m)$ down to the determination of the ground state configuration of the cadmium parent nucleus. In this case the only suitable (and reasonable) configuration for $N=61$ is $(6h)^1$ yielding the ground state $^2H_{9/2}$ with odd parity. The transition is then allowed and one may conclude that the K capture transition energy is quite small (<0.1 Mev).

The shell model is perhaps most reliable in determining the parity of ground and isomeric states. Such determinations are embodied in Tables VIII and IX for beta-transitions with and without changes in parity. Complex transitions are included only when the branching ratio has been measured, permitting the calculations of the "half-life" of the transition between ground states.

These tables exhibit remarkable features, in some respects at variance with generally accepted ideas. Excluding $_{37}Rb^{87}$, the ft values with change in parity spread out from 4.7×10^6 to 2.8×10^9 suggesting wide variations in the nuclear matrix elements involved in 1st forbidden transitions. The larger values of ft are still far too small to warrant a 3d forbidden assignment, hence must be explained by some special feature of the 1st forbidden transition. As already mentioned it is plausible that transitions with $\Delta I=\pm2$ and change in parity should appear empirically as 2nd forbidden.[25]

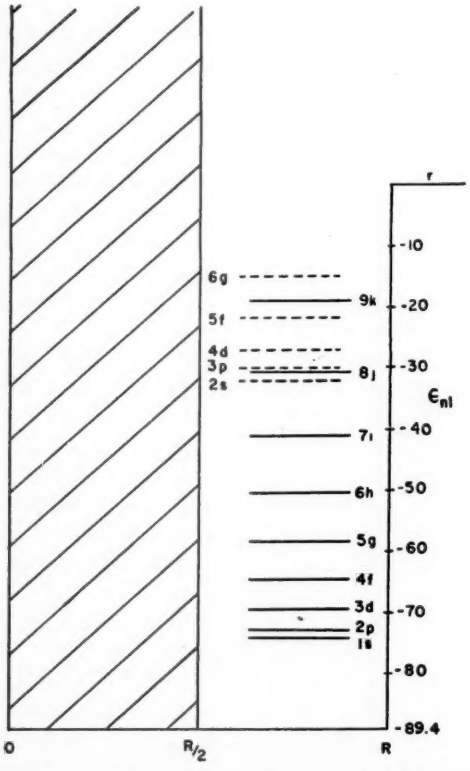

FIG. 3. Single particle energy levels in a well of finite depth, central elevation infinite. Unit of energy $\hbar^2/MR^2$.

The first group in Table IX extending from $_0n^1$ to $_{21}Sc^{41}$ is the mirror image transitions. *There is no evidence for any systematic trend with increasing atomic number.* Presumably the ground state wave functions of parent and daughter nuclei are practically identical from one end of the group to the other. The next group contains allowed singlet-triplet transitions. These two groups contain all transitions taking place within a supermultiplet (allowed and favored in Wigner's terminology). The third group is really a collection of diverse types. $_4Be^{10}$ has already been discussed in connection with the direct transition from $_{11}Na^{22}(g)$ to $_{10}Ne^{22}(g)$. The $_6C^{14}\rightarrow{}_7N^{14}$ transition is empirically 2nd forbidden although the spin changes by only one unit. Dr. H. Primakoff and one of the writers (E. F.) suggest the following explanation: the magnetic moment of $_7N^{14}$ requires a ground state containing 90 percent more or less of $^3D_1$ configurations. Since, however, an accurate calculation of the moment is not possible (because of relativistic effects) the ground state may be almost entirely $^3D_1$. The transition $^2S_0\rightarrow{}^3D_1$ is of course doubly forbidden even though the spin changes by only one unit. A small admixture of $^3S_1$ may dominate the beta-decay process and produce a close approximation to the allowed shape in the beta spectrum.[30] The remaining transition $_{15}P^{30}\rightarrow{}_{14}Si^{30}$ should be included in Wigner's allowed (unfavored) group. Here the transition is perhaps of the type $^3D_1+{}^3S_1\rightarrow{}^1S_0$ with $^3D_1$ predominant in the ground state of the parent nucleus, but not to the same extent as in $_7N^{14}(g)$.

The allowed (unfavored) group includes twenty-five examples ranging from $_8O^{19}$ to $_{59}Pr^{140}$. *Here also there is no evidence for a trend toward larger ft values with increasing atomic number.* All transitions in this group have a relatively small ft value ($\sim10^5$). In a few cases ($_{27}Co^{61}$, $_{40}Zr^{89}$, $_{46}Pd^{112}$, $_{47}Ag^{106}$, $_{49}In^{114}$, and $_{50}Sn^{121}$) the ground state configurations are uncertain because of crossovers and the classification is determined by the ft value and other relevant facts (isomerism, known spins and moments, etc.)

The absence of a trend in the allowed (unfavored) group was first noticed by Itoh.[31] A more extensive and precise analysis by Feather and Richardson[26] reveals a slight trend which might pass unnoticed in a table of ft values.

V. EIGENVALUE CALCULATIONS

Two calculations have been made to illustrate the behavior of single particle energy levels in a

[30] L. Feldman and C. S. Wu, Phys. Rev. **75**, 1286 (1949).
[31] Junkichi Itoh, Proc. Phys.-Math. Soc. Japan **22**, 531 (1940).

potential well containing a central elevation or depression. Figure 2 shows the levels in a well of infinite depth with the central half of the well occupied by an elevation ($D'>0$) or depression ($D'<0$). Another extreme situation appears in Fig. 3. Here the well depth is finite, but the central half is occupied by an elevation of infinite height. These extreme models reproduce the empirically established upward displacement of the $2s$, $3p$, and $4d$ group of levels, but fail to account for the cross-overs within the displaced group. Refinements in the shape of the potential are not likely to alter this situation.

The source of the discrepancy may be traced to the implicit incidence of configuration interaction on all the deductions and correlations of the shell model. Thus the levels traced in Fig. 1 are not true single particle levels such as might be generated by a potential function, but include the influence of all configurations which couple with the low configurations to produce the actual low states of nuclear systems. It is even plausible that the complete inversion of the $2s$, $3p$, and $4d$ levels occurring after the completion of the $5g$ shell simply expresses accurately the increasing importance of configuration interaction with increasing angular momentum. Studies of level density, based on the free particle model, show that the partial density of levels with a given angular momentum is a monatonic increasing function of angular momentum in intermediate and heavy nuclei.[32,33] Furthermore, in light nuclei, the maximum partial density occurs at $l=2$ (D states).[7] Configuration interaction should therefore, on the average, tend to depress states in the inverse order of their angular momentum (limited to $I\leqq 3$ in light nuclei).

Two relevant examples are provided by the ground states of ${}_5B^{10}$ and ${}_{11}Na^{22}$; in each Hartree type calculations place ${}^3S_1$ below ${}^3D_{1,2,3}$ and configuration interaction must be evoked to account for the observed ${}^3D_3$ ground states. Again configuration interaction is perhaps helpful in making the ground state of ${}_7N^{14}$ predominantly ${}^3D_1$.

Note added in proof.—The spin and parity assignments in the 89 and 91 series of isobars have been confirmed by recent measurements of beta-decay distribution functions (references in letter by Shull and Feenberg in this issue). These measurements support the completion of a p shell at $Z=40$ and the beginning of a d shell at $N=51$. The occurrence of long-lived isomeric states in six odd Tellurium isotopes (R. D. Hill, Washington meeting of the Physical Society, April 1949) fits neatly into the qualitative structure of Fig. 1.

[32] H. A. Bethe, Phys. Rev. **48**, 367 (1937).
[33] John Bardeen, Phys. Rev. **51**, 799 (1937).

On Spins, Moments, and Shells in Nuclei*

L. W. NORDHEIM
Duke University, Durham, North Carolina
(Received December 27, 1948)

Known values of nuclear spins and magnetic moments are used to assign orbital quantum numbers to the last odd particle. A consistent scheme is developed that permits the correlation of a wide variety of nuclear data. An interpretation is obtained of the general trends of nuclear spins, for the particular stability of nuclei containing 20, 50, or 82 neutrons or protons, for the occurrence of isomeric states, and for the allowed or forbidden character of β-decays for nuclei with odd mass numbers.

I. INTRODUCTION—NUCLEAR SHELLS

SINCE the early days of nuclear physics, attempts have been made to detect regularities in the structure of nuclei[1] in analogy to the construction principle and electron catalogue for atomic electrons. There is convincing evidence, as recently re-emphasized by Maria G. Mayer[2] for the particular stability of nuclei that contain neutrons or protons in numbers given in Table I. The differences should, of course, give the numbers of particles in subsequent closed shell configurations.

In the past, several attempts[3] have been made to explain these numbers on the basis of a one-particle picture. It is assumed that a reasonable first approximation can be obtained by having each particle moving in an average potential caused by the others. The most natural form for such a potential is in first approximation a simple well since the nuclear matter has essentially constant density and the range of the forces is smaller than the nuclear radius, at least for not too light nuclei. The order of terms in such a well with infinitely high walls, as worked out by Elsasser,[3] is given in Table II, together with the number of particle places. The principal feature of this order is that for a given total quantum number the state with the smallest number of radial nodes, i.e., the highest angular momentum, is energetically the lowest, which is just the opposite as in an atomic field. The order of states is not changed in a well with finite walls,[4] though, of course, there will be only a finite number of places.

A comparison between the numbers of Tables I and II fails to give a correlation above 20 particles. This negative result is not surprising since the one-particle picture is certainly a very crude approximation. There are so many degeneracies and the interaction between configurations is so strong that there will be an extensive mixing of many states which may change greatly the order in which new orbits are added and the character of the ground state of a particular nucleus may be largely accidental.

II. ASSIGNMENT OF ORBITS ON BASIS OF SPIN AND MAGNETIC MOMENT

There is however one more type of information available that throws light on the character of the ground states of nuclei, their spins and moments.[5] It is well known that the magnetic moments as functions of spin lie between two limits as pointed out first by Schmidt.[6] They are given by the assumption that the spin is due solely to the extra odd nucleon and that for the one limit its intrinsic spin and orbital momentum are parallel and for the

TABLE I. Nuclear configurations of particular stability.

No. of particles		2	8	20	50	82	126
Differences		6	12	30	32	44	
Shell	*I*	*II*	*III*	*IV*	*V*	*VI*	

TABLE II. Order of states and numbers of places n in a spherical potential well.

Orbit	1*s*	2*p*	3*d*	2*s*	4*f*	3*p*	5*g*	4*d*	6*h*	3*s*	5*f*	7*i*	4*p*	8*j*	6*g*	5*d*	4*s*
n	2	6	10	2	14	6	18	10	22	2	14	26	6	30	18	10	2

TABLE III. Schmidt limits for the magnetic moments of odd A nuclei in dependence on spin.

	I	1/2	3/2	5/2	7/2	9/2
Odd Z	$I=l+\frac{1}{2}$	+2.79	3.79	4.79	5.79	6.79
	$I=l-\frac{1}{2}$	−0.24	+0.17	+0.88	+1.71	+2.52
Odd N	$I=l+\frac{1}{2}$	−1.91	−1.91	−1.91	−1.91	−1.91
	$I=l-\frac{1}{2}$	+0.64	1.15	1.36	1.49	1.57

* Please see comments on this and the preceding paper in a Letter to the Editor by E. Feenberg, K. C. Hammack, and L. W. Nordheim, this issue.

[1] For a review and discussion of these attempts see H. A. Bethe and R. F. Bacher, Rev. Mod. Phys. **8**, 168 *ff.* (1936) and E. P. Wigner and E. Feenberg, Reports on Progress in Phys. **8**, 274, London (1942).

[2] Maria G. Mayer, Phys. Rev. **74**, 235 (1948).

[3] See the articles in reference 1 and particularly W. Elsasser, J. de phys. et Rad. **5**, 389, 625 (1934).

[4] See Henry Margenau, Phys. Rev. **46**, 613 (1934).

[5] The most recent and complete tabulation of nuclear spins and moments is due H. H. Goldsmith and D. R. Inglis, issued by the Brookhaven National Laboratory as report BNL-1-5, October 1, 1948. All data used here have been taken from this work.

[6] T. Schmidt, Zeits. f. Physik. **106**, 358 (1937).

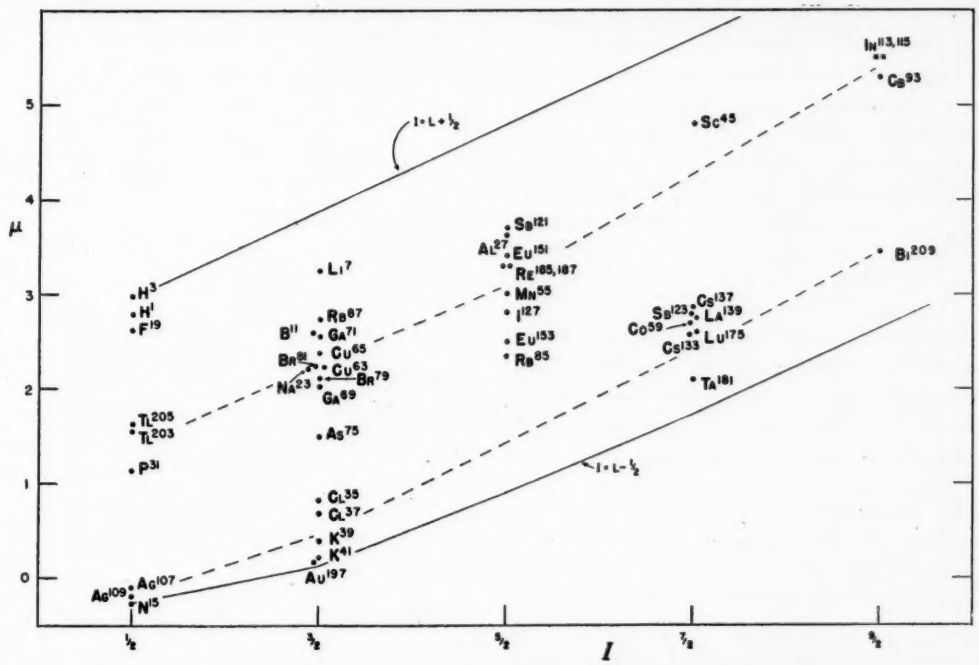

FIG. 1a. Magnetic moments and Schmidt limits as function of spin in nuclei of odd Z.

other antiparallel. The g formulas are

$$\mu_I = g_l l + g_s \quad \text{for } I = l + 1/2,$$

$$\mu_I = g_l \frac{(l+1)(2l-1)}{2l+1} - g_s \cdot \frac{2l-1}{2l+1} \quad \text{for } I = l - 1/2.$$

With an orbital $g_l = 1$ for protons and 0 for neutrons and the intrinsic moments $g_s = 2.79$ for protons and $g_s = -1.91$ for neutrons the following values for the Schmidt limits are obtained. (See Table III.)

The actual values of the magnetic moments μ lie between these limits. One has thus to conclude that the actual wave function of the odd particle is a mixture of the two possibilities, combined with states of different parity for the residual nucleus with spin zero.

Figure 1 gives a representation of the distribution of magnetic moments and of the spins of the isotopes with odd mass numbers. The Schmidt limits are indicated by the solid lines. Inspection of Fig. 1 shows that the moments fall definitely into two groups,[7] each of which lies nearer to one of the limits, though there are some nuclei which are about halfway in between. The groups are indicated by the dotted lines. The fact that these lines do not coincide with the Schmidt limits indicates, of course, that the one-particle picture is not entirely adequate. However, it seems to be worth while to investigate the pattern which results from the assignment of orbital momenta according to the groupings in Fig. 1.

In Tables IV and VI the apparent orbital moments for all nuclei of odd atomic weight with known spins are listed separately for odd protons and odd neutrons. We assign also a principal quantum number in accordance with the exclusion principle, following as far as possible the sequence of orbits from Table II. The superscripts $\pm$ indicate addition or subtraction of angular and spin momentum to the total nuclear spin. The cases of strong mixtures are indicated, and the places, where shells are filled according to Table I, are also marked. Several magnetic moments have not been measured and the assignments in these cases are subject to doubt. The choice for the two Ir isotopes has been made on the basis of the information that their moments have opposite signs, which can be reconciled with the spin values only by the orbits given in the table.

We discuss first Table IV for protons. It is very striking that, in the main, new orbits appear in a definite order, which is very similar but not quite the same as in Table II. There are frequent shifts between orbits which are energetically near to each other. It is remarkable, however, how new orbits appear after passing through the closed shell numbers of Table I. $_9F^{19}$ shows that here the $2s$ orbit is lower than $3d$. $_{21}Sc^{45}$ brings the first $4f$. The $5g$'s appear fairly solidly with $_{51}Sb^{123}$, and $_{83}Bi^{209}$ gives beautiful evidence for a $6h$ orbit.

In any attempt to interpret nuclear structure, one has to be aware of the following limitations:

[7] This has been noticed by David R. Inglis, Phys. Rev. **53**, 470 (1938).

a one-particle picture cannot be as clearcut as in the atomic or molecular case. The actual energy difference between states of different symmetry are much smaller than would result from a Hartree-Fock approximation (compare the discussion by Wigner and Feenberg, reference 1). There are always many configurations which are energetically near each other, and which may thus interact strongly. The situation is in some respects analogous to the case of the rare earths for atomic structure where also a number of competing orbits are available. It is a matter of accident which new orbit out of several possible ones will be added, and there may be re-arrangements in the sequence as heavier nuclei are built up. Also, an orbit may not be favored for single occupancy and thus may not appear explicitly as an observable last orbit, while it may be filled when two particles are available. It is thus to be expected that possible shells will have real significance only when they are just completed. It is also not unlikely that re-arrangements will not respect shell boundaries. Thus, orbits may appear before they are expected, and even a completed shell may loosen up again when a re-arrangement is accidentally favored.

The material presented in Table IV suggests strongly and quite naturally a grouping of orbits which accounts for the magic numbers of Table I up to and inclusive of shell *V*, when the above limitations are taken into account. This scheme, which we will adopt as a working hyopthesis, is given in Table V.

The shells are indicated by brackets. The shell numbers correspond also to the highest total quantum number occurring in it. There is no indication in heavier nuclei of sub-shells comprised of orbits of one kind only.** This means that new orbits are always added before the filling out of the preceding levels, except at the places given by the magic numbers. The latter are thus the more or less accidental positions where a clean break happens to be possible.

The order of levels in Table V differs only slightly from the level scheme for a potential well given in Table II. Thus one gains the impression that the one-particle picture is not quite devoid of all significance. It should be said, however, that it does seem neither necessary nor warranted to assume that one-particle wave functions can be ascribed to all individual particles in nuclei. However, such an assignment makes sense according to the evidence for the last odd particle. The exclusion principle will then still determine the nature of its wave function, though those for the inner particles may have lost all semblance to one-particle wave functions.

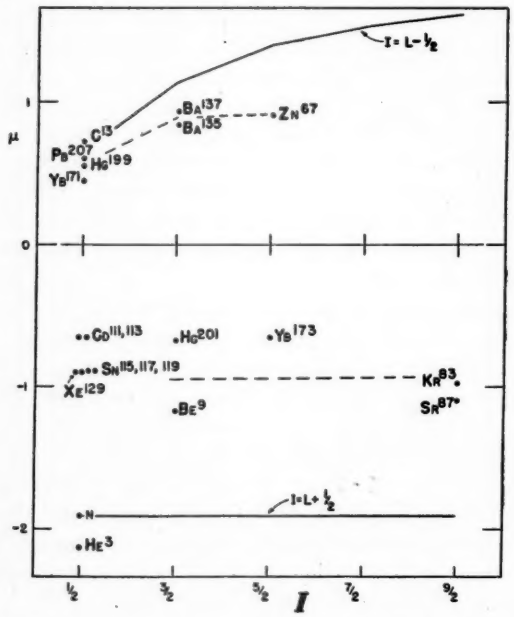

FIG. 1b. Magnetic moments and Schmidt limits as function of spin in nuclei of odd *N*.

TABLE IV. Spins *I*, magnetic moments μ, and assignment of orbital quantum numbers to the last proton in elements with odd *Z*.

Nucleus	*I*	μ	Orbit	Nucleus	*I*	μ	Orbit
$_3Li^7$	3/2	3.25	$2p^+$	$_{41}Cb^{93}$	9/2	5.3	$5g^+$
$_5B^{11}$	3/2	2.69	$2p^+$	$_{47}Ag^{107}$	1/2	−0.10	$3p^-$
$_7N^{15}$	1/2	−0.28	$2p^-$	$_{47}Ag^{109}$	1/2	−0.19	$3p^-$
$_9F^{19}$	1/2	2.63	$2s$	$_{49}In^{113}$	9/2	5.5	$5g^+$
$_{11}Na^{23}$	3/2	2.2	$2p^+ + 3d^-$	$_{49}In^{115}$	9/2	5.5	$5g^+$
$_{13}Al^{27}$	5/2	3.6	$3d^+$	$_{51}Sb^{121}$	5/2	3.7	$4d^+$
$_{15}P^{31}$	1/2	1.13	$2p^- + 2s$	$_{51}Sb^{123}$	7/2	2.8	$5g^-$
$_{17}Cl^{35}$	3/2	0.82	$3d^-$	$_{53}I^{127}$	5/2	2.8	$5f^- + 4d^+$
$_{17}Cl^{37}$	3/2	0.68	$3d^-$	$_{55}Cs^{133}$	7/2	2.58	$5g^-$
$_{19}K^{39}$	3/2	0.39	$3d^-$	$_{55}Cs^{137}$	7/2	2.86	$5g^-$
$_{19}K^{41}$	3/2	0.22	$3d^-$	$_{57}La^{139}$	7/2	2.76	$5g^-$
$_{21}Sc^{45}$	7/2	4.8	$4f^+$	$_{59}Pr^{141}$	5/2		$5f^-$
$_{23}V^{51}$	7/2		$4f^+$	$_{63}Eu^{151}$	5/2	3.4	$5d^+ + 5f^-$
$_{25}Mn^{55}$	5/2	3.0	$4d^+ + 4f^-$	$_{63}Eu^{153}$	5/2	1.5	$5f^-$
$_{27}Co^{59}$	7/2	2.7	$5g^-$	$_{65}Tb^{159}$	3/2		$5d^-$?
$_{29}Cu^{63}$	3/2	2.22	$3p^+ + 4d^-$	$_{67}Ho^{165}$	7/2		$5g^-$
$_{29}Cu^{65}$	3/2	2.38	$3p^+ + 4d^-$	$_{69}Tm^{169}$	1/2		$3s$?
$_{31}Ga^{69}$	3/2	2.02	$3p^+ + 4d^-$	$_{71}Lu^{175}$	7/2	2.6	$5g^-$
$_{31}Ga^{71}$	3/2	2.56	$3p^+ + 4d^-$	$_{73}Ta^{181}$	7/2	2.1	$5g^-$
$_{33}As^{75}$	3/2	1.5	$3p^+ + 4d^-$	$_{75}Re^{185}$	5/2	3.3	$5d^+ + 5f^-$
$_{35}Br^{79}$	3/2	2.1	$3p^+ + 4d^-$	$_{75}Re^{187}$	5/2	3.3	$5d^+ + 5f^-$
$_{35}Br^{81}$	3/2	2.27	$3p^+ + 4d^-$	$_{77}Ir^{191}$	1/2		$4p^-$
$_{37}Rb^{85}$	5/2	1.35	$4f^-$	$_{77}Ir^{193}$	3/2		$5d^-$
$_{37}Rb^{87}$	3/2	2.74	$3p^+$	$_{79}Au^{197}$	3/2	0.195	$5d^-$
$_{39}Y^{89}$	1/2		$3p^-$	$_{81}Tl^{203}$	1/2	1.55	$3s + 4p^-$
				$_{81}Tl^{205}$	1/2	1.63	$3s + 4p^-$
				$_{83}Bi^{209}$	9/2	3.45	$6h^-$

TABLE V. Average energetic order of one particle levels and shell structure for nuclei.

Orbits	(1*s*)	(2*p*)	(2*s*, 3*d*)	(4*f*, 3*p*, 4*d*)	(5*g*, 5*f*)	(6*h*, 3*s* ···)
No of places	2	6	12	30	32	44
Shell	*I*	*II*	*III*	*IV*	*V*	*VI*

** There is a possibility that a shell may be completed at *N* or *Z* equal to 40 , which could be interpreted as a filling of only the 4*f* and 3*p* levels of shell *IV*. The evidence consists in a good isotopic and isotonic spread, the frequent occurrence of new type orbits for *N* and *Z*>40, and the fairly frequent occurrence of isomers with particle number 39. However, there is no necessity for this assumption.

The above interpretation of the structure of nuclear shells is strengthened by consideration of the nature of the occurring deviations.

The only difficulty in shell *III* comes from $_{11}Na^{23}$ and the similar case of $_{15}P^{31}$, which have strongly mixed orbits and have magnetic moments which show evidence of a considerable contribution of a p orbit which regularly should not occur in this group. The explanation may be that in these cases the residual nucleus has an angular momentum different from zero.

In shell *IV* there is a group of nuclei from $_{29}Cu^{63}$ to $_{35}Br^{79}$ which have to be explained as mixtures of $3p^+$ and $4d^-$ orbits, or again, as due to the presence of angular momentum in the residual nucleus. The most remarkable nucleus in this shell is $_{27}Co^{59}$ which has definitely a $5g$ orbit. The early appearance of this orbit must be due to an accident. This is borne out by the β-decay properties of other nuclei with 27 particle groups, which demand different assignments (compare Section IV). It is not unlikely that there is an angular momentum contribution from the residual nucleus in the 27 particle configuration, which would obviate the necessity of introducing a $5g$ orbit at this early position.

The $5g$ orbits belonging regularly to shell *V* appear with fair frequency toward the end of shell *IV* ($_{41}Cb^{93}$, $_{49}In^{113}$, and $_{49}In^{115}$). It will be seen later (Section III) that this premature coming in of a new orbit from a higher shell is intimately connected with the occurrence of isomeric states. For instance, both In isotopes have such isomeric states which can be interpreted as belonging to $3p^-$ orbits as in $_{47}Ag$.

In shell *V* one finds many $5g$ and some $5f$ levels, though others occur also. The most surprising case is $_{51}Sb^{121}$ which has to be interpreted as an accidental loosening up of the preceding closed shell. Mixtures occur frequently in the middle of the shell. The case of the $_{63}Eu$ isotopes with same spin but large difference in magnetic moment is remarkable. Towards the end of this shell many levels appear corresponding to states which are higher in the sequence of Table II.

We now take up the case of odd neutron nuclei. The available material is collected in Table VI, which gives also the number of neutrons for each isotope.

The rather meager material for $N<50$ fits well within the same scheme as that for protons. We find that all odd neutron nuclei with $N<50$ have exactly the same configuration, also with respect to relative orientation of particle spin and orbital momentum, as the corresponding proton numbers. The one exception $_{36}Kr_{47}^{83}$ has an isomer which should be the configuration corresponding to $_{47}Ag^{107}$.

However, there is a striking difference between the neutron and proton cases for nuclei with larger neutron numbers. In place of $5g$ or $5f$ orbits, only orbits with low angular momentum appear. The assignment of total quantum numbers becomes thus rather doubtful since we cannot know whether higher l states are added in between, or whether the total quantum number increases. We are inclined toward the first assumption in view of the apparent closed shell of 82 neutrons. Higher angular momentum neutrons must then always be added in pairs.

There are two effects which may help to explain the difference between neutrons and protons. The electric charge in nuclei is, according to available evidence, nearly uniformly distributed over the nuclear volume. It will thus produce a quasi-elastic repulsive force which will tend to favor orbits with high angular moment. Secondly, protons have always neutron counterparts with which they can interact, while the last neutrons have no proton partners. Thus they will not move in exactly the same "average field."*** Looking at the combined

TABLE VI. Neutron numbers N, spins I, magnetic moments μ and assignment of orbital quantum numbers to the last neutron in elements with odd N.

Nucleus	N	I	μ	Orbit	Nucleus	N	I	μ	Orbit
$_4Be^9$	5	3/2	−1.18	$2p^+$	$_{70}Yb^{171}$	101	1/2	0.45	$4p^-$
$_6C^{13}$	7	1/2	0.70	$2p^-$	$_{70}Yb^{173}$	103	5/2	−0.65	$5d^+$
$_{16}S^{33}$	17	3/2		$3d^-$	$_{72}Hf^{177}$	105	≤3/2		
$_{30}Zn^{67}$	37	5/2	0.9	$4f^-$	$_{72}Hf^{179}$	107	≤3/2		
$_{34}Se^{77}$	43	1/2		$3p^-$	$_{74}W^{183}$	109	1/2		
$_{36}Kr^{83}$	47	9/2	−0.97	$5g^+$	$_{76}Os^{187}$	113	1/2		s or p
$_{38}Sr^{87}$	49	9/2	−1.1	$5g^+$	$_{78}Pt^{195}$	117	1/2		s or p
$_{42}Mo^{95}$	53	1/2		$3s$	$_{80}Hg^{199}$	119	1/2	0.55	$4p^-$
$_{48}Cd^{111}$	63	1/2	−0.65	$3s$	$_{80}Hg^{201}$	121	3/2	−0.61	$4p^+$
$_{48}Cd^{113}$	65	1/2	−0.65	$3s$	$_{82}Pb^{207}$	125	1/2	0.6	$4p^-$
$_{50}Sn^{115}$	65	1/2	−0.9	$3s$					
$_{50}Sn^{117}$	67	1/2	−0.89	$3s$					
$_{50}Sn^{119}$	69	1/2	−0.89	$3s$					
$_{54}Xe^{129}$	75	1/2	−0.90	$3s$					
$_{54}Xe^{131}$	77	3/2	+0.8	$5d^-$					
$_{56}Ba^{135}$	79	3/2	+0.84	$5d^-$					
$_{56}Ba^{137}$	81	3/2	+0.94	$5d^-$					

TABLE VII. Nuclei with isomeric states.

Odd proton	Odd neutron	Odd neutron	Odd-odd	Odd-odd
	$_{22}Ti_{23}$	$_{52}Te_{79}$	$_{21}Sc_{23}$	$_{65}Tb_{95}$
$_{33}As_{40}$	$_{20}Ca_{29}$	$_{54}Xe_{73}$	$_{25}Mn_{27}$	$_{71}Lu_{105}$
$_{39}Y_{48}$	$_{22}Ti_{29}$	$_{54}Xe_{81}$	$_{27}Co_{33}$	$_{73}Ta_{107}$
$_{39}Y_{52}$	$_{30}Zn_{39}$	$_{56}Ba_{77}$	$_{35}Br_{45}$	$_{73}Ta_{109}$
$_{41}Cb_{54}$	$_{32}Ge_{39}$	$_{66}Dy_{99}$	$_{41}Cb_{51}$	$_{77}Ir_{115}$
$_{43}Tc_{54}$	$_{32}Ge_{45}$	$_{68}Er_{101}$	$_{41}Cb_{53}$	$_{79}Au_{117}$
$_{43}Tc_{56}$	$_{34}Se_{49}$	$_{68}Er_{103}$	$_{45}Rh_{59}$	$_{81}Tl_{119}$
$_{45}Rh_{58}$	$_{36}Kr_{43}$	$_{70}Yb_{105}$	$_{47}Ag_{63}$	$_{91}Pa_{143}$
$_{47}Ag_{62}$	$_{36}Kr_{47}$	$_{78}Pt_{119}$	$_{49}In_{63}$	
$_{49}In_{64}$	$_{36}Kr_{49}$	$_{80}Hg_{117}$	$_{49}In_{65}$	even-even
$_{49}In_{66}$	$_{38}Sr_{49}$	$_{80}Hg_{119}$	$_{49}In_{67}$	$_{32}Ge_{40}$
$_{59}Pr_{82}$	$_{40}Zr_{49}$		$_{51}Sb_{71}$	$_{52}Te_{72}$
$_{69}Tm_{100}$	$_{42}Mo_{51}$		$_{51}Sb_{73}$	$_{58}Ce_{82}$
$_{69}Tm_{102}$	$_{48}Cd_{67}$		$_{55}Cs_{79}$	$_{78}Pt_{118}$
$_{73}Ta_{108}$	$_{50}Sn_{73}$		$_{55}Cs_{85}$	$_{82}Pb_{122}$
$_{75}Re_{112}$	$_{52}Te_{75}$		$_{57}La_{81}$	
$_{79}Au_{118}$	$_{52}Te_{77}$		$_{63}Eu_{89}$	

*** Compare the discussion in Bethe and Bacher, reference 1, §37.

TABLE VIII. Spin, orbit and parity assignments for nuclei in β-transitions.

(a) Allowed transitions

A and class	Initial nucleus	Orbit	Spin	Final nucleus	Orbit	Spin	γ	ΔI	Δp
35*a*	$_{16}S_{19}$	$3d^-$	3/2	$_{17}Cl_{18}$	$3d^-$	3/2		0	no
43*a*	$_{21}Sc_{22}$	$4f^+$	7/2	$_{20}Ca_{23}$	$4f^+$	7/2	γ	0	no
45*a*	$_{22}Ti_{23}$ I.T.	$4f^+$	7/2	$_{21}Sc_{24}$	$4f^+$	7/2		0	no
49*b*	$_{23}V_{26}$	$4f^+$	7/2	$_{22}Ti_{27}$	$5g^-$	7/2		1	yes
									no
51*a*	$_{25}Mn_{26}$	$4d^+ + 4f^-$	5/2	$_{24}Cr_{27}$	$5g^-$	7/2		1	
					$4d^+ + 4f^-$	5/2		0	no
57*a*	$_{28}Ni_{29}$	$3p^+ + 4d^-$	3/2	$_{27}Co_{30}$	$5g^-$	7/2		2	
					$3p^+ + 4d^-$	3/2		0	no
61*b*	$_{29}Cu_{32}$	$3p^+ + 4d^-$	3/2	$_{28}Ni_{33}$	$3p^+ + 4d^-$	3/2		0	no
63*a*	$_{30}Zn_{33}$	$3p^+ + 4d^-$	3/2	$_{29}Cu_{34}$	$3p^+ + 4d^-$	3/2		0	no
69*a*	$_{30}Zn_{39}$	$3p^-$	1/2	$_{31}Ga_{38}$	$3p^+ + 4d^-$	3/2		1	no
75*a*	$_{32}Ge_{43}$	$3p^-$	1/2	$_{33}As_{42}$	$3p^+ + 4d^-$	3/2	γ	1	no
71*c*	$_{33}As_{38}$	$3p^+ + 4d^-$	3/2	$_{32}Ge_{39}$	$3p^-$	1/2		1	no
81*c*	$_{34}Se_{47}$ I.T.	$3p^-$	1/2	$_{35}Br_{46}$	$3p^+ + 4d^-$	3/2		1	no
83*a*	$_{35}Br_{48}$	$3p^+ + 4d^-$	3/2	$_{36}Kr_{47}$ I.T.	$5g^+$	9/2		3	
					$3p^-$	1/2			no
79*c*	$_{36}Kr_{43}$	$3p^-$	1/2	$_{35}Br_{44}$	$3p^+ + 4d^-$	3/2		1	no
97*a*	$_{41}Cb_{56}$	$5g^+$	9/2	$_{42}Mo_{55}$	$3s$	1/2	γ	4	
		$3p^-$?	1/2					1	yes
93*c*	$_{42}Mo_{51}$ I.T.	$3s$	1/2	$_{41}Cb_{52}$	$5g^+$	9/2		4	
		$5g^-$	7/2					1	no
101*a*	$_{43}Tc_{58}$	$3p^-$	1/2	$_{44}Ru_{57}$	$3s$	1/2	γ	1	yes
117*a*	$_{49}In_{68}$	$5g^+$	9/2	$_{50}Sn_{67}$	$3s$	1/2		4	
		$3p^-$	1/2					0	yes
139*a*	$_{56}Ba_{83}$	$6h^-$	9/2	$_{57}La_{82}$	$5g^-$	7/2	γ	1	yes

proton and neutron evidence, we are inclined to conclude that in nuclei higher numbers of radial nodes are not as sharply penalized as in a simple potential well, particularly for neutrons. This effect is compensated partly but not entirely by the Coulomb repulsion for protons. The non-appearance of $6h$ orbits in shell V as contrasted to the early appearance of $5g$ states in shell IV seems also to indicate a discrimination against too high angular momentum values. However, the discussion of the next section indicates that the $6h$ orbits are occurring in isomeric states.

There is definitely not enough evidence to substantiate any assignment to the magic number 44 for shell VI. If one wishes to speculate and to play with numbers, one can make the observation that a ($6h3s6g4s$) configuration gives 44 places and that ($4p5d$) gives 16 additional ones which would bring us to $_{90}Th^{232}$ by taking all the orbits from Table II up to $4s$ except the very high angular momentum states $7i$ and $8j$.

There is no definite trend discernible as to the relative alignment of intrinsic spin and orbital momentum. One might perhaps say that there is in general a tendency towards antiparallelism (i.e., the minus sign has the edge) except for just added new type orbits.

III. OCCURRENCE OF ISOMERIC STATES

An interesting illustration of the way, in which the construction principle for nuclei operates, is furnished by the statistics of isomeric states. Table VII gives all nuclei with isomeric states listed in the isotope chart of the General Electric Research Laboratory.[8] The different types, odd proton, odd neutron, odd-odd, even-even, are separated, and both proton as well as neutron numbers are given.

We consider first the odd A nuclei. No isomeric states are connected with particle numbers below 20, since no high orbital momentum states are present in such nuclei. A few isomeric states occur in the twenties, where the first high spins are observed. At larger numbers the definite rule is established, with very few exceptions, that isomeric states appear at odd particle numbers which are not too far below those for completed shells. These cases are indicated in Table VII by vertical lines on the side (neutron or proton) to which the rule applies. The scarcity of isomeric states for proton

[8] Prepared by G. Friedlander and M. L. Perlman, 1948. *Note added in proof.*—The Table of Isotopes by G. T. Seaborg and I. Perlman, Rev. Mod. Phys. **20**, 585 (1948), and the new Segrè chart AECD-2111 lead to a still more convincing statistics of isomers.

TABLE VIII. (*Cont.*)

(b) First forbidden

A and class	Initial nucleus	Orbit	Spin	Final nucleus	Orbit	Spin	γ	ΔI	Δp
23*a*	$_{10}Ne_{23}$	$3d^+$	5/2	$_{11}Na_{12}$	$2p^+ + 3d^-$	3/2		1	yes
27*a*	$_{12}Mg_{15}$	$2p^- + 2s$	1/2	$_{13}Al_{14}$	$3d^+$	5/2	γ	2	yes
29*a*	$_{13}Al_{16}$	$3d^+$	5/2	$_{14}Si_{15}$	$2p^- + 2s$	1/2		2	yes
31*a*	$_{14}Si_{17}$	$3d^-$	3/2	$_{15}P_{16}$	$2p^- + 2s$	1/2		1	yes
41*a*	$_{18}A_{23}$	$4f^+$	7/2	$_{19}K_{22}$	$3d^-$	3/2	γ	2	yes
45*a*	$_{20}Ca_{25}$	$4d^+ + 4f^-$	5/2	$_{21}Sc_{24}$	$4f^+$	7/2	γ	1	yes
49*d*	$_{20}Ca_{29}$ I.T.	$3p^+ + 4d^-$	3/2	$_{21}Sc_{28}$	$4f^+$	7/2	γ	2	no
51*a*	$_{22}Ti_{29}$ I.T.	$3p^+ + 4d^-$	3/2	$_{23}V_{28}$	$4f^+$	7/2	γ	2	no
59*a*	$_{26}Fe_{33}$	$3p^+ + 4d^-$	3/2	$_{27}Co_{32}$	$5g^-$	7/2	γ	2	no?
65*a*	$_{28}Ni_{37}$	$4f^-$	5/2	$_{29}Cu_{36}$	$3p^+ + 4d^-$	3/2	γ	1	no?
71*a*	$_{32}Ge_{39}$ I.T.	$3p^-$	1/2	$_{31}Ga_{40}$	$3p^+ + 4d^-$	3/2		1	no?
89*a*	$_{37}Rb_{52}$	$4f^-$	5/2	$_{38}Sr_{51}$	$3s$	1/2	γ	2	yes
89*a*	$_{40}Zr_{49}$ I.T.	$5g^+$	9/2	$_{39}Y_{50}$	$3p^-$	1/2			
		$3s$?	1/2					0	yes
101*b*	$_{42}Mo_{59}$	$3s$	1/2	$_{43}Tc_{58}$	$3p^-$	1/2	γ	0	yes
109*a*	$_{46}Pd_{63}$	$3s$	1/2	$_{47}Ag_{62}$ I.T.	$3p^-$	1/2	γ	0	yes
115*a*	$_{48}Cd_{67}$ I.T.	$3s$	1/2	$_{49}In_{66}$ I.T.	$5g^+$	9/2	γ	4	no
131*a*	$_{53}I_{78}$	$5f^- + 4d^+$	5/2	$_{54}Xe_{77}$	$5d^-$	3/2	γ	1	yes
141*a*	$_{58}Ce_{83}$	$6h^-$	9/2	$_{59}Pr_{82}$	$5f^-$	5/2	γ	2	no
165*a*	$_{66}Dy_{99}$	$4p^+$	3/2	$_{67}Ho_{98}$	$5g^-$	7/2	γ	2	yes
187*b*	$_{74}W_{113}$	$4p^-$	1/2	$_{75}Re_{112}$	$5f^- + 5d^+$	5/2	γ	2	no

(c) Second and higher forbidden

A and class	Initial nucleus	Orbit	Spin	Final nucleus	Orbit	Spin	γ	ΔI	Δp
59*a*	$_{26}Fe_{33}$	$3p^+ + 4d^-$	3/2	$_{27}Co_{32}$	$5g^-$	7/2	γ	2	no?
87*a*	$_{37}Rb_{50}$	$4f^-$	3/2	$_{38}Sr_{49}$ I.T.	$5g^+$	9/2	γ	3	yes
89*a*	$_{38}Sr_{51}$	s	1/2	$_{39}Y_{50}$	$3p^-$	1/2			
		$5g^+$	9/2					4	yes
99*a*	$_{42}Mo_{57}$	$3s$	1/2	$_{43}Tc_{56}$ I.T.	$3p^-$	1/2	γ		
					$5g^+$	9/2		4	yes
185*b*	$_{74}W_{111}$	p^-	1/2	$_{75}Re_{110}$	$5d^+ + 5f^-$	5/2	γ	2	no

and neutron numbers between 50 and 70 and around 82 to 117 is very striking.

The interpretation of this phenomenon can be found in the observation that new orbits appear not infrequently before the completion of the preceding shell. Thus, there will be a state in which the last particle goes into the new orbit with high spin and a competing state in which the incomplete shell is added to. These two states are likely to have widely different spins, since the lowest orbits of new shells have high angular momentum coupled with a tendency for parallelism of spin and orbital momentum, while the upper states in a shell have low spins and a tendency towards antiparallelism. It cannot be predicted, of course, which of these states is the lower one.

The spread of isomeric states is fairly large, from 39 to 49 for shell *IV*; from ~69 to 81 in shell *V*; and from 117 on in shell *VI*. Neutron and proton shells behave very much alike. It is quite noticeable that certain numbers seem to favor isomerism both for neutrons and protons. This is most pronounced for 49 and to a lesser degree for 39, 47 and 79.

The reverse case of a competing state with loosening up of a shell after its completion seems practically not to occur. A once reached shell configuration seems thus to remain stable.

Our rule applies rather surprisingly also to odd-odd nuclei as is evident from the corresponding section of Table VII. This is a further indication for a marked independence of neutron and proton configurations, which emerges as an outstanding feature of the whole picture.

The cases of isomers in even-even nuclei are too few to permit any conclusions.

The above rule does not imply, of course, that isomeric states have to occur in all nuclei with not quite completed shells or that they could not occur in others. However, the preference is very pronounced.

IV. INTERPRETATION OF β-TRANSITIONS

Another group of phenomena that can be connected with the assignment of spins and orbits to nuclei is the allowed or forbidden character of β-transitions.[9]

The possibility of making assignments of spins to radio-active nuclei is based on the following observations:

(1) The spins of odd neutron nuclei with $N<50$ are generally the same as those with the same number of protons.
(2) Most spins of odd neutron nuclei with $N>50$ are low and follow a fairly definite pattern.
(3) The spin of isotopes differing by two neutrons is the same with very few exceptions.

These rules make it possible with the help of Table IV and Table VI to assign spin values and orbital quantum numbers to most nuclei of odd mass number. It is not expected, of course, that this primitive procedure will be true in all cases, and some corrections will be made later. We give the resulting assignments in Table VIII for all odd A nuclei contained in Konopinski's[9] classification of β-transitions. The transitions listed in his table have been checked with the G.E. isotope chart[8] and some isotope identifications have been corrected.

We have not included the 14 known conjugate nuclear pairs, where the number of neutrons in the product equals the number of protons in the initial state. All these nuclei should show no spin change, and all such β-transitions are allowed.

Table VIII contains, besides the nuclei with the numbers of protons (left) and neutrons (right) for the initial and final states, the spin assignments from rules 1, 2, 3. The measured spins are underlined. Different assignments are indicated below those from rules 1 to 3 in the cases where we believe that changes have to be made. All those cases will be discussed in the text. The table contains the symbol I.T. behind every isotope, which is known to possess an isomeric state, whether it is necessary for the interpretation or not. The symbol γ means, that γ-radiation is emitted in connection with the transition. The parity column, to be discussed later, indicates whether one should assume that the parity is different (yes) or the same (no) in the initial and final nucleus. The preferred parity in mixtures is always the one of the orbit given first. For instance, $2p^-+2s$ means that the parity is odd. The class symbols have the usual meaning

a isotope certain,
b mass number probable, element certain,
c one of a few mass numbers, element certain,
d element certain.

Table VIII shows at once striking correlations. The allowed transitions are in most cases connected with $\Delta I=0$ with some $\Delta I=1$. There are practically no γ-rays, if both N and Z are below 50. There are γ-rays, however, if $Z<50$ but $N>50$, that is, the neutrons and protons end in different shells. There are only a few such transitions altogether, and no allowed cases for odd A are known beyond Ba^{139}. The explanation for this rule lies in the difference of the behavior of the last proton and neutron for $Z>50$.****

Among the forbidden transitions, one finds frequently $\Delta I=2$ with some $\Delta I=1$, and γ-radiations in the majority of cases. Among the higher forbidden cases some larger spin changes are encountered. There is again a marked difference between the cases with N smaller or larger than 50.

A closer interpretation demands a comparison with theoretical selection rules, which are still rather uncertain. It can be said, however, that the material presented here is in good accord with the Gamow-Teller selection rules. In these, parity plays the essential role.

With no change in parity $\Delta I=0, \pm1$ lead to allowed transitions, and $\Delta I=\pm2, \pm3$ to second-order forbidden ones. With change in parity $\Delta I=0, \pm1, \pm2$ are all first-order forbidden and higher ΔI of third order. These rules are rather flexible, particularly in presence of γ-radiation. For the latter, there are the two possibilities that they either come from a side path, in which case only a small fraction of γ-radiation is expected, or they may also come from a more allowed path than the direct transition, in which case there should be at least one γ-ray per disintegration.

Since we ascribed orbital momenta to the last odd number, we obtain also its contribution to the parity of the ground state. It would seem likely that the residual nucleus, with spin zero, would give an even contribution to parity. However, as mentioned before, the actual magnetic moments lie between and not on the Schmidt limits, and cores of different parity have to be added to the two orbits to make a mixture of definite parity possible. Thus, no really definite statement on parity can be made, particularly in case of strong mixtures, as they occur frequently in half-filled shells. It is, however, possible to make reasonable assignments in practically all cases, though they are not always unique and may have to be revised later.

We discuss now how the parities of mixtures have been determined.

$2p^++3d^-$ for 11 particles is odd according to the first forbidden character of $_{10}Ne_{22}$;

[9] For a complete review of the theory of β-decay, see Emil J. Konopinski, Rev. Mod. Phys. 15, 209 (1943).

**** We have left out in general the consideration of the heavy naturally radioactive elements, since no spin and moments are known here. It seems that some allowed transitions occur in this group. This may be due to the circumstance that low orbital momentum states are possible here for both protons and neutrons.

$2p^-+2s$ for 15 particles is odd from the first forbidden character of $_{12}Mg_{15}$ and $_{14}Si_{17}$;

$4d^++4p^-$ for 25 particles is even from the first forbidden character of $_{20}Ca_{25}$;

$5f^-+4d^+$ in $_{53}I_{78}$ should be odd from the first forbidden character of its decay;

$3p^++4d^-$ for particle numbers between 29 and 35 is odd from the allowed character of $_{30}Zn_{39}$. Strong support for this assignment is furnished by $_{20}Ca_{29}$ and $_{22}Ti_{29}$ whose decays are first forbidden with a γ-ray in series,[10] which indicates that the transition to the ground state of the final nucleus should be second forbidden.

It is now possible to make a prediction as to the last orbit for nuclei with N or Z equal to 43. A $3p^-$ orbit as in $_{47}Ag$ accounts for $_{32}Ge_{93}$ and $_{36}Kr_{43}$ (allowed) and for $_{42}Mo_{59}$ (first forbidden).

A reversal of the energetic order with a known isomeric state can be invoked in the cases of $_{42}Mo_{51}$, and $_{49}In_{68}$ (allowed) and in $_{40}Zr_{49}$ (first forbidden). $_{35}Br_{98}$ (allowed) goes into an isomeric state of $_{36}Kr_{47}$.

A similar explanation should hold for $_{41}Cb_{56}$, (allowed) which has to be assumed to have one of the regular shell IV orbits ($3p$ or $4d$) and not the $5g$ configuration of $_{41}Cb_{52}$.

The case of $_{56}Ba_{83}$ (allowed) is interesting. It has 83 neutrons and the assignment of a $6h^-$ orbit as in $_{83}Bi$ seems to be justified, in place of the $5d^-$ of $_{56}Ba_{81}$. Similarly, $_{38}Sr_{51}$ (highly forbidden) corresponds rather to the proton case with a $5g$ orbit for $Z=51$, in place of the $3s$ orbits found in shell V for neutrons.

The nuclei with N or Z equal to 27 show definitely an anomalous behavior, which we believe to be connected with the anomalous spin and moment of $_{27}Co_{32}^{59}$. The isotope $_{26}Fe_{33}^{59}$ goes over a second forbidden transition into $_{27}Co^{59}$, accompanied by a first forbidden one with a series γ-ray. This behavior is in order, if it is assumed that the $5g^-$ configurations of Co^{59} has odd parity. This assumption can explain the allowed character of the decay of $_{23}V_{26}$. It is, however, necessary to assume that $_{24}Cr_{27}$ and $_{27}Co_{30}$ have different orbits, corresponding to the 25 and 29 configurations, in order to be in agreement with the allowed character of the decays of $_{25}Mn_{26}$ and $_{28}Ni_{29}$.

It is necessary to suppose in several cases that the decay goes into an excited state of the product nucleus with a subsequent γ-emission. This applies to most of the allowed transitions with $N>50$ (that is, protons and neutrons ending in different shells). The existence of a series γ-ray is known[11] for $_{43}Tc_{58}$. It is also proven[10] for the cases in the first forbidden group, that is, $_{20}Ca_{29}$, $_{22}Ti_{29}$, and $_{26}Fe_{33}$. We are inclined to explain the large spin change of $_{48}Cd_{67}$ (first forbidden) by series γ-rays, in place of ascribing it to the isomeric state, which would lead to an allowed transition.

The assignments for some heavy nuclei with odd N ($_{66}Dy_{99}$, $_{79}W_{111}$, and $_{74}W_{113}$) are not uniquely determined, owing to lack of information. The entries in the table are compatible with the β-decay properties. It has also to be admitted that $_{28}Ni_{37}$ and $_{32}Ge_{39}$ would be classified as allowed in place of the empirical assignment of first forbidden.

The material presented in Table VIII, after incorporation of the above considerations, looks, however, very encouraging. It seems that much useful information can be obtained by the comparison of β-decay data and orbital state assignment based on observed spins and moments. Further work on these lines is in progress.

V. CONCLUDING REMARKS

The principal aim of this investigation has been to correlate the information on nuclear states from spins and moments with other nuclear properties. There can be little doubt that such a correlation exists and that the magic numbers 20, 50, and 82 have real significance. This result is strengthened further by the discovery of interesting regularities in the distribution of quadrupole moments by W. Gordy and of neutron cross sections by H. Newson, which will be published separately.

It should be emphasized that all data used here have been taken from existing compilations, without further scrutiny. It is thus to be expected that some of the assignments will prove to be in error. One may hope, however, that corrections necessitated by new and better data, will tend more to clarify than to confuse the situation.

Most of the evidence collected here does not depend on the interpretation of shell numbers in terms of definite combinations of single particle states. The proposed level scheme is more or less a by-product and may have to be revised later. There is, for instance, the possibility that a far reaching rearrangement of levels occurs in the building up of a larger and larger nuclei, so that the sequence of states in heavy nuclei may be quite different from that in light nuclei. However, such an assumption does not seem to be necessary at the present time, since the proposed level scheme appears to be natural and reasonable.

The author wishes to thank W. Gordy, E. Greuling, H. Newson, and K. Way for stimulating discussions, and W. Goad and M. Meeks for technical help.

[10] Walke, Thompson, and Holt, Phys. Rev. **57**, 177 (1940); Walke, Williams, and Evans, Proc. Roy. Soc. **A171**, 360 (1939).
[11] W. Maurer and F. W. Ramm, Zeits. f. Physik **119**, 334 (1942).

PHYSICAL REVIEW VOLUME 75, NUMBER 12 JUNE 15, 1949

Inelastic Scattering of Low Speed Electrons from a Copper Single Crystal

PAUL P. REICHERTZ*,** AND H. E. FARNSWORTH
Brown University, Providence, Rhode Island
(Received December 13, 1948)

The energy distribution of inelastically scattered electrons from a (100) face of a copper single crystal has been investigated by the electrostatic deflection method. Using normal incidence of the primary electrons, observations were made in the neighborhood of two strong diffraction peaks in the (100) azimuth, one at 59.5-ev primary energy and colatitude angle 60°, and one at 114.5 ev and 40.5°. Discrete loss peaks were observed at about 3.0-, 6.0-, 12.3-, and 20.0-ev energy loss with the intensities depending on both primary energy and colatitude angle. An excess of inelastic scattering occurs near the elastically scattered diffraction beams so that maxima are observed in the curves giving the intensity of inelastic scattering as a function of primary energy for constant values of energy loss. Near the 59.5-ev diffraction beam the maxima of the curves for different values of energy loss occur at a constant value of primary energy. This suggests that the inelastic scattering takes place after diffraction, but the fact that the maxima occur at 56 ev instead of 59.5 ev is not understood. For inelastic scattering near the 114.5-ev diffraction beam the results are complex but are approximately explained by assuming (1) inelastic background scattering followed by diffraction, for energy losses below 10 ev, (2) the same as (1) plus diffraction followed by inelastic background scattering, for energy losses above 10 ev. Possible reasons are given for the fact that the maxima for the latter process occur 3.5 ev above the energy for the diffraction maximum.

INTRODUCTION

PREVIOUS investigations on inelastic scattering of low speed electrons from outgassed metal surfaces may be divided into two groups: (1) those using polycrystalline metals, and (2) those using metal single crystals. Results in the first group[1] indicate that there are certain discrete energy loss peaks, corresponding to more probable values of energy loss, superposed on a general background of inelastic scattering. The positions of the discrete loss peaks are a function of the metal although both the positions and intensities are observed to be independent of angle of incidence and energy of the primary electrons. These observations for copper have been accounted for by Rudberg and Slater[2] by deriving an expression for the probability of excitation by electron bombardment as a function of the two electronic levels involved in the transition. Results in the second group obtained with a silver crystal by Turnbull and Farnsworth[3] show that the intensities of both the discrete loss peaks and of the background scattering are a function of primary energy and angle of incidence when the measurements are made in the vicinity of the critical values of angle and voltage for a diffraction beam of elastically scattered electrons. The results also show that the excess background scattering which accompanies the elastic scattering of the diffraction beams, for a given solid angle, increases as the energy-loss is decreased. Further, when inelastic scattering for a constant energy loss is plotted against secondary energy rather than primary energy, the maxima in the curves for different values of energy loss occur at the same values of secondary energy. This result is to be expected if the primary electrons are first inelastically scattered without appreciable change in their direction of motion and are then diffracted by the crystal lattice. However, the discrete loss peaks appear to attain their maximum values in the neighborhood of the primary voltages required for the diffraction of electrons which would indicate that the energy loss in this case occurs after diffraction rather than before. Thus the order of the two processes, diffraction and energy loss, does not appear to be the same for the background and discrete-loss inelastic scattering. Because these observations were confined to the region of only two diffraction beams more observations are required before general conclusions can be drawn.

The purpose of the present investigation is to extend the above observations to other diffraction

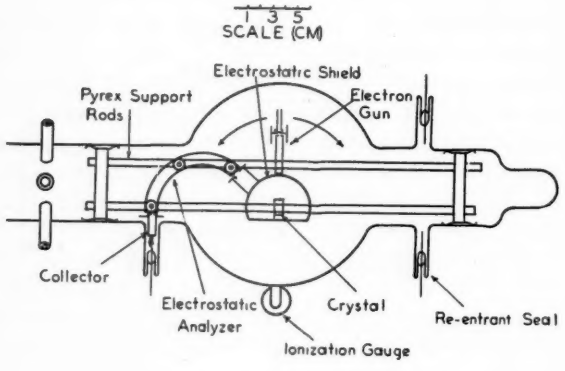

a

* Part of a dissertation presented for the degree of Doctor of Philosophy in Brown University.

** Now with the Magnolia Petroleum Company, Dallas, Texas.

[1] E. Rudberg, Phys. Rev. **50**, 138 (1936); **45**, 764 (1934); Proc. Roy. Soc. **A127**, 111 (1930); K. Svenska Vet. Akad. Handl. **7**, (1929); L. J. Haworth, Phys. Rev. **48**, 88 (1935); **42**, 906 (1932).

[2] E. Rudberg and J. C. Slater, Phys. Rev. **50**, 150 (1936).

[3] J. C. Turnbull and H. E. Farnsworth, Phys. Rev. **54**, 509 (1938).

beams and also to another crystal. The previous work was done by magnetic analysis in which the angle between the incident and reflected beam is necessarily restricted to 90 degrees and hence to angles of incidence other than normal. In the present work an electrostatic analyzer is used with which it is possible to extend the observations to diffraction beams for the case of normal incidence.

APPARATUS AND PROCEDURE

The apparatus consists of two essential units. The first is the electron gun and the crystal in its housing with provision for varying the colatitude angle of the observed scattered electrons. The second is the electrostatic analyzer and Faraday collector, which determines the energy distribution of the scattered electrons.

Figure 1a shows a diagrammatic sketch of the apparatus. The electron gun is mounted so that the primary electrons are incident normally on the crystal face, and the electron gun and crystal can be rotated as a unit by means of the magnetic control, thus changing the colatitude angle. The analyzer is placed so that scattered electrons enter it normal to the entrance slit. The whole apparatus is assembled so that the plane of rotation of the gun and crystal coincide with the plane of the analyzer. Thus the electrons travel in a plane as they move from the gun filament to the collector. The colatitude angle is measured by a scale and pointer within the tube, which permit estimates of position to 0.2°. The whole structure is assembled as a unit on a rigid frame of Pyrex rods with sheet molybdenum supports. The bulb in which the electron gun and crystal move is 16 cm in diameter and has a semi transparent film of gold evaporated onto its inner surface for purposes of electrostatic shielding. The electrical leads to the gun are connected to re-entrant seals in a small tube at the top of the main bulb which is located directly above the axis of rotation of the gun and crystal. The leads to the gun filament consist of three braided strands of No. 29 copper wire, while the leads to the accelerating chambers of the gun are one strand of the same wire. Because these leads exert an appreciable torque opposing the motion of gun and crystal, a friction arrangement is attached to the magnetic control as a means of maintaining any desired angle. Most of the metallic parts are made of molybdenum, although small amounts of nickel are used at welded joints. The apparatus was assembled with clean tools, after all parts had been cleaned chemically.

The copper crystal is one previously used by Farnsworth.[4] The front face is parallel to the (100) set of crystal planes and observations are taken in

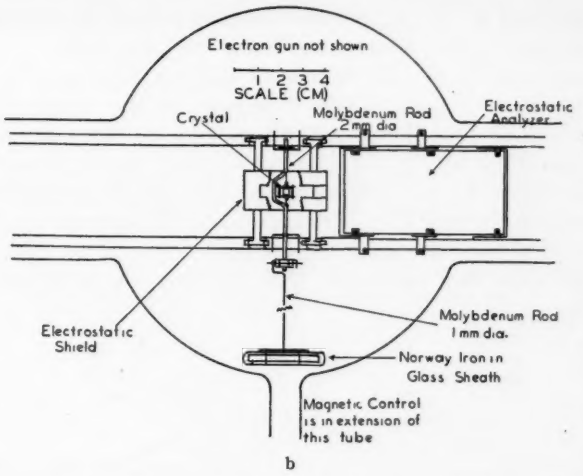

FIG. 1 (a). Schematic diagram of apparatus showing relative positions of electron gun, crystal, and electrostatic analyzer. (b). Diagram of crystal mounting and magnetic control.

the (100) azimuth. The crystal and its mounting are shown in Fig. 1b. A molybdenum plate is attached to the crystal mount so that it makes good thermal contact with the side of the crystal. The plate extends beyond the back face of the crystal and is heated by electron bombardment to outgas the crystal. The crystal can be rotated so that the separation of the plate and a fixed tungsten filament is of the order of two mm. This method of heating decreases the probability of recrystallization of the target during the bombarding process.

The electron gun is similar to that used by Farnsworth.[5] It consists of a platinum ribbon filament coated with oxides of barium, strontium, and calcium, an accelerating electrode, and a barrel containing diaphragms with rectangular openings to define the beam. The filament is shaped in the

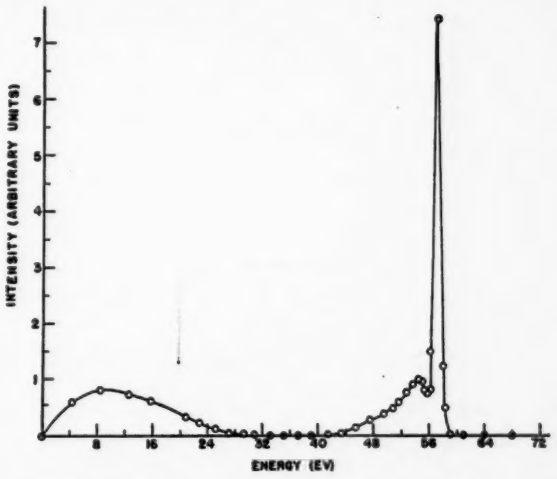

FIG. 2. Complete energy distribution curve at colatitude angle of 56° for primary energy of 57 ev.

[4] H. E. Farnsworth, Phys. Rev. **40**, 684 (1932).

[5] H. E. Farnsworth, Phys. Rev. **34**, 679 (1927).

form of a "T" to reduce the magnetic field. Three evenly spaced small tungsten wires placed over the opening in the diaphragm of the accelerating electrode decrease the field distortion in the neighborhood of the filament. The output of the gun, as measured by the total current to the crystal, is held constant for a set of readings. The defining cylinder of the electron gun, the target, and the entrance and exit slits of the analyzer are all at ground potential so that the electrons after leaving the gun and before entering the analyzer travel in a field-free space. This path is further protected by metallic shields. The distance between the exit slit of the gun and the crystal face is 40 mm.

The electrostatic analyzer is similar to that described by Hughes and McMillen[6] and has been treated theoretically by Rojansky.[7] The radii of the plates are 3.5 cm and 4.5 cm and the dimensions of the entrance and exit slits are 4×0.470 mm and 4×0.480 mm, respectively. This gives a theoretical

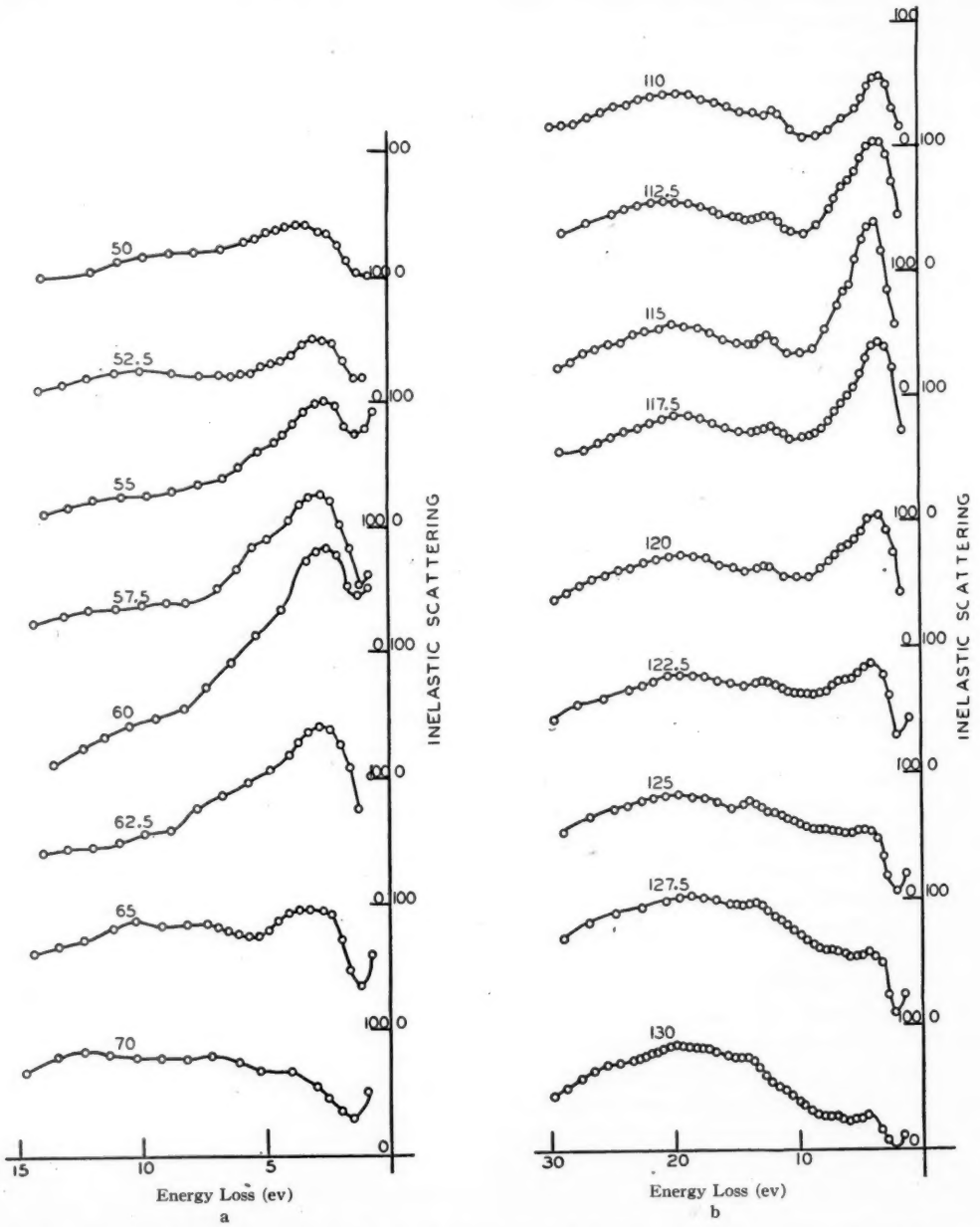

FIG. 3. Energy distribution curves of inelastically scattered electrons for the primary voltages given on the individual curves. The scattering or colatitude angle is 60° for all curves in Fig. 3a, and 40.5° for curves in Fig. 3b. The peaks for elastically scattered electrons at zero energy loss are not shown.

[6] A. L. Hughes and J. A. McMillen, Phys. Rev. **34**, 291 (1929).
[7] V. Rojansky, Phys. Rev. **34**, 284 (1929).

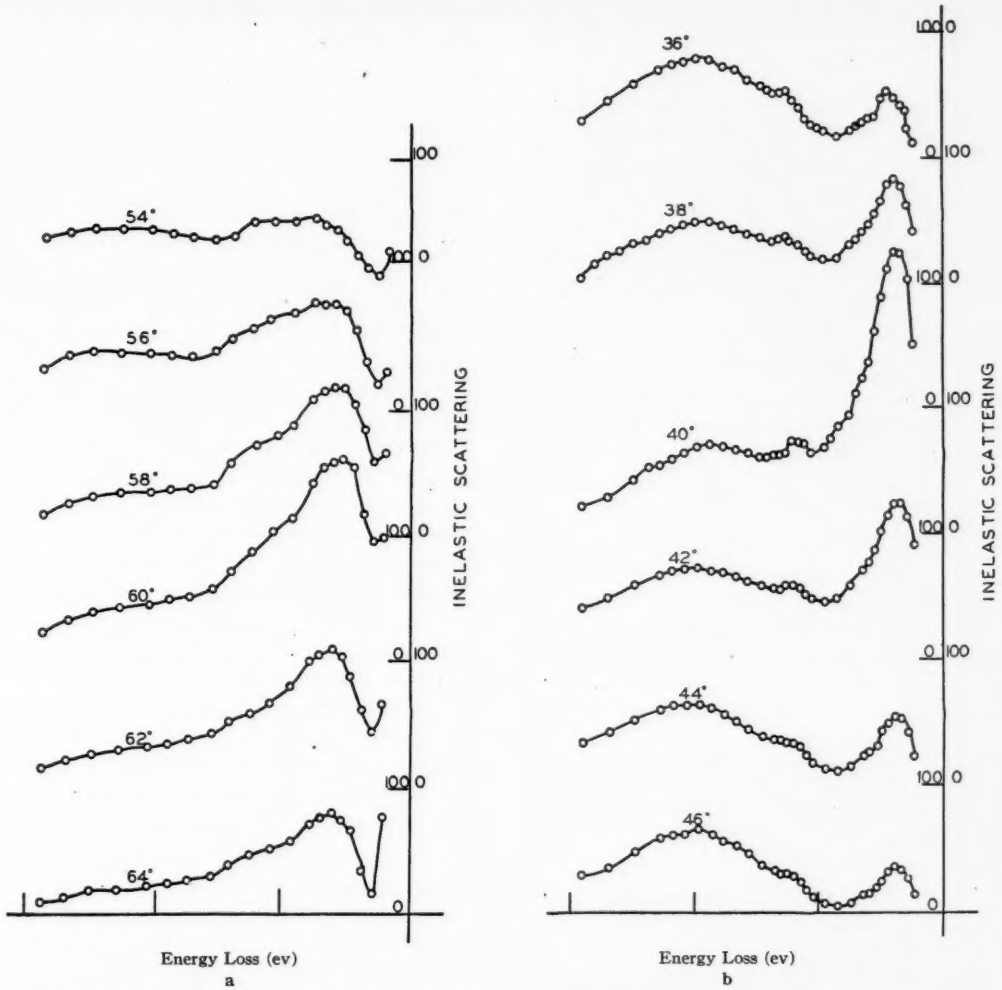

FIG. 4. Energy distribution curves of inelastically scattered electrons for the colatitude angles given on the individual curves. The primary voltage is 59.5 for all curves in Fig. 4a and 114.5 for curves in Fig. 4b.

resolving power of $\Delta V/V=0.0273$ as compared with 0.0265 for the magnetic analyzer used by Turnbull and Farnsworth and 0.009 for the electrostatic analyzer used by Rudberg. All parts of the analyzer are made of molybdenum, with the exception of platinum-iridium foil slits. The various components of the analyzer are insulated electrically from one another by thin strips of mica.

The collector is of the double wall type, with fused silica insulation between the walls. The current to the collector is measured by a balanced bridge direct current amplifier with a FP-54 tube. Used in conjunction with a galvanometer of sensitivity 10^{-10} ampere per millimeter, the amplifier has a maximum sensitivity of approximately 10^{-16} ampere per millimeter. This maximum sensitivity is required for most of the observations. The earth's magnetic field is compensated by Helmholtz coils of 1-meter diameter, and 0.5-meter separation.

During the initial period of alternate bombardment of the crystal and experimental observations on the elastic scattering, the experimental tube was pumped continuously. Pressures obtained at this point were of the order of 10^{-8} mm of mercury as measured by an ionization gauge. When the crystal had been outgassed sufficiently so that strong diffraction beams of elastically scattered electrons appeared, the tube was gettered, using RCA type Barium getters, and sealed off. Further outgassing of the crystal at dull red heat was continued at intervals during the period of making observations.

Figure 2 shows a typical energy distribution curve obtained at a colatitude angle of 56° for electrons having a primary energy of 57 ev. The elastically scattered electrons are represented by the sharp peak at the extreme right of the curve. The position of this peak serves to establish the zero on the energy loss scale for all subsequent figures. The intensity of the reflection peak is such that it cannot be plotted on the scales chosen for

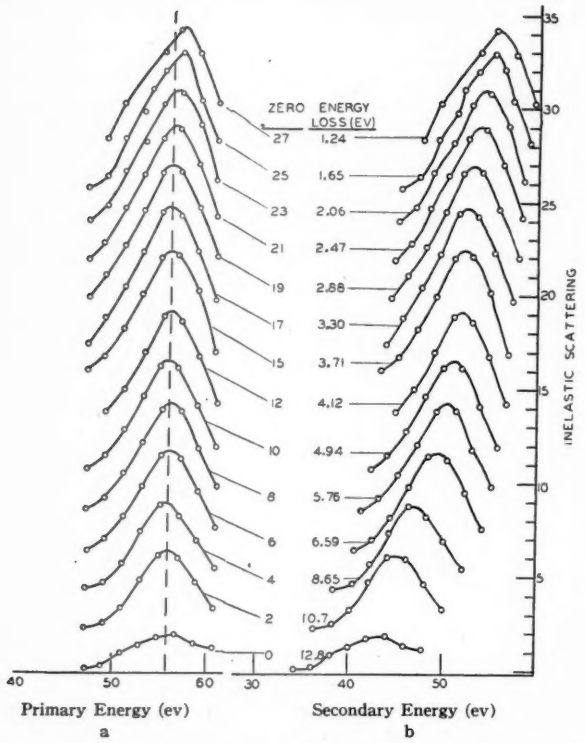

FIG. 5. Inelastic scattering for constant values of energy loss about the diffraction peak at 59.5 ev. Successive curves are shifted vertically; the zeros and energy losses are given in the figure. The same data are used for the two sets of curves but are plotted with different abscissas.

subsequent figures. However, its position was always measured in order to determine the zero on the energy loss scale.

Immediately to the left of the reflection peak is the portion of the distribution curve associated with inelastic collisions. This research is confined to a study of the character of the structure in this region of the distribution curve. The relatively broad maximum in the curve which appears at low energies is due to secondary emission. Some evidence of structure has also been found in this region for molybdenum by Haworth.[1]

The following evidence indicates that the measurements on inelastic scattering are not due to elastically scattered primaries which have reached the collector. The absence of any measurable current on the high energy side of the main reflection peak is an indication of the resolution of the analyzer. The positions of the energy loss peaks observed for the copper single crystal correspond reasonably well to similar peaks for polycrystalline copper observed by Rudberg[2] using magnetic rather than electrostatic analysis.

THE INELASTIC SCATTERING

A. The Discrete Loss Peaks

Observations were made in the neighborhood of the two diffraction peaks in the (100) azimuth which were observed to occur at 59.5-ev and 114.5-ev primary energies, with colatitude angles of 60° and 40.5°, respectively. The curves in Figs. 3a and 3b show the distribution of energy of the inelastically scattered electrons for various values of the primary voltage near two different diffraction peaks. Each curve represents the energy distribution of the secondary electrons which are inelastically reflected from the crystal, for a constant value of primary energy and of colatitude angle. A comparison of these curves for either peak shows the variation of results as the primary energy is changed from the critical value for the diffraction peak in question. The curves in the neighborhood of the peak at 59.5-ev primary energy, and shown in Fig. 3a, show clearly the presence of one discrete loss peak indicating a most probable energy loss of about 3 ev. The presence of two other discrete loss values at approximately 6 and 11 ev may also be detected, but these are not pronounced or sharp. The curves taken in the neighborhood of the second diffraction peak at 114.5-ev primary energy, Fig. 3b, show four discrete loss values at approximately 3.6, 6.0, 12.3, and 20 ev, respectively.

Both sets of curves indicate a decided dependence of intensity of the first discrete loss peak on the primary energy of the electrons. In each case this peak attains its maximum value at or near the primary voltage for the main diffraction peak. Because of the broadness, overlapping, and low intensities of the other discrete loss peaks occurring near the 59.5-ev diffraction beam, changes of their intensities with changes in primary energies are not pronounced. In the neighborhood of the other main diffraction peak at 114.5-ev primary energy the discrete loss peak at 20.0-ev energy loss attains a maximum value at two different primary energies; one at about 117.5 ev and the other at about 127.5 ev. The intensity variation of the peak at 12.3 ev is difficult to determine, but it appears that this peak also attains a maximum at two primary energies which are approximately the same as those for the 20-ev peak. These observations check with other results which are considered later.

The curves in Figs. 4a and 4b show the change in the distribution of energy of the inelastically scattered electrons as the colatitude angle is varied. Each of the curves shows the energy distribution in the inelastically scattered electrons for a constant value of primary energy and particular colatitude angle. A comparison of these curves in the vicinity of either diffraction peak shows that the first discrete loss peak is most pronounced at the colatitude angle for the diffraction peak in question.

The variations of the other weaker discrete loss peaks with colatitude angle are not well defined but appear in approximate agreement with that of the first discrete loss peak.

B. Total Scattering with Energy Loss

Examination of the curves of Figs. 3a and 3b and of Figs. 4a and 4b indicates that, disregarding the structure appearing in the curves, the background scattering is largest where the elastic scattering is largest. This is most pronounced for small values of energy loss, where the amount of extra background scattering increases with decreasing energy loss. For larger values of energy loss it is difficult to separate the background scattering from the discrete loss scattering. Accordingly, the following observations include both types of scattering.

Data were taken in the following manner to determine the dependence of the total inelastic scattering on the secondary energy of the electrons. The position of the crystal and electron gun with respect to the analyzer was set at the critical angle for the main diffraction peak. Then, starting with a primary energy below the critical value for the main peak, the potentials on the plates of the electrostatic analyzer were adjusted so that only electrons of some definite energy loss were measured. Then the primary energy was changed and the potentials on the plates of the analyzer were changed correspondingly so that again only electrons of the same energy loss were measured. In this manner points for one curve were obtained, and those for succeeding curves resulted by repeating this procedure for other values of energy loss. The experimental curves are shown in Figs. 5 and 6. Figures 5a and 5b contain curves of the total inelastic scattering plotted against both primary and secondary energy in the vicinity of the diffraction beam at 59.5 ev.

The curves in Fig. 5 show that the maxima in the neighborhood of the first diffraction peak are essentially constant in primary energy, except for several of the lower energy-loss curves, and occur at about 56 ev, instead of 59.5 ev, the value for the first diffraction peak. The fact that the maxima occur at a constant primary energy suggests that the primary electrons are diffracted before suffering energy losses of varying amounts corresponding to the background scattering. But if this were the complete explanation the maxima should occur at 59.5 ev instead of 56 ev. One possible interpretation of this discrepancy is that the effective inner potential of the crystal is greater for electrons which are first diffracted and then suffer inelastic collisions as they leave the crystal than it is for elastically diffracted electrons. There is ample evidence[8] that the effective inner potential is not constant,[9] at least in the range of primary energies below 150 ev. Also, as the energy loss becomes smaller, one would expect the process to approach that for elastically scattered electrons so that the maximum should shift toward 59.5 ev as the energy loss decreases. This shift is exhibited by the uppermost curves corresponding to energy losses less than about 2.5 ev, in Fig. 5a. However, if diffraction occurs before inelastic scattering it is difficult to understand why the diffracted electron, which later suffers an inelastic collision, should be subject to a higher value of inner potential.

Reference to the curves in Fig. 6 show that in the neighborhood of the 114.5-ev diffraction peak the results are more complicated than those just discussed. The following characteristics are to be noted. The maxima for different energy losses are not constant in either primary or secondary energy. For the larger energy-loss curves there are two maxima. For several of the curves in limited ranges of energy loss the maxima are constant in primary energy and a similar statement applies for secondary energy. For energy losses below about 10 ev, the maxima are essentially constant in secondary energy, suggesting inelastic background scattering followed by diffraction. Furthermore, the maxima occur at a secondary energy of about 114.5 ev, which is that of the second diffraction peak, as one expects for the above double process. Even in the two lowest curves, corresponding to larger energy losses, one notes maxima at approximately the above value of secondary energy. However, in the curves for energy losses greater than about 10 ev, there is a shift and then a splitting of the maxima as the energy loss increases. While one set of maxima is nearly constant in primary energy, the other set is nearly constant in secondary energy (with one exception in each case). That which is

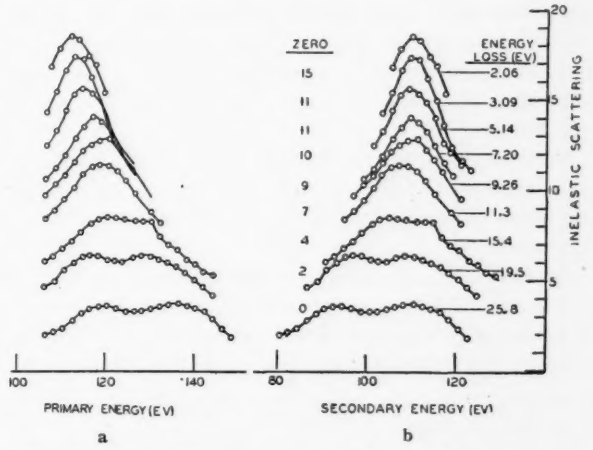

FIG. 6. Inelastic scattering for constant values of energy loss about the diffraction peak at 114.5 ev. Successive curves are shifted vertically; the zeros and energy losses are given in the figure.

[8] H. E. Farnsworth, Phys. Rev. **34**, 690 (1929).

[9] L. Sturkey (Phys. Rev. **73**, 183 (1948)) has shown that there are double values of the effective inner potential when primary electrons are incident on a set of crystal planes at the Bragg angle.

constant in primary energy suggests diffraction followed by inelastic background scattering as in the first case considered. However, in the present case the maxima occur at about 118 ev which is 3.5 ev greater than the 114.5 ev for the diffraction peak. As in the first case we may associate this difference with a variation in the effective value of inner potential. It may also be attributed to a discrete energy loss of 3.5 ev (which agrees approximately with the value for the first discrete loss peak) which precedes the diffraction. The experimental evidence is not sufficient to justify a definite conclusion. The number of observations was limited by a failure in the experimental tube.

SUMMARY

The following processes have been postulated to interpret the results:

(1) For the results in the vicinity of the 59.5-ev diffraction beam.—Diffraction followed by inelastic background scattering. However, the maxima occur at 3.5 ev below the 59.5 ev of the diffraction beam.

(2) For the results in the vicinity of the 114.5-ev diffraction beam.—(a) Inelastic background scattering followed by diffraction, for energy losses below 10 ev. The maxima occur at the secondary energy of 114.5 ev which checks with the 114.5-ev diffraction peak. (b) The same as (a) plus diffraction followed by inelastic background scattering, for energy losses above 10 ev. The maxima for the latter process occur at 118 ev instead of at 114.5 ev which corresponds to the diffraction maximum.

PHYSICAL REVIEW VOLUME 75, NUMBER 12 JUNE 15, 1949

The Surface Photoelectric Effect

R. E. B. MAKINSON
School of Physics, University of Sydney, Australia
(Received December 20, 1948)

An expression is derived for the photoelectric current produced at the surface of a metal, the conduction electrons being supposed free and the potential barrier of arbitrary shape. The validity of the common assumption that the current arising from conduction electrons of a particular momentum can be expressed as the product of an excitation function and a transmission coefficient is examined. It is concluded that the assumption is in general valid. The production in the photoelectric current of beat frequencies between spectral lines is also briefly discussed.

I. INTRODUCTION

IN discussions of the surface photoelectric effect in metals, particularly in deriving an expression for the threshold frequency at 0°K from data obtained at higher temperatures, it has frequently been assumed that the photoelectric current arising from conduction electrons of given momentum in the metal may be expressed as a product of an excitation function and the transmission coefficient of the surface barrier for the excited electrons. The excitation function is then assumed not to vary rapidly near the threshold frequency.

No general proof of the validity of this factorization appears to have been given in accessible literature, but doubts as to its validity have been expressed.[1,2]

An extension of earlier work[3] is given below in which a formal expression of great generality for the photoelectric current is derived. From this it appears that the factorization mentioned and the smooth variation of the excitation function near the threshold are in general justified. The theory is easily extended to enable discussion of the possible production of beats between spectral lines.

II. ASSUMPTIONS

If we suppose that the conduction electrons are free in the interior of the metal and neglect their interaction, the potential energy of each may be represented near the surface by a potential $V(x)$ which has some such form as shown in Fig. 1(a).

The wave function u for an electron unperturbed by incident light satisfies

$$(\hbar^2/2m)\nabla^2 u+i\hbar\partial u/\partial t-Vu=0. \quad (1)$$

Putting

$$u=u_k=\psi_k \exp(-iE_k t/\hbar), \quad (2)$$

let

$$\psi_k=\alpha_k\phi_k(x) \exp(ik_2 y+ik_3 z);$$

then

$$\phi_k''-\{p^2+(\mu/h)V(x)\}\phi_k=0,$$

where

$$p=(\mu\nu_a-k_1^2)^{\frac{1}{2}}>0, \quad \mu=8\pi^2 m/h,$$

$$k^2=k_1^2+k_2^2+k_3^2=(8\pi^2 m/h^2)(E_k+h\nu_a).$$

[1] R. H. Fowler, *Statistical Mechanics* (Cambridge University Press, London, 1936), p. 358.
[2] E. Guth and C. J. Mullin, Phys. Rev. **59**, 868 (1941).
[3] R. E. B. Makinson, Proc. Roy. Soc. **A910**, 367 (1937). The same notation is used here. Essentially the present discussion was given in a Dissertation by the author, University of Cambridge, England, 1938.

In the interior of the metal

$$\phi_k = \exp(ik_1x) + a_k \exp(-ik_1x)$$

with $|a_k| = 1$. We restrict k_1 to positive values.

At temperature $T = 0°\text{K}$, $k \leqslant k_0$ where k_0 gives the electron wave number at the top of the Fermi distribution, so that $k_0^3/3\pi^2 = n_0$, the number of conduction electrons per cm³. The normalizing factor α_k is supposed chosen so in the interior of the metal

$$2\sum_k |\psi_k|^2 = n_0,$$

i.e.,

$$\alpha_k^2 = (1/8\pi^3)dk_1dk_2dk_3 \text{ at } T = 0°\text{K}.$$

For generality in the following discussion we note that Bardeen[4] has shown that a more accurate description of the electron gas than is given above may be obtained by replacing the potential $V(x)$ in (1) by the effective potential

$$U_k(x) = V(x) - B_k(x),$$

in which

$$B_k(x) = (1+c)A_k(x),$$

the function $A_k(x)$ representing an exchange energy and $cA_k(x)$ a "correlation energy," both being dependent on k. "Each electron has, so to speak, to have its own barrier." The constant c was assigned the value 0.24 by Bardeen and calculations of $B_k(x)$ were given for sodium. We suppose therefore in the following that u satisfies the unperturbed wave equation,

$$(h^2/8\pi^2m)\nabla^2u - (h/2\pi i)\partial u/\partial t - U_k(x)u = 0, \quad (1a)$$

where the functions $U_k(x)$ are of the general form* sketched in Fig. 1(b).

We will further assume that all the barriers tend towards the form of an image-field barrier[5] of shape $-e^2/4x$ as $x \to \infty$, $B_k(x)$ vanishing faster than the latter function.

III. THE PHOTOELECTRIC CURRENT

In the presence of incident plane waves of light of frequency ν, which we may describe classically by a vector potential $\boldsymbol{A}$ and scalar potential Φ, a perturbation is introduced into (1a); thus, neglecting a term in A^2,

$$(h^2/8\pi^2m)\nabla^2u - (h/2\pi i)\partial u/\partial t - U_k(x)u = -(ihe/2\pi mc)(\boldsymbol{A}\cdot\nabla u + \tfrac{1}{2}u\nabla\cdot\boldsymbol{A}) - e\Phi u. \quad (3)$$

We may put $\Phi = 0$ and

$$A(x, y, t) = a(x) \exp\{-2\pi i\nu(y \sin\theta/c + t)\} + \text{conjugate},$$

where θ is the angle of incidence of the light and y a cartesian coordinate in the plane of the surface and the plane of incidence.

Let $u = u_k + v_k$ where u_k is the solution corresponding to (2) of the unperturbed Eq. (1a). Then to the first order

$$(h^2/8\pi^2m)\nabla^2v_k - (h/2\pi i)\partial v_k/\partial t - U_k(x)v_k = -(ihe/2\pi mc)(\boldsymbol{A}\cdot\nabla u_k + \tfrac{1}{2}u_k\nabla\cdot\boldsymbol{A}).$$

Neglecting the terms in $\exp\{-2\pi i(E_k - h\nu)t/h\}$, which correspond to stimulated emission, and putting

$$v_k = \alpha_k\vartheta_k(x) \exp\{ik_2y + ik_3z - 2\pi i(E_k + h\nu)t/h - 2\pi i\nu y \sin\theta/c\},$$

we find that ϑ_k must satisfy

$$\vartheta_k'' + \{r^2 - (\mu/h)U_k(x)\}\vartheta_k = -(4\pi ie/ch) \times \{a_x\phi_k' + i\phi_k(a_yk_2 + a_zk_3) + \tfrac{1}{2}\phi_k k a_x'\}, \quad (4)$$

on neglecting two small terms involving ν/c, where

$$r = \{k_1^2 + \mu(\nu - \nu_a)\}^{\frac{1}{2}} > 0,$$

and ν_a is now the function of k given by

$$h\nu_a = -U_k(-\infty).$$

We have to find the solution of (4) which for large positive x represents an outward stream of photoelectrons:

$$\vartheta_k = B_re^{irx}, \quad x \gg 0,$$
$$= C_re^{-iqx}, \quad x \ll 0,$$

where

$$q = (k_1^2 + \mu\nu)^{\frac{1}{2}}.$$

Let $\chi_r(x)$ be the solution of

$$\chi_r'' + \{r^2 - (\mu/h)U_k(x)\}\chi_r = 0, \quad (5)$$

which satisfies the boundary conditions

$$\chi_r = e^{-iqx}, \quad x \ll 0$$
$$= G_re^{irx} + H_re^{-irx}, \quad x \gg 0. \quad (5a)$$

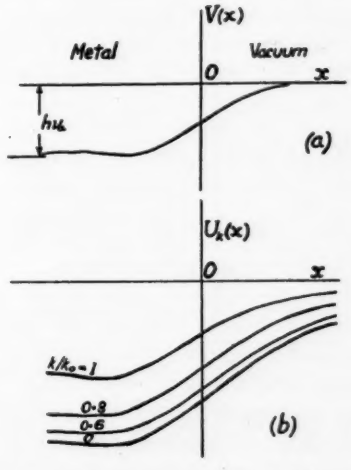

FIG. 1. (a) General shape of potential barrier at metal surface, supposed independent of electron momentum $k\hbar$. (b) Barrier dependent on k (see reference 4).

[4] J. Bardeen, Phys. Rev. **49**, 653 (1936).
* See reference 4, p. 661.
[5] J. Bardeen, Phys. Rev. **49**, 640A (1936); **58**, 727 (1940).

Multiplying both sides of (4) by χ_r, integrating from $-\infty$ to $+\infty$ with an extinction factor $e^{\Delta x}$ (Δ small), using (5) and integrating by parts, we find

$$B_r=(2\pi e/hc)M(\boldsymbol{k},\nu)/(H_r r),$$

where

$$M(\boldsymbol{k},\nu)=\int_{-\infty}^{\infty}\{a_x\chi_r\phi_k'+\tfrac{1}{2}\phi_k\chi_r a_x' +i\chi_r\phi_k(k_2a_y+k_3a_z)\}dx. \quad (6)$$

Now the photoelectric current density in $x\gg 0$ corresponding to ϑ_k is

$$dJ_x=(2eh/4\pi mi)(v_k\partial v_k^*/\partial x-v_k^*\partial v_k/\partial x) =-(eh/\pi m)|\alpha_k|^2 r|B_r|^2. \quad (7)$$

The transmission coefficient of the barrier $U_k(x)$ to the wave e^{-irx} incident from the outside (or e^{iqx} incident from inside) is

$$D(r)=q/(r|H_r|^2),$$

hence

$$dJ_x=-|\alpha_k|^2 e\cdot D(r)\cdot(4\pi e^2/hmc^2q)|M(\boldsymbol{k},\nu)|^2. \quad (7a)$$

It is to be noted that this contribution to the photoelectric current, arising from the electrons with momentum $\boldsymbol{k}\hbar$, is in the form of the product of the electronic charge, the normalizing factor $|\alpha_k|^2$, $D(r)$ the transmission coefficient of the barrier for the excited electrons, and the function $4E(\boldsymbol{k},\nu)$ where

$$E(\boldsymbol{k},\nu)=(\pi e^2/hmc^2q)|M(\boldsymbol{k},\nu)|^2. \quad (8)$$

We may describe $E(\boldsymbol{k},\nu)$ as the probability per unit time of the excitation of one electron per cm^2 of surface from an unperturbed state $\boldsymbol{k}$ to that of an outgoing photoelectron. (There are four electrons in the state $\boldsymbol{k}$ with the normalization used here.)

Integrating over all values of $\boldsymbol{k}$, we have for the photoelectric current density in e.s.u. per cm^2 at 0°K:

$$J_x=(-e/2\pi^3)\int\int\int E(\boldsymbol{k},\nu)D(r)dk_1dk_2dk_3, \quad (9)$$

the integration being taken over the hemisphere in $\boldsymbol{k}$ space: $k_1^2+k_2^2+k_3^2\leqslant k_0^2$, $k_1>0$.

In principle, the value of the vector potential $\boldsymbol{A}$ near the surface may be calculated[3] from classical wave theory and a knowledge of the electron density variation near the surface, the latter being calculable from the unperturbed wave functions u_k.

If the surface is "perfectly plane" (i.e., with irregularities small not merely in comparison with a light wave-length but with the electron wave-lengths as at a face of a perfect crystal) it may be shown[3] that a_y and a_z are nearly constant through the region in which $U_k(x)$ varies appreciably, which is much less than a light wave-length. The component a_x, on the other hand, varies rapidly in this region, inversely as the dielectric constant $\epsilon_1(x)+i\epsilon_2$ where $\epsilon_1(x)=1-ne^2/(\pi m\nu^2)$ and ϵ_2 has a small value representing damping. In this case the photoelectric current arises only from the component of the incident light polarized in the plane of incidence and vanishes for normal incidence. If, now, following Bardeen,[4] the function $U_k(x)$ is supposed to depend only on the magnitude of k and not upon its direction, the excitation function $E(k,\nu)$ simplifies to the form

$$E(k,k_1,\nu)=(e^2/64\pi hm)H_z(0)^2\times\sin^2\theta|N(k,k_1,\nu)|^2/(\nu^2 q), \quad (10)$$

where $H_z(0)$ is the amplitude of the z-component of the magnetic field at the surface and

$$N(k,k_1,\nu)=\int_{-\infty}^{\infty}(\chi_r\phi_k'-\phi_k\chi_r')/\{\epsilon_1(x)+i\epsilon_2\}dx.$$

The results obtained previously[3] for a square barrier, representing potassium, are easily seen to follow from the foregoing as a special case.

The effect of optical roughness of the surface, the scale of irregularities being greater than a light wave-length, results in emission for any polarization or angle of incidence,[6] but for monochromatic light one can show that it remains of the form

$$J=\text{const.}G(\nu)\cdot R$$

where

$$G(\nu)=(1/\nu^2)\int\int\int[D(r)/q]\times|N(k,k_1,\nu)|^2dk_1dk_2dk_3 \quad (11)$$

and R is a purely geometrical factor describing the roughness of the surface, involving also the angle of incidence and plane of polarization.

The same conclusion holds** when there exists roughness on a scale small compared with a light wave-length but large when compared with the barrier width or when both types of roughness are present together.

IV. THE EXCITATION FUNCTION

We conclude that it is legitimate in all cases to regard the photoelectric current, arising as a surface effect from electrons of a given momentum

[6] K. Mitchell, Proc. Roy. Soc. **A153**, 513 (1936).

** See reference 3. The more general barrier here considered does not affect the essentials of the discussion.

kh within the metal, as the product of an excitation function and a barrier transmission coefficient.

This formal separation is of course of little value unless the excitation function $E(\boldsymbol{k}, \nu)$ given by (8) does not in fact vary sharply with frequency in the neighborhood of the threshold frequency ν_0. We need therefore to show that the function $M(\boldsymbol{k}, \nu)$ given by (6) cannot vary sharply near ν_0.

In the integrand of (6) we see from (5a) that $\chi_r(x)$ is not critically dependent on ν near ν_0 (i.e., as $r\to 0$) except for values of x near the top of the surface barrier, but in that region the factor $\phi_k(x)$ is falling off exponentially and has become small; we are also well away from the maximum of a_x. Further, if the barrier is always of the image type for large x, as appears to be the case, the transmission coefficient $D(r)$ for the wave χ_r (an incoming wave with the transmitted portion always of unit amplitude) approaches a limit[7] only a little less than 1 as $r\to 0$. Thus G_r and H_r increase no faster than r^{-1} as $r\to 0$.

It seems clear then, that in general, the major contribution to the integral (6) arises from vaues of x where the integrand does not vary sharply with ν near ν_0 although lengthy numerical calculations would be necessary to make a quantitative statement in a particular case. We therefore expect the integral (6) and hence the excitation function to vary smoothly with frequency near the threshold.

It has sometimes been assumed[8, 9] that the excitation function is proportional to the component of electron momentum normal to the surface. Equations (8) and (10) give no support to this assumption.

It may be added that the theory of the temperature-dependence of the photoelectric current near the threshold is complicated in a different manner by the dependence, referred to above, of the effective surface barrier on the momentum of the conduction electron excited. This invalidates the expressions given by Fowler[1] and by Du Bridge, to an extent uncertain in the absence of numerical computation for particular cases. Conclusions based on discrepancies found experimentally,[10–12] for which other reasons have been advanced[13] are therefore in some doubt. Similar remarks apply to expressions which have been derived for the total energy distribution of photoelectrons.[6, 8]

[7] L. W. Nordheim, Proc. Roy. Soc. **A121**, 626 (1928).
[8] A. G. Hill, Phys. Rev. **53**, 184 (1938).
[9] H. Bradner, Phys. Rev. **71**, 269 (1947).
[10] M. M. Mann and L. A. Du Bridge, Phys. Rev. **51**, 120 (1937).
[11] R. J. Cashman, Phys. Rev. **52**, 512 (1937).
[12] C. F. J. Overhage, Phys. Rev. **52**, 1039 (1937).
[13] W. V. Houston, Phys. Rev. **52**, 1047 (1937).

V. BEATS BETWEEN SPECTRAL LINES

It has been proposed[14] to excite a resonant cavity at microwave frequencies by means of "beats" in the photoelectric current produced by two sharp adjacent spectral lines. The general expressions given above enable the possibility of this to be examined from another angle.

If we assume for simplicity that both spectral lines are perfectly sharp, with frequencies ν_1 and ν_2 we start as before from (3), putting $\Phi=0$, and

$$\boldsymbol{A}(x, y, z, t)=\boldsymbol{a}_1(x)\exp\{-2\pi i\nu_1(y\sin\theta_1/c+t)\}+\boldsymbol{a}_2(x)\exp\{-2\pi i\nu_2(y\sin\theta_2/c+t)\}+\text{conjugates.}$$

We now put

$$v_k=\alpha_k\vartheta_k^{(1)}(x)\exp\{ik_2y+ik_3z-2\pi i(E_k+h\nu_1)t/h-2\pi i\nu_1 y\sin\theta_1/c\}+\alpha_k\vartheta_k^{(2)}(x)\times\exp\{ik_2y+ik_3z-2\pi i(E_k+h\nu_2)t/h-2\pi i\nu_2 y\sin\theta_2/c\}$$

and find that $\vartheta_k^{(1)}$ and $\vartheta_k^{(2)}$ both satisfy equations of the form (4) with ν_1, ν_2 written respectively for ν. We write r_1, r_2 for r and $B_r^{(1)}$, $B_r^{(2)}$ for B_r when $\nu=\nu_1$, ν_2. Let $B_r^{(1)}=|B_r^{(1)}|\exp(i\delta_1)$, $B_r^{(2)}=|B_r^{(2)}|\times\exp(i\delta_2)$. Equation (7) for the photoelectric current arising from electrons with a particular value of $\boldsymbol{k}$ now becomes

$$dJ_x=-(eh/\pi m)|\alpha_k|^2\{r_1|B_r^{(1)}|^2+r_2|B_r^{(2)}|^2+(r_1+r_2)|B_r^{(1)}B_r^{(2)}|\cos[(r_1-r_2)x-2\pi(\nu_1-\nu_2)t+(\delta_1-\delta_2)]\}. \quad (12)$$

It is clear from (12) that, at fixed x, the current varies at the "beat" frequency. If $\nu_1-\nu_2$ is very small, so that $\nu_1\sim\nu_2\sim\nu$ say and $B_r^{(1)}\sim B_r^{(2)}$, the current oscillates sinusoidally between zero and twice its mean value, i.e., with 100 percent modulation.

However, the expression (12) has to be integrated over all values of $\boldsymbol{k}$ for which $r_{1,2}>0$. The total electron stream thus contains components with a continuous range of velocities from zero up to that of the most energetic photo-electrons ejected at frequency ν; each component is intensity-modulated, the phase $(\delta_1-\delta_2)$ of the modulation at $x=0$ varying with velocity. The percentage modulation of the total photoelectric current at the beat frequency is therefore certainly very small.

ACKNOWLEDGMENT

The writer is greatly indebted to Mr. A. H. Wilson for helpful discussions during the period when much of the above work was done.

[14] A. T. Forrester, W. E. Parkins, and E. Gerjuoy, Phys. Rev. **72**, 728 (1947); also **73**, 922 (1948).

PHYSICAL REVIEW VOLUME 75, NUMBER 12 JUNE 15, 1949

On the Classical Radiation of Accelerated Electrons

JULIAN SCHWINGER
Harvard University, Cambridge, Massachusetts
(Received March 8, 1949)

This paper is concerned with the properties of the radiation from a high energy accelerated electron, as recently observed in the General Electric synchrotron. An elementary derivation of the total rate of radiation is first presented, based on Larmor's formula for a slowly moving electron, and arguments of relativistic invariance. We then construct an expression for the instantaneous power radiated by an electron moving along an arbitrary, prescribed path. By casting this result into various forms, one obtains the angular distribution, the spectral distribution, or the combined angular and spectral distributions of the radiation. The method is based on an examination of the rate at which the electron irreversibly transfers energy to the electromagnetic field, as determined by half the difference of retarded and advanced electric field intensities. Formulas are obtained for an arbitrary charge-current distribution and then specialized to a point charge. The total radiated power and its angular distribution are obtained for an arbitrary trajectory. It is found that the direction of motion is a strongly preferred direction of emission at high energies. The spectral distribution of the radiation depends upon the detailed motion over a time interval large compared to the period of the radiation. However, the narrow cone of radiation generated by an energetic electron indicates that only a small part of the trajectory is effective in producing radiation observed in a given direction, which also implies that very high frequencies are emitted. Accordingly, we evaluate the spectral and angular distributions of the high frequency radiation by an energetic electron, in their dependence upon the parameters characterizing the instantaneous orbit. The average spectral distribution, as observed in the synchrotron measurements, is obtained by averaging the electron energy over an acceleration cycle. The entire spectrum emitted by an electron moving with constant speed in a circular path is also discussed. Finally, it is observed that quantum effects will modify the classical results here obtained only at extraordinarily large energies.

EARLY in 1945, much attention was focused on the design of accelerators for the production of very high energy electrons and other charged particles.[1] In connection with this activity, the author investigated in some detail the limitations to the attainment of high energy electrons imposed by the radiative energy loss[2] of the accelerated electrons. Although the results of this work were communicated to various interested persons,[1,3,4] no serious attempt at publication[5] was made. However, recent experiments on the radiation from the General Electric synchrotron[6] have made it desirable to publish the portion of the investigation that is concerned with the properties of the radiation from individual electrons, apart from the considerations on the practical attainment of very high energies. Accordingly, we derive various properties of the radiation from a high energy accelerated electron; the comparison with experiment has been given in the paper by Elder, Langmuir, and Pollock.

I. GENERAL FORMULAS

Before launching into the general discussion, it is well to notice an elementary derivation of the total rate of radiation, based on Larmor's classical formula for a slowly moving electron, and arguments of relativistic invariance. The Larmor formula for the power radiated by an electron that is instantaneously at rest is

$$P=\frac{2}{3}\frac{e^2}{c^3}\left(\frac{d\mathbf{v}}{dt}\right)^2=\frac{2}{3}\frac{e^2}{m^2c^3}\left(\frac{d\mathbf{p}}{dt}\right)^2. \tag{I.1}$$

Now, radiated energy and elapsed time transform in the same manner under Lorentz transformations, whence the radiated power must be an invariant. We shall have succeeded in deriving a formula for the power radiated by an electron of arbitrary velocity if we can exhibit an invariant that reduces to (I.1) in the rest system of the electron. To accomplish this, we first replace the time derivative by the derivative with respect to the invariant proper time. The differential of proper time is defined by

$$ds^2=dt^2-1/c^2(dx^2+dy^2+dz^2),$$

or

$$ds=(1-v^2/c^2)^{\frac{1}{2}}dt. \tag{I.2}$$

Secondly, we replace the square of the proper time derivative of the momentum by the invariant combination

$$(d\mathbf{p}/ds)^2-1/c^2(dE/ds)^2.$$

Hence, as the desired invariant generalization of (I.1), we have

$$P=\frac{2}{3}\frac{e^2}{m^2c^3}\left[\left(\frac{d\mathbf{p}}{ds}\right)^2-\frac{1}{c^2}\left(\frac{dE}{ds}\right)^2\right]$$
$$=\frac{2}{3}\frac{e^2}{m^2c^3}\left(\frac{E}{mc^2}\right)^2\left[\left(\frac{d\mathbf{p}}{dt}\right)^2-\frac{1}{c^2}\left(\frac{dE}{dt}\right)^2\right]. \tag{I.3}$$

The conventional form of this result is obtained on

[1] See L. I. Schiff, Rev. Sci. Inst. **17**, 6 (1946).
[2] D. Iwanenko and I. Pomeranchuk, Phys. Rev. **65**, 343 (1944).
[3] Edwin M. McMillan, Phys. Rev. **68**, 144 (1945).
[4] John P. Blewett, Phys. Rev. **69**, 87 (1946).
[5] Julian Schwinger, Phys. Rev. **70**, 798 (1946).
[6] Elder, Langmuir, and Pollock, Phys. Rev. **74**, 52 (1948).

writing

$$\mathbf{p}=\frac{m\mathbf{v}}{(1-\beta^2)^{\frac{1}{2}}},\quad E=\frac{mc^2}{(1-\beta^2)^{\frac{1}{2}}},\quad \beta=\frac{v}{c},$$

and performing the indicated differentiations. Thus

$$P=\frac{2}{3}\frac{e^2}{c^3}\frac{1}{(1-\beta^2)^3}\left[\left(\frac{d\mathbf{v}}{dt}\right)^2-\left(\frac{\mathbf{v}}{c}\times\frac{d\mathbf{v}}{dt}\right)^2\right]. \quad (I.4)$$

The two important limiting cases of these formulas are realized in the linear accelerator and the synchrotron, or betatron. In the former, the rates of momentum and energy change are connected by

$$c^2p(dp/dt)=E(dE/dt),$$

whence

$$P=\frac{2}{3}\frac{e^2}{m^2c^3}\left(\frac{dp}{dt}\right)^2=\frac{2}{3}\frac{e^2}{m^2c^3}\left(\frac{dE}{dx}\right)^2, \quad (I.5)$$

which shows that the radiated power depends only on the external force and is independent of the electron energy. The ratio of power lost in radiation to power gained from external sources is

$$P\Big/\frac{dE}{dt}=\frac{2}{3}\frac{e^2}{mc^2}\frac{dE/mc^2}{dx}, \quad (I.6)$$

for high energy electrons. It is evident that radiative losses in a linear accelerator are negligible, unless the accelerating field supplies energy of the order mc^2 in a distance equal to the classical radius of the electron! For the circular trajectory of an electron in a synchrotron,

$$P=\frac{2}{3}\frac{e^2}{m^2c^3}\left(\frac{E}{mc^2}\right)^2\left(\frac{d\mathbf{p}}{dt}\right)^2, \quad (I.7)$$

since the energy changes slowly in comparison with the vectorial momentum. Now

$$\left(\frac{d\mathbf{p}}{dt}\right)^2=\omega_0^2p^2=\frac{\omega_0}{R\epsilon}\beta^3E^2, \quad (I.8)$$

where ω_0 and R are the instantaneous angular velocity and radius of curvature. Hence,

$$P=\tfrac{2}{3}\omega_0\frac{e^2}{R}\beta^3\left(\frac{E}{mc^2}\right)^4. \quad (I.9)$$

For high energy electrons moving in a circular path, the energy radiated per revolution is

$$\delta E=(4\pi/3)(e^2/R)(E/mc^2)^4. \quad (I.10)$$

A useful form of this result is

$$\delta E_{\text{kev}}=88.5(E_{\text{Bev}})^4/R_{\text{met}} \quad (I.11)$$

where E_{Bev} is the electron energy in units of 1 Bev $=10^9$ ev, R_{met} is the radius of the electron orbit in meters, and δE_{kev} is the energy radiated per revolution in units of 1 kev $=10^3$ ev.

We shall now construct an expression for the instantaneous power radiated by an electron moving along an arbitrary prescribed path. Our procedure will be such that by introducing various forms for this result the following additional physical quantities can be obtained: the angular distribution of the radiation, the rate of radiation into the various frequencies generated by the electron, and the angular distribution of the radiation emitted at each of these frequencies.

The method is based on a consideration of the rate at which the electron does work on the electromagnetic field,

$$-\int\mathbf{j}\cdot\mathbf{E}_{\text{ret}}dv, \quad (I.12)$$

which can be conveniently divided into two essentially different parts on writing

$$\mathbf{E}_{\text{ret}}=\tfrac{1}{2}(\mathbf{E}_{\text{ret}}+\mathbf{E}_{\text{adv}})+\tfrac{1}{2}(\mathbf{E}_{\text{ret}}-\mathbf{E}_{\text{adv}}). \quad (I.13)$$

Here $\mathbf{E}_{\text{ret}}$ and $\mathbf{E}_{\text{adv}}$ are the retarded and advanced electric field intensities generated by the electron charge and current densities, ρ and $\mathbf{j}$. The first part of (I.12), derived from the symmetrical combination of $\mathbf{E}_{\text{ret}}$ and $\mathbf{E}_{\text{adv}}$, changes sign on reversing the positive sense of time and therefore represents reactive power. It describes the rate at which the electron stores energy in the electromagnetic field, an inertial effect with which we are not concerned. However, the second part of (I.12), derived from the antisymmetrical combination of $\mathbf{E}_{\text{ret}}$ and $\mathbf{E}_{\text{adv}}$, remains unchanged on reversing the positive sense of time, and therefore represents resistive power. Subject to one qualification, it describes the rate of irreversible energy transfer to the electromagnetic field, which is the desired rate of radiation. Included in the second part of (I.12) are terms which have the form of the time derivative of an acceleration dependent electron energy. The latter is completely negligible compared with the electron kinetic energy for all realizable accelerations. It will be a simple manner to eliminate these unwanted terms after evaluating the dissipative part of (I.12). Thus, the power carried away by radiation is, provisionally,

$$P=-\int\mathbf{j}\cdot\mathbf{E}dv, \quad (I.14)$$

with

$$\mathbf{E}=\tfrac{1}{2}(\mathbf{E}_{\text{ret}}-\mathbf{E}_{\text{adv}})=-\frac{1}{c}\frac{\partial}{\partial t}\mathbf{A}-\nabla\phi. \quad (I.15)$$

The expression of P in terms of the vector and scalar

potentials, $\mathbf{A}$ and ϕ, can be simplified by employing the charge conservation equation

$$\nabla\cdot\mathbf{j}+\partial\rho/\partial t=0. \tag{I.16}$$

Thus,

$$P=\int\left[\frac{1}{c}\mathbf{j}\cdot\frac{\partial\mathbf{A}}{\partial t}-\rho\frac{\partial\phi}{\partial t}\right]dv+\frac{d}{dt}\int\rho\phi dv. \tag{I.17}$$

The second term of this formula is of the acceleration energy type and may be discarded. Hence the expression for the radiated power, which still includes unwanted acceleration energy terms, becomes

$$P=\int\left[\frac{1}{c}\mathbf{j}\cdot\frac{\partial\mathbf{A}}{\partial t}-\rho\frac{\partial\phi}{\partial t}\right]dv. \tag{I.18}$$

The retarded and advanced scalar potentials can be conveniently written as

$$\phi_{\text{ret, adv}}(\mathbf{r}, t)=\int\frac{\delta\left(t'-t\pm\frac{|\mathbf{r}-\mathbf{r}'|}{c}\right)}{|\mathbf{r}-\mathbf{r}'|}\rho(\mathbf{r}', t')dv'dt', \tag{I.19}$$

where the upper sign is appropriate for the retarded potential. On introducing the Fourier integral representation of the function $\delta(t)$:

$$\delta(t)=\frac{1}{2\pi}\int_{-\infty}^{\infty}e^{i\omega t}d\omega, \tag{I.20}$$

the potentials assume the form

$$\phi_{\text{ret, adv}}(\mathbf{r}, t)=\frac{1}{2\pi}\int e^{i\omega(t'-t)}\times\frac{e^{\pm i(\omega/c)|\mathbf{r}-\mathbf{r}'|}}{|\mathbf{r}-\mathbf{r}'|}\rho(\mathbf{r}', t')dv'dt'd\omega, \tag{I.21}$$

whence

$$\phi(\mathbf{r}, t)=\frac{i}{2\pi}\int e^{i\omega(t'-t)}\times\frac{\sin\frac{\omega}{c}|\mathbf{r}-\mathbf{r}'|}{|\mathbf{r}-\mathbf{r}'|}\rho(\mathbf{r}', t')dv'dt'd\omega. \tag{I.22}$$

Similarly,

$$\mathbf{A}_{\text{ret, adv}}(\mathbf{r}, t)=\int\frac{\delta\left(t'-t\pm\frac{|\mathbf{r}-\mathbf{r}'|}{c}\right)}{|\mathbf{r}-\mathbf{r}'|}\times\frac{1}{c}\mathbf{j}(\mathbf{r}', t')dv'dt', \tag{I.23}$$

and

$$\mathbf{A}(\mathbf{r}, t)=\frac{i}{2\pi}\int e^{i\omega(t'-t)}\frac{\sin(\omega/c)|\mathbf{r}-\mathbf{r}'|}{|\mathbf{r}-\mathbf{r}'|}\times\frac{1}{c}\mathbf{j}(\mathbf{r}', t')dv'dt'd\omega. \tag{I.24}$$

It will also prove useful to write

$$\frac{\sin(\omega/c)|\mathbf{r}-\mathbf{r}'|}{|\mathbf{r}-\mathbf{r}'|}=\frac{\omega}{c}\int\exp[i(\omega/c)\mathbf{n}\cdot(\mathbf{r}-\mathbf{r}')]\frac{d\Omega}{4\pi} \tag{I.25}$$

in which $d\Omega$ is an element of solid angle associated with the direction of the unit vector $\mathbf{n}$. The resultant expressions for ϕ and $\mathbf{A}$:

$$\phi(\mathbf{r}, t)=\frac{i}{2\pi c}\int\exp[i(\omega/c)\mathbf{n}\cdot(\mathbf{r}-\mathbf{r}')-i\omega(t-t')]\times\rho(\mathbf{r}', t')dv'dt'\omega d\omega\frac{d\Omega}{4\pi},$$

$$\mathbf{A}(\mathbf{r}, t)=\frac{i}{2\pi c}\int\exp[i(\omega/c)\mathbf{n}\cdot(\mathbf{r}-\mathbf{r}')-i\omega(t-t')]\times\frac{1}{c}\mathbf{j}(\mathbf{r}', t')dv'dt'\omega d\omega\frac{d\Omega}{4\pi} \tag{I.26}$$

are a superposition of plane waves traveling with the speed c.

The total radiated power, calculated from (18), (19), and (23), is

$$P(t)=\frac{1}{2}\int\left[\rho(\mathbf{r}, t)\rho(\mathbf{r}', t')-\frac{1}{c^2}\mathbf{j}(\mathbf{r}, t)\cdot\mathbf{j}(\mathbf{r}', t')\right]\cdot\left[\frac{\delta'\left(t'-t+\frac{|\mathbf{r}-\mathbf{r}'|}{c}\right)}{|\mathbf{r}-\mathbf{r}'|}-\frac{\delta'\left(t'-t-\frac{|\mathbf{r}-\mathbf{r}'|}{c}\right)}{|\mathbf{r}-\mathbf{r}'|}\right]dvdv'dt', \tag{I.27}$$

where $\delta'(t)$ denotes the derivative of the delta-function. Alternatively, if the Fourier integral representations (I.22) and (I.24) are employed,

$$P(t)=-\frac{1}{2\pi}\int\Big[\rho(\mathbf{r},t)\rho(\mathbf{r}',t') -\frac{1}{c^2}\mathbf{j}(\mathbf{r},t)\cdot\mathbf{j}(\mathbf{r}',t')\Big]e^{i\omega(t'-t)} \times\frac{\sin\frac{\omega}{c}|\mathbf{r}-\mathbf{r}'|}{|\mathbf{r}-\mathbf{r}'|}dvdv'dt'\omega d\omega =\int_0^\infty P(\omega,t)d\omega, \quad \text{(I.28)}$$

It may be inferred that

$$P(\omega,t)=-\frac{\omega}{\pi}\int\Big[\rho(\mathbf{r},t)\rho(\mathbf{r}',t') -\frac{1}{c^2}\mathbf{j}(\mathbf{r},t)\cdot\mathbf{j}(\mathbf{r}',t')\Big]\cos\omega(t-t') \cdot\frac{\sin\frac{\omega}{c}|\mathbf{r}-\mathbf{r}'|}{|\mathbf{r}-\mathbf{r}'|}dvdv'dt' \quad \text{(I.29)}$$

represents the power radiated at the time t in a unit angular frequency range about ω. The latter statement is correct if $P(\omega, t)$ changes only slightly in a time interval equal to the reciprocal of ω, a condition that is adequately met in practice.

With the aid of (I.25), the total radiated power can also be written

$$P(t)=-\frac{1}{2\pi c}\int\Big[\rho(\mathbf{r},t)\rho(\mathbf{r}',t') -\frac{1}{c^2}\mathbf{j}(\mathbf{r},t)\cdot\mathbf{j}(\mathbf{r}',t')\Big] \times\exp\Big[i\omega\Big[t'-t+\frac{1}{c}\mathbf{n}\cdot(\mathbf{r}-\mathbf{r}')\Big]\Big] \cdot\omega^2 d\omega dvdv'dt'\frac{d\Omega}{4\omega}$$

$$=\frac{1}{c}\int\Big[\rho(\mathbf{r},t)\rho(\mathbf{r}',t') -\frac{1}{c^2}\mathbf{j}(\mathbf{r},t)\cdot\mathbf{j}(\mathbf{r}',t')\Big] \times\delta''\Big(t'-t+\frac{1}{c}\mathbf{n}\cdot(\mathbf{r}-\mathbf{r}')\Big) \cdot dvdv'dt'\frac{d\Omega}{4\pi}$$

$$=\int P(\mathbf{n},t)d\Omega. \quad \text{(I.30)}$$

Evidently,

$$P(\mathbf{n},t)=\frac{1}{4\pi c}\int\Big[\rho(\mathbf{r},t)\rho(\mathbf{r}',t') -\frac{1}{c^2}\mathbf{j}(\mathbf{r},t)\cdot\mathbf{j}(\mathbf{r}',t')\Big] \times\delta''\Big(t'-t+\frac{1}{c}\mathbf{n}\cdot(\mathbf{r}-\mathbf{r}')\Big)dvdv'dt' \quad \text{(I.31)}$$

describes the power radiated per unit solid angle in the direction $\mathbf{n}$, at the time t. Similarly, (I.30) can be written

$$P(t)=\int_0^\infty d\omega\int d\Omega P(\mathbf{n},\omega,t), \quad \text{(I.32)}$$

where

$$P(\mathbf{n},\omega,t)=-\frac{1}{4\pi^2}\frac{\omega^2}{c}\int\Big[\rho(\mathbf{r},t)\rho(\mathbf{r}',t') -\frac{1}{c^2}\mathbf{j}(\mathbf{r},t)\cdot\mathbf{j}(\mathbf{r}',t')\Big] \cdot\cos\omega\Big(t'-t+\frac{1}{c}\mathbf{n}\cdot(\mathbf{r}-\mathbf{r}')\Big)dvdv'dt' \quad \text{(I.33)}$$

represents the power radiated at time t into a unit solid angle about the direction $\mathbf{n}$ and contained in a unit angular frequency interval about the frequency ω. This interpretation is also subject to the adiabatic condition, that $P(\mathbf{n}, \omega, t)$ change only slightly in a time interval equal to the period of the radiation.

Thus far, we have dealt with the radiation of an arbitrary charge-current distribution. For a point electron of charge e, located at the variable position $\mathbf{R}(t)$,

$$\rho(\mathbf{r},t)=e\delta(\mathbf{r}-\mathbf{R}(t)),\quad \mathbf{j}(\mathbf{r},t)=e\mathbf{v}(t)\delta(\mathbf{r}-\mathbf{R}(t)), \quad \text{(I.34)}$$

where $\mathbf{v}(t)=d\mathbf{R}(t)/dt$. Our various formulas can now be simplified by performing the spatial integrations. Hence

$$P(t)=\frac{e^2}{2}\int_{-\infty}^{\infty}\Big(1-\frac{1}{c^2}\mathbf{v}(t)\cdot\mathbf{v}(t+\tau)\Big) \times\Big[\delta'\Big(\tau+\frac{|\mathbf{R}(t+\tau)-\mathbf{R}(t)|}{c}\Big) -\delta'\Big(\tau-\frac{|\mathbf{R}(t+\tau)-\mathbf{R}(t)|}{c}\Big)\Big] \times\frac{d\tau}{|\mathbf{R}(t+\tau)-\mathbf{R}(t)|}, \quad \text{(I.35)}$$

$$P(\mathbf{n},t)=\frac{e^2}{4\pi c}\int_{-\infty}^{\infty}\left(1-\frac{1}{c^2}\mathbf{v}(t)\cdot\mathbf{v}(t+\tau)\right)$$
$$\times\delta''\left(\tau-\frac{1}{c}\mathbf{n}\cdot(\mathbf{R}(t+\tau)-\mathbf{R}(t))\right)d\tau, \quad \text{(I.36)}$$

$$P(\omega,t)=-\frac{e^2\omega}{\pi}\int_{-\infty}^{\infty}\left(1-\frac{1}{c^2}\mathbf{v}(t)\cdot\mathbf{v}(t+\tau)\right)$$
$$\times\cos\omega\tau\frac{\sin\frac{\omega}{c}|\mathbf{R}(t+\tau)-\mathbf{R}(t)|}{|\mathbf{R}(t+\tau)-\mathbf{R}(t)|}d\tau, \quad \text{(I.37)}$$

$$P(\mathbf{n},\omega,t)=-\frac{e^2}{4\pi^2}\frac{\omega^2}{c}\int_{-\infty}^{\infty}\left(1-\frac{1}{c^2}\mathbf{v}(t)\cdot\mathbf{v}(t+\tau)\right)$$
$$\times\cos\omega\left(\tau-\frac{1}{c}\mathbf{n}\cdot(\mathbf{R}(t+\tau)-\mathbf{R}(t))\right)d\tau, \quad \text{(I.38)}$$

in which we have placed $t'-t=\tau$.

The total power and its angular distribution can be obtained by straightforward integration, for an arbitrary electron trajectory. We consider, for example, the evaluation of $P(\mathbf{n},t)$. It is convenient to introduce the variable

$$\gamma=\tau-\frac{1}{c}\mathbf{n}\cdot(\mathbf{R}(t+\tau)-\mathbf{R}(t))$$

for which

$$d\gamma=\left(1-\frac{1}{c}\mathbf{n}\cdot\mathbf{v}(t+\tau)\right)d\tau,$$

whence

$$P(\mathbf{n},t)=\frac{e^2}{4\pi c}\int_{-\infty}^{\infty}\frac{1-\frac{1}{c^2}\mathbf{v}(t)\cdot\mathbf{v}(t+\tau)}{1-\frac{1}{c}\mathbf{n}\cdot\mathbf{v}(t+\tau)}\delta''(\gamma)d\gamma. \quad \text{(I.39)}$$

It is now merely necessary to integrate twice by parts and observe that $\gamma=0$ implies $\tau=0$, unless the electron velocity exceeds that of light (as in the Cerenkov effect). Thus

$$P(\mathbf{n},t)=\frac{e^2}{4\pi c}\frac{1}{1-\frac{1}{c}\mathbf{n}\cdot\mathbf{v}(t)}\left[\frac{d}{d\tau}\frac{1}{1-\frac{1}{c}\mathbf{n}\cdot\mathbf{v}(t+\tau)}\right.$$
$$\left.\times\frac{d}{d\tau}\frac{1-\frac{1}{c^2}\mathbf{v}(t)\cdot\mathbf{v}(t+\tau)}{1-\frac{1}{c}\mathbf{n}\cdot\mathbf{v}(t+\tau)}\right]_{\tau=0}. \quad \text{(I.40)}$$

On performing the indicated differentiations, we obtain

$$P(\mathbf{n},t)=\frac{e^2}{4\pi c^3}\left[\frac{\dot{\mathbf{v}}^2}{\left(1-\frac{1}{c}\mathbf{n}\cdot\mathbf{v}\right)^3}\right.$$
$$\left.+2\frac{\mathbf{n}\cdot\dot{\mathbf{v}}\mathbf{v}\cdot\dot{\mathbf{v}}}{\left(1-\frac{1}{c}\mathbf{n}\cdot\mathbf{v}\right)^4}-\frac{(\mathbf{n}\cdot\dot{\mathbf{v}})^2\left(1-\frac{v^2}{c^2}\right)}{\left(1-\frac{1}{c}\mathbf{n}\cdot\mathbf{v}\right)^5}\right]$$
$$+\frac{d}{dt}\frac{e^2}{4\pi c^2}\left[-\frac{\frac{1}{c}\mathbf{v}\cdot\dot{\mathbf{v}}}{\left(1-\frac{1}{c}\mathbf{n}\cdot\mathbf{v}\right)^3}\right.$$
$$\left.+\frac{\mathbf{n}\cdot\dot{\mathbf{v}}\left(1-\frac{v^2}{c^2}\right)}{\left(1-\frac{1}{c}\mathbf{n}\cdot\mathbf{v}\right)^4}\right], \quad \text{(I.41)}$$

of which only the first term should be retained. Replacing the velocity by $\mathbf{v}=\mathbf{p}c^2/E$, we have finally,

$$P(\mathbf{n},t)=\frac{e^2}{4\pi m^2c^3}\left(\frac{mc^2}{E}\right)^2\left[\frac{\dot{\mathbf{p}}^2-\frac{1}{c^2}\dot{E}^2}{\left(1-\mathbf{n}\cdot\frac{\mathbf{p}c}{E}\right)^3}\right.$$
$$\left.-\left(\frac{mc^2}{E}\right)^2\frac{\left(\mathbf{n}\cdot\dot{\mathbf{p}}-\frac{1}{c}\dot{E}\right)^2}{\left(1-\mathbf{n}\cdot\frac{\mathbf{p}c}{E}\right)^5}\right]. \quad \text{(I.42)}$$

It can be verified that

$$P(t)=\int P(\mathbf{n},t)d\Omega=\frac{2}{3}\frac{e^2}{m^2c^3}\left(\frac{E}{mc^2}\right)^2\left[\dot{\mathbf{p}}^2-\frac{1}{c^2}\dot{E}^2\right],$$

in agreement with (I.3).

For the two extremes of linear acceleration and circular motion, the angular distribution of the radiated power is given by

$$P(\mathbf{n},t)=\frac{e^2}{4\pi m^2c^3}\dot{p}^2(1-\beta^2)^3\frac{\sin^2\vartheta}{(1-\beta\cos\vartheta)^5}, \quad \text{(I.43)}$$

and

$$P(\mathbf{n}, t)=\frac{e^2}{4\pi m^2c^3}\dot{\mathbf{p}}^2(1-\beta^2)\left[\frac{1}{(1-\beta\cos\vartheta)^3}-(1-\beta^2)\frac{\sin^2\vartheta\cos^2\vartheta}{(1-\beta\cos\vartheta)^5}\right]. \quad (I.44)$$

The angles ϑ and φ are the polar angles of a coordinate system in which the z axis coincides with the instantaneous direction of motion, and the xz plane is that of the orbital motion. It is evident that at high speeds the direction of motion is a strongly preferred direction of emission. As a simple measure of this asymmetry we consider the mean value of $\sin^2\vartheta$, defined as

$$\langle\sin^2\vartheta\rangle=\int\sin^2\vartheta P(\mathbf{n}, t)d\Omega/P(t). \quad (I.45)$$

An elementary calculation yields, for linear acceleration,

$$\langle\sin^2\vartheta\rangle=(1-\beta^2)\left[1-\tfrac{1}{2}(1-\beta^2)+\frac{3}{4}\frac{(1-\beta^2)^2}{\beta^5}\left(\log\frac{1+\beta}{1-\beta}-2\beta-\frac{2\beta^3}{3}\right)\right], \quad (I.46)$$

and, for circular motion,

$$\langle\sin^2\vartheta\rangle=(1-\beta^2)\left[1+\tfrac{1}{4}(1-\beta^2)-\frac{3}{4}\frac{1-\beta^2}{\beta^3}\left(\log\frac{1+\beta}{1-\beta}-2\beta\right)-\frac{3}{8}\frac{(1-\beta^2)^2}{\beta^5}\left(\log\frac{1+\beta}{1-\beta}-2\beta-\frac{2\beta^3}{3}\right)\right]. \quad (I.47)$$

The values of these averages, for low energy electrons, are 4/5 and 3/5, for linear and circular motion, respectively. Both types of motion yield the following limiting form for high energy electrons

$$\langle\sin^2\vartheta\rangle=1-\beta^2=(mc^2/E)^2, \quad (I.48)$$

and therefore the mean angle between the direction of emission and that of the electron's motion is

$$\bar{\vartheta}=\langle\vartheta^2\rangle^{\frac{1}{2}}=mc^2/E, \quad E/mc^2\gg1. \quad (I.49)$$

A useful form of this result is

$$\bar{\vartheta}_{\min}=1.76/E_{\text{Bev}},$$

where $\bar{\vartheta}_{\min}$ is the mean angle of emission in minutes and E_{Bev} is the electron energy in units of Bev.

The power radiated into a given frequency range necessarily depends upon the detailed motion of the electron over a time interval that is large compared with the period of radiation under consideration. However, the very narrow cone of radiation that is generated by a high energy electron suggests that only a small part of the electron trajectory is effective in producing the radiation observed in a given direction, which also implies that very high frequencies must be emitted. We therefore consider first the high frequency radiation generated by an energetic electron, in the anticipation that only the instantaneous nature of the electron's motion will be involved. Secondly, we shall derive the entire spectrum emitted by an electron moving with constant speed in a circular path.

II. HIGH FREQUENCY RADIATION BY ENERGETIC ELECTRONS

To evaluate (I.37) for $E/mc^2\gg1$, it is sufficient to write

$$\begin{aligned}|\mathbf{R}(t+\tau)-\mathbf{R}(t)|&=|\tau\mathbf{v}(t)\\&\quad+(\tau^2/2)\dot{\mathbf{v}}(t)+(\tau^3/6)\partial^2\mathbf{v}(t)/\partial t^2|\\&=(\tau^2v^2+\tau^3\mathbf{v}\cdot\dot{\mathbf{v}}+(\tau^4/4)\dot{\mathbf{v}}^2\\&\qquad+(\tau^4/3)\mathbf{v}\cdot\partial^2\mathbf{v}/\partial t^2)^{\frac{1}{2}}. \quad (II.1)\end{aligned}$$

Furthermore, $\mathbf{v}\cdot\dot{\mathbf{v}}=(d/dt)\frac{1}{2}\mathbf{v}^2$ may be placed equal to zero since v differs negligibly from c when $E/mc^2\gg1$. In a similar manner, $\mathbf{v}\cdot\partial^2\mathbf{v}/\partial t^2\simeq-\dot{\mathbf{v}}^2\simeq-c^4/R^2$. In the latter formula R is the instantaneous radius of curvature. Hence

$$|\mathbf{R}(t+\tau)-\mathbf{R}(t)|\simeq v|\tau|-\frac{1}{24}\frac{c^3}{R^2}|\tau^3| \quad (II.2)$$

and

$$P(\omega, t)=-\frac{2}{\pi}\frac{e^2\omega}{c}\int_0^\infty\left(1-\beta^2+\frac{1}{2}\frac{c^2\tau^2}{R^2}\right)\times\cos\omega\tau\sin\omega\left(\beta\tau-\frac{c^2\tau^3}{24R^2}\right)\frac{d\tau}{\tau}. \quad (II.3)$$

In writing this result, an approximation similar to (II.2) has been employed on the velocity dependent factor of (I.37):

$$\begin{aligned}1-\frac{1}{c^2}\mathbf{v}(t)\cdot\mathbf{v}(t+\tau)&=1-\frac{v^2}{c^2}-\frac{\tau}{c^2}\mathbf{v}\cdot\dot{\mathbf{v}}-\frac{\tau^2}{2c^2}\mathbf{v}\cdot\partial^2\mathbf{v}/\partial t^2\\&\simeq1-\beta^2+\frac{1}{2}\frac{c^2\tau^2}{R^2}. \quad (II.4)\end{aligned}$$

In addition, the first term of (II.2) suffices for the evaluation of the denominator in (I.37). It is now

convenient to write, approximately,

$$P(\omega,t)=\frac{1}{\pi}\frac{e^2\omega}{c}\int_0^\infty\left(1-\beta^2+\frac{1}{2}\frac{c^2\tau^2}{R^2}\right)\times\left\{\sin\left(\omega(1-\beta)\tau+\frac{\omega c^2}{24R^2}\tau^3\right)\frac{d\tau}{\tau}-\sin 2\omega\tau\frac{d\tau}{\tau}\right\}. \quad \text{(II.5)}$$

The approximation employed in the second term of (II.5) is valid provided $\omega\gg c/R$, that is, if we restrict attention to frequencies that greatly exceed the instantaneous angular frequency of the electron. To justify this statement, note that the largest values of τ that contribute to the integral in question are $\tau\sim 1/\omega$. Thus the neglected term is of the order of magnitude $\omega\tau^3c^2/R^2\sim(c/\omega R)^2\ll 1$.

To simplify the first integral in (II.5), we write

$$\tau=\frac{2R}{c}(1-\beta^2)^{\frac{1}{2}}x, \quad \text{(II.6)}$$

whence

$$P(\omega,t)=\frac{1}{\pi}\frac{e^2\omega}{c}(1-\beta^2)\left[\int_0^\infty(1+2x^2)\times\sin\tfrac{3}{2}\xi(x+\tfrac{1}{3}x^3)\frac{dx}{x}-\frac{\pi}{2}\right]. \quad \text{(II.7)}$$

In this formula, we have placed

$$\xi=\frac{2}{3}\frac{\omega R}{c}(1-\beta^2)^{\frac{1}{2}}=\frac{2}{3}\frac{\omega R}{c}\left(\frac{mc^2}{E}\right)^3 \quad \text{(II.8)}$$

and employed the well-known integral

$$\int_0^\infty\frac{\sin ax}{x}dx=\frac{\pi}{2},\quad a>0. \quad \text{(II.9)}$$

The approximation (II.2) can now be justified by considering the range of variable that is of most importance for the integral in (II.7). The essential frequencies are such that $\xi\sim 1$, or $\omega\sim(c/R)(E/mc^2)^3$. Clearly, then, the important values of x are $x\sim 1$, or $\tau\sim(R/c)(mc^2/E)$. The series (II.7) is essentially an expansion in powers of $(c\tau/R)^2\sim(mc^2/E)^2\ll 1$. Thus the neglect of higher terms in the expansion is justified provided $E/mc^2\gg 1$.

The integral contained in (II.7) can be recognized as related to the Airy integral[7]

$$\int_0^\infty\cos\tfrac{3}{2}\xi(x+\tfrac{1}{3}x^3)dx=3^{-\frac{1}{3}}K_{1/3}(\xi). \quad \text{(II.10)}$$

[7] G. N. Watson, *Bessel Functions* (The Macmillan Company, New York, 1945), p. 188.

Now

$$3^{-\frac{1}{3}}K_{1/3}(\xi)=\frac{d}{d\xi}\int_0^\infty\sin\tfrac{3}{2}\xi(x+\tfrac{1}{3}x^3)\frac{dx}{x},$$

whence

$$3^{-\frac{1}{3}}\int_\xi^\infty K_{1/3}(\eta)d\eta=\lim_{L\to\infty}\int_0^\infty\sin L(x+\tfrac{1}{3}x^3)\frac{dx}{x}-\int_0^\infty\sin\tfrac{3}{2}\xi(x+\tfrac{1}{3}x^3)\frac{dx}{x}=\frac{\pi}{2}-\int_0^\infty\sin\tfrac{3}{2}\xi(x+\tfrac{1}{3}x^3)\frac{dx}{x}. \quad \text{(II.11)}$$

Furthermore,

$$3^{-\frac{1}{3}}K_{2/3}(\xi)=\int_0^\infty x\sin\tfrac{3}{2}\xi(x+\tfrac{1}{3}x^3)dx \quad \text{(II.12)}$$

since

$$\left(\frac{d}{d\xi}+\frac{1}{3\xi}\right)K_{1/3}(\xi)=-K_{2/3}(\xi). \quad \text{(II.13)}$$

Hence

$$\int_0^\infty(1+2x^2)\sin\tfrac{3}{2}\xi(x+\tfrac{1}{3}x^3)\frac{dx}{x}-\frac{\pi}{2}=3^{-\frac{1}{3}}\left(2K_{2/3}(\xi)-\int_\xi^\infty K_{1/3}(\eta)d\eta\right)=3^{-\frac{1}{3}}\int_\xi^\infty K_{5/3}(\eta)d\eta. \quad \text{(II.14)}$$

The last simplification involves the recurrence relation

$$2\frac{d}{d\xi}K_{2/3}(\xi)+K_{1/3}(\xi)=-K_{5/3}(\xi). \quad \text{(II.15)}$$

Our final result is

$$P(\omega,t)=\frac{3^{\frac{1}{2}}}{4\pi}\frac{e^2}{R}\left(\frac{E}{mc^2}\right)^4\frac{\omega_0\omega}{\omega_c^2}\int_{\omega/\omega_c}^\infty K_{5/3}(\eta)d\eta, \quad \text{(II.16)}$$

where the critical frequency ω_c is defined by

$$\omega_c=\tfrac{3}{2}\omega_0\left(\frac{E}{mc^2}\right)^3 \quad \text{(II.17)}$$

and

$$\omega_0=c/R.$$

Before proceeding with the discussion of the formula, it is advisable to check our approximations by verifying that

$$P(t)=\int_0^\infty P(\omega,t)d\omega=\tfrac{2}{3}\omega_0\frac{e^2}{R}\left(\frac{E}{mc^2}\right)^4,$$

or that

$$\int_0^\infty \xi d\xi \int_\xi^\infty K_{5/3}(\eta)d\eta = \frac{1}{2}\int_0^\infty \xi^2 K_{5/3}(\xi)d\xi = \frac{8\pi}{3^{7/3}}.$$

This is indeed the value yielded by the formula

$$\int_0^\infty \xi^{\mu-1}K_\nu(\xi)d\xi = 2^{\mu-2}\Gamma\left(\frac{\mu-\nu}{2}\right)\Gamma\left(\frac{\mu+\nu}{2}\right). \quad \text{(II.18)}$$

In virtue of the properties of the Bessel functions of imaginary argument, the behavior of $P(\omega, t)$ is radically different, depending upon whether ω/ω_c is large or small compared with unity. For $\omega \ll \omega_c$, it is convenient to write

$$P(\omega, t) = \frac{3^{\frac{1}{2}}}{4\pi}\frac{e^2}{R}\left(\frac{E}{mc^2}\right)^4 \frac{\omega_0 \omega}{\omega_c^2} \times\left[2K_{2/3}\left(\frac{\omega}{\omega_c}\right) + \int_0^{\omega/\omega_c} K_{1/3}(\eta)d\eta - \frac{\pi}{3^{\frac{1}{2}}}\right] \quad \text{(II.19)}$$

and insert the power series expansions for small values of the argument. Thus,

$$\omega/\omega_c \ll 1 : P(\omega, t) = \frac{3^{1/6}\Gamma(\frac{2}{3})}{\pi}\frac{e^2}{R}\left(\frac{\omega}{\omega_0}\right)^{\frac{1}{3}} \times\left[1 - \frac{\Gamma(\frac{2}{3})}{2}\left(\frac{\omega}{2\omega_c}\right)^{\frac{1}{3}} + \cdots\right], \quad \text{(II.20)}$$

of which the leading term for small frequencies varies as $\omega^{\frac{1}{3}}$ and is independent of the electron energy. If $\omega/\omega_c \gg 1$, we may employ the asymptotic form for large argument in Eq. (II.16), whence

$$\omega/\omega_c \gg 1 : P(\omega, t) = \frac{3}{4}\left(\frac{3}{2\pi}\right)^{\frac{1}{2}}\frac{e^2}{R} \times\left(\frac{E}{mc^2}\right)^4 \frac{\omega_0}{\omega_c}\left(\frac{\omega}{\omega_c}\right)^{\frac{1}{2}} e^{-\omega/\omega_c} \times\left[1 + \frac{55}{72}\frac{\omega_c}{\omega} + \cdots\right]. \quad \text{(II.21)}$$

Therefore, the energy radiated into a unit frequency interval steadily increases with frequency until $\omega/\omega_c \sim 1$, after which there is a rapid decrease.[8] Since the power radiated at frequencies not in excess of ω_c is independent of E, but varies as $\omega^{\frac{1}{3}}$, the total power should vary as $\omega_c^{4/3}$, which is indeed proportional to $(E/mc^2)^4$.

Associated with the critical frequency is a wave-length

$$\lambda_c = (4\pi/3)R(mc^2/E)^3 \quad \text{(II.22)}$$

which may be written, for practical purposes, as

$$\lambda_{c,A} = 5.59(R_{\text{met}}/(E_{\text{Bev}})^3). \quad \text{(II.23)}$$

Here R_{met} and E_{Bev} have the meanings previously attributed to them, while $\lambda_{c,A}$ denotes the critical wave-length in units of $1A = 10^{-8}$ cm. Evidently an electron accelerator will be a source of high frequency radiation. It is desirable to have a simply physical explanation for the very high frequencies generated by an energetic electron. We shall base such an explanation upon the angular distribution properties of the radiation. Since the mean angle between the direction of motion and that of the radiation is $\bar{\vartheta} = mc^2/E$, the time interval during which radiation is emitted toward the observer is

$$\Delta t \sim (R/c)\bar{\vartheta}$$

being the time required for the direction of motion to move through the angle $\bar{\vartheta}$. However, the time interval for reception of the pulse by the observer differs from Δt, in virtue of the Doppler effect. The time of reception, at the point $\mathbf{r}$, of a signal generated at the time t and the point $\mathbf{R}(t)$ is

$$t' = t + \frac{|\mathbf{r} - \mathbf{R}(t)|}{c},$$

whence

$$dt' = \left(1 - \frac{\mathbf{r} - \mathbf{R}(t)}{|\mathbf{r} - \mathbf{R}(t)|}\cdot\frac{\mathbf{v}(t)}{c}\right)dt = (1 - \beta\cos\vartheta)dt.$$

Thus the time interval during which the pulse is received is of the order of magnitude

$$\Delta t' \sim (1 - \beta + \tfrac{1}{2}\bar{\vartheta}^2)\Delta t \sim (1 - \beta^2)\Delta t \sim (R/c)(mc^2/E)^3$$

and the Fourier spectrum of the pulse will contain all frequencies up to a maximum of the order of magnitude

$$\omega_c \sim 1/\Delta t' \sim (c/R)(E/mc^2)^3,$$

in agreement with our more precise considerations.

The combined spectral and angular distribution for a high energy electron can be obtained in a similar way. We write, approximately,

$$P(\mathbf{n}, \omega, t) = -\frac{e^2}{4\pi^2}\frac{\omega^2}{c}\int_{-\infty}^{\infty} \times\left(1 - \beta^2 + \frac{1}{2}\frac{c^2\tau^2}{R^2}\right)\cos\omega\left(\left(1 - \frac{\mathbf{n}\cdot\mathbf{v}}{c}\right)\tau - \frac{1}{2}\frac{\mathbf{n}\cdot\dot{\mathbf{v}}}{c}\tau^2 - \tfrac{1}{6}\mathbf{n}\cdot\frac{\partial^2\mathbf{v}/\partial t^2}{c}\tau^3\right)d\tau. \quad \text{(II.24)}$$

It will be convenient to replace the polar angles ϑ and φ by the angles ψ and χ. The former designates

[8] These qualitative results have also been obtained by L. Arzimovich and I. Pomeranchuk, J. Phys. USSR 9, 267 (1945).

the angle between the direction of emission and the instantaneous orbital plane, while χ denotes the angle, projected onto the orbital plane, between the direction of emission and direction of motion. The connection between the two sets of spherical coordinates is

$$\begin{aligned}\sin\vartheta\sin\varphi&=\sin\psi,\\ \sin\vartheta\cos\varphi&=\cos\psi\sin\chi,\\ \cos\vartheta&=\cos\psi\cos\chi.\end{aligned}\tag{II.25}$$

Hence,

$$\begin{aligned}\frac{\mathbf{n}\cdot\dot{\mathbf{v}}}{c}&=\frac{c}{R}\sin\vartheta\cos\varphi\simeq\frac{c}{R}\chi,\\ 1-\frac{\mathbf{n}\cdot\mathbf{v}}{c}&=1-\beta\cos\vartheta\simeq\tfrac{1}{2}(1-\beta^2+\psi^2+\chi^2),\\ \frac{\mathbf{n}\cdot(\partial^2\mathbf{v}/\partial t^2)}{c}&\simeq\frac{1}{c^2}\mathbf{v}\cdot(\partial^2\mathbf{v}/\partial t^2)\simeq-\frac{c^2}{R^2},\end{aligned}\tag{II.26}$$

in which approximations have been introduced based on the small angle between the directions of emission and motion. Expressed in these angular coordinates, (II.24) becomes

$$\begin{aligned}P(\mathbf{n},\omega,t)=-\frac{e^2}{4\pi^2}\frac{\omega^2}{c}\int_{-\infty}^{\infty}&\\ \times\left(1-\beta^2+\frac{1}{2}\frac{c^2\tau^2}{R^2}\right)\cos\omega&\\ \times\left(\tfrac{1}{2}(1-\beta^2+\psi^2+\chi^2)\tau\right.&\\ \left.-\frac{c\chi}{2R}\tau^2+\frac{c^2\tau^3}{6R^2}\right)d\tau.&\end{aligned}\tag{II.27}$$

To bring this integral into the standard Airy integral form, it is necessary to eliminate the term in τ^2 that occurs in the argument of the trigonometric function. We achieve this by the following substitution for τ:

$$\tau\rightarrow\tau+\frac{R}{c}\chi,\tag{II.28}$$

whence

$$\begin{aligned}P(\mathbf{n},\omega,t)=-\frac{e^2}{4\pi^2}\frac{\omega^2}{c}\int_{-\infty}^{\infty}&\\ \times\left(1-\beta^2+\tfrac{1}{2}\chi^2+\frac{1}{2}\frac{c^2\tau^2}{R^2}+\frac{c}{R}\chi\tau\right)&\\ \cdot\cos\omega\left(\tfrac{1}{2}(1-\beta^2+\psi^2)\tau+\frac{c^2}{6R^2}\tau^3\right.&\\ \left.+\frac{R}{2c}(1-\beta^2+\psi^2)\chi+\frac{R}{6c}\chi^3\right)d\tau.&\end{aligned}\tag{II.29}$$

It should now be remarked that only the distribution in the angle ψ is of interest, that in the angle χ being essentially unobservable in practice. Accordingly, we may integrate (II.29) with respect to χ to obtain $P(\psi,\omega,t)$, the power emitted per unit angle relative to the orbital plane, and per unit angular frequency, at the time t. The introduction of the variables

$$\begin{aligned}x&=(1-\beta^2+\psi^2)^{-\frac{1}{3}}\chi,\\ y&=(1-\beta^2+\psi^2)^{-\frac{1}{3}}\frac{c\tau}{R}\end{aligned}\tag{II.30}$$

yields

$$\begin{aligned}P(\psi,\omega,t)=-\frac{1}{4\pi^2}\frac{e^2}{R}\frac{\omega^2}{\omega_0^2}(1-\beta^2+\psi^2)\int_{-\infty}^{\infty}&\\ \times\left(1-\beta^2+\frac{1-\beta^2+\psi^2}{2}(x^2+y^2+2xy)\right)&\\ \cdot\cos\left[\frac{\omega R}{2c}(1-\beta^2+\psi^2)^{\frac{1}{3}}(x+\tfrac{1}{3}x^3\right.&\\ \left.+y+\tfrac{1}{3}y^3)\right]dxdy,&\end{aligned}\tag{II.31}$$

whence

$$\begin{aligned}P(\psi,\omega,t)=\frac{1}{3\pi^2}\frac{e^2}{R}\frac{\omega^2}{\omega_0^2}(1-\beta^2+\psi^2)^2&\\ \times\left[K_{2/3}{}^2\left(\frac{\omega R}{3c}(1-\beta^2+\psi^2)^{\frac{3}{2}}\right)\right.&\\ \left.+\frac{\psi^2}{1-\beta^2+\psi^2}K_{1/3}{}^2\left(\frac{\omega R}{3c}(1-\beta^2+\psi^2)^{\frac{3}{2}}\right)\right]&\end{aligned}\tag{II.32}$$

on employing (II.10), (II.12), and the identity

$$\begin{aligned}\int_0^{\infty}(1+x^2)\cos\tfrac{3}{2}\xi(x+\tfrac{1}{3}x^3)dx&\\ =\frac{2}{3\xi}\int_0^{\infty}d\sin\tfrac{3}{2}\xi(x+\tfrac{1}{3}x^3)=0.&\end{aligned}\tag{II.33}$$

This result can also be written

$$\begin{aligned}P(\psi,\omega,t)=\frac{3}{4\pi^2}\frac{e^2}{R}\left(\frac{\omega}{\omega_c}\right)^2&\\ \times\left(\frac{E}{mc^2}\right)^2\left(1+\left(\frac{E}{mc^2}\psi\right)^2\right)^2&\\ \cdot\left[K_{2/3}{}^2(\xi)+\frac{\left(\frac{E}{mc^2}\psi\right)^2}{1+\left(\frac{E}{mc^2}\psi\right)^2}K_{1/3}{}^2(\xi)\right],&\end{aligned}\tag{II.34}$$

where

$$\xi=\frac{\omega}{2\omega_c}\left(1+\left(\frac{E}{mc^2}\psi\right)^2\right)^{\frac{3}{2}}. \tag{II.35}$$

Evidently the spectrum of the radiation emitted at the angle ψ extends up to a maximum frequency

$$\sim\omega_c\left(1+\left(\frac{E}{mc^2}\psi\right)^2\right)^{-\frac{3}{2}},$$

which decreases rapidly with increasing angle if $\psi>mc^2/E$. This again implies that appreciable radiation occurs only at angles $\psi\sim mc^2/E$, which is made evident by the angular distribution function for the radiation, irrespective of frequency:

$$P(\psi,t)=\int_0^\infty P(\psi,\omega,t)d\omega$$
$$=\omega_0\frac{e^2}{R}\left(\frac{E}{mc^2}\right)^5\left(1+\left(\frac{E}{mc^2}\psi\right)^2\right)^{-5/2}$$
$$\times\left[\frac{7}{16}+\frac{5}{16}\frac{\left(\frac{E}{mc^2}\psi\right)^2}{1+\left(\frac{E}{mc^2}\psi\right)^2}\right], \tag{II.36}$$

obtained from (II.34) with the aid of the integral

$$\int_0^\infty K_\mu^2(x)x^2dx=\frac{\pi^2}{4}\frac{\frac{1}{4}-\mu^2}{\cos\pi\mu}. \tag{II.37}$$

This result agrees, of course, with that computed from $P(\mathbf{n},t)$ by integrating with respect to χ and introducing the approximations appropriate to the situation under discussion.

The synchrotron spectral measurements reported in reference 6 pertain, not to the instantaneous power spectrum individually emitted by the accelerated electrons, but rather to the spectrum averaged over an acceleration cycle. For the high energies under consideration, the electron energy varies linearly with the magnetic field. If the latter increases sinusoidally to its maximum value in an interval T,

$$E(t)=E_m\sin\frac{\pi}{2}\frac{t}{T}, \tag{II.38}$$

where E_m is the maximum electron energy. Correspondingly,

$$\omega_c(t)=\omega_m\sin^3\frac{\pi}{2}\frac{t}{T}, \tag{II.39}$$

with

$$\omega_m=(3/2)\omega_0(E_m/mc^2)^3. \tag{II.40}$$

The desired average power spectrum is given by

$$\bar{P}(\omega)=\frac{1}{T}\int_0^T P(\omega,t)dt$$
$$=\frac{3^{\frac{1}{2}}}{4\pi}\frac{e^2}{R}\frac{1}{T}\int_0^T dt\left(\frac{E(t)}{mc^2}\right)^4$$
$$\times\frac{\omega_0\omega}{\omega_c^2(t)}\int_{\omega/\omega_c(t)}^\infty K_{5/3}(\eta)d\eta. \tag{II.41}$$

It is convenient to introduce as a new variable

$$\tau=\omega_m/\omega_c(t)=\sin^{-3}\frac{\pi}{2}\frac{t}{T}. \tag{II.42}$$

With the aid of the differential relation

$$\frac{dt}{T}=\frac{2}{3\pi}(\tau^{\frac{2}{3}}-1)^{-\frac{1}{2}}\frac{d\tau}{\tau},$$

(II.41) now reads

$$\bar{P}(\omega)=\frac{3^{\frac{1}{2}}}{2\pi^2}\frac{e^2}{R}\left(\frac{E_m}{mc^2}\right)^4\frac{\omega_0\omega}{\omega_m^2}$$
$$\times\int_1^\infty\frac{\tau^{-\frac{1}{3}}}{(\tau^{\frac{2}{3}}-1)^{\frac{1}{2}}}d\tau\int_{(\omega/\omega_m)\tau}^\infty K_{5/3}(\eta)d\eta. \tag{II.43}$$

The integrals can be simplified with an integration by parts, according to

$$3\int_1^\infty d(\tau^{\frac{2}{3}}-1)^{\frac{1}{2}}\int_{(\omega/\omega_m)\tau}^\infty K_{5/3}(\eta)d\eta$$
$$=3\frac{\omega}{\omega_m}\int_1^\infty(\tau^{\frac{2}{3}}-1)^{\frac{1}{2}}K_{5/3}\left(\frac{\omega}{\omega_m}\tau\right)d\tau.$$

Therefore

$$\bar{P}(\omega)=\frac{3^{\frac{1}{2}}}{2\pi^2}\frac{e^2}{R}\left(\frac{E_m}{mc^2}\right)^4\frac{\omega_0}{\omega_m}F\left(\frac{\omega}{\omega_m}\right) \tag{II.44}$$

or

$$\bar{P}(\omega)=\frac{3^{\frac{1}{2}}}{\pi^2}\frac{e^2}{R}\frac{E_m}{mc^2}F\left(\frac{\omega}{\omega_m}\right), \tag{II.45}$$

where

$$F(x)=x^2\int_1^\infty(\tau^{\frac{2}{3}}-1)^{\frac{1}{2}}K_{5/3}(x\tau)d\tau. \tag{II.46}$$

It can be verified that the total time average power, computed from (II.44) as $\int_0^\infty\bar{P}(\omega)d\omega$, agrees with

the more direct calculation:

$$\bar{P}=\tfrac{2}{3}\omega_0\frac{e^2}{R}\left(\frac{E_m}{mc^2}\right)^4\frac{1}{T}\int_0^T\sin^4\frac{\pi}{2}\frac{t}{T}dt$$
$$=\tfrac{1}{4}\omega_0\frac{e^2}{R}\left(\frac{E_m}{mc^2}\right)^4. \tag{II.47}$$

The asymptotic form of $F(x)$ for $x\gg1$ can be computed in a straightforward manner from the known behavior of $K_{5/3}$ for large argument, with the result:

$$x\gg1: F(x)\sim\frac{\pi}{2}3^{-\frac{1}{2}}e^{-x}\left(1+\frac{7}{18}\frac{1}{x}+\cdots\right). \tag{II.48}$$

The first term in the expansion of $F(x)$ for small x is obtained from the leading term in the expansion of $K_{5/3}$:

$$x\ll1: F(x)=2^{\frac{1}{2}}\Gamma(5/3)x^{\frac{1}{2}}$$
$$\times\int_1^\infty(\tau^{\frac{2}{3}}-1)^{\frac{1}{2}}\tau^{-5/3}d\tau=2^{-\frac{1}{2}}\pi\Gamma(\tfrac{2}{3})x^{\frac{1}{2}}. \tag{II.49}$$

The corresponding average power spectrum,

$$\omega\ll\omega_m: \bar{P}(\omega)=\frac{3^{1/6}}{\pi}\Gamma(\tfrac{2}{3})\frac{e^2}{R}\left(\frac{\omega}{\omega_0}\right)^{\frac{1}{3}},$$

agrees with the first term of (II.20), the energy independent low frequency instantaneous power spectrum. To obtain further terms in an expansion, we observe that

$$\frac{d}{dx}(x^{-\frac{1}{2}}F(x))=-x^{5/3}\int^\infty\tau(\tau^{\frac{2}{3}}-1)^{\frac{1}{2}}K_{2/3}(x\tau)d\tau \tag{II.50}$$

since

$$\frac{d}{dx}(x^{5/3}K_{5/3}(x))=-x^{5/3}K_{2/3}(x). \tag{II.51}$$

By an appropriate change in variable, this becomes

$$\frac{d}{dx}(x^{-\frac{1}{2}}F(x))=-x^{-\frac{1}{2}}\int_x^\infty\xi(\xi^{\frac{2}{3}}-x^{\frac{2}{3}})^{\frac{1}{2}}K_{2/3}(\xi)d\xi, \tag{II.52}$$

and an integration with respect to x, in conjunction with (II.49), yields

$$x^{-\frac{1}{2}}F(x)-2^{-\frac{1}{2}}\pi\Gamma(\tfrac{2}{3})$$
$$=-\int_0^x\eta^{-\frac{1}{2}}d\eta\int_\eta^\infty\xi(\xi^{\frac{2}{3}}-\eta^{\frac{2}{3}})^{\frac{1}{2}}K_{2/3}(\xi)d\xi. \tag{II.53}$$

For small x, the leading terms on the right side of (II.53) are

$$-3x^{\frac{1}{2}}\int_0^\infty\xi^{4/3}K_{2/3}(\xi)d\xi+\tfrac{1}{2}x\int_0^\infty\xi^{\frac{1}{3}}K_{2/3}(\xi)d\xi$$
$$=-\frac{3}{2^{\frac{1}{3}}}\Gamma(\tfrac{1}{2})\Gamma(\tfrac{5}{6})x^{\frac{1}{2}}+2^{-4/3}\Gamma(\tfrac{1}{2})\Gamma(7/6)x,$$

whence

$$x\ll1: F(x)=2^{-\frac{1}{2}}\pi\Gamma(\tfrac{2}{3})x^{\frac{1}{2}}$$
$$\times\left[1-\frac{3}{2^{\frac{1}{2}}\pi^{\frac{1}{2}}}\frac{\Gamma(\frac{5}{6})}{\Gamma(\frac{2}{3})}x^{\frac{1}{2}}+\frac{1}{2\pi^{\frac{1}{2}}}\frac{\Gamma(7/6)}{\Gamma(\frac{2}{3})}x+\cdots\right]. \tag{II.54}$$

The approximate evaluations of $F(x)$ for large and small argument furnish a reasonable qualitative picture of the function. To obtain the complete curve, resort must be had to numerical integration. The result may be seen in Fig. 1 of reference 6, which is essentially a plot of $F(x)$.

We shall conclude this section by briefly examining under what conditions quantum phenomena will invalidate the classical considerations we have presented. This will occur when the momentum of the emitted quantum is comparable with the electron momentum. Hence, for the validity of our classical treatment, it is required that

$$\hbar\omega\ll E,\quad \omega\sim\omega_c,$$

or

$$E/mc^2\ll\left(\frac{R}{\hbar/mc}\right)^{\frac{1}{3}}. \tag{II.55}$$

For a given radius, say $R=10^2$ cm, this sets an upper limit to the electron energy, of the order of 10^{12} ev. However, it must be remembered that in a magnetic device, the radius of the orbit is related to the maximum particle energy, as restricted by the strength of attainable magnetic fields:

$$E=eHR.$$

The limitation (II.55) should thus be written

$$\frac{E}{mc^2}\ll\frac{mc^2}{(e\hbar/mc)H}, \tag{II.56}$$

which implies that, for $H=10^4$ gauss, classical theory will be adequate if the particle energy does not exceed 10^{15} ev.

III. RADIATION BY AN ELECTRON IN UNIFORM CIRCULAR MOTION

In order to obtain the complete spectrum radiated by an accelerated electron, it is necessary to specify the entire trajectory. Accordingly, we shall apply our general method to calculate the radiation properties of an electron moving with constant

speed in a circular path. Since the motion is periodic, the spectrum will consist of harmonics of the rotational angular frequency $\omega_0=v/R$. We shall obtain the total power radiated into each harmonic as well as its angular distribution.[9]

The quantities entering into the formula (I.37) for the spectral distribution are easily evaluated for circular motion. Thus

$$\mathbf{v}(t)\cdot\mathbf{v}(t+\tau)=v^2\cos\omega_0\tau, \tag{III.1}$$

and

$$|\mathbf{R}(t+\tau)-\mathbf{R}(t)|=2R\left|\sin\frac{\omega_0\tau}{2}\right|. \tag{III.2}$$

Furthermore, the periodic nature of the motion can be exploited by writing

$$\omega_0\tau=\varphi+2\pi k, \tag{III.3}$$

and replacing the integration with respect to τ from $-\infty$ to $+\infty$ by one with respect to φ from $-\pi$ to $+\pi$, combined with a summation with respect to the integer k from $-\infty$ to ∞. Thus,

$$P(\omega)=-\frac{e^2}{\pi}\frac{\omega}{\omega_0}\sum_{k=-\infty}^{\infty}\cos 2\pi\frac{\omega}{\omega_0}k \times\int_{-\pi}^{\pi}(1-\beta^2\cos\varphi)\cos\frac{\omega}{\omega_0}\varphi \times\frac{\sin[(2\omega R/c)\sin(\varphi/2)]}{2R\sin\varphi/2}d\varphi. \tag{III.4}$$

However, according to the Poisson sum formula,

$$\sum_{k=-\infty}^{\infty}\cos 2\pi\frac{\omega}{\omega_0}k=\sum_{n=-\infty}^{\infty}\delta\left(\frac{\omega}{\omega_0}-n\right), \tag{III.5}$$

in which n ranges over all integral values. Since ω is restricted to be positive, we obtain

$$P(\omega)=\sum_{n=1}^{\infty}\delta(\omega-n\omega_0)P_n \tag{III.6}$$

with

$$P_n=-n\omega_0\frac{e^2}{R}\frac{1}{2\pi}\int_{-\pi}^{\pi}(1-\beta^2\cos\varphi)\cos n\varphi \times\frac{\sin(2n\beta\sin\varphi/2)}{\sin\varphi/2}d\varphi. \tag{III.7}$$

The discrete nature of the spectrum is now exhibited, with P_n representing the power radiated into the nth harmonic. The latter can be rewritten as

$$P_n=-n\omega_0\frac{e^2}{R}\left[(1-\beta^2)\frac{1}{2\pi}\int_{-\pi}^{\pi}\times\frac{\sin(2n\beta\sin\varphi/2)}{\sin\varphi/2}\cos n\varphi d\varphi +2\beta^2\frac{1}{2\pi}\int_{-\pi}^{\pi}\sin(2n\beta\sin\varphi/2)\times\sin\varphi/2\cos n\varphi d\varphi\right]. \tag{III.8}$$

Both integrals can be expressed in terms of Bessel functions, for the operations of integration and differentiation with respect to z, applied to the equation

$$\frac{1}{2\pi}\int_{-\pi}^{\pi}\cos(z\sin\varphi/2)\cos n\varphi d\varphi=J_{2n}(z), \tag{III.9}$$

yield

$$\frac{1}{2\pi}\int_{-\pi}^{\pi}\frac{\sin(z\sin\varphi/2)}{\sin\varphi/2}\cos n\varphi d\varphi=\int_0^z J_{2n}(x)dx, \tag{III.10}$$

and

$$\frac{1}{2\pi}\int_{-\pi}^{\pi}\sin(z\sin\varphi/2)\times\sin\varphi/2\cos n\varphi d\varphi=-J_{2n}'(z). \tag{III.11}$$

Therefore

$$P_n=n\omega_0\frac{e^2}{R}\left[2\beta^2J_{2n}'(2n\beta)-(1-\beta^2)\int_0^{2n\beta}J_{2n}(x)dx\right]. \tag{III.12}$$

If the electron velocity is small compared to that of light, the dominant term in P_n is

$$\beta\ll 1: P_n=2\omega_0\frac{e^2}{R}(n+1)\frac{n^{2n+1}}{(2n+1)!}\beta^{2n+1}, \tag{III.13}$$

which makes it evident that appreciable power is radiated only into the fundamental frequency. For very large electron energies, $1-\beta^2\ll 1$, and we may place β equal to unity provided n is small compared with a critical harmonic number $n_c\sim(1-\beta^2)^{-\frac{1}{2}}$. Under these circumstances, we have

$$P_n=2n\omega_0\frac{e^2}{R}J_{2n}'(2n). \tag{III.14}$$

[9] See G. A. Schott, *Electromagnetic Radiation* (Cambridge University Press, Cambridge, 1912), pp. 109, 110.

The derivative of the Bessel function with equal order and argument can be approximated by its asymptotic form:[10]

$$J_{2n}'(2n)\sim\frac{3^{1/6}}{2\pi}\Gamma(\tfrac{2}{3})n^{-\frac{1}{3}}, \tag{III.15}$$

with an error that is only 15 percent for $n=1$, and 5 percent for $n=5$. Hence

$$1-\beta^2\ll 1,\quad n\ll n_c: P_n\simeq\frac{3^{1/6}}{\pi}\Gamma(\tfrac{2}{3})\omega_0\frac{e^2}{R}n^{\frac{1}{3}}. \tag{III.16}$$

Evidently the radiated power increases with increasing frequency. To find the behavior of P_n for very high frequencies, we must replace the Bessel functions in (III.12) by their asymptotic forms for large and comparable order and argument.[11] One thus obtains

$$n\gg 1: \int_0^{2n\beta} J_{2n}(x)dx=\frac{1}{3^{\frac{1}{3}}\pi}\int_{n/n_c}^{\infty}K_{1/3}(\eta)d\eta,$$
$$J_{2n}'(2n\beta)=\frac{1}{3^{\frac{1}{3}}\pi}\left(\frac{3}{2n_c}\right)^{\frac{1}{3}}K_{2/3}\left(\frac{n}{n_c}\right), \tag{III.17}$$

with

$$n_c=\tfrac{3}{2}(1-\beta^2)^{-\frac{3}{2}}, \tag{III.18}$$

whence

$$P_n=\frac{3^{\frac{1}{2}}}{4\pi}\omega_0\frac{e^2}{R}\frac{1}{1-\beta^2}\frac{n}{n_c^2}\int_{n/n_c}^{\infty}K_{5/3}(\eta)d\eta, \tag{III.19}$$

on employing the relation (II.15). The discrete spectrum is effectively a continuum if $n\gg 1$. The power radiated into a unit angular frequency interval is

$$P(\omega)=P_{\omega/\omega_0}\frac{1}{\omega_0} \tag{III.20}$$

which yields an expression for $P(\omega)$ that is identical with (II.16), the more general result obtained for a high energy electron traversing an arbitrary trajectory.

The combined spectral and angular distribution function, $P(\mathbf{n},\omega)$, also assumes the form characteristic of a discrete harmonic spectrum:

$$P(\mathbf{n},\omega)=\sum_{n=1}^{\infty}\delta(\omega-n\omega_0)P_n(\mathbf{n}) \tag{III.21}$$

on introducing the periodic nature of the electronic motion. Here

$$P_n(\mathbf{n})=-\frac{e^2}{4\pi^2}\frac{n^2\omega_0^3}{c}\oint\left(1-\frac{1}{c^2}\mathbf{v}(t)\cdot\mathbf{v}(t+\tau)\right)$$
$$\times\cos n\omega_0\left(\tau-\frac{1}{c}\mathbf{n}\cdot(\mathbf{R}(t+\tau)-\mathbf{R}(t))\right)d\tau, \tag{III.22}$$

in which the integration is extended over one traversal of the orbit. This quantity still involves the arbitrary initial phase of the electron in its circular path. An average with respect to t is equivalent to averaging over the initial phase. Further, the integrations with respect to t and $t+\tau=t'$ can be performed independently, which brings (III.22) into the form

$$P_n(\mathbf{n})=-\frac{e^2}{8\pi^3}\frac{n^2\omega_0^4}{c}\oint\left(1-\frac{1}{c^2}\mathbf{v}(t)\cdot\mathbf{v}(t')\right)$$
$$\times\exp\left[in\omega_0\left(t'-t-\frac{1}{c}\mathbf{n}\cdot(R(t')-\mathbf{R}(t))\right)\right]dtdt', \tag{III.23}$$

in which it is understood that the real part is to be taken. We may now conveniently introduce a special coordinate system in which the xy plane is that of the orbit, and the unit vector $\mathbf{n}$ lies in the xz plane, at an angle ψ relative to the orbital plane. In terms of the polar coordinates φ and φ' for the points $\mathbf{R}(t)$ and $\mathbf{R}(t')$, we have

$$\mathbf{n}\cdot\mathbf{R}(t)=R\cos\psi\cos\varphi,\quad \mathbf{n}\cdot\mathbf{R}(t')=R\cos\psi\cos\varphi'$$
$$\frac{1}{c^2}\mathbf{v}(t)\cdot\mathbf{v}(t')=\beta^2\cos(\varphi-\varphi'),$$

and

$$\omega_0 dt=d\varphi,\quad \omega_0 dt'=d\varphi',$$

whence

$$P_n(\psi)=\frac{e^2}{8\pi^3}\frac{n^2\omega_0^2}{c}$$
$$\times\int_0^{2\pi}(\beta^2\cos\varphi\cos\varphi'$$
$$+\beta^2\sin\varphi\sin\varphi'-1)$$
$$\times\exp[in\beta\cos\psi\cos\varphi-in\varphi]$$
$$\times\exp[-in\beta\cos\psi\cos\varphi'+in\varphi']d\varphi d\varphi'. \tag{III.24}$$

The integrals can be expressed in terms of Bessel

[10] Reference 7, p. 260.
[11] Reference 7, p. 248.

functions. From the well-known integral

$$\frac{1}{2\pi}\int_0^{2\pi} \exp[iz\cos\varphi - in\varphi]d\varphi = i^n J_n(z), \quad \text{(III.25)}$$

we derive

$$\frac{1}{2\pi}\int_0^{2\pi} \exp[iz\cos\varphi - in\varphi] \times\cos\varphi d\varphi = i^{n-1}J_n'(z), \quad \text{(III.26)}$$

and

$$\frac{1}{2\pi}\int_0^{2\pi} \exp[iz\cos\varphi - in\varphi] \times\sin\varphi d\varphi = -i^n(n/z)J_n(z) \quad \text{(III.27)}$$

by differentiation with respect to z and integration by parts, respectively. Therefore,

$$P_n(\psi) = \omega_0\frac{e^2}{R}\beta^3\frac{n^2}{2\pi}\left[(J_n'(n\beta\cos\psi))^2 + \sin^2\psi\left(\frac{J_n(n\beta\cos\psi)}{\beta\cos\psi}\right)^2\right], \quad \text{(III.28)}$$

which yields the power radiated, in the nth harmonic, into a unit solid angle at the angle ψ with the orbital plane.

For $\beta\cos\psi \ll 1$, the leading term in (III.28) is

$$\frac{1}{2\pi}\omega_0\frac{e^2}{R}\beta\frac{(n\beta/2)^{2n}}{[(n-1)!]^2}(\cos\psi)^{2n-2}(1+\sin^2\psi),$$

which shows that the power radiated decreases rapidly with increasing harmonic number in either of two situations; emission by a low energy electron in any direction, or emission by a high energy electron in a direction almost normal to the orbital plane. On the other hand, the power radiated in the orbital plane by a very high energy electron is described by

$$1-\beta^2 \ll 1 : P_n(0) = \omega_0\frac{e^2}{R}\frac{n^2}{2\pi}(J_n'(n))^2 \simeq \frac{6^{\frac{1}{2}}}{4\pi^3}(\Gamma(\tfrac{2}{3}))^2\omega_0\frac{e^2}{R}n^{\frac{1}{3}}, \quad \text{(III.29)}$$

provided $n \ll n_c$. Evidently the power radiated in this direction increases with increasing frequency. To find the behavior at very high frequencies, without restriction to $\psi = 0$, we must employ the asymptotic forms of the Bessel functions for large order and argument:

$$1-\beta^2 \ll 1, \quad \psi^2 \ll 1, \quad n \gg 1:$$

$$J_n(n\beta\cos\psi) = \frac{1}{3^{\frac{1}{2}}\pi}(1-\beta^2+\psi^2)^{\frac{1}{4}}K_{1/3}(\xi),$$

$$J_n'(n\beta\cos\psi) = \frac{1}{3^{\frac{1}{2}}\pi}(1-\beta^2+\psi^2)\,K_{2/3}(\xi), \quad \text{(III.30)}$$

where

$$\xi = \frac{n}{n_c}\left(1+\frac{\psi^2}{1-\beta^2}\right)^{\frac{3}{2}}. \quad \text{(III.31)}$$

We obtain

$$P_n(\psi) = \frac{1}{6\pi^2}\omega_0\frac{e^2}{R}n^2(1-\beta^2+\psi^2)^2 \times\left[K_{2/3}^2(\xi) + \frac{\psi^2}{1-\beta^2+\psi^2}K_{1/3}^2(\xi)\right]. \quad \text{(III.32)}$$

On replacing this quantity by

$$P(\psi, \omega) = (2\pi/\omega_0)P_{\omega/\omega_0}(\psi), \quad \text{(III.33)}$$

the power radiated into a unit angular frequency range and a unit angular interval (rather than unit solid angle), we encounter a formula that is identical with (II.32), or (II.34), the more general result obtained for a high energy electron traversing an arbitrary trajectory.

PHYSICAL REVIEW VOLUME 75, NUMBER 12 JUNE 15, 1949

On Generalizing Boson Field Theories

ALEX E. S. GREEN
Department of Physics, University of Cincinnati, Cincinnati, Ohio
(Received December 13, 1948)

If a boson field theory is generalized to admit in the field Lagrangian all the derivatives of the field coordinates up to the σth in a particularly symmetrical way, then we find that in the final expression for the interaction energy of fermions the usual interaction is replaced by a weighted sum of σ such interactions, where the relative weight factor and the boson mass associated with each interaction are given uniquely by algebraic relationships involving the constants appearing in the field Lagrangian. We thus are able to formulate a simple principle for obtaining the interaction energy according to a multiple-boson theory of the form suggested by our generalizations if the interaction energy is known for the one-boson case. The principle is then applied to the non-relativistic and relativistic interaction terms for electrons according to electrodynamic (photon) field theory, and for nucleons according to the meson field theories investigated by Kemmer. We find that in almost every case the weight factors are such that not only are the inadmissible R^{-3} and R^{-2} singularities removed, but also in three- and four-boson theory, the objectionable R^{-1} singularities. A closely related result is the fact that generalization justifies the neglect of short wave-lengths in the evaluation of the interaction and self-energy integrals.

1. THE BOSON FIELD

CONSIDER the quadratic Lagrangian density

$$L=(1/2a^2)\sum_\sigma c_\sigma a^{2\sigma} Q_{\lambda_\sigma} Q_{\lambda_\sigma}, \tag{1.1}$$

where a is a length, the c's are dimensionless natural constants, $Q(x_\nu)$ the field coordinate is a real or imaginary potential, $x_\nu=(\mathbf{r}, ict)$, $\partial_{\lambda_1}=\partial/\partial x_{\lambda_1}$ and $Q_{\lambda_\sigma}=\partial_{\lambda_1}\partial_{\lambda_2}\cdots\partial_{\lambda_\sigma}Q$. Applying the variational equation

$$ic\delta W=ic\delta\int\int L dV dt=\delta\int L d\Omega=0, \tag{1.2}$$

using

$$Q_{\lambda_\sigma}\delta Q_{\lambda_\sigma}=(-\Box)^\sigma Q\delta Q + \partial_\nu\left\{\sum_{\tau=0}^{\sigma-1}[(-\Box)^{\sigma-1-\tau}\partial_\nu Q_{\lambda_\tau}]\delta Q_{\lambda_\tau}\right\}, \tag{1.3}$$

and assuming that the potential and all derivatives up to the order $\sigma-1$ are held constant on the boundaries of the four-dimensional space, we obtain the equation of motion

$$[\textstyle\sum_\sigma c_\sigma a^{2\sigma}(-\Box)^\sigma]Q=0. \tag{1.4}$$

Alternatively, in performing the variation we may obtain the same equation of motion by using in place of Eq. (1.3), the relation

$$Q_{\lambda_\sigma}\delta Q_{\lambda_\sigma}=(-\Box)^\sigma Q\delta Q + \sum_{\tau=1}^{\sigma}\left\{\binom{\sigma}{\tau}[(-\Box)^{\sigma-\tau}Q_{\lambda_\tau}]\delta Q\right\}_{\lambda_\tau}. \tag{1.5}$$

Applying Gauss's theorem to convert successively the τ-dimensional integral of a divergence into $\tau-1$-dimensional integrals, we need only insist that the potential be held constant on the boundaries providing in four-space the Lagrangian contains only derivatives up to the fourth. This latter generalization is thus a less radical departure from the usual Hamilton's principle.

We define the energy momentum tensor $t_{\mu\nu}$ and the energy momentum four-vector P_μ by

$$\delta W=\int t_{\mu\nu}ds_\nu\delta x_\mu=P_\mu\delta x_\mu, \tag{1.6}$$

where δx_μ represents a displacement of a space-like boundary, and the potential satisfies Eq. (1.4) throughout the four-dimensional domain. Using (1.3), Gauss theorem, and

$$\delta Q_{\lambda_\tau}=-(\partial_\mu Q_{\lambda_\tau})\delta x_\mu, \tag{1.7}$$

we find that

$$ict_{\mu\nu}=L\delta_{\mu\nu}-(1/a^2)\textstyle\sum_\sigma c_\sigma a^{2\sigma} \times\left\{\sum_{\tau=0}^{\sigma-1}[(-\Box)^{\sigma-1-\tau}\partial_\nu Q_{\lambda_\tau}]\partial_\mu Q_{\lambda_\tau}\right\}. \tag{1.8}$$

These results may also be obtained by application of the formulas of Chang[1] to our particular Lagrangian. We may show without difficulty that $\partial_\nu t_{\mu\nu}=0$, thus insuring conservation of energy and momentum, and also that the antisymmetric part of $t_{\mu\nu}$ is a four-divergence.

The equation of motion of the field may be written as

$$[\Pi_\sigma(\Box-\xi_\sigma^2/a^2)]Q(x_\nu)=0, \tag{1.9}$$

where ξ_σ^2 are the roots (dimensionless) of

$$F(\xi^2)=\textstyle\sum_\tau c_\tau(-\xi^2)^\tau=0. \tag{1.10}$$

In view of the basic position of wave motion in field phenomenon, it is satisfactory that our Lagrangian leads directly to a wave equation. A solution of Eq. (1.9) is the generalized Fourier

[1] T. S. Chang, Proc. Camb. Phil. Soc. **44**, 76 (1948).

integral

$$Q(x_\nu)=(1/2\pi)^{\frac{1}{2}}\sum_\sigma\int[Q_\sigma(\mathbf{k})\exp(ik_{\sigma\nu}x_\nu)+Q_\sigma^*(\mathbf{k})\exp(-ik_{\sigma\nu}x_\nu)]d\mathbf{k}, \quad (1.11)$$

where

$$k_{\sigma\nu}=(\mathbf{k}, ik_\sigma) \text{ and } k_\sigma^2-\mathbf{k}\cdot\mathbf{k}=\xi_\sigma^2/a^2=\kappa_\sigma^2. \quad (1.12)$$

Comparing Eq. (1.12) with the energy momentum relationship of special relativity, we find that $\xi_\sigma=am_\sigma c/\hbar$ where m_σ are the masses of the bosons associated with the field. If the masses are to be real, then the c's in the Lagrangian must all have the same parity.

Using Eqs. (1.8) and (1.11) we may express the energy momentum four-vector in terms of Fourier amplitudes. As an aid to calculation we use a boundary corresponding to instantaneous space and discard all time-dependent terms. Both steps are permissible because $\partial_\nu t_{\mu\nu}=0$. We obtain

$$P_\mu=\sum_\sigma(\gamma_\sigma/c)\int k_{\sigma\mu}k_\sigma[Q_\sigma(\mathbf{k})Q_\sigma^*(\mathbf{k})+Q_\sigma^*(\mathbf{k})Q_\sigma(\mathbf{k})]d\mathbf{k}, \quad (1.13)$$

where

$$\gamma_\sigma=-\sum_\tau \tau c_\tau(-\xi_\sigma^2)^{\tau-1}=[dF/d\xi^2]_{\xi=\xi_\sigma}. \quad (1.14)$$

The γ's which arise naturally in our theory during this last calculation are factors which weight the fields associated with the different bosons. They alternate in parity, which means that alternate bosons make negative contributions to the total energy and momentum of the field. From (1.13) we see that the field Hamiltonian has the form

$$H=\sum_\sigma\gamma_\sigma\int k_\sigma^2[Q_\sigma(\mathbf{k})Q_\sigma^*(\mathbf{k})+Q_\sigma^*(\mathbf{k})Q_\sigma(\mathbf{k})]d\mathbf{k}. \quad (1.15)$$

This same expression would be obtained from a field Hamiltonian of the form

$$H=\sum_\sigma(\gamma_\sigma/2)\int\{\kappa_\sigma^2[Q_\sigma(x_\nu)]^2+[\nabla Q_\sigma(x_\nu)]^2+\pi_\sigma^2\}dV, \quad (1.16)$$

where $\pi_\sigma=\partial Q_\sigma(x_\nu)/c\partial t$. Our Hamiltonian is thus a weighted sum of σ-terms, each of the form usually used as a starting point in the treatment of the boson field.

2. THE INTERACTION OF FERMIONS

In the field theoretic treatment of the interaction of two fermions which are coupled by a boson field, one may assume that the interaction Hamiltonian involves only the potentials as (for example) in the charge-like interaction

$$H_i=gQ(x_j^a)+gQ(x_j^b), \quad (2.1)$$

or their first derivatives, as in the dipole-like interaction

$$H_i=-ga[\boldsymbol{\sigma}^a\cdot\nabla Q(x_j^a)+\boldsymbol{\sigma}^b\cdot\nabla Q(x_j^b)]. \quad (2.2)$$

The g's are coupling constants having the dimension of charge, and a is a length which must now be identified with the Compton wave-length of the fermion. In the generalized cases we simply replace $Q(x_j)$ by $\sum_\sigma Q_\sigma(x_j)$. Taking either (2.1) or (2.2) in conjunction with (1.16), we obtain, after application of a classical[2] or quantum-mechanical formalism, the chief interactions

$$V_{ab}=-\sum_\sigma(g^2/4\pi\gamma_\sigma R)\exp(-\kappa_\sigma R), \quad (2.3)$$

$$V_{ab}=a^2(\boldsymbol{\sigma}^a\cdot\nabla)(\boldsymbol{\sigma}^b\cdot\nabla)\sum_\sigma(g^2/4\pi\gamma_\sigma R)\times\exp(-\kappa_\sigma R). \quad (2.4)$$

These two special cases demonstrate the general principle governing the change in the interaction energy between fermions which takes place in going from a one-boson theory to the corresponding generalized boson theory. The principle which also follows from general considerations may be stated in two ways.

1. If a one-boson theory gives an interaction energy V, then the corresponding result according to generalized theory is $\sum_\sigma V_\sigma/\gamma_\sigma$.

2. If a one-boson theory gives an interaction energy of the form oJ where o is an operator which does not involve the Compton wave-length of the boson, then the corresponding result according to generalized theory is $o\sum_\sigma J_\sigma/\gamma_\sigma$.

The principle is changed in no way when applied to a theory based upon a vector or tensor field having a plurality of components, or a field with two or three components in isotopic space such as the charged or symmetric theories, providing each component has been introduced and treated in a manner suitable for generalization. Unfortunately, it is sometimes difficult to determine whether these conditions are fulfilled because of the variety of complicated mathematical treatments given to theories which are actually identical in physical

TABLE I. Parity of combinations for positive c's.

i	−2	−1	0	1	2	3	4	5	6
I	−	−	−	−	−	−	−	−	−
II	−	−	0	+	+	+	+	+	+
III	−	−	0	+	0	−	−	−	−
IV	−	−	0	+	0	−	0	+	+

[2] W. Pauli, *Meson Theory of Nuclear Forces* (Interscience Publishers, Inc., New York, 1946), pp. 4–7.

substance. Further, the Lagrangian used may appear quite different from a sum of our one-boson Lagrangians, yet only differ from such a sum by a four-divergence. It may also happen that actual differences in the field Lagrangian are compensated for by the auxiliary conditions or by the symmetry conditions imposed on the potentials. In cases which are doubtful, the principle may be applied on heuristic grounds.

In ordinary meson theory, J is the Yukawa potential which may be written

$$J^{\mathrm{I}}=-(g^2/4\pi a c_1\rho)\exp(-\xi\rho)$$
$$=-(g^2/4\pi a c_1)(1/\rho-\xi+\xi^2\rho/2-\xi^3\rho^2/6+\cdots), \quad (2.5)$$

where $\rho=R/a$ and $\gamma=-c_1$.

In ordinary electrodynamics, J is the Coulomb potential which is simply a special case of the above, corresponding to $\xi=0$.

For higher degrees of generalization we have, upon inserting the explicit expressions for the γ's,

$$J^{\mathrm{II}}=-(g^2/4\pi a c_2\nabla_{21}\rho)\times[\exp(-\xi_1\rho)-\exp(-\xi_2\rho)], \quad (2.6)$$

$$J^{\mathrm{III}}=-(g^2/4\pi a c_3\nabla_{21}\nabla_{31}\nabla_{32}\rho)[\nabla_{32}\exp(-\xi_1\rho)-\nabla_{31}\exp(-\xi_2\rho)+\nabla_{21}\exp(-\xi_3\rho)], \quad (2.7)$$

$$J^{\mathrm{IV}}=-(g^2/4\pi a c_4\nabla_{21}\nabla_{31}\nabla_{32}\nabla_{41}\nabla_{42}\nabla_{43}\rho)\times[\nabla_{32}\nabla_{42}\nabla_{43}\exp(-\xi_1\rho)-\nabla_{31}\nabla_{41}\nabla_{43}\exp(-\xi_2\rho)+\nabla_{21}\nabla_{41}\nabla_{42}\exp(-\xi_3\rho)-\nabla_{21}\nabla_{31}\nabla_{32}\exp(-\xi_4\rho)], \quad (2.8)$$

where $\nabla_{21}=\xi_2^2-\xi_1^2$, etc. It may be verified that these functions are static solutions of Eq. (1.4). The power series expansion of J^{I} suggests that in generalized theory we investigate the properties of $\sum_\sigma \xi_\sigma{}^i/\gamma_\sigma$ for various integral i's, a study which may be carried out by algebraic methods. It turns out that the parities of these combinations are independent of the magnitudes of the ξ's. They are given in Table I for positive c's (reverse each sign for negative c's).

Now in the various forms of field theory, J appears in interaction terms preceded by differential operators which result in combinations such as J'/R, $R(J'/R)'$, $R^{-2}(R^2J')'$, and $R^3[(J'/R)'/R]'$ (where prime denotes differentiation with respect to R). Upon carrying out these differentiations, we observe that the zeros of $\sum_\sigma \xi_\sigma{}^i/\gamma_\sigma$ occur at exactly the critical values of i, which cause the elimination of the R^{-3}, R^{-2}, and R^{-1} singularities which would ordinarily appear.[3] This remarkable result is closely related to a consequence of generalized theory which may be noted by examining the quantum field theory expression for our generalized potential, namely

$$J=[g^2/(2\pi)^3]\times\int\{\textstyle\sum_\sigma \exp[ik_{\sigma\nu}(x_\nu{}^b-x_\nu{}^a)]\}/2\mathbf{k}_\sigma{}^2\gamma_\sigma\}d\mathbf{k}. \quad (2.9)$$

Setting the times equal, and integrating over the angles in polar k space, we obtain

$$J=[g^2/(2\pi)^2]\times\int_0^\infty[\textstyle\sum_\sigma k\sin(kR)/\gamma_\sigma R(k^2+\kappa_\sigma{}^2)]dk, \quad (2.10)$$

for large values of k the integrand is

$$\textstyle\sum_\sigma[\sin(kR)/kR](1/\gamma_\sigma-\xi_\sigma{}^2/\gamma_\sigma k^2a^2+\xi_\sigma{}^4/\gamma_\sigma k^4a^4-\cdots). \quad (2.11)$$

In generalized theories this integrand vanishes strongly even in the unfavorable case for $R=0$ which arises in the self-energy calculation. If the J in Eq. (2.10) is preceded by a differential operator, then after differentiation, terms with additional k's in the numerator of the integrand will appear. In these cases it will be the zeros of $\sum_\sigma \xi_\sigma{}^i/\gamma_\sigma$ for $i=2$, 4, etc. which will make the integrand vanish for short wave-lengths. Integrating (2.10) we get our generalized potential

$$J=\textstyle\sum_\sigma(g^2/4\pi a\gamma_\sigma\rho)\exp(-\xi_\sigma\rho).$$

3. THE INTERACTION OF ELECTRONS

The field Lagrangian often used as a starting point in ordinary electrodynamics is a sum of four terms of the form (1.1) corresponding to $c_1=-1$, and all the other c's equal to zero.[4,5] The interaction energy for one photon processes which follows from the usual quantum theory is Breit's interaction,

$$V=[1-\boldsymbol{\alpha}^a\cdot\boldsymbol{\alpha}^b/2+(1/2R)\times(\boldsymbol{\alpha}^a\cdot\mathbf{R})(\boldsymbol{\alpha}^b\cdot\mathbf{R})d/dR]J=\mathfrak{B}J, \quad (3.1)$$

where J is the Coulomb potential and $\mathfrak{B}$ is Breit's operator.

To obtain the interaction energy of electrons on a generalized theory which admits second derivatives of the field coordinates, as in the theories initiated by Bopp[6] and by Podolsky,[7] we replace the Coulomb potential by the non-singular potential given by (2.6) with $\xi_1=0$. The same result follows from a detailed investigation.[8] For further generalization of electrodynamics we use (2.7) or (2.8).

A reduction of the 16-component Dirac wave equation to a 4-component Pauli form[9] shows that

[3] The reader is invited to test Table I and these results with arbitrary numbers for the ξ's.

[4] L. Rosenfeld, Zeits. f. Physik **76**, 731 (1932), Eq. (8).
[5] J. Schwinger, Phys. Rev. **74**, 1442 (1948), Eq. (1.9).
[6] F. Bopp, Ann. d. Physik **38**, 345 (1940).
[7] B. Podolsky, Phys. Rev. **62**, 68 (1942).
[8] A. E. S. Green, Phys. Rev. **72**, 628 (1947).
[9] G. Breit, Phys. Rev. **51**, 258 (1937).

the relativistic interaction terms (retardation, spin orbit, spin-spin, tensor force, and Dirac character), which arise at this stage of approximation, are associated with the derivatives of J previously listed. Thus, we find that all the R^{-3} and R^{-2} singularities vanish upon generalization as well as the R^{-1} singularities (which are here not objectionable) in the three- and four-boson cases.

4. THE INTERACTION OF NUCLEONS

The most extensive investigation of the interaction of nucleons due to one-meson fields is that of Kemmer;[10] who derived eight distinct meson interactions. After making the necessary modifications in constants, his results for neutral mesons in the non-relativistic limit may be written (in obvious notation) as

$$V_{vg}=J=-V_{sg}, \quad (4.1) \qquad V_{sf}=V_{psf}=0, \quad (4.2)$$

$$V_{vf}=2\sigma^a\cdot\sigma^b a^2R^{-2}(R^2J')'/3 - S_{ab}a^2R(J'/R)'/3=-V_{pvf}, \quad (4.3)$$

$$V_{psg}=\sigma^a\cdot\sigma^b a^2R^{-2}(R^2J')'/3 + S_{ab}a^2R(J'/R)'/3=-V_{pvg}, \quad (4.4)$$

where $S_{ab}=3(\sigma^a\cdot\mathbf{R}/R)(\sigma^b\cdot\mathbf{R}/R)-\sigma^a\cdot\sigma^b$.

We see that all of the usual Kemmer interactions become well behaved upon generalization because of the immunity of our generalized potential to singularities when subjected to the above operators. Here it is advantageous to go to the three- or four-meson case to eliminate the R^{-1} singularities which are now objectionable because of the infinite self-energies they imply.

Consider for further illustration several of Kemmer's relativistic forms.

$$V_{sg}'=-\beta^a\beta^b J, \quad (4.5)$$

$$V_{sf}'=a^2(\alpha^a\cdot\nabla)(\alpha^b\cdot\nabla)J, \quad (4.6)$$

$$V_{vg}'=[1-\alpha^a\cdot\alpha^b+(1/\kappa^2)(\alpha^a\cdot\nabla)(\alpha^b\cdot\nabla)]J. \quad (4.7)$$

The relativistic terms due to V_{sg}', V_{sf}', and the first two parts of V_{vg}' are well behaved in the generalized cases, however, a retardation term and spin orbit term arising from $(1/\kappa^2)(\alpha^a\cdot\nabla)(\alpha^b\cdot\nabla)J$ have inadmissible singularities which do not vanish upon generalization. By an alternate formalism involving, among other things, a different treatment of the supplementary conditions, the writer has obtained in this case[11] the interaction $V_{vg}'=\mathfrak{B}J$, whose relativistic terms are well behaved in the generalized cases. The complications which arise in the treatment of the supplementary conditions, however, require that the efficacy of generalization for the relativistic terms in the vector and also in the pseudo-vector case be regarded as provisional.

The fact that the generalized meson potential and its important derivatives have simple, well-behaved shapes enables us to compare qualitatively the results of the numerous possible generalized meson theories with the more successful phenomenological theories. We can thus readily find one-meson interactions which, upon generalization, will account roughly for the position of the ^3S and ^1S levels of the deuteron and the sign of the quadrupole moment. However, to arrive at quantitative conclusions concerning these and other equations would require a specific assignment of the meson masses and the g or f (or g's and f's if more than one force is used) followed by detailed numerical computations. Such a task involving a many-parameter set of numerical computations might appropriately be undertaken by a computation laboratory.

Examples of generalized potentials which correspond to meson masses which have been reported are[12,13]

$$J=\mp(A/\rho)[\exp(-0.10\rho)-1.07\exp(-0.16\rho) +0.07\exp(-0.5\rho)], \quad (4.8)$$

$$J=\mp(B/\rho)[\exp(-0.05\rho)-1.527\exp(-0.10\rho) +0.530\exp(-0.16\rho) -0.003\exp(-0.5\rho)]. \quad (4.9)$$

There is an intimate connection between generalized meson theories and mixture theories. Thus, a two-meson generalization of V_{sg} will give *exactly* the interaction obtained by mixing V_{sg} with V_{vg} where the masses are different but the couplings are equal. A three-meson generalization of V_{sg} will give *exactly* the interaction obtained by mixing two V_{sg}'s with one V_{vg} where the masses are different and the relative couplings are determined by (2.7). A similar conclusion follows for the four-meson generalization and for the other sets.

It must be noted that, although the mixture theories which have been used are the least objectionable of the relativistic theories of nuclear forces, they may be criticized (1) for their *ad hoc* nature, (2) for the inadmissible singularities which persist amongst the relativistic terms,[14] and (3) for their failure in quantitative details.[15] Generalized theories are certainly free from the first objection and quite possibly from the second. It remains to be seen whether other theoretical objections will be raised to generalization, and whether a generalized meson theory will succeed in quantitatively accounting for nuclear phenomenon.

[10] N. Kemmer, Proc. Roy. Soc. **A166**, 127 (1938).
[11] A. E. S. Green, Phys. Rev. **73**, 26 (1948).
[12] Lattes, Occhialini, and Powell, Nature **160**, 453 (1947).
[13] L. Leprince-Ringuet and M'Lheritier, J. de Phys. et rad. **7**, 66 (1946).
[14] Ning Hu, Phys. Rev. **67**, 339 (1945).
[15] W. H. Ramsey, Proc. Phys. Soc. **61**, 297 (1948).

Radially Symmetric Distributions of Matter

MAX WYMAN
Department of Mathematics, University of Alberta, Edmonton, Alberta, Canada
(Received November 22, 1948)

Several of the known solutions of the Einstein field equations are re-examined and it is shown that these solutions are special cases of more general solutions of the field equations. The explicit solution of the field equations in terms of known functions is also found for the case of Volkoff's massive spheres. In the last section of this paper a mathematical procedure for generating solutions of the field equations is outlined.

1. INTRODUCTION

IN a paper published some time ago R. C. Tolman[1] pointed out some of the difficulties in obtaining explicit solutions of Einstein's gravitational equations in terms of known analytic functions. It was pointed out how few such solutions were known, and in this paper methods were considered by means of which eight solutions were obtained. Some of these solutions had been discovered by other people using different methods. Tolman considered a sphere of fluid at rest in a coordinate system for which the line element has the form:

$$ds^2=e^{\nu}dt^2-e^{\lambda}dr^2-r^2d\theta^2-r^2\sin^2\theta d\phi^2, \qquad (1.1)$$

where λ, ν are unknown functions of r alone. For an isotropic sphere of fluid described by (1.1) the pressure p and density ρ must satisfy the relations:

$$8\pi p=e^{-\lambda}(\nu'/r+1/r^2)-1/r^2, \qquad (1.2)$$

$$8\pi p=e^{-\lambda}(\nu''/2-\lambda'\nu'/4+(\nu'-\lambda')/2r+\nu'^2/4), \qquad (1.3)$$

$$8\pi\rho=e^{-\lambda}(\lambda'/r-1/r^2)+1/r^2, \qquad (1.4)$$

$$p'=-(p+\rho)\nu'/2, \qquad (1.5)$$

where the prime denotes differentiation with respect to r.

It is well known that the equality of (1.2) and (1.3) automatically ensures that (1.5) is satisfied. For this reason the mathematical problem resolves itself into obtaining solutions of the equation resulting from the equality of (1.2) and (1.3). Since we have two unknowns λ and ν and only one equation the problem is indeterminate as it stands. In order to ensure a unique solution it is necessary to add a second relation involving λ and ν. The most satisfactory procedure would be to choose this relation by means of some physical condition, say an equation of state involving p and ρ which would then ensure that the resulting solution would be of physical interest. Tolman has pointed out however that such a procedure is almost impossible to carry through because of the complicated non-linear character of the expressions involved. For this reason, the usual procedure is to choose the auxiliary relation so that a mathematical simplification takes place in the equation to be solved. This procedure is not too satisfactory in that most of the solutions obtained in this way will not be of physical interest.

It is useful to point out one or two guiding principles in generating solutions of the field equations. If one assumes that the distribution of density $\rho=\rho(r)$ is known, then (1.4) can be integrated to determine $e^{-\lambda}$. For $e^{-\lambda}$ known, the equality of (1.2) and (1.3) results in a Riccati equation of the first order in ν'. It is of course well known that this equation is not in general solvable by quadratures but there exists an extensive literature on the equation which can be used to find solutions expressible in terms of known functions. If it is assumed that the gravitational potential e^{ν} is known, then the equality of (1.2) and (1.3) yields a linear equation of the first order in $e^{-\lambda}$. Such equations can always be solved by quadratures.

In our present paper we shall use the methods briefly outlined above to obtain several new solutions of the gravitational field equations. We shall also re-examine several of the known solutions and show how they can be generalized.

2. BOUNDARY CONDITIONS

For a line-element of the form (1.1), the Schwarzschild exterior solution is known to be:

$$e^{\nu}=e^{-\lambda}=1-2m/r, \qquad (2.1)$$

where m is the mass of the sphere as measured by its external gravitational field. For this reason any solution for e^{ν} and e^{λ} valid in the interior of this sphere must satisfy the relations:

$$e^{\nu}=e^{-\lambda}=1-2m/r_b, \qquad (2.2)$$

where r_b is the value of r at the boundary of the sphere. In addition we require the pressure p to vanish when $r=r_b$.

From (1.2) this implies:

$$e^{-\lambda}(r\nu'+1)-1=0, \quad \text{at} \quad r=r_b. \qquad (2.3)$$

Since $e^{-\lambda}$ is continuous at the boundary, the three

[1] R. C. Tolman, Phys. Rev. **55**, 364 (1939).

boundary conditions are equivalent to the requirement that e^{ν}, $e^{\nu}\nu'$, and $e^{-\lambda}$ be continuous across the boundary of the sphere. From this it is easy to see that the solutions of the field equations which we seek will be such that e^{ν} contains two arbitrary constants, and $e^{-\lambda}$ contains one such constant.

3. VOLKOFF'S MASSIVE SPHERES

When the density ρ is taken to be constant Eq. (1.4) can be integrated to give

$$e^{-\lambda}=(x-x^3+K)/x, \tag{3.1}$$

where $x=r/R$ and $R^2=3/8\pi\rho$, and K is an arbitrary constant of integration. In order to avoid a singularity at the origin, Schwarzschild took $K=0$ and proceeded to find his well-known interior solution. By means of this solution it was possible to conclude that there must be an upper limit to the size of a sphere of given density. More recently G. M. Volkoff[2] has considered non-zero values of K and has shown that solutions exist for which the possible size of the sphere increases beyond that predicted by Schwarzschild. In fact, by increasing K indefinitely the possible size also increases indefinitely. Unfortunately several of the statements in Volkoff's paper are incorrect and he did not obtain his results in as complete a form as possible.

In the above mentioned paper Volkoff obtains the equation

$$d\mathrm{P}/dx=-[(\mathrm{P}+3)(\mathrm{P}x^3+v)/2x(x-v)], \tag{3.2}$$

where P is a quantity proportional to the pressure p and $v=x^3-K$. Volkoff states that Eq. (3.2) can not be explicitly integrated in terms of known functions. This statement is incorrect as (3.2) is an equation of Riccati type for which an obvious solution is $\mathrm{P}=-3$. It is well known that Riccati equations for which one solution is known can be integrated by quadrature. In fact we shall show that the integrals involved are elliptic integrals. It is also stated that solutions exist which behave near the origin like $\mathrm{P}\sim 7K/x^3$. Since all the solutions do not behave in this manner it is obvious that a behavior of this type at the origin implies some condition involving K. This condition is not given by Volkoff, but we shall be able to obtain it by carrying through the explicit integration of the field equations.

From the boundary condition to be satisfied by $e^{-\lambda}$, (3.1) implies

$$2m/R=x_b^3-K, \tag{3.3}$$

where $x_b=r_b/R$. Numerical integration of (3.2) for several different values of K showed that $x_b\sim x_1$, where x_1 is positive solution of the equation

$$x_1-x_1^3+K=0. \tag{3.4}$$

From (3.3) it was argued that $x_b\sim x_1$ implied that

$$2m/R\sim x_1^3-K=x_1\sim x_b. \tag{3.5}$$

This argument is not correct. If we let $x=x_1-\delta$, where δ is a small correction term and drop all terms involving δ^2 we find

$$2m/R=x_1^3+3x_1^2\delta-K=x_1+3x_1^2\delta\sim x_b+3x_1^2\delta. \tag{3.6}$$

Thus for (3.5) to be correct it is necessary to show that for large value of x_1, $3x_1^2\delta$ is still small compared to x_b. As a numerical example we quote the value $K=80/7$ for which Volkoff obtains $x_b=2.39+$. Assuming that $2.39+$ means that x_b could probably be as large as 2.395 we find from (3.3) the largest possible value of $2m/R$ to be 2.31 and not $2.39+$ as quoted by Volkoff. The behavior of $2m/R$ for large values of K cannot be determined from (3.3) alone. It is not possible to discuss this behavior until the condition on K is determined which makes $\mathrm{P}\sim 7K/x^3$ for small values of x.

In order to find the general solution of the field equations we note that for constant ρ Eq. (1.5) can be integrated to give

$$8\pi(p+\rho)=ae^{-\nu/2}. \tag{3.7}$$

Adding (1.2) and (1.4) and using (3.7) we find

$$e^{-\lambda}(\nu'+\lambda')=ae^{-\nu/2}. \tag{3.8}$$

Hence

$$(d/dr)(e^{\nu/2})+(\lambda'/2)(e^{\nu/2})=(ar/2)e^{\lambda}. \tag{3.9}$$

This equation is a linear equation in $e^{\nu/2}$ whose solution is given by

$$e^{\nu}=e^{-\lambda}\left(b\int_{r_b}^{r}re^{3\lambda/2}dr+c\right)^2, \tag{3.10}$$

where $b=a/2$ and c is a second constant of integration. Thus the general solution of the field equations, for non-zero K, is:

$$\begin{aligned} e^{-\lambda}&=1-(r/R)^2+KR/r,\\ e^{\nu}&=e^{-\lambda}\left(b\int_{r_b}^{r}re^{3\lambda/2}dr+c\right)^2. \end{aligned} \tag{3.11}$$

From the boundary condition $(e^{-\lambda})_{r=r_b}=1-2m/r_b$ we immediately find that

$$K=x_b^3-2m/R, \tag{3.12}$$

where $x_b=r_b/R$. Equation (3.12) gives an interesting physical interpretation of K. If we let $M=4\pi\rho r_b^3/3$, the Newtonian expression for the mass of the sphere, then

$$K=2(M-m)/R. \tag{3.13}$$

Thus K is a measure of the discrepancy between the Newtonian and relativistic values for the mass

[2] G. M. Volkoff, Phys. Rev. 55, 413 (1939).

of the sphere. Since $e^{-\lambda}$ must be positive as $r\to 0$ we must have $K\geqslant 0$ and hence $m\leqslant M$. Thus the relativistic value of the mass is always less than or equal to the corresponding Newtonian value.

From the boundary condition $(e^{\nu})_{r=r_b}=(e^{-\lambda})_{r=r_b}$ we immediately have $c=1$. Further the continuity of $e^{\nu}\nu'$ with the corresponding Schwarzschild value at $r=r_b$ gives us

$$b=3(1-2m/r_b)^{\frac{1}{2}}/2R^2. \tag{3.14}$$

At this stage we note that we have determined the constants K, b and c in terms of m, r_b, and R. We might thus expect that a knowledge of the boundary radius and the constant density would not determine the mass since m, r_b, and R are still independent variables. It is not until we examine the internal pressure that we find another relation connecting these three variables.

Using (1.2) and (3.11) we find

$$8\pi p=-3/R^2+\left[2be^{\lambda/2}\Big/\left(b\int_{r_b}^{r}re^{3\lambda/2}dr+1\right)\right]. \tag{3.15}$$

Since $e^{\lambda/2}\to 0$ as $r\to 0$ we see that the pressure will be negative near the center of the sphere unless

$$b\int_{r_b}^{0}re^{3\lambda/2}dr+1=0. \tag{3.16}$$

Since the boundary value r_b is the first place at which the pressure vanishes we see that the pressure would be negative throughout the sphere unless (3.16) holds. From the fact that we have assumed the sphere to be in equilibrium we see that the pressure could not be negative throughout and hence (3.16) must hold in order to give a solution of physical interest. From (3.14) and (3.16) we thus find that

$$\int_0^{r_b}re^{3\lambda/2}dr=2R^2(1-2m/r_b)^{-\frac{1}{2}}/3. \tag{3.17}$$

Using (3.16) we find

$$8\pi p=-3/R^2+\left[2e^{\lambda/2}\Big/\int_0^{r}re^{3\lambda/2}dr\right]. \tag{3.18}$$

For small values of r, (3.18) implies that the pressure behaves according to the law $8\pi p\sim 7KR/r^3$. Thus the only solutions with $K\neq 0$ which will be of physical interest are those in which the pressure behaves according to the law above. Moreover, in order to obtain this behavior, relation (3.17) connecting m, r_b, and R must be valid. This is the relation which was not obtained in the Volkoff paper, and it is the relation which enables us to discuss the behavior of $2m/R$ for large values of K.

Evaluation of $\int_0^r re^{3\lambda/2}dr$

If we let $\gamma(z)$ be the Weierstrass elliptic function with invariants 12, $4(27K^2-2)$, then it is well known that

$$(d\gamma/dz)^2=(\gamma'(z))^2=4\gamma^3-12\gamma-4(27K^2-2).$$

For this reason, the substitution

$$r=3KR/(\gamma(z)-1) \tag{3.19}$$

reduces the integral

$$I=\int_0^r re^{3\lambda/2}dr \tag{3.20}$$

to

$$I=216\sqrt{3}K^2R^2\int_0^z\frac{dz}{(\gamma')^2}. \tag{3.21}$$

From (3.19), $dr=-3KR\gamma'(z)dz/(\gamma(z)-1)^2$. Thus for positive dr and dz, $\gamma'(z)$ must be taken negative. For this reason we must take

$$(4\gamma^3-12\gamma-4(27K^2-2))^{\frac{1}{2}}=-\gamma'(z).$$

By using the properties of elliptic functions, (3.21) can be evaluated to give

$$I=[4\sqrt{3}R^2/3(27K^2-4)]\{\zeta(z)-\tfrac{1}{2}(27K^2-2)z +[(2\gamma^2-(27K^2-2)\gamma-4)/\gamma']\} \tag{3.22}$$

where $\zeta(z)$ is the Weierstrass zeta function defined by $\zeta(z)=-\int\gamma(z)dz$ and the condition $\zeta(z)-1/z\to 0$ as $z\to 0$. Although (3.15) is the expression of the integral in terms of known functions, it will not be much value for numerical computation. At the present time no tables of values of the Weierstrass elliptic functions seem to be in existence. For such work numerical integration of (3.20) is still necessary.

We have previously stated that $K=0$ leads to the Schwarzschild interior solution which is expressible in terms of elementary functions. The only other value of K for which this is true is $K=2/3\sqrt{3}$. For this case

$$I=\frac{R^2}{27}\left[\frac{15z^4+25z^2+8}{z(1+z^2)^2}+15\tan^{-1}z-\frac{15\pi}{2}\right], \tag{3.23}$$

where $z=(2R-3^{\frac{1}{2}}r)^{\frac{1}{2}}/(3^{\frac{1}{2}}r)^{\frac{1}{2}}$. For this case the boundary values are $r_b/R=1.13$ and $2m/R=1.06$. For the Schwarzschild solution, $(K=0)$, the corresponding values are $r_b/R=0.944$ and $2m/R=0.838$. Thus we still find an upper limit to the size of a sphere of given density, but these upper limits are greater than those predicted by the Schwarzschild solution.

For general values of K we have from (3.1) that $x-x^3+K>0$ throughout the sphere. Thus if x_1 denotes the only positive root of $x-x^3+K=0$, we find for large values of K that $x_1<K^{\frac{1}{3}}+1/3K^{\frac{1}{3}}$.

For this reason $x_b < K^{\frac{1}{3}} + 1/3K^{\frac{1}{3}}$. Since $2m/R$ is positive, (3.12) implies $x_b > K^{\frac{1}{3}}$ and therefore $K^{\frac{1}{3}} < x_b < K^{\frac{1}{3}} + 1/3K^{\frac{1}{3}}$. With this restriction on x_b it is possible to show that

$$\lim_{K \to \infty} \int_0^{r_b} r e^{3\lambda/2} dr = \infty .$$

Hence from (3.17) $2m \to r_b$ and $2m/R \to x_b$ for large values of K.

4. DENSITY PROPORTIONAL TO A POWER OF r

In the previous section we assumed the density ρ to be constant. As a generalization we shall now assume that $\rho = ar^{N-2}$, where a and N are as yet unrestricted constants. From (1.4) we immediately find

$$e^{-\lambda} = 1 - (r/R)^N + K/r, \tag{4.1}$$

where $R^{-N} = 8\pi a/(N+1)$, and K is a constant of integration. In order to avoid a singularity at the origin we restrict $K = 0$ and $N > 0$. Thus

$$e^{-\lambda} = 1 - (r/R)^N. \tag{4.2}$$

Since $e^{-\lambda}$ must be positive we find that $r \leqslant R$. Equating (1.2) and (1.3) we find that the equation to determine ν is

$$(1-q)r^2(2\nu'' + (\nu')^2) - r\nu'(2 + (N-2)q) + 2q(2-N) = 0, \tag{4.3}$$

where $q = (r/R)^N$. The substitution

$$\nu = 2 \log y, \quad x = (1-q)^{\frac{1}{2}}$$

reduces this equation

$$(1-x^2)(d^2y/dx^2) - 2((N-2)/N)x(dy/dx) - 2((N-2)/N^2)y = 0. \tag{4.4}$$

For certain values of N, Eq. (4.4) does possess solutions which can be expressed in terms of elementary functions. However, for arbitrary values of N the general solution can only be expressed by means of the hypergeometric function $F(a, b; c; z)$ to be

$$y = AF(a, b; \tfrac{1}{2}; x^2) + BxF(a+\tfrac{1}{2}, b+\tfrac{1}{2}; \tfrac{3}{2}; x^2), \tag{4.5}$$

where

$$a = [(N-4) + (N^2 - 16N + 32)^{\frac{1}{2}}]/4N \tag{4.6}$$

$$b = [(N-4) - (N^2 - 16N + 32)^{\frac{1}{2}}]/4N \tag{4.7}$$

and A and B are arbitrary constants. For large values of N, the solution (4.4) approaches that given by

$$y = A + B \log\{(1-x)/(1+x)\}. \tag{4.8}$$

There are an infinite number of values of N for which Eq. (4.4) will have solutions which can be expressed in terms of elementary functions. For example, if one of a or b is a negative integer, at least one of the solutions can be expressed in terms of elementary functions. Similarly if one of $a+\frac{1}{2}$ or $b+\frac{1}{2}$ is a negative integer such a solution is possible. If $2(N-2)/N$ is an odd integer, it can be shown that the general solution can be expressed in terms of elementary functions. In addition to those mentioned there exist many other values of N for which a solution of this type exists. As an example we take the case $N = 4$. For this value of N the differential equation becomes

$$(1-x^2)(d^2y/dx^2) - x(dy/dx) - (1/4)y = 0. \tag{4.9}$$

The general solution of this equation is

$$y = A \sinh(\tfrac{1}{2} \arcsin x + B), \tag{4.10}$$

where A and B are arbitrary constants. This leads to

$$e^{-\lambda} = 1 - (r/R)^4,$$
$$e^{\nu} = A^2 \sinh^2[\tfrac{1}{2} \arcsin(1 - (r/R)^4)^{\frac{1}{2}} + B] \tag{4.11}$$

as a rigorous solution of the field equations. For this solution the distribution of density ρ is given by

$$8\pi\rho = 5r^2/R^4. \tag{4.12}$$

The distribution of pressure can be exactly obtained from (1.2) and (4.11) but the expression is complicated. From the boundary condition $(e^{-\lambda})_{r=r_b} = 1 - 2m/r_b$ we find that $m = r_b^5/2R^4$. Thus we see that the relativistic expression for the mass is the same as the Newtonian expression for the mass of a sphere of radius r_b corresponding to a distribution of density given by (4.12).

For most bodies the quantity r/R is extremely small. Thus one can expand the expression for e^{ν}, given in (4.11), in powers of r/R and obtain a simplified approximate solution for e^{ν}.

5. TOLMAN'S SOLUTION VI

In the paper previously mentioned, Professor Tolman determines eight solutions of the field equations, five of which were new at that time. We propose to show in the next sections of this paper, that three of these solutions can be generalized.

The sixth solution given by Professor Tolman is

$$e^{\lambda} = 2 - n^2, \quad e^{\nu} = (Ar^{1-n} - Br^{1+n})^2, \tag{5.1}$$

where A, B, and n are arbitrary constants. Corresponding to this solution the pressure p and density ρ are given by

$$8\pi p = \frac{(1-n)^2 A - (1+n)^2 B r^{2n}}{(2-n^2) r^2 (A - Br^{2n})} \tag{5.2}$$

$$8\pi\rho = \frac{(1-n^2)}{(2-n^2)r^2}. \tag{5.3}$$

Before proceeding to the generalization of this solution we should like to note some restrictions on

the parameters occurring in the solution which have not been pointed out before. Since the solution is symmetric with respect to n and $-n$, there is no loss in restricting $n \geqslant 0$. Further, to ensure that e^{λ} is positive we must have $0 \leqslant n < \sqrt{2}$. For this range of values the density given by (5.3), will be positive only if $0 \leqslant n \leqslant 1$. In the particular case $n=1$ this solution reduces to the solution corresponding to special relativity. If one leaves n, A and B as constants to be determined by the boundary conditions, then the solution does contain the proper number of arbitrary constants. However, if we desire to fix n arbitrarily independently of the boundary conditions then, of course, only two constants remain with which to satisfy the three boundary conditions. This procedure would of course immediately place a condition on the boundary conditions. In the detailed discussion of this solution Professor Tolman arbitrarily assigns the value $\frac{1}{2}$ to n. On this basis the mass m must satisfy $m=3r_b/14$. Thus the mass m becomes completely determined by the boundary radius of the sphere and no arbitrary constant remains that could be interpreted in terms of the average density of the sphere. If we choose $n=\frac{1}{2}$ we have from (5.3), $8\pi\rho=3/7r^2$, and hence the distribution of density becomes completely determined, and therefore the corresponding solution can apply at most to one sphere. We shall show that there exists a solution of the field equations which includes the present solution as a special case and in which the constant n can be arbitrarily assigned without imposing a condition on the boundary conditions. Moreover we shall show that in our new solution the range of n is not restricted to be $0 \leqslant n \leqslant 1$.

We shall retain the expression

$$e^{\nu}=(Ar^{1-n}-Br^{1+n})^2 \tag{5.4}$$

since, for fixed n, the expression still retains the proper number of arbitrary constants. Equating (1.2) and (1.3) we find that the equation to determine $e^{-\lambda}$ is

$$(r^2\nu'+2r)(d/dr)e^{-\lambda}+(2r^2\nu''+r^2\nu'^2 -2r\nu'-4)e^{-\lambda}=-4. \tag{5.5}$$

When ν is given by (5.4), Eq. (5.5) becomes a linear equation of the first order in $e^{-\lambda}$. Its solution can easily be determined to be

$$e^{-\lambda}=(2-n^2)^{-1}+ar^b[A(2-n)-B(2+n)r^{2n}]^c, \tag{5.6}$$

where a is an arbitrary constant of integration, $b=2(n^2-2)/(n-2)$ and $c=2(2-n^2)/(n^2-4)$. This solution is valid providing n does not have the value $2^{\frac{1}{2}}$ or 2. For the case $n=2$ we find

$$e^{-\lambda}=-\tfrac{1}{2}+ar\,e^{-(A/4Br^4)}, \tag{5.7}$$

$$e^{\nu}=(Ar^{-1}-Br^3)^2. \tag{5.8}$$

Similarly for $n=2^{\frac{1}{2}}$ we find

$$e^{-\lambda}=a+\log[A(2-2^{\frac{1}{2}})-B(2+2^{\frac{1}{2}})r^{2^{\frac{1}{2}}}]/r(2+2^{\frac{1}{2}}), \tag{5.9}$$

$$e^{\nu}=(Ar^{1-2^{\frac{1}{2}}}-Br^{1+2^{\frac{1}{2}}})^2, \tag{5.10}$$

where a is again an arbitrary constant of integration.

It will be noticed of course that $a=0$ in (5.6) will give the Tolman solution, and in this sense our solution will include the Tolman solution as a special case.

We have pointed out that the Tolman solution can apply only in the range $0 \leqslant n \leqslant 1$. Moreover for $n=1$ this solution reduces to that of spacial relativity. When $n=1$ in our generalized solution we find

$$e^{\nu}=(A-Br^2)^2, \tag{5.11}$$

$$e^{-\lambda}=1+ar^2(A-3Br^2)^{-\frac{1}{3}}. \tag{5.12}$$

This gives a new solution which does not reduce to the solution corresponding to special relativity unless $a=0$. Satisfying the boundary conditions we find

$$A=(1-5m/2r_b)/(1-2m/r_b)^{\frac{1}{2}}, \tag{5.13}$$

$$B=-m/2r_b^3(1-2m/r_b)^{\frac{1}{2}}, \tag{5.14}$$

$$a=-2m(1-m/r_b)^{\frac{1}{2}}/r_b^3(1-2m/r_b)^{\frac{1}{2}}, \tag{5.15}$$

where m is the mass and r_b is the boundary of the sphere. From (1.4) we find that the density ρ is given by

$$8\pi\rho=-a(A-3Br^2)^{-5/3}(3A-5Br^2). \tag{5.16}$$

For small values of m/r_b we notice that $A \sim 1$, $B \sim -m/2r_b^3$, and $a \sim -2m/r_b^3$. Thus the boundary density ρ_b will be given, approximately, by (5.16), to be $8\pi\rho_b \sim 6m/r_b^3$. Hence $m \sim 4\pi\rho_b r_b^3/3$. Thus in our solution the mass is determined by the boundary radius r_b and a physical constant ρ_b which will be determined by the physical constitution of the sphere. In the similar example of Tolman's solution it was found that the mass was determined only by the radius of the sphere, and it was shown that this solution would apply at most to one sphere. Since the parameter ρ_b still remains undetermined in our solution it will be possible to apply this solution to spheres of different physical composition.

In addition to the above we have, in our solution, been able to remove the restriction that $0 \leqslant n \leqslant 1$ which was found necessary in order that the Tolman solution should have physical significance.

6. TOLMAN'S SOLUTION V

In the same paper as mentioned before Professor Tolman gives

$$e^{-\lambda}=a-(r/R)^N, \quad e^{\nu}=b^2r^{2n}, \tag{6.1}$$

where $a=(1+2n-n^2)^{-1}$ and $N=2(1+2n-n^2)/(n+1)$ as a new solution of the field equations. In the above n, R, and b are arbitrary constants. If we take the point to view, as was taken in the previous section, that n is an arbitrary constant to be assigned independently of the boundary conditions, then the solution (6.1) does not contain the proper number of arbitrary constants to fulfill the boundary conditions. We propose to show that a solution of the field equations does exist which contains (6.1) as a special case and which contains three arbitrary constants in addition to n.

If we consider the value of $e^{-\lambda}$ to be given by the expression in (2.1) then from the equality of (1.2) and (1.3) the equation to determine ν is

$$\nu''/2-(\lambda'/4+1/2r)\nu'+\tfrac{1}{4}\nu'^2 +(e^{\lambda}/r^2-\lambda'/2r-1/r^2)=0. \quad (6.2)$$

The substitution $\nu=2\log y$ reduces this equation to

$$y''-(\lambda'/2+1/r)y'+(e^{\lambda}/r^2-\lambda'/2r-1/r^2)y=0. \quad (6.3)$$

When λ is known, this equation is a homogeneous linear equation of the second order in y. For the particular λ which we have chosen we know, from Tolman's work, that $y=r^n$ is a particular solution of (6.3). From the theory of linear equations of the second order we know that the general solution of (6.3) can therefore be obtained by a quadrature. It is not difficult to show that this general solution is

$$y=cr^n\int x^p dx/(1-x)^{\frac{1}{2}}+Br^n, \quad (6.4)$$

where $x=(1+2n-n^2)(r/R)^N$ and $p=2n/(n^2-2n-1)$. The integral occurring in (6.4) can be evaluated in terms of elementary functions only if p or $p-\frac{1}{2}$ is an integer, either positive, negative, or zero. For all values of p, (6.4) can be expressed by the hypergeometric function to be

$$y=cr^{2-n}F(\tfrac{1}{2},\, p+1;\, p+2;\, (1+2n-n^2)(r/R)^N)+Br^n. \quad (6.5)$$

For this case the resulting solution of the field equations is

$$e^{-\lambda}=(1+2n-n^2)^{-1}-(r/R)^N, \quad (6.6)$$

$$e^{\nu}=[cr^{2-n}F(\tfrac{1}{2},\, p+1;\, p+2;\, (1+2n-n^2)(r/R)^N)+br^n]^2. \quad (6.7)$$

Since the above solution degenerates to the Tolman solution of $c=0$ we thus have obtained a generalization of the Tolman solution. We note that the constants n, R, c, and b are all arbitrary. Again we can assign n in arbitrarily, and determine R, c, and b from the boundary conditions.

As examples of elementary solutions we might point out that $n=0$ results in the Schwarzschild interior solution. To illustrate a new solution we take $n=1$. Thus $N=2$, $p=-1$. For this case the hypergeometric function of (6.7) degenerates into a constant and the two particular solutions as given in (6.7) are not linearly independent. Returning to (6.4) we easily find that

$$e^{-\lambda}=\tfrac{1}{2}-(r/R)^2,$$
$$e^{\nu}=(cr\log\{(1-(1-2(r/R)^2)^{\frac{1}{2}})/(1+(1-2(r/R)^2)^{\frac{1}{2}})\}+br)^2. \quad (6.8)$$

Similarly one can obtain from (6.4) many other examples of solutions of the field equations which can be expressed in terms of the known elementary functions.

7. TOLMAN'S SOLUTION VIII

By making the mathematical assumption that $e^{-\lambda}=\text{const.}r^{-2b}e^{\nu}$, Professor Tolman was able to obtain a new solution of the field equations. The results as given by Professor Tolman are not quite complete as we shall show when we generalize the procedure introduced by him. If one replaces the above mathematical assumption by the requirement

$$e^{-\lambda}=f(r)e^{\nu}, \quad (7.1)$$

where $f(r)$ is to considered an arbitrary but known function, then it is possible to show that the final problem of solving the field equation reduces to the solution of a second-order non-homogeneous linear differential equation. Since the theory of such equations is well known this provides another general procedure worth investigating in our attempt to find solutions which are of physical interest.

Adding (1.2) and (1.4) we find

$$8\pi(p+\rho)=e^{-\lambda}(\lambda'+\nu')/r. \quad (7.2)$$

From (7.1)

$$\lambda'+\nu'=-f'(r)/f(r). \quad (7.3)$$

Hence

$$8\pi(p+\rho)=-f'(r)e^{\nu}/r. \quad (7.4)$$

From (1.5) and (7.4)

$$8\pi p'=f'(r)e^{\nu}\nu'/2r. \quad (7.5)$$

Using (1.2) and (7.1) our expression for the pressure p is given by

$$8\pi p=[f(r)e^{\nu}\nu']/r+[e^{\nu}f(r)]/r^2-1/r^2. \quad (7.6)$$

Differentiating (7.6) with respect to "r" and equating the result to the right-hand side of (7.5) we find

$$r^2f(r)(d^2e^{\nu}/dr^2)+\tfrac{1}{2}r^2f'(r)(de^{\nu}/dr) +(rf'(r)-2f(r))e^{\nu}=-2. \quad (7.7)$$

Thus with $f(r)$ considered as a known function, Eq. (7.7) becomes a linear differential equation of the second-order to determine e^{ν}.

Since the procedure outlined is purely mathematical, many of the solutions obtained in this way

will be of no physical interest. Whether or not a solution will be of physical interest will depend on a suitable choice of $f(r)$. Although we have very little to guide us in making a suitable choice of $f(r)$, there are a few clues worth pointing out. Since $e^{-\lambda}$ and e^{ν} are positive we must have that $f(r)$ is a positive function. Moreover, the boundary condition $(e^{-\lambda})_{r=r_b}=(e^{\nu})_{r=r_b}$ immediately implies $f(r_b)=1$. From Eq. (7.4) we can also see that $f'(r)$ must be negative since p, ρ, e^{ν}, and r are all positive quantities. These requirements of course provide very little restriction on our choice of $f(r)$ but at least they do provide a guide in making such a choice.

In the solution obtained by Professor Tolman, $f(r)$ was given by $f(r)=c^2r^{-2b}$. With this choice (7.7) becomes

$$r^2(d^2e^{\nu}/dr^2)-br(de^{\nu}/dr)-2(b+1)e^{\nu}=-2r^{2b}/c^2. \quad (7.8)$$

Tolman's results are complete except for the one case in which r^{2b} happens to be a solution of the homogeneous equation. The only positive value of b for which this is true is $b=1+2^{\frac{1}{2}}$. For this case the general solution of (7.8) is

$$e^{\nu}=-\{2r^{2b}\log r/c^2(3b-1)\}+\alpha r^{2b}+\beta r^{1-b}, \quad (7.9)$$

where α and β are constants of integration and $b=1+2^{\frac{1}{2}}$. From this

$$e^{-\lambda}=\{-2\log r/(3b-1)\}+\alpha c^2+\beta c^2 r^{1-3b}. \quad (7.10)$$

With the solution given by (7.9) and (7.10) Tolman's results become complete for all positive values of b. Negative values of b are of course excluded because of the fact that $f'(r)$ must be negative.

As an example of a new solution found by this method we shall take $f(r)=a-br^2$ where a and b are both positive constants. With this choice of $f(r)$ Eq. (7.7) becomes

$$r^2(a-br^2)(d^2e^{\nu}/dr^2)-br^3(de^{\nu}/dr)-2ae^{\nu}=-2. \quad (7.11)$$

An obvious solution of the non-homogeneous equation is $e^{\nu}=1/a$. In order to complete the problem we must therefore find the general solution of the homogeneous equation. For the homogeneous equation the substitution

$$e^{\nu}=r^2y, \quad x=br/a$$

reduces this equation to

$$x(1-x)(d^2y/dx^2)+((5/2)-3x)(dy/dx)-y=0. \quad (7.12)$$

This is a hypergeometric equation whose general solution can be put into the form

$$y=AF(1,1;5/2;x)+Bx^{-\frac{3}{2}}F(-\tfrac{1}{2},-\tfrac{1}{2};-\tfrac{1}{2};x), \quad (7.13)$$

where A and B are again arbitrary constants of integration. However, both of the hypergeometric functions of (7.13) can be expressed in terms of elementary functions and we find

$$y=(A/x)[(1-(1-x)/x)^{\frac{1}{2}}\arcsin x^{\frac{1}{2}}]+Bx^{-\frac{3}{2}}(1-x)^{\frac{1}{2}}. \quad (7.14)$$

This leads to the following solution of the non-homogeneous equation

$$e^{\nu}=A[1-(R^2/r^2-1)^{\frac{1}{2}}\arcsin(r/R)]+(B/r)(1-(r/R)^2)^{\frac{1}{2}}+1/a, \quad (7.15)$$

$$e^{-\lambda}=a(1-(r/R)^2)e^{\nu}. \quad (7.16)$$

In this section we have given a brief outline of a procedure that can be used to generate new solutions of the field equations. We have pointed out that the procedure is unsatisfactory in that a judicious choice of $f(r)$ must be made. It has however been possible to point out a few requirements that $f(r)$ must satisfy which help in making this choice of $f(r)$. Functions of the form $(a-br^n)^m$ and ae^{-br^n} would satisfy these restrictions, and the resulting solutions of the field equations would be worth investigating. However, in any case in which the procedure of this section is followed, a thorough investigation of the physical consequences of the solution should be made in order to determine whether or not the solution is of physical interest.

8. CONCLUSION

For the main part our paper has been a critical examination of some of the known solutions of the gravitational field equations. In many cases we were able to show that the known solutions were particular cases of a more general class of solutions of the field equations. A new method of generating solutions was outlined in Section 7 but it was pointed out that this method is still not too satisfactory from the physical point of view.

PHYSICAL REVIEW VOLUME 75, NUMBER 12 JUNE 15, 1949

Transport Phenomena in a Bose-Einstein Gas

WILLIAM BAND
Institute for the Studies of Metals, University of Chicago, Chicago, Illinois
(Received January 19, 1949)

This paper develops the formal first order perturbation theory of transport phenomena in an ideal Bose-Einstein gas.

The perturbation relaxation time is an unknown parameter in the theory. The ratio of thermal conductivity to viscosity is independent of this relaxation time; it increases discontinuously by a factor almost 2 at the Bose-Einstein condensation temperature T_λ. The isothermal Knudsen heat of transport through a small hole, classically equal to $2kT$, drops rapidly to zero as T falls to T_λ: the Bose-Einstein gas flowing isothermally through a small hole carries no heat when its temperature is below T_λ and it exhibits corresponding thermo-mechanical effects.

The mathematical analysis is carried out in terms of an approximation in which the lowest energy states of the gas are treated discretely while above an arbitrary level they are treated by an integration approximation. The treatment is capable of generalization to models in which there are anomalies in the lowest level spacings.

INTRODUCTION

As briefly reported previously[1] the transport phenomena in an ideal Bose-Einstein gas show some interesting analogies with the peculiar phenomena in liquid helium II. In the previous work only the first approximation was used, namely the integration approximation familiar in discussions of the equilibrium properties of the Bose-Einstein gas.[2] Here we proceed to the second approximation and include a finite (arbitrary) number of the lowest states from zero up to ϵ_s summed discretely. The transition temperature T_λ at which condensation in momentum space sets in depends on the energy ϵ_s chosen, and this dependence is examined in some detail.

Velocity distribution functions are set up and first order perturbations are defined. Boltzmann equations for the rate at which these perturbations tend to be removed by collisions are expressed in terms of a relaxation time τ_n. This relaxation time could in principle be calculated from quantum theoretical considerations if a definite model were adopted for the atomic forces.[3] However such a calculation would involve considerable speculation especially with regard to the collision cross section of the particles condensed into the lowest state.[4] We therefore confine ourselves to a formal development in terms of τ_n as an unknown parameter.

The perturbations here considered are such that the total number of particles in any given energy range of the continuous spectrum or in any one level in the discrete spectrum remains constant and equal to the equilibrium number. It is the spherical symmetry of the velocity distribution in each such range or level that is perturbed. It is implied here, as in all classical first-order perturbation theory, that the relaxation time of such perturbations is long compared with the relaxation time for adjustment of equilibrium between the numerical populations of the various states. This assumption may in fact be invalid below the transition temperature where, according to ideas expressed elsewhere,[5] the transition probabilities between the lowest state and the excited states may become so low that even perturbations like time dependent variations of temperature may necessarily involve disturbances of equilibrium in the numerical distribution. We shall not consider this kind of complication in the present discussion.

The energy per particle in the lowest energy state may be assumed independent of the population in that state. This is consistent with the picture of an ideal gas in an infinite enclosure and essential to the validity of statistical formulas. Under this assumption the first-order perturbation theory leads formally to the interesting result that below the transition temperature a temperature gradient produces a mass flow which cannot be prevented by any opposing pressure gradient. This is because below the temperature T_λ the condensed particles exert no pressure and the pressure of the excited particles is a single valued function of temperature and independent of the density of the gas. The temperature gradient causes excited particles to flow along with the heat current and condense into the lowest state at the point of heat removal; but there is no mechanism provided for the return flow of the lowest-state particles in spite of the concentration gradient set up. However admitting that the particles have finite size and that the energy of the lowest state is not entirely independent of its population, we are able to imagine

[1] W. Band, Phys. Rev. **75**, 339A (1949).
[2] J. E. Mayer and M. G. Mayer, *Statistical Mechanics* (John Wiley and Sons, Inc., New York, 1940).
[3] E. A. Uehling and G. E. Uhlenbeck, Phys. Rev. **43**, 552 (1933); E. A. Uehling, Phys. Rev. **46**, 917 (1943).
[4] J. de Boer and J. van Kranendonk, Physica **XIV**, 442 (1948); J. de Boer, Physica **X**, 348 (1943).
[5] L. Meyer and W. Band, Phys. Rev. **74**, 386, 394 (1948).

that the concentration gradient of lowest-state particles will drive them up the temperature gradient and so balance the mass flow of the excited particles down the temperature gradient.

The thermal conductivity of such a model is found to increase by a factor of about 2 as T drops through T_λ, but then to drop rapidly with further decrease of temperature. There is no superconductivity for heat in the ideal Bose-Einstein gas.

The viscosity of the gas is found to equal the product of relaxation time and pressure. The curve of pressure *v.* temperature decreases more rapidly below T_λ than above, and this is roughly analogous with the behavior of the viscosity in liquid helium, but there is no quantitative similarity. In particular both the heat conductivity and the viscosity are proportional to the relaxation time so that it is impossible to have a decrease in the viscosity and at the same time an increase by many orders of magnitude in the thermal conductivity no matter what anomalies one might postulate in the relaxation time. The ratio of thermal conductivity to viscosity is independent of τ_n, and this is found to have a discontinuity only just twofold at T_λ; in liquid helium the factor is about 10^5.

This is the greatest apparent difference between the transport properties of the Bose-Einstein gas and those of liquid helium. This result is quite consistent with the idea[6] that the anomalously high heat conductivity of helium II is due not directly to statistical degeneracy of any form, but to the presence of second sound waves. These waves are believed to be essentially a disturbance of equilibrium between the numerical populations of the lowest state and the excited states, which has been explicitly excluded from the present calculations.

The isothermal heat transport Q_2 carried by unit mass flowing under a pressure gradient is calculated from perturbation theory and the result checks with the thermodynamic expression $Q_2=E+PV$. Q_2 falls slowly from its classical value $2.5kT$ at high T to a limit $1.28kT_\lambda$ at T_λ.

Consider two enclosures filled with the same Bose-Einstein gas and connected by a hole so small that no significant perturbations are caused in the velocity distributions of either enclosure. In the presence of the temperature difference ΔT there will exist a pressure difference ΔP if no net mass flow is permitted through the hole. The ratio $\Delta P/\Delta T$ is sometimes called the Knudsen pressure coefficient.[7] The Knudsen isothermal heat transfer Q_1 is defined as the heat carried per unit mass in a flow due to a pressure difference across the hole but no temperature difference. Both these quantities are found from an ordinary kinetic theory calculation in terms of the Bose Einstein velocity distribution functions, and the results agree with the thermodynamic relation[8]

$$\Delta P/\Delta T=N(Q_2-Q_1)/TV.$$

The heat transfer Q_1 goes to zero rather suddenly at T_λ. This is remarkably like the thermomechanical anomaly in liquid helium flowing through fine slits:[9] it even implies a sudden increase in the Knudsen pressure coefficient, and this may be regarded as a close analogy with the so-called "fountain pressure" effect in helium II.

In the Bose-Einstein gas this effect is due entirely to the statistical degeneracy and has nothing to do with the van der Waals forces. It is due to the fact already stressed, that below T_λ the excited particles exert a pressure that is a single valued function of the temperature alone, so that if there is no temperature difference across the small hole there will be no net flow of excited particles either. It is not due to any prevention of the flow of excited particles in either direction, but merely an exact balance of flow in both directions. The only net mass flow will be composed of lowest-state particles, and the only pressure difference will be due to the dependence of the lowest energy levels on their population. The only energy transferred through the hole will be this difference in the lowest energy, and if we go to the limit of perfection in the ideal gas this vanishes; and in any case it is negligible compared with the thermal energy.

In the search for a theory of the peculiar properties of liquid helium we are confronted by the following obvious obstacle: the theory of a quantum liquid could conceivably be derived unambiguously from the theory of classical liquids by means of some form of the correspondence principle, but no really acceptable molecular theory of the classical liquid as yet exists in a form that can be handled with any degree of facility. The attempt to overcome this obstacle and to approach the quantum liquid via the classical liquid may be called the vertical approach. It is well illustrated by the recent work of Born and Green,[10] and also by the present writer's extension of J. E. Mayer's classical statistical thermodynamics of mixed liquids to include the effects of quantum degeneracy.[11]

Another simpler if less rigorous approach is however possible. The problem of the classical liquid has been attacked from the theory of the

[6] L. Meyer and W. Band, Phys. Rev. **73**, 226 (1948).

[7] M. Knudsen, Ann. d. Physik **34**, 603 (1911); S. Weber, Zeits. f. Physik **24**, 267 (1924).

[8] C. Wagner, Ann. d. Physik **V3**, 629 (1929); L. Onsager, Phys. Rev. **38**, 2265 (1931); R. S. de Groot, Physica **13**, 555 (1947).

[9] L. Meyer and W. Band, Naturwiss., in press (review of the present state of the helium II problem).

[10] M. Born and H. S. Green, Proc. Roy. Soc. **A189**, 103 (1947); **A190**, 455 (1947); **A191**, 108 (1947); **A192**, 166 (1948); and Nature **161**, 391 (1948).

[11] W. Band, J. Chem. Phys. **16**, 343 (1948).

classical solid on the one side, and from the classical gas on the other. Parallel to this attack, we may approach the quantum liquid problem from either side—the quantum solid or the quantum gas. Such a horizontal approach to the quantum liquid was employed in some early work by F. London;[12] it has one significant advantage over the vertical approach: namely that the theories of the quantum gas and the quantum solid are fairly well developed and comparatively elementary, so that the starting point is more easy to handle than for the vertical approach from the classical liquid.

In the present paper we have not attacked the problem of the quantum liquid directly, but have made a preliminary study of the transport properties of the degenerate Bose-Einstein gas in the hope that by so doing we may consolidate the horizontal approach to the quantum liquid. It is at least encouraging that some of the transport properties of the gas are found to be remarkably similar with those of helium II.

EQUILIBRIUM PROPERTIES OF THE BOSE-EINSTEIN GAS

First approximations to most of the properties of the ideal Bose-Einstein gas can be derived from a smoothed integration over the entire energy spectrum. In this paper we use instead a method similar to that due to F. London[12] in which the lowest energy states are included discretely, and only those states above some arbitrary level treated approximately by integration.

The Gibbs free energy $G=kT\ln\lambda$ is determined by

$$N/V=(4\pi/h^3)\int_{p_1}^{\infty}\{\lambda^{-1}e^{p^2/2mkT}-1\}^{-1}p^2dp+\sum_{s=0}^{z}w_s\{\lambda^{-1}e^{\epsilon_s/kT}-1\}^{-1}$$

where p_1 is the lowest momentum not included discretely, ϵ_s is the energy of the sth discrete state, w_s the weight per unit volume of the sth state, ϵ_0 and w_0 belong to the lowest state ($\epsilon_0=0$), and ϵ_z, w_z to the highest state in the discrete spectrum. For the purposes of the present paper it is convenient to express this equation in the form:

$$N/V=(4\pi/h^3)\int_{p_1}^{\infty}p^2\sum_{j=1}^{\infty}\lambda^j e^{-jp^2/2mkT}dp+\sum_{s=0}^{z}w_s\sum_{j=1}^{\infty}\lambda^j e^{-j\epsilon_s/kT}. \quad (1.1)$$

For convenience we shall call the lowest energy states the s-states and the states in the integral the n-states.

The statistical weight of the discrete state ϵ_s is the volume in momentum space between the energy levels ϵ_s and ϵ_{s+1}:

$$w_s=(4\pi/3h^3)\{(2m\epsilon_{s+1})^{\frac{3}{2}}-(2m\epsilon_s)^{\frac{3}{2}}\}=(2\pi mkT)^{\frac{3}{2}}h^{-3}(4/3(\pi)^{\frac{1}{2}})\Delta(\epsilon_{s+1}/kT)^{\frac{3}{2}}. \quad (1.2)$$

The suffix $s+1$ has been used deliberately in the last expression to permit the lowest state to be included formally. To express (1.1) in a form that is more easily handled we need a number of abbreviations and theorems that will be collected here rather than in an appendix, because without seeing them, the reader would find many of the ensuing equations meaningless. The theorems have little intrinsic mathematical importance so their proofs are not given.

Definition:

$$I(n,j)\equiv\frac{2^{n+1}/(\pi)^{\frac{1}{2}}}{1\cdot3\cdot5\cdots(2n-1)}\int_{(j\varphi)^{\frac{1}{2}}}^{\infty}Z^{2n}e^{-Z^2}dZ,\qquad \varphi\equiv\epsilon_s/kT=p_1^2/2mkT. \quad (1.3)$$

$$[n,\ j=1,\ 2,\ 3,\ \cdots]$$

$$I(0,j)\equiv(2/(\pi)^{\frac{1}{2}})\int_{(j\varphi)^{\frac{1}{2}}}^{\infty}e^{-Z^2}dZ. \quad (1.4)$$

Theorem:

$$I(n,j)=I(0,j)+e^{-j\varphi}\sum_{k=0}^{n-1}\frac{2^{n-k}/(\pi)^{\frac{1}{2}}}{1\cdot3\cdot5\cdots(2n-2k-1)}(j\varphi)^{n-k-\frac{1}{2}}. \quad (1.5)$$

The integrals $I(n,j)$ all approach unity in the limit $p_1\to0$.

Definitions:

$$\Lambda(n,m)\equiv\sum_{j=1}^{\infty}I(n,j)\lambda^j/j^m, \quad (1.6)$$

$$H(q,m)\equiv\varphi^q\sum_{j=1}^{\infty}e^{-j\varphi}\lambda^j/j^m, \quad (1.7)$$

$$H_s(q,m)\equiv\varphi_s{}^q\sum_{j=1}^{\infty}e^{-j\varphi_s}\lambda^j/j^m,\quad \varphi_s=\epsilon_s/kT. \quad (1.8)$$

Theorems:

The radius of convergence of the j-series in $\Lambda(n,m)$ is

$$\lambda=1/(1-\varphi),\ \text{all } n,\ m. \quad (1.9)$$

The series $H_s(q,m)$ all diverge when

$$\lambda\to e^{\epsilon_s/kT}. \quad (1.10)$$

[12] F. London, J. Phys. Chem. **43**, 49 (1939); Phys. Rev. **54**, 947 (1938).

The radii of convergence, $e^{\epsilon_s/kT}$ form a monotonically increasing sequence:

$$1=e^{\epsilon_0/kT}<e^{\epsilon_1/kT}<\cdots<e^{\epsilon_s/kT}<1/(1-\varphi). \quad (1.11)$$

The series $H_0(q, m)$ is thus the first to diverge as λ increases. The following theorems on the first variations of the Λ's and H's are true if p_1 is kept constant:

$$\Delta\Lambda(n, m)=\Lambda(n, m-1)\Delta\ln\lambda+\frac{2^n/(\pi)^{\frac{1}{2}}}{1\cdot3\cdot5\cdots(2n-1)}\times H(n+\tfrac{1}{2}, m-n-\tfrac{1}{2})\Delta\ln T, \quad (1.12)$$

$$\Delta H(q, m)=H(q, m-1)\Delta\ln\lambda+\{qH(q-1, m)-H(q, m-1)\}\Delta\ln\varphi, \quad (1.13)$$

$$\Delta H_s(q, m)=H_s(q, m-1)\Delta\ln\lambda+\{qH_s(q-1, m)-H_s(q, m-1)\}\Delta\ln\varphi_s. \quad (1.14)$$

Theorem:

$$\Lambda(n, m)=\Lambda(n-1, m)+\frac{2^n/(\pi)^{\frac{1}{2}}}{1\cdot3\cdot5\cdots(2n-1)}\times H(n-\tfrac{1}{2}, m-n+\tfrac{1}{2}). \quad (1.15)$$

In terms of the foregoing notation we now write (1.1) in the form:

$$N/V=(2\pi mkT)^{\frac{3}{2}}h^{-3}\left\{\Lambda(1, \tfrac{3}{2})+\sum_{s=0}^{z}(4/3(\pi)^{\frac{1}{2}})\times\Delta(\epsilon_{s+1}/kT)^{\frac{3}{2}}H_s(0, 0)\right\}. \quad (1.16)$$

The lambda-transition occurs at that temperature which forces λ to approach the smallest of the radii of convergence: namely the value unity that makes the series $H_0(0, 0)$ diverge.

The individual terms in the s-sum of (1.16) are generally exceedingly small compared with the leading Λ-term; they represent the populations of the individual discrete states, whereas the Λ-term represents the integral (or sum) over all the n-states. As soon as the value of λ is close enough to unity the population of the lowest state begins to increase, and because when $\lambda=1$, $H_0(0, 0)$ actually diverges, there is no limit to the population of this state. However λ has to be so close to unity to make $H_0(0, 0)$ comparable with the Λ term, that we can write $\lambda=1$ in all the other terms in (1.16) in order to estimate the transition temperature. This temperature, T_λ is therefore given by

$$N/V=(2\pi mkT_\lambda)^{\frac{3}{2}}h^{-3}\left\{\Lambda_c(1, \tfrac{3}{2})+\sum_{s=1}^{z}(4/3(\pi)^{\frac{1}{2}})\times\Delta(\epsilon_{s+1}/kT_\lambda)^{\frac{3}{2}}H_{sc}(0, 0)\right\}, \quad (1.17)$$

where the $s=0$ term is absent, and $\Lambda_c(1, \frac{3}{2})$ and $H_{sc}(0, 0)$ denote the values at $\lambda=1$. When T goes below T_λ the right hand side of (1.17) decreases, and the deficiency is made up by the divergent H_0 term.

In (1.17) the s-sum actually makes only a small correction to the calculation of T_λ, and it is sufficient to evaluate it to a first approximation. If we agree to keep $\epsilon_z/kT\ll1$, we have

$$H_{sc}(0, 0)=\sum_{j=1}^{\infty}e^{-j\epsilon_s/kT}\doteqdot kT/\epsilon_s. \quad (1.18)$$

To the same approximation the s-sum in (1.17) becomes

$$(4/3(\pi)^{\frac{1}{2}})\sum_{s=1}^{z}(kT/\epsilon_s)\Delta(\epsilon_{s+1}/kT)^{\frac{3}{2}}\doteqdot(2/(\pi)^{\frac{1}{2}})\sum_{s=1}^{z}(kT\epsilon_s)^{-\frac{1}{2}}\Delta\epsilon_s=(4/(\pi)^{\frac{1}{2}})\{(\epsilon_z/kT)^{\frac{1}{2}}-(\epsilon_1/kT)^{\frac{1}{2}}\}. \quad (1.19)$$

The strict requirement for the accuracy of this result is thus

$$(\epsilon_z/kT)^{\frac{1}{2}}\ll1. \quad (1.20)$$

On this understanding the transition temperature is determined by

$$N/V=(2\pi mkT_\lambda)^{\frac{3}{2}}h^{-3}\times\{\Lambda_c(1, \tfrac{3}{2})+(4/(\pi)^{\frac{1}{2}})(\epsilon_z/kT)^{\frac{1}{2}}\}. \quad (1.21)$$

Now the quantity ϵ_z is entirely arbitrary, and it is clear that the correct value of T_λ should be independent of the choice of this parameter. The approximation (1.18) will therefore presumably be acceptable if the parameter can be so chosen that T_λ has a stationary value with respect to variations of ϵ_z, all other quantities remaining fixed.

Using the definitions (1.3), (1.4), (1.6) and the theorem (1.5) we can write the bracketed expression on the right hand side of (1.21) in the form:

$$\sum_{j=1}^{\infty}\{1-P((j\varphi)^{\frac{1}{2}})+(2/(\pi)^{\frac{1}{2}})(j\varphi)^{\frac{1}{2}}e^{-j\varphi}\}j^{-\frac{3}{2}}+(4/(\pi)^{\frac{1}{2}})\varphi^{\frac{1}{2}}\equiv F(\varphi), \quad (1.22)$$

where $P(x)$ is the probability integral normalized to unity. Differentiating this with respect to φ we find, if φ is small

$$\partial F/\partial\varphi=(\varphi/\pi)^{\frac{1}{2}}. \quad (1.23)$$

This is positive and vanishes only at $\varphi=0$, but $\varphi\partial F/\partial\varphi$ remains small compared with φ for small φ. Thus any choice of φ conforming to (1.20) is such that there is no appreciable dependence of T_λ on φ.

Choosing for example $\varphi=0.01$ we have evaluated $F(\varphi)$ exactly by direct summation and compared

with the result given by integration approximation ($\varphi=0$). We find

$$F(0.01)=2.616, \quad F(0)=2.612. \tag{1.24}$$

The modification in T_λ due to this second approximation is therefore less than 0.2 percent.* Implicit in this calculation is the assumption that the volume V of the gas is large enough to ensure the presence of a considerable number (say ten or more) of energy levels in the range $0.01kT$. In fact the volume has to be less than about 10^{-16} cc before this condition would be formally violated!

We conclude that for the ideal gas the integration approximation gives sufficiently precise values for the transport properties: their computation generally involves series that converge more rapidly than those involved in the evaluation of T_λ. The numerical results given in the present paper have been calculated only on this approximation, but the formal analysis has been carried through in terms of the second approximation because it will later enable us to study the properties of special models in which any desired anomalies may be present in the lower energy levels.

Below the transition temperature T_λ the number of particles N_n in the n-states is given by

$$N_n/V=(2\pi mkT)^{\frac{3}{2}}h^{-3}\Lambda_c(1, \tfrac{3}{2}) \tag{1.25}$$

and the total number of particles in the s-states is the difference

$$\sum_{s=0}^{z} N_s/V=N/V-N_n/V. \tag{1.26}$$

However the number in the lowest state alone has to be found from a more precise calculation of the s-sums in (1.17). Provided we keep close enough to the transition temperature to allow (1.20) to remain valid, we may use (1.21) instead of (1.17) and write

$$N_0/V=N/V-(2\pi mkT)^{\frac{3}{2}}h^{-3} \times\{\Lambda_c(1, \tfrac{3}{2})+4/(\pi)^{\frac{1}{2}})(\epsilon_z/kT)^{\frac{1}{2}}\} \tag{1.27}$$

Because both $\Lambda_c(1, \frac{3}{2})$ and ϵ_z/kT depend on T below T_λ, this equation is not exactly of the same form as that given by the integration approximation, namely:

$$N_0/V=(N/V)\{1-(T/T_\lambda)^{\frac{3}{2}}\}$$

But because the T-variation of the expression in {brackets} in (1.27) is essentially proportional to its φ-variation, and because we have chosen φ at T_λ so that the φ-variation is almost zero, we may assume also that at least near to T_λ its T-variation is also almost zero. Hence the two expressions for N_0 almost coincide.

The total energy E_n of the particles in the n-states is given by

$$E_n/V=(3/2)kT(2\pi mkT)^{\frac{3}{2}}h^{-3}\Lambda(2, 5/2), \tag{1.28}$$

while the energy in any one of the s-states is given by

$$E_s/V=w_skTH_s(1, 0). \tag{1.29}$$

The general relation $P=2E/3V$ is still true here, and we can immediately write down the partial pressures due respectively to the n-particles and to each of the s-states:

$$\begin{aligned} P_n&=kT(2\pi mkT)^{\frac{3}{2}}h^{-3}\Lambda(2, 5/2)\\ P_s&=(2/3)kTw_sH_s(1, 0), \end{aligned} \tag{1.30}$$

and obtain the total pressure exerted by the gas:

$$P=kT(2\pi mkT)^{\frac{3}{2}}h^{-3}\Big\{\Lambda(2, 5/2)+\sum_{s=0}^{z}(8/9(\pi)^{\frac{1}{2}}) \times\Delta(\epsilon_{s+1}/kT)^{\frac{1}{2}}H_s(1, 0)\Big\}. \tag{1.31}$$

Using (1.16) we then find the equation of state in the more convenient form:

$$PV=NkT\frac{\Lambda(2, 5/2)+\sum_{s=0}^{z}(8/9(\pi)^{\frac{1}{2}})\Delta(\epsilon_{s+1}/kT)^{\frac{1}{2}}H_s(1, 0)}{\Lambda(1, 3/2)+\sum_{s=0}^{z}(4/3(\pi)^{\frac{1}{2}})\Delta(\epsilon_{s+1}/kT)^{\frac{1}{2}}H_s(0, 0)}. \tag{1.32}$$

Going over to the integration approximation we find

$$\begin{aligned} &T\leqslant T_\lambda, && P=\zeta(5/2)kT(2\pi mkT)^{\frac{3}{2}}h^{-3},\\ &T=T_\lambda, && P=\zeta(5/2)kT_\lambda(2\pi mkT_\lambda)^{\frac{3}{2}}h^{-3},\\ &T\geqslant T_\lambda, && P/P_\lambda=(T/T_\lambda)\zeta(3/2)\zeta(\lambda, 5/2) \div\zeta(\lambda, 3/2)\zeta(1, 5/2), \end{aligned}$$

where $\zeta(n)$ is the Riemann zeta-function

$$\sum_{j=1}^{\infty} 1/j^n$$

and $\zeta(\lambda, n)$ is an "incomplete" Reimann zeta-

* This discussion of the lambda-point differs essentially from that given by F. London and referred to above. In his treatment the discrete set of states was lumped together and the s-sum of our expression (1.1) was represented only by a single term in which the mean energy of the particles in the discrete states appeared in the exponent. The radius of divergence of this series was therefore $e^{\epsilon_s/kT}$ where $\bar{\epsilon}_s$ was the mean energy of the s-particles. London used a constant value for this mean energy $\bar{\epsilon}_s=3\epsilon_s/5$ where ϵ_s was the energy of the lowest state in the integral, or the highest discrete state. This would be correct only at high temperatures, but near the lambda-point the mean energy drops towards zero. London's calculation would lead to a value of T_λ appreciably different from the result of the integration approximation even for the ideal gas.

function:

$$\zeta(\lambda, n) \equiv \sum_{j=1}^{\infty} \lambda^j / j^n.$$

These are limiting forms of the Λ functions when φ is zero.

Figure 1 shows the temperature dependence of the parameter λ on the integration approximation, and Fig. 2 shows the pressure curves for several arbitrary values of T_λ, calculated for a gas with atoms equal in mass to those of He^4.

FIRST-ORDER PERTURBATION THEORY

The unperturbed distribution function giving the number of n-particles per unit volume in a cell $dv_x dv_y dv_z$ of velocity space (see Eq. (1.1)) is

$$f_{n0}(v)dv_x dv_y dv_z = (m/h)^3 \sum_{j=1}^{\infty} \lambda^j e^{-jmv^2/2kT} dv_x dv_y dv_z. \quad (2.1)$$

The unperturbed distribution function for particles in each s-state gives the number of particles per unit volume per unit solid angle:

$$f_{s0}(v)d\Omega = w_s H_s(0, 0)d\Omega,\ d\Omega = \sin\theta d\theta d\Phi/4\pi. \quad (2.2)$$

The first function applies to all velocities $v \geqslant p_1/m$ while the others apply only to the particular velocities v_s, respectively, the magnitudes v_s being constant in each function.

Consider the perturbations that leave the energy levels unchanged but which are of such a form that the functions become

where
$$\left.\begin{aligned} f_n(v) &= f_{n0}(v) + f_{n1}(v) \\ f_{n1}(v) &= -\tau_n v_x \partial f_{n0}(v)/\partial x \end{aligned}\right\} \quad (2.3)$$

and

where
$$\left.\begin{aligned} f_s(v) &= f_{s0}(v) + f_{s1}(v) \\ f_{s1} &= -\tau_s v_{sx} \partial f_{s0}(v)/\partial x \end{aligned}\right\} \quad (2.4)$$

$$s = 1, 2, 3 \cdots z.$$

In (2.3) $v_x = v\cos\theta$, while in (2.4) v has the magnitude $v_s = (2\epsilon_s/m)^{\frac{1}{2}}$ and $v_{sx} = v_x \cos\theta$.

These are Boltzmann type perturbation equations and involve no changes in the equilibrium populations of any given energy range or in any given discrete level. τ_n and τ_s are relaxation times for the readjustment of equilibrium in the spherical symmetry of the velocity distributions. One would like to be able to compute these times from a complete theory of collision probabilities between the atoms. However such a calculation could hardly be free of speculative elements specially with regard to the collision cross sections attributable to the particles condensed into the lowest energy level. Fortunately, the formal theory can be developed without such a calculation, the results being expressible in terms of the relaxation times as unknown parameters. For notational symmetry we retain all the τ_s as distinct, but eventually only τ_0 for the lowest state will be considered as possibly different from the others.

It will further be supposed that the relaxation times are long compared with the relaxation time, which must also exist in principle, for adjustment of equilibrium between the relative numerical populations of the various states: in other words all the perturbation functions contain the same value of the equilibrium parameter λ at any given point in space.

This last assumption may in fact be invalid below the lambda-point, according to ideas developed elsewhere:[5] the transition probabilities between particles in the lowest state and those in the excited states may become so low as to cause trouble. We shall not consider this kind of complication in the present paper.

Using the above perturbed distribution functions we obtain for the net flow of particles per second

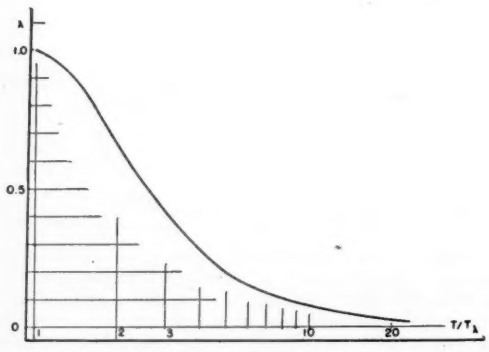

FIG. 1. The temperature dependence of the statistical parameter λ calculated on the integration approximation.

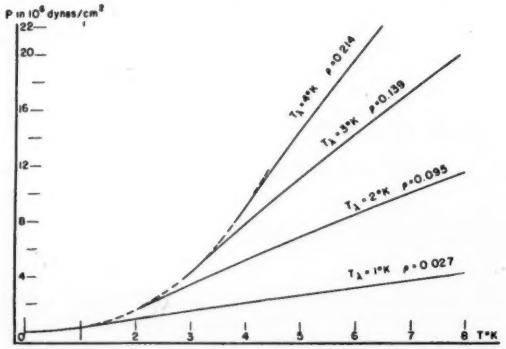

FIG. 2. The pressure-temperature curves for several arbitrary densities calculated for a gas with atoms equal in mass to those of He^4.

across unit area in x-direction:

$$J=*\int\int\int_{-\infty}^{\infty}* v\cos\theta f_{n1}(v)dv_xdv_ydv_z + \sum_{s=0}^{z}\int_{\theta=0}^{\pi}\int_{\Phi=0}^{2\pi} v_s\cos\theta f_{s1}(v)d\Omega, \quad (2.5)$$

where the integral sign $*\int\int\int*$ is intended to indicate that the integration is to be taken only over the region in velocity space *outside* of the sphere of radius $v_z=(2\epsilon_z/m)^{\frac{1}{2}}$. To handle this and similar integrals we use the following additional theorem:

$$*\int\int\int_{-\infty}^{\infty}* v_x^2v^{2n}\sum_{j=1}^{\infty} j\lambda^j e^{-jmv^2/2kT}dv_xdv_ydv_z = (4/3)(\pi)^{\frac{1}{2}}(2kT/m)^{n+5/2}\left\{\frac{1\cdot3\cdot5\cdots(2n+3)}{2^{n+3}}\right\}\times\sum_{j=1}^{\infty} I(n+2,j)\lambda^j/j^{n+\frac{1}{2}}. \quad (2.6)$$

This theorem permits (2.5) to be written out:

$$J=-\tau_n(kT/m)(2\pi mkT)^{\frac{1}{2}}h^{-3}\times\{\Lambda(2,3/2)d\ln\lambda/dx+(5/2)\Lambda(3,5/2)d\ln T/dx\} -\sum_{s=0}^{z}(2\tau_s/3)(kT/m)w_sH_s(1,-1)\times\{d\ln\lambda/dx-d\ln\varphi_s/dx\}. \quad (2.7)$$

The net flow of energy per second across unit area is similarly

$$W=*\int\int\int_{-\infty}^{\infty}* \tfrac{1}{2}mv^2v\cos\theta f_{n1}(v)dv_xdv_ydv_z + \sum_{s=0}^{z}\int_{\theta=0}^{\pi}\int_{\Phi=0}^{2\pi}\epsilon_sv_s\cos\theta f_{s1}(v)d\Omega \quad (2.8)$$

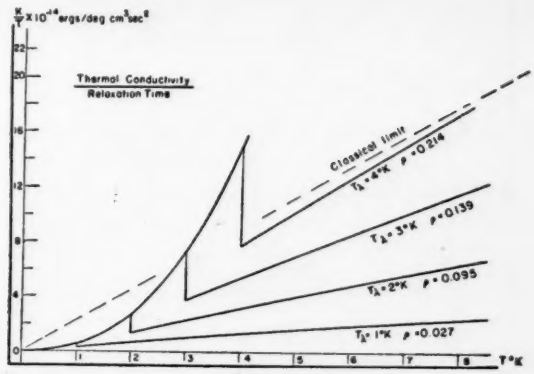
Thermal Conductivity
Relaxation Time
Classical limit
T_λ = 4°K ρ = 0.214
T_λ = 3°K ρ = 0.139
T_λ = 2°K ρ = 0.095
T_λ = 1°K ρ = 0.027
T °K

FIG. 3. Thermal conductivity curves for a gas with atoms equal in mass to those of He^4.

and again using (2.6) this can be written in the form:

$$W=-(\tau_n/m)(kT)^2(2\pi mkT)^{\frac{1}{2}}h^{-3}\times\{(5/2)\Lambda(3,5/2)d\ln\lambda/dx+(35/4)\Lambda(4,7/2)d\ln T/dx\} -\sum_{s=1}^{z}(2/3)(\tau_s/m)(kT)^2w_sH_s(2,-1)\times\{d\ln\lambda/dx-d\ln\varphi_s/dx\}. \quad (2.9)$$

Expressed in terms of the temperature gradient, we may write (2.9) as

$$W=-(d\ln T/dx)(\tau_n/m)(kT)^2(2\pi mkT)^{\frac{1}{2}}h^{-3}\times\left[\left\{(5/2)\Lambda(3,5/2)+\sum_{s=0}^{z}(8/9(\pi)^{\frac{1}{2}})(\tau_s/\tau_n)\times\Delta(\epsilon_{s+1}/kT)^{\frac{1}{2}}H_s(2,-1)\right\}d\ln\lambda/d\ln T +\left\{(35/4)\Lambda(4,7/2)+\sum_{s=0}^{z}(8/9(\pi)^{\frac{1}{2}})\times(\tau_s/\tau_n)\Delta(\epsilon_{s+1}/kT)^{\frac{1}{2}}H_s(2,-1)\right\}\right]. \quad (2.10)$$

The thermal conductivity is to be measured in the absence of any net mass flow, and this condition, namely $J=0$, used in (2.7) determines the variation of $\ln\lambda$. Thus:

$$J=0,\quad d\ln\lambda/d\ln T=-\frac{(5/2)\Lambda(3,5/2)+\sum_{s=0}^{z}(8/9(\pi)^{\frac{1}{2}})(\tau_s/\tau_n)\Delta(\epsilon_{s+1}/kT)^{\frac{1}{2}}H_s(1,-1)}{\Lambda(2,3/2)+\sum_{s=0}^{z}(8/9(\pi)^{\frac{1}{2}})(\tau_s/\tau_n)\Delta(\epsilon_{s+1}/kT)^{\frac{1}{2}}H_s(1,-1)}. \quad (2.11)$$

At sufficiently high temperatures (2.11) reduces to 5/2 and the thermal conductivity becomes:

$$T\gg T_\lambda,\quad K=W\div dT/dx=-(5/2)(\tau_n/m)(N/V)k^2T.$$

Generally on the integration approximation we find

$$T\gtrsim T_\lambda,\quad K=-(5/4)(k^2T/m)(N/V)\times[7\zeta(\lambda,7/2)/\zeta(\lambda,3/2)-5\{\zeta(\lambda,5/2)/\zeta(\lambda,3/2)\}^2]. \quad (2.12)$$

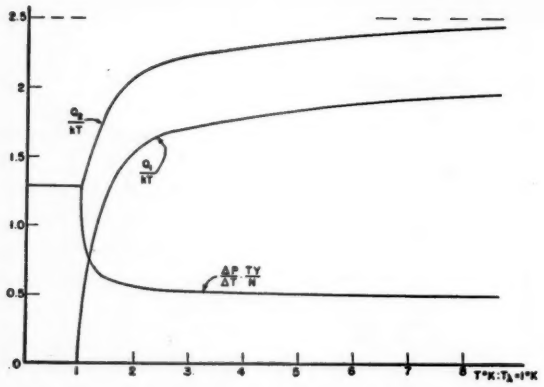

FIG. 4. The heat content, the Knudsen isothermal heat of transport, and the Knudsen pressure coefficient in units of kT plotted against T/T_λ.

Below T_λ we run into the difficulty that $\Delta \ln\lambda$ must remain zero and it is actually impossible to satisfy (2.11). In other words Eq. (1.31) leads to a pressure that is a single valued function of T only below T_λ, and a decrease of volume or an increase of density can only result in increasing the density of the population in the lowest state, and these do not contribute to the pressure. Physically we have to suppose that the mass flow given by (2.7) can actually be balanced by a return current of particles in the lowest state, although this cannot appear in the formal analysis. On this understanding we can still define a conductivity below T_λ, and putting $\Delta \ln\lambda=0$ in (2.9) we find

$$T\leqslant T_\lambda,\quad K=-(35/4)(\tau_n/m)(N_n/V)k^2T \times\Lambda_c(4,\,7/2)/\Lambda_c(1,\,3/2). \tag{2.13}$$

There is thus apparently a discontinuity of the conductivity by a factor of almost 2 as T drops through the transition temperature. Figure 3 shows the curves drawn from the integration approximation.

As discussed in the Introduction, nothing like superconductivity for heat is to be expected in the ideal gas.

The isothermal heat transport accompanying mass flow is derived from (2.9) by writing $\Delta T=0$ and dividing the result by the value of J obtained from (2.7) also with $\Delta T=0$. The result is

$$Q_s\equiv(W/J)_{T=\text{const.}}=kT\frac{(5/2)\Lambda(3,\,5/2)+\sum_{s=0}^{z}(8/9(\pi)^{\frac{1}{2}})(\tau_s/\tau_n)\Delta(\epsilon_{s+1}/kT)^{\frac{1}{2}}H_s(2,\,-1)}{\Lambda(2,\,3/2)+\sum_{s=0}^{z}(8/9(\pi)^{\frac{1}{2}})(\tau_s/\tau_n)\Delta(\epsilon_{s+1}/kT)^{\frac{1}{2}}H_s(1,\,-1)} \tag{2.14}$$

or on the integration approximation

$$Q_2=5kT\zeta(\lambda,\,5/2)/2\zeta(\lambda,\,3/2). \tag{2.15}$$

This curve is shown on Fig. 4. At very high temperatures it coincides with the classical result $Q_2=5kT/2$.

If (1.28), (1.29) and (1.31) are used with the approximation (1.18) and (1.19) in (2.14) we arrive at the thermodynamic relation

$$NQ_2/V=E/V+P. \tag{2.16}$$

There is no marked discontinuity in Q_2 at T_λ.

From the same perturbation theory we can compute the viscosity of the gas. We set up the unperturbed distribution functions in the form

$$f_{n0}(v)=(m/h)^3\sum_{j=1}^{\infty}\lambda^j\exp[-jm(\mathbf{v}+\mathbf{u})^2/2kT], \tag{2.17}$$

$$f_{s0}(v)=w_s\sum_{j=1}^{\infty}\lambda^j\exp[-jm(\mathbf{v}_s+\mathbf{u})^2/kT],\qquad s=0,\,1,\,\cdots z,$$

where $\mathbf{u}$ means the speed of flow of the gas at a distance y from the wall, and $\mathbf{v}$ is the velocity of the particle relative to stationary coordinates. We allow u to depend on y so that $\partial u/\partial y$ is a constant. We then allow perturbations such that

$$\left.\begin{aligned} f_n(v)&=f_{n0}(v)+f_{n1}(v)\\ f_{n1}(v)&=-\tau_n v_y\partial f_{n0}(v)/\partial y.\end{aligned}\right\} \tag{2.18}$$

where

We then find the flow of x-momentum across a surface normal to the y-direction, and this finally gives the coefficient of viscosity as the ratio of the momentum transfer to the velocity gradient

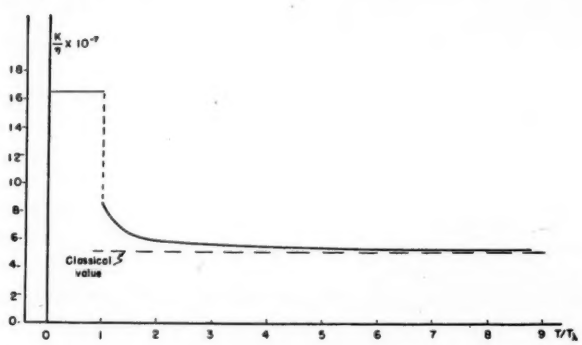

FIG. 5. The ratio of thermal conductivity to viscosity as a function of T/T_λ.

$\partial u/\partial y$. The result turns out to be

$$\eta=\tau_n P_n \Lambda(3, 5/2)/\Lambda(2, 5/2) + \sum_{s=0}^{z} \tau_s P_s(\epsilon_s/kT). \quad (2.19)$$

We note specially that the lowest state contributes nothing to the viscosity because it exerts no pressure. At high temperatures (2.19) reduces to the simple result:

$$T \gg T_\lambda, \quad \eta=\tau_n P. \quad (2.20)$$

This agrees with the classical kinetic theory if we use the classical expression for the mean free path and mean speed with which to express the relaxation time. Generally the integration approximation gives

$$T \gtrsim T_\lambda \text{ and } T<T_\lambda, \quad \eta=\tau_n P \quad (2.21)$$

a result which holds for all temperatures.

The most significant consequence of these calculations is obtained by taking the ratio between K and η, because this is independent of τ. Figure 5 shows the curve. There is a discontinuity of about two-fold at T_λ, but K/η remains finite below T_λ so that it is clear that no assumed anomaly in τ_n at T_λ could give both superfluidity and superconductivity for heat below the transition temperature.

THE KNUDSEN PHENOMENA

Exclude from the range of integration the region of momentum space in which the total momentum is less than p_1 so that

$$p_x^2+p^2 \gtrsim p_1^2 \quad \text{where} \quad p^2 \equiv p_y^2+p_z^2. \quad (3.1)$$

The number of n-particles with x-momentum within the range p_x to p_x+dp_x incident per second on unit area normal to the x-axis is

$$n(p_x)dp_x=(\pi/3m)p_x dp_x \int_\rho^\infty \sum_{j=1}^{\infty} \lambda^j \times e^{-j(p^2+p_x^2)/2mkT} dp^2, \quad (3.2)$$

where

$$\left.\begin{aligned} &\rho^2=p_1^2-p_x^2 \quad \text{if} \quad |p_x|<|p_1| \\ \text{or} \quad &\rho^2=0 \quad \text{if} \quad |p_x| \gtrsim |p_1|. \end{aligned}\right\} \quad (3.3)$$

This integral can be written in the form

$$n(_n \equiv \int_0^\infty n(p_x)dp_x = 2\pi m(kT)^2 h^{-3} \times \{H(0, 2)+H(1, 1)\} \quad (3.4)$$

and equals the total number of n-particles striking unit area per second.

Assuming spherical isotropy of the velocity distribution in each s-state, it is easy to calculate the number of such particles striking unit area:

$$n(_s = \tfrac{1}{4}(N_s/V)(p_s/m) = \tfrac{1}{4} w_s (2kT/m)^{\frac{1}{2}} H_s(\tfrac{1}{2}, 0). \quad (3.5)$$

The pressure exerted by the gas can be obtained from these by integrating expressions like $2p_x$ times (3.2). The results confirm Eq. (1.30). The kinetic energy carried by the particles arriving per second per unit area is found by integrating the expression, for the n-states:

$$\epsilon(_n = \int (1/2m)(p^2+p_x^2) n(p_x) dp_x. \quad (3.6)$$

The result is

$$\epsilon(_n = 4\pi m(kT)^3 h^{-3} \times \{H(0, 3)+H(1, 2)+\tfrac{1}{2}H(2, 1)\}. \quad (3.7)$$

For the s-states, where each s-particle carries the same energy for any given value of s, we find the energy arriving per second per unit area:

$$\epsilon(_s = \tfrac{1}{2} w_s (1/2m)^{\frac{1}{2}} (kT)^3 H_s(\tfrac{3}{2}, 0). \quad (3.8)$$

To obtain the Knudsen phenomena, consider two enclosures filled with the gas at slightly different pressures and temperatures, and connected by a hole so small that no appreciable disturbance in the mean velocity distribution of the gas occurs in either enclosure in the immediate neighborhood of the hole. The net mass flow through such a hole is its area multiplied by the first variation of the number

$$n(\equiv n(_n + \sum_{s=0}^{z} n(_s. \quad (3.9)$$

The condition for a steady state, zero net mass flow, is

$$\Delta n(= 0. \quad (3.10)$$

Put this condition in (3.4), (3.5) and (3.9) and find the following value for the variation of $\ln\lambda$ as between the two enclosures:

$$\frac{\Delta \ln\lambda}{\Delta \ln T} = -\frac{2H(0, 2)+2H(1, 1)+H(2, 0)+\sum_{s=0}^{z}(2/3)\Delta(\epsilon_{s+1}/kT)^{\frac{1}{2}} H_s(\frac{3}{2}, -1)}{H(0, 1)+H(1, 0)+\sum_{s=0}^{z}(2/3)\Delta(\epsilon_{s+1}/kT)^{\frac{1}{2}} H_s(\frac{1}{2}, -1)}. \quad (3.11)$$

We next write out the first variation of the pressure (1.31) and use the theorems (1.12) to (1.14). Then obtain the pressure difference between the two enclosures required to prevent a net mass flow under the temperature difference ΔT, by using (3.11) in the first variation of the pressure. The

result is the Knudsen pressure coefficient:

$$V\Delta P/Nk\Delta T=\frac{\Lambda(2,\tfrac{3}{2})+\sum_{s=0}^{z}(8/9(\pi)^{\frac{1}{2}})\Delta(\epsilon_{s+1}/kT)^{\frac{1}{2}}H_s(1,-1)}{\Lambda(1,\tfrac{3}{2})+\sum_{s=0}^{z}(4/3(\pi)^{\frac{1}{2}})\Delta(\epsilon_{s+1}/kT)^{\frac{1}{2}}H_s(0,0)}\frac{\Delta\ln\lambda}{\Delta\ln T}$$

$$+\frac{(5/2)\Lambda(3,5/2)+\sum_{s=0}^{z}(8/9(\pi)^{\frac{1}{2}})\Delta(\epsilon_{s+1}/kT)^{\frac{1}{2}}\{H_s(0,0)-H_s(1,-1)+H_s(1,0)\}}{(5/2)\Lambda(3,5/2)+\sum_{s=0}^{z}(8/9(\pi)^{\frac{1}{2}})\Delta(\epsilon_{s+1}/kT)^{\frac{1}{2}}H_s(2,-1)}Q_2. \quad (3.12)$$

At sufficiently high temperatures most of the terms in this expression become negligible and we find the classical result:

$$T\gg T_\lambda,\quad \Delta P/\Delta T=(Nk/V)(5/2-2)$$
$$=\tfrac{1}{2}Nk/V. \quad (3.13)$$

On the integration approximation

$$H(0,m)=\zeta(\lambda,m)$$

while $H(n,m)=0$, $n\neq 0$. Therefore in place of (3.11) we have

$$\Delta\ln\lambda/\Delta\ln T=-2\zeta(\lambda,2)/\zeta(\lambda,1) \quad (3.11a)$$

while the Knudsen pressure coefficient becomes

$$V\Delta P/Nk\Delta T=5Q_2/2-2\zeta(\lambda,2)/\zeta(\lambda,1). \quad (3.12a)$$

The isothermal Knudsen heat transfer is obtained from the isothermal variation of the energy flow

$$\epsilon(\equiv\epsilon(_n+\sum_{s=0}^{z}\epsilon(_s. \quad (3.14)$$

We use (3.7) and (3.8) and divide the result by the isothermal first variation of $n($ given by (3.9) to obtain the mean energy per particle flowing on average across the hole when there is a pressure difference but no temperature difference. This is the isothermal Knudsen heat transfer Q_1 and we find that

$$Q_1/kT \text{ is exactly equal to } -\Delta\ln\lambda/\Delta\ln T$$

as given by the expression (3.11). We may write this on the integration approximation:

$$Q_1/kT=2\zeta(\lambda,2)/\zeta(\lambda,1). \quad (3.15)$$

The curve in Fig. 4 is drawn from this equation. It has the classical value 2 at sufficiently high temperatures.

From quasi-thermodynamics it is expected that

$$V\Delta P/Nk\Delta T=(Q_2-Q_1)/kT \quad (3.16)$$

and it is obvious that the integration approximation, represented by (2.15), (3.12a) and (3.15) that this relation is identically satisfied. If we use the more exact expressions, and accept the same approximation as in (1.18) for evaluating the corrections, we easily confirm that (3.16) is again satisfied.

The actual value of Q_1 given by (3.15) is of considerable interest. The denominator becomes infinite at T_λ and remains infinite at lower temperatures, so that the heat transferred through the small hole vanishes there. The same result follows on the second approximation. Inspecting (3.11), which yields this second approximation for Q_1, we note that the series

$$H(2,0) \quad \text{and} \quad \sum_{s=0}^{z} w_s H_s(\tfrac{3}{2},-1)$$

become the dominant terms in the numerator, while the series

$$H(1,0) \quad \text{and} \quad \sum_{s=0}^{z} w_s H_s(\tfrac{1}{2},-1)$$

are the dominant terms in the denominator. The ratio of these terms is not greater than ϵ_z/kT, and in fact equals the mean energy of the lowest states divided by kT, when $T\leqslant T_\lambda$. The mean energy vanishes at and below the lambda-point, because of the greatly increased population of the lowest state, so that again we obtain the same result: *the Bose-Einstein gas cannot transport heat during isothermal flow through a small hole at temperatures below the lambda transition.*

The writer is happy to express his gratitude to Dr. Lothar Meyer, Dr. J. W. Stout, and Dr. Lester Guttman for numerous discussions.

Letters to the Editor

PUBLICATION of brief reports of important discoveries in physics may be secured by addressing them to this department. The closing date for this department is five weeks prior to the date of issue. No proof will be sent to the authors. The Board of Editors does not hold itself responsible for the opinions expressed by the correspondents. Communications should not exceed 600 words in length.

Non-Radiating Maxwell Waves

GRANVILLE A. PERKINS
Carbide and Carbon Chemicals Corporation, New York, New York
May 4, 1949

SINCE Bohr's suggestion of steady states, many attempts have been made to describe, mathematically, non-radiating electrodynamic oscillations, including non-radiating solutions of Maxwell's field equations. However, no one seems to have pointed out that a single restriction, consistent with those equations and equivalent to zero permeability, puts them in a form for which *all solutions* are non-radiating.

It is assumed that Maxwell's field equations are correct, with their original physical interpretations. It is also assumed that a component portion of the field, particularly that associated with transitions between states, can be described by the usual Maxwell-Lorentz equations. There is abundant evidence, however, of non-radiating oscillation within a steady state, and for brevity only the non-radiating oscillatory portion of the field will be here described. In Eqs. (1) and (2) Maxwell's **D** is replaced by $\mathbf{E}+4\pi\mathbf{P}$ and **B** by $\mathbf{H}+4\pi\mathbf{M}$; **u** and ρ are considered to be zero for this portion of the field.

$$\text{curl}\mathbf{H}=\dot{\mathbf{E}}/c+4\pi\dot{\mathbf{P}}/c \tag{1}$$
$$\text{curl}\mathbf{E}=-\dot{\mathbf{H}}/c-4\pi\dot{\mathbf{M}}/c \tag{2}$$
$$\mathbf{H}=\text{curl}\mathbf{A}-\text{grad}\Omega \tag{3}$$
$$4\pi\mathbf{M}=\text{curl}\mathbf{Q}+\text{grad}\Omega \tag{4}$$
$$\mathbf{E}=-\text{grad}\phi-\dot{\mathbf{A}}/c-\dot{\mathbf{Q}}/c \tag{5}$$
$$\text{div}\mathbf{A}+\dot{\phi}/c=0. \tag{6}$$

The potentials are unusual, but (3), (4) and (5) are obviously consistent with (1) and (2). Equation (6) is also easily proved to be consistent by standard methods. From the above equations the following inhomogeneous wave equations are obtained:

$$\nabla^2\phi-\ddot{\phi}/c^2=4\pi\,\text{div}\mathbf{P}-\text{div}\dot{\mathbf{Q}}/c \tag{7}$$
$$\nabla^2\mathbf{A}-\ddot{\mathbf{A}}/c^2=-4\pi\dot{\mathbf{P}}/c+\ddot{\mathbf{Q}}/c^2. \tag{8}$$

Equations (7) and (8) are as general as (1) and (2), but for the oscillation under discussion we make the particular restriction, compatible with (1)–(8):

$$\mathbf{Q}=-\mathbf{A}. \tag{9}$$

Equations (7) and (8) reduce to:

$$\nabla^2\phi=4\pi\,\text{div}\mathbf{P} \tag{10}$$
$$\nabla^2\mathbf{A}=-4\pi\dot{\mathbf{P}}/c. \tag{11}$$

These equations are easily solved for any given oscillation of $\dot{\mathbf{P}}$ and div**P**, and the solutions are non-radiating because there is no wave equation. The non-radiative character of similar equations is well established in classical theory. Presumably Ω vanishes, but even if it does not, it cannot make Eqs. (10) and (11) radiative.

The assumption, here, of the correctness of classical theory does not include that portion of classical theory specifically applying to the electron, such as the Lorentz electron theory. On the contrary, one may consider the time average of charge density, ρ, to be distributed according to Schrödinger's equation, with a superposed charge density $-\text{div}\mathbf{P}$, which oscillates with twice the de Broglie frequency, without radiation. This is entirely consistent with classical (pre-electron) electromagnetic theory, and accordingly the total instantaneous charge density at any point is $\rho-\text{div}\mathbf{P}$, which may be considered to vary in the range between 0 and 2ρ. Any motion of the electron as a whole gives rise to the convection current density, **u**, which is connected with radiation according to the Maxwell-Lorentz equations.

Present study indicates that a comprehensive theory can be formulated along these lines, the time-dependence of the charge density removing the chief difficulties encountered by such theories in the past.

Neutron-Hydrogen Mass Difference from the D–D Reactions*

A. V. TOLLESTRUP, F. A. JENKINS,** W. A. FOWLER, AND C. C. LAURITSEN
Kellogg Radiation Laboratory, California Institute of Technology, Pasadena, California
April 26, 1949

THE energy release in the reactions

$$D^2+D^2\rightarrow H^3+H^1+Q_1 \tag{1}$$
$$D^2+D^2\rightarrow He^3+n^1+Q_2 \tag{2}$$

has been determined by measurement of the energy of the singly charged H^3 and He^3 ions produced in a heavy ice target at a known angle with a deuteron beam of well-defined energy. The results have been used to evaluate the neutron-hydrogen mass difference as follows:

$$n^1-H^1=(Q_1-Q_2)+(H^3-He^3).$$

The mass difference of H^3 and He^3 is taken from measurements on the maximum energy of the β-rays from tritium. Two recent determinations[1,2] give a weighted mean of 18.3 ± 0.3 kev. In the second reference it is shown that the neutrino mass is less than 1.0 kev and hence can be disregarded in these calculations.

Deuterons mono-energetic to better than 0.1 percent were obtained from an electrostatic accelerator and analyzer previously described.[3] The analyzer was calibrated by measurements on the strong gamma-ray resonance in $F^{19}(p\alpha', \gamma)O^{16}$ which has been carefully standardized by Herb *et al.*[4] at 873.5 kev. The target was produced by allowing D_2O vapor to enter the target chamber adjacent to a flat face on a copper rod which was kept at liquid air temperature. The D_2O vapor condensed on the rod continuously thus insuring a fresh target surface at all times. Oil vapors were trapped out of the system by means of a liquid air trap at the diffusion pump.

The H^3 and He^3 ions were detected with a scintillation counter. The ZnS screen[5] was located in the vacuum system. Fluorescent light from the scintillations was collected by a hemispherical mirror, brought out through a Lucite window, and focused on the cathode of a 931-A electron multiplier. The pulses from the electron multiplier were amplified $\sim10^4$ times. A discriminator was used to eliminate the dark current pulses.

The energies of the H^3 and He^3 ions emerging from the target in the angular interval 134.5°–141.1° were measured by means of a double-focusing magnetic spectrometer.[6] In one set of measurements the energy of the doubly charged He^3 ions was also measured. For accurate comparison of the results for reactions (1) and (2), the majority of the observations were made on singly charged He^3 ions. The magnetic field in the spectrometer, which was determined by means of

a null reading fluxmeter,[7] could be held fixed to 0.05 percent and reproduced to 0.3 percent. Since the energies of the H^3 and He^3 ions are very dependent upon angle, the angular opening of 6.6° was the major factor in determining the experimental resolution (4 percent in energy).

The spectrograph was calibrated by observing the maximum energy protons and deuterons scattered into the spectrograph from a copper target and from the oxygen of the D_2O target. The energy of protons scattered from copper is almost independent of angle, whereas the energy of deuterons scattered from oxygen is very dependent upon angle. Thus it is possible to determine the fluxmeter calibration and also to check the direct measurement of the angle of observation.

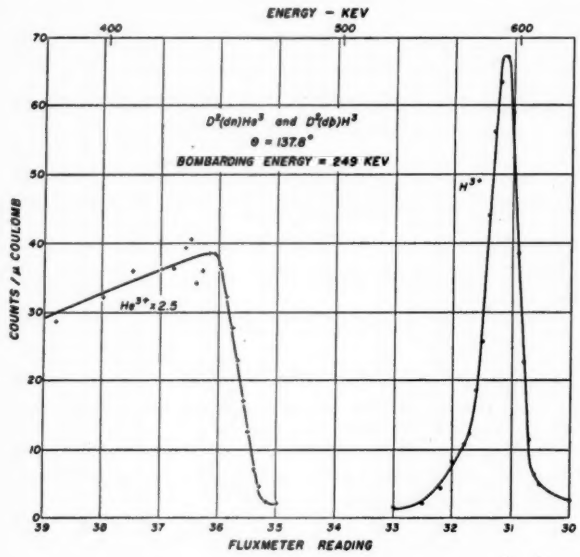

FIG. 1. Energies of H^3 and He^3 ions.

Figure 1 shows curves obtained with deuterons at a bombarding energy of 249 kev. The target was about 30 kev thick for the deuterons. This figure was ascertained by comparing the neutron intensity with that from a thick target. All runs were made while the neutron count was slowly increasing, which indicated that fresh ice was being deposited. The target was very thick for the He^3 ions due to the large stopping cross section of the target atoms for helium ions. The curve for the H^3 ions is similar to a thin target curve even though the target was ~30 kev thick for these ions. This apparent contradiction can be explained by the fact that at the mean angle of 137.8°, the energy of the H^3 particles increases with decreasing incident deuteron energy. Thus H^3 particles formed deep in the target receive more energy than those formed at the surface. However, those formed deep in the target must expend energy to reach the surface of the target. For thin smooth targets, calculations indicate that the H^3 particles entering the spectrograph from the surface have slightly greater energy than those from deeper in the target. This is contingent on the target being turned at such an angle that the paths for penetration of the deuterons and reemergence of the H^3 are nearly equal. A careful study of the results at different target angles confirmed this conclusion. Because of irregularities in the target surface, presumably arising from its crystalline nature, a few particles from deep in the target escape from the target with energies greater than those from the surface. This accounts for the "fillet" on the leading edge of the H^3 peak. The effect was more pronounced for thick targets, as was expected. For this reason only thin targets were employed, and the extrapolation of the front edge of the H^3 curve was taken as corresponding to the energy of particles entering at the minimum acceptance angle of the spectrograph, 134.5°. The slope of the front edge is consistent with the resolution expected from the spectrograph entrance and exit windows and from the dependence of the energy of the H^3 on angle. A small correction gave the energy for those entering at the mean acceptance angle of 137.8°. The corrected values agreed with the energy at the peak of the curve. An additional correction for one-half the energy equivalent of the target thickness was made. The point of half-maximum intensity on the "thick" target curves for He^3 was taken as corresponding to the energy of those He^3 ions leaving the surface of the target at 137.8°. The extrapolated end points of the He^3 curves properly corrected gave the same results. Fourteen separate curves were obtained at five different bombarding voltages. The weighted averages are $Q_1=4.036\pm0.022$ Mev, $Q_2=3.265\pm0.018$ Mev, $Q_1-Q_2=771\pm6$ kev.

The probable errors were computed by combining the observed statistical errors, which were very small, with estimated systematic errors. The systematic probable errors assumed were 0.3° in angle of observation, 0.6 percent in observed energy, and 0.2 percent in energy of deuterons. The small error in Q_1-Q_2 is obtained because only the difference between the H^3 and He^3 energies is significant in determining this number. The results for Q_2 are substantially in agreement with other recent determinations.[8] The value for Q_1 is significantly higher than the value $3.98\pm.02$ previously determined.[9] The above data yield $n^1-H^1=789\pm6$ kev. This is in satisfactory agreement with the recent determinations from (p, n) reaction thresholds of 776 ± 10[10] and 782 ± 2 kev.[11] Combined with the mass spectroscopic[12] value for $2H^1-H^2=1.432\pm.002$ Mev, one obtains the binding energy of the deuteron as $2.221\pm.006$ Mev which is somewhat lower than the value $2.235\pm.009$ recently determined by Bell and Elliott.[13]

* This work was assisted by the joint program of the ONR and AEC.
** While on leave from the University of California.
[1] S. C. Curran, J. Angus, and A. L. Cockroft, Phil. Mag. **40**, 53 (1949).
[2] G. C. Hanna and B. Pontecorvo, Phys. Rev. **75**, 983 (1949).
[3] W. A. Fowler, C. C. Lauritsen, and T. Lauritsen, Rev. Sci. Inst. **18**, 818 (1947).
[4] R. G. Herb, S. C. Snowdon, and O. Sala, Phys. Rev. **75**, 246 (1949).
[5] Furnished by RCA, phosphor type 33Z20-A.
[6] C. W. Snyder, C. C. Lauritsen, W. A. Fowler, and S. Rubin, Phys. Rev. **74**, 1564A (1948).
[7] C. C. Lauritsen and T. Lauritsen, Rev. Sci. Inst. **19**, 916 (1948).
[8] H. V. Argo, Phys. Rev. **74**, 1293 (1948); D. L. Livesey and D. H. Wilkinson, Proc. Roy. Soc. **195**, 123 (1948).
[9] M. L. Oliphant, A. R. Kempton, and Lord Rutherford, Proc. Roy. Soc. **149**, 406 (1935); M. S. Livingston and H. A. Bethe, Rev. Mod. Phys. **9**, 245 (1937).
[10] W. E. Shoupp, B. Jennings, and K. H. Sun, Phys. Rev. **75**, 1 (1949).
[11] A. Hemmendinger, *et al.* private communication. R. F. Taschek, G. A. Jarvis, H. V. Argo, and A. Hemmendinger, Phys. Rev. **75**, 1268 (1949).
[12] K. T. Bainbridge, National Research Council Preliminary Report No. 1, Nuclear Science Series (1948).
[13] R. E. Bell and L. G. Elliott, Phys. Rev. **74**, 1552 (1948).

Note on the Use of the Shock Tube as an Intermittent Supersonic Wind Tunnel*

GEORGE RUDINGER
Cornell Aeronautical Laboratory, Inc., Buffalo, New York
May 6, 1949

THE use of a shock tube as an intermittent supersonic wind tunnel was discussed in a recent letter.[1] An expression was given for the ratio of the pressures on the two sides of the shock which would just make the flow behind the shock supersonic with respect to the tube.

In two notes published more recently elsewhere,[2,3] it was shown that there exists a maximum Mach number which can be produced behind a shock wave advancing into a gas at rest. For an infinite pressure ratio across the shock this limiting Mach number was shown to be 1.89 for air.

This is considerably lower than the value of 2.42 shown in the sample photograph of reference 1 and this apparent incompatibility will be discussed in the following.

It is known[4] that breaking a diaphragm which separates regions of different pressures in a tube produces a shock wave and an expansion wave traveling in opposite directions, and an interface moving between them in the direction of the shock wave. Across the interface, pressure and flow velocity remain constant while the temperature may change. In the region between the shock wave and the interface, the limiting value of Mach number applies while no such limit exists for the gas between the interface and the expansion wave. The gas between the shock wave and the interface is compressed by the former, and therefore, its temperature is raised. If the shock strength is increased to infinity, both the temperature and the flow velocity behind the shock become infinite in such a way, however, that the Mach number approaches the finite limit stated above. If subscripts c and e are used to refer to the compression and expansion chambers, respectively, and if the speed of sound before breaking the diaphragm is denoted by a the pressure ratio across the shock (defined so as to be greater than unity) which will just produce sonic flow in the region between the interface and the expansion wave may be computed as

$$y=1+\frac{\gamma_e(\gamma_e+1)+\gamma_e[(\gamma_e+1)^2+8(\gamma_c+1)a_e/a_c]^{\frac{1}{2}}}{2(\gamma_c+1)a_e/a_c}.$$

(Note that $y=1/\xi$ of reference 1 $=\lambda$ of references 2 and 3.)

For the special case of $a_e=a_c$ and $\gamma_e=\gamma_c=1.4$, this formula yields $y=3.16$. This compares with a pressure ratio of 4.76 to produce sonic flow between the shock wave and the interface computed from the relation given in reference 1. In other words, it is possible to obtain supersonic flow in a shock tube even though the shock is not strong enough to produce supersonic flow immediately behind itself. The Mach number in the region following the interface will always be higher than that in the region following the shock unless the temperature in the compression chamber was so high initially that even after expansion, the speed of sound in the expanded region was still higher than in the compression region between the shock and the interface.

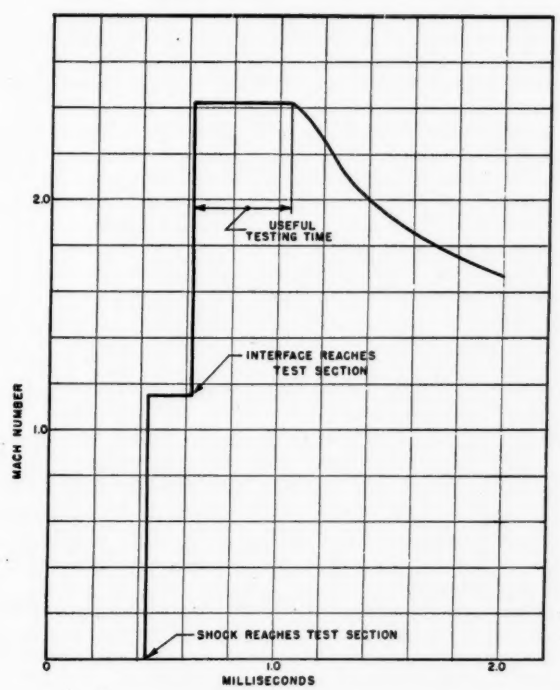

FIG. 1. Variation of Mach number with time at the test section of a shock tube.

To illustrate how the Mach number in a shock tube may reach the value 2.42 presented in reference 1, an example was worked out by means of the method of characteristics. The shock tube was assumed to be filled with air ($\gamma=1.4$) and the initial conditions for pressure, and speed of sound were $p_c/p_e=106$, and $a_c=a_e=350$ m/sec. The length of the compression chamber was taken as 0.70 m and the test section located at a distance of 0.35 m from the position of the diaphragm. The tube was assumed long enough to eliminate effects from wave reflection. Figure 1 shows the value of Mach number at the test section as function of time. As soon as the shock passes the test section the Mach number becomes 1.15. About 200 microseconds later the interface reaches the test section and the Mach number is increased to 2.42. This value is then maintained for about 400 microseconds after which the Mach number decreases gradually. It is seen that using the flow following the interface not only eliminates the Mach number limitation but also may lead to a useful testing time which is considerably longer than that corresponding to the flow ahead of the interface.

The fact that there may be two distinct supersonic Mach numbers occurring during one shock tube experiment is, perhaps, not generally realized and some of the observed transients during which steady supersonic flow is established may, in part at least, be due to the passage of the interface.

* These comments are based on related work on non-stationary gas flow which is being supported by ONR through Project SQUID.

[1] C. W. Mautz, F. W. Geiger, and H. T. Epstein, Phys. Rev. **74**, 1872 (1948).
[2] F. Cap, J. Chem. Phys. **17**, 106 (1949).
[3] B. W. Augenstein, J. Chem. Phys. **17**, 429 (1949).
[4] R. Courant and K. O. Friedrichs, *Supersonic Flow and Shock Waves* (Interscience Publishers, Inc., New York, 1948), p. 181.

Shape of the Beta-Spectra of Sr^{90} and Y^{90} *

E. N. JENSEN AND L. JACKSON LASLETT
Institute for Atomic Research and Department of Physics, Iowa State College, Ames, Iowa
April 26, 1949

THE beta-spectra of Sr^{90} and Y^{90} have been examined in this laboratory, using the magnetic lens spectrometer previously described,[1] and were found to exhibit a shape similar to that recently reported by Langer and Price[2] for the forbidden transition of Y^{91}.

The $Sr^{90}-Y^{90}$ spectra were first investigated here using a composite source,[3] in equilibrium, mounted on a thin Formvar-polystyrene film carried by a Lucite holder. The observational data were corrected at low energies for the transmission of the window of the Geiger-Müller counter; the correction factor for this window, which would pass electrons of energies of 12 kev, was estimated by determining the effect of additional foils in front of the counter and was significant only for electrons of kinetic energy below 230 kev. For making comparisons with the theoretical momentum distributions, carefully computed values of the Fermi function were used which were in very good agreement with the values obtained by the use of Bethe's[4] approximation.

A Kurie plot of the data obtained with the composite source is shown in Fig. 1, in which the points for the spectrum due to Sr^{90} alone were obtained by subtraction of the estimated contribution from the Y^{90} component. The non-linearity of the curves thus obtained indicates that the spectra of these two activities differ significantly in shape from that expected for allowed transitions and frequently found for forbidden spectra. To obtain more definitive data on the spectrum of Sr^{90} alone, a portion of the strontium activity was separated from the composite source and examined in the spectrometer. A Kurie plot of the data so obtained, after correction for residual Y^{90}, is shown in Fig. 2. The non-linear character of this graph resembles closely that illustrated by Fig. 1.

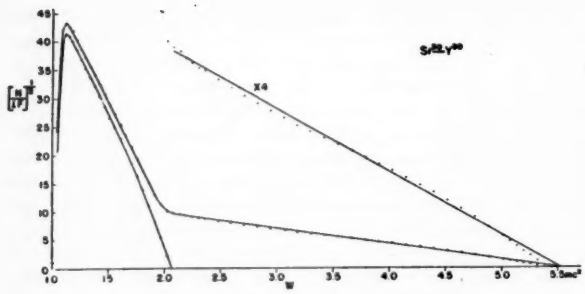

FIG. 1. Kurie plot, $(N/IF)^{\frac{1}{2}}$ *vs.* W, of beta-spectrum obtained with composite $Sr^{90}-Y^{90}$ source.

On the basis of the theory of shell-structure in nuclei, as developed by Feenberg and Hammack,[5] it would be reasonable to consider these transitions to involve a spin change of two units, together with a parity change. Introduction of the factor

$$a=(W^2-1)+(W_0-W)^2,$$

which is theoretically appropriate[6] for transitions of this type, leads to the modified Kurie plots shown in Fig. 3. The linearity

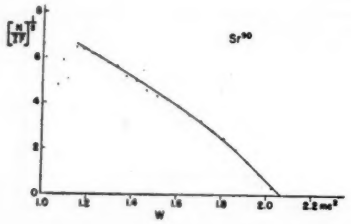

FIG. 2. Kurie plot of beta-spectrum obtained with separated Sr^{90} source.

thus obtained affords evidence that the transitions are of the type indicated, for which the special form found for the spectrum becomes in agreement with that predicted theoretically. These spectra are of perhaps particular interest in that the initial Sr^{90} nucleus and that of the final Zr^{90} product are each of the *even-even* type.

The upper limits found for the Sr^{90} and Y^{90} spectra are, from Fig. 3, 2.05 mc^2 (0.53$_7$-Mev kinetic energy) and 5.37 mc^2 (2.23-Mev kinetic energy), respectively. These values, determined in light of the special form found for the spectra, differ not inappreciably from those reported by Meyerhof,[7] whose data also, however, give some indication of the same type of departure from the conventional spectral shape as that reported here.

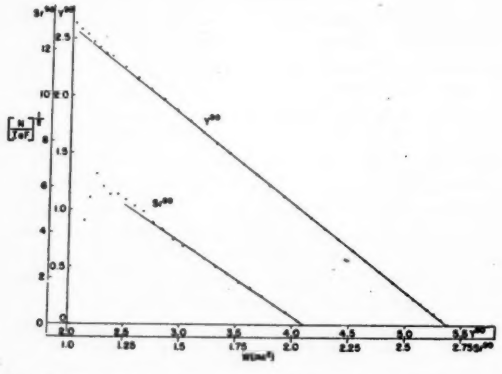

FIG. 3. Modified Kurie plots, $(N/IaF)^{\frac{1}{2}}$ *vs.* W, for the upper, or Y^{90} portion of the beta-spectrum obtained with the composite source and of the spectrum obtained with the separated Sr^{90} source.

We wish to indicate our appreciation of the assistance by Dr. A. F. Voigt and his associates in the Radiochemistry section of this Laboratory for their help in the separation of the Sr^{90} activity and our thanks to Dr. J. M. Keller, Dr. J. F. Carlson, and Mr. A. Paskin for helpful discussions concerning the theoretical aspects of the work. The assistance of Mr. R. T. Nichols in recording and computing the data and of Mr. E. R. Rathbun, Jr., in construction of the Geiger-Müller tubes is also gratefully acknowledged.

* Contribution No. 65 from the Institute for Atomic Research and Department of Physics, Iowa State College, Ames, Iowa. Work was performed at the Ames Laboratory of the Atomic Energy Commission.

[1] Jensen, Laslett, and Pratt, Phys. Rev. **75**, 458 (1949). The use of this instrument for the study of beta-ray spectra has been checked by the use of a P^{32} sample, and found to give data consistent with the results of other investigators.

[2] L. M. Langer and H. C. Price, Jr., Phys. Rev. **75**, 1109 (1949). We are greatly indebted to Dr. Langer for kindly sending us a copy of his manuscript in advance of its publication and for calling to our attention the applicability of a special type of energy dependence for the Y^{91} beta-transition.

[3] This source was kindly furnished in high specific activity by Dr. C. W. Sherwin, of the University of Illinois, who has been especially interested in the beta-spectrum of Y^{90} in connection with his neutrino-recoil experiments. The active material was grounded electrically, by means of a line of silver paint, to avoid charging effects during the observations.

[4] H. A. Bethe and R. F. Bacher, Rev. Mod. Phys. **8**, 194 (1936).

[5] E. Feenberg and K. C. Hammack, private communication of work now scheduled for publication. We are indebted to Dr. Feenberg for correspondence concerning this work and for pointing out the inapplicability of the usual $f \cdot t$ selection criterion for disintegrations of the type considered here. Dr. Feenberg has recently indicated that results similar to ours have been obtained at Washington University by Braden, Slack, and Shull.

[6] E. J. Konopinski, Rev. Mod. Phys. **15**, 227 (1943); E. J. Konopinski and G. E. Uhlenbeck, Phys. Rev. **60**, 308–20 (1941).

[7] W. E. Meyerhof, Phys. Rev. **74**, 621 (1948).

Determination of the Energy Distribution of Bremsstrahlung from 19.5 Mev Electrons*

H. W. KOCH AND R. E. CARTER**
Physics Department, University of Illinois, Urbana, Illinois
April 25, 1949

THE bremsstrahlung spectrum has been measured for 19.5 Mev electrons produced by a betatron and directed against a 0.005-in. thick platinum target. The relative intensity of the x-rays as a function of energy was determined from the energy distribution of the pair electrons produced in the gas of a cloud chamber, which was air. Since the pair production cross section is known for a low Z material (air) to better than 10 percent at energies between 1 and 20 Mev,[1] the x-ray intensity spectrum from platinum can be reliably inferred from the pair electron spectrum.

Two reports on determinations of betatron x-ray spectra have been published.[2] Neither work permits a conclusive test of the Bethe-Heitler bremsstrahlung theory applied to electrons of 19.5 Mev energy.

In the present experiment, the x-rays from the betatron target are collimated by means of a tapered hole in a 16-in. thick lead wall. The defining aperture for the rays was the $\frac{1}{8}$-in. diameter entrance opening of the collimator, which defined an x-ray beam whose total angle was 0.24°. The half-intensity total angle of the x-rays from the thin betatron target was approximately 6°.

Pair electrons produced in an air pressure of 1.4 atmospheres were curved by a magnetic field of 1540 gausses. 40,000 stereoscopic pictures were taken on 35 millimeter film. Of this total number, 10,300 pictures have been analyzed. Data were obtained on approximately 1300 pair electrons produced in the field of a nucleus and 33 pair electrons produced in the field of an electron.

The analysis of pair energies was divided into two parts: (1) The direct image of the film was carefully reprojected on a plane normal to the cloud-chamber magnetic field direction. The x and y coordinates of the pair origin, the radii of the pair particle arcs, and the corresponding chord lengths were measured. (2) The film was reprojected through the original

camera-mirror system into three dimensions. The z coordinate of the pair origin, the dip angles for both electron and positron helical tracks, and the angle between the individual particles and the incoming quantum were measured.

From the two sets of information, the electron and the positron helices could be completely specified in space. The detailed specification of tracks was necessary in order to determine the sensitivity of the experimental apparatus to detect or to discriminate against certain energy ranges of pairs. The selection or omission criteria for pairs are based on the minimum chord length required to measure accurately a given particle radius and on the maximum allowable dip angle of a particle helix. Weighting factors have been obtained as a function of particle energy which are applied to each pair kept for the final data. The weighting factors correct for the tracks omitted due to the selection criteria.

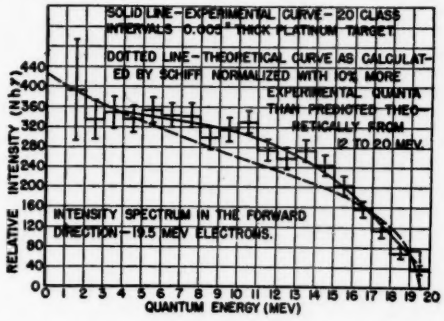
SOLID LINE—EXPERIMENTAL CURVE—20 CLASS INTERVALS 0.005" THICK PLATINUM TARGET
DOTTED LINE—THEORETICAL CURVE AS CALCULATED BY SCHIFF NORMALIZED WITH 10% MORE EXPERIMENTAL QUANTA THAN PREDICTED THEORETICALLY FROM 12 TO 20 MEV.
INTENSITY SPECTRUM IN THE FORWARD DIRECTION—19.5 MEV ELECTRONS.
RELATIVE INTENSITY (N h ν)
QUANTUM ENERGY (MEV)

FIG. 1. X-ray intensity spectrum as deduced from corrected pair spectrum obtained with a total of 1130 pairs.

Figure 1 shows the x-ray intensity spectrum as deduced from the corrected pair spectrum obtained with a total of 1130 pairs. The dotted line is the theoretically predicted intensity spectrum in the forward direction and for a thin platinum target as calculated by Schiff using the Bethe-Heitler theory.[3] The theoretical curve has been normalized by providing for 10 percent more experimental quanta than theoretically predicted from 12 to 20 Mev.[4]

The experimental histogram shows an apparent difference in shape from the theoretical curve, which can possibly be attributed to the approximations of the Bethe-Heitler calculations. The difference in shape indicates relatively more experimental quanta in the middle energy ranges. This conclusion has been found to be independent of the type of normalization used.

Results have also been obtained on the positron fractional energy, the particle-quantum angles, and pairs produced in the field of an electron. The data provide a consistent picture of pair and triplet production and serve to test the reliability of the weighting factor principles used for correcting the x-ray spectral distribution.

The authors are indebted to Professors C. S. Robinson and A. T. Nordsieck for their invaluable suggestions and help. Mr. George Modesitt capably performed much of the tedious analysis.

* Assisted by the joint program of the ONR and the AEC.
** Now at the Los Alamos Scientific Laboratory, Los Alamos, New Mexico.
[1] See G. D. Adams, Phys. Rev. **74**, 1707 (1948) and C. L. Cowan, Phys. Rev. **74**, 1841 (1948) for the latest results and the references in the literature. The theoretical pair production cross section for air is within 3 percent of the experimental value at energies between 10.9 and 18.7 Mev according to the results of the first reference.
[2] Lasich and Riddiford, J. Sci. Inst. **24**, 177 (1947). Bosley, Craggs, Nash, and Payne, Nature **161**, 1022 (1948).
[3] Private communication from Professor L. I. Schiff. See also L. I. Schiff, Phys. Rev. **70**, 87 (1946).
[4] L. H. Lanzl, J. S. Laughlin, and L. S. Skaggs, Phys. Rev. **74**, 1261 (1948).

Contraction of the Instantaneous Orbit at Injection in a Betatron

F. F. HEYMANN
Research Department, Metropolitan-Vickers Electrical Company, Ltd., Manchester, England
April 26, 1949

KERST[1] has given what appears to be a satisfactory explanation of the mechanism by which the electron beam in a betatron is caused to miss the injector for the first few revolutions after injection. According to this theory, an electron loses an amount of energy $\Delta E = LdI/dt$ electron volts per revolution, where L is the effective self-inductance of the electron beam, and dI/dt is the rate at which the current in the beam increases. This loss in energy causes the orbit radius to contract by an amount[1]

$$\Delta E/E = 2(1-n)\Delta r/r. \tag{1}$$

In the betatron under discussion, $n = \frac{3}{4}$, which reduces Eq. (1) to

$$\Delta r/r = 2\Delta E/E \tag{2}$$

where r is the radius of the instantaneous orbit.

Kerst suggests that, in order to enhance this process, energy might be abstracted from the electron beam externally by passing a rapidly changing current through conductors placed above and below the orbit. This procedure has been carried out by Adams[2] who has reported an improvement of 100 percent in the output of a 20 Mev betatron.

A method of orbit contraction has been achieved on a 20 Mev betatron constructed in this Laboratory by the process of applying a negative bias to the silver coating of the vacuum chamber, relative to the anode of the injector. The azimuthal component of the field due to the potential difference between the anode and the silver coating is strong over a small region immediately in front of the injector, and decreases gradually over a considerable fraction of a revolution. The effect of this field may be examined qualitatively by discussing these two regions of the field separately.

In the strong field immediately in front of the injector, the orbit contracts so rapidly in space that the electrons cannot follow it without oscillation, so that any advantage due to this contraction is nullified.

This oscillation is prevented by advancing the phase of the injector pulse, so that in practice, the major effect of this region of the field is to subtract from the injector voltage. In the weaker and more extended region of the field, the instantaneous orbit contracts less rapidly in space, and the electrons are better able to follow this contraction without severe oscillation. It is this region of the field which is responsible for causing electrons to miss the injector on subsequent revolutions.

When injection takes place under these conditions, each electron loses an amount of energy corresponding to some

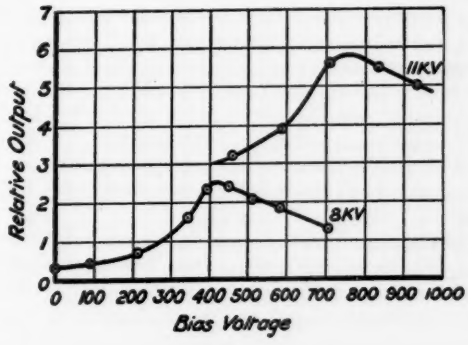

FIG. 1.

fraction of the bias voltage during the first revolution it makes, so that the radius of its instantaneous orbit is reduced correspondingly. On subsequent revolutions, it receives an impulse radially outwards each time it passes the injector. The oscillations set up by this impulse are, however, thought to be relatively small, because of the large gradient of the field near the injector. If the contraction is large enough, electrons will not enter the high potential region in the vicinity of the gun.

The results obtained in tests carried out at injector voltages of 8 and 11 kev respectively, are illustrated in Fig. 1. To obtain points on these curves, the filament current and injector phasing were in each case adjusted for maximum output. It was noticed that the optimum emission was reduced considerably as the bias voltage was increased, as is illustrated in Fig. 2. This seems to indicate that, as the bias is increased,

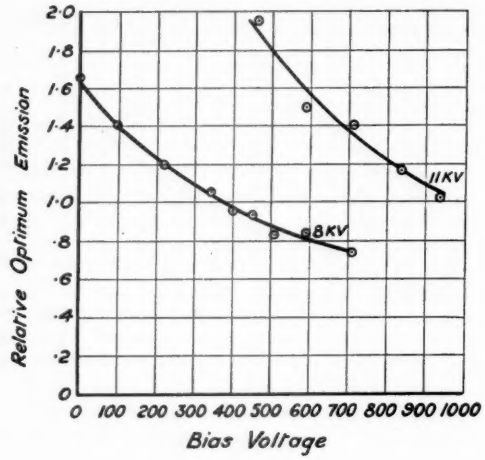

FIG. 1.

less of the contraction due to the Kerst mechanism is needed in order to miss the injector. With 11 kev applied to the injector, it was impossible to obtain a measurable output at zero bias, without increasing the filament current to a dangerously high value.

It is difficult to estimate the fraction of the bias voltage which is effective in producing orbit contraction. An upper limit to the contraction may be found by assuming that the whole of the bias voltage is effective. In this case, the maxima of the curves in Fig. 1 correspond to 2.1 cm and 2.7 cm contraction for 8 and 11 kev respectively. ($r \simeq 20$ cm.)

It was thought that the increase in output might be due to improved focusing of the beam produced by the field in the vacuum chamber, but this seems to be ruled out by the following considerations: The silver coating in the betatron under discussion is split into two isolated sections with the injector placed in the middle of the first section. The currents collected at the two segments were observed separately. The ratio between these currents did not vary by more than 20 percent when the bias was varied. Thus, since the bias does not appreciably improve the fraction of the total emission which manages to reach the further section of the vacuum chamber, it seems probable that the angular spread of the beam emerging from the injector is not appreciably improved by the bias.

With the optimum bias required for 11 kev injector voltage, the x-ray output of the betatron was 9 roentgens/min. at 1 meter, measured in a Victoreen thimble chamber shielded by a $\frac{1}{4}''$ lead sheath with $\frac{3}{8}$ full excitation on the magnet.

[1] D. W. Kerst, Phys. Rev. **74**, 503 (1948).
[2] G. D. Adams, Rev. Sci. Inst. **19**, 607 (1948).

Evidence for a Change in the Nature of Work-Hardening at Small Strains*

J. S. KOEHLER AND T. H. BLEWITT**
Department of Physics, Carnegie Institute of Technology, Washington, D. C.
May 4, 1949

A THEORY of work-hardening using a type of crystalline imperfection known as a dislocation has been given by G. I. Taylor.[1] Taylor supposed that dislocations originate at the surface of the mosaic blocks and that they move through the material until they are stopped at some high internal stress such as a mosaic block boundary or near another dislocation. As the deformation of an initially unstrained crystal proceeds the density of dislocations increases since in Taylor's theory each dislocation on the average contributes a small but finite plastic strain. Simultaneously the stress required for further deformation increases because of the increasing stress field resulting from the large numbers of dislocations present. Taylor supposes that the dislocation density is uniform throughout the material and that most of the dislocations are trapped in the specimen.

There is now considerable evidence that deformation on slip bands is of importance particularly in the initial deformation of a well annealed single crystal. Since slip bands are easily resolved in an ordinary microscope the units responsible for this deformation are therefore more widely spaced than the dislocations used by Taylor. Heidenreich and Shockley[2] obtained electron microscope and electron diffraction pictures of pure aluminum single crystals. After 5 percent extension they observed slip bands separated by about 4μ. At small strains they indicate that the slip bands consist of a single step whereas at larger strains the bands consist of fine parallle laminae about 200A thick. The maximum relative shearing displacement of two neighboring laminae was about 2000A. Heidenreich and Shockley found that the material in the slip bands was sufficiently distorted so that it gave no Kikuchi lines whereas the material between the slip bands gave Kikuchi lines. After 6 percent extension the slip bands were from 1 to 2μ apart and no Kikuchi lines were observed. Blewitt[3] has measured the increase in the electrical resistance of ordered single crystals of $AuCu_3$ during tensile tests in which only single slip occurred. In agreement with Sachs and Weerts[4] he finds that the resolved stress-strain curve consists essentially of two intersecting straight lines; the resolved shearing stress increases slightly in going from a resolved shearing strain of 0 percent to 10 percent whereas when the strain is larger than 10 percent the stress increases rapidly with increasing strain. Blewitt's preliminary data indicates a similar change in the resistance increase produced by coldwork. The increase in the electrical resistance was small for resolved shearing strains less than 10 percent. For larger strains an increase in the residual resistance was found. For a resolved shearing strain of 22 percent the increase amounted to about 2 percent of the initial residual resistance. Miller and Milligan[5] have obtained stress-strain curves for pure aluminum and silver single crystals at small strains. Their data shows changes in the sign of the curvature at extensions of less than 1 percent. Sachs and Weerts[6] have also observed a similar change using single crystals of copper, silver, and gold. Dehlinger and Kochendörfer[7] measured x-ray line widths on polycrystalline rolled copper specimens; after correcting for changes in particle size they found that the average internal stress is negligible until a 5 percent reduction is achieved; the internal stress increases rapidly for larger strains. In other words, there is considerable evidence that the mechanism of flow and hardening alters when the strain exceeds a few percent.

In summary one finds that for small strains the deformation seems to occur by a shearing displacement at the slip bands. The rate of work-hardening seems to be low for this case and

according to Heidenreich and Shockley the distortion seems to be confined to the immediate vicinity of the slip bands. Somewhere in the range of strain from 1 percent to 20 percent the behavior changes, the strains become more homogeneously distributed, the rate of work-hardening increases, and the average of the internal strains over the volume increases rapidly. It may be that at large strains the deformation is sufficiently homogeneous that Taylor's theory can be applied. It seems that the limiting amount of deformation at the slip bands before severe work-hardening begins can be increased by increasing the temperature, by decreasing drastically the rate of strain, and by the use of solid solutions.[8]

There are a number of leading questions which we would like to ask: Does the stress-strain curve remain relatively flat as long as the slip bands consist of a single step; does the stress begin to rise when the slip bands change from a single step to one or more laminae? Does slip continue to occur at a slip band throughout the entire course of deformation? Do new slip bands appear throughout the course of deformation? At large strains is all of the strain accounted for by the relative shearing displacement of neighboring laminae or should one suppose that a portion of the strain is associated with a Taylor dislocation lattice? For deformations at low temperatures does the maximum shearing displacement at a step depend on the size of the specimen?

We would like to thank Professor F. Seitz for several helpful discussions.

* Supported by the Office of Naval Research.
** AEC Fellow in the Physical Sciences.
[1] G. I. Taylor, Proc. Roy. Soc. **145**, 362 (1934).
[2] R. D. Heidenreich and W. Shockley, Bristol Conference on the Strength of Solids, p. 57, Physical Society of London (1947).
[3] T. H. Blewitt and J. S. Koehler, Cambridge meeting Am. Phys. Soc. (June 1949).
[4] G. Sachs and J. Weerts, Zeits. f. Physik **67**, 507 (1931).
[5] R. F. Miller and W. E. Milligan, Trans. AIME **124**, 229 (1937).
[6] G. Sachs and J. Weerts, Zeits. f. Physik **62**, 473 (1930).
[7] U. Dehlinger and A. Kochendörfer, Zeits. f. Krist. **101**, 134 (1939); Zeits. f. Metallkunde **31**, 231 (1939); A. Kochendörfer, Zeits. f. Krist. **101**, 149 (1939).
[8] Schmid and Boas, *Kristalplastizität* (Verlag, Julius Springer, Berlin, 1935), p. 157; R. F. Miller and W. E. Milligan (see reference 5, p. 242); C. F. Elam, *Distortion of Metal Crystals* (Oxford University Press, London, 1935), p. 79, Fig. 45 (α-brass).

The Positron Decay of F^{18}

J. P. Blaser, F. Boehm, P. Marmier
Department of Physics, Swiss Federal Institute of Technology, Zürich, Switzerland
May 2, 1949

THE positron spectrum of F^{18} has been investigated by different authors with rather contradictory results. Snell[1] and Yasaki and Watanabe[2] found a simple spectrum with upper limit between 500 and 700 kev using absorption and cloud-chamber methods. Knox[3] could not find any evidence for nuclear γ-rays. A detailed investigation by means of a cloud chamber has been carried out recently by Zah-Wei Ho,[4] who described a twofold complex β^+-spectrum with upper limits at 950 ± 50 kev (20 percent) and 600 ± 100 kev (80 percent). In addition this author found a 1.4 Mev γ-ray together with some low energy γ-radiation.

A study of this problem with a magnetic β-spectrometer seems desirable. Thin sources of high specific activity are required herefor. A well suited F^{18}-source has been obtained by irradiation of a thin mica foil (muscovite: $KAl_3Si_3H_2O_{12}$) with protons from the cyclotron. A few minutes after bombardment all short periods arising from Al, Si and O have practically disappeared and only two periods of respectively 112 ± 1 minutes and 8 days remain. The negligibly weak 8 days activity can be assigned to Ca^{41} produced in the reaction $K(p, n)Ca$. The 112 minutes period showing β^+-activity arises from F^{18} formed by (p, n)-reaction of O^{18}. In spite of the low isotopic abundance of O^{18} the resulting activity is sufficient for spectrometer measurements. The source used for the magnetic lens spectrometer was a 1.6 mg/cm² mica foil activated directly with a 5.5 Mev proton beam of 1 μA and 6 mm in diameter.

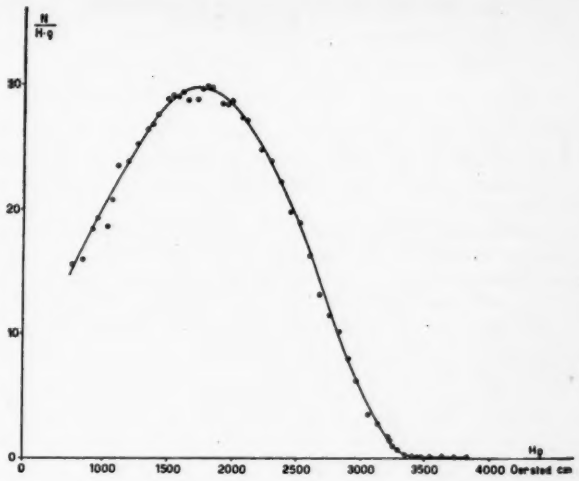

FIG. 1. Positron momentum distribution of F^{18}.

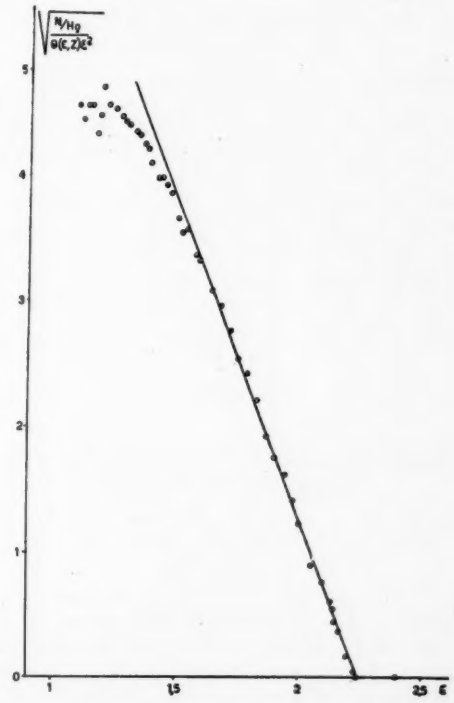

FIG. 2. Kurie plot of the positron spectrum of F^{18}.

Figure 1 shows the momentum distribution of the positrons. The Kurie plot (Fig. 2) indicates an upper limit of 635 ± 15 kev and brings to evidence that the β-spectrum is simple. With $W_0=2.24$ mc² the ft-value is found to be $ft=4100$ characterizing an allowed transition. The mass difference of F^{18} minus O^{18} becomes 0.001781 ± 0.000016 atomic mass units.

[1] A. H. Snell, Phys. Rev. **51**, 143 (1937).
[2] T. Yasaki and S. Watanabe, Nature **141**, 787 (1938).
[3] W. J. Knox, Phys. Rev. **74**, 1192 (1948).
[4] Zah-Wei Ho, Comptes Rendus **226**, 1187 (1948).

On the Hot-Wire Length Correction

STANLEY CORRSIN AND LESLIE S. G. KOVASZNAY
Department of Aeronautics, The Johns Hopkins University, Baltimore, Maryland
May 4, 1949

TWO of the conclusions reached by F. N. Frenkiel[1] concerning the effect of finite length of a hot-wire anemometer upon measurement of turbulence intensity appear to be in error:

(1) Although $1/I_b^2(\equiv\langle e^2\rangle_{Av}/\langle e_0^2\rangle_{Av})$, the ratio of mean square measured voltage to ideal mean square voltage (for $R_y(s)=1$) approaches zero as $1/l$ when the wire length l approaches infinity, still the longitudinal turbulent energy measured by this hot-wire does not approach zero. The measured energy is proportional to $\langle e^2\rangle_{Av}=\langle e_0^2\rangle_{Av}/I_b^2$, and since $\langle e_0^2\rangle_{Av}\sim l^2$, $\langle e^2\rangle_{Av}$ increases proportionally to l as $l\to\infty$.

(2) A Gaussian longitudinal correlation function does not lead to $I_b=1$ when the turbulence is isotropic. If we substitute $R_x=\exp\{-\pi x^2/4L_x^2\}$ into the special form for isotropic turbulence, i.e.

$$1/I_b^2=\frac{1}{l}\int_0^l R_x(s)ds$$

we find

$$\frac{1}{I_b^2}=\frac{L_x}{l}\operatorname{erf}\left\{\frac{(\pi)^{\frac{1}{2}}}{2}\frac{l}{L_x}\right\}$$

which is less than unity when $l>0$. In fact, it is physically obvious that for any turbulent flow $1/I_b^2<1$ whenever the fluctuations are not perfectly correlated all along the hot-wire. This can also be seen immediately from a sketch of the general length-correction integrand, $[(l-s)R_y(s)]$.

It should furthermore be noted that in the two expressions for measured correlation as a function of true correlation (either the general relation for $R_{b,y}$ or the additional relation for isotropic turbulence), there is zero error due to finite wire length when the true correlation function is Gaussian.

[1] F. N. Frenkiel, Phys. Rev. **75**, 1263 (1949).

Elastic Constants and Internal Loss of Single Nickel Crystals

R. M. BOZORTH, W. P. MASON, H. J. MCSKIMIN, AND J. G. WALKER
Bell Telephone Laboratories, Murray Hill, New Jersey
April 29, 1949

SINCE the elastic constants of single nickel crystals have never been measured and are of some interest in magnetic studies, the velocities and approximate attenuations have been measured for two single nickel crystals. In preparing the crystals, 750 grams of electrolytic nickel of high purity (0.04 percent Co, 0.002 percent Fe) were melted in an alumina crucible (dextron bond, Norton ATM409) in a molybdenum wound resistance furnace in pure dry hydrogen. The bottom of the crucible was placed in the hottest part of the furnace and the charge melted. The furnace was cooled at the rate of 8°C/hour until the metal was well below the melting point. Several single crystals of 50 to 75 grams each were obtained and were carefully cut from the ingot with a thin carborundum wheel. The surfaces were etched, and the orientation determined approximately by reflection of light from the etch pits, which were of the (111) form. Surfaces were cut parallel to the (100) and (110) planes as nearly as possible, and were tested by x-rays using back reflection, then corrected by careful grinding and etching to within a few minutes of arc of the desired plane.

The crystal upon which most of the measurements were made was cut in the form of a disk about 2.5 cm in diameter and 0.472 cm thick, the circular surfaces being parallel to the (110) planes. The other crystal used for check purposes had its two major surfaces parallel to the (110) plane and 3.13 cm apart, and two other surfaces parallel to (001) and 1.35 cm apart. Other surfaces were irregular.

The velocities and attenuations were measured by pulsing methods. The most satisfactory arrangement, shown by Fig. 1,

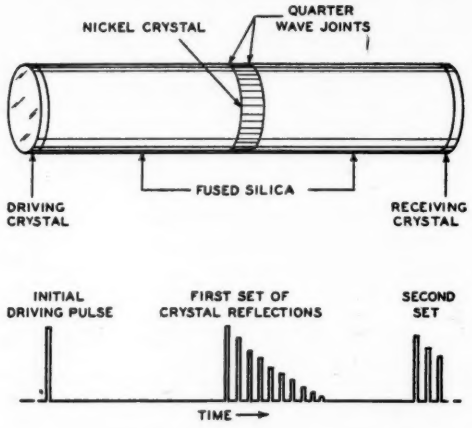

FIG. 1.

consisted in soldering longitudinal or shear wave crystals to the ends of two one-inch fused silica rods and connecting the nickel crystal to the polished ends of the rods by an approximate quarter wave-length of a poly-α-methyl styrene liquid and film of polystyrene. This provided a low mechanical impedance on either side of the nickel crystal, and a longitudinal or shear wave in the crystal was reflected back and forth giving a series of pulses in time and amplitude, from which the velocity and attenuation could be measured. The silica rods were long enough so that reflections from the ends did not arrive in time to interfere with the multiple pulses in the crystal. The most satisfactory way to determine the velocity was by making the pulses considerably longer than the time between reflections and adjusting the frequency until all the pulses added in phase. A number of such frequencies were determined, using the wide frequency range possible with the soldered crystals, and the number of wavelengths corresponding to each frequency determined. By this method a velocity determination good to better than one percent was possible with a crystal thickness of 0.5 cm.

TABLE I. Orientations and elastic constants.

Direction of propagation	Direction of particle motion	Type of mode	Equation for velocity	Measured velocity	Elastic constants (dynes/cm²)
110	110	Long.	$v=[(c_{11}+c_{12}+2c_{44})/2\rho]^{\frac{1}{2}}$	6.06×10^5 cm/sec.	$c_{11}+c_{12}+2c_{44}=6.53\times10^{12}$
110	110	Shear	$v=[(c_{11}-c_{12})/2\rho]^{\frac{1}{2}}$	2.26×10^5	$c_{11}-c_{12}=0.90\times10^{12}$
110	001	Shear	$v=[c_{44}/\rho]^{\frac{1}{2}}$	3.65×10^5	$c_{44}=1.185\times10^{12}$
100	100	Long.	$v=[c_{11}/\rho]^{\frac{1}{2}}$	5.30×10^5	$c_{11}=2.50\times10^{12}$
100	010	Shear	$v=[c_{44}/\rho]^{\frac{1}{2}}$	3.65×10^5	$c_{44}=1.185\times10^{12}$

All three constants were derived from measurements made along the single [110] direction. Calculations show that a longitudinal and two shear waves can be generated, all having different velocities. There is no coupling between the longitudinal and shear modes so that shear motions are at right angles to the direction of propagation whereas the longitudinal motion is along the direction of motion. Table I shows the orientations, the associated elastic constants, the velocities determined and the calculated elastic constants, with $\rho=8.90$. From it one has the following values of elastic constants accurate to within a percent.

$c_{11}=2.50\times10^{12}$ dynes/cm^2; $c_{12}=1.60\times10^{12}$; $c_{44}=1.185\times10^{12}$.

The anisotropy factor $2c_{44}/(c_{11}-c_{12})$, is equal to 2.63.

The absorption is very high for a single metal crystal, indicating damping of the magnetic type. The two crystals gave somewhat different results but agreed in showing a considerably higher damping for shear waves than for longitudinal. Within the experimental error the attenuation measured was proportional to the square of the frequency, indicating a damping due to micro-eddy currents. At 10 megacycles the Q's for the first three orientations of the table were

$$Q_1=\frac{\pi}{\delta_1}=385;\quad Q_2=90;\quad Q_3=85.$$

A New Type of Focusing in a Magnetic Lens Field

HILDING SLÄTIS AND KAI SIEGBAHN
Nobel Institute for Physics, Stockholm, Sweden
May 2, 1949

SINCE some time ago we have been using a β-lens spectrometer (see Fig. 1) which operates according to a new

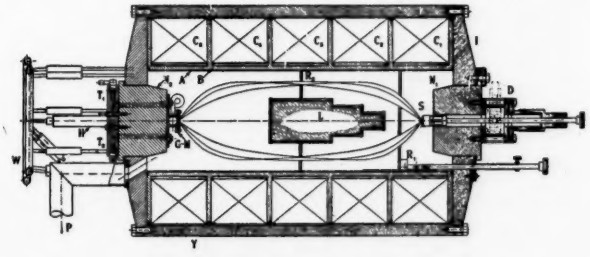

FIG. 1. Section of the β-spectrometer.

focusing principle. This was actually found when we were investigating the possibilities of decreasing the spherical abberation error by changing the field form along the axis of the lens. Such investigations have been made in our laboratory before.[1] Besides ordinary measurements of line profiles with G-M counters we also used a photographic tracing technique to investigate the behavior of the different electron paths in the spectrometer. This method was previously used here in another connection to study electron paths in a spectrometer.[2] We have found that if the magnetic gradient in the spectrometer is made sufficiently strong (the magnetic field having a minimum halfway between source and counter) a first or intermediate ring-formed "image" of the source is obtained midway between source and detector. If a ring-formed shutter is placed here, which transmits the beam, a second *point* image is formed at the G-M slit (see Fig. 2). It is found that quite a substantial solid angle of the total radiation can be utilized at a good resolving power. Thus at a resolving power of 4 percent a transmission of ~8 percent can be obtained. Furthermore, another essential advantage is that an ordinary small counter still can be used since we get essentially a point image. If wanted the resolution can, of course, be increased.

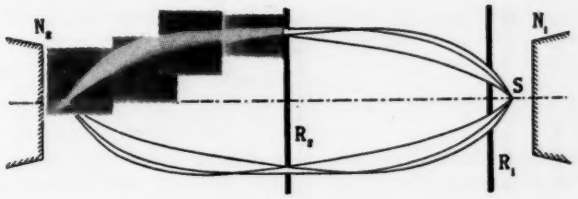

FIG. 2. A photographic record of the focused electron beam.

Thus we have also adjusted the spectrometer for a resolving power of 1.7 percent.

Some general features of this focusing system may briefly be mentioned here. To a certain radius of the central ring baffle a certain magnetic field gradient is related. In our case this gradient was found simply by changing the ratio of the current $I_{2,3,4}$ through the coils 2, 3, 4, to the current I through all coils at a given radius of central shutter. A series of measurements of this kind is given in Fig. 3. As can be seen, there

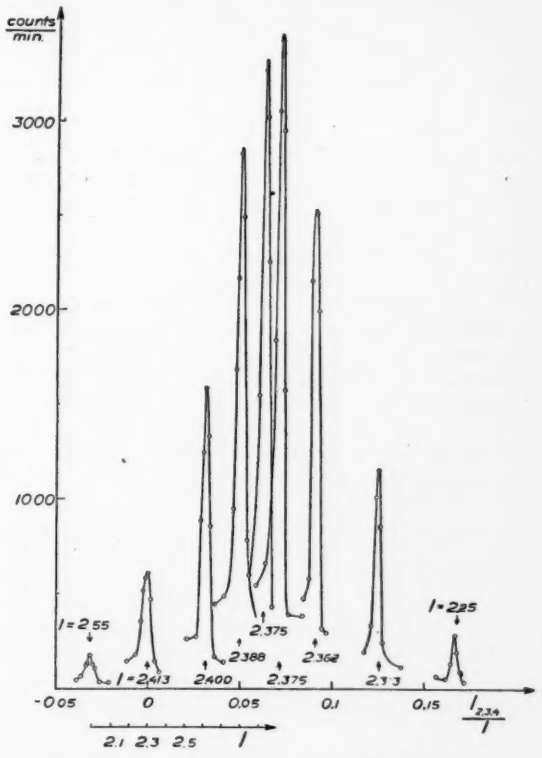

FIG. 3. Adjustment of the magnetic gradient for a given radius of the central shutter.

is a very pronounced maximum at a ratio of these two currents equal to 1:15 for the radius used. Another interesting feature is the strong dependence of the number of counts in the detector on the position of the source. Actually, if the source is moved only a few mm from its correct position no electrons will hit the G-M slit and be counted, no matter what the current is. This means that scattered radiation emanating from other places than the source will not contribute to the counting.

A full description of the spectrometer is given in Arkiv. für Fysik.

[1] Kai Siegbahn, Phil. Mag. **XXXVIII**, 162 (1946).
[2] Hilding Slätis, Arkiv. f. Mat., Astr. o. Fysik **32A**, No. 20 (1945).

On the Production of Cosmic-Ray Stars in the Stratosphere*

J. J. LORD AND MARCEL SCHEIN
Department of Physics, University of Chicago, Chicago, Illinois
April 27, 1949

THE effect upon the cosmic radiation of absorbing material covering photographic plates has been measured in the stratosphere through the use of free balloons. Ilford C2 Boron loaded emulsions 100 microns in thickness were employed. The balloons rose rapidly (900 ft. per min.) then remained at an almost constant altitude corresponding to 5 cm of Hg pressure for about 11.7 hours, and finally descended at approximately the same rate. A constant temperature regulator was used to keep the temperature of the plates at approximately 20°C.

The apparatus, Fig. 1, consisted of Pb plates covering four 2 in.×2 in. photographic plates (1), (2), (3), and (4). The plates were covered respectively with 0, 3.6, 14.3, and 46.6 grams per cm² of Pb directly above each photographic plate.

The rates of occurrence of events in the emulsions is shown in Fig. 2 where curve (A) shows the number of protons entering from outside the emulsion with range $\geqslant 300$ microns and stopping in the emulsion, (B) the number of stars of more than 3 tracks, and (C) the number of stars of more than 4 tracks. Only stars with at least one track longer than 100 microns were considered.

An analysis of the protons with a range $\geqslant 300$ microns and stopping in the emulsion shows that 78 percent originate outside of the emulsion, 15 percent from stars in the emulsion, and 7 percent originate from the emulsion but not from stars (probably largely from neutron collisions with protons in the emulsion).

It has been found in previous long exposures of plates in the stratosphere that the amount and location of matter greatly affects the number of events occurring in the photographic emulsion. The effects due to radiations from the Pb in this experiment can be estimated by a comparison with 2 plates which were placed in a gondola of negligible mass 25 feet above the one containing the lead. The following changes were noted in passing from these upper two plates to Plate (1) of Fig. 1: (a) The frequency of protons stopping with a range greater than 100 microns and that of stars of 2 and 3 prongs increased by a factor of approximately 1.5; (b) the frequency of stars of more than 4 prongs remained the same within 15 percent. This shows that from the lead there is an appreciable increase in the secondary radiation with energies capable of producing stars with 2 and 3 prongs. Since stars at these high altitudes are thought to be produced predominately by nucleons, the energy of these must be of the order of magnitude

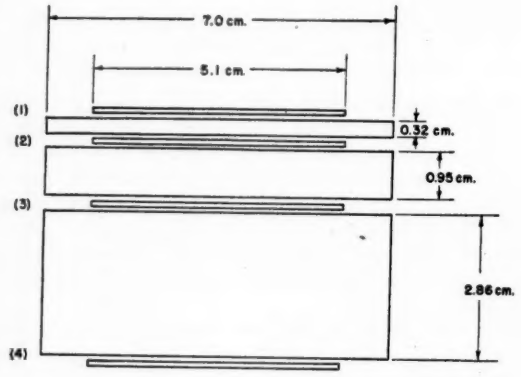

FIG. 1. Arrangement of lead plates and photographic plates.

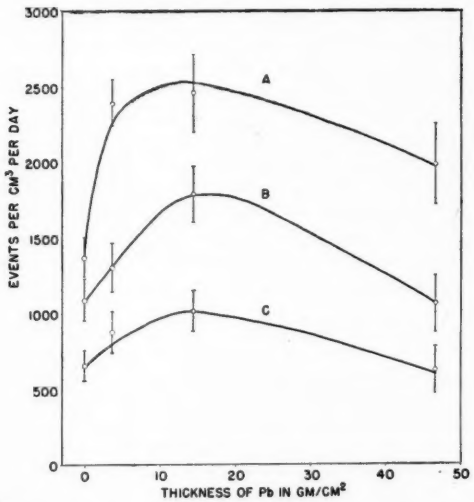

FIG. 2. Rates of occurrence of events in the photographic emulsions. (A) Number of protons entering from outside with range $\geqslant 300$ microns and stopping in the emulsions; (B) number of stars of more than three tracks; (C) number of stars of more than four tracks.

of 100 Mev. It then follows that about $\frac{1}{3}$ of the flux of these low energy nucleons in Plate (1) is coming from below. It can also be shown by a simple calculation that the frequency with which stars are produced by the forward and backward radiations will reach a maximum at the lead thickness corresponding to 15 g/cm² which is in accordance with the experimental observations as shown in Fig. 2. The average number of secondary nucleons of an energy of about 100 Mev does not have to be very large in each encounter in the Pb to produce the observed maxima.

Transition effects of stars in plates covered with Pb have been previously reported at mountain elevations.[1] The great bulk of nearby matter contributes sufficient secondary radiations such that the transition effect is considerably reduced as compared to that measured in balloons where only a small amount of material was located in the neighborhood of the equipment.

The above described investigation shows that close to the top of the atmosphere, the stars of less than 4 prongs must be produced, in addition to nucleons entering from the outside, by secondaries generated in the material placed around the photographic emulsion. Preliminary results obtained using carbon and paraffin indicate that this effect is strongly dependent upon atomic number and is considerably smaller in light materials than in Pb.

* Assisted by the joint program of the ONR and AEC.
[1] W. Heitler, C. F. Powell, and H. Heitler, Nature **146**, 65 (1940); G. Bernardini, G. Cortini, and A. Manfredini, Phys. Rev. **74**, 485 (1948).

Intensity of Cosmic-Ray Stars and Slow Mesons in the Stratosphere*

J. J. LORD AND MARCEL SCHEIN
Department of Physics, University of Chicago, Chicago, Illinois
April 27, 1949

THE variation with altitude of events occurring in photographic emulsions has been measured through the use of free balloons in the stratosphere. Ilford C2 Boron loaded plates 100 microns in thickness were used for all of the measurements reported herein. Four balloon flights were selected for which the apparatus remained for long periods at nearly constant altitudes. The atmospheric pressure-time curves for two of these flights are shown in Fig. 1. The flights

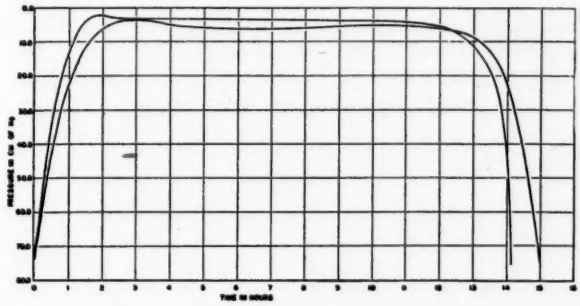

FIG. 1. Pressure time curves for two of the flights.

allowed for the determination of the rates of production of nuclear disintegrations in the emulsions at four different altitudes. This was accomplished by first assuming the duration of the exposure to be equal to the time at which the pressure was less than 9 cm of Hg and then the altitude was taken to be the time average value in this interval. This gave as pressure altitudes 1.1, 3.2, 5.0, and 5.8 cm of Hg. Using the altitude dependence as found by this means, a more accurate numerical integration of the intensity of events occurring in the emulsions multiplied by time was made over the exact trajectories of the balloons. This calculation then made it possible to assign reliable intensity values for the pressure-altitudes indicated.

Since the location and amounts of nearby material effects the intensities of events in the plates, the measurements at 1.1 cm and 5.0 cm of Hg pressure were made using the uppermost plate in practically identical arrangements as described previously.[1] The arrangements for the measurements at 3.2 cm and 5.8 cm of Hg pressure consisted of plates removed from nearby matter. It was shown previously[1] that this will not lead to a change of more than 15 percent in the intensities of stars of more than 4 prongs.

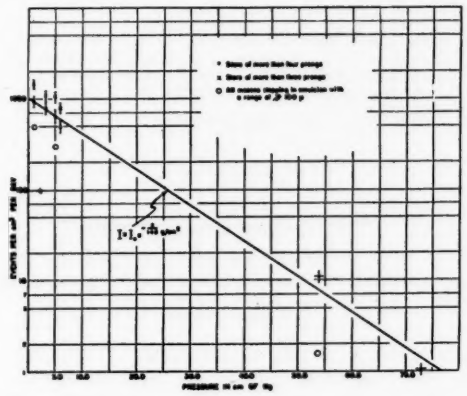

FIG. 2. Variation with altitude of occurrence of stars of more than four tracks and mesons stopping in the emulsion with a range in excess of 100 microns.

In Fig. 2, the variation with altitude is given for stars of more than four tracks and mesons stopping in the emulsion with a range in excess of 100 microns. All stars had at least one track longer than 100 microns.

These measurements above 6 cm of Hg pressure give a general indication of the altitude dependence of stars in the higher atmosphere. Assuming that the variation of star intensity with altitude is an exponential function of the atmospheric pressure, the points in Fig. 2 give sufficient trend to strongly indicate that the straight line drawn though these points in the stratosphere and extending through those at lower elevations[2] represent the star intensity as a function of pressure over 98 percent of the atmosphere. This curve then corresponds to an absorption coefficient of the star producing radiation of 148 grams per cm^2. This is in general agreement with ionization chamber measurements of bursts corresponding to nuclear disintegrations.[3]

The points in Fig. 2, showing the intensities of all mesons stopping in the emulsion, were obtained with two identical pieces of apparatus (Plate (1) of Fig. 1 of the preceding paper) at 1.1 cm and 5.0 cm of Hg pressure. The point at 54 cm of Hg pressure was obtained by Powell and his collaborators[2] from plates exposed under very different conditions from those in the stratosphere. Hence, this only gives a rough indication of how the slow meson intensity varies with altitude.

* Assisted by the joint program of ONR and AEC.

[1] J. J. Lord and M. Schein, preceding paper.

[2] Lattes, Occhialini, and Powell, Nature **160**, 453 (1947). D. H. Perkins, Nature **160**, 707 (1947).

[3] B. Rossi, Rev. Mod. Phys. **20**, 552 (1948).

Isotopic Weight Doublet in the $B_2{}^{11}D_6$ and O_2 Mass Spectrum

FRANCIS J. NORTON
General Electric Research Laboratory, Schenectady, New York

April 30, 1949

THE mass spectrometer such as is used in abundance measurements[1] can in special circumstances show resolution within a single mass peak. This was observed, as shown by the recorded spectrum (Fig. 1a) for partially deuterated

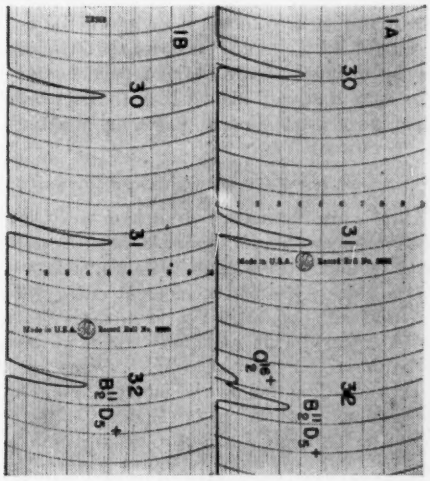

FIG. 1. (a) Spectrum of diborane with admixture of air; (b) with air removed.

diborane, $B_2{}^{11}D_6$, in the presence of a very small amount of air. The mass 32 peak consisting of the ions $B_2{}^{11}D_5{}^+$ and $O_2{}^{16+}$ is a doublet. After condensing the diborane by liquid nitrogen, the air in the sample was pumped away, and the sample readmitted to the spectrometer. The spectrum (Fig. 1b) was now found, representing the upper portion of the diborane mass spectrum in the absence of oxygen.

The isotopic weight of the $B_2{}^{11}D_5{}^+$ ion is 32.0994, from the values[2] for D and B^{11}, and $O_2{}^{16+}$ is, of course, 32.0000. This large difference—nearly 10 percent of a mass unit—shows in this doublet. The deuterium was obtained through the Isotopes Division, U. S. Atomic Energy Commission.

[1] A. O. Nier, Rev. Sci. Inst. **11**, 212 (1940).

[2] J. Mattauch, *Nuclear Physics Tables* (Interscience Publishers, Inc., New York, 1946).

An Interpretation of Mixed Showers

SATIO HAYAKAWA
Research Institute, Central Meteorological Observatory, Tokyo, Japan
May 5, 1949

A REMARKABLE experiment on mixed showers carried out by Chao[1] forces us to add some considerations to our previous note.[2] In *I* we emphasized that there had been few cases where multiple cascade showers had been found in a mixed shower. Chao's experiment, however, shows that such cases are rather more frequent than the cases of single core.

First we should remark the following characteristic features of the results of (A). Firstly, the smaller the size of the cascade shower, the lower is its initiating position in the cloud chamber. This seems to mean that his apparatus is selective and records more showers of larger size, because the considerable part of single cascade showers, which are supposed to have small size and initiate from upper lead plates, may be missed from the observation. The observed ratio of single and multiple cores in (A) may not represent the actual value. Secondly, initiating particles are almost all ionizing. This fact is not only in contradiction with experiments hitherto carried out,[3] but also very difficult to understand in view of the symmetry between charged and neutral particles in nuclear events, although some dissymmetry can be expected if some electromagnetic interaction between an incident ionizing particle and a matter nucleus might be effective for producing mixed showers.

In spite of the above unclear points, it is certain that more cases of multiple cores are occurring than expected in *I*. Now we must consider once more the possibility of these showers with multiple cores by the decay process of neutral nuclear mesons or of C-mesons which are expected to be produced by a nuclear collision if we adopt the hypothesis of Sakata[4] and Pais.[5] Taketani remarks that C-meson may be produced by incident heavy charged particles with a rather large cross section though smaller than that of charge acceleration.[6] The most predominant diverging angle of produced C-mesons is estimated as

$$\theta_c=[(\mu c/k)^2+(\mathrm{Mc}/p)^2]^{\frac{1}{2}} \tag{1}$$

where M and μ are the masses of nucleon and C-meson and p and k their momenta respectively. In most cases $k\sim 5$ Bev/c and p may be about a few tens of Bev/c, since we may consider that a half or less of the incident energy of nucleon is lost by a nuclear encounter. For such cases (1) is approximated by $\theta_c \gtrsim \mathrm{Mc}/p$. This angle may not be inconsistent with the observation of (A), in which at least one cascade shower has almost the same direction as the incident one. On the other hand, the explanation in terms of the decay of neutral nuclear mesons is very difficult because they are emitted with so large angular divergence that the above feature can hardly be accounted for. Now the produced C-meson should immediately disintegrate into a pair of an electron and a positron. One of the pair particles with energy ϵ_1 has the angle θ_1 with the parent if the latter has energy E:

$$\theta_1 \approx \mu c^2/(\epsilon_1 E)^{\frac{1}{2}}. \tag{2}$$

This leads to a relation between the diverging angle and the energy for two disintegration particles:

$$\theta_1/\theta_2=(\epsilon_2/\epsilon_1)^{\frac{1}{2}}. \tag{3}$$

Now the energy of a disintegration ray is estimated from the size of its initiating cascade shower. Then it is seen that this relation is satisfied in few cases of (A). The result of (A) shows that the cascade showers with larger angular divergences have not so small sizes as expected by (3). This discussion is also valid to the case of nuclear neutral mesons.

The above consideration seems still to rule out the role of decay process in mixed showers. As for angular distribution, our charge acceleration process discussed in *I* may be consistent with the new experimental result. The angular distribution of emitted photons by this process is given by[7]

$$d(\cos\theta)u^2(1-\cos^2\theta)/(1-u\cos\theta)^2,$$

which results in the most predominate angle

$$\theta_a \sim \mathrm{Mc}/p. \tag{4}$$

This may approximately explain the observed angular divergences for the momentum of a few tens of Bev/c. But the probability of accompanying the emission of a photon by a nuclear encounter, about 20 percent for the energy under consideration, may be too small to explain the rather frequent occurrence of two or more cores, even if the first remark above is taken into consideration. Furthermore, the large angular divergence taking place in the case of multiple cores cannot be explained by the charge acceleration of the incident fast nucleon, too. Thus it is suggested to introduce the charge acceleration process of produced charged mesons, which are believed to be emitted with large angle. This process may be considerably reduced by interference effect as mentioned in *I*, but in convenient circumstances such a process may be possible, for example when one of the produced mesons has a larger velocity or a larger angle than the others. This possibility, however, appears to contradict with Williams' conclusion,[8] that there is only a single core in an extensive air shower which would be caused by the same mechanism. Such a difficulty might be avoided by considering that in extreme high energy region as that met with in the case of air showers, too many mesons are produced to emit photons without interference, or subcores do not contribute to his experiment because of too large emitted angles. It is very regrettable that our semi-classical and intuitive theory prevents further progression to such problems.

The author expresses his hearty thanks to Prof. Tomonaga, Dr. Taketani, and Mr. Koba for their valuable discussions.

[1] C. Y. Chao, Phys. Rev. **75**, 581 (1949); **74**, 962 (1948). These papers will be cited as (A).
[2] S. Hayakawa, Phys. Rev. **75**, 1759 (1949). This paper will be cited as *I*.
[3] W. B. Fretter, Phys. Rev. **73**, 41 (1948).
[4] S. Sakata, Prog. Theor. Phys. **2**, 145 (1947).
[5] A. Pais, Phys. Rev. **68**, 227 (1945).
[6] M. Taketani, private conversation. O. Hara and M. Tatsoka, Prog. Theor. Phys. **3**, 369 (1948); O. Hara, private communication.
[7] Hayakawa, Miyamoto, and Tomonaga, Jour. Phys. Soc. Japan **2**, 199 (1947), formula (4.35).
[8] R. W. Williams, Phys. Rev. **74**, 1789 (1948).

Cosmic-Ray Underground

SATIO HAYAKAWA AND SIN-ITIRO TOMONAGA
Central Meteorological Observatory and Tokyo Bunrika Daigaku, Tokyo, Japan
May 5, 1949

IN a previous note[1] one of the authors (S.H.) pointed out that the remarkable bend of the intensity-depth curve of the underground cosmic-rays can be accounted for by pi-mu decay and on this basis a rough estimation of the life of pi-mesons was made.[2] In the meanwhile the life of pi-mesons was determined at Berkeley for artificially produced mesons and we found that our estimated life agrees well with this result. It becomes thus of interest to treat the problem in a more precise manner. According to the current picture pi-mesons are produced by the primary cosmic-ray particles, presumably protons or heavier nuclei, on colliding with air nuclei and these mesons disintegrate into mu-mesons on falling down through the atmosphere. In this decay process almost all of pi-mesons of lower energies are transformed into mu-mesons at sea level, whereas only a little part of pi-mesons of higher energies are converted into mu-mesons. This results in that the energy spectrum of mu-mesons at sea level has a bend which manifests itself as the bend of the intensity-depth curve of the

underground cosmic-rays. Since the position of the bend of the energy spectrum depends on the life of pi-mesons, the latter can be determined from the position of the intensity-depth curve. In this way the life of pi-mesons was estimated in the previous note, but, as this calculation was carried out only roughly in that the energy spectra of pi- and mu-mesons were not properly considered, we now improve the calculation taking into account also the energy loss of mu-mesons passing through the earth crust.

We now carry through the calculation in the following way. We assume that the energy spectrum of pi-mesons when they are produced be of the form

$$\text{const.}E^{-\gamma-1}dE. \tag{1}$$

These pi-mesons are produced in proportion to the intensity of the primary particles which decrease with increasing depth from the top of the atmosphere as

$$I=I_0\exp(-l/\Lambda), \tag{2}$$

l being the atmospheric depth and Λ the mean free path of the primaries. In calculating the spectrum of mu-mesons produced by these pi-mesons we first neglect the absorption of pi-mesons in the atmosphere. Of course, this does not correspond to the actual case but we can thus obtain in some way an extreme value for the intensity of mu-mesons. The calculation was then performed assuming that the absorption of pi-mesons in the atmosphere is just as large as that of the primary particles.

The energy spectrum of mu-mesons having been obtained, we can calculate the intensity-depth curve if the range-energy relation of the mu-meson is known. In order to determine this relation we estimate the energy loss of mu-mesons passing through the matter on the plausible assumption that the energy loss is caused by ionization, emission of bremsstrahlung and creation of pairs. Then the required intensity-depth curve is obtained by substituting the energy expressed as the function of range into the integral energy spectrum of mu-mesons at sea level.

The calculated intensity-depth relation is given in Fig. 1. The theoretical curves in the figure have been calculated by assuming the following numerical values for various constants: the mass of pi- and mu-mesons are 286 and 217 times electron mass, the mean life of pi-mesons is 1×10^{-8} sec.,[3] $\gamma=1.8$, and $\Lambda=125$ g cm^{-2}. The upper curve is the result by neglecting the absorption in the atmosphere and the lower is that obtained by assuming that this absorption is just as large as the absorption of the primary particles. The broken lines indicate the corresponding curves neglecting the radiation and pair-creation processes of mu-mesons. The experimental results of Wilson[4] and Nishina *et al.*,[5] marked by × and 0, are found to lie between the two theoretical curves. In view of our imperfect knowledge about the production and absorption of pi-mesons as well as of the statistical inaccuracy in their mean lifetime, we cannot yet draw any decisive conclusion from our result, but our result seems to show that the life of pi-mesons measured at Berkeley for the artificial mesons does not contradict the cosmic-ray data so that we may identify the cosmic-ray mesons with mesons produced at Berkeley. Our result seems further to show that no extra process other than the known electromagnetic ones is needed to explain the behavior of deep rays so far as the present status of our experimental knowledge is concerned.

A detailed account will be published in the Progress of Theoretical Physics.

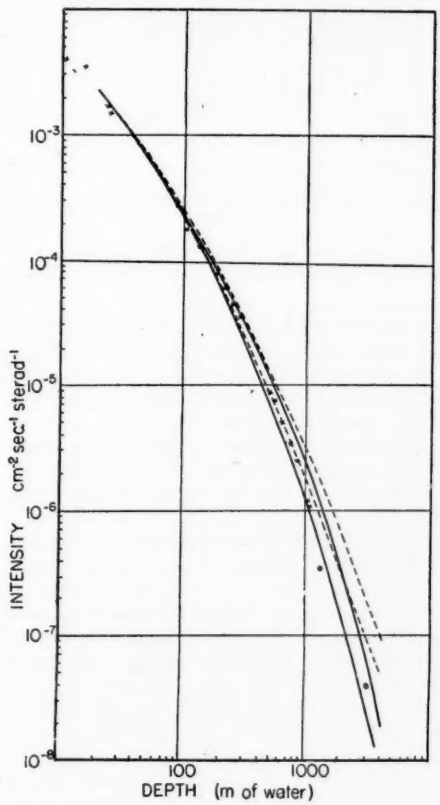

FIG. 1 Intensity-depth relation.

[1] S. Hayakawa, Prog. Theor. Phys. **3**, 199 (1948).
[2] K. I. Greisen, Phys. Rev. **73**, 521 (1948).
[3] J. R. Richardson, Phys. Rev. **74**, 1720 (1948).
[4] V. C. Wilson, Phys. Rev. **53**, 337 (1938).
[5] Nishina, Sekido, Miyazaki, and Masuda, Phys. Rev. **59**, 401 (1941); Y. Miyazaki, to be published.

Crystal Interactions in Ferromagnetic Resonance

WILLIAM FULLER BROWN, JR.
Sun Physical Laboratory, Newtown Square, Pennsylvania
March 30, 1949

RADO[1] has recently attempted to correct for magnetic interactions between crystal grains in the theory of ferromagnetic resonance. His correction does not contain the anisotropy constant—a fatal defect, since for crystals of zero magnetic anisotropy the correction must vanish.

Rado's method was to replace the applied magnetic field by a "local" field, the formula for which he took from a calculation by Néel[2] on the approach to saturation. A calculation identical with Néel's was published earlier by Holstein and Primakoff;[3] their Eq. (25) contains the formula quoted (incorrectly[4]) in Rado's letter. Even earlier, I had used a similar method in a related problem.[5] Each such problem requires separate investigation; no single local field formula can claim general validity. In the work cited, I derived several such formulas, each valid for a different type of deviating force. Rado's problem requires direct treatment.

Consider an ellipsoidal specimen with principal axes Ox, Oy, Oz; demagnetizing factors L, M, N; large constant applied field (O, O, H_o); small alternating applied field (h_{ox}, h_{oy}, O); magnetization of constant magnitude J_s in variable direction (α, β, γ) with $\alpha\ll1$, $\beta\ll1$, $\gamma\doteq1-\frac{1}{2}(\alpha^2+\beta^2)$; anisotropy and stress energy density (to the second order of small quantities)

$$w(x, y, z, \alpha, \beta)=g_1\alpha+g_2\beta+\tfrac{1}{2}(g_{11}\alpha^2+2g_{12}\alpha\beta+g_{22}\beta^2), \tag{1}$$

where the g's are functions of (x, y, z).

The dynamic generalization of Eqs. (32) of reference 5 is

$$\begin{aligned} C\nabla^2\alpha-(J_sH+g_{11})\alpha-g_{12}\beta+J_sH_x'-J_s\dot{\beta}/\gamma_o&=g_1-J_sh_{ox},\\ C\nabla^2\beta-g_{12}\alpha-(J_sH+g_{22})\beta+J_sH_y'+J_s\dot{\alpha}/\gamma_o&=g_2-J_sh_{oy}. \end{aligned} \tag{2}$$

Here γ_o is Kittel's[6] γ, the ratio of magnetic moment to angular momentum; $H=H_o-NJ_s$; $\mathbf{H}'$ is the magnetizing force due to the transverse magnetization and to eddy currents and is related to α and β by the usual electromagnetic equations. When $h_{oz}=h_{oy}=0$ and $\dot{\alpha}=\dot{\beta}=0$, there are no eddy currents, and $\mathbf{H}'$ may be derived from a scalar potential U; then Eq. (2) reduces to the previous equations if, as before, the second-order terms in w are neglected. When there is no magnetic anisotropy or internal stress, all the g's vanish; then the solution for a polycrystalline aggregate is identical with that for a single crystal, provided eddy current fields are negligible.

Since the equations are linear, the contributions of (g_1, g_2) and of (h_{oz}, h_{oy}) to α, β, and $\mathbf{H}'$ may be found separately and superposed. The former is time-independent; this is the static problem treated in references 2, 3, 5. The terms in g_{11} etc. are important only for a crystal with Oz a direction of easy magnetization; in the calculation of Holstein and Primakoff, these and the terms in C are neglected. The object is to evaluate the mean squares of α and β over the specimen volume: then $\gamma_{av}=1-\frac{1}{2}[(\alpha^2)_{av}+(\beta^2)_{av}]$. It is in the integrations incidental to this mean-square evaluation that the function quoted by Rado emerges.

The complexity of this calculation is due to the variation of g_1 and g_2 with position. In the evaluation of the $\mathbf{h}_o$ term such complexity is lacking, since h_{oz} and h_{oy} are independent of (x, y, z). If the terms in g_{11} etc. are again neglected, if the time factor is $e^{j\omega t}$, and if eddy current fields are negligible, this problem is solved by a uniform α and β that produce uniform transverse magnetizing forces $H_x'=-J_sL\alpha$, $H_y'=-J_sM\beta$. For the alternating part of (α, β), Eqs. (2) therefore reduce to

$$\begin{aligned}(H+LJ_s)\alpha+(j\omega/\gamma_o)\beta&=h_{oz},\\ -(j\omega/\gamma_o)\alpha+(H+MJ_s)\beta&=h_{oy};\end{aligned}\qquad(3)$$

and if the determinant of this system is set equal to zero, Kittel's resonance condition is obtained. To this approximation, therefore, magnetic interactions between the crystals have no effect on the resonance condition.

If the terms in g_{11} etc. are appreciable, interaction enters; but there is no obvious reason why the function that occurs in the resonance condition in this problem should have any simple relation to the function that occurs in the mean squares in the static problem. The order of magnitude of the effect could perhaps be estimated by carrying out the calculation for a few special cases, such as plane parallel crystal boundaries or isolated spherical inclusions. If the effect is not negligible, the simplest procedure is to make it negligible by increasing H_o.

[1] George T. Rado, Phys. Rev. **75**, 893 (1949).
[2] L. Néel, C. R. Acad. Sci. Paris **220**, 814 (1945); J. de Physique **9**, 193 (1948).
[3] T. Holstein and H. Primakoff, Phys. Rev. **59**, 388 (1941).
[4] See correction by Rado, Phys. Rev. **75**, 1451 (1949).
[5] William Fuller Brown, Jr., Phys. Rev. **58**, 736 (1940). See also Phys. Rev. **59**, 528 (1941); **60**, 139 (1941).
[6] Charles Kittel, Phys. Rev. **71**, 270 (1947); **73**, 155 (1948).

Radiations from Lu^{177}

DONALD G. DOUGLAS
Radiation Laboratory, McGill University, Montreal, Canada
May 4, 1949

SAMPLES of "Specpure"* Lu_2O_3 irradiated in the Chalk River pile, have been studied with a thin lens spectrometer. Secondary electrons from lead, gold and tin radiators reveal the presence of three gamma-rays of energies 112.2 ± 0.6, 206.3 ± 1.0, and 317.3 ± 1.5 kev, the former two of comparable intensity, the latter much weaker. X-radiation agreeing well in energy with characteristic K radiation of Hf has also been observed.

A Kurie plot of the beta-spectrum intersecting the abscissa at 495 ± 5 kev is straight for only the upper 100 kev. Regarding the departure from straightness as an indication of complexity, two lower end points at 169 ± 10, and 366 ± 25 kev, are obtained. These end points taken with the three gamma-rays are consistent with the decay scheme shown in Fig. 1.

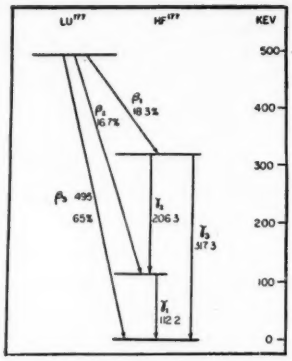

FIG. 1. Proposed decay scheme for Lu^{177}.

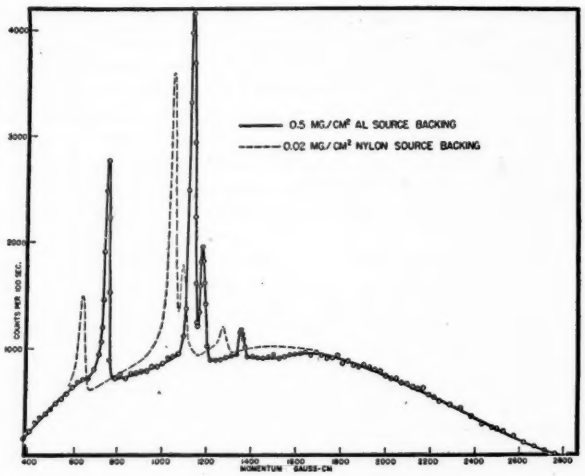

FIG. 2. Beta-spectrum of Lu^{177}. The dotted curve shows the effect of source charging.

Four conversion lines have been found at energies 46.9 ± 0.5, 101.8 ± 0.6, 109.9 ± 0.6, and 141.4 ± 0.8 kev (Fig. 2). The first three arise respectively from K, L, and M, conversion of the 112.2 kev gamma-ray, the last from K conversion of the 206.3 kev gamma-ray. Since addition of the electron binding energies of Hf gives better agreement with the gamma-energies found from the photoelectron spectrum than does addition of Lu binding energies it can be stated that the gamma-rays follow the beta-rays.

The end point 495 kev is to be compared with values 440, 520, 470 kev obtained by other workers[1] using absorption and cloud chamber methods. A gamma-ray energy 0.2 Mev, obtained by absorption,[1] is in agreement with that of 206.3 kev reported here. The weak 1.3 Mev gamma-ray found by Wilkinson and Hicks probably arises from an impurity. Values 6.8, 6.6 and 6.9 days have been reported for the half life.[1] A source was observed for 400 hours and the value 6.98 ±0.10 days obtained. There was no evidence of any contaminating activity differing appreciably in half life.

The great importance of using a well grounded source was demonstrated.[2] A typical run using an ungrounded Nylon backed source is shown by the dotted curve in Fig. 2. All the

lines are shifted toward lower energies. Later runs revealed even greater shifts, as much as 19 kev for the 46.9 kev line. Line positions were always closely reproducible when thin aluminum backing was used.

Source thicknesses for the beta-spectrum were estimated to be less than 0.1 mg/cm². Nylon windows 0.08 mg/cm² were used to close the argon-ethylene filled counter used as detector. No correction was made for window absorption.

The author is indebted to Professor J. S. Foster, Director of this Laboratory, for his keen interest in this work, and to Mr. J. S. Fraser for many valuable discussions and for assistance in taking spectrometer data.

* Obtained from Johnson Matthey, London, England.

[1] G. T. Seaborg and I. Perlman, Rev. Mod. Phys. **20**, 585 (1948).
[2] C. H. Braden *et al.*, Phys. Rev. **74**, 1539 (1948).

Anomalies in the Microwave Spectrum of Methyl Cyanide and Methyl Iso-Cyanide

HARALD H. NIELSEN
Mendenhall Laboratory of Physics, The Ohio State University, Columbus, Ohio
April 25, 1949

THE microwave spectra of methyl cyanide and methyl iso-cyanide have been studied by Gordy[1] who has observed three lines in the former case and four lines in the latter case which can be shown to originate with rotational transitions in an excited vibration state. The electric moment lies along the axis of symmetry so that $\Delta K=0$. From the general positions of the lines in the spectrum Gordy has identified them with transitions $J=1\rightarrow J=2$.

The lines observed by Gordy occur at the frequencies 36870.94 mc, 36903.40 mc and 36942.15 mc in the spectrum of methyl cyanide and at 40313.37 mc, 40364.07 mc, 40366.55 mc and 40424.49 mc in the spectrum of methyl iso-cyanide. The general pattern in the former case consists of two lines separated by a frequency interval of about 72 mc with a third line almost in the center of these. In the latter example the two extreme lines are separated by an interval of about 111 mc with two lines near the center of these separated by an interval of 1.5 mc. These patterns cannot be explained on the basis of a rigid symmetric rotator, but require that certain degeneracies be removed.

It seems reasonable to suppose that the excited vibration states which here are involved are the frequencies ω_8 in the two molecules, namely 380 cm^{-1} and 290 cm^{-1}. These are doubly degenerated perpendicular vibrations and associated with each of them there exists one unit of internal angular momentum of vibration. A Coriolis interaction between vibration and rotation splits the levels where $K\neq 0$ into two components, the separation between components being $Kh/2\pi^2 I_{zz}c$. Examination of the Hamiltonian for a symmetric molecule reveals that the component state corresponding to the situation where the molecular framework remains at rest (i.e., $K=l$) may further be split by an l-type doubling.[2]

The magnitude of the l-type doubling may be calculated accurately only when the normal coordinate problem has been solved and the shape of the molecule is known. An estimate may nevertheless, be made which may be regarded as a fair approximation. Taking B to be 0.335 cm^{-1} and $\omega_8=290$ cm^{-1} for methyl cyanide these splittings may be estimated to be about 0.0047 cm^{-1} and 0.0015 cm^{-1} respectively for the states $J=1$ and $J=2$. The appropriate selection rule yields a pattern like the one observed with the two extreme lines separated by about 0.0031 cm^{-1} (93 mc) and two lines near the center separated by a much smaller interval of the order of 3×10^{-5} cm^{-1} (1.0 mc). For methyl cyanide the splittings for $J=1$ and $J=2$ are respectively predicted to be 0.003 cm^{-1} and 0.001 cm^{-1} and the line pattern will be similar to the former, the extreme lines in the pattern being here separated by about 0.002 cm^{-1} (i.e. 60 mc) with two lines near the center, their separation being about 1.3×10^{-5} cm^{-1} (i.e. 0.4 mc). Since the two central lines would have the same frequency except for centrifugal distortion it is proposed that the single line observed by Gordy in the latter case is in reality two unresolved lines. Because of the roughness of the approximation the agreement with experiment is regarded as satisfactory. A further check is the comparison of the interval between the extreme lines in the two cases. Experimentally this ratio is about 0.65 and the theory indicates a ratio of 0.64.

The theory of l-type doubling in polyatomic molecules will be discussed in detail later with specific applications to the above two molecules.

The author wishes to express his gratefulness to Professor Walter Gordy for having made his measurements available to him.

[1] Walter Gordy, private communication.
[2] It is found that in the original work of Nielsen and Shaffer (J. Chem. Phys. **11**, 140 (1943)) an error in sign was introduced. Two terms of equal magnitude which were cancelled against each other should have been added together. When this correction is made the coefficient of the matrix element in the case of a linear molecule becomes $(Be^2/2\omega_8)[1+4\Sigma_{s'}\xi_{ss'}^2\lambda_s/(\lambda_{s'}-\lambda_s)]$, where $\lambda_s=4\pi^2c^2\omega_s^2$, instead of $(Be^2/2\omega_8)$. This change appears to bring the theoretical relations for l-type splitting in linear molecules into substantial agreement with experiment.

Polarization of the Vacuum

JERZY RAYSKI*
N. Copernicus University, Torun, Poland
April 7, 1949

THE problem of the vacuum polarization and the closely connected question of the photon self-energy has recently caused much confusion. As is well known, Heisenberg[1] obtained for the photon self-energy a logarithmic divergence while Wentzel[2] found a finite but non-zero value. On the other hand Schwinger[3] believes that there is no doubt in the gauge invariance of the formalism and demonstrates that the photon self-energy is strictly zero.

The reason for this discrepancy is as follows: The proofs of the gauge invariance are based on the assumption that the Schrödinger equation possesses a solution. But in frames of the quantized field theory (at least in case of two coupled fields), this assumption is obviously not true. The quantized field equations possess no solution and, after the unitary transformations, the gauge invariance must be restored again (similarly to the mass and charge constants which must be restored by renormalization).

The basic expressions for the vacuum polarization containing products of $\bar{\Delta}$ and $\Delta^{(1)}$ functions and their derivatives are mathematically meaningless at the light cone[4] so that by formal operations on non-existing integrals one may obtain any result one likes. The most straightforward evaluation yields for the photon self-energy a quadratically divergent result. Heisenberg obtained a logarithmic divergence only because he arbitrarily subtracted a part of the effect.

In order to give a mathematical meaning to such expressions as e.g. products of $\bar{\Delta}$ and $\Delta^{(1)}$ functions on the light cone a special regularizing procedure is needed. This may be achieved by replacing $\bar{\Delta}\Delta^{(1)}$ by a (finite) sum

$$\bar{\Delta}(m_0)\cdot\Delta^{(1)}(m_0)\rightarrow\sum_i C_i\bar{\Delta}(m_i)\Delta^{(1)}(m_0).$$

m_0 is the mass of the electron while m_i, $i=1, 2, \cdots$ play only an auxiliary role and are assumed to tend to infinity. C_i are constants ($C_0=1$) such that

$$\sum C_i=0, \quad \sum C_i m_i^2=0. \tag{I}$$

The above mentioned procedure secures the consistency of the calculations but, on the other hand, means a departure from the wave equation. It cannot be considered as a theory but rather as a provisional remedy.[4]

Another possibility, which seems promising, is to combine several charged fields with different transformation character of their field functions.[5] The photon self-energy due to the interaction with electrons is negative while the same quantity due to the interaction with charged scalar particles is positive. Both are quadratically divergent so that a compensation is possible. The conditions for compensation show a remarkable analogy with the conditions (I) for regularization and may be considered as conditions for the existence of a solution of the Schrödinger equation.

* Present address: Eidg. Techn. Hochschule, Zürich.
[1] W. Heisenberg, Zeits. f. Physik **90**, 209 (1934).
[2] G. Wentzel, Phys. Rev. **74**, 1070 (1948).
[3] J. Schwinger, Phys. Rev. **75**, 651 (1949).
[4] An extensive report on invariant regularization, criticism of relativistic electrodynamics, etc. is in preparation by W. Pauli and F. Villars. To appear probably in Rev. Mod. Phys. The present author is indebted to both authors for the opportunity of seeing their paper before publication.
[5] J. Rayski, Acta Phys. Polonica **IX**, 129 (1948).

Paramagnetic Resonance Spectra of Five Chromic Sulfate Alums

B. Bleaney*
Clarendon Laboratory, Oxford, England
April 27, 1949

THE anomalous behavior at low temperatures of the paramagnetic resonance spectra of ammonium and potassium chromic alums previously reported[1] has been further investigated by measurements at small intervals of wave-length between 3 cm and 10 cm. In addition, rubidium, cesium and methylamine chromic alums have been studied for comparison. The spectra of these five alums at low temperatures show fundamental differences in character, corresponding to the following groupings:

Group 1. Rubidium, cesium and methylamine chromic alums.—These alums exhibit the "normal" chromic alum spectrum at all temperatures down to 20°K. By "normal spectrum" is meant that associated with a predominantly cubic crystalline electric field on which is superimposed a small trigonal component with symmetry about the (111) axis. The presence of such a field was originally deduced by Van Vleck,[2] and the room temperature spectra of all the chromic alums so far studied[3–6] conform to this type. The splittings between the two doublets of the spin quadruplet deduced from this spectrum at various temperatures are listed in Table I. As the

Table I. Splittings (cm^{-1}) in various chromic alums at low temperatures.

Temperature	Ammonium	Potassium	Rubidium	Cesium	Methylamine
290°K*	0.135	0.12	0.165	0.145	0.165
193°K	0.085	0.055	0.126	0.134	
90°K	0.035	{0.26 {0.15±.01	0.108±.002	0.133±.002	0.170±.003
	transition point				
80°K	{0.314±.003 {0.242±.003				
20°K	{0.317±.003 {0.240±.003	{0.270±.003 {0.15 ±.01	0.108±.002	0.133±.002	0.170±.003

* Values at 290°K are from unpublished work of Bagguley and Griffiths (see reference 6). Probable error where not given is ±0.005 cm^{-1}.

alum is cooled from room temperature, the splitting decreases somewhat (except in the case of the largest monovalent ion CH_3NH_3) but becomes constant below 90°K. Since the splitting is sensitive to very small distortions of the octohedron of water molecules around the Cr^{+++} ion, its temperature dependence is probably associated with thermal contraction, which becomes zero at low temperatures. No further change in the splitting is anticipated below 20°K; the small discrepancy between the value given for the cesium alum and that of 0.138±0.002 cm^{-1} obtained by Benzie and Cooke[7] from paramagnetic relaxation measurements at 1°K may be due to a contribution from spin-spin interaction to the specific heat greater than that calculated from pure dipolar interaction.

Group 2. Ammonium chromic alum.—No further measurements have been made on the "normal" spectrum observed at high temperatures, but analysis of the unresolved line at 90°K indicates a splitting just above the transition point of about 0.03_5 cm^{-1}. Below the transition point the spectrum is quite different, and it was previously assumed, in virtue of Kramers' theorem, that the splitting of 0.314 cm^{-1} measured by plotting the transitions back into zero magnetic field was the only one present. Continuation of this plotting to longer wave-lengths has revealed, however, the presence of a second splitting equal to 0.242±0.003 cm^{-1}. It seems necessary to ascribe these two splittings to different ions in the unit cell which must, therefore, be substantially different in structure from the high temperature modification. The splittings are in substantial agreement with the average value of 0.27±0.01 cm^{-1} of Benzie and Cooke,[7] if the two types of ion are present in roughly equal proportions, as is suggested by the relative intensities of the absorption peaks in the paramagnetic resonance spectrum.

Group 3. Potassium chromic alum.—The splitting deduced from the high temperature spectrum falls to a minimum value of about 0.03_5 cm^{-1} at 160°K. There is no sudden transition at this temperature, however, but as the temperature is lowered side peaks in the spectrum appear whose intensity increases steadily down to 20°K without marked change in position. This process is reversible without observable hysteresis if the temperature is increased again. As with the ammonium salt two splittings are observed, but they are much more different in magnitude (see Table I). The resemblance[1,5] to the normal spectrum with a splitting of *ca.* 0.17 cm^{-1} (which would agree well with measurements by other methods[8–10]) is thus only superficial, and the relative intensities of the various peaks are not of the right order of magnitude.

No satisfactory explanation of this behavior of the potassium salt has been propounded which can be reconciled with the following facts: (a) The specific heat of the spin system, as determined from paramagnetic relaxation measurements,[8] is the same at 90°K as at helium temperatures, and considerably lower than calculated from the two splittings unless a much smaller fraction of the ions have the higher splitting than have the lower value. This latter is not suggested by the relative intensities in the paramagnetic spectrum. The intensities are all abnormally low, however, and it may be that a proportion of the ions have yet another splitting too small to observe. On the other hand, no such distribution of splittings could account for the plateau in the entropy curve at 0.05°K found by de Klerk, Steenland and Gorter[11] falling below $R\log_e 2$, which seems to require that the Kramers degeneracy be partly lifted.

Van Vleck[2] has shown that the splitting in the chromic alums is due partly to the direct field of the more distant atoms and partly to the distortion of the local octohedron of water molecules. The distortion required (0.03 A.U.) is so small that it may well change sufficiently with temperature as the crystal contracts to account for the temperature dependent part of the splitting. The contribution from the more distant atoms should be substantially independent of temperature, and is estimated by Van Vleck as about 0.05 cm^{-1}. It may be significant that the minimum splitting in both the ammonium and potassium alums is 0.03_5 cm^{-1}, and that this represents the effect of the more distant atoms.

The behavior of the paramagnetic resonance spectra of these alums at low temperatures is similar to that observed in the optical spectra by Kraus and Nutting,[12] especially in the "shattering" of the ammonium alum, and the gradual transition in intensity from the high to the low temperature spectrum in the potassium alum. It may be that x-ray analysis will reveal structural differences such as those found in the aluminum alums[13] which can be correlated with the magnetic behavior. A further unexplained peculiarity of the alums is the Debye-type electrical relaxation discovered by Guillien.[14] Unfortunately his measurements do not cover a sufficient number of alums to detect correlatable differences in behavior.

* Present address: Lyman Laboratory of Physics, Harvard University, and Research Laboratory of Electronics, Massachusetts Institute of Technology, Cambridge, Massachusetts.

[1] Bleaney and Penrose, Proc. Phys. Soc. **60**, 395 (1948).
[2] J. Van Vleck, J. Chem. Phys. **7**, 61 (1939).
[3] Bagguley and Griffiths, Nature **160**, 532 (1947).
[4] Weiss, Whitmer, Torrey, and Hsiang, Phys. Rev. **72**, 975 (1947). Whitmer, Weidner, Hsiang, and Weiss, Phys. Rev. **74**, 1478 (1948).
[5] D. Halliday and J. Wheatley, Phys. Rev. **74**, 1712 (1948).
[6] Bagguley and Griffiths (to be published).
[7] Benzie and Cooke (to be published).
[8] See Gorter, *Paramagnetic Relaxation* (Elsevier Publishing Company, Inc., New York, 1947).
[9] B. Bleaney, unpublished, quoted by Van Vleck, Phys. Rev. **57**, 426 (1940).
[10] Casimir, de Haas, and de Klerk, Physica **6**, 365 (1939).
[11] de Klerk, Steenland, and Gorter, Nature **161**, 678 (1948).
[12] D. L. Kraus and G. C. Nutting, J. Chem. Phys. **9**, 133 (1941).
[13] Lipson, Proc. Roy. Soc. **151**, 347 (1935).
[14] Guillien, Comptes Rendus **209**, 21 (1939); **213**, 991 (1941); **217**, 443 (1943).

Microwave Magnetic Resonance Absorption in Oxygen

ROBERT BERINGER AND J. G. CASTLE, JR.
Sloane Physics Laboratory, Yale University, New Haven, Connecticut*
May 3, 1949

WE have detected the absorption arising from magnetic dipole transitions between adjacent Zeeman components of the rotational levels of the oxygen molecule. The apparatus is essentially a microwave analogue of the radio-frequency nuclear magnetic resonance method.[1] Power from a frequency-stabilized 9360 mc/sec. oscillator is coupled into an oxygen-filled, cylindrical cavity placed in a uniform axial magnetic field. The cavity resonates in the TM011 mode so that the r-f and d.c. magnetic fields are perpendicular. A Wollaston wire bolometer is coupled to the cavity and forms one arm of a d.c. bridge. The axial magnetic field has a small 30 cycle/sec. modulation component so that in the region of an absorption line the microwave power into the bolometer is modulated, producing a 30 cycle/sec. unbalance signal in the bridge. This signal is amplified by a high-gain tuned amplifier and impressed on a lock-in mixer whose d.c. output indicates the magnitude and sign of the derivative of the absorption line (i.e., $d\chi''/dH$, where χ'' is the imaginary part of the magnetic susceptibility).

At atmospheric pressure two broad absorption lines were found for fields ranging up to 9 kilogauss. As the pressure was lowered these showed increasingly complex fine-structure. At an oxygen pressure of 1.5 cm Hg twenty-seven partially resolved components could be identified in the region from 5.4 kilogauss to the highest fields used. They showed no simple regularities in spacing, which varied from 380 to 60 gauss, or in intensity, which varied by at least a factor five. The half-widths of several of the larger lines could be determined; they range from 40 to 80 gauss and do not show the expected linear dependence with the field. Further, the half-widths are greater than those deduced from the pressure broadening of the 0.5-cm absorption band[2] of O_2 by factors ranging from 4 to 8. The largest resolved lines at the 1.5-cm pressure have χ'' values estimated to be 3×10^{-10} c.g.s. Noise fluctuations are about two percent of this.

As might be expected, the spectrum is not in accord with the low field Zeeman theory. Assuming pure Hund case (b) coupling in the $^3\Sigma$ ground state of O_2, the low field Zeeman formula predicts an absorption line at 6.9 kilogauss arising from $\Delta M=\pm1$ transitions between the Zeeman levels of the $J=1$ and 2 components of the $K=1$ rotational state, and a line at 10.3 kilogauss for the $K=3$, $J=2$ levels, as well as other lines at higher fields. However, even at 6.9 kilogauss the spin energy is a third of the average level-spacing in the spin triplets. Thus one expects a partial Paschen-Back effect for the fields used in the experiments. A more complete analysis of the line positions and intensities requires a high field Zeeman theory for molecular triplet states.

* Assisted by the ONR.

[1] Purcell, Torrey, and Pound, Phys. Rev. **69**, 37 (1946).
[2] J. H. Van Vleck, Phys. Rev. **71**, 413 (1947); R. Beringer, Phys. Rev. **70**, 53 (1946).

Three-Photon Annihilation of an Electron-Positron Pair

A. ORE AND J. L. POWELL
Institute for Nuclear Studies, University of Chicago, Chicago, Illinois
April 29, 1949

AFTER we had submitted the proof of our paper by the above title,[1] it came to our attention that this subject has recently been discussed by L. D. Landau, E. M. Lifshits, and I. Pomeranchuk.[2]

Landau and Pomeranchuk's work includes a discussion of allowed and forbidden annihilation processes. The earlier work by J. Pirenne and by J. A. Wheeler, to which we refer in our paper, as well as the conclusions which we have drawn from a detailed study of the special case of the three-photon annihilation, are in agreement with the general results of these authors.

However, Lifshits gives a formula for the differential cross section for three-photon annihilation which is in apparent disagreement with our result. As a consequence, he finds a lifetime of the triplet ground state of the positronium atom (8.8×10^{-8} sec.) which is shorter than ours by a factor 1.6.

Unfortunately, the brevity of Lifshits' report does not permit a comparison of the methods of calculation, and we have been unable to discover the source of the discrepancy.

[1] A. Ore and J. L. Powell, Phys. Rev. **75**, 1696 (1949).
[2] L. D. Landau, Dokl. Akad. Nauk, SSSR **60** (No. 2), 207 (1948). E. M. Lifshits, Dokl. Akad. Nauk, SSSR **60**, 211 (1948). I. Pomeranchuk, Dokl. Akad. Nauk, SSSR **60**, 213 (1948). See also Physics Abstracts **A52**, p. 125, abstr. 1005, 1006, 1007 (1949).

Electrolytic Deposits of Po in Extremely Dilute Solutions

M. HAISSINSKY, H. FARAGGI, A. COCHE, AND P. AVIGNON
Institut du Radium, Paris
March 16, 1949

DURING the course of experiments which we are carrying out on the electrochemical behavior of radio-elements in extremely dilute solutions (between 10^{-10} and 10^{-14}N) we have made some observations which we think present an interest for nuclear physics research.

We obtain polonium deposits, either by electrolysis of its acid solutions (HNO_3, 1.5N) or by spontaneous deposition on surfaces of Au, Ag, Pt or Ni. After having measured the deposited quantity by means of a linear amplifier, the electrode is applied to an Ilford Nuclear Research plate type C2, and, after development, an examination of the plate enables us to establish the distribution of the Po atoms on the surface and that of the alpha ranges. This latter is generally based on

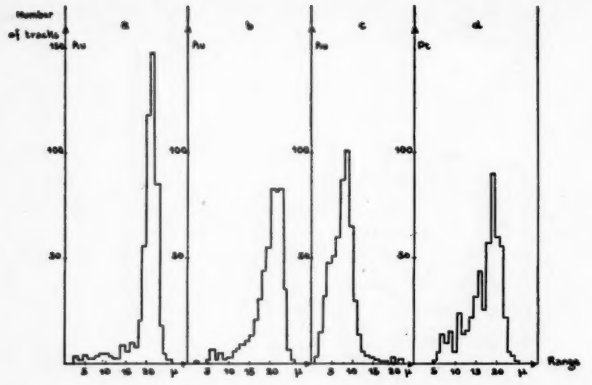

Initial cone: $0.44 \cdot 10^{-9}$N $0.11 \cdot 10^{-9}$N 10^{-10}N 10^{-12}N
Po deposit/cm²: 0.06 e.s.u. $0.67 \cdot 10^{-4}$ e.s.u. $0.68 \cdot 10^{-4}$ e.s.u. $0.42 \cdot 10^{-4}$ e.s.u.

FIG. 1. Distribution of α ranges.

measurements of about 500 traces. The deposits correspond, except where the contrary is indicated, to $4-5\times10^{-5}$ esu/cm² (initial alpha emission of 60 to 80 particles min./cm² or 10^{-11} mg/cm²). Note that the quantity necessary to cover 1 cm² of uniform monomolecular layer is 2650 e.s.u.

When the electrolysis is carried out in 10 cm³ of a solution containing 1.5 esu Po in order to obtain a deposit on gold of 0.06 e.s.u./cm² a range distribution is obtained as given by Fig. 1*a*, where a well-defined peak is found corresponding to 21.5μ (in the Ilford emulsion) and which is just the normal alpha-range for Po according to our calibration. However a not negligible number of tracks are found which possess ranges inferior to the normal value: e.g. 2.6 percent of 14.5μ, 1 percent of 9.4μ etc.

If the deposit in the same solution is stopped at an intensity of 60α/min. cm² (4.10^{-5} e.s.u./cm²), the distribution is considerably changed (Fig. 1*b*): the peak is here broader and corresponds to 19.5μ and the number of shortened tracks is much greater. In much more dilute solutions the deformation is more strongly accentuated, the maximum range and the distribution varying with the origin and the "history" of the metal, and probably with other experimental conditions. The quantitative reproductibility is consequently quite mediocre. As an example we reproduce the statistics corresponding to a deposit on gold foil in solution 10^{-13}N (Figs. 1*c* and 2). The

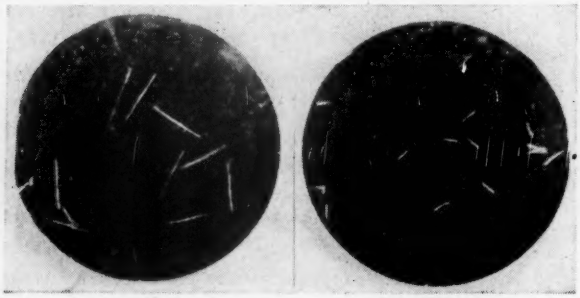

FIG. 2. 10^{-10}N 10^{-13}N
Po deposits on gold, in solution.

peak here is only of 7.5μ. An analogous distribution was found for deposits obtained in 10^{-14}N solutions.

For deposits on Ag obtained under similar conditions to those just described (10^{-13}N) we have observed a nearly normal distribution (analogous to that shown in Fig. 1*a*). On Pt and on Ni, the distribution is intermediate between Au and Ag.

It is interesting to note that traces of nearly the same length tend to be grouped together on the various parts of the surface. Furthermore, in the more concentrated solutions (5×10^{-12} to 10^{-10}N) we frequently observed stars which correspond to aggregations containing thousands of Po atoms, and whose centers often seem to be situated at a certain depth inside the electrode. Our solutions being strongly acid, the possibility is excluded of considering the stars as of a radio-colloidal origin.

These experiments clearly show that a fraction of the Po atoms, the proportion varying with the conditions and especially with the nature of the support, slightly penetrates the interior of the metal. This signifies a partial absorption of the alpha-rays with a shortening of their ranges. The phenomenon is certainly related to the surface structure and could be explained by the existence of "active centers" postulated for the interpretation of the kinetic and energetic results for deposits obtained in extremely dilute solutions.[1]

We think that our results explain the observations of Chang[2] on the existence of numerous groups of reduced tracks in the alpha-"spectrum" of Po. Chang's conclusions have been severely criticized by Feather[3] and by Zajac, Broda, and Feather[4] and have not been confirmed in the more recent experiments of Wadey.[5] This author attributes the groups to the diffusion of Po in the metal, but the normal diffusion at room temperature is undetectable, according to the measurements of Rona and Schmidt;[6] $D<10^{-14}$ cm²/day. Our experiments show that what has been observed by Chang is not the fine structure of the alpha-rays but the ultra-fine structure of the surface. They permit one to predict that the proportions of the feeble energy components of Chang's "spectrum" would strongly increase with the diminution of the source intensity.

Details of this research and its electrochemical aspects will shortly be described in the Journal de Physique et le Radium.

[1] M. Haissinsky, *Electrochimie des radioëléments* (Actualités Scientifiques No. 1009, Paris, 1946).
[2] W. Y. Chang, Phys. Rev. **69**, 60 (1946).
[3] N. Feather, Phys. Rev. **70**, 88 (1946).
[4] B. Zajac, E. Broda and N. Feather, Proc. Phys. Soc. **60**, 501 (1948).
[5] W. G. Wadey, Phys. Rev. **74**, 1846 (1948).
[6] Rona and Schmidt, Wien. Ber. **136**, 65 (1927).

The Forbidden Beta-Decay of Sr^{90} and Y^{90} *

CHARLES H. BRADEN, LEWIS SLACK, AND FRANKLIN B. SHULL
Washington University, St. Louis, Missouri
April 28, 1949

THE isotope Sr^{90} is a fission product which decays by β^--emission to Y^{90}. The half-life is $8\cdot10^8$ seconds and the energy release, including rest mass, is 2.04 mc² (kinetic energy 531 kev). The daughter product, Y^{90}, decays by β^--emission to Zr^{90}. The half-life for this transition is $2.25\cdot10^5$ seconds and the energy release is 5.40 mc² (kinetic energy 2.25 Mev). No gamma-radiation is observed. The decay scheme is pictured in Fig. 1 together with spin values and

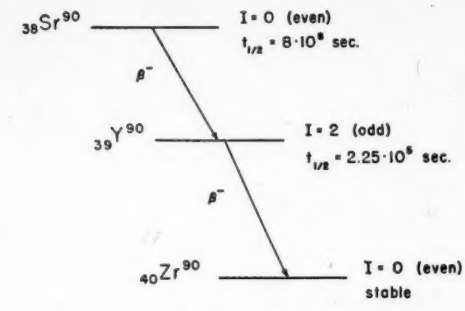

FIG. 1. Decay scheme for Sr^{90} and Y^{90}, showing spin and parity assignments as suggested in text.

parities as explained below. The arguments are based on two assumptions: (1) Gamow-Teller selection rules govern the beta-decay process, and (2) the nuclear shell model[1] is a reliable guide in the region $Z\sim40$ and $N\sim50$.

The nucleus $_{40}Zr^{90}$ contains closed shells of 40 protons and 50 neutrons. Thus, $I=0$ and the parity is even in the ground state.

$_{39}Y^{90}$ is an odd-odd nucleus. It is characterized by a $(3p)^{-1}(4d)^1$ configuration in the notation of Feenberg and Hammack. Thus, the ground state parity is *odd*.

$_{38}Sr^{90}$ is an even-even nucleus. It is characterized by a $(3p)^{-2}(4d)^2$ configuration. In the ground state the parity is even and, most probably, $I=0$.

Both beta-transitions are associated with change of parity. Thus by G-T rules, both are first-forbidden or both are third-forbidden. The *ft* product for the first transition is $\sim10^9$ and for the second $\sim10^8$. These values are appropriate for first-forbidden transitions with $\Delta I=\pm2^{(1-2)}$, but are too small for third-forbidden. Consequently, $I=2$ in the ground state of Y^{90}.

Thus the two beta-transitions of Fig. 1 should produce peculiar energy distributions similar to those found in Y^{91}, Cs^{137}, K^{42}, and Rb^{86} by various investigators.[2-7] In such cases the energy distribution differs[8] from the allowed form by a factor $G\sim(W_0-W)^2+(W^2-1)$.

A carrier-free sample of Sr^{90} was obtained from Oak Ridge. This sample had been aged to permit an associated 55-day activity of Sr^{89} to die out. Three spectra were measured: (1) Sr^{90} and Y^{90} in equilibrium together, (2) Sr^{90} alone, and (3) Y^{90} alone. For the latter two runs, the isotopes were chemically separated by a method due to Kurbatov and Kurbatov.[9] Samples were prepared for the spectrometer by evaporation from solution on thin Zapon films, following the insulin technique of Langer.[10]

The spectra were measured in the double-focusing spectrometer described by Kurie, Osoba, and Slack.[11] In the interests of higher counting rates, a wide counter window (0.25 in.) was used, which dropped the resolving power to 1 percent. The window was Zapon film of 3- to 4-kev stopping power, and was supported lengthwise by a single 5-mil wire. A pressure regulator[12] was used to avoid loss of counter pressure caused by window leakage.

The results are shown as FK (Fermi-Kurie) plots in Fig. 2 for Sr^{90} and in Fig. 3 for Y^{90}. As indicated in Fig. 2, the Sr^{90} data was obtained by subtracting the Y^{90} distribution curve from that for an equilibrium mixture of both Sr^{90} and Y^{90}.

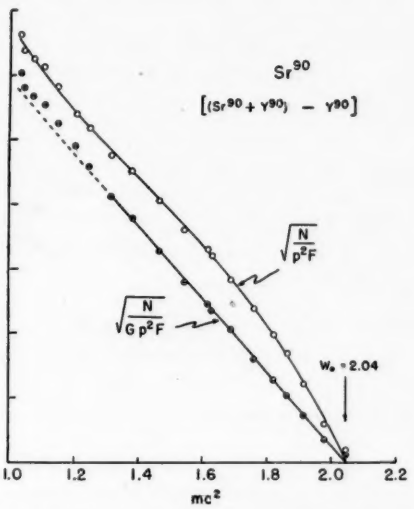

FIG. 2. Sr^{90} FK plots. "Allowed" plot (upper) and "forbidden" plot (lower), with ordinates as indicated.

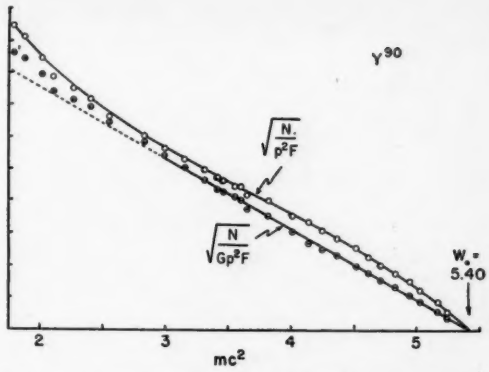

FIG. 3. Y^{90} FK plots. "Allowed" plot (upper) and "forbidden" plot (lower), with ordinates as indicated.

The upper curve in each figure (labeled $[N/p^2F]^{\frac{1}{2}}$) is a conventional or "allowed" FK plot, i.e., computed as though the transition were allowed. The lower curve in each figure (labeled $[N/Gp^2F]^{\frac{1}{2}}$) is a "forbidden" FK plot, i.e., computed as though the transition were first-forbidden, with $\Delta I=\pm2$ (yes). The near-straightness of the latter pair of plots confirms the assignment of spins and parities shown in Fig. 1.[13]

* Assisted by the joint program of the ONR and the AEC.

[1] E. Feenberg and K. C. Hammack, Phys. Rev. **75**, 1964 (1949).
[2] F. B. Shull and E. Feenberg, Phys. Rev. **75**, 1768 (1949).
[3] L. M. Langer and H. C. Price, Jr., Phys. Rev. **75**, 1109 (1949).
[4] A. C. G. Mitchell and C. L. Peacock, Phys. Rev. **75**, 1272 (1949).
[5] J. S. Osoba, Phys. Rev. (in press).
[6] A. C. G. Mitchell (private communication); see also Zaffarano, Kern, and Mitchell, Phys. Rev. **74**, 682 (1948), especially Fig. 4.
[7] K. Siegbahn, Arkiv. f. Mat., Astr. o. Fys. **34B**, No. 4 (1946).
[8] E. J. Konopinski and G. E. Uhlenbeck, Phys. Rev. **60**, 308 (1941).
[9] J. D. Kurbatov and M. N. Kurbatov, J. Phys. Chem. **46**, 441 (1942).
[10] L. M. Langer, Rev. Sci. Inst. **20**, 216 (1949).
[11] Kurie, Osoba, and Slack, Rev. Sci. Inst. **19**, 771 (1948).
[12] Ter-Pogossian, Townsend, and Robinson (to be published in Rev. Sci. Inst.).
[13] Similar results and conclusions are reported by L. J. Laslett and E. Jensen and by L. M. Langer (private communications).

The Forbidden Beta-Decay of Sr^{89}*

LEWIS SLACK, CHARLES H. BRADEN, AND FRANKLIN B. SHULL
Washington University, St. Louis, Missouri
April 28, 1949

THE isotope Sr^{89} decays by β^- emission to Y^{89} with a half-life of $4.75\cdot10^6$ seconds. The energy release, including rest mass, is 3.93 mc^2, so that the maximum electron kinetic energy is 1.50 Mev. No gamma-radiation is observed. The *ft* product for the beta-transition is $4.9\cdot10^8$.

Using the nuclear shell model notation of Feenberg and Hammack,[1] the Sr^{89} ground state is characterized by a $(3p)^{-2}(4d)^1$ configuration, so its parity is even. The ground state of Y^{89} is characterized by a $(3p)^{-1}$ configuration, so its parity is odd. The beta-transition between ground states, therefore, involves a parity change, and the transition is first-forbidden by Gamow-Teller rules. The large *ft* value favors a spin change of 2 units.[1,2]

A beta-transition for which $\Delta I=\pm2$ (yes) yields an electron energy distribution which differs from that for an allowed transition by a factor $G\sim(W_0-W)^2+(W^2-1)$, if it is assumed that Gamow-Teller rules apply to the beta-process.[3] Such distributions have been observed previously for Y^{91}, Cs^{137}, Rb^{86}, Sr^{90}, Y^{90}, and K^{42}.[2,3,4-10] If the above reasoning is correct, the Sr^{89} spectrum should display a similar forbidden "shape."

The spectrum was measured in the magnetic double-focusing spectrometer.[11] A source of Sr^{89}, containing also some Sr^{90}

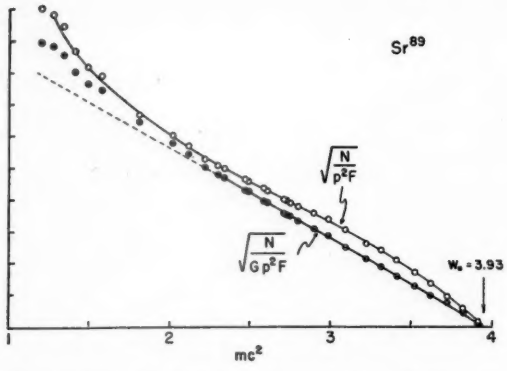

FIG. 1. Sr^{89} FK plots. "Allowed" plot (upper) and "Forbidden" plot (lower), with ordinates as indicated.

and Y^{90}, was obtained from Oak Ridge. Contributions to the spectrum from Sr^{90} and Y^{90} have been subtracted from the data. The data are shown in Fig. 1 in the form of FK (Fermi-Kurie) plots. The ordinate for the upper curve ("allowed" plot) is $(N/p^2F)^{\frac{1}{2}}$ and for the lower ("forbidden" plot) is $(N/Gp^2F)^{\frac{1}{2}}$. No attempt has been made to use a closer approximate form of G because of the relatively high value of W_0.[6] The upper curve shows the characteristic upward bulge for energies higher than $W_0/2$. The lower curve is satisfactorily straight, and confirms the prediction made above.[12]

Goldsmith and Inglis[13] list the spin of Y^{89} as 1/2(?), (original source of this value is not mentioned). If true, the spin of Sr^{89} ground state is 5/2. These spin values are in harmony with the nuclear shell model.

* Assisted by the joint program of the ONR and the AEC.
[1] E. Feenberg and K. C. Hammack, Phys. Rev. **75**, 1964 (1949).
[2] F. B. Shull and E. Feenberg, Phys. Rev. **75**, 1768 (1949).
[3] E. J. Konopinski and G. E. Uhlenbeck, Phys. Rev. **60**, 308 (1941).
[4] L. M. Langer and H. C. Price, Jr., Phys. Rev. **75**, 1109 (1949).
[5] A. C. G. Mitchell and C. L. Peacock, Phys. Rev. **75**, 1272 (1949).
[6] J. S. Osoba, Phys. Rev. (in press).
[7] Braden, Slack, and Shull (preceding letter).
[8] Zaffarano, Kern, and Mitchell, Phys. Rev. **74**, 682 (1948), and private communication from Dr. Mitchell.
[9] K. Siegbahn, Arkiv. f. Math., Astr. o. Fysik **34B**, No. 4 (1946).
[10] Private communications from L. J. Laslett and E. Jensen.
[11] Kurie, Osoba, and Slack, Rev. Sci. Inst. **19**, 771 (1948).
[12] Similar results have been observed by L. J. Lazlett and L. M. Langer (private communication).
[13] H. H. Goldsmith and D. R. Inglis, *The Properties of Atomic Nuclei I.*, Brookhaven National Lab. (1948).

Measurements Concerning the Vapor-Liquid Equilibrium of Solutions of He^3 in He^4 below 2.19°K

K. W. TACONIS AND J. J. M. BEENAKKER
Kamerlingh Onnes Laboratory, University, Leyden, Holland
AND
ALFRED O. NIER AND L. T. ALDRICH
University of Minnesota, Minneapolis, Minnesota
April 22, 1949

A SMALL vessel having a volume of 0.33 cm^3 had condensed in it a known amount of helium in which the He^3 concentration was about 5×10^{-4}. The vessel was placed in a bath of normal liquid helium and the vapor pressure difference, Δp, between the vessel and bath was measured while the vapor and liquid in the vessel were effectively stirred. In the top of the vessel we inserted a ground copper plug just below the capillary tube which connects the vessel with the apparatus outside the cryostat. The plug gives the helium film sufficient means for creeping out of the vessel, leaving the He^3 below the plug.[1] The film helium could be pumped out of the capillary by means of a Toeppler pump, and mass spectrometric analysis of this gas confirmed that no measurable amount of He^3 was going out. Thus the pumping effected a very considerable increase in the He^3 concentrations inside of the vessel.

If one assumes (a) perfect solution, i.e. independence of the energy of one atom of He^3 or He^4 of the concentration, (b) liquid helium to be a two fluid system with He^3 soluble in the normal fluid only, and (c) helium to act as a perfect gas in the vapor phase, then a determination of Δp as a function of the known He^3 content at constant temperature (below the λ-point) enables one to test the relations which follow.

According to Henry

$$p_3 = N_3{}^L\pi_3/(N_3{}^L+N_4{}^{nL}) \quad (1)$$

and

$$p_4 = N_4{}^{nL}\pi_4/(N_3{}^L+N_4{}^{nL}) \quad (2)$$

in which p_3 and p_4 are the partial pressures of the two isotopes in the vapor, $N_3{}^L$ and $N_4{}^{nL}$ the number of molecules of He^3 and normal fluid He^4 in the liquid, π_3 and π_4 the saturated vapor pressures. We derive from (1) and (2):

$$p_3/p_4 = N_3{}^L\pi_3/N_4{}^{nL}\pi_4 \quad (3)$$

and

$$\Delta p = p_3+p_4-\pi_4 = N_3{}^L(\pi_3-\pi_4)/(N_3{}^L+N_4{}^{nL}). \quad (4)$$

Accepting provisionally Tisza's relation $N_4{}^{nL}/N_4{}^L = \alpha = S/S_\Lambda$ (S is the entropy of the pure He^4 at the temperature used and S_Λ its entropy at the λ-point), we were able to calculate from the measured value of Δp at each temperature the absolute and relative concentrations in liquid and vapor, i.e.: $C_L = N_3{}^L/N_4{}^L$, $C_V = p_3/p_4$, $X_L = N_3{}^L/(N_3{}^L+N_4{}^L)$ and $X_V = p_3(p_3+p_4)$.

TABLE I. $T = 1.75$°K.

Δp mm Hg	$K_L 10^4$	$X_V 10^3$	$N_3{}^L\cdot10^8$	$N_3{}^V\cdot10^8$	$N_3{}^{tot}\cdot10^8$
0.16	5	16	435	22	457
0.33	10	35	284	88	372
0.54	17	58	221	172	393
0.67	21	70	189	219	408
0.78	24	80	168	258	426
0.84	26	85	130	280	410
0.91	28	91	84	306	390
1.11	35	112	35	390	425

The so calculated values of X_L and X_V together with the known volumes of vapor and liquid in the vessel made it possible to compute the total number of molecules He^3 present in the vessel. We could finally compare this number with our original amount of He^3, *viz.*: 440×10^{-8} mole.

Table I shows in column 6 the number of $N_3{}^{tot}$ at 1.75°K, which is, considering the accuracy of measurement, quite satisfactory. Similar isotherms were investigated at 2.0 and 1.9°K and analogous results were obtained. Lowering the temperature at constant filling gave again a good confirmation of our assumption. At 1.2°K we reached concentrations in the vapor as high as about 70 percent for a liquid concentration of 2 percent.

On the whole our chief assumption that He^3 is soluble in the normal fluid fraction of helium II appears to be remarkably well realized. Details will be published in Physica.

[1] Daunt, Probst, Johnston, Aldrich, and Nier, Phys. Rev. **72**, 502 (194.7)

A Search for Crystals That Exhibit Conduction Pulses Under Alpha-Particle Bombardment

A. J. AHEARN
Bell Telephone Laboratories, Murray Hill, New Jersey
April 23, 1949

AFTER conduction pulses were observed in diamond[1] under polonium alpha-particle bombardment, a search was made for other crystals that exhibit this phenomenon. The choice of crystal species that were selected for test was

guided by desiderata outlined elsewhere,[2] where such species were available.

The experimental techniques employed were like those reported earlier.[1] In most cases, specimens 0.25×0.25×0.020 inch with polished major faces were used. Conduction pulses were sought by applying the voltage first across electrodes separated by a gap of 0.002 inch on one face of the specimen and next across the electrodes on the opposite major faces of the specimen.

The first stage of the amplifier was put inside the experimental tube thereby attaining an input capacity of 10 to 15 $\mu\mu$f. With an estimated noise level of about 20 microvolts r.m.s. a 40 microvolt alpha-conduction pulse would be about the minimum that could be detected visually.

All measurements were made at room temperature. In general, at least two specimens of each species were tested. In many cases, the specimens probably were single crystals as they were cut from much larger crystalline pieces of the material. When the specimens were prepared from relatively small samples they may have been polycrystalline but in all probability the grain size was at least as large as the electrode separation.

Table I lists the species in which conduction pulses were observed. In general, no quantitative measurements either of counting efficiency or of pulse size were made. The species are listed in Table I in the order of decreasing response to alpha-particle bombardment. This rough classification is based on visual observations of the pulses as they are displayed on a cathode-ray oscilloscope.

The crystal species with which alpha-conduction pulses were not observed are listed in Table II. In most of these cases, a potential of at least 300 volts was applied in each of the two test procedures.

These negative results were obtained with a limited number of specimens of each species. In a number of cases indicated in Table II negative results in similar tests have been reported also by other investigators. This failure to observe conduction pulses even where confirmed by other workers does not necessarily preclude the possibility that sufficiently favorable conditions are attainable under which some or all of these species might yield positive results.

TABLE I. Species in which conduction pulses were observed.

1. Diamond
2. Sphalerite[a] (ZnS, cubic form)
   Wurzite[b] (ZnS, hexagonal form)
   Greenockite (CdS)[c,d]
3. Cinnabar (HgS)
4. Periclase[e] (MgO)
5. Stibnite (Sb_2S_3)
   Realgar (As_2S_2)
   Carborundum[f] (SiC)

[a] A. J. Ahearn, Phys. Rev. **73**, 524 (1948).
[b] Synthetic zinc sulfide through courtesy of Dr. J. M. Jauch, University of Iowa, Iowa City, Iowa.
[c] Synthetic cadmium sulfide prepared by Dr. R. Frerichs (see reference d) and supplied through courtesy of Dr. R. J. Cashman, Northwestern University, Evanston, Illinois.
[d] For other published work on bombardment conductivity in cadmium sulfide see R. Frerichs, Phys. Rev. **72**, 594 (1947). Report of Conference on Scintillation Counters and Crystal Counters, Rochester, New York, 1948; G. J. Goldsmith and K. Lark-Horowitz, Phys. Rev. **75**, 526 (1949).
[e] Synthetic crystals through courtesy of Dr. E. G. Rochow, General Electric Company and Norton Company, Niagara Falls, Canada.
[f] Synthetic crystals possessing an unusually high resistivity through courtesy of Dr. G. Busch, Zürich University, Switzerland.

TABLE II. Species in which alpha-conduction pulses were not observed.

Arsenic Trioxide*	Wulfenite
Orpiment	Mica
Sapphire*	Magnesium Meta Aluminate*
Topaz	Naphthalene*
Beryl	Orthoclase
Emerald	Potassium Bromide
Tourmaline	Rochelle Salt[a,*]
Barium Titanate*	Pyrargyrite
Apatite	Quartz
Calcite[a]	Sodium Chloride[a]
Fluorite[a]	Sodium Nitrate*
Lithium Fluoride[a,*]	Sulfur[a,b]
Cerusite	Titanium Dioxide[c,*]
Crocoite	Zinc Manganese Ferrite*

Potassium chloride* (also natural crystals)
Scheelite[d,*] (also natural crystals)
50 other species† of ionic crystals including tartrates, halides, sulfates, etc. of both organic and inorganic cations.

* Synthetic crystal.
[a] R. Hofstadter (Nucleonics, May, 1949) reports similar negative results.
[b] W. Jentschke (Phys. Rev. **73**, 77 (1948)) reports similar negative results with sulfur and alkali halides.
[c] Courtesy of Dr. R. Dahlstrom, National Lead Company, South Amboy, New Jersey.
[d] Courtesy of Linde Air Products Company.
† In order to conserve space, these species are not itemized since they are less common than those specifically listed in Table II. However the complete list will gladly be furnished on request.

[1] Wooldridge, Ahearn, and Burton, Phys. Rev. **71**, 913 (1947). A. J. Ahearn, Phys. Rev. **73**, 1113 (1948).
[2] K. G. McKay, Phys. Rev. **74**, 1606 (1948).

In^{118} and In^{119} Produced by Photo-Disintegration of Tin*

R. B. DUFFIELD AND J. D. KNIGHT
Department of Physics, University of Illinois, Urbana, Illinois
April 28, 1949

THE irradiation of tin with 17.5-Mev x-rays has been previously shown to produce 13-second In^{116} and 117-minute In^{117} by (γ, p) reactions.[1] An examination of the indium activities produced by the irradiation of tin with 23-Mev betatron x-rays at this laboratory has led to the identification of two additional periods which can be assigned to In^{118} and In^{119} on the basis of evidence outlined below. The properties of these two isotopes are summarized in Table I.

TABLE I. Properties of In^{118} and In^{119}.

Isotope	Made by	Observed half-life	Decay
In^{118}	$Sn^{119}(\gamma, p)$	4.5±0.5 min.	β^- 1.5 Mev γ
In^{119}	$Sn^{120}(\gamma, p)$	17.5±1 min.	β^- 2.7 Mev no γ

The identity of the In^{118} was established by an 8-minute irradiation with 23-Mev x-rays of a sample of tin foil enriched to 78.5 percent in Sn^{119}.[2] This sample decayed with a 4.5±0.5

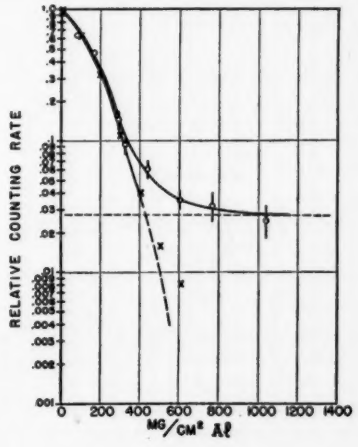

FIG. 1. Aluminum absorption curve of radiation from In^{118}.

minute half-life, after subtraction of a long-lived background (~4 percent) and the 40-minute Sn^{123} contribution (~5 percent).

An aluminum absorption curve was run on this activity by making a number of separate identical irradiations of the tin foil and following each decay through a different thickness of aluminum. The absorption curve is shown in Fig. 1. The tin sample used in these irradiations had a thickness of 80 mg/cm². Analysis of the curve as shown in the figure gave a beta-component with a range of approximately 670 mg/cm² of aluminum corresponding to an energy of 1.5±0.2 Mev, plus a gamma-ray background amounting to approximately 3 percent of the beta-counting rate. The beta-ray range and energy were estimated by a Feather analysis, using as reference standard a sample of P^{32} mocked up to resemble the In^{118} source in self-absorption.

There was not sufficient intensity for a lead absorption curve, although measurements taken through 1.0 g/cm² and 4.6 g/cm² of lead gave counting rates equal within experimental error to that of the thick absorber background in Fig. 1.

The In^{119} was identified by 23-Mev irradiation of a sample of tin foil enriched to 95.4 percent in Sn^{120}, followed by dissolution of the foil and precipitation of indium as indium hydroxide from hot 2 M sodium hydroxide solution. The precipitate showed a pure 17.5±1 minute decay. An aluminum absorption curve on a second portion of the irradiated Sn^{120} foil is shown in Fig. 2. A Feather analysis carried out as described above

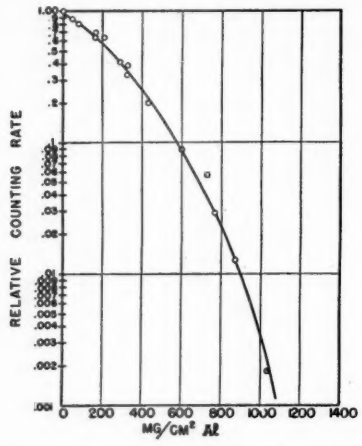

FIG. 2. Aluminum absorption curve of radiation from In^{119}.

gave a beta-range of 1350 mg/cm² of aluminum, corresponding to 2.7±0.2 Mev. Gamma-rays, if present at all, had a counting rate less than 0.001 that of the beta-counting rate.

* Assisted by the joint program of ONR and AEC.
[1] O. Hirzel and W. Waffler, Helv. Phys. Acta **20**, 373 (1947).
[2] The enriched Sn^{119} and Sn^{120} used in this investigation were supplied by Carbide and Carbon Chemicals Corporation, Y-12 Plant, Oak Ridge, Tennessee, and obtained on allocation from the Isotopes Division of the Atomic Energy Commission.

Note on Dirac's Theory of Magnetic Poles

M. N. SAHA
Institute of Nuclear Physics, Calcutta University, Calcutta, India
May 2, 1949

IN a note bearing the above heading, Professor H. A. Wilson[1] has described a simple method for finding out the value of Dirac's free magnetic poles. I may point out that this method was described by me nearly thirteen years ago[2] in a paper "On the origin of mass in neutrons and protons." I may just quote the result:

"It was Dirac who first showed that quantum mechanics demands the existence of free magnetic poles, having the pole strength (or magnetic charge) $ch/4\pi e=e/2\alpha$, where α=Sommerfeld fine-structure constant. Recently, the present author deduced the existence of free magnetic poles from very simple considerations. If we take a point charge e at A and a magnetic pole μ at B, classical electrodynamics tells us that the angular momentum of the system about the line $\overline{AB}$ is just $e\mu/c$. Hence following the quantum logic, if we put this $=\frac{1}{2}\cdot h/2\pi$, the fundamental unit of angular momentum, we have $\mu=ch/4\pi e=e/2\alpha$ which is just the result obtained by Dirac."

[1] H. A. Wilson, Phys. Rev. **75**, 308 (1949).
[2] Ind. J. Phys. **10**, 145 (1936).

Note on Proposed Schemes for Nuclear Shell Models*

EUGENE FEENBERG AND KENYON C. HAMMACK
Washington University, St. Louis, Missouri
AND
L. W. NORDHEIM
Duke University, Durham, North Carolina
February 23, 1949

THE two papers by the present writers[1,2] on nuclear shell structure, cover very similar ground, such as assignment of orbital configurations on basis of spins and magnetic moments, statistics of isomerism, and the character of β-transitions. Both papers suggest level schemes to account for the empirically found regularities in nuclear structure. The two schemes are, however, not identical, and even a third proposal has been made by Maria G. Mayer,[3] on basis of the data collected in references 1 and 2. It may thus be of value to explain the relations between these papers.

The basis of all the considerations on shell structure is the observation that the level schemes in a simple potential well give a good account of the regularities of nuclear structure for neutron and proton numbers below 20. Such regularities persist also for heavier nuclei, though they do not correlate with the simple well scheme. These facts suggest, however, that a rearrangement of levels may be successful.

TABLE I. Proposed schemes for nuclear shells.

No. of particles in nucleus	8	20	50	82
No. of particles in shell	2+6	12	30	32
Feenberg and Hammack	$(1s)^2(2p)^6$	$(2s)^2(3d)^{10}$ / $(1s)^2(2p)^6$ $(3d)^{10}$	$(4f)^{14}(5g)^{18}$	$(6h)^{22}(4d)^{10}$
Nordheim	$(1s)^2(2p)^6$	$(2s)^2(3d)^{10}$	$(4f)^{14}(3p)^6(4d)^{10}$	$(5g)^{18}(5f)^{14}$
Mayer	$(1s)^2(2p)^6$	$(2s)^2(3d)^{10}$	$(4f)^{14}(3p)^6(5g_{9/2})^{10}$	$(5g_{7/2})^8(4d)^{10}(3s)^2(6h_{11/2})^{12}$
Order of levels in potential well	1s, 2p, 3d, 2s, 4f, 3p, 5g, 4d, 3s, 6h, 5f, 4p, 7i			

In the scheme of Feenberg and Hammack, the rearrangement consists in a pushing up of orbits with radial nodes, such as 2*s*, 3*p*, 4*d*, which progresses more and more for heavier nuclei. Thus, the level scheme is somewhat different for light and heavy nuclei. A qualitative explanation for this tendency is given by the repulsive action of the Coulomb forces on protons, which will cause a decrease in density of nuclear matter at the center of heavy nuclei.

In Nordheim's scheme, the rearrangement is in the opposite sense; that is, radial nodes are not penalized as much as in a potential well. This may also be described as a discrimination against high orbital momentum states. The latter may be caused by the strong interaction between the nuclear particles,

since a rigid or liquid nucleus as a whole would have no orbital momentum in its lowest state.

The scheme proposed by Mayer follows exactly the order in a potential well. It achieves the breaks at the correct places by the assumption of a very strong spin-orbit coupling at high angular momentum values.

A summary of the three schemes is given in Table I. All three schemes give, of course, the empirical shell numbers and a statistical correlation with observed spins and moments. A decision between the schemes may be hoped for through discussion of new data which may tend to tip the scales in a definite direction, or by more theoretical work. Among the latter would be a refined calculation of the effects of the Coulomb forces on the density distribution in a nucleus, improved treatment of the many body problem, and better understanding of the spin-orbit coupling in nuclei.

It should be emphasized that the existence and the characteristics of nuclear shell structure have become now much more clearly established than formerly in spite of the ambiguities in their interpretation. Particularly there is a definite correlation between spin and shell structure. This does not mean necessarily that the individual particle model is better than hitherto assumed. The shell structure in nuclei, is, however, so pronounced an effect that one may hope to obtain an interpretation even on basis of such a crude approximation as the individual particle model.

* This letter has been written on request by the editor of the Physica Review, who received the papers, reference 1 and 2, by the same mail.

[1] Eugene Feenberg and Kenyon C. Hammack, Phys. Rev. **75**, 1877 (1949).
[2] L. W. Nordheim, Phys. Rev. **75**, 1894 (1949).
[3] Maria G. Mayer, Phys. Rev. **75**, 1969 (1949).

On Closed Shells in Nuclei. II

MARIA GOEPPERT MAYER
Argonne National Laboratory and Department of Physics, University of Chicago, Chicago, Illinois

February 4, 1949

THE spins and magnetic moments of the even-odd nuclei have been used by Feenberg[1,2] and Nordheim[3] to determine the angular momentum of the eigenfunction of the odd particle. The tabulations given by them indicate that spin orbit coupling favors the state of higher total angular momentum. If strong spin-orbit coupling, increasing with angular momentum, is assumed, a level assignment different from either Feenberg or Nordheim is obtained. This assignment encounters a very few contradictions with experimental facts and requires no major crossing of the levels from those of a square well potential. The magic numbers 50, 82, and 126 occur at the place of the spin-orbit splitting of levels of high angular momentum.

Table I contains in column two, in order of decreasing binding energy, the levels of the square well potential. The quantum number gives the number of radial nodes. Two levels of the same quantum number cannot cross for any type of potential well, except due to spin-orbit splitting. No evidence of any crossing is found. Column three contains the usual spectroscopic designation of the levels, as used by Nordheim and Feenberg. Column one groups together those levels which are degenerate for a three-dimensional isotropic oscillator potential. A well with rounded corners will have a behavior in between these two potentials. The shell grouping is given in column five, with the numbers of particles per shell and the total number of particles up to and including each shell in column six and seven, respectively.

Within each shell the levels may be expected to be close in energy, and not necessarily in the order of the table, although the order of levels of the same orbital angular momentum and different spin should be maintained. Two exceptions, $_{11}Na^{23}$ with spin 3/2 in stead of the expected $d_{5/2}$, and$_{25}$ Mn^{55} with 5/2 instead of the expected $f_{7/2}$, are the only violations.

Table II lists the known spins and orbital assignments from magnetic moments[4] when these are known and unambiguous, for the even-odd nuclei up to 83. Beyond 83 the data is limited and no exceptions to the assignment appear.

Up to Z or $N=20$, the assignment is the same as that of Feenberg and Nordheim. At the beginning of the next shell, $f_{7/2}$ levels occur at 21 and 23, as they should. At 28 the $f_{7/2}$ levels should be filled, and no spins of 7/2 are encountered any more in this shell. This subshell may contribute to the stability of Ca^{48}. If the $g_{9/2}$ level did not cross the $p_{1/2}$ or $f_{5/2}$

TABLE I.

Osc. No.	Square well	Spect. term	Spin term	No. of states	Shells	Total No.
0	$1s$	$1s$	$1s_{1/2}$	2	2	2
			$1p_{1/2}$	4		
1	$1p$	$2p$	$1p_{3/2}$	2	6	8
	$1d$	$3d$	$1d_{5/2}$	6		
2			$1d_{3/2}$	4	12	
	$2s$	$2s$	$2s_{1/2}$	2		20
			$1f_{7/2}$	8	8?	28?
	$1f$	$4f$	$1f_{5/2}$	6		
3			$2p_{3/2}$	4	22	
	$2p$	$3p$	$2p_{1/2}$	2		
			$1g_{9/2}$	10		50
	$1g$	$5g$	$1g_{7/2}$	8		
4			$2d_{5/2}$	6		
	$2d$	$4d$	$2d_{3/2}$	4	32	
	$3s$	$3s$	$3s_{1/2}$	2		
			$1h_{11/2}$	12		82
	$1h$	$6h$				
			$1h_{9/2}$	10		
5			$2f_{7/2}$	8		
	2	$5f$	$2f_{5/2}$	6		
			$3p_{3/2}$	4	44	
	$3p$	$4p$	$3p_{1/2}$	2		
			$1i_{13/2}$	14		126
	$1i$	$7i$				
			$1i_{11/2}$			
6	$2g$	$6g$				
	$3d$	$5d$				
	$4s$	$4s$				

levels, the first spin of 9/2 should occur at 41, which is indeed the case. Three nuclei with N or $Z=49$ have $g_{9/2}$ orbits. No s or d levels should occur in this shell and there is no evidence for any.

The only exception to the proposed assignment in this shell is the spin 5/2 instead of 7/2 for Mn^{55}, and the fact that the magnetic moment of $_{27}Co^{59}$ indicates a $g_{7/2}$ orbit instead of the expected $f_{7/2}$.

In the next shell two exceptions to the assignment occur. The spin of 1/2 for Mo^{95} with 53 would be a violation, but is experimentally doubtful. The magnetic moment of Eu^{153} indicates $f_{5/2}$ instead of the predicted $d_{5/2}$. No $h_{11/2}$ levels appear. It seems that these levels are filled in pairs only,

which does not seem a serious drawback of the theory as this tendency already shows up at the filling of the $g_{9/2}$ levels. Otherwise, the agreement is satisfactory. The shell begins with $_{51}$Sb, which has two isotopes with $d_{5/2}$ and $g_{7/2}$ levels, respectively, as it should. The thallium isotopes with 81 neutrons and a spin of 1/2 indicate a crossing of the $h_{11/2}$ and $3s$ levels. This is not surprising, since the energies of these levels are close together in the square well. The assignment

TABLE II. Spins of even-odd nuclei.

No. of neutrons or protons	Element	Odd protons: Mass No. orbit	Odd protons: Mass No. orbit	Odd neutron: Element	Odd neutron: Mass No. orbit	O=neutron X=proton: s 1/2	p 3/2	d 5/2	f 7/2	g 9/2	h	No. odd p or n	Levels
1	H	1 s	3 s	He	3 s	⊗						1	$1s$
3	Li	7 p					X					3	$p_{3/2}$
5	B	11 p		Be	9 p		⊗					5	
7	N	15 p		C	13 p	⊗						7	$p_{1/2}$
9	F	19 s				X						9	
11	Na	23					X					11	$d_{5/2}$
13	Al	27 d						X				13	
15	P	31				X						15	$s_{1/2}$
17	Cl	35 d	37 d	S	33		⊗					17	$d_{3/2}$
19	K	39 d	41 d				X					19	
21	Sc	45 f							X			21	$f_{7/2}$
23	V	51							X			23	
25	Mn	55						X				25	
27	Co	59 g							X			27	
29	Cu	63	65				X					29	$p_{3/2}$
31	Ga	69					X					31	
33	As	75					X					33	
35	Br	79	81				X					35	$f_{5/2}$
37	Rb	85 f(5/2)	87 p(3/2)	Zn	67 f		X	⊗				37	
39	Y	89				X						39	$p_{1/2}$
41	Cb	93 g								X		41	$g_{9/2}$
43	Tc			Se	77	O						43	
45	Rh											45	
47	Ag	107 p	109 p	Kr	83 g	X				O		47	
49	In	113 g	115 g	Sr	87 g					⊗		49	
51	Sb	121 d(5/2)	123 g(7/2)					X	X			51	$g_{7/2}$
53	I	127		Mo	95	O		X				53	$d_{5/2}$
55	Cs	133 g	137 g						X			55	
57	La	139 g							X			57	
59	Pr	141						X				59	
61	Pm											61	
63	Eu	151	153 f	Cd	111 s	O		X				63	
65	Tb	159		Cd	s, Sn s	O	X					65	$h_{11/2}$
67	Ho	165		Sn	117 s	O			X			67	
69	Tm			Sn	119 s	⊗						69	
71	Lu	175 g							X			71	
73	Ta	181 g							X			73	
75	Re	185	187	Xe	129 s	O		X				75	
77	Ir	191 (1/2)	193 (3/2)	Xe	131 d	X	⊗					77	$d_{3/2}$
79	Au	197 d		Ba	135 d		⊗					79	
81	Tl	203	205	Ba	137 d	X	O					81	$s_{1/2}$
83	Bi	209 A								X		83	$h_{9/2}$

demands that there be no spins of 9/2 in this shell, and none have been found. No f or p levels should occur and, except for Eu^{153}, there is no indication of any.

The spin and magnetic moment of $_{83}$Bi, indicating an $h_{9/2}$ state, is a beautiful confirmation of the correct beginning of the next shell. Here information begins to be scarce. The spin and magnetic moment of Pb^{207} with 125 neutrons interpret as $p_{1/2}$. This is the expected end of the shell since $7i$ and $4p$ have practically the same energy in the square well model. No spins of 11/2 and no s, d, or g orbits should occur in this shell, and the data indicates none.

The prevalence of isomerism towards the end of a shell, noticed by Feenberg and Nordheim, is easily understood by this assignment. These are the regions where levels with very different spins are adjacent. These ground and isomeric states should also have different parity.

Thanks are due to Enrico Fermi for the remark, "Is there any indication of spin-orbit coupling?" which was the origin of this paper.

[1] Eugene Feenberg, Phys. Rev. **75**, 320 (1949).
[2] Eugene Feenberg and K. C. Hammack, Phys. Rev. **75**, 1877 (1949).
[3] Lothar Nordheim, Phys. Rev. **75**, 1894 (1949). The author is indebted to these authors for having obtained copies of both references 2 and 3 before publication.
[4] H. H. Goldsmith and D. R. Inglis, *The Properties of Atomic Nuclei.I.* (Information and Publications Division, Brookhaven National Laboratory.)

Erratum: Charged Particles Emitted by Carbon Bombarded by 90-Mev Neutrons

[Phys. Rev. **75**, 1274 (1949)]

KEITH BRUECKNER AND WILSON M. POWELL
Radiation Laboratory, Department of Physics, University of California, Berkeley, California

THROUGH inadvertance, the curve for the energy distribution of protons leaving the carbon target was omitted. It is presented here.

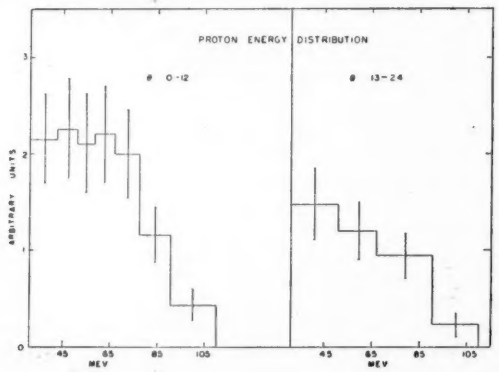

FIG. 2 (a) Energy distribution of the protons leaving carbon within 12° of the neutron beam. (b) Energy distribution of the protons leaving carbon with angles between 13° and 24° from the neutron beam. The errors indicated are standard deviations based only on the number of tracks used to determine the values.

Author Index to Volume 75

References with (A) are to abstracts of papers presented at meetings of the American Physical Society, and those with (T) designate title only. References with (L) are to Letters to the Editor.

Abraham, Bernard M. (see Osborne, Darrell W.)—988(L)
Adair, R. K. (see Bockelman, C. K.)—336(A)
——, **H. H. Barschall, C. K. Bockelman, and O. Sala.** Total cross section of Be, O, Na, and Ca for fast neutrons—1124
Adams, E. N., II (see Avery, R.)—1106(L)
Adams, G. D. (see Kerst, D. W.)—330(A)
Adams, Sam (see Burkhart, L. E.)—83
Adel, Arthur. Comparison of atmospheric methane content above Flagstaff, Arizona, and Columbus, Ohio—322(L)
—— Concerning the abundance of atmospheric carbon monoxide—1766(L)
—— Excited-state bands in atmospheric spectra—1262(L)
—— Ozonosphere temperatures from ground stations—1333(A)
Adelman, Frank L. and Stanley B. Jones. Stars in photographic emulsions initiated by heavy negative mesons—1468(A)
Ahearn, A. J. Search for crystals that exhibit conduction pulses under alpha-particle bombardment—1966(L)
—— (see Newton, R. R.)—103
Albert, R. D. (see Wu, C. S.)—315(L), 1107(L)
—— **and C. S. Wu.** Beta-ray spectra of Cu^{64}—1286(A)
Alburger, David E. Beta-ray spectrum of K^{40}—1442(L)
—— Gamma-rays from deuteron reactions—51
Alcock, N. Z. and D. G. Hurst. Neutron diffraction by gases—1609(L)
Aldrich, L. T. (see Lane, C. T.)—46
—— (see Taconis, K. W.)—1966(L)
Aldrich, R. W. (see Sack, H. S.)—1285(A)
Alexander, Ben H. Undercooling and nucleation of liquid metals—343(A)
Alfvén, Hannes. On the solar origin of cosmic radiation—1732
——, **R. D. Richtmyer, and E. Teller.** On the origin of cosmic rays—892(L)
Alger, R. S. (see von Hippel, A.)—1282(A)
Allen, A. (see Sun, K. H.)—1302(A)
Allen, James S., H. R. Paneth, and A. H. Morrish. Electron-neutrino angular correlation in the beta-decay of He^6—570
Allen, K. W. and J. T. Dewan. Light-charged particle emitted in fission—337(A)
Allison, H. W. (see Moore, George E.)—347(A)
Alpert, D. (see Krasik, S.)—1281(T)
Alpert, Nelson L. Study of phase transitions by means of nuclear magnetic resonance phenomena—398——Erratum—1271(L)
Alpher, Ralph A. and Robert C. Herman. Remarks on the evolution of the expanding universe—1089, 1333(A)
——, **R. Herman, and G. A. Gamow.** Erratum: thermonuclear reactions in the expanding universe—701(L)
——, **R. C. Herman, and G. A. Gamow.** On the origin of the elements—332(A)
Alvarez, Luis W. Nitrogen 12—1815
—— N^{17}, a delayed neutron emitter—1127
Alzofon, F. E. Relativistic treatment of neutron-proton elastic scattering in the Born approximation—1773(L)
Amsterdam, M. F. (see Miller, B. L.)—1325(A)
Anderson, Carl D. (see Leighton, Robert B.)—1432, 1466(A)
—— see Seriff, Aaron J.)—1466(A)
——, **Robert B. Leighton, and Aaron J. Seriff.** Decay products and the mass of the mesotron—1466(A)
Anderson, P. W. On the anomalous line-shapes in the ammonia inversion spectrum at high pressures—1450(L)
Anderson, Paul A. Work function of lithium—1205
Andrews, C. L. Diffraction patterns of electromagnetic waves near rods and apertures—346(A)
Angello, Stephen J. Electrical properties of cuprous oxide rectifier cells below room temperature—1310(A)
Anslow, Gladys A. and Ruth C. Shea. Association bands in the ultraviolet spectra of N—H...O bridged polymers—1318(A)
Antonoff, George and Robert J. Conan. Density of water as function of temperature—1303(A)
Apker, L. (see Taft, E.)—344(A), 1181
Araki, Gentaro. On the difficulty of the meson theory of nuclear forces—1101(L)
—— On the vector and pseudovector theories of nuclear forces—1262(L)
Arfken, G. B. (see Hatcher, R. D.)—1389
Argo, H. V. (see Taschek, R. F.)—1268(L)
Arnold, G. P., V. W. Myers, and A. H. Weber. Effect of crystal orientation on the scattering of slow neutrons—217
Arnold, Robert D. (see Kip, Arthur F.)—1556
—— **and Arthur F. Kip.** Paramagnetic resonance absorption in two sulfates of copper—1199
Ashworth, J. N. (see Ferry, John D.)—1284(A)
Augenstein, Bruno W. Passage of finite amplitude pressure waves through temperature discontinuities—521(L)
Avery, R. and E. N. Adams II. Exchange moments of H^3 and He^3—1106(L)
Avignon, P. (see Haissinsky, M.)—1963(L)
Axel, P. and S. M. Dancoff. Classification of isomeric transitions—1297(A)

Bailey, V. A. Space-charge wave amplification effects—1104(L)
Bainbridge, Kenneth T. Fringing field corrections for magnetic sector lenses and prisms—216(A)
—— Isotopic weights—215(T)
Bak, Börge, Erik Stenberg Knudsen, and Erhardt Madsen. Microwave absorption of some organic vapors—1622(L)
Baker, W. O. (see Mason, W. P.)—936, 1285(A)
——, **W. P. Mason, and J. H. Heiss.** Dynamics of polymer solutions and the deformation of separate macromolecules—1301(A)
Ballou, J. W. and J. C. Smith. Acoustic measurements of polymer physical properties—1284(A)
Ballou, N. E. Alpha-radioactivity in elements lighter than bismuth—1105(L)
—— (see Wolfe, R. D.)—527(L)
Band, William. Transport phenomena in a Bose Einstein gas—339(A), 1937
Barber, W. C. East-west asymmetry and latitude effect of cosmic rays at altitudes up to 33,000 feet—590
Bardeen, John. Physical principles involved in the transistor, a semiconductor triode—327(T)
—— Pressure change of resistance of tellurium—1777(L)
—— (see Pearson, G. L.)—865
—— **and W. H. Brattain.** Characteristics of the transistor—703(T)
—— **and W. H. Brattain.** Physical principles involved in transistor action—1208

Bargmann, V. Remarks on the determination of a central field of force from the elastic scattering phase shifts—301
Barkas, Walter H. Production ratio of positive and negative mesons for various cyclotron target materials—1467(A)
—— Threshold energy for meson production—1109(L)
Barker, E. C. (see Snell, Arthur H.)—1290(A)
Barker, F. C. and R. E. Peierls. On the definition of the "effective range" of nuclear forces—312(L)
Barker, R. S., W. O. Seifert, and J. H. Dillon. Kinetic concept of elasticity—1300(A)
Barnes, S. W. (see Ingram, M.)—1765(L)
——, **A. F. Clark, G. B. Collins, C. L. Oxley, R. L. McCreary, J. B. Platt, and S. N. VanVoorhees.** Note on the Rochester cyclotron—983(L)
Barnóthy, J. Theoretical values of mass and life-time of mesons—1458(A)
Barschall, H. H. (see Adair, R. K.)—1124
—— (see Bockelman, C. K.)—336(A)
—— (see Gittings, H. T.)—1610(L)
—— **and R. F. Taschek.** Angular distribution of 14-Mev neutrons scattered by protons—342(A), 1819
Baumhoff, L. (see Horning, W.)—370
Beach, Louis A., Charles L. Peacock, and Roger G. Wilkinson. Beta- and gamma-radiation of Ta^{182}—329(A)
——, **Charles L. Peacock, and Roger G. Wilkinson.** Gamma-rays of W^{187} in the low energy region—211(L)
Beams, J. W. (see Snoddy, L. B.)—1324(A)
Beard, C. I. and B. P. Dailey. Stark spectrum and dipole moment of HNCS—1318(A)
Beard, D. B. (see Morrison, P.)—1332(A)
Bearden, J. A. (see Schwarz, G.)—1304(A)
—— **and G. L. Rogosa.** Single crystals *vs.* double crystal x-ray spectrometers—1304(A)
Beatty, J. R. and J. M. Davies. Time and stress effects in the behavior of rubber at low temperature—1314(A)
Beatty, Suzanne van Dijke. Table of interplanar spacings for different target materials for the back reflection region—700(L)
Beck, Carl A. Near ultraviolet absorption spectrum of hydroquinone catechol and resorcinol vapor—334(A)
Becker, M. and H. Y. Fan. Photovoltaic effect of P—N barriers produced in germanium by α- and deuteron bombardment—1631(A)
Becker, R. A. (see McElhinney, J.)—542
Bedell, Frederick. What led to the founding of the American Physical Society—1456(T), 1601
Bederson, B. (see Fisher, L. H.)—1324(A), 1615(L)
Beeck, Otto. New concept of catalytic hydrocarbon reactions from isotopic tracer studies—1456(T)
Beeman, W. W. (see Petree, Marcella Cooper)—1628(A)
Beenakker, J. J. M. (see Taconis, K. W.)—1966(L)
Belinfante, Frederik J. Positon theory—1633(A)
—— Quantum-electrodynamics—337(A), 1321(A)
Bell, E. E. (see Chen, I-Shan)—1113(A)
—— (see Cleveland, Forrest F.)—334(A)
Bell, P. R. (see Kelley, G. G.)—1290(A)
Benedict, W. S. Centrifugal stretching in H_2O and D_2O—1317(A)
Benfield, A. E. Possible magnetic field of a rotating metallic body containing a stress gradient—211(L)
Benson, W. K., Jr., R. L. Mather, B. J. Moyer, and Joseph Yater. Radiation field of the 184-cyclotron—1470(A)
Benton, A. and E. L. Kinsey. Absorption spectrum of neodynium bromate crystals—888(L)
Berger, Martin and Gerhart Groetzinger. Consideration of multiple scattering in the evaluation of cloud-chamber tracks—342(A)
Bergmann, Peter G. Non-linear field theories—680
Beringer, Robert and J. G. Castle, Jr. Microwave magnetic resonance absorption in oxygen—1963(L)
Berlin, T. H. (see Kac, M.)—1298(A)
Berman, A. I. Method for increasing the safe power input of x-ray tubes—1457(A)
Bernardini, G. On the positive excess of the penetrating component in cosmic rays—1335(A)
—— On the star-producing radiation and the absorption of the nucleonic component—1328(A)
Bernstein, S., J. B. Dial, C. P. Stanford, and T. E. Stephenson. Total cross sections of small samples of Hf, Er, Ni^{58}, and Ni^{60} from neutron crystal spectrometer measurements—1302(A)
Berry, Chester R. Disorder in thin films of silver and silver iodide formed on silver bromide crystals—1299(A)
Berry, H. W. Scattering of fast argon atoms in argon gas—913
Bethe, H. A. and C. Longmire. On the experimental value of the fine structure constant—306
Bickford, L. R., Jr. Magnetic resonance absorption in magnetite as a function of temperature—1298(A)
Biehl, A. T. (see Roesch, W. C.)—1457(A)
——, **H. V. Neher, and W. C. Roesch.** Latitude dependence of cosmic rays at 33,000 feet—1457(A)
——, **H. V. Neher, and Wm. C. Roesch.** Note on the east-west effect—688(L)
Billmeyer, F. W., Jr., and W. H. Stockmayer. Method of measuring molecular weight distribution breadth—1307(A)
Biondi, Manfred A. and Sanborn C. Brown. Measurements of ambipolar diffusion in helium—1700
Bishop, A. S. Meson mass measurements. Part II. Experimental results—1468(A)
Biswas, Sukumar. On the Geiger-Nuttall relationship—530(L)
Bitter, F. Magnetic resonance frequencies for several nuclei—1326(A)
Bjorklund, R. (see Moyer, B. J.)—1470(A)
Blachman, Nelson M. and Ernest D. Courant. Correction and addendum: scattering of particles by the gas in a synchrotron—315(L)
Black, Robert F. (see Duckworth, Henry E.)—1438(L), 1616(L)
Blair, J. Morris, George Freier, E. E. Lampi, and William Sleator, Jr. Scattering of deuterons by helium at deuteron energies from 0.9 to 3.5 Mev—1678
Blair, J. S. Electro-disintegration of nuclei—907(L)
Blake, F. G., Jr. Gas bubbles as cavitation nuclei—1313(A)
Blaser, J. P., F. Boehm, and P. Marmier. Positron decay of F^{18}—1953(L)
Blatt, John M. Theoretical analysis of ionization chamber data on large air showers—1584
—— (see Jackson, J. D.)—1296(A)
—— **and J. D. Jackson.** Some calculations concerning neutron-proton scattering—341(A)
Blau, M. Grain density in nuclear tracks—1327(A)
—— Grain density in photographic tracks of heavy particles—279
Bleakney, W. (see Fletcher, C. H.)—1294(A)
——, **D. K. Weimer, and C. H. Fletcher.** Experimental measurement of the density field in the Mach reflection of shock waves—1294(A)
Bleaney, B. Paramagnetic resonance spectra of five chromic sulphate alums—1962(L)
Blewett, John P. Propagation of electromagnetic waves guided by magnetic materials—1288(A)
—— (see Plotkin, Martin)—1288(A)

Blewett, M. Hildred. Effects of eddy currents on the field of the cosmotron magnet—1288(A)
Blewitt, T. H. (see Koehler, J. S.)—1952(L)
Bloembergen, N. Fine structure of the proton magnetic resonance in $CuSO_4 \cdot 5H_2O$—1326(A)
Bloom, Evelyn G. (see Mohler, Fred L.)—1332(A)
Blunt, R. F., W. F. Love, and E. N. Skomal. Dielectric properties of barium titanate at low temperatures—1299(A)
Bockelman, C. K. (see Adair, R. K.)—1124
——, **R. K. Adair, H. H. Barschall, and O. Sala.** Total cross section of Be, N, O, Na, and Ca for fast neutrons—336(A)
Bockhop, D., A. C. Helmholz, S. D. Softky, J. W. Rose, and T. Breakey. Excitation functions from deuteron bombardment of Cu—1469(A)
Boehm, F. (see Blaser, J. P.)—1953(L)
Bøggild, J. K. and L. Minnehagen. Cloud-chamber study of the disintegration of lithium by slow neutrons—782
Bohm, D. Note on a theorem of Bloch concerning possible causes of superconductivity—502
—— (see Gross, E. P.)—1323(A)
—— **and E. P. Gross.** Excitation and damping of plasma oscillations—1323(A)
—— **and E. P. Gross.** Theory of plasma oscillations. A. Origin of medium-like behavior—1851
—— **and E. P. Gross.** Theory of plasma oscillations. B. Excitation and damping of oscillations—1864
Bonner, T. W. (see Whaling, Ward)—688(L)
——, **J. E. Evans, J. C. Harris, and G. C. Phillips.** Neutrons and gamma-rays from the disintegration of C^{12} by deuterons—1401
——, **J. E. Evans, and J. E. Hill.** Accurate determination of the threshold for the nuclear reaction $C^{12}(d, n)N^{13}$—1398
Boom, R. W. (see Claassen, R. S.)—331(A)
Borst, Lyle B. Nuclear reactor at Brookhaven National Laboratory—330(A)
—— (see Floyd, J. J.)—328(A), 1106(L)
Bottom, Virgil E. Electrical properties of highly purified tellurium—1310(A)
Bouricius, W. G. (see Breit, G.)—1029
Bouwkamp, C. J. On the transmission coefficient of a circular aperture—1608(L)
Bowen, Theodore (see Schein, Marcel)—339(A)
Bowers, W. A. and Nathan Rosen. H^3 and the mass of the neutrino—523(L)
Boyer, R. F. Compatibility, efficiency, and permanence of plasticizers—1314(A)
Bozorth, R. M. (see Williams, H. J.)—155
——, **W. P. Mason, H. J. McSkimin, and J. G. Walker.** Elastic constants and internal loss of single nickel crystals—1954(L)
Braden, Charles H. (see Slack, Lewis)—1965(L)
——, **Lewis Slack, and Franklin B. Shull.** Forbidden beta-decay of Sr^{90} and Y^{90}—1964(L)
Bradner, Hugh. Photographic plate confirmation of high energy deuterons from 90-Mev neutrons on carbon—1467(A)
—— (see Ehckrotte, Warren)—1467(A)
Bradt, H. L. (see Kaplon, M. F.)—1329(A)
—— **and B. Peters.** Nuclear collisions of heavy cosmic-ray primaries—1779(L)
Bragg, J. K. (see Goldstein, J. H.)—1453(L)
—— **and S. Golden.** Interaction of nuclear electric quadrupole moments and molecular rotation in asymmetric top molecules. II. Approximate methods for first-order coupling—735
—— **and A. H. Sharbaugh.** Microwave spectrum of formaldehyde—1774(L)
Bratenahl, A., R. H. Hildebrand, C. E. Leith, and B. J. Moyer. Elastic scattering of 90-Mev neutrons—1466(A)
Brattain, R. Robert. Spectroscopic determination of molecular structure—1456(T)
Brattain, W. H. (see Bardeen, J.)—703(T), 1208
—— **and H. B. Briggs.** Optical constants of germanium in the infra-red and visible—1705
Breakey, T. (see Bockhop, D.)—1469(A)
Breckenridge, R. G. Low frequency dispersion in ionic crystals containing foreign ions—1282(A)
Breit, G. (see Hatcher, R. D.)—1389
—— **and W. G. Bouricius.** Boundary conditions and range of force for S state of two protons—1029
—— **and R. E. Meyerott.** Hyperfine structure of the ground term of hydrogen—1447(L)
Bretscher, E. and A. P. French. Low energy cross section of the $D - T$ reaction and angular distribution of the alpha-particles emitted—1154
Brice, B. A. Performance of a light scattering photometer for determining high molecular weights—1307(A)
Bridge, H. S. and B. Rossi. Further experiments on cosmic-ray bursts—810
Briggs, H. B. (see Brattain, W. H.)—1705
Brillouin, L. Interaction between waves and electrons traveling together—1281(T)
—— **and H. P. Iskenderian.** Termodynamics of a thermomagnetic generator—1325(A)
Brockman, Frank G. (see Dowling, P. H.)—1298(A)
——, **P. H. Dowling, and Walter G. Steneck.** Anomalous behavior of the dielectric constant of a ferromagnetic ferrite at the magnetic Curie point—1440(L)
——, **P. H. Dowling, and Walter G. Steneck.** Magnetic properties of a ferromagnetic ferrite (part I)—1298(A)
Brode, Robert B. Mass of the cosmic-ray mesotrons—904(L)
—— (see Retallack, J. Gordon)—1716
Brody, James K. (see Fred, Mark)—1772(L)
Brosi, A. R., T. W. DeWitt, and H. Zeldes. Decay of 8-day iodine^{131} to a metastable state of xenon^{131}—1615(L)
Brown, Alexander. X-ray diffraction studies on the stretching and relaxation of polyethylene—1330(A)
Brown, F. W., III, P. J. Harris, and A. L. Klein. Life tests on self-quenching Geiger-Mueller tubes with halogen and polyatomic gases as quenching agents—1461(A)
Brown, H. (see Longmire, C.)—264, 328(A), 1102(L)
—— **and V. Perez-Mendez.** Beta-spectrum of A^{41}—1276(L)
—— **and V. Perez-Mendez.** Production of radioactive gases by deuteron bombardment of gaseous targets—1286(A)
Brown, J. (see Richards, J.)—331(A)
Brown, James (see Lind, David A.)—1544, 1633(A)
Brown, Richard M. and E. M. Purcell. Nuclear magnetic resonance in weak fields—1262(L)
Brown, Sanborn C. (see Biondi, Manfred A.)—1700
—— (see MacDonald, A. D.)—411, 1324(A)
Brown, William Fuller, Jr. Crystals interactions in ferromagnetic resonance—1959(L)
—— Irreversible magnetic effects of stress—147
Broxon, James W. Magnetic moments of sunspots—349(A), 606
—— Relation of the cosmic radiation to sunspot magnetic moments—341(A), 612
Brueckner, Keith, Walter Hartsough, Evans Hayward, and Wilson M. Powell. Neutron-proton scattering at 90 Mev—555
—— **and Wilson M. Powell.** Charged particles emitted by carbon bombarded by 90-Mev neutrons—1274(L)
——Erratum—1970(L)

Brunton, D. C. and G. C. Hanna. Energy distribution of fission fragments from U^{235} and U^{233}—1632(A)
—— **and G. C. Hanna.** Fission fragment energies in U^{235} and U^{233}—990(L)
Buchanan, James O. Separation of argon 36 by thermal diffusion—1332(A)
Buchdahl, R. (see Merz, E.)—1315(A)
——, **L. E. Nielsen, and Rita Levreault.** Dynamic mechanical properties of some high polymers—1284(A)
Buck, J. H. (see White, J. R.)—1619(L)
Bueche, A. M. and P. Debye. Scattering by inhomogeneous solids—1308(A)
Burcham, W. E. and Joan M. Freeman. Short-range alpha-particles from fluorine and lithium bombarded by protons—1756
Burfening, John, Eugene Gardner, and C. M. G. Lattes. Positive mesons produced by the 184-inch Berkeley cyclotron—382
Burg, Anton B. (see Gordy, Walter)—208(L), 1325(A)
Burgy, M. T. (see Hughes, D. J.)—344(A), 565
Burkhart, L. E., W. F. Peed, and E. J. Spitzer. K spectra of element 61—86
——, **George Stukenbroeker, and Sam Adams.** Isotope shifts in uranium spectra—83
Butement, F. D. S. Radioactive gadolinium and terbium isotopes—1276(L)
Butler, J. W., J. E. Evans, C. W. Malich, and J. R. Risser. Neutrons from the $Be^9(d, n)B^{10}$ reaction—1291(A)
Byatt, W. J., F. T. Rogers, Jr., and Arthur Waltner. On the beta-particle spectrum from the decay of tritium—909(L)

Cahn, Julius H. Electron velocity distribution function in high frequency alternating fields including electronic interactions—838
—— Electronic interaction in electrical discharges in gases—293
—— Electrostatic interaction in d.c. discharges in gases—346(A)
Callen, H. B. Electric breakdown in ionic crystals—1282(A)
Campbell, E. C., W. M. Good, and W. A. Strauser. Stopping of fission fragments in gases—1292(A)
Carney, Rose A. and Forrest F. Cleveland. Vibrational spectrum of hexachloroethane—333(A)
Carter, R. E. (see Koch, H. W.)—1950(L)
Case, K. M. Divergences in field theory—1440(L)
—— Equivalence theorems for meson-nucleon couplings—1306(A)
Cashin, W. M. and P. Debye. Determination of molecular weights and sizes by absorption—1307(A)
Castle, J. G., Jr. (see Beringer, Robert)—1963(L)
Chamberlain, Owen. Neutron diffraction in liquid elements—1471(T)
Chambre, P. L. (see Schaaf, S. A.)—1293(A)
Chandrasekhar, S. On the decay of isotropic turbulence—1454(L)
—— Theory of statistical and isotropic turbulence—896(L)
Chang, Chih-san (see Ch'en, Shang-yi)—81
Chang, T. S. Relativistic field theories—967
Chang, W. Y. Evidence of low energy gamma-rays (1–5 Mev) from stopped negative mesons—1315(A)
Chao, C. Y. Mixed cosmic-ray showers at sea level—581
Chapman, R. M. (see Migeotte, M. V.)—1611(L)
Chapman, Seville. Mechanisms of charge generation in thunderclouds—1333(A)
Chen, I-Shan and E. E. Bell. Measurement and analysis of some infra-red bands of HCN—1113(A)
Ch'en, Shang-yi and Chih-san Chang. Absorption spectrum of dense lithium vapor—81
Cheng, Lin-Sheng (see Yu, Fu-Chun)—1287(A)
Cherry, D. D. and C. S. Shyman. On meteor speed measurements by the radio Doppler method at low frequencies—1441(L)
Chew, Geoffrey F. and M. L. Goldberger. Analysis of low energy proton-proton scattering experiments—1466(A)
—— **and M. L. Goldberger.** Nuclear reactions produced by high energy neutrons—1456(T)
—— **and Marvin L. Goldberger.** On the analysis of nucleon-nucleon scattering experiments—1637
Chipman, D. (see Warren, B. E.)—1629(A)
Christian, R. S. Analysis of neutron-proton scattering with tensor forces—1675
—— **and E. Hart.** Neutron-proton scattering—1465(A)
Christy, R. F. Angular distribution of γ-rays from lithium—1464(A)
—— (see Latter, R.)—1459(A)
Chu, K. Y. and M. L. Wiedenbeck. Radiations from Hf^{181}—226
Claassen, R. S. and R. W. Boom. Temperature dependence of efficiency of a naphthalene scintillation counter—331(A)
Clark, A. F. (see Barnes, S. W.)—983(L)
Clark, Harold E. Excitation of mercury vapor by positive alkali ions—334(A)
Clark, R. K. and G. Failla. Absolute determination of the emission rate of beta-rays—328(A)
Cleveland, Forrest F. (see Carney, Rose A.)—333(A)
—— (see Kreusch, E.)—334(A)
—— (see Rosser, Shirley E.)—333(A)
—— (see Zietlow, James P.)—333(A)
—— (see Ziomek, Joseph S.)—334(A)
——, **K. W. Greenlee, and E. E. Bell.** Infra-red absorption spectrum of dimethyldiacetylene—334(A)
Cocconi, G. Some properties of the cosmic-ray ionizing particles that generate penetrating showers—1074
—— **and V. Cocconi Tongiorgi.** Density spectrum of extensive air showers of cosmic rays—1058
——, **V. Cocconi Tongiorgi, and K. Greisen.** Penetrating particles in extensive cosmic-ray air showers—1063
Coche, A. (see Haissinsky, M.)—1963(L)
Coffin, Victor H. and Clarence E. Bennett. Precise measurements of the molar refraction of carbon dioxide and its variation with density—215(A)
Cohen, E. Richard. Proton scattering by Li^7 and Be^9—1463(A)
Cohen, M. H. (see Hull, G. F.)—1311(A)
Cohen, Martin J. Observations at sea level with a self-controlled cloud chamber—1329(A)
Cole, Robert H. and Paul M. Gross, Jr. Wide range capacitance-conductance bridge—1312(A)
Collins, C. B. (see Macnamara, J).—532(L)
Collins, G. B. (see Barnes, S. W.)—983(L)
Conan, Robert J. (see Antonoff, George)—1303(A)
Conant, F. S., G. L. Hall, and G. R. Thurman. Relationship between Gough-Joule coefficients and moduli of vulcanized rubbers—1314(A)
Cook, C. Sharp (see Moe, David)—1270(L)
—— (see Robinson, J. Eugene)—1099(L)
—— (see Ter-Pogossian, Michel)—995
Cook, Leslie J., Edwin M. McMillan, Jack M. Peterson, and Duane C. Sewell. Total cross sections of nuclei for 90-Mev neutrons—7
Cook, Richard K. and Pearl G. Weissler. Measurement of the piezoelectric constants of alpha- and beta-quartz—1283(A)

Cool, R. L., E. C. Fowler, J. C. Street, W. B. Fowler, and R. D. Sard. Cloud-chamber study of mesons stopping in aluminum foils—1275(L)
Coon, J. H. He^3 isotopic abundance—1355
—— **and R. A. Nobles.** Disintegration of He^3 and N^{14} by thermal neutrons—1358
——, **R. F. Taschek, and S. G. Forbes.** Angular distribution of 14-Mev neutrons scattered by deuterons—1465(A)
Cork, B., L. Johnston, and C. Richman. Apparatus for measuring proton-proton scattering at 32 Mev using proportional counters—1465(A)
Cork, J. M., H. B. Keller, W. C. Rutledge, A. E. Stoddard, and J. Sazynski. Radioactivity induced in ytterbium by neutron bombardment—1133
——, **H. B. Keller, J. Sazynski, W. C. Rutledge, and A. E. Stoddard.** Electron spectrum of iodine 131—1621(L)
——, **H. B. Keller, J. Sazynski, W. C. Rutledge, and A. E. Stoddard.** Gamma-rays from tantalum 182—1778(L)
——, **H. B. Keller, J. Sazynski, A. Stoddard, and W. C. Rutledge.** Gamma-radiation from neutron activated ytterbium—1287(A)
Corrsin, Stanley. Some measurements in a round turbulent jet—1282(T)
—— **and Leslie S. G. Kovasznay.** On the hot-wire length correction—1954(L)
Corson, E. M. On a new equation of state—1264(L)
—— On problems involving permutation degeneracy—1266(L)
Coryell, C. D. (see Floyd, J. J.)—328(A)
——, **L. E. Glendenin, and R. R. Edwards.** Distribution of nuclear charge in fission—337(A)
Courant, Ernest D. (see Blachman, Nelson M.)—315(L)
Cowan, G. R. and D. R. Hornig. Thickness of a shock front in a gas—1294(A)
Cowley, J. M. Short-range order in Cu_3Au—1629(A)
Cranberg, L. and J. Halpern. Calibration of photographic emulsions for low energy electrons—1328(A)
Crane, H. R. Discharge of a Geiger counter at voltages above the plateau—985(L)
—— (see Wiedenbeck, M. L.)—1268(L)
Crawford, M. F., A. L. Schawlow, W. M. Gray, and F. M. Kelly. Nuclear moments of silver—1112(L)
——, **H. L. Welsh, and J. L. Locke.** Infra-red absorption of oxygen and nitrogen induced by intermolecular forces—1607(L)
Creagan, R. J. Q values from alpha-particle bombardment of boron—1292(A)
Critchfield, C. L. and D. C. Dodder. On the scattering of protons in hydrogen—419
Crittenden, E. C., Jr., and R. I. Strough. Limiting sensitivity of instruments for displaying the magnetic hysteresis loops of small specimens—1630(A)
Cross, Paul C. (see Grady, Harold R.)—1450(L)
Crouch, G. E., Jr. Ferromagnetic resonance in iron oxides—525(L)
Curtis, N. W. and L. S. Osborne. Sensitivity of physically developed nuclear emulsion tracks to specific ionization—1327(A)
Czyzak, S. J. and A. Wattenberg. Diffraction of slow neutrons by liquid D_2O—1634(A)

Dabbs, J. W. T. (see Moak, C. D.)—1770(L)
Dacey, John E. (see Paine, Roger W., Jr.)—1301(A)
——, **Roger W. Paine, Jr., and Clark Goodman.** Nuclear shielding studies—1301(A)
Dailey, B. P. (see Beard, C. I.)—1318(A)
——, **H. Minden, and R. G. Shulman.** Torsion vibrational states of CH_3CF_3—1319(A)
Dancoff, S. M. (see Axel, P.)—1297(A)
—— **and S. D. Drell.** Electrostatic scattering of neutrons—341(A)
Danielson, G. C. and R. E. Rundle. Structure of ferroelectric $BaTiO_3$—1630(A)
Darling, B. T. and J. E. Garvey. Water drop model of radioactive alpha-decay—1296(A)
Darrow, K. K. Linguistics of solid-state physics—1625(T)
Daunt, J. G., C. V. Herr, and A. A. Silvidi. Performance of a simple helium liquefier—1113(A)
Davidson, W. L. (see Wollan, E. O.)—1348
Davies, J. M. (see Beatty, J. R.)—1314(A)
Davis, Leverett, Jr., and Jesse L. Greenstein. Polarization of starlight by interstellar dust particles in a galactic magnetic field—1605(L)
—— **and R. V. Langmuir.** Betatron injection—1457(A)
Davis, R. H. and J. D. Graves. Optical method for improving the counting efficiency of scintillation counters—1461(A)
Davison, Perry W. Energy levels in sulfur nuclei—757
DeBenedetti, S. (see McGowan, F. K.)—1761(L)
deBethune, A. J. (see Present, R. D.)—1050
de Bretteville, A., Jr. (see Rosenblum, P.)—1305(A)
——, **N. J. Field, and S. B. Levin.** Optical interference phenomena and cinema-micrography of barium titanate crystals—1625(T)
Debye, P. Soap solutions—1308(A)
—— (see Bueche, A. M.)—1308(A)
—— (see Cashin, W. M.)—1307(A)
De Juren, J. (see Knable, N.)—1470(A)
Delano, Victor and Clark Goodman. Shielding measurements in concrete—1301(A)
Demers, Pierre and Roger Mathieu. Direct photometry on tracks in the photographic emulsion—1327(A)
DeSorbo, W. (see Fiske, M.D.)—1311(A)
—— (see Horn, F. H.)—1311(A)
—— (see Youngblood, J. F.)—1311(A)
Deutsch, Martin and Arne Hedgran. Decay of Co^{55}—1443(L)
Dewan, J. T. (see Allen, K. W.)—337(A)
DeWitt, T. W. (see Brosi, A. R.)—1615(L)
Dial, J. B. (see Bernstein, S.)—1302(A)
Dickinson, W. C. and T. F. Wimett. Magnetic moment of Be^9—1769(L)
Dickson, Donald. Radar techniques in high speed x-ray moving pictures—1635(T)
Dickson, R. (see Russell, B. R.)—1628(A)
Dillon, J. H. (see Barker, R. S.)—1300(A)
Diven, B. C. (see McElhinney, J.)—542
Dodder, D. C. (see Critchfield, C. L.)—419
Donoghue, J. J., E. Gerjuoy, and R. E. Vollrath. Rupture strength of benzene—1456(A)
Donoghue, W. F. (see Hafner, E. M.)—331(A)
Douglas, Donald G. Radiations from Lu^{177}—1960(L)
Dow, W. G. (see Reifman, A.)—1311(A)
Dowling, P. H. (see Brockman, Frank G.)—1298(A), 1440(L)
—— **and Frank G. Brockman.** Magnetic properties of a ferromagnetic ferrite (part II)—1298(A)
Drell, S. D. Magnetic internal conversion coefficient—132, 338(A)
—— (see Dancoff, S. M.)—341(A)
Driscoll, Raymond L. (see Thomas, Harold A.)—902(L), 992(L)
Duckworth, Henry E. Some possible rare stable isotopes—1438(L)
——, **Robert F. Black, and Richard F. Woodcock.** New stable isotope of platinum—1438(L)
——, **Robert F. Black, and Richard F. Woodcock.** Search for stable Pd^{100}, W^{178}, and Pb^{203}—1616(L)

Duffendack, O. S. Physics in an industrial laboratory—1635(T)
Duffield, R. B. (see McElhinney, J.)—542
—— **and J. D. Knight.** In^{118} and In^{119} produced by photo-disintegration of tin—1967(L)
—— **and J. D. Knight.** Radioactive silver isotopes produced by photo-disintegration of cadmium—1465(A), 1613(L)
DuMond, Jesse W. M. Inappreciable effect of Compton shifted scattering, within a gamma-ray source, on precision wave-length determinations with the focusing crystal spectrometer—1266(L)
—— Recent changes and additions in the consistency diagram of the natural atomic constants—1267(L)
—— (see Lind, David A.)—1544, 1633(A)
—— (see Watson, Bernard B.)—505, 1305(A)
——, **D. A. Lind, and B. B. Watson.** Precision measurement of the wave-length and spectral profile of the annihilation radiation from Cu^{64} with the two-meter focusing curved crystal spectrometer—1226, 1304(A)
du Pré, F. K. (see Hutner, R. A.)—345(A)
—— (see Rittner, E. S.)—345(A)
Dyson, F. J. Radiation theories of Tomonaga, Schwinger, and Feynman—486
—— S-matrix in quantum electrodynamics—1736
Dyson, J. P. (see Graves, J. D.)—1461(A)

Edlén, B. and K. Lidén. Note on the arc spectrum of lithium—890(L)
Edwards, H. D. (see Gilliam, O. R.)—1014
Edwards, R. R. (see Coryell, C. D.)—337(A)
Eggen, D. T. and M. L. Pool. Radioactive isotopes of Rh and Pd—1464(A)
Eggler, C. (see Hughes, D. J.)—515, 1285(A)
Ehckrotte, Warren and Hugh Bradner. Recoils of active fluorine^{18} from 184-in. cyclotron bombardment—1467(A)
Ehrenhaft, Felix. Further experimental proofs of the existence of single magnetic poles—1334(A)
—— New phenomena of radiation in magnetic fields—1628(A)
Einbinder, Harvey. Application of Jacobians to statistical thermodynamics. Part I. The explicit calculation of thermodynamic functions—1335(A)
—— Application of Jacobians to statistical thermodynamics. Part II. The theory of thermodynamic fluctuations—1335(A)
—— On the hydrodynamic stability of flame fronts—1313(A)
Eisenstein, A. and J. R. Young. Oxide cathode interface and coating voltages—347(A)
Eisenstein, J. (see Rohrlich, F.)—705
Ekstein, H. New approximation method in scattering phase caalculations—1322(A)
Eldridge, John A. Strings, poles and the electron—1614(L)
Ellis, Cecil B. Survey of nuclear energy possibilities—330(A)
Elmore, W. C. and R. Hofstadter. Temperature dependence of scintillations in sodium iodide crystals—203(L)
Emmerich, Werner S. and J. D. Kurbatov. Beta-decay spectrum of Ag^{110}—1446(L)
Engelkemeir, Antoinette G., W. H. Hamill, Mark G. Inghram, and W. F. Libby. Half-life of radiocarbon (C^{14})—1825
Epstein, H. T. On the existence of micelles in organic acid monolayers—1628(A)
Erickson, K. W., J. L. Fowler, and E. J. Stovall, Jr. Differential cross section for reaction $D(d, n)He^3$ for 10-Mev bombarding energy—894(L)
Erikson, Henry A. and E. L. Hill. Note on the one-electron states of diatomic molecules—29
Errett, Daryl (see Rieke, F. F.)—346(A)
Estermann, I. Resistivity of germanium samples at liquid helium temperatures—1625(T)
——, **A. Foner, and J. E. Zimmerman.** Resistivity of germanium samples at liquid helium temperatures—1631(A)
——, **W. J. Leivo, and O. Stern.** Change in density of potassium chloride crystals upon irradiation with x-rays—627
Evans, J. E. (see Bonner, T. W.)—1398, 1401
—— (see Butler, J. W.)—1291(A)
—— (see Whaling, Ward)—688(L)
——, **C. W. Malich, and J. R. Risser.** Neutrons and gamma-radiation from deuteron bombardment of Be—1161
Everhart, G. G. (see Gittings, H. T.)—1610(L)
—— (see Taschek, R. F.)—1361

Fahy, Edward F. and Marcel Schein. Observations on large cosmic-ray bursts at an altitude of 3500 meters—207(L)
—— **and Marcel Schein.** Origin of large cosmic-ray bursts at an altitude of 3500 meters—340(A)
Failla, G. (see Clark, R. K.)—328(A)
Fairbank, Henry A. Helium three isotope at liquid helium temperature—215(T)
—— (see Lane, C. T.)—46
Fairbank, W. M. Surface resistance of superconductors at microwave frequencies—215(T)
Fan, H. Y. Theory of photovoltaic effect of $P-N$ barrier in a semi-conductor—1631(A)
—— (see Becker, M.)—1631(A)
Fankuchen, I. (see Miller, E.)—1314(A)
Fano, U. and P. R. Karr. Approach to spectral equilibrium in the penetration of x-rays—1303(A)
Faraggi, H. (see Haissinsky, M.)—1963(L)
Farnsworth, H. E. (see Reichertz, Paul P.)—1902
Fatehally, R. A. (see Garlick, G. F. J.)—1446(L)
Faust, W. R. and M. H. Johnson. Multiple Compton scattering—467
Feenberg, Eugene. Nuclear shell structure and isomerism—320(L)
—— (see Shull, Franklin B.)—1768(L)
—— **and Kenyon C. Hammack.** Interpretation of nuclear shell structure—332(A)
—— **and Kenyon C. Hammack.** Nuclear shell structure—1877
——, **Kenyon C. Hammack, and L. W. Nordheim.** Note on proposed schemes for nuclear shell models—1968(L)
Feer, Daniel B. Emission of radiation in the disintegration of mesons—731
Felber, F. (see Richards, J.)—331(A)
Feld, Bernard T. Angular correlations in successive nuclear α-γ-emission and the excited state of Li^7—1618(L)
—— On the inelastic scattering of fast neutrons—1115
—— On the interpretation of neutron inelastic scattering data—1302(A)
Feldman, David and Julian Schwinger. Radiative correction to the Klein-Nishina formula—338(A)
Feldman, L. and C. S. Wu. Beta-ray spectra of C^{14}—1286(A)
Fermi, Enrico. On the origin of the cosmic radiation—1169
—— **and L. Marshall.** Spin dependence of slow neutron scattering by deuterons—578
Fernbach, S., R. Serber, and T. B. Taylor. Scattering of high energy neutrons by nuclei—1352

Ferry, John D., J. N. Ashworth, and W. M. Sawyer. Rigidities of polyisobutylene and polyvinyl acetate solutions from wave propagation measurements—1284(A)
Feshbach, Herman (see Goldstein, Herbert)—1306(A)
—— **and William Rarita.** Tensor forces and the triton binding energy—1384
—— **and V. F. Weisskopf.** On the scattering of fast neutrons—342(A)
Feynman, R. P. Theory of positrons—1321(A)
——, **N. Metropolis, and E. Teller.** Equations of state of elements based on the generalized Fermi-Thomas theory—1561
Field, N. J. (see de Bretteville, A. P.)—1625(T)
Fillmore, Franklin (see Panofsky, Wolfgang K. H.)—1465(A)
Filosofo, I. and A. Rostagni. On the liberation of ions by electron bombardment—1269(L)
Finkelstein, R. J. On the quantization of a unitary field theory—1079
Fireman, E. L. Measurement of the half-life of double beta-decay from $_{50}Sn^{124}$—323(L)
—— On the decay of K^{40}—1447(L)
Fisher, L. H. and B. Bederson. Formative time lags in spark breakdown—1324(A)
—— **and B. Bederson.** Search for the transition of streamer to Townsend form of spark in air—1615(L)
Fiske, M. D. (see Horn, F. H.)—1311(A)
—— (see Youngblood, J. F.)—1311(A)
——, **W. DeSorbo, F. H. Horn, and J. F. Youngblood.** General Electric low temperature laboratory. Part I. The building and general facilities—1311(A)
Fletcher, C. H. (see Bleakney, W.)—1294(A)
——, **D. K. Weimer, and W. Bleakney.** Shock tube for the study of transient gas flow—1294(A)
Fletcher, J. C. and H. K. Forster. Energy of the disintegration product of a light mesotron—204(L)
Fletcher, R. Impulse breakdown of air in the 10^{-9}-sec. range—1324(A)
Flory, L. E. Electronic storage of information—1281(T)
Flory, Paul J., Norman Rabjohn, and Marcia C. Shaffer. Dependence of the tensile strength of vulcanized rubber on the degree of cross-linking—1300(A)
Floyd, J. J. and L. B. Borst. Energy of beta-rays from K^{40}—1106(L)
——, **C. D. Coryell, and L. B. Borst.** Radioactive decay of K^{40}—328(A)
Foldy, Leslie L. Electromagnetic properties of nucleons—1625(T)
—— Multiple scattering with energy loss—311(L)
—— On the scattering of low energy γ-rays by protons—1634(A)
—— Single production of mesons by γ-rays near threshold—1633(A)
—— **and R. E. Marshak.** Production of π-mesons in nucleon-nucleon collisions—1307(A), 1493
Foley, H. M. (see Wu, Ta-You)—1305(A), 1681
Foner, A. (see Estermann, I.)—1631(A)
Forbes, S. G. (see Coon, J. H.)—1465(A)
Forró, M. Compton-Getting effect of cosmic radiation—1458(A)
Forsbergh, P. W., Jr. Phase transitions in barium titanate—1299(A)
Forster, H. K. (see Fletcher, J. C.)—204(L)
Fowler, E. C. (see Cool, R. L.)—1275(L)
Fowler, J. L. (see Erickson, K. W.)—894(L)
Fowler, W. A. (see Thomas, R. G.)—1463(A), 1612(L)
—— (see Tollestrup, A. V.)—1463(A), 1947(L)
—— (see Woodbury, E. J.)—1462(A)
——, **C. C. Lauritsen, and S. Rubin.** Inelastic scattering of protons from Li^7—1471(A)
——, **C. C. Lauritsen, and S. Rubin.** Scattering of protons by lithium—1463(A)
Fowler, W. B. (see Cool, R. L.)—1275(L)
Francis, J. E., Jr. (see McGowan, F. K.)—1761(L)
Franklin, E. G. (see Nier, Alfred O.)—346(A)
Franzen, W., J. Halpern, and W. E. Stephens. Ionization chamber observation of the reaction $N^{14}(n, p)C^{14}$—1292(A)
Fraser, L. W. (see Van Allen, J. A.)—1315(A)
Fred, Mark, Frank S. Tomkins, and James K. Brody. Isotope shift in the helium spectrum—1772(L)
Freeman, Joan M. (see Burcham, W. E.)—1756
Freier, George (see Blair, J. Morris)—1678
——, **Eugene Lampi, W. Sleator, and J. H. Williams.** Angular distribution of 1- to 3.5-Mev protons scattered by He^4—342(A), 1345
——, **E. E. Lampi, and J. H. Williams.** Neutron yield from $Li^7(p, n)Be^7$—901(L)
Freier, Phyllis (see Ney, E. P.)—340(A)
——, **E. J. Lofgren, E. P. Ney, and F. Oppenheimer.** Star production at high altitudes—340(A)
——, **E. P. Ney, and F. Oppenheimer.** Cosmic ray induced nuclear stars at high altitudes—1451(L)
——, **Edward P. Ney, and Frank Oppenheimer.** Energies of heavy nuclei in cosmic rays—991(L)
French, A. P. (see Bretscher, E.)—1154
French, J. B. and V. F. Weisskopf. Electromagnetic shift of energy levels—338(A), 1240
Frenkiel, F. N. Influence of the length of a hot wire on the measurements of turbulence—1263(L)
—— Influence of the length of wires on the measurement of turbulence with a hot-wire anemometer—1314(A)
Fretter, William B. Cloud-chamber observations of penetrating shows in lead at 3020 meters—1330(A)
Friedlander, G. (see Hill, R. D.)—324(L)
Frisch, David H. Calculation of interaction integrals in Wigner's theory of heavy nuclei—1297(A)
—— (see Weisskopf, V. F.)—1297(A)
Fujimoto, Y. and Y. Yamaguchi. On the cosmic-ray stars—1776(L)
Furry, W. H. and James N. Snyder. On the stimulated decay of mesons—1265(L)
Fusfeld, Herbert I. Apparatus for rapid measurement of internal friction—1626(A)

Gallagher, Georges (see Rouault, Marcel)—1319(A)
Gamow, G. A. (see Alpher, R. A.)—332(A), 701(L)
Gangnes, A. V., J. F. Jenkins, Jr., and J. A. Van Allen. Cosmic-ray intensity above the atmosphere—57——Erratum—892(L)
Garbuny, M. (see Shoupp, W. E.)—336(A)
Gardner, Eugene. Meson mass measurements. Part I. Experimental method—1468(A)
—— Stars in photographic emulsions initiated by alpha-particles—379
—— (see Burfening, John)—382
—— **and Vincent Peterson.** Stars in photographic emulsions initiated by deuterons. Part I. Experimental—364
Garlick, G. F. J. and R. A. Fatehally. Measurement of particle energies with scintillation counters—1446(L)
Garrett, Milan W. Field or search coils combining loops and solenoids—1297(A)
Garvey, J. E. (see Darling, B. T.)—1296(A)
George, Waller (see LaTorre, Richard)—1309(A)
Gerjuoy, E. (see Donoghue, J. J.)—1456(A)
Germain, Lawrence S. Range spectrum of cosmic-ray mesotrons—1458(A)
Ghiorso, A. (see Meinke, W. W.)—314(L)
—— (see Perlman, I.)—1096
Ghormley, J. A. (see Jenks, G. H.)—701(L)
Gideon, Donald N. (see Kurbatov, J. D.)—328(A)

——, **W. C. Miller, and B. Waldman.** Nuclear isomerism of selenium produced by x-rays—329(A)
Gilliam, O. R., H. D. Edwards, and Walter Gordy. Microwave investigations of methyl fluoride, fluoroform, and phosphorus trifluoride—1014
Gilmore, G. D. (see Spencer, R. S.)—1300(A)
Ginsburg, N. Infra-red emission spectra of molecules—1317(A)
Gittings, H. T. (see Taschek, R. F.)—1361
——, **H. H. Barschall, and G. G. Everhart.** Inelastic scattering of 14.5-Mev neutrons by lead—1610(L)
——, **R. F. Taschek, A. R. Ronzio, E. Jones, and W. J. Masilun.** Relative sensitivities of some organic compounds for scintillation counters—205(L)
Gladding, E. K. (see Remington, W. R.)—1330(A)
Glaser, H. (see Rogosa, G. L.)—1304(A)
Glendenin, L. E. Nuclear closed shell effects in fission—337(A)
—— (see Coryell, C. D.)—337(A)
Gluckstern, R. L. and Lloyd Smith. On the injection of ions in the bevatron—1467(A)
Gold, Louis. On the directional character of the long-range order parameter—1265(L)
—— Superlattice lines of the second kind and their relation to the apparent discrepancy in the x-ray analysis of the structure of Heusler alloy—1629(A)
Goldberg, Leo (see Mohler, Orren C.)—520(L)
Goldberger, Marvin L. (see Chew, Geoffrey F.)—1456(T), 1466(A), 1637
Golden, S. (see Bragg, J. K.)—735
Goldhaber, Gerson. Gamma-ray spectrum from $F^{19} + H^1$ using photographic emulsions containing D_2O—336(A)
Goldhaber, M. Excited states of nuclei—327(T)
Goldman, J. E. Influence of atomic order on magnetic properties—1625(T)
—— (see Smoluchowski, R.)—1299(A)
—— **and R. Smoluchowski.** Effect of ordering on magnetostriction and magnetization—1299(A)
—— **and R. Smoluchowski.** Influence of order on the saturation magnetic moment—310(L)
—— **and R. Smoluchowski.** Magnetostriction and order-disorder—140
Goldsmith, G. J. and K. Lark-Horovitz. Cadmium sulfide as a crystal counter—526(L)
Goldstein, Herbert and Herman Feshbach. On the interaction of a nucleon with a pseudoscalar field—1306(A)
Goldstein, J. H. and J. K. Bragg. Nuclear quadrupole effects in the microwave spectrum of the asymmetric top molecule, vinyl chloride—1453(L)
Goldstein, Louis (see King, L. D. P.)—1302(A), 1366
—— **and W. H. Lane.** On proton-proton scattering models—1296(A)
Goldstein, N. (see Hughes, D. J.)—1781
Golian, S. E., C. Y. Johnson, E. H. Krause, M. L. Kuder, G. J. Perlow, and C. A. Schroeder. V-2 cloud-chamber observation of a multiply charged primary cosmic ray—524(L)
Good, W. M. (see Campbell, E. C.)—1292(A)
Goodman, Clark (see Dacey, John E.)—1301(A)
—— (see Delano, Victor)—1301(A)
—— (see Paine, Roger W., Jr.)—1301(A)
Gordy, Walter (see Gilliam, O. R.)—1014
—— (see Smith, Alex. G.)—260
——, **Harold Ring, and Anton B. Burg.** Erratum: nuclear spins and quadrupole moments of B^{10} and B^{11}—208(L)
——, **Harold Ring, and A. B. Burg.** Nuclear moments of B^{10} and B^{11}—1325(A)
Goucher, F. S. Some electrical and photoelectric studies of $p-n$ junctions in silicon and germanium—1625(T)
Grady, Harold R., Paul C. Cross, and Gilbert W. King. Hydrogen sulfide bands at 10200 cm^{-1}—1450(L)
Gráf, T. Erratum: significance of the radioactivity of potassium in geophysics. II—534(L)
Graham, John W. (see Torreson, O. W.)—208(L)
Graves, J. D. (see Davis, R. H.)—1461(A)
—— (see Koch, G. E.)—1461(A)
—— **and J. P. Dyson.** Laboratory alpha-scintillation counter—1461(A)
Gray, D. E. Problem of abstracting the periodical literature of physics—327(T)
Gray, W. M. (see Crawford, M. F.)—1112(L)
Green, Alex E. S. Consequences of generalized meson field theories—332(A)
—— On generalizing boson field theories—1926
Green, G. K., H. S. Snyder, and L. W. Smith. Dynamic magnetic measurements on cosmotron magnet model—1289(A)
Greenblatt, M. H. Microwave secondary electron multiplier—1324(A)
Greenlee, K. W. (see Cleveland, Forrest F.)—334(A)
Greenspan, Martin. Attenuation of sound in rarefield helium—197(L)
Greenstein, Jesse L. (see Davis, Leverett, Jr.)—1605(L)
Gregg, E. C., Jr. Variation of the equilibrium radius with time in a flux-forced field-biased betatron—1633(A)
Gregory, B. (see Tinlot, John)—519(L), 520(L)
Greisen, K. Range of cascade showers in lead—1071
—— (see Cocconi, G.)—1063
Greuling, E. (see Levy, Paul W.)—819
Grey, Jerry and Arthur Kantrowitz. Theoretical study of a proposed high intensity molecular beam source—1331(A)
Griffith, B. A. and J. P. Stanley. On the numerical calculation of the internal conversion in the K-shell; the electric dipole case—534(L)——Erratum—1110(L)
Grilly, E. R. (see Sydoriak, S. G.)—303
——, **E. F. Hammel, and S. G. Sydoriak.** Approximate densities of liquid He^3 between 1.27° and 2.79°K—1103(L)
Grinstead, Robert R. and Don M. Yost. Ferromagnetic alloys in the system copper-manganese-indium—984(L)
Groetzinger, Gerhart (see Berger, Martin)—342(A)
—— (see Kahn, David)—906(L)
—— (see McClure, Gordon W.)—340(A)
—— **and Gordon W. McClure.** Difference in the E-W asymmetry of the hard component of the cosmic radiation for particles of opposite charge—349(A)
——, **Fred Ribe, and Lloyd Smith.** Cloud-chamber tracks of positive particles branching from beta-rays—342(A)
Gross, E. P. (see Bohm, D.)—1323(A), 1851, 1864
—— **and D. Bohm.** Medium-like behavior and theory of plasma oscillations—1323(A)
Gross, Paul M., Jr. (see Cole, Robert H.)—1312(A)
Grunlund, Jean M. (see Yaffe, L.)—699(L)
Gugelot, P. C. Spectrum and angular distribution of neutrons from $Be + p$—1291(A)
Gupta, S. (see Majumdar, R. C.)—1788
Gurevitch, M. On the stability of the isobaric pair In^{115}–Sn^{115}—767
Guth, Eugene. Ferromagnetism and rubber elasticity—1625(T)
—— (see Ivey, D. G.)—1284(A)
—— (see Witte, R. S.)—1284(A)
—— (see Zapp, Robert L.)—1300(A)
—— **and H. M. James.** Relations between the problems of rubber elasticity, phase-change, and ferromagnetism—1314(T)
Gwinn, H. R. (see Hibbs, R. F.)—533(L)

Hadley, J., E. Kelly, C. Leith, E. Segrè, C. Wiegand, and H. York. Experiments on $N-P$ scattering with 90- and 40-Mev neutrons—351

Haeff, Andrew V. On the origin of solar radio noise—1333(A), 1546
Hafner, E. M. (see Heydenburg, N. P.)—1147
——, **W. F. Donoghue, and H. Snyder.** New proton spectrometer—331(A)
Hahn, E. E., B. R. Russell, and P. H. Miller, Jr. Conductivity of sintered and single crystals of zinc oxide semiconductor—1631(A)
Hainer, R. M. (see King, Gilbert W.)—1320(A)
—— (see McMahon, H. O.)—1320(A), 1459(A)
——, **Gilbert W. King, and H. O. McMahon.** Infra-red absorption spectrum of cholesterol at low temperatures—1320(A)
Haissinsky, M., H. Faraggi, A. Coche, and P. Avignon. Electrolytic deposits of Po in extremely dilute solutions—1963(L)
Hall, G. L. (see Conant, F. S.)—1314(A)
Hall, Harvey (see Halpern, Otto)—910(L), 1322(A)
Hall, M. B. and W. E. Mochel. Infra-red studies of neoprene—1330(A)
Hall, R. N. (see Woodbury, E. J.)—1462(A)
Hall, T. A. and S. D. Warshaw. Note on the determination of the rates of energy loss of H^1 and H^2 nuclei in gold and aluminum—891(L)
Halliday, David (see Wheatley, John)—1412
Halpern, J. (see Cranberg, L.)—1328(A)
—— (see Franzen, W.)—1292(A)
Halpern, Otto. Depolarization of neutrons during diffusion—1633(A)
—— Double refraction and polarization of neutron beams—343(A)
—— Thermodynamic theory of the magnetic transition curve of superconductors—1460(A)
—— **and Harvey Hall.** Coherent scattering of radiation and negative energy states—910(L)
—— **and Harvey Hall.** Relativistic theory of radiation scattering—1322(A)
Halsey, G. D., Jr. Non-linear viscous elasticity and secondary bond rupture—1300(A)
Hamermesh, Bernard and Albert Wattenberg. Angular distribution of photo-neutrons from deuterium and beryllium—1290(A)
Hamermesh, Morton. General treatment of methods for the production of polarized neutrons—1281(T)
—— Total reflection of neutrons on cobalt—1766(L)
Hammack, Kenyon C. (see Feenberg, Eugene)—332(A), 1877, 1968(L)
Hammel, E. F. (see Grilly, E. R.)—1103(L)
—— (see Sydoriak, S. G.)—303
Hamill, W. H. (see Engelkemeir, Antoinette G.)—1825
Hanna, G. C. (see Brunton, D. C.)—990(L), 1632(A)
—— (see Pontecorvo, B.)—982(L)
——, **D. H. W. Kirkwood, and B. Pontecorvo.** High multiplication proportional counters for energy measurements—985(L)
—— **and B. Pontecorvo.** β-spectrum of H^3—983(L)
——, **B. Pontecorvo, and D. H. W. Kirkwood.** Low energy radiations in proportional counters—330(A)
Hanna, S. S. (see Krone, R. W.)—335(A)
—— **and D. R. Inglis.** On the excited states of Li^7—1767(L)
Hanson, A. O. Energies of neutrons from MsTh-D, La-D, Y-Be, and Sb-Be photo-neutron sources—1794
—— (see McElhinney, J.)—542
Harkins, William D. and Martin Popelka, Jr. Principle of regularity and continuity of nuclear series—332(A)
Harman, W. D. (see Hibbs, R. F.)—533(L)
Harris, J. C. (see Bonner, T. W.)—1401
Harris, P. J. (see Brown, F. W., III)—1461(A)
Harrison, R. J. On the thermodynamics of the fountain effect in liquid helium II—1311(A)
Harrison, S. W. (see Hutter, R. G. E.)—1281(T)
Hart, E. (see Christian, R.)—1465(A)
Hartman, Philip and Aurel Wintner. On the intuitive approach to the spectrum of a wave equation—1452(L)
Hartsough, Walter (see Brueckner, Keith)—555
——, **Evans Hayward, and Wilson M. Powell.** Some preliminary cloud-chamber photographs of artificial mesons—905(L)
Harvalik, Zaboj V. X-ray diffraction patterns of some inorganic salts crystallized at the critical temperature of water as solvent—1283(A)
Hatcher, R. D., G. B. Arfken, and G. Breit. *S*-wave proton-proton scattering from 0.2 to 40 Mev for the Yukawa and Gauss error potentials—1389
Hausner, Henry H. Temperature coefficient of resistance of sintered semiconductors—1310(A)
Havens, W. W., Jr. (see Melkonian, Edward)—1295(A)
—— (see Rainwater, L. J.)—1295(A)
—— (see Ruderman, I. W.)—895(L), 1296(A)
—— **and L. J. Rainwater.** Slow neutron velocity spectrometer studies: Al, Cr, C, Fe, Ni—1296(A)
Haxel, Otto, J. Hans D. Jensen, and Hans E. Suess. On the "magic numbers" in nuclear structure—1766(L)
Hayakawa, Satio. Interpretation of mixed showers—1958(L)
—— On the origin of high energy photons—1759
—— **and Sin-itiro Tomonaga.** Cosmic-ray underground—1958(L)
Hayashi, Chushiro. Stars built on the shell source model—1619(L)
Hayden, Richard J. (see Inghram, Mark G.)—693(L)
——, **David C. Hess, Jr., and Mark G. Inghram.** Isotopic constitution of ytterbium—322(L)
——, **John H. Reynolds, and Mark G. Inghram.** Reactions induced by slow neutron irradiation of europium—1500
Haynes, J. R. and W. Shockley. Investigation of hole injection in transistor action—691(L)
Hayward, Evans. Energy spectrum of the delayed neutrons from O^{17}—917
—— (see Brueckner, Keith)—555
—— (see Hartsough, Walter)—905(L)
Hayward, R. W. (see Helmholz, A. C.)—1469(A)
—— **and A. C. Helmholz.** Study of Cd^{115} isomers—1469(A)
Hazen, W. E., C. A. Randall, and O. L. Tiffany. Vertical intensity at 10,000 feet of ionizing particles that produce penetrating showers—694(L)
Hedgran, Arne (see Deutsch, Martin)—1443(L)
—— (see Siegbahn, Kai)—523(L)
Hees, George W. and Harold Jacobs. Secondary emission from barium oxide as a function of temperature and activation—1312(A)
Heiman, W. J. (see Orth, D. A.)—1100(L)
Heiss, J. H. (see Baker, W. O.)—1301(A)
—— (see Mason, W. P.)—936, 1285(A)
Heitler, Walter (see Slotnick, Murray)—1645
Heller, R. B. (see Hughes, D. J.)—344(A), 565
—— (see Saxon, D.)—330(A), 909(L)
Heller, Wilfried. Determination of the shape of particles from dityndallism—1308(A)
Heller, W. and W. Wojtowicz. Studies on the size and shape of tactoids—343(A)
Helmholz, A. C. (see Bockhop, D.)—1469(A)
—— (see Hayward, R. W.)—1469(A)
——, **R. W. Hayward, and C. L. McGinnis.** Radioactivities of Ag^{111}, Cd^{111}, and In^{111}—1469(A)
Helsel, R. G. On the canonical reduction of quadratic forms—1088
Hemmendinger, Arthur. Erratum: disintegration of Be^8—1267(L)

—— (see Taschek, R. F.)—1268(L), 1361, 1464(A)
——, **G. A. Jarvis, and R. F. Taschek.** Interaction of protons with tritium—1291(A)
Herb, R. G., S. C. Snowdon, and O. Sala. Absolute voltage determination of three nuclear reactions—246
Hereford, Frank L. Heavily ionizing radiation at a 4300-meter altitude—1316(A)
—— Intensity of heavily ionizing penetrating particles at 4300-meter altitude—923
—— (see Pomerantz, Martin A.)—1316(A)
Herman, Robert C. (see Alpher, Ralph A.)—332(A), 701(L), 1089, 1333(A)
Herr, C. V. (see Daunt, J. G.)—1113(A)
Herring, Conyers. Some simple theorems on the free energies of crystal surfaces—344(A)
Herz, R. H. Recording of electron tracks in photographic emulsions—478
Hess, David C., Jr. (see Hayden, Richard J.)—322(L)
—— (see Inghram, Mark G.)—693(L)
Heydenburg, N. P., D. R. Inglis, W. D. Whitehead, Jr., and E. M. Hafner. Proton resonances in the deuteron bombardment of carbon—1147
Heymann, F. F. Contraction of the instantaneous orbit at injection in a betatron—1951(L)
Hibbs, R. F., J. W. Redmond, H. R. Gwinn, and W. D. Harman. Natural abundance measurements on germanium—533(L)
Hicks, Harry G. (see Wilkinson, Geoffrey)—696(L), 1370, 1687
Hildebrand, R. H. (see Bratenahl, A.)—1466(A)
Hill, A. G. (see Strandberg, M. W. P.)—827
Hill, E. L. (see Erikson, Henry A.)—29
Hill, J. E. (see Bonner, T. W.)—1398
—— (see Shoupp, W. E.)—785
Hill, R. D., G. Scharff-Goldhaber, and G. Friedlander. Internal conversion electrons from metastable Te^{125}—324(L)
Hillier, James. Present status of electron microscopy—703(T)
Hincks, E. P. and B. Pontecorvo. On the decay products of the μ-meson—341(A)
—— **and B. Pontecorvo.** Penetrating of μ-meson decay electrons and their bremsstrahlung radiation—698(L)
Hipple, John A. (see Reese, R. M.)—1332(A)
—— (see Thomas, Harold A.)—902(L), 992(L)
—— **and H. A. Thomas.** Time-of-flight mass spectrometer with varying field—1616(L)
Hoerlin, Herman. Sensitivity of x-ray films in the 10-kv to 250-kv range—1304(A)
Hofstadter, Robert. Crystal and scintillation counters—703(T)
—— Detection of gamma-rays with thallium-activated sodium iodide crystals—796——Erratum—1611(L)
—— (see Elmore, W. C.)—203(L)
—— (see Milton, J. C. D.)—1289(A)
——, **J. C. D. Milton, and J. A. McIntyre.** Pulse size distributions in scintillation counters—1290(A)
Hoke, G. R. (see Shutt, R. P.)—1329(A)
Holden, A. N. (see Yager, W. A.)—1630(A)
——, **C. Kittel, F. R. Merritt, and W. A. Yager.** Microwave resonance absorption in a paramagnetic organic compound—1614(L)
——, **C. Kittel, and W. A. Yager.** Microwave magnetic resonance absorption in a nickel salt near 1.25 cm—1443(L)
Hollomon, J. H. Kinetics of nucleation applied to solid-state problems—1281(T)
Holmes, J. E. R., J. Y. Mei, and R. S. Turgel. Search for nuclear isomers with half-lives between a millisecond and a second—889(L)
Holstein, T. Space-charge controlled diffusion in gaseous discharges—1323(A)
Honig, Richard E. On the isomerization of hydrocarbons by electron impact—1319(A)
Horn, F. H. (see Fiske, M. D.)—1311(A)
—— (see Youngblood, J. F.)—1311(A)
——, **W. DeSorbo, M. D. Fiske, and J. F. Youngblood.** General Electric low temperature laboratory. Part II. Liquefaction cycles for hydrogen and helium—1311(A)
Hornig, D. F. (see Cowan, G. R.)—1294(A)
—— (see Mair, R. D.)—1283(A)
—— (see Wagner, E. L.)—1282(A)
Horning, W. and L. Baumhoff. Stars in photographic emulsions initiated by deuterons. Part II. Theoretical—370
Hornyak, W. F. (see Lauritsen, T.)—1462(A)
—— (see Rasmussen, V. K.)—1462(A)
—— **and T. Lauritsen.** Beta-decay spectra of B^{12} and Li^8—1462(A)
Horton, C. W. On the diffraction of a plane wave by a semi-infinite conducting sheet—1263(L)
Hsu, K. N. and T. M. Hu. Scattering of high energy neutrons by protons with non-central interaction—987(L)
Hu, T. M. (see Hsu, K. N.)—987(L)
Hu, Ning. Correction to nucleon scattering from virtual meson emission—1305(A)
—— Erratum: on the application of Heisenberg's theory of S-matrix to the problems of resonance scattering and reactions in nuclear physics—1449(L)
Huang, Su-Shu. Variational method for the continuous wave function of an electron in the field of a neutral atom—980(L)
Hubbard, H. W. $Al^{27}(d, \alpha p)Na^{24}$ cross section—1470(A)
Huddleston, C. M. (see Hughes, D. J.)—515
Hudgens, J. E., Jr., and W. S. Lyon. Radiation from columbium 95—206(L)
Hudspeth, Emmett L. and Charles P. Swann. Comparison of $Li(p, \gamma)$ with a $F(p, \gamma)$ resonance—1291(A)
—— **and Charles P. Swann.** Value of the $Li(p, \gamma)$ resonance—1272(L)
Huggins, M. L. Macromolecular nomenclature—1330(A)
Hughes, D. J., M. T. Burgy, R. B. Heller, and J. W. Wallace—344(A), 565
—— **and C. Eggler.** Spectrum of Be^{10} by absorption—1285(A)
——, **C. Eggler, and C. M. Huddleston.** Beta-spectrum of Be^{10}—515
——, **W. D. B. Spatz, and N. Goldstein.** Capture cross sections for fast neutrons—1781
Hughes, D. S., W. L. Pondrom, and R. L. Mims. Transmission of elastic pulses in metal rods—1552
Hughes, S. G. and W. E. Stephens. Coincidences in Be^{10} beta-rays—1286(A)
Hull, G. F., Jr., M. H. Cohen, and R. W. Terhune. Characteristics of bridges between electric contacts—1311(A)
Humphreys, R. F. (see Motz, H. T.)—1289(A)
Hung, C. S. Thermionic emission from oxide cathodes: retarding and accelerating fields—1281(T)
Hunter, G. T. and H. T. Richards. Angular yield of neutrons from the D-D reaction—335(A)
Hunter, Joseph L. Measurements of ultrasonic absorption in viscous liquids—1627(A)
Huntington, H. B. Surface energies for a free electron metal—1627(A)
Hurst, D. G. (see Alcock, N. Z.)—1609(L)
Hutchison, Clyde A., Jr. Magnetic susceptibility of BeO—465
—— Paramagnetic resonance absorption in crystals colored by irradiation—1769(L)

Hutchison, Dwight A. Efficiency of the electrolytic separation of nitrogen isotopes—1303(A)
Hutner, R. A. (see Rittner, E. S.)—345(A)
——, **E. S. Rittner, and F. K. du Pré.** Concerning the work of polarization in ionic crystals of the NaCl type. II. Polarization around two adjacent charges in the rigid lattice—345(A)
Hutter, R. G. E. and S. W. Harrison. High current-density electron beams—1281(T)

Imber, O. (see Zerfoss, S.)—320(L)
Infeld, L. (see Schild, A.)—1323(A)
Ingersoll, J. G. (see Strandberg, M. W. P.)—1524
Inghram, Mark G. Special properties of active isotopes identified by the mass spectrometer—1281(T)
—— (see Engelkemeir, Antoinette G.)—1825
—— (see Hayden, Richard J.)—322(L), 1500
——, **Richard J. Hayden, and David C. Hess, Jr.** Isotopic constitution of dysprosium—693(L)
Inglis, D. R. Meson exchange and spin-orbit coupling in nuclei—1767(L)
—— (see Hanna, S. S.)—1767(L)
—— (see Heydenburg, N. P.)—1147
—— (see Krone, R. W.)—335(A)
—— (see Resnick, Robert)—1291(A)
Ingram, M. and S. W. Barnes. Observations on the blood of cyclotron workers—1765(L)
Irvine, John W., Jr., and Raymond C. Sangster. Purification and comparison of some organic phosphors for scintillation counters—1460(A)
Ise, John, Jr. Extensive penetrating showers of cosmic rays—1458(A)
Iskenderian, H. P. (see Brillouin, L.)—1325(A)
Ivey, D. G., B. A. Mrowca, and E. Guth. Velocity and attenuation of supersonic waves in natural and synthetic rubbers—1284(A)
Izard, Emmette F. (see Kolb, Harry J.)—1331(A), 1331(A)

Jackson, J. David (see Blatt, John M.)—341(A)
—— **and J. M. Blatt.** Some calculations on proton-proton scattering—1296(A)
Jacobi, Thomas H. Thermionic and photoelectric emission with moderate applied electric fields, employing a two-step potential barrier—1599
Jacobs, Harold (see Hees, George W.)—1312(A)
—— (see Wolk, Bernard)—1312(A)
—— **and Armand P. LaRocque.** Effects of various barium compounds with respect to cold cathode behavior as a function of life in a glow discharge—347(A)
——, **Armand P. LaRocque, and Alfred Mazzei.** Barium fluoride as a cold cathode in an argon glow discharge—1312(A)
Jacobson, Louis (see Overstreet, Roy)—231
Jaffé, George. Statistical theory of liquids. III—184
Jaffe, Hans. Primary and secondary pyroelectric effect in lithium sulfate monohydrate—1625(A)
James, H. M. (see Guth, E.)—1314(T)
Jarvis, G. A. (see Hemmendinger, A.)—1291(A)
—— (see Taschek, R. F.)—1268(L), 1361, 1464(A)
Jauch, J. M. Phenomenological quantum electrodynamics—327(T)
—— (see Watson, K. M.)—1249
Jehle, Herbert. Specificity of interaction between pairs of identical large molecules—348(A)
—— Two-component wave equations—1609(L)
Jen, C. K. Paschen-Back effect in NH_3 and N_2O microwave spectra—1319(A)
Jenkins, F. A. (see Tollestrup, A. V.)—1947(L)
Jenkins, J. F., Jr. (see Gangnes, A. V.)—57, 892(L)
Jenks, G. H., J. A. Ghormley, and F. H. Sweeton. Measurement of the half-life and average energy of tritium decay—701(L)
Jennings, B. (see Shoupp, W. E.)—1, 336(A)
—— (see Sun, K. H.)—1302(A)
Jensen, Erling N. and L. Jackson Laslett. Shape of the beta-spectra of Sr^{90} and Y^{90}—1949(L)
——, **L. Jackson Laslett, and William W. Pratt.** Application of a magnetic lens spectrometer to the measurement of gamma-radiation from Zn^{65} and Co^{60}—458
Jensen, J. Hans D. (see Haxel, Otto)—1766(L)
Jesse, William P. and John Sadauskis. Alpha-particle ionization in argon and in air and the range-energy curves—1110(L)
Johnson, C. Y. (see Golian, S. E.)—524(L)
Johnson, L. R. (see Zerfoss, S.)—320(L)
Johnson, M. H. (see Faust, W. R.)—467
—— **and G. T. Rado.** Ferromagnetism at very high frequencies. II. Method of measurement and processes of magnetization—841
Johnson, Natalie S. (see Johnson, Wm. W. A.)—1320(A)
Johnson, Thomas H. Photographic neutron detector of high sensitivity—1301(A)
Johnson, V. A. Theory of resistivity and Hall effect in semiconducting anisotropic crystals—1631(A)
Johnson, Wm. W. A., Natalie S. Johnson, and Daniel P. Norman. Band emission spectra of polymers, effects of curing time—1320(A)
Johnston, Francis and John E. Willard. Maximum positron to negatron ratio in the decay of Cl^{36}—528(L)
Johnston, L. (see Cork, B.)—1465(A)
Jones, E. (see Gittings, H. T.)—205(L)
Jones, Stanley B. (see Adelman, Frank L.)—1468(A)
—— **and R. S. White.** Yield of negative mesons produced by high energy alpha-particles as a function of alpha-particle energy—1468(A)
Jones, W. (see Shoupp, W. E.)—336(A)
Jordan, W. H. (see Kelley, G. G.)—1290(A)
Juárez, Antonio Romero. Periods of motion in periodic orbits in the equatorial plane of a magnetic dipole—137
Jungerman, J. and S. C. Wright. Kinetic energy release in fission induced by high energy neutrons—1470(A)

Kac, Mark. Statistical analysis of random functions—1282(T)
—— **and T. H. Berlin.** Mathematical model of a ferromagnet—1298(A)
Kahn, David and Gerhart Groetzinger. Upper limit for the (d, H^3) reaction in phosphorus—906(L)
Kallmann, Hartmut. Quantitative measurements with scintillation counters—623
Kamel, R. Measurement of the internal friction of solids—1606(L)
Kane, E. O. (see Shanley, T. J. B.)—1317(A)
Kantrowitz, Arthur (see Grey, Jerry)—1331(A)
Kaplan, Nathan (see Yagoda, Herman)—339(A), 1328(A)
Kaplon, M. F., B. Peters, and H. L. Bradt. Nuclear explosions in photographic emulsions produced by primary cosmic rays—1329(A)
Karle, Isabella. Studies of internal motion and molecular structure by electron diffraction—1625(T)
Karplus, Robert and A. Harry Sharbaugh. Second-order Stark effect of methyl chloride—889(L)——Erratum—1449(L)
Karr, P. R. (see Fano, U.)—1303(A)
Karraker, D. G. (see Reynolds, Frederick L.)—313(L)
Kê, T'ing-Sui. On the mechanism of the embrittlement of copper by bismuth—1626(A)
Keighton, W. B. (see Mandeville, C. E.)—221, 329(A), 1528
—— (see Woo, Y. H.)—1286(A)

Keller, H. B. (see Cork, J. M.)—1133, 1287(A), 1621(L), 1778(L)
Kelley, G. G., W. H. Jordan, and P. R. Bell. Waveforms associated with the discharge of a Geiger tube—1290(A)
Kelly, E. L. Experimental determinations of stopping powers using alpha-particles of 15 to 37 Mev—1006
—— (see Hadley, J.)—351
—— **and E. Segrè.** Some excitation functions of bismuth —999
Kelly, F. M. (see Crawford, M. F.)—1112(L)
Kern, Bernard D. (see Zaffarano, Daniel J.)—1632(A)
——, **A. C. G. Mitchell, and Daniel J. Zaffarano.** Beta- and gamma-rays of antimony 125—1287(A)
Kern, W. P. (see Weisz, P. B.)—899(L)
Kerst, D. W., G. D. Adams, H. W. Koch, and C. S. Robinson. Betatron model—330(A)
Kimball, G. E. (see Weingarten, I. R.)—1325(A)
King, A. L. and R. W. Lawton. Elasticity of soft body tissues—1281(T)
King, Gilbert W. (see Grady, Harold R.)—1450(L)
—— (see Hainer, R. M.)—1320(A)
—— (see McMahon, H. O.)—1320(A), 1459(A)
——, **H. O. McMahon, and R. M. Hainer.** Infra-red absorption spectra of some polymers at liquid helium temperatures—1320(A)
King, L. D. P. and Louis Goldstein. On the absorption of slow neutrons by He_3 nuclei—1302(A)
—— **and Louis Goldstein.** Total cross section of the He_3 nucleus for slow neutrons—1366
Kinsey, E. L. (see Benton, A.)—888(L)
Kip, Arthur F. (see Arnold, Robert D.)—1199
—— **and Robert D. Arnold.** Ferromagnetic resonance at microwave frequencies in an iron single crystal—1556
Kirkwood, D. H. W. (see Hanna, G. C.)—330(A), 985(L)
—— (see Pontecorvo, B.)—982(L)
Kirsch, M. (see Yaffe, L.)—699(L)
Kittel, Charles. Interpretation of the thermal conductivity of glasses—972
—— Recent developments in ferromagnetism—1625(T)
—— (see Holden, A. N.)—1443(L), 1614(L)
—— (see Yager, W. A.)—1630(A)
Klein, A. L. (see Brown, F. W., III)—1461(A)
Klein, David (see Lind, David A.)—1544, 1633(A)
Klein, M. M. and W. Perl. Calculation of compressible flow past an ellipsoid of revolution by an integral method—1293(A)
Klein, Martin J. and L. Tisza. Critical point fluctuations —1303(A)
Klick, Clifford C. and James H. Schulman. Absence of photo-conductivity in tungstate phosphors—1606(L)
Knable, N., J. De Juren, and B. J. Moyer. Nuclear cross sections for 90-Mev neutrons—1470(A)
Knight, G. B. and R. L. Macklin. Radiations of uranium Y—34
Knight, J. D. (see Duffield, R. B.)—1465(A), 1613(L), 1967(L)
Knox, William J. Relative cross sections for nuclear reactions induced by high energy neutrons in light elements—537
Knudsen, Erik Stenberg (see Bak, Börge)—1622(L)
Koch, G. E. and J. D. Graves. Effects of temperature on naphthalene and anthracene scintillation counters—1461(A)
Koch, H. W. (see Kerst, D. W.)—330(A)
—— **and R. E. Carter.** Determination of the energy distribution of bremsstrahlung from 19.5-Mev electrons—1950(L)
Kock, W. E. Wave propagation in dipole arrays—1635(T)
Koehler, J. S. Calculation of the changes in the conductivity of metals produced by cold-work—106, 327(T)
—— Calculation of the effects produced by soluble impurities on the damping of metals—1626(A)
—— (see Marx, J. W.)—1309(A)
—— **and T. H. Blewitt.** Evidence for a change in the nature of work-hardening at small strains—1952(A)
Kohn, W. Approach to perturbation theory by the variation iteration method—1322(A)
Kolb, Harry J. and Emmette F. Izard. Dilatometric studies of high polymers I. Second-order transition temperature—1331(A)
—— **and Emmette F. Izard.** Dilatometric studies of high polymers II. Crystallization of aromatic polyesters—1331(A)
Kovasznay, Leslie S. G. Optical methods of measuring turbulence—1282(T)
—— (see Corrsin, Stanley)—1954(L)
Krasik, S., D. Alpert, and A. O. McCoubrey. Initiation and maintenance fields of a microwave discharge—1281(T)
Kratz, H. R. Principal series of potassium, rubidium, and cesium in absorption—1844
Krause, E. H. (see Golian, S. E.)—524(L)
Kreusch, E., J. S. Ziomek, and Forrest F. Cleveland. Vibrational spectra of *trans*-dichloroethylene—334(A)
Krimm, S. (see Stein, R. S.)—1301(A)
Krisberg, N. L. and M. L. Pool. Radioactive scandium and vanadium—1286(A), 1693
Kroll, Norman M. Covariant Hamiltonian formulation of field theory and the transformation to the interaction representation—1321(A)
—— **and Willis E. Lamb, Jr.** On the self-energy of a bound electron—388
Krone, R. W., S. S. Hanna, and D. R. Inglis. Angle dependence of the reaction $Li^6(d, p)Li^7$—335(A)
Krueger, H. H. A., D. Meneghetti, C. R. Ringo, and L. Winsberg. Effect of small angle scattering on neutron cross-section measurements—1098(L)
Kruger, P. Gerald (see Phillips, J. A.)—1289(A)
Krzywoblocki, M. Z. On the correlation tensors in compressible fluids—1293(A)
Kuczynski, G. C. Determination of the coefficient of self-diffusion without radioactive tracers—1309(A)
—— Effect of tension upon the electrical resistivity of metals and alloys—1335(A)
—— Sintering of metallic particles—344(A)
Kuder, M. L. (see Golian, S. E.)—524(L)
Kundu, D. N. (see Pool, M. L.)—337(A)
—— **and M. L. Pool.** Columbium 96—1690
—— **and M. L. Pool.** $(p, n):(p, \gamma)$ and $(d, n):(d, 2n)$ reaction cross sections by using enriched Mo—336(A)
Kunkel, Wulf. Dust electrostatics—1460(A)
Kurbatov, J. D. (see Emmerich, Werner S.)—1446(L)
—— (see Yu, Fu-Chun)—1287(A)
—— **and Donald Gideon.** Disintegration of Mn^{54} into the isobar Fe^{54}—328(A)
Kusch, P. On the nuclear electric quadrupole moment of Li^6—887(L)
—— (see Taub, H.)—1326(A), 1481
—— **and H. Taub.** On the g_J values of the alkali atoms—1477
Kyhl, R. L. (see Strandberg, M. W. P.)—270

Laitone, E. V. Detached shock wave in front of a conical nose at supersonic speeds—1294(A)
Lamb, Willis E., Jr. (see Kroll, Norman M.)—388
—— (see Retherford, R. C.)—1325(A)
—— (see Skinner, Miriam)—1325(A)

—— **and R. C. Retherford.** Formation of metastable H atoms by electron bombardment of H_2—1332(A)
Lamer, V. K. Some current misconceptions of N. L. Sadi Carnot's memoir and cycle—1281(T)
Lampi, Eugene E. (see Blair, J. Morris)—1678
—— (see Freier, George)—342(A), 901(L), 1345
Landau, L. On the theory of superfluidity—884(L)
Landé, Alfred. Physical significance of the reciprocal lattice—1113(A)
Lander, J. J. Polymorphism and anion rotational disorder in alkaline earth carbonates—1282(T)
Landon, H. H. (see Smith, Charles S.)—1625(A)
Lane, C. T., Henry A. Fairbank, L. T. Aldrich, and Alfred O. Nier. On the He^3-He^4 equilibrium below the λ-point—46
Lane, W. H. (see Goldstein, L.)—1296(A)
Langer, Lawrence M. Shape of the beta-spectrum of RaE—328(A)
—— **and H. Clay Price, Jr.** Shape of the beta-spectrum of the forbidden transition of yttrium 91—1109(L)
Langer, Rudolph E. Note on the theory of vibration-rotation interaction—792
—— On the wave equation with small quantum numbers —1573
Langmuir, R. V. (see Davis, Leverett, Jr.)—1457(A)
Lark-Horovitz, K. (see Goldsmith, G. J.)—526(L)
LaRocque, Armand P. (see Jacobs, Harold)—347(A), 1312(A)
Laslett, L. Jackson (see Jensen, Erling N.)—458, 1949(L)
Lassen, N. O. Angular distribution of protons from photo-disintegration of the deuteron—1099(L)
—— On the energy loss by fission fragments along their path—1762(L)
LaTorre, Richard and Waller George. Plastic deformation of filaments at constant true strain rates—1309(A)
Latter, R. and R. F. Christy. Decay time of π-meson—1459(A)
Lattes, C. M. G. Meson mass measurements. Part III. Discussion of results—1468(A)
—— (see Burfening, John)—382
Lauritsen, C. C. (see Fowler, W. A.)—1463(A), 1471(A)
—— (see Rasmussen, V. K.)—199(L)
—— (see Thomas, R. G.)—1463(A), 1612(L)
—— (see Tollestrup, A. V.)—1463(A), 1947(L)
Lauritsen, T. (see Hornyak, W. F.)—1462(A)
—— (see Rasmussen, V. K.)—199(L), 1462(A)
—— **and W. F. Horynak.** Converter thickness corrections in gamma-ray spectroscopy—1462(A)
Lawson, A. W. New techniques in high pressure research 1625(T)
Lawson, James L. 88-Mev gamma-ray cross sections—433
Lawton, R. W. (see King, A. L.)—1281(T)
Lazarus, David. Propagation of elastic waves in some cubic crystals as a function of external pressure—1625(A)
Leaf, Boris. Use of pressure in thermodynamics—339(A)
Leavitt, C. P. (see Valley, G. E.)—201(L)
——, **G. E. Valley, and J. A. Vitale.** High altitude high pressure cloud-chamber pictures—1328(A)
Lee, T. D., M. Rosenbluth, and C. N. Yang. Interaction of mesons with nucleons and light particles—905(L)
Lehovec, Kurt. On the hole current in the germanium transistor—1100(L)
Leighton, Robert B. (see Anderson, Carl D.)—1466(A)
—— (see Seriff, Aaron J.)—1466(A)
——, **Carl D. Anderson, and Aaron J. Seriff.** Energy spectrum of mesotron decay electrons—1466(A)
——, **Carl D. Anderson, and Aaron J. Seriff.** Energy spectrum of the decay particles and the mass and spin of the mesotron—1432
Leith, C. E. (see Bratenhal, A.)—1466(A)
—— (see Hadley, J.)—351
Leivo, W. J. (see Estermann, I.)—627
Lengel, J. H. (see Mohler, Fred L.)—1332(A)
Levin, S. B. (see de Bretteville, A. P.)—1625(T)
Levine, Harold and Julian Schwinger. On the theory of diffraction by an aperture in an infinite plane screen. II—1423
—— **and Julian Schwinger.** On the transmission coefficient of a circular aperture—1608(L)
Levinger, Joseph S. Analysis of neutrons in extensive showers—1540
Levinson, Norman. Determination of the potential from the asymptotic phase—1445(L)
Levinthal, C., E. A. Martinelli, and A. Silverman. Inelastic scattering of protons—1467(A)
Levinthal, E. C. Relative magnetic moments of H^1 and H^2—1464(A)
Levreault, Rita (see Buchdahl, R.)—1284(A)
Levy, Paul W. and E. Greuling. Radiations from 2.7-day Au^{198}—819
Libby, W. F. (see Engelkemeir, Antoinette G.)—1825
Lidén, K. (see Edlén, B.)—890(L)
Liebermann, L. N. Second viscosity of liquids—1415
Lilly, Robert C. (see Parmley, Thomas J.)—619
Lin, C. C. (see von Kármán, T.)—1282(T)
Lind, David A. (see DuMond, Jesse W. M.)—1226, 1304(A)
—— (see Watson, Bernard B.)—505, 1305(A)
——, **James Brown, David Klein, David Muller, and Jesse DuMond.** Precision gamma-ray wave-length measurements on I^{131} with the 2-meter curved crystal focusing spectrometer—1633(A)
——, **James Brown, David Klein, David Muller, and Jesse DuMond.** Precision measurements of gamma-rays from I^{131} with the 2-meter focusing curved crystal spectrometer—1544
Locke, J. L. (see Crawford, M. F.)—1607(L)
Loeb, L. B. Certain principles governing mechanisms of electrical discharges derived from corona studies—1456(T)
Lofgren, E. J. (see Freier, P. S.)—340(A)
—— (see Ney, E. P.)—340(A)
Long, V. A. (see Whaley, R. M.)—341(A)
Longini, R. L. Intrinsic efficiency of fluorescence excited by electron bombardment—335(A)
Longmire, Conrad L. On simultaneous beta-gamma emission from nuclei—15
—— (see Bethe, H. A.)—306
—— **and H. Brown.** Screening and relativistic effects on beta-spectra—264, 328(A)——Erratum—1102(L)
Lord, Jere J. and Marcel Schein. Intensity of cosmic-ray stars and slow mesons in the stratosphere—1956(L)
—— **and Marcel Schein.** Nuclear disintegrations and mesons in the stratosphere—340(A)
—— **and Marcel Schein.** On the production of cosmic-ray stars in the stratosphere—1956(L)
Love, W. F. (see Blunt, R. F.)—1299(A)
Low, W. (see Townes, C. H.)—1318(A)
—— **and C. H. Townes.** O^{17} and S^{36} in the rotational spectrum of OCS—529(L)
—— **and C. H. Townes.** Stark effect in symmetric top molecules with nuclear quadrupole coupling—1319(A)
Lowen, I. S. and N. Tralli. Magnetic multipole internal conversion—529(L)
Luttinger, J. M. Magnetic moments of the neutron and proton—309(L)
—— On the magnetic moments of the nucleons in meson theory—1277(L)
Lyon, W. S. (see Hudgens, J. E., Jr.)—206(L)

Ma, S. T. Relativistic formulation of the quantum theory of radiation—535(L)
—— Vacuum polarization—1264(L)
MacDonald, A. D. and Sanborn C. Brown. High frequency gas discharge breakdown in helium—411
—— **and Sanborn C. Brown.** Microwave gas discharge breakdown in helium—1324(A)
MacIntyre, W. J. Decay of scintillations in calcium fluoride crystals—1439(L)
—— Resolving times of naphthalene and polystyrene counters—1290(A)
Macklin, R. L. (see Knight, G. B.)—34
Macnamara, J., C. B. Collins, and H. G. Thode. Mass spectrometer determination of the half-life of Xe^{133}—532(L)
Madansky, Leon (see Pidd, R. W.)—1175
—— **and R. W. Pidd.** On the characteristics of the parallel plate spark counter—346(A)
Madorsky, S. L., S. Straus, Dorothy Thompson, and Laura Williamson. Pyrolysis of hydrocarbon polymers —1331(A)
Madsen, Erhardt (see Bak, Börge)—1622(L)
Maienschein, Fred (see Meem, J. Lawrence, Jr.)—1632(A)
—— **and J. Lawrence Meem, Jr.** Coincidence studies on Au^{199}—1632(A)
Mair, R. D. and D. F. Hornig. Vibrational spectrum of crystalline benzene—1283(A)
Majumdar, R. C. and S. Gupta. Meson fields and the equation of motion of a spinning particle—1788
Makinson, R. E. B. Surface photoelectric effect—1908
Malich, C. W. (see Butler, J. W.)—1291(A)
—— (see Evans, J. E.)—1161
Mandeville, C. E. Characteristic radiation of praseodymium (142)—1017, 1287(A)
—— (see Woo, Y. H.)—1286(A)
——, **M. V. Scherb, and W. B. Keighton.** Radiations from Cd^{115} and $*In^{115}$—329(A)
——, **M. V. Scherb, and W. B. Keighton.** Radiations from Cd^{115}, $*In^{115}$, and Hf^{181}—221
—— **and E. Shapiro.** Disintegration scheme of cerium (141)—1834
—— **and E. Shapiro.** Some characteristics of antimony (125)—897(L)
——, **Y. H. Woo, M. V. Scherb, W. B. Keighton, and E. Shapiro.** Radiations from Ge^{77} and Ge^{71}—1528
Marin, Joseph (see Sauer, John A.)—1285(A)
Mark, H. (see Miller, E.)—1314(A)
Markham, Jordan J. Effect of surface states on the temperature variation of the work function of semiconductors—1310(A)
—— **and P. H. Miller, Jr.** Effect of surface states on the temperature variation of the work function of semiconductors—959
Marmier, P. (see Blaser, J. P.)—1953(L)
Marquez, L. (see Orth, D. A.)—1100(L)
Marshak, R. E. Beta-decay of Be^{10} and theory of beta-decay—513, 1285(A)
—— On mesons π and μ—700(L)
—— (see Foldy, L. L.)—1307(A), 1493
—— (see Wightman, A. S.)—1306(A)
Marshall, L. Alpha-particles from fission as recorded by photographic emulsions—1339
—— (see Fermi, E.)—578
Martin, B. (see ter Haar, D.)—1298(A)
Martinelli, E. A. (see Levinthal, C.)—1467(A)
Marx, J. W. Effect of dissolved hydrogen on the decrement and the elastic constants of copper—1626(A)
—— **and J. S. Koehler.** Damping of single crystals of lead and copper—1309(A)
Masilun, W. J. (see Gittings, H. T.)—205(L)
Mason, F. D. (see Stephenson, S. T.)—1711
Mason, W. P. (see Baker, W. O.)—1301(A)
—— (see Bozorth, R. M.)—1954(L)
——, **W. O. Baker, H. J. McSkimin, and J. H. Heiss.** Measurement of shear elasticity and viscosity of liquids at ultrasonic frequencies—936
——, **W. O. Baker, H. J. McSkimin, and J. H. Heiss.** Measurement of the mechanical properties of polymer liquids by ultrasonic methods—1285(A)
Mather, R. L. (see Benson, W. K., Jr.)—1470(A)
Mathieu, Roger (see Demers, Pierre)—1327(A)
Mattern, John (see Sharbaugh, A. Harry)—1102(L)
Matthews, P. T. Generalized Schrödinger equation in the interaction representation—1270(L)
Matthias, B. T. New ferroelectric crystals—1771(L)
—— **and J. N. Richardson.** Ferroelectricity in barium titanate—703(T)
May, Albert, J. H. McMillen, and J. C. Woodhull. Cavity pressure and cavitation number after vertical water-entry of a sphere—1313(A)
Mayer, J. E. Electron affinities from equilibrium measurements—1282(T)
Mayer, Maria Goeppert. On closed shells in nuclei. II—1969(L)
Mazzei, Alfred (see Jacobs, Harold)—1312(A)
McClure, Gordon W. (see Groetzinger, Gerhart)—349(A)
—— **and Gerhart Groetzinger.** Production of neutrons by the capture of cosmic-ray mesons—340(A)
McConaghie, Virginia Marie and Harald H. Nielsen. Study of the high frequency fundamental bands in the spectrum of AsH_3 and AsD_3—633
McCoubrey, A. O. (see Krasik, S.)—1281(T)
McCreary, R. L. (see Barnes, S. W.)—983(L)
McElhinney, J., A. O. Hanson, R. A. Becker, R. F. Duffield, and B. C. Diven. Thresholds for several photonuclear reactions—542
McGinnis, C. L. (see Helmholz, A. C.)—1469(A)
McGowan, F. K., S. DeBenedetti, and J. E. Francis, Jr. On the measurement of short-lived isomers of nuclei—1761(L)
McIntyre, J. A. (see Hofstadter, R.)—1290(A)
McKay, K. G. (see Newton, R. R.)—103
McKenzie, K. M. Acceleration of protons in the 184-inch Berkeley cyclotron—1471(T)
McMahon, H. O. (see Hainer, R. M.)—1320(A)
—— (see King, Gilbert W.)—1320(A)
——, **R. M. Hainer, and Gilbert W. King.** Low temperature infra-red transmission cell—1320(A)
——, **Gilbert W. King, and R. M. Hainer.** Automatic slit-width adjuster for an infra-red spectrometer—1459(A)
McMath, Robert R. (see Mohler, Orren C.)—520(L)
McMillan, Edwin M. Report of initial performance of the Berkeley synchrotron—1471(T)
—— (see Cook, Leslie J.)—7
McMillen, J. H. (see May, Albert)—1313(A)
McReynolds, Andrew W. Effect of stress and deformation on the martensite transformation—1309(A)
—— Martensite reaction—703(T)
McSkimin, H. J. (see Bozorth, R. M.)—1954(L)
—— (see Mason, W. P.)—936, 1285(A)
Meem, J. Lawrence, Jr. (see Maienschein, Fred)—1632(A)
—— **and Fred Maienschein.** Preliminary investigation of radiations from I^{124}—1632(A)
Mei, J. Y. (see Holmes, J. E. R.)—889(L)
Meijer, Robert R. On the absorption of slow neutrons by rhodium—773
Meiners, Edwin P., Jr., David R. Smith, and Lewis Slack. Angular distribution of photo-neutrons—1632(A)
Meinke, W. W., A. Ghiorso, and G. T. Seaborg. Three additional collateral alpha-decay chains—314(L)

Meissner, K. W., L. G. Mundie, and P. H. Stelson. Erratum: structure of the ^2D terms of the arc spectrum of lithium—891(L)
Meister, Arnold G. Force constants for the CBr_3H, CBr_3D, and CBr_4 molecules—333(A)
—— (see Zietlow, James P.)—333(A)
Melkonian, Edward, L. J. Rainwater, and W. W. Havens, Jr. Precise determination of the slow neutron cross section for the free proton—1295(A)
Meneghetti, David (see Krueger, H. H. A.)—1098(L)
—— (see Winsberg, Lester)—975
Meng, C. Y. (see Strandberg, M. W. P.)—1524
Merritt, F. R. (see Holden, A. N.)—1614(L)
—— (see Yager, W. A.)—318(L), 1630(A)
Merz, E., L. Nielsen, and R. Buchdahl. Mechanical properties of polystyrene films cast from solvents—1315(A)
Merz, Walter J. Dielectric behavior of $BaTiO_3$ single-domain crystals—687(L)
Metropolis, N. (see Feynman, R. P.)—1561
Meyer, H. A., G. Schwachheim, A. Wataghin, and G. Wataghin. On the nature of mesons in penetrating showers—908(L)
Meyerott, R. E. (see Breit, G.)—1447(L)
Migeotte, Marcel V. Fundamental band of carbon monoxide at 4.7 μ in the solar spectrum—1108(L)
—— **and R. M. Chapman.** On the question of atmospheric ammonia—1611(L)
Miles, John W. On electromagnetic diffraction through a plane screen—695(L)
Miller, B. L. and M. F. Amsterdam. Microwave electron accelerator using two resonant cavities—1325(A)
Miller, Charles G. Corona studies in nitrogen, oxygen, and mixtures—1460(A)
Miller, E., I. Fankuchen, and H. Mark. Polymerization in the solid state—1314(A)
Miller, Edward E. Field measurement of average optical transmission—335(A)
Miller, Franklin, Jr. Proposed loading of piano strings for improved tone—1113(A)
Miller, P. H., Jr. (see Hahn, E. E.)—1631(A)
—— (see Markham, Jordan J.)—959
—— (see Russell, B. R.)—1628(A)
Miller, Walter C. (see Gideon, D. N.)—329(A)
—— (see Schillinger, Edwin J., Jr.)—900(L)
—— **and Bernard Waldman.** Investigation of bremsstrahlung by means of the nuclear isomerism of indium—329(A), 425
Milton, J. C. D. (see Hofstadter, R.)—1290(A)
—— **and R. Hofstadter.** Luminescent spectra of phosphors useful in scintillation counters—1289(A)
Mims, R. L. (see Hughes, D. S.)—1552
Minden, H. (see Dailey, B. P.)—1319(A)
Minnehagen, L. (see Bøggild, J. K.)—782
Misener, A. D. Fluid properties of liquid helium—215(T)
Mitchell, Allan C. G. (see Kern, Bernard D.)—1287(A)
—— (see Peacock, Charles L.)—1272(L)
—— (see Zaffarano, Daniel J.)—1632(A)
—— **and Charles L. Peacock.** On the Cs^{137} disintegration scheme—197(L)
Moak, C. D. and J. W. T. Dabbs. Neutron capture γ-rays from Cd—1770(L)
Mochel, W. E. (see Hall, M. B.)—1330(A)
Moe, David, George E. Owen, and C. Sharp Cook. On the gamma-radiation from I^{131}—1270(L)
Mohler, Fred L., Evelyn G. Bloom, E. J. Wells, Jr., J. H. Lengel, and C. Edward Wise. Double charged ion spectra in mass spectra of hydrocarbons—1332(A)
Mohler, Orren C., Robert R. McMath, and Leo Goldberg. Excited-state bands of atmospheric CO_2—520(L)
Montgomery, C. G. and D. D. Montgomery. Coincident bursts in small ionization chambers—980(L)
—— **and D. D. Montgomery.** Ionization bursts as a function of chamber area—1329(A)
Montgomery, D. D. (see Montgomery, C. G.)—980(L), 1329(A)
Montgomery, R. A. Measurements of the absolute intensity of cosmic radiation at sea level—1407
Moore, George E., H. W. Allison, and James Morrison. Production of free alkaline earth metal in simple vacuum tube filaments—347(A)
Morris, Peter A. (see Swann, W. F. G.)—1317(A)
Morrish, A. H. (see Allen, James S.)—570
Morrison, Adair (see Pickup, Eric)—686(L), 1328(A)
—— **and Eric Pickup.** Studies of cosmic-ray phenomena in nuclear research emulsions—1328(A)
Morrison, James (see Moore, George E.)—347(A)
Morrison, P. and D. B. Beard. He^3 and the origin of terrestrial helium—1332(A)
Morrissey, R. and C. S. Wu. Beta-ray spectrum of RaE—1288(A)
Moshinsky, M. and E. P. Wigner. Interaction by boundary conditions—1322(A)
Motz, H. T. and R. F. Humphreys. Masses of nuclei from neon to chlorine—1289(A)
Moyer, Burton J. (see Benson, W. K., Jr.)—1470(A)
—— (see Bratenahl, A.)—1466(A)
—— (see Knable, N.)—1470(A)
—— (see Parmley, Thomas J.)—619
——, **H. F. York, and R. Bjorklund.** High energy gamma-radiation from 184-cyclotron target—1470(A)
Mrowca, B. A. (see Ivey, D. G.)—1284(A)
—— (see Witte, R. S.)—1284(A)
Muether, H. R. (see Sherr, R.)—282, 328(A)
Muller, David (see Lind, David A.)—1544, 1633(A)
Mundie, L. G. (see Meissner, K. W.)—891(L)
Munk, Max M. Reversal theorem of linearized supersonic aerodynamics—1293(A)
Murphy, Thomas (see Torreson, O. W.)—208(L)
Myers, Vernon W. Forces between ammonia molecules and the second virial coefficient for ammonia—1620(L)
—— (see Arnold, G. P.)—217
—— **and A. Wattenberg.** "Cross-over transitions" in Cl^{38}, Co^{60}, Br^{82}, and Sb^{124}—992(L)

Nafe, John E. (see Nelson, Edward B.)—343(A), 1194
Nakano, Yoshihiro (see Umeda, Kwai)—1621(L)
Neher, H. V. Energy of cosmic-ray particles from ionization chamber and counter telescope data—1458(A)
—— (see Biehl, A. T.)—688(L), 1457(A)
—— (see Roesch, W. C.)—1457(A)
Nelson, Edward B. and John E. Nafe. Hyperfine structure of tritium—343(A), 1194
Newton, Amos S. Fission of thorium with alpha-particles—17
—— Formation of U^{232} by helium ions on thorium—209(L)
Newton, Robert R. Space charge effects in bombardment conductivity through diamond—234
——, **A. J. Ahearn, and K. G. McKay.** Observation of the ferro-electric Barkhausen effect in barium titanate—103
Ney, Edward P. (see Freier, Phyllis)—340(A), 991(L), 1451(L)
——, **P. Freier, E. J. Lofgren, and F. Oppenheimer.** Observations on heavy nuclei in cosmic radiation—340(A)
Nielsen, Harald H. Anomalies in the microwave spectrum of methyl cyanide and methyl iso-cyanide—1961(L)
—— (see McConaghie, Virginia Marie)—633
—— (see Stewart, Hugh B.)—640
Nielsen, L. E. (see Buchdahl, R.)—1284(A)
—— (see Merz, E.)—1315(A)

Niemiec, Thaddeus. Method of measurement of small periodic displacements and its application to determining the piezoelectric constants of potassium dihydrogen arsenate—215(A)
Nier, Alfred O. (see Lane, C. T.)—46
—— (see Taconis, K. W.)—1966(L)
——, **T. R. Roberts, and E. G. Franklin.** Double focusing mass spectrometer—346(A)
Nobles, R. A. (see Coon, J. H.)—1358
Nordheim, L. W. On spins, moments and shells in nuclei —1297(A), 1894
—— (see Feenberg, Eugene)—1968(L)
—— (see Roberg, Jane)—444
Norman, Daniel P. (see Johnson, Wm. W. A.)—1320(A)
Norton, Francis J. Isotopic weight doublet in the $B_2{}^{11}D_6$ and O_2 mass spectrum—1957(L)
Nosawa, Reikichi. Electronic eigenfunctions in ionic crystals—1102(L)
Nowick, A. S. Longitudinal vibration of bars with non-linear internal friction—1626(A)

Ogata, K. Isotopic weights of medium elements—200(L)
Okayama, Taisuke. On the mesic charge—308(L)
O'Neil, H. T. Reflection and refraction of plane shear waves in viscoelastic media—928
O'Neill, G. F. (see Shutt, R. P.)—1329(A)
Oppenheimer, Frank (see Freier, Phyllis)—340(A), 991(L), 1451(L)
—— (see Ney, E. P.)—340(A)
Ore, A. and J. L. Powell. Three-photon annihilation of an electron-positron pair—1696, 1963(L)
Orowan, E. Brittle fracture of triaxial stresses—1625(T)
Orth, D. A., L. Marquez, W. J. Heiman, and D. H. Templeton. Radioactive thallium isotopes produced from gold—1100(L)
Osborne, Darrell W., Bernard Weinstock, and Bernard M. Abraham. Comparison of the flow of isotopically pure liquid He^3 and He^4—988(L)
Osborne, L. S. (see Curtis, N. W.)—1327(A)
Osborne, M. F. M. Charged Bose-Einstein particles in a magnetic field—339(A)
—— Quantum theory restrictions on the general theory of relativity—1457(A), 1579
Ostrander, R. S. (see Van Allen, J. A.)—1315(A)
Overstreet, Roy, Louis Jacobson, and P. R. Stout. Evidence for a new isotope of potassium—231
Overton, W. C., R. H. Pry, R. W. Schmitt, and C. F. Squire. Ultrasonic velocity of longitudinal and transverse waves in metallic beryllium at low temperatures —1309(A)
Owen, G. E. Conductivity of dilute water solutions near the critical temperature—1303(A)
Owen, George E. (see Moe, David)—1270(L)
—— (see Slack, L.)—1448(L)
Oxley, C. L. (see Barnes, S. W.)—983(L)

Paine, Roger W., Jr. (see Dacey, John E.)—1301(A)
——, **John E. Dacey, and Clark Goodman.** Determination of absolute neutron intensities—1301(A)
Pais, A. and G. E. Uhlenbeck. On the interaction of charged spin O particles with the electromagnetic field —1321(A)
Pake, G. E. Nuclear magnetic resonance in studies of solids—1625(T)
—— Nuclear resonance line widths as functions of temperature—327(T)
—— **and E. M. Purcell.** Erratum: line shapes in nuclear paramagnetism—534(L)
Paneth, H. R. (see Allen, James S.)—570
Panofsky, Wolfgang K. H. and Franklin Fillmore. Camera for *P-P* scattering at 32 Mev—1465(A)
Parmley, Thomas J., Burton J. Moyer, and Robert C. Lilly. Radioactivities of some high mass isotopes of cobalt—619
Patterson, G. N. Theory of the shock tube—1294(A)
Peacock, Charles L. (see Beach, Louis A.)—211(L), 329(A)
—— (see Mitchell, Allan C. G.)—197(L)
—— **and Allan C. G. Mitchell.** Disintegration of Cs^{137}—1292(L)
—— **and Roger G. Wilkinson.** Radiations of W^{187} and Au^{199} in the low energy region—329(A)
Peakes, Bayard P. Electron does not exist—1629(A)
Pearson, G. L. and J. Bardeen. Electrical properties of pure silicon and silicon alloys containing boron and phosphorus—865
——, **J. D. Struthers, and H. C. Theuerer.** Correlation of Geiger-counter and Hall-effect measurements in alloys containing germanium and radioactive antimony 124—344(A)
Peck, E. R. Infra-red recording spectrograph of high resolution, yielding precise wave-length measurements —327(T)
Peed, W. F. (see Burkhart, L. E.)—86
Peierls, R. E. (see Barker, F. C.)—312(L)
Pellam, J. R. Investigations of pulsed second sound in liquid helium II—1183
Pensak, L. Conductivity induced by electron bombardment in thin insulating films—472
Perez, Mendez V. (see Brown, H.)—1276(L), 1286(A)
Perkins, Granville A. Non-radiating Maxwell waves—1947(L)
Perl, W. (see Klein, M. M.)—1293(A)
Perlman, I., A. Ghiorso, and G. T. Seaborg. Relation between half-life and energy in alpha-decay—1096
Perlman, M. L. Yields of some photo-nuclear reactions—988(L)
Perlow, G. J. (see Golian, S. E.)—524(L)
Peters, B. (see Bradt, H. L.)—1779(L)
—— (see Kaplon, M. F.)—1329(A)
Peterson, Jack M. (see Cook, Leslie J.)—7
Peterson, Vincent. Absolute cross section for production of heavy negative mesons by 380-Mev alpha-particles—1469(A)
—— (see Gardner, Eugene)—364
Petree, Marcella Cooper and W. W. Beeman. X-ray *K*-absorption edge of calcium in the metal and some compounds—1628(A)
Phillips, Anne N., Louis Rosen, and R. F. Taschek. Upper limits of the fission cross sections of bismuth, lead, mercury, gold, iridium, and tungsten for 14-Mev neutrons—919
Phillips, G. C. (see Bonner, T. W.)—1401
Phillips, J. A. and P. Gerald Kruger. On the production of ± electron pairs in the field of an electron—1289(A)
Piccioni, Oreste. π-μ-meson-distinction with G-M counters—1281(T)
Pickup, Eric (see Morrison, Adair)—1328(A)
—— **and Adair Morrison.** Emissions of mesons in the cosmic stars in photographic emulsions—686(L)
—— **and Adair Morrison.** Some cosmic-ray events in photographic emulsions—1328(A)
Pidd, R. W. (see Madansky, Leon)—346(A)
—— **and Leon Madansky.** Some properties of the parallel plate spark counter I—1175
Pierce, J. R. Broad-band oscilloscope tube—1282(T)
Pike, Eugene W. and Thomas R. Silverberg. Analog computers for functions of many variables—1333(A)
Placzek, G. Theory of slow neutron scattering—1295(A)
Platt, J. B. (see Barnes, S. W.)—983(L)
Plotkin, Martin and John P. Blewett. Ferromagnetic ferrites for a cosmotron accelerating unit—1288(A)

Polachek, H. and R. J. Seeger. On the refraction of a shock-wave at an air-water interface—1294(A)
Pollard, E. C., V. L. Sailor, and L. D. Wyly. Particle groups from the bombardment of aluminum by deuterons—725
Pomerantz, Martin A. Properties at very high altitudes of cosmic radiation at large zenith angles, and verification of a consequence of Liouville's theorem—1335(A)
—— Properties of cosmic radiation at very high altitudes —69
—— Properties of cosmic radiation in the lower atmosphere—1721
—— **and Frank L. Hereford.** Detection of heavy particles in the primary cosmic radiation—1316(A)
Pondrom, W. L. (see Hughes, D. S.)—1552
Pontecorvo, B. (see Hanna, G. C.)—330(A), 983(L), 985(L)
—— (see Hincks, E. P.)—341(A), 698(L)
——, **D. H. W. Kirkwood, and G. C. Hanna.** Nuclear capture of L_I electrons—982(L)
Pool, M. L. (see Eggen, D. T.)—1464(A)
—— see Krisberg, N. L.)—1286(A), 1693
—— (see Kundu, D. N.)—336(A), 1690
—— **and D. N. Kundu.** Relative cross-section measurements for the identification of Tc^{92} and Tc^{93}—337(A)
Popelka, Martin, Jr. (see Harkins, William D.)—332(A)
Poss, H. L. On the magnetic moments of C^{13}, F^{19}, Tl^{203}, and Tl^{205}—600
Powell, John L. Note on the bremsstrahlung produced by protons—32
—— (see Ore, A.)—1696, 1963(L)
Powell, Wilson M. Cloud-chamber analysis of the particles coming from carbon when bombarded by 90-Mev neutrons—1456(T)
—— (see Brueckner, Keith)—555, 1274(L), 1970(L)
—— (see Hartsough, Walter)—905(L)
Pratt, William W. (see Jensen, Erling N.)—458
Present, R. D. and A. J. deBethune. Separation of a gas mixture flowing through a long tube at low pressure—1050
Preston, Melvin A. Electrostatic interaction and low energy particles in alpha-radioactivity—90
Price, H. Clay, Jr. (see Langer, Lawrence M.)—1109(L)
Price, W. J. Erratum: acoustical birefringence—992(L)
—— Ultrasonic measurements on rochelle salt crystals—946
Prim, R. C. New superposition principle in gas dynamics —1293(A)
Primakoff, H. (see Slack, L.)—1448(L)
Proctor, W. G. Magnetic moment of Tl^{203}—522(L)
Protzman, Thomas F. Transition temperatures of methyl methylmethacrylate polymers at ultrasonic frequencies —1627(A)
Pry, R. H. (see Overton, W. C.)—1309(A)
Purcell, E. M. (see Brown, Richard M.)—1262(L)
—— (see Pake, G. E.)—534(L)

Rabi, I. I. (see Rainwater, L. J.)—1295(A)
Rabjohn, Norman (see Flory, Paul J.)—1300(A)
Rado, George T. Domain interactions in the theory of ferromagnetic resonance—893(L)——Erratum and addendum—1451(L)
—— (see Johnson, M. H.)—841
Rainwater, W. J. (see Havens, W. W., Jr.)—1296(A)
—— (see Melkonian, Edward)—1295(A)
—— (see Ruderman, I. W.)—895(L), 1296(A)
——, **I. I. Rabi, and W. W. Havens, Jr.** Interaction of neutrons with electrons in bismuth—1295(A)
Ramsey, Norman F. New molecular beam magnetic resonance method—1326(A)
Randall, C. A. (see Hazen, W. E.)—694(L)
Rarita, William (see Feshbach, Herman)—1384
Rasmussen, V. K., W. F. Hornyak, and T. Lauritsen. Gamma-radiation and nuclear pairs from $F^{19} + p$—1462(A)
——, **C. C. Lauritsen, and T. Lauritsen.** Doppler broadening of a gamma-ray line—199(L)
Rayski, Jerzy. Polarization of the vacuum—1961(L)
Read, W. T. (see Shockley, W.)—692(L)
Redman, W. C. Angular distribution of end-group protons from $B^{10} + d$—1292(A)
Redmond, J. W. (see Hibbs, R. F.)—533(L)
Reese, R. M. and J. A. Hipple. Loss of ions in magnetic analyzer as affected by initial kinetic energy—1332(A)
Reichertz, Paul P. and H. E. Farnsworth. Inelastic scattering of low speed electrons from a copper single crystal—1902
Reifman, A. and W. G. Dow. Theory and application of the variable voltage probe for exploration of the ionosphere—1311(A)
Remington, W. R. and E. K. Gladding. Equilibria in the dyeing of Nylon with acid dyes—1330(A)
Resnick, Robert and D. R. Inglis. Angular distribution of $Li^6(d, \alpha)\alpha$—1291(A)
Retallack, J. Gordon and Robert B. Brode. Mass of cosmic-ray mesotrons—1716
Retherford, R. C. (see Lamb, W. E., Jr.)—1332(A)
—— **and W. E. Lamb, Jr.** Shift of the $2^2S_{\frac{1}{2}}$ state in hydrogen and deuterium—1325(A)
Reynolds, Frederick L., D. G. Karraker, and D. H. Templeton. Mass spectrographic assignment of rubidium isotopes—313(L)
Reynolds, George T. Detection of cosmic-ray particles by scintillation counters—1317(A)
Reynolds, John H. (see Hayden, Richard J.)—1500
Reynolds, S. E. (see Workman, E. J.)—347(A)
—— **and E. J. Workman.** Electrical charge separation produced by rapid freezing of rainwater—347(A)
Ribe, Fred (see Groetzinger, Gerhart)—342(A)
Richards, H. T. (see Hunter, G. T.)—335(A)
—— (see Smith, R. V.)—335(A)
—— **and R. V. Smith.** *P-N* reactions for argon and neon —336(A)
Richards, J., J. Brown, F. Felber, and D. Saxon. On making thin Nylon films—331(A)
Richardson, J. M. Quantum theory of ferromagnetic resonance—1630(A)
—— (see Matthias, B. T.)—703(T)
Richman, C. (see Cork, B.)—1465(A)
Richtmyer, R. D. (see Alfven, H.)—892(L)
—— **and Edward Teller.** On the origin of cosmic rays—1729
Rieke, F. F. and Daryl Errett. Measurement of electron mobility by means of pulse techniques—346(A)
Rightmire, B. G. Mechanism of steady-state creep in metals—1627(A)
Ring, Harold (see Gordy, Walter)—208(L), 1325(A)
Ringo, C. R. (see Krueger, H. H. A.)—1098(L)
Riseman, Jacob. Inter-relationship of some of the hydrodynamic properties of flexible molecules in solution—1308(A)
Risser, J. R. (see Butler, J. W.)—1291(A)
—— (see Evans, J. E.)—1161
Rittner, E. S. (see Hutner, R. A.)—345(A)
——, **R. A. Hutner, and F. K. du Pré.** Concerning the work of polarization in ionic crystals of the NaCl type. I. Polarization around a single charge in the rigid lattice—345(A)
Roberg, Jane and L. W. Nordheim. Angular and lateral spread of cosmic-ray showers—444
Roberts, B. W., Jr. Structure and short range order for low temperature Ag_3Al—1629(A)

Roberts, Shepard. Dielectric constant of barium titanate at high temperatures—989(L)
Roberts, T. R. (see Nier, Alfred O.)—346(A)
Robinson, C. S. (see Kerst, D. W.)—330(A)
Robinson, J. E. (see Sydoriak, S. G.)—118
Robinson, J. Eugene (see Ter-Pogossian, Michel)—995
——, **Michel Ter-Pogossian, and C. Sharp Cook.** Gamma-rays from Na^{24} and V^{48}—1099(L)
Roesch, Wm. C. (see Biehl, A. T.)—688(L), 1457(A)
——, **A. T. Biehl, and H. V. Neher.** Measurements of cosmic-ray intensity at high altitudes—1457(A)
Rogers, F. T., Jr. (see Byatt, W. J.)—909(L)
—— (see Waltner, Arthur)—1445(L)
Rogosa, G. L. (see Bearden, J. A.)—1304(A)
—— **and H. Glaser.** X-ray absorption edges of tantalum —1304(A)
Rohrlich, F. and J. Eisenstein. Neutron-proton and neutron-neutron scattering at high energies—705
Ronzio, A. R. (see Gittings, H. T.)—205(L)
Rose, J. W. (see Bockhop, D.)—1469(A)
Rose, M. E. Electron-neutrino correlation in heavy elements—1444(L)
—— On the production of nuclear polarization—213(L)
—— Scattering and absorption of neutrons by polarized nuclei—213(L)
Rosen, Louis (see Phillips, Anne N.)—919
——, **F. K. Tallmadge, and J. H. Williams.** Range distribution of the charged particles from the *D-D* reactions for 10-Mev deuterons: differential elastic scattering cross section at 40 degrees, 30 degrees, and 20 degrees in the laboratory system—1632(A)
Rosen, Nathan (see Bowers, W. A.)—523(L)
Rosenblum, E. S. Sector type double-focusing magnetic spectrometer—1628(A)
Rosenblum, P. and A. de Bretteville, Jr. Accurate simple recording microphotometer—1305(A)
Rosenbluth, Marshall N. Model for nuclear capture of μ-mesons—532(L)
—— (see Lee, T. D.)—905(L)
Rosser, Shirley E. and Forrest F. Cleveland. Vibrational spectra of some tribromomethanes—333(A)
Rossi, B. (see Bridge, H. S.)—810
Rostagni, A. (see Filosofo, I.)—1269(L)
Roth, Louise. Fluorescence of anthracene excited by high energy radiation—983(L)
Rothstein, Jerome. Cathode vapor and anchoring of the cathode spot—1336(A)
—— Cathode vapor, the discontinuous glow-arc transition, and arc stability—1335(A)
—— Estimation of Hg-type arc spot temperature—1323(A)
Rouault, Marcel and Georges Gallagher. Electron diffraction by gas molecules. Results on the structure of ethyl alcohol and ethyl mercaptan—1319(A)
Roy, R. R. Emission of protons from boron and argon on bombardment with Po-α-particles—1775(L)
Rubin, Sylvan. 10-Mev magnetic proton spectrograph—1459(A)
—— (see Fowler, W. A.)—1463(A), 1471(A)
—— (see Thomas, R. G.)—1612(L)
Ruderman, I. W., W. W. Havens, Jr., T. I. Taylor, and L. R. Rainwater. Scattering of slow neutrons by paramagnetic crystals—895(L), 1296(A)
Rudinger, George. Note on the use of the shock tube as an intermittent supersonic wind tunnel—1948(L)
Rundle, R. E. (see Danielson, G. C.)—1630(A)
Russell, B. R. (see Hahn, E. E.)—1631(A)
——, **R. Dickson, and P. H. Miller, Jr.** Noise spectrum analyzer—1628(A)
Rutledge, W. C. (see Cork, J. M.)—1133, 1287(A), 1621(L), 1778(L)
Ryder, E. J. and W. Shockley. Interpretation of dependence of resistivity of germanium on electric field—310(L)
Ryu, Norio (see Shinohara, Kenichi)—1762(L)

Sachs, R. G. Erratum: Phenomenological theory of exchange currents in nuclei—1605(L)
Sack, H. S. and R. W. Aldrich. Elastic losses of elastomers at ultrasonic frequencies—1285(A)
Sadauskis, John (see Jesse, William P.)—1110(L)
Safford, R. W. and A. M. Thorndike. Cosmic-ray particle of charge two or greater—903(L)
Saha, M. N. Note on Dirac's theory of magnetic poles—1968(L)
Sailor, Vance L. Energy levels in Ca^{41} and the mass difference between A^{40} and Ca^{40}—1836
—— Proton energies from $K^{39,41}(d, p)K^{40,42}$—1292(A)
—— (see Pollard, E. C.)—725
Sala, O. (see Adair, R. K.)—1124
—— (see Bockelman, C. K.)—336(A)
—— (see Herb, R. G.)—246
Salvini, G. and G. Tagliaferri. Local production of the penetrating particles in extensive showers—1112(L)
Sangster, Raymond C. (see Irvine, John W., Jr.)—1460(A)
Sard, R. D. Neutrons correlated with charged cosmic-ray particles—327(T)
—— (see Cool, R. L.)—1275(L)
Sauer, John A. and Joseph Marin. Creep and damping properties of polystyrene—1285(A)
Sawyer, W. M. (see Ferry, John D.)—1284(A)
Saxon, D. (see Richard, J.)—331(A)
—— **and R. Heller.** Gamma-rays following Au^{198} β-decay —330(A), 909(L)
Sazynski, J. (see Cork, J. M.)—1133, 1287(A), 1621(L), 1778(L)
Schaaf, S. A. and P. L. Chambre. On converging viscous flow in a wedge—1293(A)
Schafroth, R. Radiative corrections to the Klein-Nishina-formula—1111(L)
Scharff-Goldhaber, G. (see Hill, R. D.)—324(L)
Schawlow, A. L. (see Crawford, M. F.)—1112(L)
Schein, Marcel (see Fahy, Edward F.)—207(L), 340(A)
—— (see Lord, Jere J.)—340(A), 1956(L), 1956(L)
——, **Victor H. Yngve, and Theodore Bowen.** Absorption of the hard component of the cosmic radiation in the stratosphere—339(A)
Schenck, J. (see Stroud, W. G.)—1316(A)
Scherb, M. V. (see Mandeville, C. E.)—221, 329(A), 1528
—— (see Woo, Y. H.)—1286(A)
Schiff, L. I. Radiation accompanying meson creation—1459(A)
Schild, A. and L. Infeld. Geodesic postulate and field equations in general relativity—1323(A)
Schillinger, Edwin J., Jr., Bernard Waldman, and Walter C. Miller. Scintillation counting with chrysene—900(L)
Schmitt, R. W. (see Overton, W. C.)—1309(A)
Schroeder, C. A. (see Golian, S. E.)—524(L)
Schulman, James H. (see Klick, Clifford C.)—1606(L)
Schulz, L. G. Index of refraction of evaporated films of LiF—345(A)
—— Structure and growth of evaporated LiF films on amorphous substrates—1284(A)
Schwachheim, G. (see Meyer, H. A.)—908(L)
Schwarz, G. and J. A. Bearden. High frequency limit of the continuous x-ray spectrum—1304(A)
Schwarzmann, Gertrude. On the hydrogen spectrum—1334(A)
Schwarzschild, Martin. Turbulence in the atmospheres of stars—1282(T)

Schwinger, Julian. On radiative corrections to electron scattering—898(L)
—— On the classical radiation of accelerated electrons—1912
—— Quantum electrodynamics. II. Vacuum polarization and self-energy—651
—— (see Feldman, David)—338(A)
—— (see Levine, Harold)—1423, 1608(L)
Scott, W. T. Distribution of arc-chord differences in scattered particle tracks—1763(L)
—— Statistical distribution of arc-chord differences in scattered particle tracks—1327(A)
—— (see Snyder, H. S.)—1296(A)
Seaborg, G. T. (see Meinke, W. W.)—314(L)
—— (see Perlman, I.)—1096
Seeger, R. J. (see Polachek, H.)—1294(A)
Segrè, E. (see Hadley, J.)—351
—— (see Kelly, E. L.)—999
—— **and C. E. Wiegand.** Experiments on the effect of atomic electrons on the decay constant of Be^{7}—39
Seidl, F. G. P. Interpretation of the resonance scattering of neutrons by cobalt in terms of the Breit-Wigner equation—1508
Seifert, W. O. (see Barker, R. S.)—1300(A)
Seitz, Frederick. Fundamental aspects of diffusion in solids—327(T)
—— Multiplication of electrons in crystals by high electrostatic fields—1625(T)
—— Theory of electron multiplication in crystals—1283(A)
Serber, R. Spins of the mesons—1459(A)
—— (see Fernbach, S.)—1352
Seriff, Aaron J. (see Anderson, Carl D.)—1466(A)
—— (see Leighton, Robert B.)—1432, 1466(A)
——, **Robert B. Leighton, and Carl D. Anderson.** On nuclear capture of negative mesotrons—1466(A)
Sewell, Duane C. (see Cook, Leslie J.)—7
Seymour, David (see Swann, W. F. G.)—1317(A)
Shafer, H. Jerome. Physical optic analysis of the schlieren method—1313(A)
Shaffer, Marcia C. (see Flory, Paul J.)—1300(A)
Shanley, T. J. B., E. O. Kane, and J. A. Wheeler. Influence on the cosmic-ray spectrum of five heavenly bodies—1317(A)
Shapiro, E. (see Mandeville, C. E.)—897(L), 1528, 1834
Shapiro, Maurice M. Photographic emulsion method of measuring relative fission cross sections—1327(A)
Sharbaugh, A. Harry (see Bragg, J. K.)—1774(L)
—— (see Karplus, Robert)—889(L), 1449(L)
—— **and John Mattern.** Microwave spectrum of methyl bromide—1102(L)
Shaw, A. E. New measurement of the packing fractions of the nickel isotopes—1011
—— Packing fractions of the nickel isotopes—331(A)
Shea, Ruth C. (see Anslow, Gladys A.)—1318(A)
Sherk, P. M. Bound electron creation in the decay of tritium—789
Sherr, R., H. R. Muether, and M. G. White. New radioactive isotope of oxygen—328(A)
——, **H. R. Muether, and M. G. White.** Radioactivity of C^{10} and O^{14}—282
Sherwin, Chalmers W. Neutrinos from P 32—1799
—— Recoils from neutrino emission—327(T)
Shinohara, Kenichi and Norio Ryu. Polarization of electrons—1762(L)
Shive, John N. Double-surface transistor—689(L)
Shockley, William. Electronic theory of the transistor—1282(T)
—— (see Haynes, J. R.)—691(L)
—— (see Ryder, E. J.)—310(L)
—— (see Suhl, H.)—1617(L)
—— (see Williams, H. J.)—155, 178
—— **and W. T. Read.** Quantitative predictions from dislocation models of crystal grain boundaries—692(L)
Shoupp, W. E. (see Sun, K. H.)—1302(A)
—— **and J. E. Hill.** Thresholds for fast neutron fission in thorium and uranium—785
——, **B. Jennings, W. Jones, and M. Garbuny.** Absolute measurement of the $Li^{7}(p, n)$ threshold voltage—336(A)
——, **B. Jennings, and K. H. Sun.** Threshold and resonances in $C^{14}(p, n)N^{14}$ reaction and energy levels of N^{15}—1
Shrader, E. F. (see Strough, R. I.)—1628(A)
Shull, C. G. (see Wollan, E. O.)—1348
—— **and Sidney Siegel.** Neutron diffraction studies of order-disorder in alloys—1008
—— **and E. O. Wollan.** Spin-dependent neutron scattering by various nuclei—1302(A)
Shull, Franklin B. (see Braden, Charles H.)—1964(L)
—— (see Slack, Lewis)—1965(L)
—— **and Eugene Feenberg.** Interpretation of the K^{42} radioactivity—1768(L)
Shulman, R. G. (see Dailey, B. P.)—1319(A)
—— **and C. H. Townes.** Stark effects in OCS—1318(A)
Shutt, R. P., G. R. Hoke, W. A. Tuttle, and G. F. O'Neill. Some cloud chamber photographs obtained with a high pressure cloud chamber—1329(A)
Shyman, C. S. (see Cherry, D. D.)—1441(L)
Sidhu, S. S. (see Winsberg, Lester)—975
Siegbahn, Kai. Radiation from 225-day Ag^{110}—1277(L)
—— (see Slätis, Hilding—318(L), 1955(L)
—— **and Arne Hedgran.** γ-radiation from Au^{198}—523(L)
Siegel, Sidney. Effect of neutron bombardment on order in the alloy Cu_3Au—1823
—— (see Shull, C. G.)—1008
Siegert, A. J. F. Approach to equilibrium in Ehrenfest's "wind-tree" model—1322(A)
Silverberg, Thomas R. (see Pike, Eugene W.)—1333(A)
Silverman, A. (see Levinthal, C.)—1467(A)
Silvidi, A. A. (see Daunt, J. G.)—1113(A)
Simmons, James W. (see Smith, Alex. G.)—260
Sinha, M. S. Photograph of a shower produced by a π-meson and a π-μ-decay—1757
Sitte, K. Note on the light-particle hypotheses of penetrating particles in extensive cosmic-ray showers—340(A)
Skinner, Miriam and W. E. Lamb, Jr. Anomalous fine structure in singly ionized helium—1325(A)
Skomal, E. N. (see Blunt, R. F.)—1299(A)
Slack, Lewis (see Braden, Charles H.)—1964(L)
—— (see Meiners, Edwin P., Jr.)—1632(A)
——, **Charles H. Braden, and Franklin B. Shull.** Forbidden beta-decay of Sr^{89}—1965(L)
——, **G. E. Owen, and H. Primakoff.** On the maximum β-energy release in tritium—1448(L)
Slätis, Hilding and Kai Siegbahn. Disintegration of Hg^{203}—318(L)
—— **and Kai Siegbahn.** New type of focusing in a magnetic lens field—1955(L)
Sleator, William, Jr. (see Blair, J. Morris)—1678
—— (see Freier, George)—342(A), 1345
Slotnick, Murray. Neutron-electron interaction—1295(A)
—— **and Walter Heitler.** Charge density and magnetic moments of the nucleons—1645
Smart, J. S. Effects of nuclear stability on the formation of the chemical elements—1379
Smith, A. H. Temperature dependence of the work function of semiconductors—953
Smith, Alex. G., Walter Gordy, James W. Simmons, and William V. Smith. Microwave spectroscopy in the region of three to five millimeters—260

Smith, C. S. Grain and interphase boundaries in metals—1625(T)
Smith, Charles S. and H. H. Landon. Thermal expansion of $Li_2SO_4 \cdot H_2O$—1625(A)
Smith, David R. (see Meiners, Edwin P., Jr.)—1632(A)
Smith, J. C. (see Ballou, J. W.)—1284(A)
Smith, L. W. (see Green, G. K.)—1289(A)
Smith, Lloyd (see Gluckstern, R. L.)—1467(A)
—— (see Groetzinger, Gerhart)—342(A)
Smith, R. V. (see Richards, H. T.)—336(A)
—— **and H. T. Richards.** *P-N* threshold for deuterium—335(A)
Smith, William V. (see Smith, Alex. G.)—260
Smoluchowski, R. Recent developments in knowledge of order-disorder phenomena—1625(T)
—— (see Goldman, J. E.)—140, 310(L), 1299(A)
—— (see Wu, T. L.)—345(A)
—— **and J. E. Goldman.** Theory of the effect of ordering of magnetic properties—1299(A)
—— **and T. L. Wu.** Internal friction and slip in thin single aluminum crystals—345(A)
Snell, Arthur H., E. C. Barker, and R. L. Sternberg. Photo-disintegration of deuterium and beryllium by the gamma-rays of Na^{24} and Ga^{72}—1290(A)
Snoddy, L. B. and J. W. Beams. Pulsed electron beam for high speed photography—1324(A)
Snowdon, S. C. (see Herb, R. G.)—246
Snyder, Hartland S. Cascade theory—906(L)
—— On the external polarization of the vacuum—1623(L)
—— (see Green, G. K.)—1289(A)
—— (see Hafner, E. M.)—331(A)
—— **and W. T. Scott.** New calculations of multiple scattering—1296(A)
Snyder, James N. (see Furry, W. H.)—1265(L)
Softky, S. D. (see Bockhop, D.)—1469(A)
Spatz, W. D. B. (see Hughes, D. J.)—1781
Spencer, R. S. and G. D. Gilmore. Equation of state for polystyrene—1300(A)
Spiers, J. A. Scattering of slow neutrons by deuterium gas—1765(L)
Spitzer, E. J. (see Burkhart, L. E.)—86
Sproull, R. L. Preparation and electrical conductivity of barium oxide crystals—1282(T)
Squire, C. F. (see Overton, W. C.)—1309(A)
Standil, S. (see Yaffe, L.)—699(L)
Stanford, C. P. (see Bernstein, S.)—1302(A)
Stanley, J. P. (see Griffith, B. A.)—534(L), 1110(L)
Stanley, James K. Diffusion of carbon in alpha-iron—1627(A)
Stein, R. S., S. Krimm, and A. V. Tobolsky. Relationship between structure, mechanical properties and birefringence in polymeric materials—1301(A)
Steinberger, J. On the range of the decay electrons of cosmic-ray mesons—1315(A)
—— On the range of the electrons in meson decay—1136
Stelson, P. H. (see Meissner, K. W.)—891(L)
Steneck, Walter G. (see Brockman, Frank G.)—1298(A), 1440(L)
Stephens, W. E. (see Franzen, W.)—1292(A)
—— (see Hughes, S. G.)—1286(A)
Stephenson, S. T. and F. D. Mason. Continuous x-ray spectrum from 8A to 14A—1711
Stephenson, T. E. (see Bernstein, S.)—1302(A)
Stern, O. (see Estermann, I.)—627
Sternberg, R. L. (see Snell, Arthur H.)—1290(A)
Sternheimer, R. M. On the compressibility of metallic cesium—888(L)
Stewart, Hugh B. and Harald H. Nielsen. Infra-red bands in the spectrum of difluoromethane—640
Stockmayer, W. H. (see Billmeyer, F. W., Jr.)—1307(A)
Stoddard, A. E. (see Cork, J. M.)—1133, 1287(A), 1621(L), 1778(L)
Stout, P. R. (see Overstreet, Roy)—231
Stout, Robert W. Radioactivity of K^{40}—1107(L)
Stovall, E. J., Jr. (see Erickson, K. W.)—894(L)
Strandberg, M. W. P., C. Y. Meng, and J. G. Ingersoll. Microwave absorption spectrum of oxygen—1524
——, **T. Wentink, Jr., and A. G. Hill.** Microwave spectrum of carbonyl selenide—827
——, **T. Wentink, Jr., and R. L. Kyhl.** Rotational absorption spectrum of OCS—270
Straus, S. (see Madorsky, S. L.)—1331(A)
Strauser, W. A. (see Campbell, E. C.)—1292(A)
Street, J. C. (see Cool, R. L.)—1275(L)
Stroud, W. G. (see Winckler, J. R.)—1316(A)
——, **J. R. Winckler, and J. Schenck.** Directional intensity of cosmic rays at high altitudes. I. Instrumentation—1316(A)
Strough, R. I. (see Crittenden, E. C., Jr.)—1630(A)
—— **and E. F. Shrader.** High current pulse generator using mechanical energy storage—1628(A)
Struthers, J. D. (see Pearson, G. L.)—344(A)
Stukenbroeker, George (see Burkhart, L. E.)—83
Suess, Hans E. (see Haxel, Otto)—1766(L)
Sugarman, Nathan. Characteristics of the fission product Cs^{135}—1473
—— Presence of a new long-lived Cs isotope in fission—1287(A)
Suhl, H. and W. Shockley. Concentrating holes and electrons by magnetic fields—1617(L)
Sun, K. H. (see Shoupp, W. E.)—1
——, **B. Jennings, W. E. Shoupp, and A. Allen.** On the delayed neutron emitter $_7N^{17}$—1302(A)
Swann, Charles P. (see Hudspeth, Emmett L.)—1272(L), 1291(A)
Swann, W. F. G., Peter A. Morris, and David Seymour. Latitude effect at high latitudes and high altitudes—1317(A)
Sweeton, F. H. (see Jenks, G. H.)—701(L)
Sydoriak, S. G. (see Grilly, E. R.)—1103(L)
——, **E. R. Grilly, and E. F. Hammel.** Condensation of pure He^3 and its vapor pressures between 1.2° and its critical point—303
—— **and J. E. Robinson.** Magnetic susceptibility of zinc at liquid helium temperatures—118
Symon, K. R. Fluctuations in energy loss of fast charged particles passing through matter—332(A)
Szelenyi, Tibor Z. Determination of the mass of N_7^{16} by means of interpolation—1105(L)

Taconis, K. W., J. J. M. Beenakker, Alfred O. Nier, and L. T. Aldrich. Measurements concerning the vapor-liquid equilibrium of solutions of He^3 in He^4 below 2.19° K—1966(L)
Taft, E. and L. Apker. Photoelectric determination of the Fermi level at amorphous arsenic surfaces—1181
—— **and L. Apker.** Photoelectric determination of the Fermi level at surfaces of amorphous arsenic—344(A)
Tagliaferri, G. (see Salvini, G.)—1112(L)
Tallmadge, F. K. (see Rosen, L.)—1632(A)
Taschek, R. F. (see Barschall, H. H.)—342(A), 1819
—— (see Coon, J. H.)—1465(A)
—— (see Gittings, H. T.)—205(L)
—— (see Hemmendinger, A.)—1291(A)
—— (see Phillips, Anne N.)—919
——, **A. Hemmendinger, and G. A. Jarvis.** Cross sections for the reaction $T^3(d, n)He^4$ from 1 to 2.5 Mev and its use as a neutron source—1464(A)
——, **G. A. Jarvis, H. V. Argo, and A. Hemmendinger.** Neutron-hydrogen mass difference from the $T^3(p, n)He^3$ reaction threshold—1268(L)

——, **G. A. Jarvis, A. Hemmendinger, G. G. Everhart, and H. T. Gittings.** Study of the interaction of protons with tritium—1361
Taub, A. H. On exact solutions of the Dirac equations—1322(A)
—— (see Kusch, P.)—1477
——**and P. Kusch.** Magnetic moment of the proton—1326(A), 1481
Taylor, T. B. (see Fernbach, S.)—1352
Taylor, T. I. (see Ruderman, I. W.)—895(L), 1296(A)
Taylor, William J. Symmetry coordinates in molecules and crystals—1283(A)
Teller, Edward (see Alfven, H.)—892(L)
—— (see Feynman, R. P.)—1561
—— (see Richtmyer, R. D.)—1729
Temmer, G. M. Excitation functions for (α, n), $(\alpha, 2n)$, $(\alpha, 3n)$ reactions on indium—1464(A)
Templeton, D. H. (see Orth, D. A.)—1100(L)
—— (see Reynolds, Frederick L.)—313(L)
ter Haar, D. Possible experimental verification of the statistics of He^3—1444(L)
—— (see Wergeland, H.)—1310(A)
——**and B. Martin.** Statistics of the three-dimensional ferromagnet—1298(A)
——**and H. Wergeland.** Viscosity of mixtures of He_3 and He_4—886(L)
Terhune, R. W. (see Hull, G. F.)—1311(A)
Ter-Pogossian, Michel (see Robinson, J. Eugene)—1099(L)
——, **J. Eugene Robinson, and C. Sharp Cook.** Disintegration of Se^{75}—995
Thackeray, E. R. Absorption spectrum of atomic sodium—1840
Theuerer, H. C. (see Pearson, G. L.)—344(A)
Thode, H. G. (see Macnamara, J.)—532(L)
Thomas, Harold A. (see Hipple, J. A.)—1616(L)
——, **R. L. Driscoll, and J. A. Hipple.** Determination of e/m from recent experiments in nuclear resonance—992(L)
——, **Raymond L. Driscoll, and John A. Hipple.** Measurements of the proton moment in absolute units—902(L)
Thomas, R. G., W. A. Fowler, and C. C. Lauritsen. Beryllium-proton reactions and scattering—1463(A)
——, **S. Rubin, W. A. Fowler, and C. C. Lauritsen.** Beryllium-proton reactions and scattering—1612(L)
Thompson, Dorothy (see Madorsky, S. L.)—1331(A)
Thompson, R. W. Disintegration of mesons—1315(A)
Thorndike, A. M. (see Safford, R. W.)—903(L)
Thornton, Robert. Recent experimental work at the Radiation Laboratory—1456(T)
Thurman, G. R. (see Conant, F. S.)—1314(A)
Tiffany, O. L. (see Hazen, W. E.)—694(L)
Ting, Yu, Roy C. Weidler, and Dudley Williams. Microwave absorption spectra of paramagnetic salts—980(L)
Tinlot, John and B. Gregory. Absorption of penetrating shower primaries—519(L)
——**and B. Gregory.** Correlation of penetrating showers with air showers—520(L)
Tiomno, J. (see Wheeler, John A.)—1306(A)
——**and John A. Wheeler.** On the coupling of μ-mesons with nucleons—1306(A)
Tisza, L. On the theory of superfluidity—885(L)
—— (see Klein, Martin J.)—1303(A)
Tobey, A. R. Neutron production by cosmic rays at sea level—894(L)
Tobias, C. A. Determination of the rate of biochemical reactions—1460(A)
Tobolsky, A. V. (see Stein, R. S.)—1301(A)
Tollestrup, A. V., F. A. Jenkins, W. A. Fowler, and C. C. Lauritsen. Neutron-hydrogen mass difference from the D-D reactions—1947(L)
——, **C. C. Lauritsen, and W. A. Fowler.** Disintegration energy of Be^8—1463(A)
Tomkins, Frank S. (see Fred, Mark)—1772(L)
Tomonaga, Sin-itiro (see Hayakawa, Satio)—1958(L)
Tongiorgi, Vanna Cocconi. Neutrons in the extensive air showers of the cosmic radiation—1532
—— (see Cocconi, G.)—1058, 1063
Torreson, O. W., Thomas Murphy, and John W. Graham. Rock magnetism as a clue to earth's magnetic history—208(L)
Torrey, Henry C. Pulse method for nuclear magnetic resonance—1326(A)
Townes, C. H. (see Low, W.)—529(L), 1319(A)
—— (see Shulman, R. G.)—1318(A)
——**and W. Low.** O^{17} and S^{36} in the rotational spectrum of OCS—1318(A)
Tralli, N. (see Lowen, I. S.)—529(L)
Truesdell, C. Recent continuum theories of fluid dynamics—1293(A)
Trump, J. G. and R. J. Van de Graaff. Secondary emission of electrons by high energy electrons—44
Turgel, R. S. (see Holmes, J. E. R.)—889(L)
Tuttle, W. A. (see Shutt, R. P.)—1329(A)

Uhlenbeck, G. E. (see Pais, A.)—1321(A)
Umeda, Kwai and Yoshihiro Nakano. Solid solubility effect of metallic surface friction—1621(L)

Valley, G. E. (see Leavitt, C. P.)—1328(A)
——, **C. P. Leavitt, and J. A. Vitale.** Cloud-chamber evidence of a meson-nucleus interaction—201(L)
——**and J. A. Vitale.** Counter controlled high pressure cloud chamber—1328(A)
Van Allen, J. A. (see Gangnes, A. V.)—57, 892(L)
——, **L. W. Fraser, and R. S. Ostrander.** Nature of the primary cosmic radiation as revealed by transition effects in lead and within the atmosphere—1315(A)
Van de Graaff, R. J. (see Trump, J. G.)—44
Van Horn, David D. X-ray investigation of iron-rich iron tungsten alloys—1630(A)
Van Hove, L. Relativistic terms in the interaction between nucleons in pseudoscalar and vector meson theory—1519
Van Name, F. W., Jr. Measurement of the radioactive decay constant of ThC′ using a coincidence method—100
Vanselow, W. (see Wilson, M. J.)—1144
VanVoorhees, S. N. (see Barnes, S. W.)—983(L)
Vitale, J. A. (see Leavitt, C. P.)—1328(A)
—— (see Valley, G. E.)—201(L), 1328(A)
Vollrath, R. E. (see Donoghue, J. J.)—1456(A)
von Hippel, A. and R. S. Alger. Breakdown of solid dielectrics by electron avalanches—1282(A)
von Kármán, T. and C. C. Lin. Statistical theory of isotropic turbulence—1282(T)
von Laue, M. Present state of physics in Germany—327(T)

Wada, W. W. Čerenkov radiation effect in meson theory—981(L)
Wagner, E. L. and D. F. Hornig. On the structure of ammonium halides and the nature of the λ-point transition—1282(A)
Wahl, Donald. Plastic deformation of crystals—1627(A)
Waldman, Bernard. Excitation of nuclei by x-rays and electrons—327(T)
—— (see Gideon, D. N.)—329(A)
—— (see Miller, Walter C.)—329(A), 425
—— (see Schillinger, Edwin J., Jr.)—900(L)
Walker, J. H. (see Bozorth, R. M.)—1954(L)

Wall, L. A. Mass spectrometric study of copolymer pyrolyses—1331(A)
Wallace, J. W. (see Hughes, D. J.)—344(A), 565
Waltner, Arthur (see Byatt, W. J.)—909(L)
—— **and F. T. Rogers, Jr.** On the beta-particle spectrum from the decay of radium *E*—1445(L)
Warburton, F. W. Comets and the reciprocal force—1471(A)
—— Relative electrodynamics—1456(A)
Warren, B. E. and D. Chipman. Long-range order in β-brass—1629(A)
Warshaw, S. D. (see Hall, T. A.)—891(L)
Wataghin, A. (see Meyer, H. A.)—908(L)
Wataghin, G. On the showers of mesons and nucleons—693(L)
—— (see Meyer, H. A.)—908(L)
Watson, Bernard B. (see DuMond, Jesse W. M.)—1226, 1304(A)
——, **William J. West, David A. Lind, and Jesse W. M. DuMond.** Precision study of the tungsten *K* spectrum using the 2-meter focusing curved crystal spectrometer—505, 1305(A)
Watson, K. M. and J. M. Jauch. Phenomenological quantum electrodynamics. Part III. Dispersion—1249
Wattenberg, Albert (see Czyzak, S. J.)—1634(A)
—— (see Hamermesh, Bernard)—1290(A)
—— (see Myers, V.)—992(L)
Way, Katharine. Neutron and proton binding energies in the region of lead—1448(L)
Weber, A. H. (see Arnold, G. P.)—217
Wei, John Pao-ngo. Narrow air showers—1330(A)
Weidler, Roy C. (see Ting, Yu)—980(L)
Weimer, D. K. (see Bleakney, W.)—1294(A)
—— (see Fletcher, C. H.)—1294(A)
Weinberg, Joseph W. Equation of state as an eigenvalue problem—338(A)
—— Magnetic scattering of elementary nucleons—348(A)
Weingarten, I. R. and G. E. Kimball. Untuned cavity microwave spectroscope using bolometer detectors—1325(A)
Weinreich, O. A. Activation phenomena of thoria cathodes—1312(A)
Weinstein, Alexander. On transonic flows—1293(A)
Weinstock, Bernard (see Osborne, Darrell W.)—988(L)
Weisskopf, V. F. (see Feshbach, H.)—342(A)
—— (see French, J. B.)—338(A), 1240
—— **and David H. Frisch.** Application of charge-symmetrical nuclear forces to Wigner's theory of heavy nuclei—1297(A)
Weissler, Alfred. Depolymerization by ultrasonic irradiation: the role of cavitation—1313(A)
Weissler, Pearl G. (see Cook, Richard K.)—1283(A)
Weisz, P. B. and W. P. Kern. Measurements of behavior and mobility of polyatomic ions—899(L)
Wells, E. J., Jr. (see Mohler, Fred L.)—1332(A)
Welsh, H. L. (see Crawford, M. F.)—1607(L)
Welton, T. A. Alternative subtraction formalism for quantum electrodynamics—1321(A)
Wentink, T., Jr. (see Strandberg, M. W. P.)—270, 827
Wentzel, Gregor. Polarization effects of vector-mesons—1810
Wergeland, H. (see ter Haar, D.)—886(L)
—— **and D. ter Haar.** Viscosity of mixtures of He_3 and He_4—1310(A)
Wert, Charles A. Precipitation from supersaturated solid solutions of C and N in α-iron—1626(A)
West, William J. (see Watson, Bernard B.)—505, 1305(A)
Whaley, R. M. and V. A. Long. Diurnal and seasonal variation in frequency of occurrence of small cosmic-ray bursts—341(A)
Whaling, Ward, J. E. Evans, and T. W. Bonner. Neutrons from deuteron bombardment of Li^6—688(L)
Wheatley, John and David Halliday. Paramagnetic absorption in single crystals of copper sulfate pentahydrate—1412
Wheeler, John A. (see Shanley, T. J. B.)—1317(A)
—— (see Tiomno, J.)—1306(A)
—— (see Wightman, A. S.)—1306(A)
—— **and J. Tiomno.** On the spin of π- and μ-mesons—1306(A)
Wheeler, L. P. Early work of Willard Gibbs—1281(T)
White, J. R. and J. H. Buck. Discrepancies between physically and chemically determined atomic weights for the elements between silver-47 and iodine-53—1619(L)
White, M. G. Design of the Brookhaven high energy proton synchrotron—1288(A)
—— (see Sherr, R.)—282, 328(A)
White, R. S. (see Jones, Stanley B.)—1468(A)
Whitehead, W. D., Jr. (see Heydenburg, N. P.)—1147
Wick, G. C. On the space distribution of slow neutrons—738
—— Theorem on cross sections—1459(A)
Wiedenbeck, M. K. (see Chu, K. Y.)—226
—— **and H. R. Crane.** Delayed emission of electrons from the cathode in a counter when operated above the plateau—1268(L)
Wiegand, C. E. (see Hadley, J.)—351
—— (see Segrè, E.)—39
Wightman, A. S., R. E. Marshak, and J. A. Wheeler. Absorption of negative pi-mesons in hydrogen—1306(A)
Wigner, E. P. (see Moshinsky, M.)—1322(A)
Wijsman, Robert A. Breakdown probability of a low pressure gas discharge—833
Wilkinson, Geoffrey. Radioactive isotopes of platinum and gold—1019
—— **and Harry G. Hicks.** Hf^{175}, a new radioactive isotope of hafnium—696(L)
—— **and Harry G. Hicks.** Radioactive isotopes of the rare earths. I. Experimental techniques and thulium isotopes—1370
—— **and Harry G. Hicks.** Radioactive isotopes of the rare earth elements. II. Neodymium isotopes—1687
Wilkinson, Roger G. (see Beach, Louis A.)—211(L), 329(A)
—— (see Peacock, Charles L.)—329(A)
Willard, John E. (see Johnston, Francis)—528(L)
Williams, Clarke. Experimental facilities to be available at the Brookhaven nuclear reactor—1289(A)
Williams, Dudley (see Ting, Yu)—980(L)
—— (see Zimmerman, John R.)—198(L), 699(L)
Williams, G. C. Combustion-generated turbulence in relation to flame propagation—1282(T)
Williams, H. J., R. M. Bozorth, and W. Shockley. Magnetic domain patterns on single crystals of silicon iron—155
—— **and W. Shockley.** Simple domain structure in an iron crystal showing a direct correlation with the magnetization—178
Williams, J. H. Nuclear scattering—1625(T)
—— (see Freier, George)—342(A), 901(L), 1345
—— (see Rosen, L.)—1632(A)
Williamson, Laura (see Madorsky, S. L.)—1331(A)
Willoughby, A. B. Chi square test as a criterion for testing halogen-filed Geiger tubes—1461(A)
Wilson, E. Bright, Jr. Calculation of molecular force constants—1317(A)
Wilson, H. A. Note on Dirac's theory of magnetic poles—309(L)
Wilson, M. J. and W. Vanselow. Procedure for processing nuclear-track emulsions—1144

Wimett, T. F. (see Dickinson, W. C.)—1769(L)
Winckler, J. R. (see Stroud, W. G.)—1316(A)
—— **and W. G. Stroud.** Directional intensity of cosmic rays at high altitudes. II. Interpretation—1316(A)
Winkler, Ernst H. Analytical studies of the Mach-Zehnder interferometer—1314(A)
Winsberg, Lester (see Krueger, H. H. A.)—1098(L)
——, **David Meneghetti, and S. S. Sidhu.** Total neutron cross sections of compounds with different crystalline structures—975
Wintner, Aurel (see Hartman, Philip)—1452(L)
Wise, C. Edward (see Mohler, Fred L.)—1332(A)
Witmer, Enos E. Masses of the mesons—348(A)
—— Nuclear magnetic moments as integral multiples of a natural unit—349(A)
—— Nuclear reaction energies as integral multiples of a natural unit—1289(A)
Witte, R. S., B. A. Mrowca, and E. Guth. Velocity and attenuation of sound in butyl and Gr-S rubbers—1284(A)
Wojtowicz, W. (see Heller, W.)—343(A)
Wolfe, R. D. and N. E. Ballou. Yields of the platinum group radio-isotopes in the high energy helium-ion bombardment of uranium—527(L)
Wolfenstein, Lincoln. Polarization of *d-d* neutrons—342(A)
—— Theory of proposed reactions involving polarized protons—1664
Wollan, E. O. (see Shull, C. G.)—1302(A)
——, **W. L. Davidson, and C. G. Shull.** Neutron diffraction study of the structure of ice—1348
Wolk, Bernard and Harold Jacobs. Micro analysis of gas in cathode coating assemblies—1312(A)
Woo, Y. H. (see Mandeville, C. E.)—1528
——, **C. E. Mandeville, M. V. Scherb, and W. B. Keighton.** Slow neutron induced activities of germanium—1286(A)
Wood, Darwin L. New measurements of the infra-red fundamental bands of NH_3—1113(A)
Wood, Elizabeth A. Optical and x-ray studies of ferroelectric domains in barium titanate—703(T)
Woodbury, E. J., R. N. Hall, and W. A. Fowler. Cross sections for $C^{12}(p\gamma)$ and $N^{14}(p\gamma)$ reactions at low energy—1462(A)
Woodcock, Richard F. (see Duckworth, Henry E.)—1438(L), 1616(L)
Woodhull, J. C. (see May, Albert)—1313(A)
Workman, E. J. (see Reynolds, S. E.)—347(A)
—— **and S. E. Reynolds.** Electrical phenomena resulting from the freezing of dilute aqueous solutions—347(A)
Worth, Donald C. Coincidence measurement of neutron energy—903(L), 1303(A)
Wouters, L. Detection of very high energy protons by means of anthracene scintillation counters—1470(A)
Wouthuysen, S. A. Theoretical remarks on nuclear disruptions by primary cosmic rays—1329(A)
Wright, S. C. (see Jungerman, J.)—1470(A)
Wu, C. S. (see Albert, R. D.)—1286(A)
—— (see Feldman, L.)—1286(A)
—— (see Morrissey, R.)—1288(A)
—— **and R. D. Albert.** Beta-ray spectra of Cu^{64}—315(L)
—— **and R. D. Albert.** Beta-ray spectra of Cu^{64} and the ratio of $N+/N-$—1107(L)
Wu, T. L. (see Smoluchowski, R.)—345(A)
—— **and R. Smoluchowski.** New criterion of slip in single Al crystals—345(A)
Wu, Ta-You and H. M. Foley. Symmetrical meson theory of nuclear forces—1305(A), 1681
Wyly, L. D. Angular yield of protons from $N^{14}(dp)N^{15}$—1292(A)
—— (see Pollard, E. C.)—725
Wyman, Max. Radially symmetric distributions of matter—1930

Yadoff, Oleg. On the mechanism of conductivity of electricity according to modern physical theories—1334(A)
Yaffe, L., M. Kirsch, S. Standil, and Jean M. Grunlund. The chain $_{56}Ba^{130}(n, \gamma)_{56}Ba^{131} \rightarrow {}_{55}Cs^{131} \rightarrow {}_{54}Xe^{131}$—699(L)
Yager, W. A. Additional ferromagnetic resonance absorption measurements on Supermalloy—316(L)
—— (see Hoden, A. N.)—1443(L), 1614(L)
—— **and F. R. Merritt.** Ferromagnetic resonance absorption in Heusler alloy—318(L)
——, **F. R. Merritt, A. N. Holden, and C. Kittel.** Microwave magnetic resonance absorption in chrome alum at 1.25 cm—1630(A)
Yagoda, Herman and Nathan Kaplan. Lithium borate-loaded emulsions as neutron detectors—1328(A)
—— **and Nathan Kaplan.** Pretreatment of nuclear emulsions for cosmic-ray exposures—339(A)
Yamaguchi, Y. (see Fujimoto, Y.)—1776(L)
Yamakawa, K. A. Suggested slow neutron crystal counter—1774(L)
Yang, C. N. (see Lee, T. D.)—905(L)
Yater, Joseph (see Benson, W. K., Jr.)—1470(A)
Yevick, George J. Interaction Hamiltonian for photon, meson, and nucleon fields—1450(L)
—— Interaction of photon-meson, and nucleon fields—1305(A)
Yngve, Victor H. (see Schein, Marcel)—339(A)
York, Herbert F. Secondary particles from various nuclei bombarded with 90-Mev neutrons—1467(A)
—— (see Hadley, J.)—351
—— (see Moyer, B. J.)—1470(A)
Yost, Don M. (see Grinstead, Robert R.)—984(L)
Young, J. R. (see Eisenstein, A.)—347(A)
Youngblood, J. F. (see Fiske, M. D.)—1311(A)
—— (see Horn, F. H.)—1311(A)
——, **W. DeSorbo, M. D. Fiske, and F. H. Horn.** General Electric low temperature laboratory. Part III. d.c. power facilities—1311(A)
Yu, Fu-Chun, Lin-Sheng Cheng, and J. D. Kurbatov. Disintegration of Ag 110 into isobars Pd 110 and Cd 110—1287(A)
Yukawa, H. Models and methods in the meson theory—1281(T)

Zachariasen, W. H. Study of new elements by x-ray diffraction methods—327(T)
Zaffarano, Daniel J. (see Kern, Bernard D.)—1287(A)
——, **Allan C. G. Mitchell, and Bernard D. Kern.** Disintegration of iodine^{131}—1632(A)
Zapp, Robert L. and Eugene Guth. Reinforcement and swelling of butyl rubber-filler systems—1300(A)
Zeldes, H. (see Brosi, A. R.)—1615(L)
Zener, Clarence. Relation between residual strain energy and the elastic moduli—345(A)
Zerfoss, S., L. R. Johnson, and O. Imber. Single crystal growth of scheelite—320(L)
Zietlow, James P., Forrest F. Cleveland, and Arnold G. Meister. Vibrational spectra of some trichloromethanes—333(A)
Zimmerman, J. E. (see Estermann, I.)—1630(A)
Zimmerman, John R. and Dudley Williams. Magnetic moment of aluminum^{27}—198(L)
—— **and Dudley Williams.** Nuclear gyromagnetic ratios of Be^9, Rb^{85}, Rb^{87}, and Cs^{133}—699(L)
Ziomek, Joseph S. (see Kreusch, E.)—334(A)
—— **and Forrest F. Cleveland.** Thermodynamic properties of diiodoacetylene and some symmetrical-top acetylenes—334(A)

Analytic Subject Index to Volume 75

References with (A) are to abstracts of papers presented at meetings of the American Physical Society. References with (L) are to Letters to the Editor.

Acoustics (see also **Ultrasonics**)
- Attenuation in rubbers, R. S. Witte, B. A. Mrowca, and E. Guth—1284(A); D. G. Ivey, B. A. Mrowca, and E. Guth—1284(A)
- Attenuation of sound in helium, Martin Greenspan—197(L)
- Erratum: acoustical birefringence, W. J. Price—992(L)
- Finite amplitude pressure waves, Bruno W. Augenstein—521(L)
- Loading of piano strings for improved tone, Franklin Miller, Jr.—1113(A)
- Plane shear waves in viscoelastic media, H. T. O'Neil—928
- "Second" sound in He *II*, J. R. Pellam—1183
- Shear elasticity and viscosity of liquids, W. P. Mason, W. O. Baker, H. J. McSkimin, and J. H. Heiss—936
- Transonic flows, Alexander Weinstein—1293(A)
- Ultrasonic absorption in viscous liquids, Joseph L. Hunter—1627(A)
- Ultrasonic measurements on rochelle salt crystals, W. J. Price—946
- Velocity of waves in metallic Be, W. C. Overton, R. H. Pry, R. W. Schmitt, and C. F. Squire—1309(A)

Aerodynamics (see also **Hydrodynamics**)
- Linearized supersonic aerodynamics, Max M. Munk—1293(A)
- Shock wave, conical nose at supersonic speeds, E. V. Laitone—1294(A)

Alloys (see **Crystalline states**)

Arcs (see **Discharge of electricity in gases**)

Astrophysics
- Band of CO in solar spectrum, Marcel V. Migeotte—1108(L)
- Comets and reciprocal force, F. W. Warburton—1471(A)
- Evolution of expanding universe, Ralph A. Alpher and Robert C. Herman—1089, 1333(A)
- Excited-state bands in atmospheric spectra, Arthur Adel—1262(L)
- Magnetic moments of sunspots, James W. Broxon—349(A), 606
- Meteor speed measurements by radio, D. D. Cherry and C. S. Shyman—1441(L)
- Polarization of starlight, Leverett Davis, Jr., and Jesse L. Greenstein—1605(L)
- Shell model of stars, Chushiro Hayashi—1619(L)
- Solar radio noise, Andrew V. Haeff—1333(A), 1546
- Thermonuclear reactions in expanding universe, R. A. Alpher, R. Herman, and G. A. Gamow—701(L)

Atmosphere (see **Meteorology**)

Atomic mass (see **Isotopes**)

Barkhausen effect (see **Magnetic properties**)

Biophysics
- Average optical transmission through plants, Edward E. Miller—335(A)
- Interaction between pairs of identical large molecules, Herbert Jehle—348(A)
- Unusual cells in blood of cyclotron workers, M. Ingram and S. W. Barnes—1765(L)

Boson theory
- Generalizing boson field theories, Alex E. S. Green—1926

Chemical reactions
- Biochemical reactions, rate of, C. A. Tobias—1460(A)

Colloids (see also **Polymerization, properties of polymers**)
- Shape of particles, Wilfried Heller—1308(A)

Conductivity, electrical (see **Electrical conductivity; Discharge of electricity in gases**)

Constants, physical, standards
- E/m from experiments in nuclear resonance, H. A. Thomas, R. L. Driscoll, and J. A. Hipple—992(L)
- Fine structure constant, H. A. Bethe and C. Longmire—306
- Particle of charge two or greater, R. W. Safford and A. M. Thorndike—903(L)
- Recent changes, Jesse W. M. DuMond—1267(L)

Cosmic radiation
- Absorption of hard component, Marcel Schein, Victor H. Yngve, and Theodore Bowen—339(A)
- Absorption of shower primaries, John Tinlot and B. Gregory—519(L)
- Analysis of ionization chamber data, John M. Blatt—1584
- Bremsstrahlung produced by protons, John L. Powell—32
- Bursts, experiments on, H. S. Bridge and B. Rossi—810
- Bursts as function of chamber area, C. G. Montgomery and D. D. Montgomery—1329(A)
- Bursts at 3500 meters, Edward F. Fahy and Marcel Schein—207(L), 340(A)
- Cascade theory, Hartland S. Snyder—906(L)
- Coincident bursts, C. G. Montgomery and D. D. Montgomery—980(L)
- Collisions of heavy primaries, H. L. Bradt and B. Peters—1779(L)
- Compton-Getting effect, M. Forró—1458(A)
- Correlation of showers, John Tinlot and B. Gregory—520(L)
- Decay products, mass of mesotron, Carl D. Anderson, Robert B. Leighton, and Aaron J. Seriff—1466(A)
- Decay products of μ-meson, E. P. Hincks and B. Pontecorvo—341(A)
- Density of extensive air showers, G. Cocconi and V. Cocconi Tongiorgi—1058
- Detection by scintillation counters, George T. Reynolds—1317(A)
- Directional intensity at high altitudes, J. R. Winckler and W. G. Stroud—1316(A)
- Disintegration of mesons, R. W. Thompson—1315(A)
- Disintegrations and mesons in stratosphere, Jere J. Lord and Marcel Schein—340(A)
- Diurnal and seasonal variation, small bursts, R. M. Whaley and V. A. Long—341(A)
- East-west asymmetry and latitude effect, W. C. Barber—590
- E-W asymmetry, particles of opposite charge, Gerhart Groetzinger and Gordon W. McClure—349(A)
- East-west effect, A. T. Biehl, H. V. Neher, and Wm. C. Roesch—688(L)
- Energies of heavy nuclei, Phyllis Freier, Edward P. Ney, and Frank Oppenheimer—991(L)
- Energy of mesotron decay electrons, Robert B. Leighton, Carl D. Anderson, and Aaron J. Seriff—1466(A)
- Energy of particles, H. V. Neher—1458(A)
- Events in photographic emulsions, Eric Pickup and Adair Morrison—1328(A)
- Explosions in emulsions, M. F. Kaplon, B. Peters, and H. L. Bradt—1329(A)
- Extensive penetrating showers, John Ise, Jr.—1458(A)

Gamma-rays (1–5 Mev) from stopped negative mesons, W. Y. Chang—1315(A)
Heavily ionizing penetrating particles, Frank L. Hereford—923
Heavy nuclei, E. P. Ney, P. Freier, E. J. Lofgren, and F. Oppenheimer—340(A); Martin A. Pomerantz and Frank L. Hereford—1316(A)
Heavy particles in primary radiation, Martin A. Pomerantz and Frank L. Hereford—1316(A)
High pressure cloud-chamber pictures, C. P. Leavitt, G. E. Valley, and J. A. Vitale—1328(A)
Influence of five heavenly bodies, T. J. B. Shanley, E. O. Kane, and J. A. Wheeler—1317(A)
Instrumentation for high altitudes, W. G. Stroud, J. R. Winckler, and J. Schenck—1316(A)
Intensity above atmosphere, A. V. Gangnes, J. F. Jenkins, Jr., and J. A. Van Allen—57, 892(L)
Intensity at high altitudes, W. C. Roesch, A. T. Biehl, and H. V. Neher—1457(A)
Intensity at sea level, R. A. Montgomery—1407
Ionizing radiation at 4300 meters, Frank L. Hereford—1316(A)
Latitude dependence at 33,000 feet, A. T. Biehl, H. V. Neher, and W. C. Roesch—1457(A)
Latitude effect, W. F. G. Swann, Peter A. Morris, and David Seymour—1317(A)
Light-particle hypotheses of penetrating particles, K. Sitte—340(A)
In lower atmosphere, Martin A. Pomerantz—1721
Magnetic moments of sunspots, James W. Broxon—349(A), 606
Mass of mesotrons, Robert B. Brode—904(L); J. Gordon Retallack and Robert B. Brode—1717
Meson-nucleus interaction, cloud-chamber evidence, G. E. Valley, C. P. Leavitt, and J. A. Vitale—201(L)
Mesons in showers, H. A. Meyer, G. Schwachheim, A. Wataghin, and G. Wataghin—908(L)
Mesons in stars, Eric Pickup and Adair Morrison—686(L)
Mesons π and μ, R. E. Marshak—700(L)
Mesons stopping in aluminum foils, R. L. Cool, E. C. Fowler, J. C. Street, W. B. Fowler, and R. D. Sard—1275(L)
μ-meson decay electrons, bremsstrahlung radiation, E. P. Hincks and B. Pontecorvo—698(L)
Narrow air showers, John Pao-ngo Wei—1330(A)
Neutrons in extensive showers, Vanna Cocconi Tongiorgi—1532; Joseph S. Levinger—1540
Nuclear disruptions by primary rays, S. A. Wouthuysen—1329(A)
Origin of photons, Satio Hayakawa—1759
Origin of radiation, Enrico Fermi—1169; Hannes Alfvén—1732
Origin of rays, H. Alfvén, R. D. Richtmyer, and E. Teller—892(L); R. D. Richtmyer and Edward Teller—1729
Particles that produce penetrating showers, W. E. Hazen, C. A. Randall, and O. L. Tiffany—694(L)
Penetrating particles in showers, G. Cocconi, V. Cocconi Tongiorgi, and K. Greisen—1063
Periodic orbits in equatorial plane of magnetic dipole, Antonio Romero Juárez—137
Phenomena in nuclear emulsions, Adair Morrison and Eric Pickup—1328(A)
Photographs with high pressure cloud chamber, R. P. Shutt, G. R. Hoke, W. A. Tuttle, and G. F. O'Neill—1329(A)
Positive excess of penetrating component, G. Bernardini—1335(A)
Pretreatment of nuclear emulsions, Herman Yagoda and Nathan Kaplan—339(A)
Primary radiation, transition effects, J. A. Van Allen, L. W. Fraser, and R. S. Ostrander—1315(A)
Production of neutrons, Gordon W. McClure and Gerhart Groetzinger—340(A); A. R. Tobey—894(L)
Production of penetrating particles in showers, G. Salvini and G. Tagliaferri—1112(L)
Properties at high altitudes, Martin A. Pomerantz—69
Properties of particles that generate penetrating showers, G. Cocconi—1074
Properties of radiation at large zenith angles, Martin A. Pomerantz—1335(A)
Radiation accompanying meson creation, L. I. Schiff—1459(A)
Range of decay electrons of mesons, J. Steinberger—1315(A)
Range of electrons in meson decay, J. Steinberger—1136
Range of showers in Pb, K. Greisen—1071
Range spectrum of mesotrons, Lawrence S. Germain—1458(A)
Relation to sunspot magnetic moments, James W. Broxon—341(A), 612
Sea level cloud chamber, Martin J. Cohen—1329(A)
Shower by π-meson and π-μ-decay, M. S. Sinha—1757
Showers at sea level, C. Y. Chao—581
Showers in Pb at 3020 meters, William B. Fretter—1330(A)
Showers, interpretation, Satio Hayakawa—1958(L)
Showers of mesons and nucleons, G. Wataghin—693(L)
Spread of showers, Jane Roberg and L. W. Nordheim—444
Star-producing radiation, G. Bernardini—1328(A)
Star production at high altitudes, P. S. Freier, E. J. Lofgren, E. P. Ney, and F. Oppenheimer—340(A); P. Freier, E. P. Ney, and F. Oppenheimer—1451(L)
Stars and bursts, Y. Fujimoto and Y. Yamaguchi—1776(L)
Stars and mesons in stratosphere, J. J. Lord and Marcel Schein—1956(L)
Stars in stratosphere, J. J. Lord and Marcel Schein—1956(L)
Stimulated decay of mesons, W. H. Furry and James N. Snyder—1265(L)
Underground radiation, Satio Hayakawa and Sin-itiro Tomonaga—1958(L)
V-2 cloud-chamber observation of multiply charged primary ray, S. E. Golian, C. Y. Johnson, E. H. Krause, M. L. Kuder, G. J. Perlow, and C. A. Schroeder—524(L)

Cosmology
Radially symmetric distributions of matter, Max Wyman—1930

Cross section, measurements, theory (see also **Scattering of electrons, neutrons, and ions**)
For $Al^{27}(d, \alpha p)Na^{24}$, H. W. Hubbard—1470(A)
Of Be, N, O, Na, and Ca for fast neutrons, C. K. Bockelman, R. K. Adair, H. H. Barschall, and O. Sala—336(A); R. K. Adair, H. H. Barschall, C. K. Bockelman, and O. Sala—1124
For $C^{12}(p\gamma)$ and $N^{14}(p\gamma)$ reactions at low energy, E. J. Woodbury, R. N. Hall, and W. A. Fowler—1462(A)
Cross-section measurements, identification of Tc^{92} and Tc^{93}, M. L. Pool and D. N. Kundu—337(A)
D-T reaction and angular distribution of alpha-particles, E. Bretscher and A. P. French—1154
Effect of small angle scattering, H. H. A. Krueger, D. Meneghetti, C. R. Ringo, and L. Winsberg—1098(L)
For electromagnetic *n-n*, *n-p*, and *p-p* scattering, Joseph W. Weinberg—348(A)

Cross section, measurements, theory (continued)
For fast neutrons, D. J. Hughes, W. D. B. Spatz, and N. Goldstein—1781
Gamma-rays for 88 Mev, James L. Lawson—433
For Hf, Er, Ni^{58}, and Ni^{60}, S. Bernstein, J. B. Dial, C. P. Stanford, and T. E. Stephenson—1302(A)
Of He_3 for slow neutrons, L. D. P. King and Louis Goldstein—1366
Of nuclei for 90-Mev neutrons, Leslie J. Cook, Edwin M. McMillan, Jack M. Peterson, and Duane C. Sewell—7; N. Knable, J. De Juren, and B. J. Moyer—1470(A)
$(p, n):(p, \gamma)$ and $(d, n):(d, 2n)$ reaction cross sections, D. N. Kundu and M. L. Pool—336(A)
Precise determination, n-p cross section, Edward Melkonian, L. J. Rainwater, and W. W. Havens, Jr.—1295(A)
For production of negative mesons, Vincent Peterson—1469(A)
For reaction $D(d, n)He^3$, K. W. Erickson, J. L. Fowler, and E. J. Stovall, Jr.—894(L)
For reaction $T^3(d, n)He^4$, neutron source, R. F. Taschek, A. Hemmendinger, and G. A. Jarvis—1464(A)
Relative cross sections, high energy neutrons on light elements, William J. Knox—537
Slow neutron studies, W. W. Havens, Jr. and L. J. Rainwater—1296(A)
Theorem on cross sections, G. C. Wick—1459(A)
Total neutron cross sections, polycrystalline substances, Lester Winsberg, David Meneghetti, and S. S. Sidhu—975

Crystal structure
Of ammonium halides, λ-point transition, E. L. Wagner and D. F. Hornig—1282(A)
Of evaporated LiF films, L. G. Schulz—1284(A)
Of ferroelectric $BaTiO_3$, G. C. Danielson and R. E. Rundle—1630(A)
Of Heusler alloy, superlattice lines, Louis Gold—1629(A)
Inorganic salts at critical temperature of water, Zaboj V. Harvalik—1283(A)
Interplanar spacings of different materials for back reflection, Suzanne van Dijke Beatty—700(L)
Of iron tungsten alloys, David D. Van Horn—1630(A)
Significance of reciprocal lattice, Alfred Landé—1113(A)
Slip in single Al crystals, T. L. Wu and R. Smoluchowski—345(A)
Structure of ice by neutron diffraction, E. O. Wollan, W. L. Davidson, and C. G. Shull—1348
Symmetry coordinates in crystals, William J. Taylor—1283(A)

Crystalline state
Alloys containing Ge and Sb^{124}, G. L. Pearson, J. D. Struthers, and H. C. Theuerer—344(A)
Breakdown by electron avalanches, A. von Hippel and R. S. Alger—1282(A)
Copper-manganese-indium alloys, Robert R. Grinstead and Don M. Yost—984(L)
Damping of metals, soluble impurities, J. S. Koehler—1626(A)
Density change of KCl crystals upon irradiation, I. Estermann, W. J. Leivo, and O. Stern—627
Diffusion of carbon in alpha-iron, James K. Stanley—1627(A)
Directional character of long-range order parameter, Louis Gold—1265(L)
Dislocation models of crystal grain boundaries, W. Shockley and W. T. Read—692(L)
Disorder in films of Ag, Chester R. Berry—1299(A)
Elastic constants of Ni crystals, R. M. Bozorth, W. P. Mason, H. J. McSkimin, and J. G. Walker—1954(L)
Electric breakdown, H. B. Callen—1282(A)
Electrical phenomena, freezing of dilute solutions, E. J. Workman and S. E. Reynolds—347(A)
Electrical properties of silicon and silicon alloys, G. L. Pearson and J. Bardeen—865
Electron multiplication in crystals, Frederick Seitz—1283(A)
Electronic eigenfunctions in ionic crystals, Reikichi Nosawa—1102(L)
Embrittlement of Cu by Bi, T'ing-Sui Kê—1626(A)
Fermi level at arsenic surfaces, photoelectric determination, E. Taft and L. Apker—344(A), 1181
Ferroelectric crystals, B. T. Matthias—1771(L)
Ferromagnetic resonance absorption, Heusler alloy, W. A. Yager and F. R. Merritt—318(L)
Ferromagnetic resonance absorption, Supermalloy, W. A. Yager—316(L)
Free energies of crystal surfaces, Conyers Herring—344(A)
Inelastic scattering of electrons from copper single crystal, Paul P. Reichertz and H. E. Farnsworth—1902
Internal friction, measurement, R. Kamel—1606(L)
Long range order in β-brass, B. E. Warren and D. Chipman—1629(A)
Low frequency dispersion in ionic crystals, R. G. Breckenridge—1282(A)
Magnetostriction and order-disorder, J. E. Goldman and R. Smoluchowski—140
Order-disorder in alloys, neutron diffraction, C. G. Shull and Sidney Siegel—1008
Order in alloy Cu_3Au, effect of neutron bombardment, Sidney Siegel—1823
Phase transitions in barium titanate, P. W. Forsbergh, Jr.—1299(A)
Photoconductivity in tungstate phosphors, Clifford C. Klick and James H. Shulman—1606(L)
Polarization around a charge in rigid lattice, E. S. Rittner, R. A. Hutner, and F. K. du Pré—345(A)
Polarization around two charges in rigid lattice, R. A. Hutner, E. S. Rittner, and F. K. du Pré—345(A)
Polymerization in solid state, E. Miller, I. Fankuchen, and H. Mark—1314(A)
Pyroelectric effect in $Li_2SO_4 \cdot H_2O$, Hans Jaffe—1625(A)
Resonance absorption in colored crystals, Clyde A. Hutchison, Jr.—1769(L)
Scintillations in calcium fluoride crystals, W. J. MacIntyre—1439(L)
Short-range order for low temperature Ag_3Al, B. W. Roberts, Jr.—1629(A)
Short-range order in Cu_3Au, J. M. Cowley—1629(A)
Single crystal of scheelite, $CaWO_4$, S. Zerfoss, L. R. Johnson, and O. Imber—320(L)
Sintering of metallic particles, G. C. Kuczynski—344(A)
Size and shape of tactoids, W. Heller and W. Wojtowicz—343(A)
Solubility and metallic friction, Kwai Umeda and Yoshihiro Nakano—1621(L)
Steady-state creep in metals, B. G. Rightmire—1627(A)
Supersaturated solid solutions of C and N in α-iron, Charles A. Wert—1626(A)
Surface energies for free electron metal, H. B. Huntington—1627(A)
Thermal expansion of $Li_2SO_4 \cdot H_2O$, Charles S. Smith and H. H. Landon—1625(A)

Dielectric constants (see **Dielectrics and dielectric properties**)
Dielectrics and dielectric properties
Anomalous behavior at Curie point, Frank G. Brockman, P. H. Dowling, and Walter G. Steneck—1440(L)
Of $BaTiO_3$ single-domain crystals, Walter J. Merz—687(L)
Of barium titanate at high temperatures, Shepard Roberts—989(L)
Of barium titanate at low temperatures, R. F. Blunt, W. F. Love, and E. N. Skomal—1299(A)
Breakdown by electron avalanches, A. von Hippel and R. S. Alger—1282(A)
Electric breakdown, H. B. Callen—1282(A)
Low frequency dispersion in ionic crystals, R. G. Breckenridge—1282(A)
Diffraction of electrons (see **Electron diffraction**)
Diffraction of neutrons (see **Neutron diffraction**)
Diffraction of radiation
By aperture in infinite plane, Harold Levine and Julian Schwinger—1423
Diffraction through plane screen, John W. Miles—695(L)
Of plane wave by semi-infinite conducting sheet, C. W. Horton—1263(L)
Near rods and apertures, C. L. Andrews—346(A)
Transmission coefficient of circular aperture, C. J. Bouwkamp—1608(L); Harold Levine and Julian Schwinger—1608(L)
Diffusion (see also **Thermal diffusion**)
Ambipolar diffusion in He, Manfred A. Biondi and Sanborn C. Brown—1700
Of carbon in alpha-iron, James K. Stanley—1627(A)
Coefficient of self-diffusion, G. C. Kuczynski—1309(A)
Separation of A^{36} by thermal diffusion, James O. Buchanan—1332(A)
Discharge of electricity in gases
Anchoring of cathode spot, Jerome Rothstein—1336(A)
BaF as cold cathode, Harold Jacobs, Armand P. LaRocque, and Alfred Mazzei—1312(A)
Breakdown probability, Robert A. Wijsman—833
Cold cathode behavior, barium compounds, Harold Jacobs and Armand P. LaRocque—347(A)
Corona in N_2, O_2, and mixtures, Charles G. Miller—1460(A)
Discharge of counter at voltages above plateau, H. R. Crane—985(L)
Electron velocity distribution function, Julius H. Cahn—838
Electronic interaction in discharges, Julius H. Cahn—293, 346(A)
Excitation and damping of plasma oscillations, D. Bohm and E. P. Gross—1864
Glow-arc transition and arc stability, Jerome Rothstein—1335(A)
High frequency breakdown in He, A. D. MacDonald and Sanborn C. Brown—411, 1324(A)
Impulse breakdown of air, R. Fletcher—1324(A)
Liberation of ions by electron bombardment, I. Filosofo and A. Rostagni—1269(L)
Hg-type arc spot temperature, Jerome Rothstein—1323(A)
Plasma oscillations, effects of collisions, D. Bohm and E. P. Gross—1323(A)
Plasma oscillations, medium-like behavior, D. Bohm and E. P. Gross—1851
Plasma oscillations, thermal motions, E. P. Gross and D. Bohm—1323(A)
Space-charge amplification effects, V. A. Bailey—1104(L)
Space-charge controlled diffusion, T. Holstein—1323(A)
Time lags in spark breakdown, L. H. Fisher and B. Bederson—1324(A)
Transition, streamer and Townsend mechanism, L. H. Fisher and B. Bederson—1615(L)
Disintegration and excitation of nucleus (see also **Radioactivity**)
Absolute voltage determination of nuclear reactions, R. G. Herb, S. C. Snowdon, and O. Sala—246
Alpha particles from F and Li bombarded by protons, W. E. Burcham and Joan M. Freeman—1756
Angle dependence of reaction $Li^6(d, p)Li^7$, R. W. Krone, S. S. Hanna, and D. R. Inglis—335(A)
Angular distribution of γ-rays from Li, R. F. Christy—1464(A)
Angular distribution of $Li^6(d, \alpha)\alpha$, Robert Resnick and D. R. Inglis—1291(A)
Angular distribution of photo-neutrons, Bernard Hamermesh and Albert Wattenberg—1290(A)
Angular distribution, protons from $B^{10} + d$, W. C. Redman—1292(A)
Angular yield of neutrons, *D-D* reaction, G. T. Hunter and H. T. Richards—335(A)
Angular yield of protons, $N^{14}(dp)N^{15}$, L. D. Wyly—1292(A)
$_{56}Ba^{130}(n, \gamma)_{56}Ba^{131} \rightarrow {}_{55}Cs^{131} \rightarrow {}_{54}Xe^{131}$, L. Yaffe, M. Kirsch, S. Standil, and Jean M. Grunlund—699(L)
Of Be^8, erratum, Arthur Hemmendinger—1267(L)
Be proton reactions, R. G. Thomas, S. Rubin, W. A. Fowler, and C. C. Lauritsen—1612(L); A. V. Tollestrup, C. C. Lauritsen, and W. A. Fowler—1463(A)
Bombardment of Al by deuterons, E. C. Pollard, V. L. Sailor, and L. D. Wyly—725
Capture of L_I electrons, B. Pontecorvo, D. H. W. Kirkwood, and G. C. Hanna—982(L)
Comparison of $Li(p, \gamma)$ with $F(p, \gamma)$ resonance, Emmett L. Hudspeth and Charles P. Swann—1291(A)
"Cross-over transitions" in Cl^{38}, Co^{60}, Br^{82}, and Sb^{124}, V. Myers and A. Wattenberg—992(L)
Cross sections of *D-T* reaction and angular distribution of alpha-particles, E. Bretscher and A. P. French—1154
(d, H^3) reaction in phosphorus, upper limit, David Kahn and Gerhart Groetzinger—906(L)
Decay of tritium, bound electron creation, P. M. Sherk—789
Disintegrations and mesons in stratosphere, Jere J. Lord and Marcel Schein—340(A)
Distribution of particles from D-D reactions, L. Rosen, F. K. Tallmadge, and J. H. Williams—1632(A)
Electro-disintegration, J. S. Blair—907(L)
Energy of disintegration product of light mesotron, J. C. Fletcher and H. K. Forster—204(L)
Energy of neutrons from photo-neutron sources, A. O. Hanson—1794
Excitation functions, deuterons on Cu, D. Bockhop, A. C. Helmholz, S. D. Softky, J. W. Rose, and T. Breakey—1469(A)
Excitation functions for (α, n), $(\alpha, 2n)$, $(\alpha, 3n)$ reactions on indium, G. M. Temmer—1464(A)
Excitation functions of Bi, E. L. Kelly and E. Segrè—999
Excited Li^7, S. S. Hanna and D. R. Inglis—1767(L)
Gamma-radiation and nuclear pairs from $F^{19} + p$, V. K. Rasmussen, W. F. Hornyak, and T. Lauritsen—1462(A)
Gamma-ray spectrum from $F^{19} + H^1$, Gerson Goldhaber—336(A)
Gamma-rays from deuteron reactions, David E. Alburger—51

Disintegration and excitation of nucleus (continued)
Of He^3 and N^{14} by thermal neutrons, J. H. Coon and R. A. Nobles—1358
High energy deuterons from 90-Mev neutrons on C, H. Bradner—1467(A)
High energy gamma-radiation from 184-cyclotron, B. J. Moyer, H. F. York, and R. Bjorklund—1470(A)
Interaction of protons with tritium, A. Hemmendinger, G. A. Jarvis, and R. F. Taschek—1291(A); R. F. Taschek, G. A. Jarvis, A. Hemmendinger, G. G. Everhart, and H. T. Gittings—1361
Ionization chamber, $N^{14}(n, p)C^{14}$, W. Franzen, J. Halpern, and W. E. Stephens—1292(A)
Of Li by slow neutrons, J. K. Bøggild and L. Minnehagen—782
$Li(p, \gamma)$ resonance, Emmett L. Hudspeth and Charles P. Swann—1272(L)
$Li^7(p, n)$ threshold voltage, W. E. Shoupp, B. Jennings, W. Jones, and M. Garbuny—336(A)
Magnetic internal conversion coefficient, S. D. Drell—338(A)
Neutron yield from $Li^7(p, n)Be^7$, G. Freier, E. E. Lampi, and J. H. Williams—901(L)
Neutrons and gamma-radiation from $Be^9 + H^2$, J. E. Evans, C. W. Malich, and J. R. Risser—1161
Neutrons and gamma-rays from disintegration of C^{12} by deuterons, T. W. Bonner, J. E. Evans, J. C. Harris, and G. C. Phillips—1401
Neutrons from Cd, C. D. Moak and J. W. T. Dabbs—1770(L)
Neutrons from deuteron bombardment of Li^6, Ward Whaling, J. E. Evans, and T. W. Bonner—688(L)
Nuclear reaction energies, integral multiples, Enos E. Witmer—1289(A)
Particles emitted by C bombarded by neutrons, Keith Brueckner and Wilson M. Powell—1274(L), 1970(L)
Precision gamma-ray measurements on I^{131}, David A. Lind, James Brown, David Klein, David Muller, and Jesse DuMond—1633(A)
Proton energies, $K^{39,41}(d, p)K^{40,42}$, V. L. Sailor—1292(A)
P-N reactions for A and Ne, H. T. Richards and R. V. Smith—336(A)
P-N threshold for deuterium, R. V. Smith and H. T. Richards—335(A)
Proton resonances in deuteron bombardment of C, N. P. Heydenburg, D. R. Inglis, W. D. Whitehead, Jr., and E. M. Hafner—1147
Protons from B and A on bombardment by α, R. R. Roy—1775(L)
Q values, $B(\alpha p)C$, R. J. Creagan—1292(A)
Radio-isotopes in helium-ion bombardment of U, R. D. Wolfe and N. E. Ballou—527(L)
Recoils of active F^{18}, Warren Ehckrotte and Hugh Bradner—1467(A)
Secondary particles, bombardment by 90-Mev neutrons, Herbert F. York—1467(A)
Of Se^{75}, Michel Ter-Pogossian, J. Eugene Robinson, and C. Sharp Cook—995
Stars in emulsions initiated by alpha-particles, Eugene Gardner—379
Stars in emulsions initiated by deuterons, experimental, Eugene Gardner and Vincent Peterson—364
Stars in emulsions initiated by deuterons, theoretical, W. Horning and L. Baumhoff—370
Stars initiated by negative mesons, Frank L. Adelman and Stanley B. Jones—1468(A)
Survey of nuclear energy possibilities, Cecil B. Ellis—330(A)
Threshold and resonances in $C^{14}(p, n)N^{14}$, energy levels of N^{15}, W. E. Shoupp, B. Jennings, and K. H. Sun—1
Threshold for $C^{12}(d, n)N^{13}$, T. W. Bonner, J. E. Evans, and J. E. Hill—1398
Unusual cells in blood of cyclotron workers, M. Ingram and S. W. Barnes—1765(L)
Doppler effect
Broadening of gamma-ray line, V. K. Rasmussen, C. C. Lauritsen, and T. Lauritsen—199(L)
Dynamics
Linearization of non-linear systems—1334(A)

Elasticity
Compressibility of metallic Cs, R. M. Sternheimer—888(L)
Constants of copper, dissolved hydrogen, J. Marx—1626(A)
Creep and damping of polystyrene, John A. Sauer and Joseph Marin—1285(A)
Damping of single crystals, J. W. Marx and J. S. Koehler—1309(A)
Elastic losses of elastomers, H. S. Sack and R. W. Aldrich—1285(A)
Elastic waves in cubic crystals, David Lazarus—1625(A)
Kinetic concept, R. S. Barker, W. O. Seifert, and J. H. Dillon—1300(A)
Mechanical and birefringence properties, R. S. Stein, S. Krimm, and A. V. Tobolsky—1301(A)
Of Ni crystals, R. M. Bozorth, W. P. Mason, H. J. McSkimin, and J. G. Walker—1954(L)
Plane shear waves in viscoelastic media, H. T. O'Neil—928
Plastic deformation of crystals, Donald Wahl—1627(A)
Plastic deformation of filaments, Richard LaTorre and Waller George—1309(A)
Of polystyrene films, E. Merz, L. Nielsen, and R. Buchdahl—1315(A)
Residual strain energy and elastic moduli, Clarence Zener—345(A)
Rigidities of polyisobutylene and polyvinyl acetate solutions, John D. Ferry, J. N. Ashworth, and W. M. Sawyer—1284(A)
Rupture strength of benzene, J. J. Donoghue, E. Gerjuoy, and R. E. Vollrath—1456(A)
Shear elasticity and viscosity of liquids, W. P. Mason, W. O. Baker, H. J. McSkimin, and J. H. Heiss—936
Slip in single Al crystals, T. L. Wu and R. Smoluchowski—345(A); R. Smoluchowski and T. L. Wu—345(A)
Of some high polymers, R. Buchdahl, L. E. Nielsen, and Rita Levreault—1284(A)
Steady-state creep in metals, B. G. Rightmire—1627(A)
Stress and deformation, martensite transformation, Andrew W. McReynolds—1309(A)
Tensile strength of vulcanized rubber, Paul J. Flory, Norman Rabjohn, and Marcia C. Shaffer—1300(A)
Time and stress effects in rubber, J. R. Beatty and J. M. Davies—1314(A)
Transmission of pulses in rods, D. S. Hughes, W. L. Pondrom, and R. L. Mims—1552
Work-hardening at small strains, J. S. Koehler and T. H. Blewitt—1952(L)
Electrical conductivity and resistance
Bombardment conductivity of diamond, Robert R. Newton—234
Bridges between electric contacts, G. F. Hull, Jr., M. H. Cohen, and R. W. Terhune—1311(A)
Changes produced by cold-work, J. S. Koehler—106

Concentrating holes and electrons by magnetic fields, H. Suhl and W. Shockley—1617(L)
Of crystals under α-particle bombardment, A. J. Ahearn—1966(L)
Of dilute solutions near critical temperature, G. E. Owen—1303(A)
Double-surface transistor, John N. Shive—689(L)
Effect of tension, G. C. Kuczynski—1335(A)
Fermi level at surfaces of amorphous arsenic, E. Taft and L. Apker—344(A), 1181
Of Ge at low temperatures, I. Estermann, A. Foner, and J. E. Zimmerman—1631(A)
Of Ge, electric field, E. J. Ryder and W. Shockley—310(L)
Hole current in Ge transistor, Kurt Lehovec—1100(L)
Hole injection in transistor action, J. R. Haynes and W. Shockley—691(L)
Induced by electron bombardment in insulating films, L. Pensak—472
Magnetic transition curve of superconductors, Otto Halpern—1460(A)
Mechanism of conductivity, Oleg Yadoff—1334(A)
Oxide rectifier cells below room temperature, Stephen J. Angello—1310(A)
Pressure change of resistance of Te, J. Bardeen—1777(L)
Principles in transistor action, J. Bardeen and W. H. Brattain—1208
Of purified Te, Virgil E. Bottom—1310(A)
Semiconducting anisotropic crystals, V. A. Johnson—1631(A)
Of silicon and silicon alloys, G. L. Pearson and J. Bardeen—865
Of sintered and single crystals of zinc oxide, E. E. Hahn, B. R. Russell, and P. H. Miller, Jr.—1631(A)
Of sintered semiconductors, Henry H. Hausner—1310(A)
Superconductivity, causes of, D. Bohm—502

Electrodynamics (see **Electromagnetic theory**)

Electromagnetic theory (see also **Quantum electrodynamics**)
Diffraction by aperture in infinite plane, Harold Levine and Julian Schwinger—1423
Diffraction through plane screen, John W. Miles—695(L)
Electromagnetic waves guided by magnetic materials, John P. Blewett—1288(A)
Non-radiating waves, Granville A. Perkins—1947(L)
Periodic orbits in equatorial plane of magnetic dipole, Antonio Romero Juárez—137
Radiation of accelerated electrons, Julian Schwinger—1912
Relative electrodynamics, F. W. Warburton—1456(A)

Electron diffraction
Structure of ethyl alcohol and ethyl mercaptan, Marcel Rouault and Georges Gallagher—1319(A)

Electrons (see also **Positrons** and **E/m**)
Magnetic properties, John A. Eldridge—1614(L)
Polarization, Kenichi Shinohara and Norio Ryu—1762(L)
Three-photon annihilation of electron-positron pair, A. Ore and J. L. Powell—1696, 1963(L)

Electrons in metals
Existence, Bayard P. Peakes—1629(A)

Electrons, positive (see **Positrons**)

Electrons, secondary
From BaO, George W. Hees and Harold Jacobs—1312(A)
By high energy electrons, J. G. Trump and R. J. Van de Graaff—44

Electrostatics
Dust electrostatics, Wulf Kunkel—1460(A)
Electrical charge separation produced by freezing of rainwater, S. E. Reynolds and E. J. Workman—347(A)
Electrical phenomena, freezing of dilute solutions, E. J. Workman and S. E. Reynolds—347(A)

Elements
Formation of elements, nuclear stability, J. S. Smart—1379
Origin of elements, R. A. Alpher, R. C. Herman, and G. A. Gamow—332(A)
Regularity and continuity of nuclear series, William D. Harkins and Martin Popelka, Jr.—332(A)

E/m
From experiments in nuclear resonance, H. A. Thomas, R. L. Driscoll, and J. A. Hipple—992(L)

Energy states of atoms (see also **Spectra, atomic**)
Electromagnetic shift of energy levels, J. B. French and V. F. Weisskopf—1240

Equations of state
Based on generalized Fermi-Thomas theory, R. P. Feynman, N. Metropolis, and E. Teller—1561
As eigenvalue problem, Joseph W. Weinberg—338(A)
For polystyrene, R. S. Spencer and G. D. Gilmore—1300(A)

Errata
Acoustical birefringence, W. J. Price—992(L)
On application of Heisenberg's theory of *S*-matrix to problems of resonance scattering and reactions in nuclear physics, Ning Hu—1449(L)
Charged particles emitted by carbon bombarded by 90-Mev neutrons, Keith Brueckner and Wilson M. Powell—1970(L)
Cosmic-ray intensity above atmosphere, A. V. Gangnes, J. F. Jenkins, Jr., and J. A. Van Allen—892(L)
Detection of gamma-rays with thallium-activated sodium iodide crystals, Robert Hofstadter—1611(L)
Disintegration of Be^8, Arthur Hemmendinger—1267(L)
Domain interactions in theory of ferromagnetic resonance, George T. Rado—1451(L)
Line shapes in nuclear paramagnetism, G. E. Pake and E. M. Purcell—534(L)
Nuclear spins and quandupole moments of B^{10} and B^{11}, Walter Gordy, Harold Ring, and Anton B. Burg—208(L)
On numerical calculation of internal conversion in *K*-shell; the electric dipole case, B. A. Griffith and J. P. Stanley—1110(L)
Phenomenological theory of exchange currents in nuclei, R. G. Sachs—1605(L)
Scattering of particles by gas in synchrotron, Nelson M. Blachman and Ernest D. Courant—315(L)
Screening and relativistic effects on beta-spectra, C. Longmire and H. Brown—1102(L)
Second-order Stark effect of methyl chloride, Robert Karplus and A. Harry Sharbaugh—1449(L)
Significance of radioactivity of K in geophysics, T. Gráf—534(L)
Structure of ^2D terms of arc spectrum of lithium, K. W. Meissner, L. G. Mundie, and P. H. Stelson—891(L)
Study of phase transitions by means of nuclear magnetic resonance phenomena, Nelson L. Alpert—1271(L)
Thermonuclear reactions in expanding universe, R. A. Alpher, R. Herman, and G. A. Gamow—701(L)

Excitation of atoms and molecules
Bands of atmospheric CO_2, Orren C. Mohler, Robert R. McMath, and Leo Goldberg—520(L)

Excitation of atoms and molecules (continued)
Formation of metastable H atoms by electron bombardment, W. E. Lamb, Jr. and R. C. Retherford—1332(A)
Of Hg vapor by positive alkali ions, Harold E. Clark—334(A)

Field theory (see also **Quantum electrodynamics**)
Covariant Hamiltonian formulation, Norman M. Kroll—1321(A)
Generalized meson field theories, Alex E. S. Green—332(A)
Generalized Schrödinger equation, P. T. Matthews—1270(L)
Interaction of charged spin O particles with electromagnetic field, A. Pais and G. E. Uhlenbeck—1321(A)
Quantization of unitary field theory, R. J. Finkelstein—1079
Relativistic field theories, T. S. Chang—967
Films, properties of
Conductivity induced by electron bombardment, L. Pensak—472
Disorder in films of Ag, Chester R. Berry—1299(A)
Growth of evaporated LiF films, L. G. Schulz—1284(A)
Index of refraction of films of LiF, L. G. Schulz—345(A)
Properties of polystyrene films, E. Merz, L. Nielsen, and R. Buchdahl—1315(A)
Fine structure (see **Spectra**, etc., and **Hyperfine structure**)
Fission of nucleus
Alpha-particles recorded by photographic emulsions, L. Marshall—1339
Of Cs^{135}, Nathan Sugarman—1473
Closed shell effects, L. E. Glendenin—337(A)
Distribution of charge, C. D. Coryell, L. E. Glendenin, and R. R. Edwards—337(A)
Energy distribution of fragments, D. C. Brunton and G. C. Hanna—990(L), 1632(A)
Energy loss of fragments, N. O. Lassen—1762(L)
Energy release, high energy neutrons, J. Jungerman and S. C. Wright—1470(A)
Fission cross sections, photographic emulsion, Maurice M. Shapiro—1327(A)
Light-charged particle emitted, K. W. Allen and J. T. Dewan—337(A)
Limits of fission cross sections of Bi, Pb, Hg, Au, I, and W for 14-Mev neutrons, Anne N. Phillips, Louis Rosen, and R. F. Taschek—919
Long-lived Cs isotope, Nathan Sugarman—1287(A)
Radio-isotopes in helium-ion bombardment of U, R. D. Wolfe and N. E. Ballou—527(L)
Stopping of fragments in gases, E. C. Campbell, W. M. Good, and W. A. Strauser—1292(A)
Of thorium with alpha-particles, Amos S. Newton—17
Thresholds for neutrons fission in Th and U, W. E. Shoupp and J. E. Hill——785
Fluid dynamics (see also **Hydrodynamics** and **Aerodynamics**)
Cavitation, water-entry of sphere, Albert May, J. H. McMillen, and J. C. Woodhull—1313(A)
Continuum theories, C. Truesdell—1293(A)
Converging viscous flow, S. A. Schaaf and P. L. Chambre—1293(A)
Correlation tensors in compressible fluids, M. Z. Krzywoblocki—1293(A)
Depolymerization by irradiation, role of cavitation, Alfred Weissler—1313(A)
Flow past an ellipsoid, M. M. Klein and W. Perl—1293(A)
Gas bubbles as cavitation nuclei, F. G. Blake, Jr.—1313(A)
Non-linear theories, Peter G. Bergmann—680
Stability of flame fronts, Harvey Einbinder—1313(A)
Transonic flows, Alexander Weinstein—1293(A)
Fluorescence
Of anthracene, Louise Roth—983(L)
Intrinsic efficiency, electron bombardment, R. L. Longini—335(A)
Friction
Damping of metals, soluble impurities, J. S. Koehler—1626(A)
Internal friction and slip, R. Smoluchowski and T. L. Wu—345(A)
Internal friction, measurement, R. Kamel—1606(L); Herbert I. Fusfeld—1626(A)
Longitudinal vibration, non-linear internal friction, A. S. Nowick—1626(A)
Solid solubility effect, Kwai Umeda and Yoshihiro Nakano—1621(L)

Geophysics
Magnetic field of rotating metallic body, A. E. Benfield—211(L)
Of K^{40}, age of earth, erratum, T. Gráf—534(L)
Rock magnetism, earth's magnetic history, O. W. Torreson, Thomas Murphy, and John W. Graham—208(L)
Gyromagnetization (see **Magnetic properties**)

Hall effect
In alloys containing Ge and Sb^{124}, G. L. Pearson, J. D. Struthers, and H. C. Theuerer—344(A)
Concentrating holes and electrons by magnetic fields, H. Suhl and W. Shockley—1617(L)
Of purified Te, Virgil E. Bottom—1310(A)
Semiconducting anisotropic crystals, V. A. Johnson—1631(A)
In Si and alloys containing B and P, G. L. Pearson and J. Bardeen—865
High voltage tubes and machines (see **Methods and instruments**)
Hydrodynamics
Isotropic turbulence, S. Chandrasekhar—896(L), 1454(L)
Hyperfine structure (see also **Nuclear moments and spin**)
g_J values of alkali atoms, P. Kusch and H. Taub—1477
Ground term of hydrogen, G. Breit and R. E. Meyerott—1447(L)
Of tritium, Edward B. Nelson and John E. Nafe—1194

Instruments (see **Methods and instruments**)
Ionization
Range-energy curves for alpha-particle, William P. Jesse and Sadauskis—1110(L)
Ions, mobility
Of polyatomic ions, P. B. Weisz and W. P. Kern—899(L)
Isobars
Masses of $B_2{}^{11}D_6$ and O_2, Francis J. Norton—1957(L)
Neutron-hydrogen mass difference, R. F. Taschek, G. A. Jarvis, H. V. Argo, and A. Hemmendinger—1268(L)
Stability of isobaric pair, M. Gurevitch—767
Isomers, molecular
Isomerization by electron impact, Richard E. Honig—1319(A)
Isomers, nuclear (see also **Nuclear structure** and **Radioactivity**)

Bremsstrahlung, nuclear isomerism of In^{115}, Walter C. Miller and Bernard Waldman—329(A), 425
Of Cd^{115}, R. W. Hayward and A. C. Helmholz—1469(A)
Classification of transitions, P. Axel and S. M. Dancoff—1297(A)
With half-lives between millisecond and second, J. E. R. Holmes, J. Y. Mei, and R. S. Turgel—889(L)
Of Se produced by x-rays, D. N. Gideon, W. C. Miller, and B. Waldman—329(A)
Shell structure and isomerism, Eugene Feenberg—320(L)
Short-lived, F. K. McGowan, S. DeBenedetti, and J. E. Francis, Jr.—1761(L)

Isotopes
Abundance measurements on Ge, R. F. Hibbs, J. W. Redmond, H. R. Gwinn, and W. D. Harman—533(L)
Of Dy, Mark G. Inghram, Richard J. Hayden, and David C. Hess, Jr.—693(L)
Electrolytic separation, Dwight A. Hutchison—1303(A)
Formation of U^{233}, Amos S. Newton—209(L)
He^3 abundance, J. H. Coon—1355
He^3 and origin of terrestrial He, P. Morrison and D. B. Beard—1332(A)
He^3-He^4 equilibrium below the λ-point, C. T. Lane, Henry A. Fairbank, L. T. Aldrich, and Alfred O. Nier—46
Isotopic weights of Cr, Fe, Zn, and Br, K. Ogata—200(L)
Mass and abundance of O^{17} and S^{36}, W. Low and C. H. Townes—529(L); C. H. Townes and W. Low—1318(A)
Mass difference between A^{40} and Ca^{40}, Vance L. Sailor—1836
Mass difference of *n*-*p*, A. V. Tollestrup, F. A. Jenkins, W. A. Fowler, and C. C. Lauritsen—1947(L)
Mass of N_7^{16} by interpolation, Tibor Z. Szelenyi—1105(L)
Masses of nuclei, Ne to Cl, H. T. Motz and R. F. Humphreys—1289(A)
New isotope of potassium, Roy Overstreet, Louis Jacobson, and P. R. Stout—231
Packing fractions of Ni, A. E. Shaw—331(A); 1011
Physically and chemically determined weights, discrepancies, J. R. White and J. H. Buck—1519(L)
Of Pt, Henry E. Duckworth, Robert F. Black, and Richard F. Woodcock—1438(L)
Possible rare stable isotopes, Henry E. Duckworth—1438(L)
Regularity and continuity of nuclear series, William D. Harkins and Martin Popelka, Jr.—332(A)
Of Rb, Frederick L. Reynolds, D. G. Karraker, and D. H. Templeton—313(L)
Search for Pd^{100}, W^{178}, and Pb^{202}, Henry E. Duckworth, Robert F. Black, and Richard F. Woodcock—1616(L)
Separation of A^{36} by thermal diffusion, James O. Buchanan—1332(A)
Separation of gases by flow through long tube, R. D. Present and A. J. deBethune—1050
Of Yb, Richard J. Hayden, David C. Hess, Jr., and Mark G. Inghram—322(L)

Kinetic theory
Transport phenomena in Bose Einstein gas, William Band—339(A), 1937

Liquids (see also **Hydrodynamics**)
Condensation of pure He^3, vapor pressure and critical point, S. G. Sydoriak, E. R. Grilly, and E. F. Hammel—303
Critical point fluctuations, Martin J. Klein and L. Tisza—1303(A)
Density of liquid He^3, E. R. Grilly, E. F. Hammel, and S. G. Sydoriak—1103(L)
Density of water, temperature, George Antonoff and Robert J. Conan—1303(A)
Flow of isotopically pure liquid He^3 and He^4, Darrell W. Osborne, Bernard Weinstock, and Bernard M. Abraham—988(L)
Fountain effect in helium II, R. J. Harrison—1311(A)
He^3-He^4 equilibrium below λ-point, C. T. Lane, Henry A. Fairbank, L. T. Aldrich, and Alfred O. Nier—46
Pulsed second sound in He II, J. R. Pellam—1183
Rupture strength of benzene, J. J. Donoghue, E. Gerjuoy, and R. E. Vollrath—1456(A)
Second viscosity of liquids, L. N. Liebermann—1415
Statistical theory, George Jaffé—184
Theory of superfluidity, L. Landau—884(L); L. Tisza—885(L)
Undercooling of liquid metals, Ben H. Alexander—343(A)
Vapor-liquid equilibrium of He^3 in He^4, K. W. Taconis, J. J. M. Beenakker, Alfred O. Nier, and L. T. Aldrich—1966(L)
Viscosity of He_3 and He_4, D. ter Haar and H. Wergeland—886(L); H. Wergeland and D. ter Haar—1310(A)

Magnetic properties (see also **Nuclear moments and spin**)
Copper-manganese-indium, ferromagnetic alloys, Robert R. Grinstead and Don M. Yost—984(L)
Dielectric constant of ferromagnetic ferrite, Frank G. Brockman, P. H. Dowling, and Walter G. Steneck—1440(L)
Dirac's theory of magnetic poles, H. A. Wilson—309(L); M. N. Saha—1968(L)
Domain interactions, George T. Rado—893(L); 1451(L); William Fuller Brown, Jr.—1959(L)
Domain patterns on crystals of silicon iron, H. J. Williams, R. M. Bozorth, and W. Shockley—155
Domain structure in iron, H. J. Williams and W. Shockley—178
Of electrons, John A. Eldridge—1614(L)
Existence of single poles, Felix Ehrenhaft—1334(A)
Of ferrite, Frank G. Brockman, P. H. Dowling, and Walter G. Steneck—1298(A); P. H. Dowling and Frank G. Brockman—1298(A)
Ferroelectric Barkhausen effect in barium titanate, R. R. Newton, A. J. Ahearn, and K. G. McKay—103
Ferroelectric crystas, B. T. Matthias—1771(L)
Ferromagnetic resonance, J. M. Richardson—1630(A)
Ferromagnetic resonance absorption, Heusler alloy, W. A. Yager and F. R. Merritt—318(L)
Ferromagnetic resonance absorption, Supermalloy, W. A. Yager—316(L)
Ferromagnetic resonance in iron crystal, Arthur F. Kip and Robert D. Arnold—1556
Ferromagnetic resonance in iron oxides, G. E. Crouch, Jr.—525(L)
Ferromagnetism at high frequencies, M. H. Johnson and G. T. Rado—841
Gyromagnetic ratios of Be^9, Rb^{85}, Rb^{87}, and Cs^{133}, John R. Zimmerman and Dudley Williams—699(L)
Irreversible effects of stress, William Fuller Brown, Jr.—147
Magnetic field of rotating metallic body, A. E. Benfield—211(L)
Magnetic refraction of neutrons at domain boundaries, D. J. Hughes, M. T. Burgy, R. B. Heller, and J. W. Wallace—344(A)

Magnetic properties (continued)
Magnetostriction and order-disorder, J. E. Goldman and R. Smoluchowski—140, 310(L), 1299(A); R. Smoluchowski and J. E. Goldman—1299(A)
Model of ferromagnet, M. Kac and T. H. Berlin—1298(A)
Nuclear magnetic resonance in weak fields, Richard M. Brown and E. M. Purcell—1262(L)
Paramagnetic absorption in crystals of copper sulfate pentahydrate, John Wheatley and David Halliday—1412
Paramagnetic resonance absorption in sulfates of copper, Robert D. Arnold and Arthur F. Kip—1199
Resonance absorption in magnetite, L. R. Bickford, Jr.—1298(A)
Susceptibility of BeO, Clyde A. Hutchison, Jr.—465
Susceptibility of Zn at low temperatures, S. G. Sydoriak and J. E. Robinson—118
Three-dimensional ferromagnet, D. ter Haar and B. Martin—1298(A)
Magnetostriction (see **Magnetic properties**)
Mass defects (see **Isotopes** and **Isobars**)
Mass ratios (see **Isotopes** and **Isobars**)
Mass spectroscopy
Double charged ions, hydrocarbons, Fred L. Mohler, Evelyn G. Bloom, E. J. Wells, Jr., J. H. Lengel, and C. Edward Wise—1332(A)
Study of copolymer pyrolyses, L. A. Wall—1331(A)
Time of flight mass spectrometer, J. A. Hipple and H. A. Thomas—1616(L)
Mechanics, quantum—general
Central field of force from phase shifts, V. Bargmann—301
Determination of potential from asymptotic phase, Norman Levinson—1445(L)
Dirac's theory of magnetic poles, H. A. Wilson—309(L)
Ferromagnetic resonance, J. M. Richardson—1630(A)
Heisenberg's theory of S-matrix, Ning Hu—1449(L)
Interaction by boundary conditions, M. Moshinsky and E. P. Wigner—1322(A)
Mesic charge, Taisuke Okayama—308(L)
Perturbation theory by variation iteration method, W. Kohn—1322(A)
Problems involving permutation degeneracy, E. M. Corson—1266(L)
Self energy of bound electron, Norman M. Kroll and Willis E. Lamb, Jr.—388
Solution of differential equation, Rudolph E. Langer—792
Spectrum of wave equation, intuitive approach, Philip Hartman and Aurel Wintner—1452(L)
Two component wave equations, Herbert Jehle—1609(L)
Wave equation with small quantum numbers, Rudolph E. Langer—1573
Wave function of electron in field of atom, Su-Shu Huang—980(L)
Mechanics, quantum—nuclear
Effective range of nuclear forces, F. C. Barker and R. E. Peierls—312(L)
Electron-neutrino correlation in heavy elements, M. E. Rose—1444(L)
Interaction Hamiltonian, George J. Yevick—1450(L)
Mechanics, statistical
Charged particles in magnetic field, M. F. M. Osborne—339(A)
Equation of state as eigenvalue problem, Joseph W. Weinberg—338(A)
Equilibrium in Ehrenfest's "wind-tree" model, A. J. F. Siegert—1322(A)
New equation of state, E. M. Corson—1264(L)
Transport phenomena in Bose Einstein gas, William Band—1937
Verification of statistics of He^3, D. ter Haar—1444(L)
Mesons (see also **Cosmic radiation**)
Absorption of pi-mesons in H_2, A. S. Wightman, R. E. Marshak, and J. A. Wheeler—1306(A)
Capture of negative mesotrons, Aaron J. Seriff, Robert B. Leighton, and Carl D. Anderson—1466(A)
Čerenkov radiation effect, W. W. Wada—981(L)
Cloud-chamber photographs of artificial mesons, Walter Hartsough, Evans Hayward, and Wilson M. Powell—905(L)
Coupling of μ-mesons with nucleons, J. Tiomno and John A. Wheeler—1306(A)
Decay products, mass of mesotron, Carl D. Anderson, Robert B. Leighton, and Aaron J. Seriff—1466(A)
Decay products of μ-meson, E. P. Hincks and B. Pontecorvo—341(A)
Decay time of π-meson, R. Latter and R. F. Christy—1459(A)
Disintegration of mesons, R. W. Thompson—1315(A)
Emission of radiation in disintegration, Daniel B. Feer—731
Energy of decay electrons, Robert B. Leighton, Carl D. Anderson, and Aaron J. Seriff—1466(A)
Energy spectrum of decay particles, mass and spin, Robert B. Leighton, Carl D. Anderson, and Aaron J. Seriff—1432
Gamma-rays (1–5 Mev) from stopped negative mesons, W. Y. Chang—1315(A)
Generalized meson field theories, Alex E. S. Green—332(A)
Interaction of fields, George J. Yevick—1305(A)
Interaction with nucleons, T. D. Lee, M. Rosenbluth, and C. N. Yang—905(L)
Magnetic moment of proton, H. Taub and P. Kusch—1481
Mass and life-time, J. Barnóthy—1458(A)
Mass in cosmic rays, J. Gordon Retallack and Robert B. Brode—1717
Mass measurements, Robert B. Brode—904(L); A. S. Bishop—1468(A); Eugene Gardner—1468(A); C. M. G. Lattes—1468(A)
Masses, Enos E. Witmer—348(A)
Mesic charge, Taisuke Okayama—308(L)
Meson fields, motion of spinning particle, R. C. Majumdar and S. Gupta—1788
Meson-nucleon coupling, K. M. Case—1306(A)
Mesons π and μ, R. E. Marshak—700(L)
Mesons stopping in aluminum foils, R. L. Cool, E. C. Fowler, J. C. Street, W. B. Fowler, and R. D. Sard—1275(L)
Nuclear capture of μ-mesons, Marshall N. Rosenbluth—532(L)
Nucleon scattering, virtual meson emission, Ning Hu 1305(A)
π-mesons in nucleon collisions, L. L. Foldy and R. E. Marshak—1307(A), 1493
Polarization of vector-mesons, Gregor Wentzel—1810
Positive mesons produced by cyclotron, John Burfening, Eugene Gardner, and C. M. G. Lattes—382
Production by γ-rays near threshold, L. L. Foldy—1633(A)
Pseudoscalar meson field, Herbert Goldstein and Herman Feshbach—1306(A)
Radiation accompanying meson creation, L. I. Schiff—1459(A)
Range of electrons in meson decay, J. Steinberger—1136

Range spectrum, Lawrence S. Germain—1458(A)
Ratio of positive and negative mesons, Walter H. Barkas—1467(A)
Spin of π- and μ-mesons, John A. Wheeler and J. Tiomno—1306(A)
Spins of mesons, R. Serber—1459(A)
Stars initiated by negative mesons, Frank L. Adelman and Stanley B. Jones—1468(A)
Stimulated decay of mesons, W. H. Furry and James N. Snyder—1265(L)
Symmetrical theory of nuclear forces, Ta-You Wu and H. M. Foley—1305(A), 1681
Theory of nuclear forces, Gentaro Araki—1101(L)
Threshold energy for production, Walter H. Barkas—1109(L)
Yield of negative mesons, Stanley B. Jones and R. S. White—1468(A)

Metals (see **Crystalline state**)

Meteorology
Atmospheric ammonia, M. V. Migeotte and R. M. Chapman—1611(L)
Atmospheric methane content, Arthur Adel—322(L)
CO in atmosphere, Arthur Adel—1766(L)
Charge generation in thunderclouds, Seville Chapman—1333(A)
Dust electrostatics, Wulf Kunkel—1460(A)
Electrical charge separation produced by freezing of rainwater, S. E. Reynolds and E. J. Workman—347(A)
Ozonosphere temperatures, Arthur Adel—1333(A)

Methods and instruments
Absolute neutron intensities, Roger W. Paine, Jr., John E. Dacey, and Clark Goodman—1301(A)
Acoustic measurements of polymer physical properties, J. W. Ballou and J. C. Smith—1284(A)
Alpha-scintillation counter, J. D. Graves and J. P. Dyson—1461(A)
Analog computers for functions of many variables, Eugene W. Pike and Thomas R. Silverberg—1333(A)
Arc-chord differences, W. T. Scott—1763(L)
Average optical transmission through plants, Edward E. Miller—335(A)
Betatron injection, Leverett Davis, Jr. and R. V. Langmuir—1457(A)
Betatron model, D. W. Kerst, G. D. Adams, H. W. Koch, and C. S. Robinson—330(A)
Biochemical reactions, rate of, C. A. Tobias—1460(A)
Bremsstrahlung, nuclear isomerism of indium, Walter C. Miller and Bernard Waldman—329(A), 425
Brookhaven proton synchroton, M. G. White—1288(A)
Cadmium sulfide as crystal counter, G. J. Goldsmith and K. Lark-Horovitz—526(L)
Calibration of emulsions for low energy electrons, L. Cranberg and J. Halpern—1328(A)
Camera for p-p scattering, Wolfgang K. H. Panofsky and Franklin Fillmore—1465(A)
Canonical reduction of quadratic forms, R. G. Helsel—1088
Capacitance-conductance bridge, Robert H. Cole and Paul M. Gross, Jr.—1312(A)
Cavity microwave spectroscope, I. R. Weingarten and G. E. Kimball—1325(A)
Chi square test for Geiger tubes, A. B. Willoughby—1461(A)
Coefficient of self-diffusion, G. C. Kuczynski—1309(A)
Coincidence measurement of neutron energy, Donald C. Worth—903(L)
Concentration of U isotopes, L. E. Burkhart, George Stukenbroeker, and Sam Adams—83
Conduction under α-particle bombardment, A. J. Ahearn—1966(L)
Conductivity of diamond, space charge effects, Robert R. Newton—234
Converter thickness corrections, gamma-ray spectroscopy, T. Lauritsen and W. F. Hornyak—1462(A)
Cosmotron accelerating unit, Martin Plotkin and John P. Blewett—1288(A)
Cosmotron magnet model, G. K. Green, H. S. Snyder, and L. W. Smith—1289(A)
Counting efficiency of scintillation counters, R. H. Davis and J. D. Graves—1461(A)
Crystal structure by neutron diffraction, E. O. Wollan, W. L. Davidson, and C. G. Shull—1348
Current pulse generator, R. I. Strough and E. F. Shrader—1628(A)
Delayed emission of electrons in counter, M. L. Wiedenbeck and H. R. Crane—1268(L)
Density field in Mach reflection, W. Bleakney, D. K. Weimer, and C. H. Fletcher—1294(A)
Deposits of Po, M. Haissinsky, H. Faraggi, A. Coche, and P. Avignon—1963(L)
Detection of gamma-rays with crystals, Robert Hofstadter—796, 1611(L)
Determination of molecular weights of polymers, W. M. Cashin and P. Debye—1307(A)
Discharge of counter at voltages above plateau, H. R. Crane—985(L)
Distribution of arc-chord differences in particle tracks, W. T. Scott—1327(A)
Double focusing mass spectrometer, Alfred O. Nier, T. R. Roberts, and E. G. Franklin—346(A)
Double-surface transistor, John N. Shive—689(L)
Eddy currents, field of cosmotron magnet, M. Hildred Blewett—1288(A)
Electromagnetic waves guided by magnetic materials, John P. Blewett—1288(A)
Electron mobility by pulse techniques, F. F. Rieke and Daryl Errett—346(A)
Electron multiplication in crystals, Frederick Seitz—1283(A)
Electron tracks in emulsions, R. H. Herz—478
Emission rate of beta-rays, R. K. Clark and G. Failla—328(A)
Equilibrium radius in field-biased betatron, E. C. Gregg, Jr.—1633(A)
Experimental facilities, Brookhaven nuclear reactor, Clarke Williams—1289(A)
Ferromagnetism at high frequencies, M. H. Johnson and G. T. Rado—841
Fission cross sections, photographic emulsion, Maurice M. Shapiro—1327(A)
Fringing field corrections for magnetic lenses, Kenneth T. Bainbridge—216(A)
Gas in cathode coating assemblies, Bernard Wolk and Harold Jacobs—1312(A)
Grain density in tracks of heavy particles, M. Blau—279, 1327(A)
Helium liquefier, J. G. Daunt, C. V. Herr, and A. A. Silvidi—1113(A)
High energy protons, anthracene scintillation counters, L. Wouters—1470(A)
High intensity molecular beam source, Jerry Grey and Arthur Kantrowitz—1331(A)
High multiplication proportional counters, G. C. Hanna, D. H. W. Kirkwood, and B. Pontecorvo—985(L)
High pressure cloud chamber, G. E. Valley and J. A. Vitale—1328(A)
Hole current in Ge transistor, Kurt Lehovec—1100(L)
Hole injection in transistor action, J. R. Haynes and W. Shockley—691(L)

Methods and instruments (continued)
Hot wire anemometer, turbulence, F. N. Frenkiel—1263(L); Stanley Corrsin and Leslie S. G. Kovasznay—1954(L)
Infra-red transmission cell, H. O. McMahon, R. M. Hainer, and Gilbert W. King—1320(A)
Injection of ions in bevatron, R. L. Gluckstern and Lloyd Smith—1467(A)
Internal friction, rapid measurement, Herbert I. Fusfeld—1626(A)
Ionosphere probe, A. Reifman and W. G. Dow—131¹(A)
Life tests on self-quenching tubes, F. W. Brown, III, P. J. Harris, and A. L. Klein—1461(A)
Light scattering photometer, B. A. Brice—1307(A)
Lithium borate emulsions as neutron detectors, Herman Yagoda and Nathan Kaplan—1328(A)
Loss of ions in magnetic analyzer, R. M. Reese and J. A. Hipple—1332(A)
Low temperature laboratory, general facilities, M. D. Fiske, W. DeSorbo, F. H. Horn, and J. F. Youngblood—1311(A)
Low temperature laboratory, liquefaction, F. H. Horn, W. DeSorbo, M. D. Fiske, and J. F. Youngblood—1311(A)
Low temperature laboratory, power facilities, J. F. Youngblood, W. DeSorbo, M. D. Fiske, and F. H. Horn—1311(A)
Mach-Zehnder interferometer, Ernst H. Winkler—1314(A)
Magnetic hysteresis loops of small specimens, E. C. Crittenden, Jr., and R. I. Strough—1630(A)
Magnetic lens, Hilding Slätis and Kai Siegbahn—1955(L)
Magnetic lens spectrometer, gamma-radiation from Zn^{65} and Co^{60}, Erling N. Jensen, L. Jackson Laslett, and William V. Pratt—458
Magnetic spectrometer, double focusing, E. S. Rosenblum—1628(A)
Mass spectrometer determination of half-life, J. Macnamara, C. B. Collins, and H. G. Thode—532(L)
Mechanical properties of polymer liquids, W. P. Mason, W. O. Baker, H. J. McSkimin, and J. H. Heiss—1285(A)
Microwave electron accelerator, B. L. Miller and M. F. Amsterdam—1325(A)
Microwave electron multiplier, M. H. Greenblatt—1324(A)
Mobility of polyatomic ions, P. B. Weisz and W. P. Kern—899(L)
Molecular beam magnetic resonance, Norman F. Ramsey—1326(A)
Molecular weight measurements, F. W. Billmeyer, Jr. and W. H. Stockmayer—1307(A)
Naphthalene and anthracene scintillation counters, effects of temperature, G. E. Koch and J. D. Graves—1461(A)
Naphthalene and polystyrene counters, William J. MacIntyre—1290(A)
Naphthalene scintillation counter, R. S. Claassen and R. W. Boom—331(A)
Neutron source, R. F. Taschek, G. A. Jarvis, A. Hemmendinger, G. G. Everhart, and H. T. Gittings—1361
Noise spectrum analyzer, B. R. Russell, R. Dickson, and P. H. Miller, Jr.—1628(A)
Note on Rochester cyclotron, S. W. Barnes, A. F. Clark, G. B. Collins, C. L. Oxley, R. L. McCreary, J. B. Platt, and S. N. VanVoorhees—983(L)
Nuclear reactor at Brookhaven, Lyle B. Brost—330(A)
Nuclear shielding studies, John E. Dacey, Roger W. Paine, Jr., and Clark Goodman—1301(A)
Nuclear-track emulsions, processing of, M. J. Wilson and W. Vanselow—1144
Nylon films, J. Richards, J. Brown, F. Felber, and D. Saxon—331(A)
Orbit at injection in betatron, F. F. Heymann—1951(L)
Organic phosphors for scintillation counters, John W. Irvine, Jr., and Raymond C. Sangster—1460(A)
Parallel plate spark counter, Leon Madansky and R. W. Pidd—346(A); R. W. Pidd and Leon Madansky—1175
Particle energies, scintillation counters, G. F. J. Garlick and R. A. Fatehally—1446(L)
Perturbation theory by variation iteration method, W. Kohn—1322(A)
Photographic emulsions containing D_2O, Gerson Goldhaber—336(A)
Photographic neutron detector, Thomas H. Johnson—1301(A)
Photometry on tracks in emulsion, Pierre Demers and Roger Mathieu—1327(A)
Piezoelectric constants of alpha- and beta-quartz, Richard K. Cook and Pearl G. Weissler—1283(A)
Plastic deformation of filaments, Richard LaTorre and Waller George—1309(A)
Power input of x-ray tubes, cooling, A. I. Berman—1457(A)
Pretreatment of nuclear emulsions, Herman Yagoda and Nathan Kaplan—339(A)
Production of nuclear polarization, M. E. Rose—213(L)
Proportional counters, low energy radiations, G. C. Hanna, B. Pontecorvo, and D. H. W. Kirkwood—330(A)
Proton moment in absolute units, Harold A. Thomas, Raymond L. Driscoll, and John A. Hipple—902(L)
Proton-proton scattering, proportional counters, B. Cork, L. Johnston, and C. Richman—1465(A)
Proton spectrograph, magnetic, Sylvan Rubin—1459(A)
Proton spectrometer, E. M. Hafner, W. F. Donoghue, and H. Snyder—331(A)
Pulse method for nuclear magnetic resonance, Henry C. Torrey—1326(A)
Pulsed electron beam for high speed photography, L. B. Snoddy and J. W. Beams—1324(A)
Radiation field of 184-cyclotron, W. K. Benson, Jr., R. L. Mather, B. J. Moyer, and Joseph Yater—1470(A)
Reaction cross sections by using enriched Mo, D. N. Kundu and M. L. Pool—336(A)
Reaction $T^3(d, n)He^4$ as neutron source, R. F. Taschek, A. Hemmendinger, and G. A. Jarvis—1464(A)
Recording microphotometer, P. Rosenblum and A. de Bretteville, Jr.—1305(A)
Schlieren method, analysis of, H. Jerome Shafer—1313(A)
Scintillation counters, Hartmut Kallmann—623
Scintillation counters, pulse size, R. Hofstadter, J. C. D. Milton, and J. A. McIntyre—1290(A)
Scintillation counters, sensitivities of organic compounds, H. T. Gittings, R. F. Taschek, A. R. Ronzio, E. Jones, and W. J. Masilun—205(L)
Scintillation counters, spectra of phosphors, J. C. D. Milton and R. Hofstadter—1289(A)
Scintillation counting with chrysene, Edwin J. Schillinger, Jr., Bernard Waldman, and Walter C. Miller—900(L)
Scintillations in calcium fluoride crystals, W. J. MacIntyre—1439(L)
Scintillations in NaI crystals, W. C. Elmore and R. Hofstadter—203(L)

Search coils combining loops and solenoids, Milan W. Garrett—1297(A)
Sensitivity of nuclear emulsion tracks to specific ionization, N. W. Curtis and L. S. Osborne—1327(A)
Sensitivity of x-ray films, Herman Hoerlin—1304(A)
Separation of gases by flow through long tube, R. D. Present and A. J. deBethune—1050
Shielding in concrete, Victor Delano and Clark Goodman—1301(A)
Shock tube, transient gas flow, C. H. Fletcher, D. K. Weimer, and W. Bleakney—1294(A)
Short half-lives of radioactive elements, E. Segrè and C. E. Wiegand—39
Short-lived isomers, F. K. McGowan, S. DeBenedetti, and J. E. Francis, Jr.—1761(L)
Single crystal of scheelite, $CaWO_4$, S. Zerfoss, L. R. Johnson, and O. Imber—320(L)
Sintering of metallic particles, G. C. Kuczynski—344(A)
Slit-width adjuster for infra-red spectrometer, H. O. McMahon, Gilbert W. King, and R. M. Hainer—1459(A)
Slow neutron counter, K. A. Yamakawa—1774(L)
Small periodic displacements, Thaddeus Niemiec—215(A)
Space-charge amplification effects, V. A. Bailey—1104(L)
Stopping powers for alpha-particles of 15 to 37 Mev, E. L. Kelly—1006
Supersonic wind tunnel, George Rudinger—1948(L)
Telemetering, W. G. Stroud, J. R. Winckler, and J. Schenck—1316(A)
Thermomagnetic generator, L. Brillouin and H. P. Iskenderian—1325(A)
Time of flight mass spectrometer, J. A. Hipple and H. A. Thomas—1616(L)
Transistor action, J. Bardeen and W. H. Brattain—1208
Turbulence with hot-wire anemometer, F. N. Frenkiel 1314(A)
Waveforms, Geiger tube, G. G. Kelley, W. H. Jordan, and P. R. Bell—1290(A)

Microwaves (see **Electromagnetic theory** and **Spectra, microwave**)

Mobility of ions (see **Ions, mobility**)

Molecular structure and constants (see also **Spectra, molecular,** etc.)
Bands of atmospheric CO_2, Orren C. Mohler, Robert R. McMath, and Leo Goldberg—520(L)
Centrifugal stretching, W. S. Benedict—1317(A)
Force constants for CBr_3H, CBr_3D, and CBr_4, Arnold G. Meister—333(A)
Forces between ammonia molecules, Vernon Myers—1620(L)
Molecular force constants, E. Bright Wilson, Jr.—1317(A)
One-electron states of diatomic molecules, Henry A. Erikson and E. L. Hill—29
Quadrupole moments and molecular rotation, first-order coupling, J. K. Bragg and S. Golden—735
Structure of ethyl alcohol and ethyl mercaptan, Marcel Rouault and Georges Gallagher—1319(A)
Symmetry coordinates in molecules, William J. Taylor—1283(A)
Thermodynamic properties of diiodoacetylene, Joseph S. Ziomek and Forrest F. Cleveland—334(A)
Torsion vibrational states of CH_3CF_3, B. P. Dailey, H. Minden, and R. G. Shulman—1319(A)

Moments, of particles (see also **Nuclear moments and spin**)

Neutrino (see also **Radioactivity; Scattering of electrons, neutrons, and ions**)
Electron-neutrino angular correlation, beta-decay of He^6, James J. Allen, H. R. Paneth, and A. H. Morrish—570
H^3 and mass of neutrino, W. A. Bowers and Nathan Rosen—523(L)
From P 32, Chalmers W. Sherwin—1799

Neutrons
Absolute intensities, Roger W. Paine, Jr., John E. Dacey, and Clark Goodman—1301(A)
Absorption by rhodium, Robert R. Meijer—773
From $Be^9(d, n)B^{10}$, J. W. Butler, J. E. Evans, C. W. Malich, and J. R. Risser—1291(A)
Delayed emitter, N^{14}, Luis W. Alvarez—1127; K. H. Sun, B. Jennings, W. E. Shoupp, and A. Allen—1302(A)
Depolarization during diffusion, Otto Halpern—1633(A)
From deuteron bombardment of Li^6, Ward Whating, J. E. Evans, and T. W. Bonner—688(L)
Double refraction and polarization of neutrons, Otto Halpern—343(A)
Energy of neutrons from photo-neutron sources, A. O. Hanson—1794
Energy spectrum of delayed neutrons from O^{17}, Evans Hayward—917
From γ-rays Cd, C. D. Moak and J. W. T. Dabbs—1770(L)
Interaction of protons with tritium, A. Hemmendinger, G. A. Jarvis, and R. F. Taschek—1291(A)
Lithium borate emulsions as neutron detectors, Herman Yagoda and Nathan Kaplan—1328(A)
Magnetic refraction at domain boundaries, D. J. Hughes, M. T. Burgy, R. B. Heller, and J. W. Wallace—344(A); 565
Neutron energies, coincidence measurement, D. C. Worth—1303(A)
Neutrons from $Be + p$, P. C. Gugelot—1291(A)
Photographic neutron detector, Thomas H. Johnson—1301(A)
Polarization of d-d neutrons, Lincoln Wolfenstein—342(A)
Production by cosmic rays, A. R. Tobey—894(L)
Space distribution of slow neutrons, G. C. Wick—738
Spin dependence of slow neutron scattering by deuterons, E. Fermi and L. Marshall—578
Total reflection on Co, Morton Hamermesh—1766(L)
Yield from $Li^7(p, n)Be^7$, G. Freier, E. E. Lampi, and J. H. Williams—901(L)

Neutron diffraction
By gases, N. Z. Alcock and D. G. Hurst—1609(L)
By liquid D_2O, S. J. Czyzak and A. Wattenberg—1634(A)
Order-disorder in alloys, C. G. Shull and Sidney Siegel—1008

Nuclear moments and spin (see also **Hyperfine structure**)
Of Be^9, W. C. Dickinson and T. F. Wimett—1769(L)
Of B^{10} and B^{11}, Walter Gordy, Harold Ring, and Anton B. Burg—208(L); 1325(A)
Charge density and magnetic moments, Murray Slotnick and Walter Heitler—1645
Fine structure constant, H. A. Bethe and C. Longmire—306
Fin structure of proton magnetic resonance, N. Bloembergen—1326(A)
Gyromagnetic rations of Be^9, Rb^{85}, Rb^{87}, and Cs^{133}, John R. Zimmerman and Dudley Williams—699(L)
Magnetic moment of Al^{27}, John R. Zimmerman and Dudley Williams—198(L)

Nuclear moments and spin (continued)
Magnetic moment of proton, H. Taub and P. Kusch—1326(A)
Magnetic moment of Tl^{203}, W. C. Proctor—522(L)
Magnetic moments of C^{13}, F^{19}, Tl^{203}, and Tl^{205}, H. L. Poss—600
Magnetic moments of H^1 and H^2, E. C. Levinthal—1464(A)
Magnetic moments of nucleons, J. M. Luttinger—309(L)
Moments as integral multiples of natural unit, Enos E. Witmer—349(A)
Nuclear magnetic resonance in weak fields, Richard M. Brown and E. M. Purcell—1262(L)
Of nucleons in meson theory, J. M. Luttinger—1277(L)
Phase transitions, magnetic resonance phenomena, Nelson L. Alpert—398, 1271(L)
Proton moment in absolute units, Harold A. Thomas, Raymond L. Driscoll, and John A. Hipple—902(L)
Quadrupole moment of Li^6, P. Kusch—887(L)
Resonance frequencies, F. Bitter—1326(A)
Of Ag, M. F. Crawford, A. L. Schawlow, W. M. Gray, and F. M. Kelly—1112(L)
Spins, moments, and shells, L. W. Nordheim—1297(A)
Of tritium, Edward B. Nelson and John E. Nafe—1194
Nuclear structure (see also **Disintegration of nucleus** and **Radioactivity**)
Absolute voltage determination of nuclear reactions, R. G. Herb, S. C. Snowdon, and O. Sala—246
Of Al^{28} and Mg^{25}, E. C. Pollard, V. L. Sailor, and L. D. Wyly—725
Binding energies in region of Pb, Katharine Way—1448(L)
Bremsstrahlung, nuclear isomerism of In^{115}, Walter C. Miller and Bernard Waldman—329(A), 425
Of Ce (141), C. E. Mandeville and E. Shapiro—1834
Charge-symmetrical forces, Wigner's theory of heavy nuclei, V. F. Weisskopf and David H. Frisch—1297(A)
Effective range of nuclear forces, F. C. Barker and R. E. Peierls—312(L)
Energy levels in Ca^{41}, Vance L. Sailor—1836
Energy levels in S, Perry W. Davison—757
Energy levels of N^{15}, W. E. Shoupp, B. Jennings, and K. H. Sun—1
Exchange moments of H^3 and He^3, R. Avery and E. N. Adams II—1106(L)
Formation of elements, nuclear stability, J. S. Smart—1379
Hyperfine structure of tritium, Edward B. Nelson and John E. Nafe—343(A)
Interaction integrals, heavy nuclei, David H. Frisch—1297(A)
Of Li^7, angular correlations, α-γ-emission, Bernard T. Feld—1618(L)
"Magic numbers," Otto Haxel, J. Hans D. Jensen, and Jans E. Suess—1766(L)
Masses of nuclei Ne to Cl, H. T. Motz and R. F. Humphreys—1289(A)
Meson theory of nuclear forces, Gentaro Araki—1101(L)
Shell structure, Eugene Feenberg and Kenyon C. Hammack—332(A), 1877; Maria Goeppert Mayer—1969(L); Eugene Feenberg, Kenyon C. Hammack, and L. W. Nordheim—1968(L)
Shell structure and isomerism, Eugene Feenberg—320(L)
Spin-orbit coupling, D. R. Inglis—1767(L)
Spins, moments and shells, L. W. Nordheim—1894
Stability of isobaric pair, M. Gurevitch—767
Symmetrical meson theory of nuclear forces, Ta-You Wu and H. M. Foley—1681
Tensor forces and triton binding energy, Herman Feshbach and William Rarita—1384
Threshold for $C^{12}(d, n)N^{13}$, T. W. Bonner, J. E. Evans, and J. E. Hill—1398
Vector and pseudovector theories, Gentaro Araki—1262(L)
Water drop model, alpha-decay, B. T. Darling and J. E. Garvey—1296(A)
Nucleons
Charge density and magnetic moments, Murray Slotnick and Walter Heitler—1645
Interaction between nucleons, meson theory, L. Van Hove—1519
Production of π-mesons in collisions, L. L. Foldy and R. E. Marshak—1493

Optical constants and properties
Of germanium films, W. H. Brattain and H. B. Briggs—1705
Index of refraction of films of LiF, L. G. Schulz—345(A)
Molar refraction of carbon dioxide, Victor H. Coffin and Clarence E. Bennett—215(A)
Scattering by inhomogeneous solids, A. M. Bueche and P. Debye—1308(A)
Soap solutions, P. Debye—1308(A)

Packing fraction (see also **Isotopes**)
Of Ni isotopes, A. E. Shaw—331(A), 1011
Pair production
In field of electron, J. A. Phillips and P. Gerald Kruger—1289(A)
Paschen-Back effect (see **Zeeman effect**)
Phosphorescence
Spectra of phosphors, J. C. D. Milton and R. Hofstadter—1289(A)
Photo-conductivity
In tungstate phosphors, Clifford C. Klick and James H. Schulman—1606(L)
Photo-disintegration
Angular distribution of photo-neutrons, Bernard Hamermesh and Albert Wattenberg—1290(A); Edwin P. Meiners, Jr., David R. Smith, and Lewis Slack—1632(A)
Angular distribution of protons, disintegration of deuteron, N. O. Lassen—1099(L)
Of Cd, R. B. Duffield and J. D. Knight—1465(A), 1613(L)
"Cross-over transitions" in Cl^{38}, Co^{60}, Br^{82}, and Sb^{124}, V. Myers and A. Wattenberg—992(L)
Of D and Be, Arthur H. Snell, E. C. Barker, and R. L. Sternberg—1290(A)
Of Sn, production of In^{118} and In^{119}, R. B. Duffield and J. D. Knight—1967(L)
Thresholds, J. McElhinney, A. O. Hanson, R. A. Becker, R. B. Duffield, and B. C. Diven—542
Yields of some reactions, M. L. Perlman—988(L)
Photoelectric effect and properties; cells
Applied electric fields, two-step potential barrier, Thomas H. Jacobi—1599
Fermi level at arsenic surfaces, E. Taft and L. Apker—344(A), 1181
Surface effect, R. E. B. Makinson—1908
Surface states, work function of semiconductors, Jordan J. Markham—1310(A)
Work function of semiconductors, temperature dependence, A. H. Smith—953

Work function of semiconductors, temperature variation, surface states, Jordan J. Markham and P. H. Miller, Jr.—959
Photography (see also **Methods and instruments**)
Electron tracks in emulsions, R. H. Herz—478
Grain density in tracks of heavy particles, M. Blau—279
Photovoltaic effect
Photovoltaic effect in Ge by α- and deuteron bombardment, M. Becker and H. Y. Fan—1631(A)
Theory, p-n barrier in semiconductor, H. Y. Fan—1631(A)
Piezoelectric effect
Constants of alpha- and beta-quartz, Richard K. Cook and Pearl G. Weissler—1283(A)
Of potassium dihydrogen arsenate, Thaddeus Niemiec—215(A)
Plasticity
Plastic deformation of crystals, Donald Wahl—1627(A)
Polymerization, properties of polymers
Band emission spectra of polymers, Wm. W. A. Johnson, Natalie S. Johnson, and Daniel P. Norman—1320(A)
Butyl rubber-filler systems, Robert L. Zapp and Eugene Guth—1300(A)
Crystallization of aromatic polyesters, Harry J. Kolb and Emmette F. Izard—1331(A)
Depolymerization by irradiation, role of cavitation, Alfred Weissler—1313(A)
Determination of molecular weights, W. M. Cashin and P. Debye—1307(A)
Dynamics of polymer solutions, W. O. Baker, W. P. Mason, and J. H. Heiss—1301(A)
Equilibria in dyeing of Nylon, W. R. Remington and E. K. Gladding—1330(A)
Gough-Joule coefficients and moduli of rubbers, F. S. Conant, G. L. Hall, and G. R. Thurman—1314(A)
Infra-red absorption spectra at low temperatures, Gilbert W. King, H. O. McMahon, and R. M. Hainer—1320(A)
Macromolecular nomenclature, M. L. Huggins—1330(A)
Mass spectrometric study of copolymer pyrolyses, L. A. Wall—1331(A)
Micelles in organic acid monolayers, H. T. Epstein—1628(A)
Properties of flexible molecules, Jacob Riseman—1308(A)
Properties of plasticizers, R. F. Boyer—1314(A)
Pyrolysis of hydrocarbon polymers, S. L. Madorsky, S. Straus, Dorothy Thompson, and Laura Williamson—1331(A)
Second-order transition temperature, Harry J. Kolb and Emmette F. Izard—1331(A)
Soap solutions, P. Debye—1308(A)
In solid state, E. Miller, I. Fankuchen, and H. Mark—1314(A)
Time and stress effects in rubber, J. R. Beatty and J. M. Davies—1314(A)
Transition temperatures of methyl methylmethacrylate polymers, Thomas F. Protzman—1627(A)
Viscous elasticity and bond rupture, G. D. Halsey, Jr.—1300(A)
X-ray diffraction, stretching and relaxation of polyethylene, Alexander Brown—1330(A)
Positrons
Theory, R. P. Feynman—1321(A); Frederik J. Belinfante—1633(A)
Three-photon annihilation of electron-positron pair, A. Ore and J. L. Powell—1696, 1963(L)
Proceedings of the American Physical Society
Founding of Society, Frederick Bedell—1601
Metropolitan Section, Columbia University, New York City, October 22, 1948—703
New England Section, Bowdoin College, Brunswick, Maine, October 23, 1948—215
Chicago, Illinois, Meeting, November 26–27, 1948—325
Annual Meeting, New York City, January 26–29, 1949—1279
Berkeley, California, Meeting, February 3–5, 1949—1456
Ohio Section, Columbus, Ohio, February 14, 1949—1113
Cleveland, Ohio, Meeting, March 10–12, 1949—1624
Metropolitan Section, Bell Telephone Laboratories, Murray Hill, New Jersey, March 25, 1949—1635
Protons
Reactions involving polarized protons, Lincoln Wolfenstein—1664

Quantum electrodynamics (see also **Field theory**)
Dispersion, K. M. Watson and J. M. Jauch—1249
Divergences in field theory, K. M. Case—1440(L)
Fields of vector mesons with negligible mass, Frederik J. Belinfante—1321(A)
Generalized quantum-electrodynamics, Frederik J. Belinfante—337(A)
Klein-Nishina formula, correction, David Feldman and Julian Schwinger—338(A)
Magnetic internal conversion coefficient, S. D. Drell—338(A)
Polarization of vacuum, Julian Schwinger—651; S. T. Ma—1264(L); Hartland S. Snyder—1623(L); Jerzy Rayski—1961(L)
Radiation theories, F. J. Dyson—486
Radiative corrections to Klein-Nishina-formula, R. Schafroth—1111(L)
S-matrix, F. J. Dyson—1736
Self-energy of bound electron, Norman M. Kroll and Willis E. Lamb, Jr.—388
Shift of energy levels, J. B. French and V. F. Weisskopf—338(A)
Subtraction formalism, T. A. Welton—1321(A)
Theory of positrons, R. P. Feynman—1321(A)
Quantum mechanics (see **Mechanics, quantum**)

Radiation
Annihilation radiation from Cu^{64}, J. W. M. DuMond, D. A. Lind, and B. B. Watson—1226
Bremsstrahlung from 19.5-Mev electrons, H. W. Koch and R. E. Carter—1950(L)
Bremsstrahlung produced by protons, John L. Powell—32
In magnetic fields, Felix Ehrenhaft—1628(A)
Phenomenological electrodynamics, dispersion, K. M. Watson and J. M. Jauch—1249
Radio (see also **Ionosphere**)
Meteor speed measurements by radio, D. D. Cherry and C. S. Shyman—1441(L)
Solar radio noise, Andrew V. Haeff—1333(A), 1546
Radioactivity (see also **Disintegration of nucleus**)
α-decay, water drop model, B. T. Darling and J. E. Garvey—1296(A)
α-radioactivity, elements lighter than Bi, N. E. Ballou—1105(L)
Of Sb^{125}, C. E. Mandeville and E. Shapiro—897(L)
Of A^{41}, H. Brown and V. Perez-Mendez—1276(L)
Of At^{210}, excitation functions of Bi, E. L. Kelly and E. Segrè—999
Of Be^{10}, D. J. Hughes and C. Eggler—1285(A)

Radioactivity (continued)
β- and gamma-rays of Sb^{125}, Bernard D. Kern, A. C. G. Mitchell, and Daniel J. Zaffarano—1287(A)
β-decay of Be^{10}, R. E. Marshak—513, 1285(A)
β-decay of B^{12} and Li^{8}, W. F. Hornyak and T. Lauritsen—1462(A)
β^{+}-decay of F^{18}, J. P. Blaser, F. Boehm, and P. Marmier—1953(L)
β-decay of Ag^{110}, Werner S. Emmerich and J. D. Kurbatov—1446(L)
β-decay of Sr^{89}, Lewis Slack, Charles H. Braden, and Franklin B. Shull—1965(L)
β-energy release in tritium, L. Slack, G. E. Owen, and H. Primakoff—1448(L)
β-particles from tritium, W. J. Byatt, F. T. Rogers, Jr., and Arthur Waltner—909(L)
β-ray spectra of C^{14}, L. Feldman and C. S. Wu—1286(A)
β-ray spectra of Cu^{64}, C. S. Wu and R. D. Albert—1107(L); R. D. Albert and C. S. Wu—1286(A)
β-spectra of Sr^{90} and Y^{90}, E. N. Jensen and L. Jackson Laslett—1949(L); Charles H. Braden, Lewis Slack, and Franklin B. Shull—1964(L)
β-spectrum of Be^{10}, D. J. Hughes, C. Eggler, and C. M. Huddleston—515
β-spectrum of H^{3}, G. C. Hanna and B. Pontecorvo—983(L)
β-spectrum of RaE, Lawrence M. Langer—328(A); R. Morrissey and C. S. Wu—1288(A); Arthur Waltner and F. T. Rogers, Jr.—1445(L)
Of C^{10} and O^{14}, R. Sherr, H. R. Muether, and M. G. White—282, 328(A)
Of Ce (141), C. E. Mandeville and E. Shapiro—1834
Of Cs^{137}, Allan C. G. Mitchell and Charles L. Peacock—197(L); Charles L. Peacock and Allan C. G. Mitchell—1272(L)
Of Co isotopes, Thomas J. Parmley, Burton J. Moyer, and Robert C. Lilly—619
Of Co^{55}, Martin Deutsch and Arne Hedgran—1443(L)
Coincidence studies on Au^{199}, Fred Maienschein and J. Lawrence Meem, Jr.—1632(A)
Coincidences in Be^{10} beta-rays, S. G. Hughes and W. E. Stephens—1286(A)
Of Cb^{95}, J. E. Hudgens, Jr. and W. S. Lyon—206(L)
Of Cb^{96}, D. N. Kundu and M. L. Pool—1690
Of Cu^{64}, C. S. Wu and R. D. Albert—315(L)
Decay constant of ThC', F. W. Van Name, Jr.—100
Decay of I^{131} to metastable Xe^{131}, A. R. Brosi, T. W. DeWitt, and H. Zeldes—1615(L)
Decay of K^{40}, E. L. Fireman—1447(L)
Decay of tritium, bound electron creation, P. M. Sherk—789
Delayed neutron emission, K. H. Sun, B. Jennings, W. E. Shoupp, and A. Allen—1302(A)
Detection of gamma-rays with crystals, Robert Hofstadter—796
Doppler broadening of gamma-ray line, V. K. Rasmussen, C. C. Lauritsen, and T. Lauritsen—199(L)
Double beta-decay from $_{50}Sn^{124}$, E. L. Fireman—323(L)
Effect of atomic electrons on decay constant, E. Segrè and C. E. Wiegand—39
Electron-neutrino angular correlation, beta-decay of He^{6}, James S. Allen, H. R. Paneth, and A. H. Morrish—570
Electron spectra of I^{131}, J. M. Cork, H. B. Keller, J. Sazynski, W. C. Rutledge, and A. E. Stoddard—1621(L)
Electrostatic interaction, alpha-radioactivity, Melvin A. Preston—90
Emission rate of beta-rays, R. K. Clark and G. Failla—328(A)
Of Eu isotopes, Richard J. Hayden, John H. Reynolds, and Mark G. Inghram—1500
Forbidden transition of Yt^{91}, Lawrence M. Langer and H. Clay Price, Jr.—1109(L)
Of Gd and Tb, F. D. S. Butement—1276(L)
γ-radiation from Au^{198}, Kai Siegbahn and Arne Hedgran—523(L)
γ-radiation from Zn^{65} and Co^{60}, Erling N. Jensen, L. Jackson Laslett, and William W. Pratt—458
γ-ray spectroscopy, T. Lauritsen and W. F. Hornyak—1462(A)
γ-rays following Au^{198} β-decay, D. Saxon and R. Heller—330(A), 909(L)
γ-rays from I^{131}, precision measurements, David A. Lind, James Brown, David Klein, David Muller, and Jesse DuMond—1544
γ-rays from Na^{24} and V^{48}, J. Eugene Robinson, Michel Ter-Pogossian, and C. Sharp Cook—1099(L)
γ-rays from Ta, J. M. Cork, H. B. Keller, J. Sazynski, W. C. Rutledge, and A. E. Stoddard—1778(L)
γ-rays of W^{187}, Louis A. Beach, Charles L. Peacock, and Roger G. Wilkinson—211(L)
Gases by deuteron bombardment, H. Brown and V. Perez-Mendez—1286(A)
Geiger-Nuttall relationship, Sukumar Biswas—530(L)
Of Ge^{77} and Ge^{71}, C. E. Mandeville, Y. H. Woo, M. V. Scherb, W. B. Keighton, and E. Shapiro—1528
Of Hf^{175}, Geoffrey Wilkinson and Harry G. Hicks—696(L)
Half-life and energy in alpha-decay, I. Perlman, A. Ghiorso, and G. T. Seaborg—1096
Half-life and energy of tritium decay, G. H. Jenks, J. A. Ghormley, and F. H. Sweeton—701(L)
Half-life of C^{14}, Antoinette G. Engelkemeir, W. H. Hamill, Mark G. Inghram, and W. F. Libby—1825
Half-life of Xe^{133}, J. Macnamara, C. B. Collins, and H. G. Thode—532(L)
Half-lives between millisecond and second, J. E. R. Holmes, J. Y. Mei, and R. S. Turgel—889(L)
Internal conversion electrons from metastable Te^{125}, R. D. Hill, G. Scharff-Goldhaber, and G. Friedlander—324(L)
Of I^{124}, J. Lawrence Meem, Jr., and Fred Maienschein—1632(A)
Of I^{131}, David Moe, George E. Owen, and C. Sharp Cook—1270(L); Daniel J. Zaffarano, Allan C. G. Mitchell, and Bernard D. Kern—1632(A)
Of Lu^{177}, Donald G. Douglas—1960(L)
Magnetic internal conversion coefficient, S. D. Drell—132
Magnetic multipole internal conversion, I. S. Lowen and N. Tralli—529(L)
Of Mn^{54}, isobar Fe^{54}, J. D. Kurbatov and Donald Gideon—328(A)
Of Hg^{203}, Hilding Slätis and Kai Siegbahn—318(L)
Of Nd isotopes, Geoffrey Wilkinson and Harry G. Hicks—1687
Neutron induced activities of Ge, Y. H. Woo, C. E. Mandeville, M. V. Scherb, and W. B. Keighton—1286(A)
Of N^{12}, Luis W. Alvarez—1815
Numerical calculation of internal conversion, electric dipole case, B. A. Griffith and J. P. Stanley—534(L), 1110(L)
Of Pt and Au, Geoffrey Wilkinson—1019
Positron to negatron ratio in decay of Cl^{36}, Francis Johnston and John E. Willard—528(L)
Of K^{40}, J. J. Floyd, C. D. Coryell, and L. B. Borst—328(A); Robert W. Stout—1107(L); David E. Alburger—1442(L)

Of K^{40}, age of earth, erratum, T. Gráf—534(L)
Of K^{40}, energy of beta-rays, J. J. Floyd and L. B. Brost —1106(L)
Of K^{42}, Franklin B. Shull and Eugene Feenberg—1768(L)
Of K^{43}, Roy Overstreet, Louis Jacobson, and P. R. Stout—231
Of Pr^{142}, C. E. Mandeville—1017, 1287(A)
Radiations from 2.7-day Au^{198}, Paul W. Levy and E. Greuling—819
Radiations from Cd^{115}, $*In^{115}$, and Hf^{181}, C. E. Mandeville, M. V. Scherb, and W. B. Keighton—221, 329(A)
Radiations from Hf^{181}, K. Y. Chu and M. L. Wiedenbeck—226
Range-energy curves for alpha-particles, William P. Jesse and John Sadauskis—1110(L)
Of rare earths, thulium isotopes, Geoffrey Wilkinson and Harry G. Hicks—1370
Of Rh and Pd, D. T. Eggen and M. L. Pool—1464(A)
Of Sc and V, N. L. Krisberg and M. L. Pool—1286(A), 1693
Screening effects on beta-spectra, C. Longmire and H. Brown—264, 328(A), 1102(L)
Of Ag^{110}, Kai Siegbahn—1277(L); Fu-Chun Yu, Lin-Sheng Cheng, and J. D. Kurbatov—1287
Of Ag^{111}, Cd^{111}, and In^{111}, A. C. Helmholz, R. W. Hayward, and C. L. McGinnis—1469(A)
Of Ag^{113} and Ag^{115}, R. B. Duffield and J. D. Knight—1465(A), 1613(L)
Simultaneous beta-gamma emission, Conrad L. Longmire—15
Stopping powers for alpha-particles of 15 to 37 Mev, E. L. Kelly—1006
Superposition principle, R. C. Prim—1293(A)
Of Ta^{182}, Louis A. Beach, Charles L. Peacock, and Roger G. Wilkinson—329(A)
Of Tl from Au, D. A. Orth, L. Marquez, W. J. Heiman, and D. H. Templeton—1100(L)
Three collateral alpha-decay chains, W. W. Meinke, A. Ghiorso, and G. T. Seaborg—314(L)
Of W^{187} and Au^{199}, Charles L. Peacock and Roger G. Wilkinson—329(A)
Uranium Y, G. B. Knight and R. L. Macklin—34
Of Yb, J. M. Cork, H. B. Keller, J. Sazynski, A. Stoddard, and W. C. Rutledge—1287(A)
Of Yb by neutrons, J. M. Cork, H. B. Keller, W. C. Rutledge, A. E. Stoddard, and J. Sazynski—1133

Rectifier (see **Electrical conductivity and resistance**)

Relativity
Evolution of expanding universe, R. A. Alpher and R. C. Herman—1333(A)
Formulation of quantum theory of radiation, S. T. Ma —535(L)
Geodesic postulate, field equations, A. Schild and L. Infeld—1323(A)
Quantum theory restrictions on general theory, M. F. M. Osborne—1457(A), 1579
Radially symmetric distributions of matter, Max Wyman—1930
Radiation scattering, Otto Halpern and Harvey Hall—1322(A)
Relativistic field theories, T. S. Chang—967
Solutions of Dirac equations, A. H. Taub—1322(A)

Resistance, electrical (see **Electrical conductivity and resistance**)

Scattering of atoms and molecules
Fast argon atoms in argon, H. W. Berry—913

Scattering of electrons, neutrons, and ions (see also **Electron diffraction**)
Absorption of slow neutrons by He_3 nuclei, L. D. P. King and Louis Goldstein—1302(A)
Analysis of nucleon-nucleon scattering, Geoffrey F. Chew and Marvin L. Goldberger—1637
Angular distribution, neutrons by protons, H. H. Barschall and R. F. Taschek—342(A)
Arc-chord differences, W. T. Scott—1763(L)
Be-H reactions and scattering, R. G. Thomas, W. A. Fowler, and C. C. Lauritsen—1463(A); R. G. Thomas, S. Rubin, W. A. Fowler, and C. C. Lauritsen—1612(L)
Cloud-chamber tracks of positive particles, Gerhart Groetzinger, Fred Ribe, and Lloyd Smith—342(A)
Crystal orientation, scattering of neutrons, G. P. Arnold, V. W. Myers, and A. H. Weber—217
Of D by He, J. Morris Blair, George Freier, E. E. Lampi, and William Sleator, Jr.—1678
Double refraction and polarization of neutrons, Otto Halpern—343(A)
Elastic scattering of neutrons, A. Bratenahl, R. H. Hildebrand, C. E. Leith, and B. J. Moyer—1466(A)
Electrostatic scattering of neutrons, S. M. Dancoff and S. D. Drell—341(A)
Energy loss of fast charged particles, K. R. Symon—332(A)
Energy loss of H^1 and H^2 nuclei in Au and Al, T. A. Hall and S. D. Warshaw—891(L)
Of fast neutrons, H. Feshbach and V. F. Weisskopf—342(A)
By gas in synchroton, Nelson M. Blachman and Ernest D. Courant—315(L)
Of high energy neutrons, S. Fernbach, R. Serber, and T. B. Taylor—1352
Inelastic, of fast neutrons, Bernard T. Feld—1115
Inelastic, of electrons from copper single crystal, Paul P. Reichertz and H. E. Farnsworth—1902
Inelastic, of protrons, C. Levinthal, E. A. Martinelli, and A. Silverman—1467(A)
Line shapes in nuclear paramagnetism, erratum, G. E. Pake and E. M. Purcell—534(L)
Magnetic scattering of elementary nucleons, Joseph W. Weinberg—348(A)
Multiple scattering, H. S. Snyder and W. T. Scott—1296(A)
Multiple scattering in cloud-chamber tracks, Martin Berger and Gerhart Groetzinger—342(A)
Multiple scattering in photographic emulsions, Leslie L. Foldy—311(L)
Neutron-electron interaction, M. Slotnick—1295(A)
Neutron inelastic scattering data, Bernard T. Feld—1302(A)
Neutron-proton calculations, J. M. Blatt and J. D. Jackson—341(A)
Neutron-proton scattering, R. Christian and E. Hart—1465(A); R. S. Christian—1675
Neutron-proton scattering at 90 Mev, Keith Brueckner, Walter Hartsough, Evans Hayward, and Wilson M. Powell—555
N-p scattering with 90- and 40-Mev neutrons, J. Hadley, E. Kelly, C. Leith, E. Segrè, C. Wiegand, and H. York—351
Neutron scattering at high energies, F. Rohrlich and J. Eisenstein—705
Of neutrons by D, J. H. Coon, R. F. Taschek, and S. G. Forbes—1465(A); J. A. Spiers—1765(L)
Neutrons by paramagnetic crystals, I. W. Ruderman, W. W. Havens, Jr., T. I. Taylor, and L. J. Rainwater—895(L), 1296(A)
Of neutrons by polarized nuclei, M. E. Rose—213(L)

Scattering of electrons, neutrons, and ions (continued)
Neutrons by protons, angular distribution, H. H. Barschall and R. F. Taschek—1819
Of neutrons by protons with non-central interaction, K. N. Hsu and T. M. Hu—987(L)
Neutrons with electrons in Bi, L. J. Rainwater, I. I. Rabi, and W. W. Havens, Jr.—1295(A)
Polarization of *d-d* neutrons, Lincoln Wolfenstein—342(A)
Of protons by Li, W. A. Fowler, C. C. Lauritsen, and S. Rubin—1463(A)
Protons by Li^7 and Be^9, E. Richard Cohen—1463(A); W. A. Fowler, C. C. Lauritsen, and S. Rubin—1471(A)
Proton-proton experiments, analysis, G. F. Chew and M. L. Goldberger—1466(A)
Proton proton scattering, calculations, J. D. Jackson and J. M. Blatt—1296(A)
Proton-proton scattering models, L. Goldstein and W. H. Lane—1296(A)
Protons scattered by He^4, angular distribution, George Freier, Eugene Lampi, W. Sleator, and J. H. Williams—342(A), 1345
Radiative corrections to electron scattering, Julian Schwinger—898(L)
Range of force for *S* state of two protons, G. Breit and W. G. Bouricius—1029
Reactions involving polarized protons, Lincoln Wolfenstein—1664
Relativistic treatment, *n-p* scattering, F. E. Alzofon—1773(L)
Resonance scattering of neutrons by Co, F. G. P. Seidl—1508
S-wave proton-proton scattering, R. D. Hatcher, G. B. Arfken, and G. Breit—1389
Scattering of neutrons by Pb, H. T. Gittings, H. H. Barschall, and G. G. Everhart—1610(L)
Scattering of protons in hydrogen, C. L. Critchfield and D. C. Dodder—419
Scattering phase calculations, approximation method, H. Ekstein—1322(A)
Slow neutron scattering, G. Placzek—1295(A)
Space distribution of slow neutrons, G. C. Wick—738
Spin dependence of slow neutron scattering by deuterons, E. Fermi and L. Marshall—578
Spin-dependent neutron scattering, C. G. Shull and E. O. Wollan—1302(A)
Theorem on cross sections, G. C. Wick—1459(A)
Wave function of electron in field of atom, Su-Shu Huang—980(L)

Scattering of radiation
Coherent scattering and negative energy states, Otto Halpern and Harvey Hall—910(L)
By inhomogeneous solids, A. M. Bueche and P. Debye—1308(A)
Of low energy γ-rays by protons, L. L. Foldy—1634(A)
Multiple Compton scattering, W. R. Faust and M. H. Johnson—467
Relativistic theory, Otto Halpern and Harvey Hall—1322(A)

Secondary electrons (see **Electrons, secondary**)

Semiconductors (see **Electrical conductivity and resistance**)

Shock waves
At air-water interface, H. Polachek and R. J. Seeger—1294(A)
Conical nose at supersonic speeds, E. V. Laitone—1294(A)
Finite amplitude pressure waves, Bruno W. Augenstein—521(L)
Mach reflection, W. Bleakney, D. K. Weimer, and C. H. Fletcher—1294(A)
Theory of shock tube, G. N. Patterson—1294(A)
Thickness, G. R. Cowan and D. F. Hornig—1294(A)

Solid state (see **Crystalline state**)

Sound (see **Acoustics**)

Spectra, absorption
Association bands in ultraviolet spectra of bridged polymers, Gladys A. Anslow and Ruth C. Shea—1318(A)
Atmospheric ammonia, M. V. Migeotte and R. M. Chapman—1611(L)
Of atmospheric methane, Arthur Adel—322(L)
Of crystalline benzene, R. D. Mair and D. R. Hornig—1283(A)
Of dense Li vapor, Shang-yi Ch'en and Chih-san Chang—81
Of dimethyldiacetylene, Forrest F. Cleveland, K. W. Greenlee, and E. E. Bell—334(A)
Fundamental bands in AsH_3 and AsD_3, Virginia Marie McConaghie and Harald H. Nielsen—633
Of H_2S, Harold R. Grady, Paul C. Cross, and Gilbert W. King—1450(L)
Of hydroquinone catechol and resorcinol vapor, Carl A. Beck—334(A)
Induced by intermolecular forces, M. F. Crawford, H. L. Welsh, and J. L. Locke—1607(L)
Infra-red of cholesterol at low temperatures, R. M. Hainer, Gilbert W. King, and H. O. McMahon—1320(A)
Infra-red bands of difluoromethane, Hugh B. Stewart and Harald H. Nielsen—640
Magnetic resonance of chromic alums, B. Bleaney—1962(L)
Microwave magnetic resonance absorption in nickel salt, A. N. Holden, C. Kittel, and W. A. Yager—1443(L)
Microwave spectrum of carbonyl selenide, M. W. P. Strandberg, T. Wentink, Jr., and A. G. Hill—827
Of neodymium bromate crystals, A. Benton and E. L. Kinsey—888(L)
Of neoprene, M. B. Hall and W. E. Mochel—1330(A)
O^{17} and S^{36} in rotational spectrum of OCS, W. Low and C. H. Townes—529(L), 1318(A)
Principal series of K, Rb, and Cs, H. R. Kratz—1844
Resonance absorption in paramagnetic compound, A. N. Holden, C. Kittel, F. R. Merritt, and W. A. Yager 1614(L)
Rotational spectrum of OCS, M. W. P. Strandberg, T. Wentink, Jr., and R. L. Kyhl—270
Of Na, E. R. Thackeray—1840
Of some polymers at low temperatures, Gilbert W. King, H. O. McMahon, and R. M. Hainer—1320(A)

Spectra, atomic
Electromagnetic shift of energy levels, J. B. French and V. F. Weisskopf—1240
Fine structure in singly ionized He, Miriam Skinner and W. E. Lamb, Jr.—1325(A)
Isotope shift in He, Mark Fred, Frank S. Tomkins, and James K. Brody—1772(L)
Isotope shifts in U, L. E. Burkhart, George Stukenbroeker, and Sam Adams—83
Shift of $2^2S_{1/2}$ state in H and D, R. C. Retherford and W. E. Lamb, Jr.—1325(A)
Structure of ^2D terms of arc spectrum of Li, B. Edlen and K. Liden—890(L); K. W. Meissner, L. G. Mundie, and P. H. Stelson—891(L)

Spectra, general
Hydrogen spectrum, Gertrude Schwarzmann—1334(A)

Spectra, microwave
Absorption of organic vapors, Börge Bak, Erik Stenberg Knudsen and Erhardt Madsen—1622(L)
Absorption spectrum of O_2, M. W. P. Strandberg, C. Y. Meng, and J. G. Ingersoll—1524
Of carbonyl selenide, M. W. P. Stranberg, T. Wentink, Jr., and A. G. Hill—827
Ferromagnetic resonance in iron crystal, Arthur F. Kip and Robert D. Arnold—1556
Of formaldehyde, J. K. Bragg and A. H. Sharbaugh—1774(L)
Magnetic resonance absorption in chrome alum, W. A. Yager, F. R. Merritt, A. N. Holden, and C. Kittel—1630(A)
Magnetic resonance absorption in nickel salt, A. N. Holden, C. Kittel, and W. A. Yager—1443(L)
Magnetic resonance absorption in O_2, Robert Beringer and J. G. Castle, Jr.—1963(L)
Of CH_3Br, A. Harry Sharbaugh and John Mattern—1102(L)
Of CH_3F, CHF_3, and PF_3, O. R. Gilliam, H. D. Edwards, and Walter Gordy—1014
Of methyl cyanide and iso-cyanide, Harald H. Nielsen—1961(L)
Nuclear quadrupole effects, J. H. Goldstein and J. K. Bragg—1453(L)
Paramagnetic absorption in copper sulfate pentahydrate, John Wheatley and David Halliday—1412
Paramagnetic resonance absorption in copper sulfate, Robert D. Arnold and Arthur F. Kip—1199
Of paramagnetic salts, Yu Ting, Roy C. Weidler, and Dudley Williams—980(L)
Paschen-Back effect in NH_3 and N_2O, C. K. Jen—1319(A)
Region of three to five mm, Alex. G. Smith, Walter Gordy, James W. Simmons, and William V. Smith—260
Resonance absorption in paramagnetic compound, A. N. Holden, C. Kittel, F. R. Merritt, and W. A. Yager—1614(L)

Spectra, molecular (see also **Molecular structure and constants**)
Ammonia inversion spectrum, P. W. Anderson—1450(L)
Analysis of bands of HCN, I-Shan Chen and E. E. Bell—1113(A)
Band of CO in solar spectrum, Marcel V. Migeotte—1108(L)
Excited-state bands in atmosphere, Arthur Adel—1262(L)
Fundamental bands of NH_3, Darwin L. Wood—1113(A)
Of hexachloroethane, Rose A. Carney and Forrest F. Cleveland—333(A)
Infra-red, N. Ginsburg—1317(A)
Nuclear quadrupole effects, J. H. Goldstein and J. K. Bragg—1453(L)
Of some tribromomethanes, Shirley E. Rosser and Forrest F. Cleveland—333(A)
Of some trichloromethanes, James P. Zietlow, Forrest F. Cleveland, and Arnold G. Meister—333(A)
Of trans-dichloroethylene, E. Kreusch, J. S. Ziomek, and Forrest F. Cleveland—334(A)

Spectroscopy, technique
Microwave spectroscopy, Alex. G. Smith, Walter Gordy, James W. Simmons, and William V. Smith—260
Slit-width adjuster for infra-red spectrometer, H. O. McMahon, Gilbert W. King, and R. M. Hainer—1459(A)

Stark effect
Dipole moment of HNCS, C. I. Beard and B. P. Dailey—1318(A)
In symmetric top molecules, W. Low and C. H. Townes—1319(A)
Second-order in methyl chloride, Robert Karplus and A. Harry Sharbaugh—889(L), 1449(L)
Stark effects in OCS, R. G. Shulman and C. H. Townes—1318(A)

Statistical mechanics (see **Mechanics, statistical**)

Superconductivity (see **Electrical conductivity and resistance**)

Thermal conductivity
Thermal conductivity of glasses, Charles Kittel—972

Thermal diffusion
Separation of A^{36} by thermal diffusion, James O. Buchanan—1332(A)

Thermal expansion
Of $Li_2SO_4 \cdot H_2O$, Charles S. Smith and H. H. Landon—1625(A)

Thermionic emission; Emitting surfaces
Applied electric fields, two-step potential barrier, Thomas H. Jacobi—1599
Free alkaline earth metal in filaments, George E. Moore, H. W. Allison, and James Morrison—347(A)
Gas in cathode coating assemblies, Bernard Wolk and Harold Jacobs—1312(A)
Oxide cathode interface and coating voltages, A. Eisenstein and J. R. Young—347(A)
Thoria cathodes, O. A. Weinreich—1312(A)

Thermodynamics
Calculation of thermodynamic functions, Harvey Einbinder—1335(A)
Fountain effect in helium II, R. J. Harrison—1311(A)
Pressure in thermodynamics, Boris Leaf—339(A)
Properties of diiodoacetylene and some symmetrical-top acetylenes, Joseph S. Ziomek and Forrest F. Cleveland—334(A)
Theory of fluctuations, Harvey Einbinder—1335(A)
Of thermomagnetic generator, L. Brillouin and H. P. Iskenderian—1325(A)

Ultrasonics (see also **Acoustics**)
Absorption in viscous liquids, Joseph L. Hunter—1627(A)
Attenuation of sound in helium, Martin Greenspan—197(L)

Viscosity
Of mixtures of He_3 and He_4, D. ter Haar and H. Wergeland—886(L); H. Wergeland and D. ter Haar—1310(A)
Second viscosity of liquids, L. N. Liebermann—1415

Work function (see also **Thermionic emission; Photoelectric effect**)
Of Li, Paul A. Anderson—1205
Of semiconductors, Jordan J. Markham—1310(A)

X-rays, absorption, diffraction, scattering, reflection, refraction, and polarization
Absorption edges of Ta, G. L. Rogosa and H. Glaser—1304(A)
γ-ray cross sections, 88 Mev, James L. Lawson—433
K absorption edge of Ca, Marcella Cooper Petree and W. W. Beeman—1628(A)
Spectral equilibrium, penetration of x-rays, U. Fano and P. R. Karr—1303(A)

X-rays, emission (see also **X-rays, spectra and spectroscopy,** etc.)
Bremsstrahlung from 19.5-Mev electrons, H. W. Koch and R. E. Carter—1950(L)
Continuous spectrum from 8A to 14A, S. T. Stephenson and F. D. Mason—1711
Frequency limit of spectrum, G. Schwarz and J. A. Bearden—1304(A)
Investigation of bremsstrahlung, Walter C. Miller and Bernard Waldman—329(A), 425
Precision study of tungsten K spectrum, Bernard B. Watson, William J. West, David A. Lind, and Jesse W. M. DuMond—505; Jesse W. M. DuMond —1266(L)
X-rays, spectra and spectroscopy, wave-length measurements (see also **X-rays, emission**)
K spectra of element 61, L. E. Burkhart, W. F. Peed, and E. J. Spitzer—86
Precision gamma-ray measurements on I^{131}, David A. Lind, James Brown, David Klein, David Muller, and Jesse DuMond—1633(A)
Precision measurements, radiation from Cu^{64}, Jesse W. M. DuMond, David A. Lind, and Bernard B. Watson—1304(A)
Precision measurements, W$K\alpha$, Bernard B. Watson, William J. West, David A. Lind, and Jesse W. M. DuMond—505, 1305(A)
Sensitivity of x-ray films, Herman Hoerlin—1304(A)
Single crystal *vs.* double crystal spectrometers, J. A. Bearden and G. L. Rogosa—1304(A)
X-rays, tubes, apparatus
Power input of tubes, A. I. Berman—1457(A)

Zeeman effect
Paschen-Back effect in NH_3 and N_2O microwave spectra, C. K. Jen—1319(A)

THE AMERICAN INSTITUTE OF PHYSICS

INCORPORATED

57 East 55th Street New York 22, N.Y.

MEMBER SOCIETIES:

American Physical Society
KARL K. DARROW, *Secretary*, Columbia University, New York 27, New York

Optical Society of America
ARTHUR C. HARDY, *Secretary*, Massachusetts Institute of Technology, Cambridge 39, Massachusetts

Acoustical Society of America
WALLACE WATERFALL, *Secretary*, 57 East 55th Street, New York 22, New York

Society of Rheology
EARL K. HUNTER, *Secretary*, Institute of Textile Technology, Charlottesville, Virginia

American Association of Physics Teachers
R. F. PAUSHTER, *Secretary*, University of Illinois, Urbana, Illinois

AFFILIATED SOCIETIES:

American Society for X-Ray and Electron Diffraction
Electron Microscopy Society of America
Physical Society of Pittsburgh
Physics Club of Chicago
Physics Club of Philadelphia
Cleveland Physics Society
Physics Club of the Lehigh Valley

ASSOCIATES:

Over seventy-five leading industrial enterprises and other institutions which contribute to the support of the Institute.

JOURNALS:

The Physical Review
JOHN T. TATE, *Editor*, University of Minnesota, Minneapolis, Minnesota

Reviews of Modern Physics
J. W. BUCHTA, *Editor*, University of Minnesota, Minneapolis, Minnesota

Journal of the Optical Society of America
GEORGE R. HARRISON, *Editor*, Massachusetts Institute of Technology, Cambridge, Massachusetts

The Journal of the Acoustical Society of America
FLOYD A. FIRESTONE, *Editor*, 3818 Fessenden Street, N.W., Washington, D. C.

American Journal of Physics
THOMAS H. OSGOOD, *Editor*, Michigan State College, East Lansing, Michigan

The Review of Scientific Instruments
GAVIN P. HARNWELL, *Editor*, Randal Morgan Laboratory of Physics, University of Pennsylvania, Philadelphia, Pennsylvania

The Journal of Chemical Physics
JOSEPH E. MAYER, *Editor*, Kent Chemical Laboratory, University of Chicago, Chicago 37, Illinois

Journal of Applied Physics
ELMER HUTCHISSON, *Editor*, Case Institute of Technology, Cleveland 6, Ohio

Physics Today
DAVID A. SAXON, *Editor*, American Institute of Physics, 57 East 55 Street, New York 22, New York

OFFICERS

GEORGE R. HARRISON, *Chairman*
Massachusetts Institute of Technology

WALLACE WATERFALL, *Secretary*
The Celotex Corporation

GEORGE B. PEGRAM, *Treasurer*
Columbia University

JOHN T. TATE, *Director on Publications*
University of Minnesota

GOVERNING BOARD

LUIS W. ALVAREZ
J. W. BEAMS
WALLACE R. BRODE
E. U. CONDON
W. F. FAIR, JR.
HARVEY FLETCHER
GEORGE R. HARRISON
W. V. HOUSTON
PAUL KIRKPATRICK
PAUL E. KLOPSTEG
F. W. LOOMIS
PHILIP M. MORSE
J. R. OPPENHEIMER
GEORGE B. PEGRAM
HAROLD K. SCHILLING
JOHN T. TATE
WALLACE WATERFALL
M. W. WHITE
A. G. WORTHING

Consultant on Printing
MELVIN LOOS

ADMINISTRATIVE STAFF

HERBERT A. BARTKY, *Director*

THEODORE VOORHEES, *Business Manager*

RUTH F. BRYANS, *Publication Manager*

[illegible] HOVERSADEN, *Office Manager*

ELLEEN B. NEUBAUER, *Circulation Manager*

The American Institute of Physics was founded in 1931 as a federation of leading societies in the field of Physics. It combines into one operating agency those functions on behalf of physics which can best be done by the Societies jointly. Its purpose is the advancement and diffusion of physics and its applications to human welfare. To this end it publishes for itself or the Societies the nine journals listed on this page; promotes unity and effectiveness of effort among all who are interested in physics; renders numerous direct services to physicists and to the public; and cooperates with government agencies, national associations, educational institutions, technical industries, and others in such manner as to realize the opportunities and fulfill the responsibilities of physics as an important and constructive human activity.